

**Nuclearity and  $\pi$ - $\pi$  Interaction Effects on Olefin Polymerization and  
Coordination Chemistry**

Thesis by  
Jessica Sampson

In Partial Fulfillment of the Requirements  
for the Degree of Doctor of Philosophy

CALIFORNIA INSTITUTE OF TECHNOLOGY  
Pasadena, California

2019  
Defended December 11, 2018

© 2019  
Jessica Sampson  
ORCID: 0000-0001-5273-6843

*Dedicated to every cat I've ever loved.  
Maybe the real PhD was the friends we made along the way.*

## ACKNOWLEDGEMENTS

Without the influence of a great many teachers I would not be writing these acknowledgements on my PhD! thesis, nor be the person I am now, and so any acknowledgements must start with those people. I have had the immense pleasure of growing up in a small town with a large science footprint. With the guidance and assistance of my middle and high school science teachers, Mary Koike, Brian Montgomery, and Brian Hanna, I was able to learn about aquatic toxicology while working for Northwestern Aquatic Sciences and soldering while working for Dr. Haru Matsumoto. As a result of organic chemistry with Profs Yamamoto and Mrksich and inorganic chemistry with Profs Hillhouse, Jordan, and Hopkins at the University of Chicago, though, I pursued synthetic chemistry, which I have grown to love and appreciate beyond my initial fascination. A particular thank you must go to Prof. Richard Jordan at the University of Chicago for the privilege of working in his lab on olefin polymerization catalysis and for greatly influencing how I think about NMR. At Caltech I have learned so much about so many different aspects of and subjects within science and chemistry while working for Prof. Theodor Agapie, both through the breadth of projects pursued and through the breadth of projects that I have had the opportunity to pursue. For these opportunities and what I have learned while working for Theo, I have so much gratitude.

It takes a village to make a thesis and without the many people in the Agapie group and in the CCE Division who have facilitated data collection, data interpretation, scheduling, caffeine, and every other necessary component of research, it is very hard to imagine how anything would ever have been accomplished. Thank you to Dave VanderVelde for help with NMR data acquisition, interpretation, for the privilege of being an NMR GLA for three years, and for answering my questions about how Bruker



instruments work. Thank you to Mike and Larry for helping me with X-ray data collection and refinement, helping me with pretty atrocious disordered solvents, and collecting EAs. A particular thank you to Larry for answering all of my questions over the last few months as I tried to finish things up. Thank you to Dr. Nate Siladke for all your help with figuring out to dispose of hazardous waste, safe chemical storage, and how to improve the lab safety culture. Thank you to Mona and Naseem for help with mass spec data collection and thank you to Alice in the Grubbs group for help with GPC. Thank you to Rick Germond in the Central Warehouse for helping us get N<sub>2</sub> over long weekends and fielding so many annoying requests. Thank you to Ryan Ribson, Dr. Brian Sanders and Dr. Jay Winkler for help with fluorescence and fluorescence decay measurements. Many, many thank yous to Margarita Davis, Pat Anderson, Lynne Martinez, Linda Syme and Julianne Just for help with scheduling this whole thing. Finally, thank you to the staff at Broad Café for helping facilitate early morning to early afternoon coffees and pastries.

None of the polymerization data collection could have been completed without the group of Dr. M. Naseem Akhtar at KFUPM. Thank you to everyone there for helping us, particularly E. A. Jaseer and Rajesh Theravalappil, with GPC acquisition, running polymerization trials, and for your insight into the project directions should be performed.

Within the Agapie group I have overlapped with a lot of very talented chemists. I have worked closely with Dr. Madalyn Radlauer, Dr. Gyeongshin Choi, Diane Rafizadeh, Shuoyan Xiong, and Ryan Ribson. Thank you to all of you for your insights and patience. Thank you also to everyone with whom I have shared space for your patience as well, particularly Marcus Low, Dr. Aimee Bryan, Dr. Jihae Park, Dr. Paul Kelley, Dr. Justin Henthorn, Dr. Josh Buss, Dr. Naoki Shida, Shuoyan Xiong, Meaghan Bruenig, Heui

Beom Lee, and Angela Shiau. To everyone else: thank you so much for your suggestions and help and for listening.

One of the greatest privileges in my time at Caltech is the support that I have received from friends and family. I would not be graduating without the support of my parents, Nicky and David and my brother Daniel; my extended family; my friends from Newport, Alex, Ilana, Hannah, Dana, Zach, Molly, and Logan; my friends from Chicago, Kathryn, Max, Gerry, Josh, and Rob; my friends at Caltech, Jeremy, Tonia, Bekah, and Kelsea; and, last but not least, all of my cats, Opal, Ariel, and Onyx. Thank you to everyone for listening and caring and eating food with me.

A completely serious thank you to everything that got me through the last year and a half: Hollow Knight, Friends at the Table, Opal, Waypoint radio and Twitch streams, Dr. Jan Aura, the Marielda, Twilight Mirage, Pyre, and Journey soundtracks, Captain America: The Winter Soldier, breakfast burritos from Tom's, seasoned fries and potstickers from TeaSpots, the BLTs from Europeane and Ginger, Broad Café, Pasadena Public Library, Destiny 2, Celeste, Hyper Light Drifter, Pokenoya, Trader Joe's Irish Breakfast Tea, whoever introduced me to bullet journaling and the Pomodoro method, my allergist, the Sufjan Stevens discography, octopi, and lizards.

Finally, my deep and profound gratitude to Jeremy, Bekah, Tonia, Alison, my parents, Larry, Mike, Aoshu, Mary, and Joey for your help during December 2018 and January and February 2019. I absolutely could not have finished this thesis without eating nachos with Bekah for a week, sleeping on Jeremy's air mattress for a week, without Mike and Larry's help with the final measurements, without Alison's help with all the administrative nonsense, and without the support of everyone else. Thank you also to the Dean's Office and Brian Stoltz for their help with getting the thesis approved.

## ABSTRACT

This thesis details work performed on the use of secondary coordination sphere effects to impact olefin polymerization activity and tacticity control and the coordination chemistry of Y, Fe, and Cu. Chapter One provides a general introduction and summary of each chapter. Chapter Two describes work in collaboration with KFUPM on nuclearity effects in Zr bisamine bisphenolate complexes. Chapter Three describes the coordination chemistry of arene-appended Y di(pyridyl) pyrrolide complexes and the olefin polymerization activity of tris(dimethylamido) Ti, Zr, and Hf di(pyridyl) pyrrolide complexes. Appendix A describes the effects of bulky trialkylsilyl, triphenylsilyl, and diphenyl(alkyl)silyl substituents on the tacticity control of monozirconium amine bis(phenolate) complexes in 1-hexene polymerization. Appendix B describes the synthesis and structures of miscellaneous dizirconium amine bis(phenolate) complexes which could not be isolated in sufficient purity for olefin polymerization tests. Appendix C describes the synthesis, electrochemistry, and reduction of mesityl-substituted di(pyridyl) NHC supported Fe complexes. Appendix D describes the preparation, solid-state structures, and electrochemistry of di(pyridyl) pyrrolide and di(pyridyl) NHC Cu(I) and Cu(II) complexes displaying  $\pi$ - $\pi$  interactions in the solid state. Appendix E describes work towards the synthesis of di(pyridyl) guanidinate proligands and metal complexes supported by di(pyridyl) urea, monopyridyl and di(pyridyl) N-heterocyclic olefin and N-heterocyclic vinylidene ligands for use in Lewis acid assisted olefin polymerization. Appendix F includes relevant spectra.

## PUBLISHED CONTENT AND CONTRIBUTIONS

Sampson, J.; Choi, G.; Akhtar, M.N.; Jaseer, E.A.; Theravalappil, R.; Al-Muallem, H.A.; and Agapie, T. “Olefin Polymerization by Dinuclear Zirconium Catalysts Based on Rigid Teraryl Frameworks: Effects on Tacticity and Copolymerization Behavior” *Organometallics* **2017**, *36*, 1915-1928. DOI: 10.1021/acs.organomet.7b00015

J.R.S. participated in the development of the project, synthesis of the bisamine bisphenolate Zr complexes, 1-hexene polymerizations, crystal data collection and solution, data analysis, and participated in the preparation and writing of the manuscript.

## TABLE OF CONTENTS

<b>Dedication</b>	<b>iii</b>
<b>Acknowledgements</b>	<b>iv</b>
<b>Abstract</b>	<b>vii</b>
<b>Published Content and Contributions</b>	<b>viii</b>
<b>Table of Contents</b>	<b>ix</b>
<b>List of Figures</b>	<b>xii</b>
<b>List of Schemes</b>	<b>xvi</b>
<b>List of Tables</b>	<b>xviii</b>
 <b>Chapter 1</b>	 <b>1</b>
General Introduction	
 <b>Chapter 2</b>	 <b>7</b>
Olefin Polymerization by Dinuclear Zirconium Catalysts Based on Rigid Teraryl Frameworks: Effects on Tacticity and Copolymerization Behavior	
Abstract	8
Introduction	9
Results	12
Discussion	28
Conclusions	34
Experimental Section	35
References	54
 <b>Chapter 3</b>	 <b>57</b>
Early Metal Di(pyridyl) Pyrrolide Complexes with Second Coordination Sphere Arene- $\pi$ Interactions: Substrate Binding and Ethylene Polymerization	
Abstract	58
Introduction	59
Results and Discussion	62
Conclusions	91
Experimental Section	92
References	110
 <b>Appendix A</b>	 <b>115</b>
Tacticity Control in 1-Hexene Polymerization by Amine Bis(phenolate) Zirconium Catalysts with Bulky Silyl Substituents	
Abstract	116
Introduction	117
Results	119
Discussion	123
Conclusions	124

Experimental Section	125
References	135
<b>Appendix B</b>	<b>136</b>
Preparation of Bimetallic Amine Bis(phenolate) Zr Complexes	
Abstract	137
Introduction	138
Results	139
Discussion	148
Conclusions	149
Experimental Section	150
References	156
<b>Appendix C</b>	<b>157</b>
Coordination Chemistry and Intramolecular $\pi$ - $\pi$ Interactions in Di(pyridyl) NHC and Di(pyridyl) Pyrrolide Supported Fe Complexes	
Abstract	158
Introduction	159
Results	163
Discussion	175
Conclusions	176
Experimental Section	177
References	187
<b>Appendix D</b>	<b>188</b>
Synthesis and Electrochemistry of Di(pyridyl) NHC and Di(pyridyl) Pyrrolide Cu(I) and Cu(II) Complexes	
Abstract	189
Introduction	190
Results	193
Discussion	215
Conclusions	218
Experimental Section	219
References	227
<b>Appendix E</b>	<b>230</b>
Synthesis and Attempted Metalations of $\mu_2$ -NNX (X = O, N, C) Ligands to Support Potential Heterobimetallic Olefin Polymerization Catalysts	
Abstract	231
Introduction	232
Results	235
Discussion	244
Conclusions	245
Experimental Section	246

References	252
<b>Appendix F</b>	<b>254</b>
Spectra	
Chapter 2	255
Chapter 3	270
Appendix A	284
Appendix B	395
Appendix C	298
Appendix D	304
Appendix E	320
<b>About the author</b>	<b>325</b>
CV	326

## LIST OF FIGURES

<b>Chapter 2</b>	
<b>Figure 2.1</b>	10
Selected examples of previously-reported dinuclear polymerization catalysts	
<b>Figure 2.2</b>	11
Compounds prepared and evaluated	
<b>Figure 2.3</b>	15
Solid-state structure of <b>2.11</b>	
<b>Figure 2.4</b>	16
Solid-state structure of <b>2.12</b>	
<b>Figure 2.5</b>	18
Solid-state structure of <b>2.20</b>	
<b>Figure 2.6</b>	31
Comparison of tacticity control by dinuclear catalysts and by monometallic catalysts	
<b>Figure 2.7</b>	33
Plot of the ratio of comonomer incorporation by the bimetallic catalyst to the monometallic catalyst according to the length of the comonomer	
 <b>Chapter 3</b>	
<b>Figure 3.1</b>	59
Examples of ligands incorporating secondary sphere effects	
<b>Figure 3.2</b>	60
Examples of terpyridine-supported complexes displaying $\pi$ - $\pi$ interactions in the solid state	
<b>Figure 3.3</b>	61
Di(pyridyl) pyrrolide ligands bearing flanking aryl groups for $\pi$ - $\pi$ interaction with substrates	
<b>Figure 3.4</b>	66
Solid-state structure of <b>3.14</b>	
<b>Figure 3.5</b>	68
Solid-state structure of <b>3.16</b>	
<b>Figure 3.6</b>	71
Solid-state structure of <b>3.18</b>	
<b>Figure 3.7</b>	74
Preliminary solid-state structure of <b>3.21</b>	
<b>Figure 3.8</b>	76
Solid-state structure of <b>3.22</b>	
<b>Figure 3.9</b>	77
Solid-state structure of <b>3.23</b>	
<b>Figure 3.10</b>	78
Solid-state structure of <b>3.24</b>	



<b>Figure 3.11</b>	80
Solid-state structure of <b>3.25</b>	
<b>Figure 3.12</b>	81-82
Solid-state structure of <b>3.31</b>	
<b>Appendix A</b>	
<b>Figure A.1</b>	117
Kol-type amine bis(phenolate) Zr catalysts for 1-hexene polymerization	
<b>Appendix B</b>	
<b>Figure B.1</b>	141
Solid-state structure of <b>B.6</b>	
<b>Figure B.2</b>	143
Solid-state structure of <b>B.7</b>	
<b>Figure B.3</b>	146
<sup>1</sup> H NMR spectra of a C <sub>2</sub> symmetric <i>para</i> -terphenyl supported dizirconium complex, the C <sub>1</sub> isomer of <b>B.15</b> , and C <sub>s</sub> isomer of <b>B.15</b>	
<b>Figure B.4</b>	147
Solid-state structure of one of the C <sub>s</sub> isomers of <b>B.15</b>	
<b>Appendix C</b>	
<b>Figure C.1</b>	159
Examples of two-coordinate Fe complexes	
<b>Figure C.2</b>	160-
Solid-state structures of <b>C.E</b> and <b>C.F</b>	161
<b>Figure C.3</b>	165
Solid-state structure of <b>C.8</b>	
<b>Figure C.4</b>	166
Solid-state structure of <b>C.9</b>	
<b>Figure C.5</b>	169
Solid-state structure of <b>C.10</b>	
<b>Figure C.6</b>	170
Solid-state structure of <b>C.11</b>	
<b>Figure C.7</b>	171
CV of <b>C.11</b> in acetonitrile	
<b>Figure C.8</b>	172
CV of <b>C.10</b> in acetonitrile	
<b>Figure C.9</b>	173
Reduction of <b>C.11</b> with 0, 1, and 2 equiv. Cp* <sub>2</sub> Co	
<b>Figure C.10</b>	174
Solid-state structure of <b>C.12</b>	

<b>Appendix D</b>	
<b>Figure D.1</b>	191
Examples of heteroleptic Cu(I) phenanthroline complexes exhibiting intramolecular $\pi$ - $\pi$ interactions in the solid state	
<b>Figure D.2</b>	192
Examples of DPP and DPI Cu(I) complexes	
<b>Figure D.3</b>	195
UV-Vis spectra of <b>D.3</b> and <b>D.4</b> in THF	
<b>Figure D.4</b>	197
Solid-state structure of <b>D.2</b>	
<b>Figure D.5</b>	198
Solid-state structure of <b>D.3</b>	
<b>Figure D.6</b>	199
Solid-state structure of the lithium salt of <b>D.1</b>	
<b>Figure D.7</b>	200
Solid-state structure of <b>D.4</b>	
<b>Figure D.8</b>	204
Solid-state structure of <b>D.7</b> with iodide counteranion	
<b>Figure D.9</b>	205
Preliminary solid-state structure of <b>D.7</b> with triflate counteranion	
<b>Figure D.10</b>	206
Solid-state structure of <b>D.8</b>	
<b>Figure D.11</b>	207
CV of <b>D.3</b> in THF	
<b>Figure D.12</b>	208
Partial CV of <b>D.4</b> in THF	
<b>Figure D.13</b>	208
CV of <b>D.7</b> with NaI in CH <sub>3</sub> CN	
<b>Figure D.14</b>	209
CV of <b>D.8</b> in CH <sub>3</sub> CN	
<b>Figure D.15</b>	211
Solid-state structure of the acetonitrile-bound <b>D.11(MeCN)</b>	
<b>Figure D.16</b>	212
Solid-state structure of the co-crystallized acetonitrile-bound <b>D.11(MeCN)</b> with the one-electron oxidized <b>D.3+</b>	
<b>Figure D.17</b>	213
Solid-state structure of <b>D.11</b>	
<b>Appendix E</b>	
<b>Figure E.1</b>	233
Examples of polymerization catalysts incorporating Lewis Acid binding sites	
<b>Figure E.2</b>	234
Targeted di(pyridyl) guanidine and di(pyridyl) NHV catalysts for ethylene-polar- $\alpha$ -olefin copolymerization	

<b>Figure E.3</b>	236
Solid-state structure of <b>E.1</b>	
<b>Figure E.4</b>	237
Solid-state structure of mono(zinc) complex <b>E.7</b>	
<b>Figure E.5</b>	238
Solid-state structure of tri(zinc) complex <b>E.8</b>	
<b>Figure E.6</b>	243
$^1\text{H}$ NMR of the product of <b>E.23</b> with $\text{Pd}(\text{OAc})_2$ in $\text{C}_6\text{D}_6$	

## LIST OF SCHEMES

<b>Chapter 2</b>	
<b>Scheme 2.1</b>	13
Preparation of proligands	
<b>Scheme 2.2</b>	13
Synthesis of phenol ligand precursors featuring <i>ortho</i> -Si <sup><i>i</i></sup> Pr <sub>3</sub>	
<b>Scheme 2.3</b>	17
Synthesis of monozirconium bisamine bisphenolate complexes featuring <i>ortho</i> -Si <sup><i>i</i></sup> Pr <sub>3</sub> substituents	
<b>Chapter 3</b>	
<b>Scheme 3.1</b>	63
Preparation of aryl-substituted di(pyridyl) pyrrole proligands	
<b>Scheme 3.2</b>	63
Preparation of tri- <i>iso</i> -propylsilylethynyl substituted anthracene boronic ester	
<b>Scheme 3.3</b>	65
Preparation of bis(tetramethyldisilylazide)yttrium complexes and subsequent transmetallation upon treatment with AlR <sub>3</sub>	
<b>Scheme 3.4</b>	70
Synthesis and reactivity of (dialkyl)yttrium complex <b>3.18</b>	
<b>Scheme 3.5</b>	79
Synthesis of tris(dimethylamido) Ti, Zr, and Hf complexes	
<b>Scheme 3.6</b>	87
Potential products of activation of (DPP <sup>Ar</sup> )M(NMe <sub>2</sub> ) <sub>3</sub> precatalysts	
<b>Appendix A</b>	
<b>Scheme A.1</b>	120
Synthesis of silyl-substituted amine bis(phenolate) proligands and their corresponding Zr benzyl complexes	
<b>Appendix B</b>	
<b>Scheme B.1</b>	140
Preparation of the mixture of C <sub>s</sub> and C <sub>2</sub> isomers of 9,10-anthracenyl-diyl linked dizirconium complexes	
<b>Scheme B.2</b>	142
Synthesis of water decomposition product <b>B.7-H<sub>2</sub>O</b>	
<b>Scheme B.3</b>	145
Synthesis of <i>meta</i> -terphenyl-supported dizirconium complexes and their corresponding proligands	

<b>Appendix C</b>	
<b>Scheme C.1</b>	160
Preparation of homoligated Fe(II) di(pyridyl) pyrrolide complexes as developed by Dr. Gyeongshin Choi	
<b>Scheme C.2</b>	163
Synthesis of di(pyridyl) NHC proligand <b>C.3</b>	
<b>Scheme C.3</b>	164
Routes pursued for the synthesis of (DPC)HBF <sub>4</sub> ( <b>C.6</b> )	
<b>Scheme C.4</b>	165
Synthesis of mono-ligated Fe(II) dichloride complexes <b>C.8</b> and <b>C.9</b>	
<b>Scheme C.5</b>	167
Synthesis of homoligated DPC and DPI Fe complexes from the corresponding protonated proligands	
<b>Scheme C.2</b>	168
Other routes explored for the synthesis of <b>C.10</b>	
<b>Scheme C.3</b>	173
Stoichiometric reduction of <b>C.11</b> in CD <sub>3</sub> CN	
<b>Appendix D</b>	
<b>Scheme D.1</b>	194
Preparation of DPP-ligated Cu(I) and Cu(II) complexes	
<b>Scheme D.2</b>	202
Preparation of DPI-ligated Cu(I) complexes	
<b>Scheme D.3</b>	210
Oxidation of <b>D.4</b> with AgBF <sub>4</sub> in THF	
<b>Appendix E</b>	
<b>Scheme E.1</b>	235
Attempted preparation of proligand <b>E.4</b> from <b>E.1</b>	
<b>Scheme E.2</b>	237
Preparation of Zn <sup>2+</sup> chloride complexes supported by the di(pyridyl) urea proligand <b>E.6</b> as developed by Diane Rafizadeh	
<b>Scheme E.3</b>	239
Potential routes to proligand <b>E.4</b> through ring closing of diamine <b>E.9</b>	
<b>Scheme E.4</b>	240
Routes to proligand <b>E.17</b> from the corresponding NHC precursor.	
<b>Scheme E.5</b>	240
Preparation of di(pyridyl) N-heterocyclic olefin <b>E.19</b>	
<b>Scheme E.6</b>	241
Preparation of monopyridyl NHO <b>E.23</b>	
<b>Scheme E.7</b>	242
Attempted routes towards the preparation of <b>E.23</b> -bound metal complexes	

## LIST OF TABLES

<b>Chapter 2</b>	
<b>Table 2.1</b>	21-22
1-Hexene and Propylene Homopolymerizations	
<b>Table 2.2</b>	24
Ethylene-propylene copolymerization by <b>2.22</b>	
<b>Table 2.3</b>	25
Ethylene Homopolymerizations and Ethylene-Propylene Copolymerizations	
<b>Table 2.4</b>	27
1-Hexene and 1-Tetradecene Copolymerizations	
<b>Table 2.5</b>	53
Crystal and refinement data for <b>2.11</b> , <b>2.12</b> , and <b>2.20</b>	
<b>Chapter 3</b>	
<b>Table 3.1</b>	85
Ethylene polymerization by (DPP <sup>Ar</sup> )M(NMe <sub>2</sub> ) <sub>3</sub> precatalysts	
<b>Table 3.2</b>	88
Ethylene-1-hexene copolymerization trials by (DPP <sup>Ar</sup> )M(NMe <sub>2</sub> ) <sub>3</sub> precatalysts	
<b>Table 3.3</b>	89
Large-scale ethylene and ethylene-1-hexene copolymerizations by <b>3.25</b>	
<b>Table 3.4</b>	104
Complete small-scale ethylene polymerization results	
<b>Table 3.5</b>	105
Complete ethylene-1-hexene copolymerization results	
<b>Table 3.6</b>	107
Crystal and refinement data for <b>3.14</b> and <b>3.16</b>	
<b>Table 3.7</b>	108
Crystal and refinement data for <b>3.18</b> , <b>3.19</b> , and <b>3.20</b>	
<b>Table 3.8</b>	109
Crystal and refinement data for <b>3.23</b> , <b>3.24</b> , and <b>3.31</b>	
<b>Appendix A</b>	
<b>Table A.1</b>	121
1-hexene polymerization by monozirconium amine bis(phenolate) complexes	
<b>Table A.2</b>	122
Ethylene polymerization by monozirconium amine bis(phenolate) complexes	
<b>Appendix B</b>	
<b>Table B.1</b>	155
Crystal and refinement data for <b>B.6</b> , <b>B.7</b> , and <b>B.14</b>	

**Appendix C**

<b>Table C.1</b>	185
------------------	-----

Crystal and refinement data for complexes **C.8**, **C.9**, and **C.10**

<b>Table C.2</b>	186
------------------	-----

Crystal and refinement data for complexes **C.11** and **C.12**

**Appendix D**

<b>Table D.1</b>	224
------------------	-----

Crystal and refinement data for complexes **D.2**, **D.3**, and **D.4**

<b>Table D.2</b>	225
------------------	-----

Crystal and refinement data for complexes **D.7/I**, **D.7/OTf**, and **D.8**

<b>Table D.3</b>	226
------------------	-----

Crystal and refinement data for complexes **D.11(MeCN)**, **D.11(MeCN)/D3+**, and **D.11**

**Appendix E**

<b>Table E.1</b>	251
------------------	-----

Crystal and refinement data for complexes **E.1**, **E.7**, and **E.8**

## **CHAPTER 1**

### GENERAL INTRODUCTION



This text describes work on the development of new ligand systems for allosteric control in olefin polymerization, substrate activation, and coordination chemistry. Ligands featuring sites for coordination of multiple metal centers,  $\pi$ - $\pi$  interactions, and Lewis acid interactions were specifically targeted. The synthesis of these prolignands, their corresponding transition metal complexes, and the chemistry of such complexes in ethylene and  $\alpha$ -olefin polymerization, activation of substrates featuring extended  $\pi$ -systems, and in coordination chemistry and photochemical studies will be described herein.

Dizirconium amine(bisphenolate) supported by a rigid ter(aryl) framework were initially described by a previous Agapie group graduate student, Dr. Madalyn Radlauer. While she was able to demonstrate that greatly increased tacticity control in 1-hexene polymerization could be achieved using catalysts with small, electron-withdrawing substituents, catalysts bearing large substituents or different central aryl substituents were not explored in this initial work. Amine bis(phenolate) supported mono- and dizirconium complexes featuring *meta*-terphenyl backbones and *ortho* triethylsilyl, tri(*iso*-propyl)silyl, triphenylsilyl, diphenyl-*tert*-butylsilyl, and diphenyl(methyl)silyl substituents with both tetramethylphenyl and 9,10-anthracenyldiyl linkers were prepared (Chapter 2 and Appendices A and B). Monozirconium complexes bearing these substituents were prepared and it was found that activation of the precatalyst bearing an *ortho*-triphenylsilyl substituent lead to poly-1-hexene with 53 % *mmmm*, while the catalysts generated from precatalysts bearing diphenyl(*tert*-butyl)silyl and diphenyl(methyl)silyl substituents produced poly-1-hexene with only 21 % and 15 % *mmmm* (Appendix A). Tetramethylphenyl-linked dizirconium complexes bearing these and other trialkyl(silyl) substituent and 9,10-anthracenyldiyl-linked dizirconium complexes bearing halogen and

alkyl substituents were prepared; however, the  $C_2$  and  $C_s$  metalation isomers could not be separated.

Single isomers of tri(*iso*-propyl)silyl substituted dizirconium complexes linked by the tetramethylphenyl and 9,10-anthracenyldiyl groups could be isolated (Chapter 2). These were tested for 1-hexene homopolymerization under stoichiometric and superstoichiometric conditions and were found to produce poly-1-hexene with enhanced tacticity control and activity over their related monozirconium controls. In conjunction with the group of Dr. M. Naseem Akhtar at King Fahd University of Petroleum and Minerals in Dhahran, Saudi Arabia, such complexes were also tested for their propylene and ethylene homopolymerization activity and their behavior in ethylene- $\alpha$ -olefin copolymerization. With the  $C_2$  symmetric dizirconium catalysts tested for copolymerization it was found that enchainment of the  $\alpha$ -olefin comonomer was more efficient for propylene and 1-hexene as compared with monozirconium catalysts, while enchainment of 1-tetradecene was more efficient for the monozirconium catalysts as compared with the corresponding dizirconium catalysts.

To explore the role of  $\pi$ - $\pi$  interactions on early metal activation of substrates bearing extended  $\pi$  systems, a series of Al, Y, Ti, Zr, and Hf complexes supported by anthracenyl- and mesityl-substituted di(pyridyl) pyrrolide (DPP) complexes were prepared and structurally-characterized. (Chapter 3). Yttrium bis(tetramethyldisilylazide) complexes bearing both mesityl and 9-anthracenyl substituents were prepared and the latter structurally-characterized. Treatment of the mesityl-substituted complex with either  $AlMe_3$  or  $AlEt_3$  lead to DPP transmetalation from Y to Al based on both NMR and X-ray crystallographic characterization of the products of those reactions. Protonolysis of a more soluble version of the 9-anthracenyl-substituted DPP proligand bearing 10-tri(*iso*-propyl)silylethynyl groups allowed access to a bis(neosilyl) Y complex, reaction of which

with ethynyltrimethylsilyl and indole allowed access to the corresponding bis(acetylide) and bis(indolide) complexes. X-ray crystallographic characterization of the latter complex shows distances consistent with  $\pi$ - $\pi$  interactions between the DPP anthracenyl substituents and the indolide ligands, indicating that this ligand scaffold and strategy can be used for  $\pi$ - $\pi$  interaction-directed substrate activation. With the Y complexes, however, relatively facile intermolecular ligand activation limits their utility and substrate scope.

A series of group IV tris(dimethylamido) complexes supported by these DPP ligands bearing aromatic substituents were also prepared and tested for ethylene polymerization activity (Chapter 3). While Dr. Gyeongshin Choi, a previous postdoc in the Agapie group, had demonstrated that  $\text{ZrCl}_3$  complexes of the DPP ligand could be prepared and structurally-characterized, the insolubility of such complexes lead to poor synthetic reproducibility. As a result the more soluble tris(dimethylamido) complexes were prepared. X-ray crystallographic characterization of one of the Ti complexes indicated that binding of only one pyridine arm in the solid-state, while X-ray characterization of a water decomposition product of one of the Zr complexes demonstrated binding of both pyridine arms. Given the equivalent aromatic, pyridine, and dimethylamido resonances observed in the NMR spectra of all tris(dimethylamido) complexes, this indicates that exchange of the pyridine donors of the DPP ligands is fast on the NMR time scale. Upon activation with 200 equiv.  $\text{AlMe}_3$  and 3 equiv.  $[\text{CPh}_3][\text{B}(\text{C}_6\text{F}_5)_4]$  the Zr complexes showed moderate activity and produced low molecular weight products with broad molecular weight distributions, while the Ti complexes produced polyethylene with higher activity and higher molecular weights, also with very broad molecular weight distributions.

Elaborating on these studies of mono(DPP) early metal complexes and previous work by Dr. Gyeongshin Choi on the preparation of bis(DPP) Fe(II) and Cu(II)

complexes, Fe(II) and Cu(I) complexes supported by mesityl-substituted di(pyridyl) NHC ligands and Cu(I) complexes supported by the mesityl-substituted DPP ligand were prepared to probe the effects of  $\pi$ - $\pi$  interactions on their coordination chemistry and photochemistry (Appendices C and D). The homoligated Fe(II) complexes of mesityl-substituted di(pyridyl)imidazole (DPI) and di(pyridyl)imidazoline (DPC) ligands were prepared and characterized in the solid state by X-ray diffraction. While the solid state structure of the bis(DPC) Fe(II) complex featured a six-coordinate Fe center with coordination to all three donors of each ligand, the solid state structure of the bis(DPI) Fe(II) complex featured a four-coordinate Fe center with dissociation of one pyridine arm from each ligand. Reduction of the bis-DPC Fe(II) complex by two equivalents of  $\text{Cp}^*_2\text{Co}$  in acetonitrile resulted in formation of a neutral four-coordinate complex which was characterized both by X-ray diffraction studies.

Bis(DPI) and bis(DPP) mono- and dicopper(I) and copper(II) complexes were also prepared and structurally characterized in addition to related heteroligated phenanthroline-DPP Cu(I) (Appendix D). Four-coordinate Cu(I) centers were observed in all structurally-characterized Cu(I) complexes with dissociation of two pyridine arms in the monocopper complexes and coordination of two pyridine arms to an additional Cu(I) center in the dicopper complexes. Reversible one-electron oxidations were observed for all Cu(I) complexes by cyclic voltammetry. Furthermore, upon oxidation of the heteroligated phenanthroline-DPP complex, however, binding of both pyridine arms was observed by X-ray crystallography. Preliminary work on the study of their photochemistry has been performed by another Agapie group graduate student Ryan Ribson and Gray group postdoc Brian Sanders, however, these studies are ongoing. Distances consistent with  $\pi$ - $\pi$  interactions were observed between at least two of the mesityl-substituents and the backbone of the other DPI or DPC ligands in all of the Cu and Fe complexes,

suggesting that formation of such interactions may not be sufficiently-stabilizing to influence the number of donors to which the metal center is coordinated, their formation can influence the metal geometry.

In conjunction with these studies of DPC and DPI ligands, a series of di(pyridyl) urea, guanidine, and N-heterocyclic olefin ligands were targeted to support potential heterobimetallic polymerization catalysts with  $\mu_2$ -O, N, and C moieties between the active catalysts and pendant Lewis acids. While di(pyridyl) ureas could be generated and work by SURF student Diane Rafizadeh demonstrated demonstrated that they could support dizinc(II) complexes with a  $\mu_2$ -O motif, their conversion into the corresponding di(pyridyl) guanidines was not achieved. Similarly, while oxidation of the DPI ligand with hexachloroethane allowed access to the corresponding 2-chloroimidazolium, conversion to the corresponding guanidine was not observed in preliminary studies. Di(pyridyl) N-heterocyclic olefins could be accessed by condensation of the N,N'-substituted ethylenediamine and deprotonation of the resulting 2-methylimidazolinium; however, promising metalation results were only observed using  $\text{Pd}(\text{OAc})_2$  and purification of the resulting complex could not be achieved.

## CHAPTER 2

OLEFIN POLYMERIZATION BY DINUCLEAR ZIRCONIUM CATALYSTS BASED ON RIGID  
TERARYL FRAMEWORKS: EFFECTS ON TACTICITY AND COPOLYMERIZATION BEHAVIOR

Adapted with permission from *Organometallics*, **2017**, 36, 1915.  
Copyright 2017 American Chemical Society.

**ABSTRACT**

Toward gaining insight into the behavior of bimetallic catalysts for olefin polymerization, a series of structurally related binuclear zirconium catalysts with bisamine bisphenolate and pyridine bisphenolate ligands connected by rigid teraryl units were synthesized. Anthracene-9,10-diyl and 2,3,5,6-tetramethylbenzene-1,4-diyl were employed as linkers. Bulky  $\text{Si}^i\text{Pr}_3$  substituents were used in the position ortho to the phenolate oxygen. Pseudo- $C_s$  and  $C_2$  symmetric isomers are observed for the binuclear complexes of bisamine bisphenolate ligands. In general, binuclear catalysts show higher isotacticity compared to the monozirconium analogues, with some differences between isomers. Amine bisphenolate-supported dizirconium complexes were found to be moderately active (up to  $1.5 \text{ kg mmol}_{\text{Zr}}^{-1} \text{ h}^{-1}$ ) for the polymerization of 1-hexene to isotactically enriched poly-1-hexene (up to 45% *mmmm*) in the presence of stoichiometric trityl or anilinium borate activators. Moderate activity was observed for the production of isotactically enriched polypropylene (up to  $2.8 \text{ kg mmol}_{\text{Zr}}^{-1} \text{ h}^{-1}$  and up to 25.4% *mmmm*). The previously proposed model for tacticity control based on distal steric effects from the second metal site is consistent with the observed behavior. Bisamine bisphenolate supported complexes are active for the production of polyethylene in the presence of MAO with activities in the range of  $1.1\text{--}1.6 \text{ kg mmol}_{\text{Zr}}^{-1} \text{ h}^{-1}$  and copolymerize ethylene with  $\alpha$ -olefins. The size of the olefin affects the level of incorporation differently between monometallic and bimetallic catalysts for the bisamine bisphenolate system. The ratio of the incorporation levels with dinuclear vs mononuclear catalysts decreases with increasing comonomer size. This effect is attributed to steric pressure provided by the distal metal center on the larger olefin in dinuclear catalysts.

## INTRODUCTION

Dinuclear early and late transition metal catalysts have been studied for improved performance in polyolefin synthesis.<sup>1</sup> Enhanced activity, incorporation of  $\alpha$ -olefins, tolerance to functional groups, and tacticity control are among the benefits demonstrated for dinuclear catalysts compared to related mononuclear catalysts. Enhanced activity and 1-hexene incorporation were reported for dizirconium catalysts supported by dimethylsilyl-linked cyclopentadienyl-amide ligands linked via an alkane-diyl chain (**2.A**, Figure 2.1).<sup>2</sup> Increased 1-hexene incorporation was reported with dizirconium complexes supported by fused phenoxy-imine ligands (**2.B**).<sup>3</sup> Pyridine-amide dihafnium complexes with naphthalene-based linkers show enhanced activity for polymerization of ethylene with 1-octene, higher molecular weights, and increased incorporation of the comonomer (**2.C**).<sup>4</sup> Enhanced  $\alpha$ -olefin incorporation by double-decker type dinickel phenoxy-imine catalysts (**2.D**)<sup>5</sup> and enhanced activity for 1-hexene polymerization with enhanced chain straightening by related double-decker  $\alpha$ -diimine dipalladium catalysts have been reported (**2.E**).<sup>6</sup> We have reported enhanced incorporation of unprotected amino olefins and enhanced amine tolerance with dinickel phenoxy-imine catalysts linked via *para*- and *meta*-terphenyl moieties (**2.F**).<sup>7</sup>

Multinuclear catalysts have also been explored for tacticity control, in particular with early metals, though to a much lesser extent than mononuclear systems.<sup>8,9</sup> Dizirconium bis-propagators supported by amidinate ligands (**2.G**) exhibit similar stereoselectivity in the presence of  $\text{ZnEt}_2$  as in its absence in contrast with monometallic catalysts which typically exhibit lower selectivity in the presence of the chain transfer reagent.<sup>10</sup> Dinuclear titanocene complexes (**2.H**) show enhanced syndiotacticity in styrene polymerization relative to the corresponding monotitanium catalysts.<sup>11</sup>



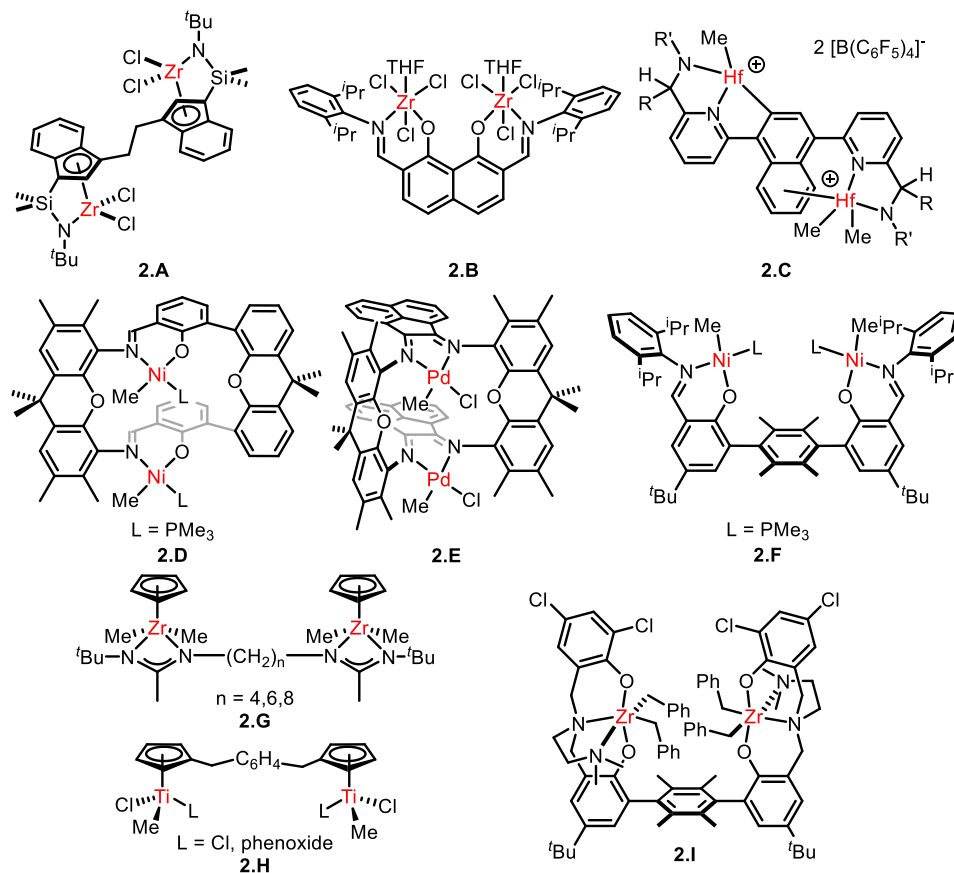


**Figure 2.1.** Selected example of previously-reported dinuclear polymerization catalysts.

Dr. Madalyn Radlauer in the Agapie Group previously reported that bimetallic zirconium amine bisphenolate complexes supported by a rigid *para*-terphenyl linker polymerize propylene and 1-hexene with enhanced activity and tacticity control.<sup>12</sup> Dinuclear **2.I** has activities of up to  $10^3 \text{ kg mmol}_{\text{Zr}}^{-1} \text{ h}^{-1}$  in 1-hexene polymerization and produce poly-1-hexene with  $>75\%$  *mmmm*. The greater activities and isoselectivities of these complexes is attributed to both the ligand environment around each isolated metal center and to the interactions of the growing polymer chain with the sterics of the distal metal center. For comparison, the original  $C_s$  symmetric bisamine bisphenolate system reported by Kol and coworkers has activities of up to  $10^2 \text{ kg mmol}_{\text{Zr}}^{-1} \text{ h}^{-1}$  and produces atactic poly-1-hexene.<sup>13</sup>

Related  $C_2$  symmetric catalysts produce >95% isotactic poly-1-hexene, but with significantly lower activity, though  $C_1$  symmetric versions show enhanced activity with lower isoselectivity.<sup>14</sup> The previous report demonstrated that dizirconium bisamine bisphenolate complexes with bulkier *t*-butyl substituents were less active and produced poly-1-hexene and polypropylene with lower tacticity control compared to complexes with smaller chloride substituents. A combination of steric effects, including the distal pressure of the second metal and the difference in size between the small chloride substituent and the large aryl substituent that also serves as linker was proposed to account for the observed changes in activity and tacticity between mono- and dinuclear catalysts. Variations in the electronic properties of the substituents likely contribute to differences in behavior among the various monometallic or bimetallic catalysts. As options to replace the chloride substituent with a smaller one are very limited, the opposite strategy of significantly increasing the steric bulk is appealing. To gain further insight into structure-function correlations of these dinuclear catalysts, determining the effect of the type of linker employed is desirable. Herein we report the synthesis and characterization of the dizirconium bisamine bisphenolate and (Figure 2.2), and their ethylene, propylene, 1-hexene, and 1-tetradecene homo- and copolymerization behavior.

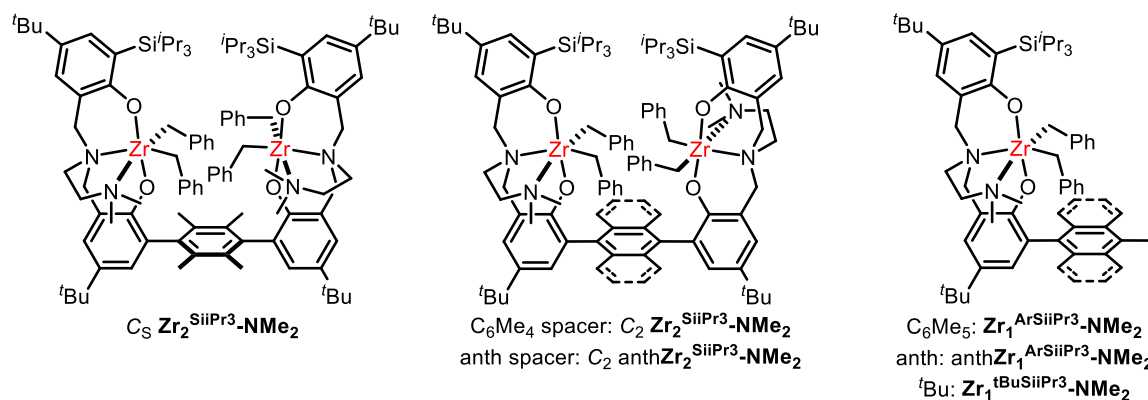
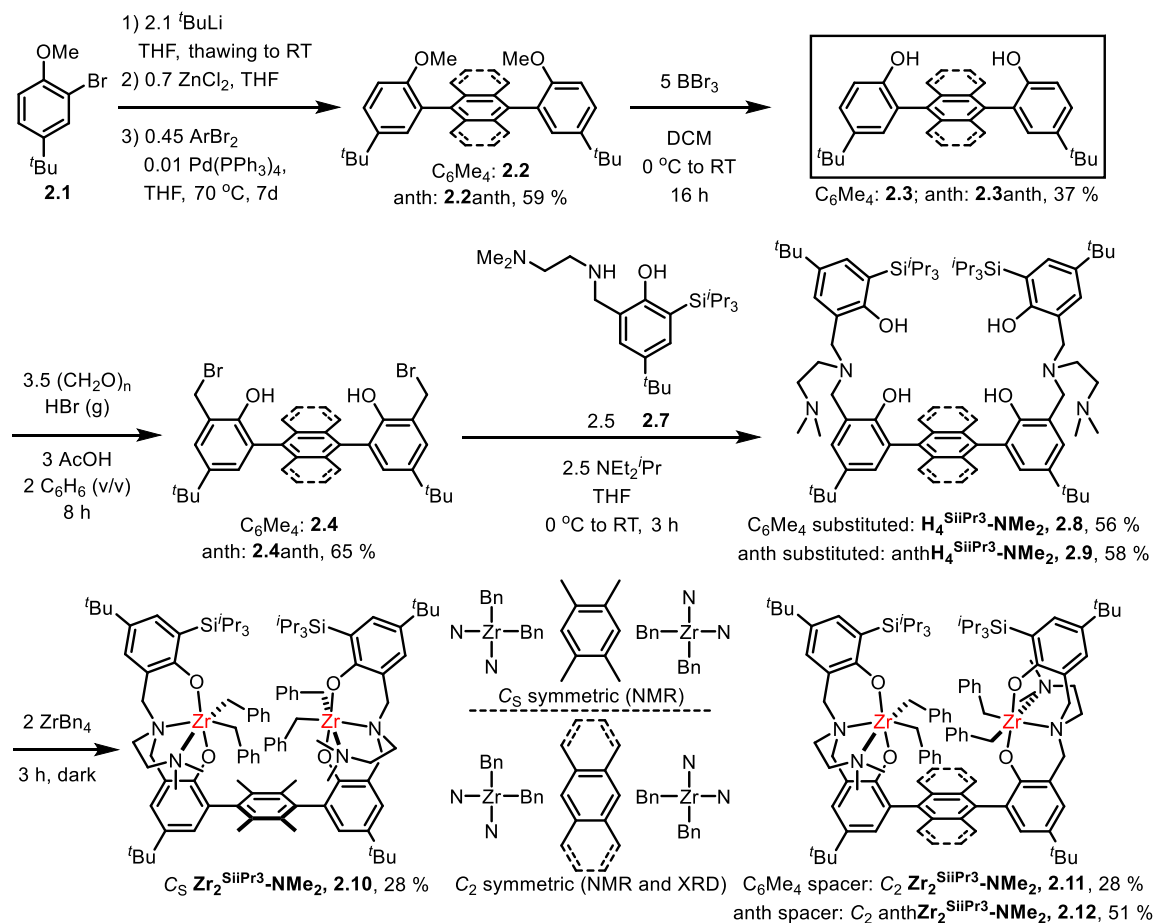


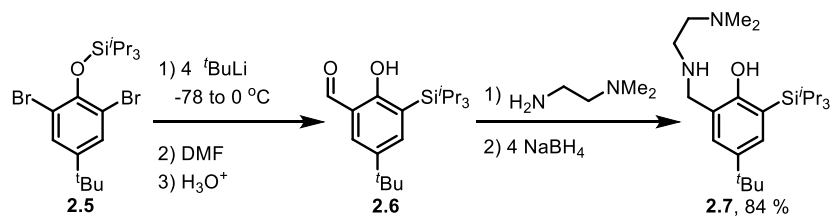
**Figure 2.2.** Compounds prepared and evaluated in this study.

## RESULTS

Dinuclear amine bisphenolate complexes based on a *para*-terphenyl framework were synthesized analogously to the previously reported catalysts<sup>12</sup> (Scheme 2.1). Double Negishi coupling of 2-bromo-4-*tert*-butylanisole with 1,4-dibromo-2,3,5,6-tetramethylbenzene or 9,10-dibromoanthracene affords the corresponding terphenyl compounds **2.2** and **2.2anth** with tetramethylphenyl and anthracenyl linkers. Upon removal of protecting groups with boron tribromide, the *syn* and *anti* atropisomers of the resulting phenols (**2.3** and **2.3anth**) were separated by column chromatography. The *syn* atropisomers were further treated with paraformaldehyde and gaseous hydrogen bromide to afford ligand precursors **2.4** and **2.4anth**. Ligand precursor **2.7** was synthesized starting with the silylation of 2,6-dibromo-4-*tert*-butyphenol (Scheme 2.2). Subsequent *retro*-Brook rearrangement and quench with DMF affords tri-*iso*-propyl substituted salicylaldehyde **2.6**. Reductive amination of this species with N,N-dimethylethylenediamine affords **2.7**. Reaction of **2.4** and **2.4anth** with **2.7** in the presence of NEtPr<sub>2</sub> produces the desired proligands H<sub>4</sub><sup>SiiPr<sub>3</sub></sup>-NMe<sub>2</sub> (**2.8**) and anthH<sub>4</sub><sup>SiiPr<sub>3</sub></sup>-NMe<sub>2</sub> (**2.8anth**) which were purified by column chromatography and isolated in moderate yields (~57%).



**Scheme 2.1.** Preparation of proligands and dinuclear complexes **2.10**, **2.11**, and **2.12**.



**Scheme 2.2.** Synthesis of phenol ligand precursors featuring *ortho*- $\text{Si}^i\text{Pr}_3$  substituents.

Dizirconium complexes supported by these new binucleating ligands were prepared by protonolysis of the phenolic proligands with two equivalents of tetrabenzylzirconium, resulting in a mixture of  $\text{C}_s$  and  $\text{C}_2$  symmetric metalation isomers. Metalation of **2.8** affords that mixture in a roughly one to one ratio. Solubility differences between the two isomers

allowed isolation of the  $C_s$  complex (in up to 95% purity) and the  $C_2$  complex (analytically pure) following recrystallization, each in roughly 25% overall yield. The structure of  $C_2$ - $\text{Zr}_2^{\text{SiPr}_3}\text{-NMe}_2$  (**2.11**) was confirmed by single crystal X-ray diffraction (XRD) analysis (Figure 3). The two Zr centers adopt similar geometries to those seen in previously-reported mono- and bimetallic complexes with bisamine bisphenolate ligands. The distance between the two metal centers is 7.74 Å, longer by more than 0.1 Å than in the solid state structure of  $\text{Zr}_2^{\text{Cl}_4}\text{-NMe}_2$  (7.62 Å) which has the longest distance between the two metal centers of the previously-reported dinuclear complexes linked by terphenyl frameworks. The slightly longer distance between the metal centers may be due to the bulky substituents applying steric pressure on the benzyl ligands. Metalation of **2.9** afforded the  $C_2$  symmetric complex in 85% purity based on  $^1\text{H}$  NMR analysis of the crude reaction mixture. Low temperature metalation improved this to 95%. Recrystallization of this mixture affords analytically pure  $C_2$  isomer. The identity of the isolated complex, **2.12**, was confirmed by XRD (Figure 3). The two Zr centers again adopt similar coordination environments to those in previously-reported Zr complexes of bisamine bisphenolate ligands. The overall geometry of the dinuclear species is similar to that of **2.11** complex. The Zr-Zr distance (7.604 Å) is shorter by more than 0.1 Å compared to the tetramethylphenyl-linked complex. The slightly shorter metal-metal distance may be a consequence of the anthracene linker being flatter than tetramethylbenzene, and alleviating some steric constraints in the cavity between the two metal centers. The proligand  $\text{H}_4^{\text{SiPr}_3}\text{-NEt}_2$  was also prepared; a similar ratio of  $C_s$  and  $C_2$  metalation isomer was obtained in comparison with **2.11**.

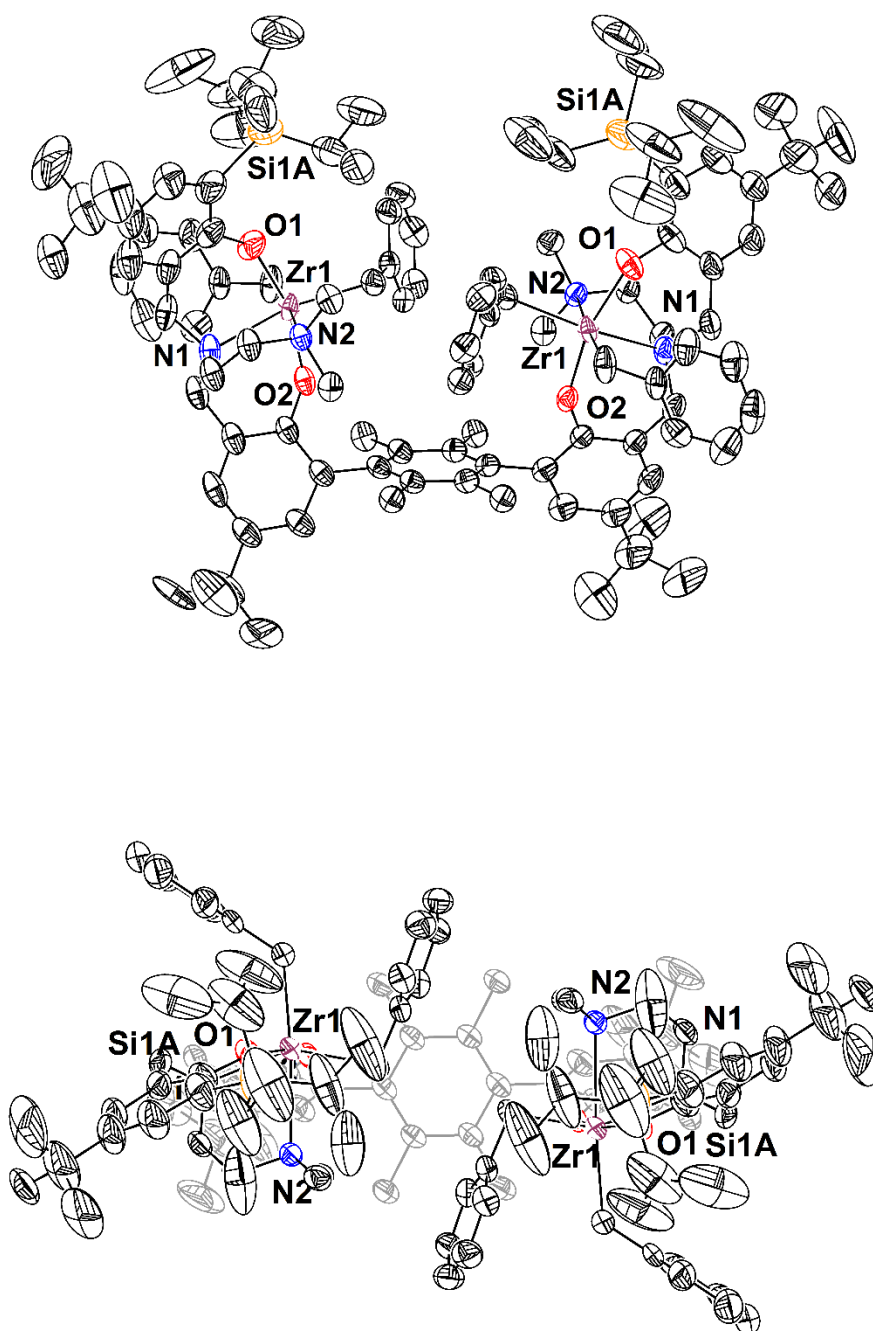


**Figure 2.3.** Solid-state structure of **2.11**. Ellipsoids are drawn at the 50 % probability level and hydrogen atoms are omitted for clarity.

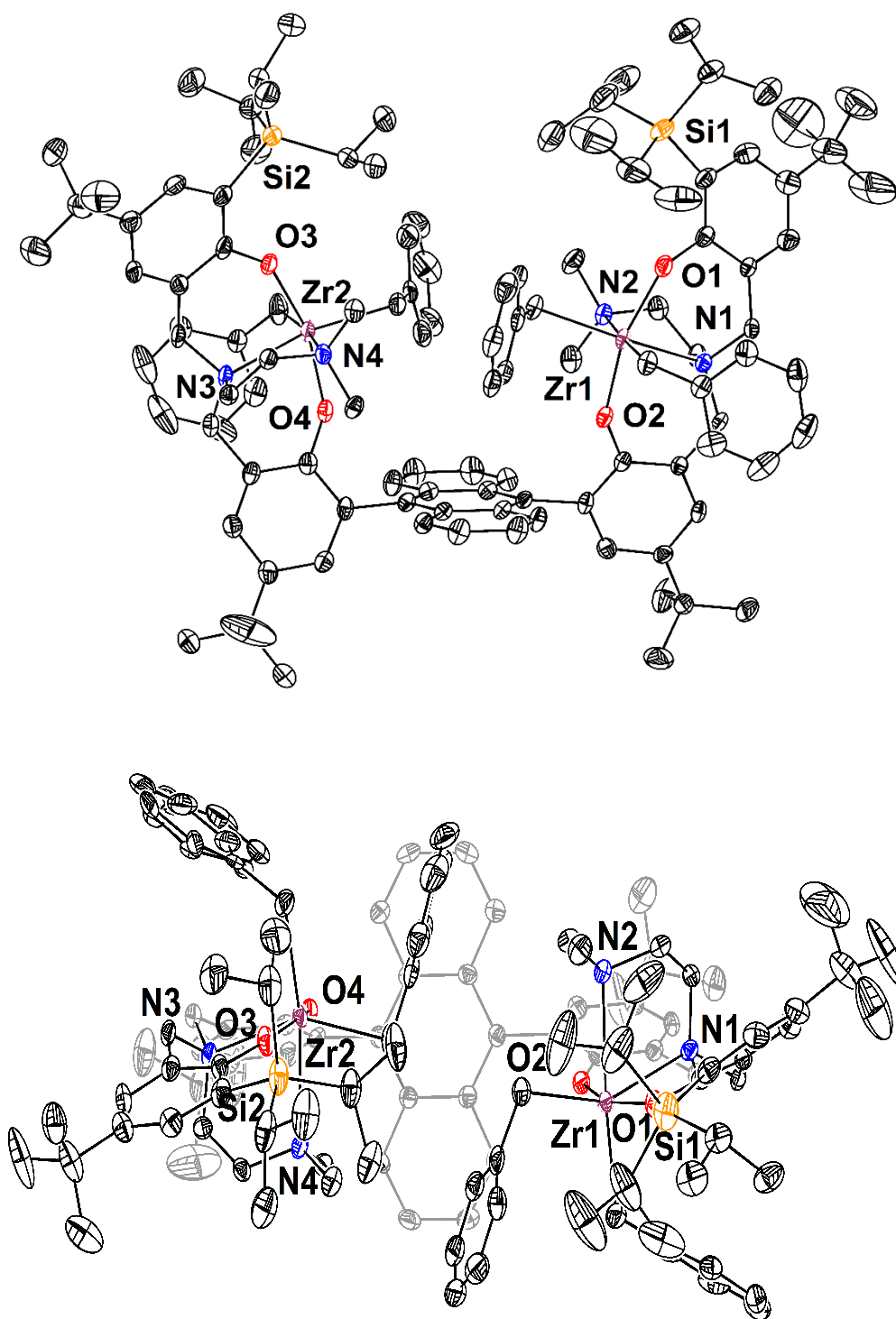
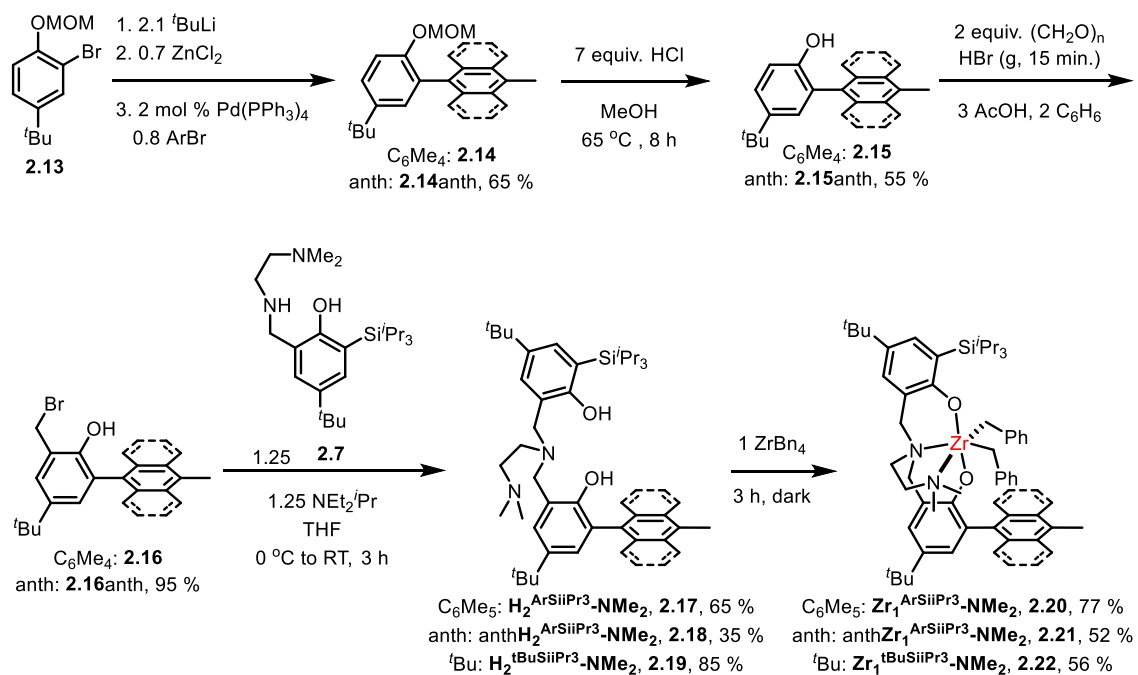


**Figure 2.4.** Solid-state structure of 2.12. Ellipsoids are drawn at the 50 % probability level and hydrogen atoms are omitted for clarity.

Monozirconium amine bis(phenolate) complexes bearing the tri(*iso*-propyl)silyl substituent were also prepared as a comparison to the dizirconium catalyst (Scheme 2.3). The mononucleating proligands were prepared analogously to the dinucleating proligands and the monometallic complexes **2.20**, **2.21**, and **2.22** were synthesized by protonolysis of the corresponding proligand with 1 equiv. ZrBn<sub>4</sub>. The structure of **2.20** was also confirmed by XRD (Figure 2.5).



**Scheme 2.3.** Synthesis of monozirconium bisamine bisphenolate complexes featuring *ortho*-Si*i*Pr<sub>3</sub> substituents.



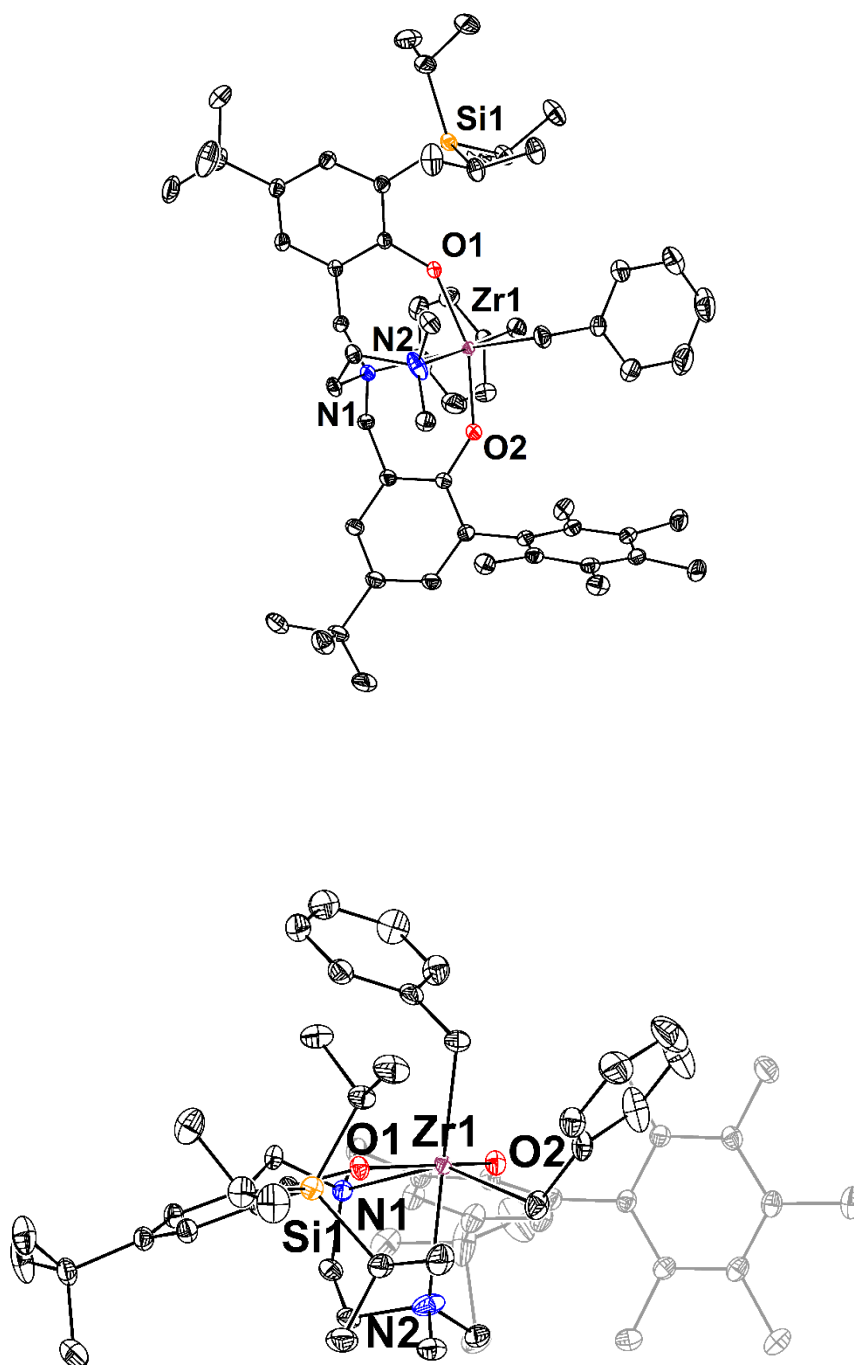


**Figure 2.5.** Solid-state structure of 2.20. Ellipsoids are drawn at the 50 % probability level and hydrogen atoms are omitted for clarity.

**1-Hexene and Propylene Homopolymerization.** The precatalyst performance in 1-hexene polymerization was tested under three sets of conditions: upon activation with stoichiometric amounts of  $[\text{CPh}_3][\text{B}(\text{C}_6\text{F}_5)_4]$  or  $[\text{HNMe}_2\text{Ph}][\text{B}(\text{C}_6\text{F}_5)_4]$ , and with excess MAO. The bimetallic bisamine bisphenolate complexes show moderate activity and produce isotactically enriched poly-1-hexene in the presence of stoichiometric  $[\text{CPh}_3][\text{B}(\text{C}_6\text{F}_5)_4]$  and  $[\text{HNMe}_2\text{Ph}][\text{B}(\text{C}_6\text{F}_5)_4]$  activators. **2.11** and **2.12** generate poly-1-hexene with ca. 30% *mmmm* content with activities in the range of  $0.77 - 1.5 \text{ kg mmol}^{-1} \text{ h}^{-1}$  (Table 2.1, entries 7-8 and 13-14). In the presence of MAO as a cocatalyst the activity of both **2.10** and **2.11** is improved, but the tacticity control is lowered to only 15% *mmmm* (Table 2.1, entry 9). **2.10** has improved tacticity control, producing poly-1-hexene with 45% *mmmm* content in the presence of  $[\text{CPh}_3][\text{B}(\text{C}_6\text{F}_5)_4]$  and  $[\text{HNMe}_2\text{Ph}][\text{B}(\text{C}_6\text{F}_5)_4]$  (Table 2.1, entries 4-6). In contrast, **2.11** has overall lower isotacticity (34% *mmmm*) for 1-hexene homopolymerization in the presence of the borate counteranion as compared to the  $C_s$  isomer, though with improved activity (Table 2.1, entries 4-6 vs. 7-9). All dinuclear catalysts show a slight improvement in activity in the presence of  $[\text{HNMe}_2\text{Ph}][\text{B}(\text{C}_6\text{F}_5)_4]$  compared to  $[\text{CPh}_3][\text{B}(\text{C}_6\text{F}_5)_4]$ . Monometallic **2.20** shows lower activities and similar tacticities to the dinuclear catalysts, except in the presence of the MAO cocatalyst where the monometallic catalyst shows higher tacticity control. Comparing **2.21** and **2.12** for 1-hexene polymerization, the dinuclear precatalyst shows significantly greater tacticity control (between 28 and 42% *mmmm* vs. between 3 and 5% *mmmm* for **2.21**). **2.12** has similar activity and isotacticity compared to **2.11** in the presence of the stoichiometric activators.

In collaboration with the group of Prof. M. Naseem Akhtar at King Fahd University of Petroleum and minerals, the activity of both mono- and dinuclear complexes were tested

for propylene polymerization in the presence of superstoichiometric MAO. **2.10**, **2.11**, and **2.12** show moderate activity ( $1.9 - 2.8 \text{ kg mmol}_{\text{Zr}}^{-1} \text{ h}^{-1}$ ) for propylene polymerization at  $60^\circ\text{C}$  in toluene in the presence of excess MAO at 5 bar propylene pressure (Table 2.1, entries 17, 18, and 20). These catalysts produce low tacticity polypropylene. **2.10** shows slightly lower tacticity control with 18.8% *mmmm* as compared to 25.4% and 23.8% for **2.11** and **2.12** (Table 1, entries 17, 18, and 20). Both **2.20** and **2.21** have lower activity ( $0.55$  and  $0.96 \text{ kg mmol}_{\text{Zr}}^{-1} \text{ h}^{-1}$  respectively) than the dinuclear catalysts and show lower tacticity control (ca. 14% *mmmm*) (Table 2.1, entries 16 and 19).

Table 2.1. 1-Hexene and Propylene Homopolymerizations<sup>a</sup>

Entry	Catalyst	Monomer	Activator	Yield <sup>b</sup>	Activity <sup>c</sup>	% <i>mmmm</i> <sup>d</sup>
1	<b>2.20</b>	1-Hexene	[CPh <sub>3</sub> ][B(C <sub>6</sub> F <sub>5</sub> ) <sub>4</sub> ]	0.076	0.11	34
2	<b>2.20</b>	1-Hexene	[HNMe <sub>2</sub> Ph][B(C <sub>6</sub> F <sub>5</sub> ) <sub>4</sub> ]	0.046	0.069	37
3	<b>2.20</b>	1-Hexene	MAO	0.116	0.17	40
4	<b>2.10</b>	1-Hexene	[CPh <sub>3</sub> ][B(C <sub>6</sub> F <sub>5</sub> ) <sub>4</sub> ]	0.067	0.10	45
5	<b>2.10</b>	1-Hexene	[HNMe <sub>2</sub> Ph][B(C <sub>6</sub> F <sub>5</sub> ) <sub>4</sub> ]	0.238	0.36	45
6	<b>2.10</b>	1-Hexene	MAO	0.613	0.92	10
7	<b>2.11</b>	1-Hexene	[CPh <sub>3</sub> ][B(C <sub>6</sub> F <sub>5</sub> ) <sub>4</sub> ]	0.513	0.77	34
8	<b>2.11</b>	1-Hexene	[HNMe <sub>2</sub> Ph][B(C <sub>6</sub> F <sub>5</sub> ) <sub>4</sub> ]	0.596	0.89	34
9	<b>2.11</b>	1-Hexene	MAO	0.676	1.0	15
10	<b>2.21</b>	1-Hexene	[CPh <sub>3</sub> ][B(C <sub>6</sub> F <sub>5</sub> ) <sub>4</sub> ]	0.036	0.054	5
11	<b>2.21</b>	1-Hexene	[HNMe <sub>2</sub> Ph][B(C <sub>6</sub> F <sub>5</sub> ) <sub>4</sub> ]	0.046	0.069	3
12	<b>2.21</b>	1-Hexene	MAO	0.204	0.31	4
13	<b>2.12</b>	1-Hexene	[CPh <sub>3</sub> ][B(C <sub>6</sub> F <sub>5</sub> ) <sub>4</sub> ]	0.870	1.3	28
14	<b>2.12</b>	1-Hexene	[HNMe <sub>2</sub> Ph][B(C <sub>6</sub> F <sub>5</sub> ) <sub>4</sub> ]	0.980	1.5	33
15	<b>2.12</b>	1-Hexene	MAO	0.860	1.3	42
16	<b>2.20</b>	Propylene	MAO	5.5	0.55	14

17	<b>2.10</b>	Propylene	MAO	19	1.9	19
18	<b>2.11</b>	Propylene	MAO	22	2.2	25
19	<b>2.21</b>	Propylene	MAO	9.6	0.96	15
20	<b>2.12</b>	Propylene	MAO	28	2.8	24

<sup>a</sup>1-Hexene polymerizations were run with 4.0  $\mu\text{mol}$  Zr, 1 equiv.  $[\text{B}(\text{C}_6\text{F}_5)_4]$  activator or 250 equiv. dried MAO, and 5000 equiv. (2.5 mL) 1-hexene in 2.5 mL PhCl for 10 min and propylene polymerizations were run with 10  $\mu\text{mol}$  Zr, 1000 equiv. (2.5 mL) MAO and 5 bar propylene in 85 mL toluene for 60 min in a 250 mL reactor; <sup>b</sup>Yield in g; <sup>c</sup>Activity in  $\text{kg mmol}_{\text{Zr}}^{-1} \text{h}^{-1}$  <sup>d</sup>From integration of the  $^{13}\text{C}\{^1\text{H}\}$  NMR spectra.

The ethylene homopolymerization of all complexes was investigated in the presence of excess MAO by the group of Dr. M. Naseem Akhtar (Table 2.3). Initial optimization with monometallic **2.22** indicated that addition of  $\text{AlMe}_3$  resulted in loss of activity in ethylene-propylene copolymerization. Improved yield was obtained at 60 °C in the presence of MAO alone (Table 2.2). **2.20** and **2.21** both have slightly improved activities (1.6 and 1.5  $\text{kg mmol}_{\text{Zr}}^{-1} \text{h}^{-1}$  respectively) (Table 2.3, entries 1 and 4) though not very different from **2.10**, **2.11**, and **2.12** (1.1 – 1.4  $\text{kg mmol}_{\text{Zr}}^{-1} \text{h}^{-1}$ ) (Table 2.3, entries 2, 3, and 5). Under these conditions, though, high PDIs (between 15 and 47, with multimodal distributions in some instances) were observed for all catalysts; the  $M_N$  values were higher for the bimetallic catalysts (between 17.2 kDa and 26.7 kDa) as compared with the monometallic catalysts (between 4.7 kDa and 8.6 kDa). The high  $T_M$  values support the formation of linear polymers under these conditions with all catalysts.<sup>22</sup>

Ethylene-propylene copolymerization behavior was tested by the group of Dr. M. Naseem Akhtar at KFUPM in the presence of excess MAO under 5 bar total pressure with a 1:3 C<sub>2</sub>:C<sub>3</sub> flow ratio (Table 2.3). Initial optimization with **2.22** indicated that under these conditions propylene was incorporated well with relatively high overall activity (Table 2.2). **2.10**, **2.11**, and **2.12** more effectively incorporate propylene than the corresponding monometallic complexes under these conditions. While **2.20** incorporates only 25% propylene, **2.10** and **2.11** incorporate 52% and 40% respectively and show slightly enhanced activity (2.1 and 2.0 kg mmol<sub>Zr</sub><sup>-1</sup> h<sup>-1</sup> respectively vs. 1.5 kg mmol<sub>Zr</sub><sup>-1</sup> h<sup>-1</sup> for **2.20**) (Table 2.3, entries 10-12). Similarly, **2.21** incorporates 36% propylene while **2.12** incorporates 49% propylene (Table 2.3, entries 13-14). Both anthracene-substituted complexes show enhanced activity and propylene incorporation compared with the phenyl-substituted complexes (36% C<sub>3</sub> for **2.21** vs. 25% C<sub>3</sub> for **2.20** (Table 2.3, entry 13 vs. entry 10) and 49% C<sub>3</sub> for **2.12** vs. 40% C<sub>3</sub> for **2.11** (Table 2.3, entry 14 vs. entry 12)). In the presence of propylene, lower PDI values were observed for these bisamine bisphenolate complexes (between 4.6 and 6.7) compared with ethylene homopolymerization; the M<sub>N</sub> values were higher for the bimetallic catalysts (between 10.6 and 12.2 kDa for the bimetallics and between 3.6 and 7.8 kDa for the monometallics), though the effect is less dramatic than in the ethylene homopolymerizations.

**Table 2.2.** Ethylene-propylene copolymerization by **2.22**.<sup>a</sup>

	<b>C2:C3</b>	<b>Temp</b> (°C)	<b>Coactivator</b>	<b>Time</b> (min)	<b>Yield</b> (g)	<b>Activity</b> (kg mmol <sub>Zr</sub> <sup>-1</sup> h <sup>-1</sup> )	<b>% I<sup>b</sup></b>
1	50:50	30	AlMe <sub>3</sub>	60	3	0.3	32
2	50:50	30	None	60	8	0.8	34
3	50:50	60	None	60	16	1.6	22
4	50:50	80	None	60	14	1.4	43
5	25:75	30	None	38	5	0.8	46
6	25:75	60	None	60	11	1.1	45
7	25:75	80	None	60	13	1.3	35

<sup>a</sup>Polymerizations were run with 10 μmol Zr in 60 mL toluene in the presence of 1000 equiv. (2.5 mL) MAO and 5 bar total pressure; <sup>b</sup>Percentage incorporation of propylene from <sup>13</sup>C{<sup>1</sup>H} NMR integration

**Table 2.3.** Ethylene Homopolymerizations and Ethylene-Propylene Copolymerizations<sup>a</sup>

	<b>Catalyst</b>	<b>% C<sub>2</sub> Feed</b>	<b>% C<sub>3</sub> Feed</b>	<b>Yield (g)</b>	<b>Activity (kg mmol<sub>Zr</sub><sup>-1</sup> h<sup>-1</sup>)</b>	<b>M<sub>N</sub> (kDa)</b>	<b>PDI<sup>b</sup></b>	<b>T<sub>M</sub> (°C)</b>	<b>% I<sup>c</sup> (C<sub>3</sub>)</b>
1	<b>2.20</b>	100	0	16	1.6	4.7	47	133	--
2	<b>2.10</b>	100	0	11	1.1	17	23	134	--
3	<b>2.11</b>	100	0	14	1.4	27	29	133	--
4	<b>2.21</b>	100	0	15	1.5	8.6	15	132	--
5	<b>2.12</b>	100	0	14	1.4	21	32	134	--
10	<b>2.20</b>	25	75	15	1.5	3.6	6.0	76	25
11	<b>2.10</b>	25	75	21	2.1	12	6.6	108	52
12	<b>2.11</b>	25	75	20	2.0	11	6.7	111	40
13	<b>2.21</b>	25	75	24	2.4	7.8	4.6	-- <sup>e</sup>	36
14	<b>2.12</b>	25	75	24	2.4	12	6.3	110	49

<sup>a</sup>Polymerizations were run with 10  $\mu$ mol Zr in 85 mL toluene in the presence of 1000 equiv.

(2.5 mL) MAO and 5 bar ethylene at 60 °C; <sup>b</sup>PDI determined from GPC measurements, where

PDI is defined as  $M_w/M_n$ ; <sup>c</sup>Calculated from DSC measurements; <sup>d</sup>Percentage incorporation of

propylene from  $^{13}\text{C}\{^1\text{H}\}$  NMR integration; <sup>e</sup>Not measured.



Ethylene-1-hexene copolymerization was investigated by Dr. M. Naseem Akhtar at KFUPM in the presence of excess MAO, 3 bar ethylene, and  $1.6 \times 10^4$  equiv. of 1-hexene (Table 2.4). The monometallic catalysts **2.20** and **2.21** both incorporate 1-hexene well (19% and 28% respectively) with similar activity as in the presence of the propylene comonomer (Table 2.4, entries 1 and 4). While the  $C_2$  **2.11** and **2.12** show modest increases (to 22% and 30%, Table 2.4, entries 3 and 5) in comonomer incorporation relative to the monometallic analogs, **2.10** incorporates less of this comonomer than either the  $C_2$  dizirconium complexes or the monozirconium complexes (12% 1-hexene incorporation, Table 2.4, entry 2). PDI values for these catalysts are large under these conditions, with the  $M_n$  values for the polymers obtained from the bimetallic catalysts generally higher compared with the  $M_n$  values from the monometallic catalysts.

To evaluate the effect of comonomer size on incorporation level between mono- and dinuclear catalysts, ethylene-1-tetradecene copolymerizations were also performed by the group of Dr. M. Naseem Akhtar at KFUPM using the bisamine bisphenolate catalysts in the presence of MAO, 3 bar ethylene, and 7900 equiv. of 1-tetradecene. **2.20** has lower activity under these conditions than in the presence of propylene or 1-hexene comonomers, and incorporates 1-tetradecene at 7% level (Table 2.4, entry 10). Both **2.10** and **2.11** have similar activities under these conditions, though the incorporation of the comonomer is lower with the dinuclear catalysts than with the mononuclear catalysts (ca. 6% for **2.10** and ca. 3% for **2.11**). Similarly, **2.12** incorporates around 7% of 1-tetradecene (Table 2.4, entries 11-12), while **2.21** incorporates more (9%, Table 2.4, entry 13). Again, higher  $M_N$  values are obtained with the bimetallic catalysts as compared to the monometallic, though the PDI values remain fairly high for all catalysts under these conditions.

**Table 2.4.** 1-Hexene and 1-Tetradecene Copolymerizations<sup>a</sup>

	<b>Catalyst</b>	<b>Comonomer</b>	<b>Yield</b> (g)	<b>Activity</b> (kg mmol <sub>Zr</sub> <sup>-1</sup> h <sup>-1</sup> )	<b>M<sub>N</sub></b> (kDa)	<b>PDI<sup>b</sup></b>	<b>T<sub>M</sub></b> (°C)	<b>% I<sup>c</sup></b>
1	<b>2.20</b>	1-Hexene	15	1.5	2.2	3.6	104	19
2	<b>2.10</b>	1-Hexene	19	1.9	5.9	3.7	99	12
3	<b>2.11</b>	1-Hexene	20	2.0	8.8	12	105	22
4	<b>2.21</b>	1-Hexene	24	2.4	7.1	3.4	--	28
5	<b>2.12</b>	1-Hexene	19	1.9	11	8.8	104	30
10	<b>2.20</b>	1-Tetradecene	9.7	0.97	17	8.8	61	7
11	<b>2.10</b>	1-Tetradecene	20	2.0	41			6
12	<b>2.11</b>	1-Tetradecene	20	2.0	39	26	104	3
13	<b>2.21</b>	1-Tetradecene	25	2.5	12	2.7	110	10
14	<b>2.12</b>	1-Tetradecene	23	2.3	22	6.6	105	7

<sup>a</sup>Polymerizations were run with 10  $\mu$ mol Zr in 65 mL toluene in the presence of 1000 equiv. (2.5 mL) MAO and 3 bar ethylene and 20 mL ( $1.6 \times 10^4$  equiv.) 1-hexene or 20 mL (7900 equiv.) 1-tetradecene at 60 °C; <sup>b</sup>Yield in g; <sup>c</sup>Activity reported in kg mmol<sub>Zr</sub><sup>-1</sup> h<sup>-1</sup>; <sup>d</sup>M<sub>N</sub> and PDI determined from GPC measurements, where M<sub>N</sub> is reported in kDa and PDI is defined as M<sub>w</sub>/M<sub>N</sub>; <sup>e</sup>Reported in °C, from DSC measurements; <sup>f</sup>% incorporation of the comonomer determined from <sup>13</sup>C{<sup>1</sup>H} NMR integration.

## DISCUSSION

Generally, the mononuclear catalysts show significantly lower activity and tacticity control compared to the dinuclear analogs. These differences may be explained in terms of the distal steric effect of the second metal, limiting anion association and degrees of freedom for olefin insertion<sup>12</sup>. The observed differences between **2.10** and **2.11** suggests that the particular coordination environment of the distal metal center affects reactivity, despite being remote. The shape of the cavity between the two metal centers has consequences on both tacticity and activity.

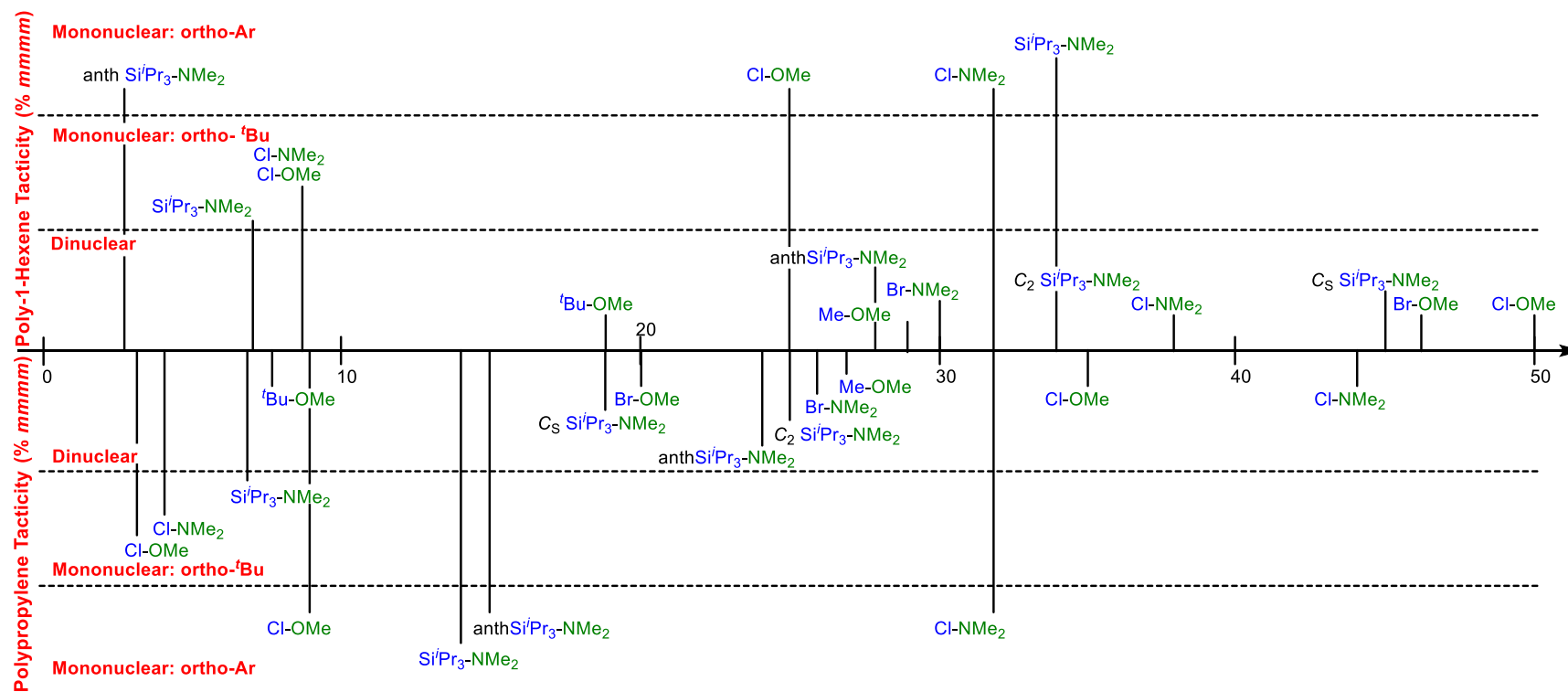
In comparison with the previously-reported complexes bearing *ortho*-pentamethylphenyl substituents, **2.20** shows a decrease in activity relative to  $\text{Zr}_1^{\text{ArCl}_2}\text{-NMe}_2$  ( $1.5 - 1.9 \text{ kg mmol}_{\text{Zr}}^{-1} \text{ h}^{-1}$ ) with fairly similar tacticity control in 1-hexene polymerization (24 -25% *mmmm* for  $\text{Zr}_1^{\text{ArCl}_2}\text{-OMe}$  and 31 - 32% *mmmm* for  $\text{Zr}_1^{\text{ArCl}_2}\text{-NMe}_2$ , Figure 4).<sup>12</sup> **2.21** shows significantly lower tacticity control as compared to these catalysts. For propylene polymerization upon activation with MAO, however, **2.20** and **2.21** show similar tacticity control, both lower than  $\text{Zr}_1^{\text{ArCl}_2}\text{-NMe}_2$ . The <sup>t</sup>Bu-substituted catalysts generally show very low tacticity control. The lower activity of the new catalysts is consistent with the previous observation of higher 1-hexene polymerization activities from complexes bearing ligands with electron-withdrawing substituents.<sup>12,21</sup> The lack of significant improvements in tacticity control for **2.20** and **2.21** could result from one or several features of the previously-proposed mechanism, including site epimerization and selectivity of monomer insertion based on steric control of polymer orientation by the bulk of the aryl substituent. With the more bulky Si<sup>t</sup>Pr<sub>3</sub> substituents, the difference between the two phenolates is less pronounced, potentially leading to less control of polymer chain orientation. The more spherical <sup>t</sup>Bu substituent does not

provide efficient tacticity control likely because it is less expansive compared to the pentamethylphenyl and anthracenyl substituents.

In comparison with the previously-reported bimetallic catalysts supported by amine bisphenolate ligands bearing the bulky *ortho-tert*-butyl substituent ( $\text{Zr}_2^{\text{tBu}_2}\text{-OMe}$ ), the new  $C_2$  symmetric complexes have similar activities for 1-hexene polymerization ( $\sim 1 \text{ kg mmol}_{\text{Zr}}^{-1} \text{ h}^{-1}$ ) but produce significantly more isotactic poly-1-hexene in the presence of the stoichiometric activators (19% *mmmm* for  $\text{Zr}_2^{\text{tBu}_2}\text{-OMe}$ , Figure 2.6). **2.12** shows similar tacticity control (28 % *mmmm*) to the previously-reported  $C_s$  and  $C_2 \text{Zr}_2^{\text{Me}_4}\text{-OMe}$  and to  $C_2 \text{Zr}_2^{\text{Br}_4}\text{-NMe}_2$  (28 – 30% *mmmm*). **2.10** and **2.11** produce similarly isotactically-enriched polymer (34 and 45 % *mmmm*) to that seen for the more sterically-open  $\text{Zr}_2^{\text{Cl}_4}\text{-NMe}_2$ ,  $\text{Zr}_2^{\text{Cl}_4}\text{-OMe}$ , and  $\text{Zr}_2^{\text{Br}_4}\text{-OMe}$  catalysts at room temperature (35 to 50 % *mmmm*), albeit with lower activity. Both **2.12** and **2.11** have similar activity for propylene homopolymerization as  $C_2 \text{Zr}_2^{\text{tBu}_2}\text{-OMe}$ , (ca.  $2 \text{ kg mmol}_{\text{Zr}}^{-1} \text{ h}^{-1}$ ) but with improved tacticity control (24 – 25% *mmmm* vs. 6 – 8% *mmmm*). The new complexes with  $\text{Si}^i\text{Pr}_3$  substituents show similar tacticity control in propylene polymerization as  $\text{Zr}_2^{\text{Br}_4}\text{-OMe}$ ,  $\text{Zr}_2^{\text{Br}_4}\text{-NMe}_2$ , and  $\text{Zr}_2^{\text{Me}_4}\text{-OMe}$ . Importantly, an extensive set of dinuclear catalysts were compared to mononuclear versions, and in *all* cases, the dinuclear catalysts show improvement in tacticity control (Figure 2.6). This suggests that the steric pressure provided by the coordination environment of the second metal restricts the orientation of the polymeryl chain and incoming olefin better than possible in analogous mononuclear systems. Overall, within the series of dinuclear catalysts, increasing steric bulk *ortho* to the phenolate oxygen away from the linker does not benefit control of tacticity. The smallest substituent, chloride, displays the highest degree of tacticity control. This behavior is consistent with the highest *mmmm* content resulting from maximizing the difference in steric profile relative to the linker, with the smaller chloride substituents *ortho* to the phenolate oxygen having the largest impact. The

much larger silyl substituents likely make the two phenolate sides more similar and less discriminating with respect to interaction with the polymeryl chain and the incoming monomer and, therefore, decrease tacticity control.

**Figure 2.6.** (Next page) Comparison of tacticity control by dinuclear catalysts with substituents *ortho* to phenoxide oxygens shown in blue and pendant donors, L, in green and by monometallic catalysts with either *ortho*-aryl substituents ( $\text{Ar} = \text{C}_6\text{Me}_5$  or 9-methylantracenyl) or *ortho*-tert-butyl substituents. 1-hexene polymerizations were run with  $[\text{CPh}_3][\text{B}(\text{C}_6\text{F}_5)_4]$  and propylene polymerizations were run with excess MAO as activators. Legend at bottom provides graphical representations of catalysts and abbreviations under each class of compounds.



Both **2.12** and **2.21** incorporate more of all of the  $\alpha$ -olefin comonomers than the corresponding **2.11** and **2.20** suggesting that the anthracene substituents are not as sterically bulky to the zirconium centers compared to methylated aryl substituents. Comparison of comonomer incorporation levels with  $C_2$  dinuclear vs. mononuclear catalysts reveals a systematic trend. The dizirconium catalysts incorporate 1.4-2.1 times the small propylene comonomer compared to the mononuclear versions, but incorporate the larger 1-hexene comonomer similarly. With 1-tetradecene, however, both the dinuclear  $C_2$  catalysts incorporate less of the comonomer than the corresponding monozirconium catalysts (Figure 2.7). **2.10** does not show a similar behavior. Overall, the  $C_2$  dinuclear catalysts relative to the mononuclear analogs show a decrease in comonomer incorporation with increasing size of the olefin (Figure 2.7). This is consistent with the distal steric bulk of the second metal disfavoring larger comonomer incorporation. This trend is inconsistent with the  $\alpha$ -olefin having an agostic interaction with the second metal center as previously proposed for dinuclear catalysts **2.A** (Figure 2.1).<sup>2</sup> The longer chain olefins are expected to be able to better accommodate such distal agostic interactions and incorporate in higher levels with dinuclear compared to mononuclear catalysts, which is not observed. The proposed steric effect is further supported by the difference in the magnitude of the effects between anthracene and tetramethylbenzene linkers. Plotting the ratio of  $\alpha$ -olefin incorporation with dinuclear vs mononuclear analogs, the tetramethylbenzene linker shows a more pronounced effect with the increasing size of the olefin, which correlates with a higher steric pressure on the incoming olefin from the methyl-substituted linker compared to flatter anthracene (Figure 2.7).

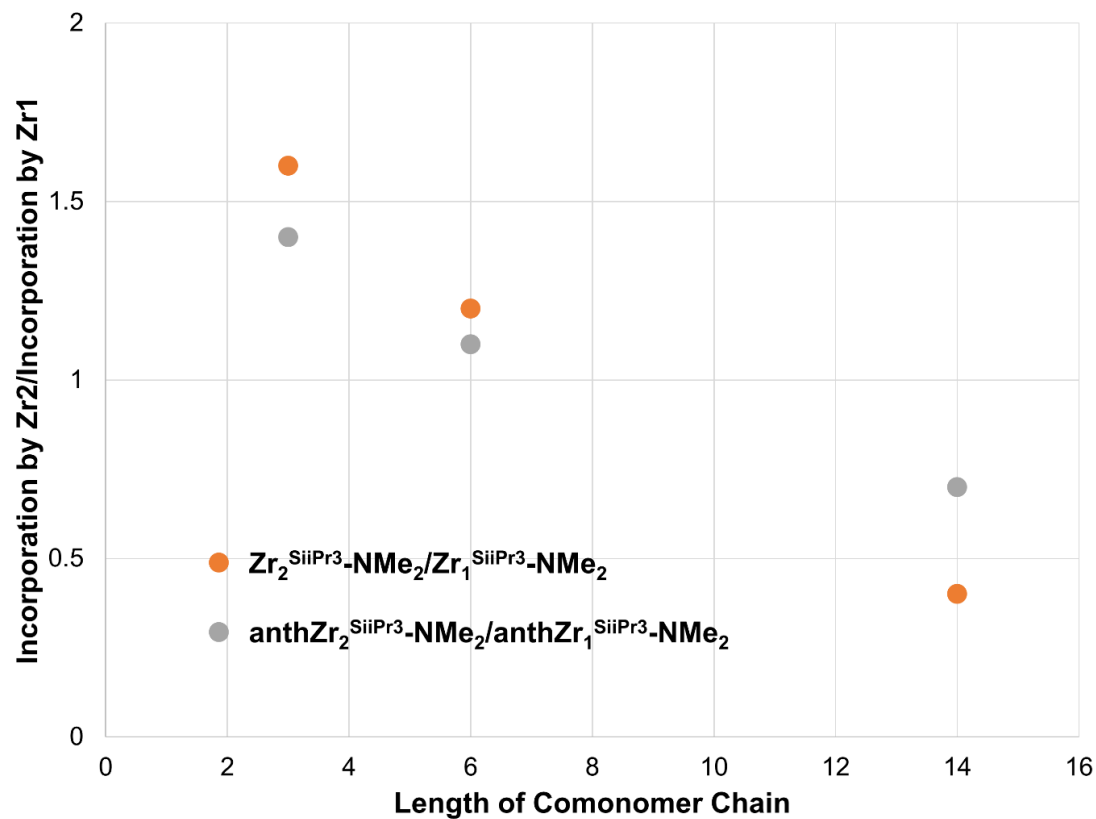


**Figure 2.7.** Plot of the ratio of comonomer incorporation by the bimetallic catalyst to monometallic catalyst according to the length of the comonomer.



## CONCLUSIONS

Mono- and dinuclear Zr benzyl complexes supported by pyridine bisphenolate and bisamine bisphenolate ligands featuring bulky  $\text{SiR}_3$  ( $\text{R} = \text{Pr, Ph}$ ) substituents were prepared and studied for olefin polymerization catalysis. With these compounds, an extensive series of dinuclear olefin polymerization catalysts and their mononuclear analogs is available for structure function studies. Generally, the dinuclear systems show better control of tacticity, although only modest levels of isotacticity were achieved. The distal steric effect caused by the second metal is proposed to lead to improved tacticity control for dinuclear complexes. Of the ligands studied, the largest steric difference between the substituents on the two phenolate ligands bound to the same metal correlates with best tacticity control. This results from a small rather than very large substituent on the phenoxide that is not connected to the linker. Ethylene- $\alpha$ -olefin copolymerization studies revealed that the longer-chain olefins are incorporated at lower levels by dinuclear compared to mononuclear catalysts relative to shorter-chain olefins. This effect is also consistent with steric effects caused by the second metal, and not with a distal agostic interaction. Overall, the reported studies provide fundamental insight into the advantages of dinuclear vs mononuclear catalysts for olefin polymerization, in particular related to control of tacticity and comonomer incorporation.

## EXPERIMENTAL SECTION

*General Notes.* All air- and water-sensitive compounds were manipulated under N<sub>2</sub> or Ar using standard Schlenk or glovebox techniques. Solvents for air- and moisture-sensitive reactions were dried by the method of Grubbs. Chlorobenzene and 1-hexene for polymerization with stoichiometric activators were refluxed over CaH<sub>2</sub> for greater than 72 h, vacuum transferred, and run over activated alumina plugs prior to use. [CPh<sub>3</sub>][B(C<sub>6</sub>F<sub>5</sub>)<sub>4</sub>] and [HNMe<sub>2</sub>Ph][B(C<sub>6</sub>F<sub>5</sub>)<sub>4</sub>] were purchased from Strem and used without further purification. 1-bromo-2,3,4,5,6-pentamethylbenzene,<sup>23</sup> 9-bromo,10-methylanthracene,<sup>24</sup> 2-Bromo-4-*tert*-butyl-1-(methoxymethoxy)benzene (**2.9**),<sup>7a</sup> **2.16tBu**,<sup>25</sup> 2,6-dibromo-4-*tert*-butylphenol,<sup>26</sup> and compounds **2.4** and **2.10**<sup>12</sup> were prepared according to literature procedure. Ethylene (99.999%) and propylene (99.999%) were passed through purification columns containing molecular sieves and oxygen scavenger. Toluene, 1-hexene, and 1-tetradecene for polymerizations were purchased from Sigma Aldrich and dried over 4 Å MS prior to use. MAO (30 wt.% in toluene) was purchased from Chemtura. Deuterated solvents were purchased from Cambridge Isotopes Lab, Inc.; CDCl<sub>3</sub> and 1,1,2,2-tetrachloroethane-d<sub>2</sub> were used without further purification; C<sub>6</sub>D<sub>6</sub> was distilled from purple Na/benzophenone ketyl and filtered over activated alumina prior to use. <sup>1</sup>H and <sup>13</sup>C spectra were recorded on Varian Mercury 300, Varian INOVA-300, 400, or 500 spectrometers or Bruker Cryoprobe 400. <sup>1</sup>H and <sup>13</sup>C chemical shifts are reported relative to residual solvent resonances. Elemental analysis was performed on a Perkin-Elmer 2400 CHNS/O Analyser and samples were taken from representative batches prepared in an N<sub>2</sub>-filled glovebox.

**Synthesis of tetrabenzylzirconium.** In the glovebox, a round bottom was charged with a stirbar, 60 mL Et<sub>2</sub>O, and benzylmagnesium chloride (126 mL, 1.9 M in

Et<sub>2</sub>O, 126 mmol, 4.2 equiv.) and frozen in the cold well. ZrCl<sub>4</sub> (7.043 g, 30.22 mmol, 1 equiv.) was added to the top of the thawing solution in 3 portions. The resulting suspension yellow suspension was stirred 1 h, warming, then capped with a septum and stored at -35 °C without stirring. After 8 h, volatiles were removed and the residue was extracted with toluene and filtered over Celite. Concentration of the filtrate resulted in the formation of microcrystalline orange solids which were suspended in Et<sub>2</sub>O, collected by filtration, and dried under vacuum to afford the desired product (8.89 g, 19.5 mmol, 65 %).

**Synthesis of compounds 2.5 and 2.6** was performed according to the literature.<sup>27</sup>

**Synthesis of compound 2.7.** To a solution of **6** (4.530 g, 13.54 mmol, 1 equiv.) in methanol (54 mL) N,N-dimethylethylenediamine (1.8 mL, 16.5 mmol, 1.2 equiv.) was added and the reaction heated to 70 °C for 12 h. Volatiles were removed and the residue was taken up in methanol (54 mL) and NaBH<sub>4</sub> (2.2043 g, 58.27 mmol, 4.3 equiv.) was added in several portions, then the reaction stirred 4 h. The resulting colorless solution was concentrated and HCl (2N) added to quench. 1 M NaOH was added in small portions to bring to pH~7 and the white suspension was extracted thrice with DCM. Combined organics were washed with water, dried with MgSO<sub>4</sub>, filtered, and evaporated to afford the product as a purple oil which was used without further purification (4.600 g, 11.31 mmol, 84 %). <sup>1</sup>H NMR (500 MHz, CDCl<sub>3</sub>) δ 7.31 (d, *J* = 2.5 Hz, 1H), 6.97 (d, *J* = 2.5 Hz, 1H), 3.96 (s, 2H), 2.73 (m, 2H), 2.48 (m, 2H), 2.27 (s, 6H), 1.50 (m, 3H), 1.28 (s, 9H), 1.09 (d, *J* = 7.63 Hz, 18H). Note: <sup>1</sup>H NMR resonances corresponding to the N-H and O-H are not observed, likely due to exchange with trace water. <sup>13</sup>C NMR (126 MHz, CDCl<sub>3</sub>) δ 161.13 (Ar), 140.11 (Ar), 133.12 (Ar), 126.29 (Ar), 120.56 (Ar), 120.48 (Ar), 58.20 (ArCH<sub>2</sub>), 45.41 (CH<sub>2</sub>), 45.31 (CH<sub>2</sub>), 33.90 (C(CH<sub>3</sub>)<sub>3</sub>), 31.66 (C(CH<sub>3</sub>)<sub>3</sub>), 19.01

(Si(CH(CH<sub>3</sub>)<sub>2</sub>)<sub>3</sub>), 11.83 (Si(CH(CH<sub>3</sub>)<sub>3</sub>). HRMS (FAB+) calcd for C<sub>24</sub>H<sub>47</sub>N<sub>2</sub>OSi (M+H)<sup>+</sup>: 407.3458. Found: 407.3476. **Preparation of 2.8.** To a solution of **2.4** (613.4 mg, 1.508 mmol, 2.5 mmol) and NEt<sup>*t*</sup>Pr<sub>2</sub> (0.21 mL, 1.506 mmol, 2.5 equiv.) in THF (15 mL) at 0 °C, **2.7** (375.8 mmol, 0.6096 mmol, 1 equiv.) in THF (21 mL) was added over the course of several minutes. The reaction was stirred 3 h, warming, then volatiles were removed under reduced pressure. The residue was dissolved in DCM and washed with K<sub>2</sub>CO<sub>3</sub> (2x), water, and brine. The combined organics were dried with MgSO<sub>4</sub>, filtered, and evaporated. Purification by column chromatography (3:2 EtOAc:Hexanes(v/v), R<sub>F</sub> ~0.2) and lyophilization from benzene afforded **H<sub>4</sub><sup>SiiPr<sub>3</sub></sup>-NMe<sub>2</sub>** as a white solid (434.8 mg, 56.2%). <sup>1</sup>H NMR (400 MHz, CDCl<sub>3</sub>) δ 9.53 (br s, 4H, OH), 7.34 (d, *J*=2.9 Hz, 2H, Ar-*H*), 7.15 (d, *J*=2.2 Hz, 2H, Ar-*H*), 7.08 (d, *J*=2.2 Hz, 2H, Ar-*H*), 7.05 (d, *J*=2.4 Hz, 2H, Ar-*H*), 3.78 (s, 4H, ArCH<sub>2</sub>), 3.74 (s, 4H, ArCH<sub>2</sub>), 2.66 (m, 4H, CH<sub>2</sub>), 2.57 (m, 4H, CH<sub>2</sub>), 2.24 (s, 12H, ArCH<sub>3</sub>), 2.00 (s, 12H, N(CH<sub>3</sub>)<sub>2</sub>), 1.50 (m, 6H, SiCH(CH<sub>3</sub>)<sub>2</sub>), 1.32 (s, 18H, C(CH<sub>3</sub>)<sub>3</sub>), 1.31 (s, 18H, C(CH<sub>3</sub>)<sub>3</sub>), 1.07 (d, *J*= 7.5 Hz, 36H, SiCH(CH<sub>3</sub>)<sub>2</sub>). <sup>13</sup>C NMR (101 MHz, CDCl<sub>3</sub>) δ 160.47 (Ar), 151.31 (Ar), 141.62 (Ar), 140.25 (Ar), 137.48 (Ar), 133.73 (Ar), 133.06 (Ar), 129.40 (Ar), 128.16 (Ar), 127.63 (Ar), 126.48 (Ar), 121.90 (Ar), 120.63 (Ar), 120.41 (Ar), 58.16 (CH<sub>2</sub>), 56.95 (CH<sub>2</sub>), 55.57 (CH<sub>2</sub>), 49.81 (CH<sub>2</sub>), 45.32 (N(CH<sub>3</sub>)<sub>2</sub>), 34.24 (ArC(CH<sub>3</sub>)<sub>3</sub>), 34.08 (ArC(CH<sub>3</sub>)<sub>3</sub>), 31.88 (ArC(CH<sub>3</sub>)<sub>3</sub>), 19.27 (SiCH(CH<sub>3</sub>)<sub>2</sub>), 17.99 (ArCH<sub>3</sub>), 11.94 (SiCH(CH<sub>3</sub>)<sub>2</sub>). HRMS (FAB+) calcd for C<sub>80</sub>H<sub>131</sub>O<sub>4</sub>N<sub>4</sub>Si<sub>2</sub> (M+H)<sup>+</sup>: 1267.971. Found: 1267.970.

**Preparation of Zr<sub>2</sub><sup>SiiPr<sub>3</sub></sup>-NMe<sub>2</sub> (C<sub>s</sub> and C<sub>2</sub> symmetric).** Proligand **2.8** (201.4 mg, 0.1588 mmol, 1 equiv.) in toluene (2.5 mL) was added to a stirred solution of ZrBn<sub>4</sub> (144.7 mg, 0.3175 mmol, 2 equiv.) in toluene (3 mL) and the reaction stirred in the dark at room temperature for 3 h. Volatiles were removed *in vacuo* and the crude material fractionated

between pentane, diethyl ether, and benzene. The ether fraction afforded primarily the  $C_s$  symmetric isomer (**2.10**) with circa 12% of the  $C_2$  symmetric isomer (80.0 mg, 0.0442 mmol, 28 %). The benzene fraction afforded primarily the  $C_2$  symmetric isomer (**2.11**), which was cleanly isolated following recrystallization from toluene/pentane (81.8 mg, 0.0452 mmol, 28%). X-Ray quality crystals of the  $C_2$  isomer were grown by vapor diffusion of pentane into toluene at -35 °C. **2.10**:  $^1\text{H}$  NMR (400 MHz,  $\text{C}_6\text{D}_6$ )  $\delta$  7.73 (d,  $J=2.6$  Hz, 2H, Ar-*H*) , 7.45 (d,  $J=2.6$  Hz, 2H Ar-*H*), 7.27 (m, 4H, Ar-*H*), 7.17 (d,  $J=2.5$  Hz, 2H, Ar-*H*), 7.12 (d,  $J=2.2$  Hz, 2H, Ar-*H*), 7.03 (m, 4H, Ar-*H*), 6.93 (m, 4H, Ar-*H*), 6.81 (t,  $J=7.4$  Hz, 2H, Ar-*H*), 6.69 (t,  $J=7.4$  Hz, 2H, Ar-*H*), 3.90 (d,  $J=13.4$  Hz, 2H,  $\text{CH}_2$ ), 3.74 (d,  $J=13.4$  Hz, 2H,  $\text{CH}_2$ ), 2.93 (s, 6H,  $\text{ArCH}_3$ ), 2.75 (d,  $J=13.4$  Hz, 2H,  $\text{ArCH}_2$ ), 2.65 (d,  $J=13.4$  Hz, 2H,  $\text{ArCH}_2$ ), 2.56 (s, 6H,  $\text{ArCH}_3$ ), 2.40 (m, 4H), 2.29 (m, 4H), 2.07- 1.99 (m, 6H), 1.78 (m, 4H), 1.54-1.34 (m, 84H), 0.99 (br m, 2H).  $^{13}\text{C}$  NMR (101 MHz,  $\text{CDCl}_3$ )  $\delta$  165.43 (Ar), 157.36 (Ar), 152.14 (Ar), 146.00 (Ar), 141.56 (Ar), 140.42 (Ar), 140.18 (Ar), 135.38 (Ar), 134.67 (Ar), 132.06 (Ar), 131.06 (Ar), 130.76 (Ar), 129.11 (Ar), 129.04 (Ar), 126.38 (Ar), 126.06 (Ar), 125.57 (Ar), 125.14 (Ar), 122.24 (Ar), 121.69 (Ar), 119.88 (Ar), 70.82 ( $\text{CH}_2$ ), 65.10 ( $\text{CH}_2$ ), 64.83 ( $\text{CH}_2$ ), 64.05 ( $\text{CH}_2$ ), 60.39 ( $\text{CH}_2$ ), 51.50 ( $\text{CH}_2$ ), 34.28 ( $\text{C}(\text{CH}_3)_3$ ), 34.16 ( $\text{C}(\text{CH}_3)_3$ ), 31.90 ( $\text{C}(\text{CH}_3)_3$ ), 20.30, 19.99, 19.89, 19.83, 19.39, 13.15 ( $\text{SiCH}(\text{CH}_3)_2$ ). Anal. Calcd  $\text{C}_{108}\text{H}_{154}\text{N}_4\text{O}_4\text{Si}_2\text{Zr}_2$ : C, 71.63; H, 8.57, N, 3.09. Found: C, 71.65; H, 8.81; N, 3.41. **2.11**:  $^1\text{H}$  NMR (500 MHz,  $\text{CD}_2\text{Cl}_2$ )  $\delta$  7.42 (d,  $J=2.2$  Hz, 2H, Ar-*H*), 7.18 (d,  $J=2.3$  Hz, 2H, Ar-*H*), 7.08 (m, 4H, Ar-*H*), 7.02 (m, 6H, Ar-*H*), 6.99 (d,  $J=2.2$  Hz, 2H, Ar-*H*), 6.83-6.77 (m, 6H, Ar-*H*), 6.63 (m, 6H, Ar-*H*), 3.62 (d,  $J=13.5$  Hz, 2H,  $\text{CH}_2$ ), 3.42 (d,  $J=13.5$  Hz, 2H,  $\text{CH}_2$ ), 2.85 (d,  $J=13.9$  Hz, 2H,  $\text{CH}_2$ ), 2.77 (d,  $J=13.7$  Hz, 2H,  $\text{CH}_2$ ), 2.66 (br m, 2H,  $\text{CH}_2$ ), 2.58 (s, 6H,  $\text{ArCH}_3$ ), 2.30 (br s, 2H,  $\text{CH}_2$ ) 2.25 (s, 6H,  $\text{ArCH}_3$ ), 2.04-1.99 (m, 4H,  $\text{CH}_2$ ), 1.89-1.84 (m, 6H), 1.78 (br m, 2H), 1.52 (m, 8H), 1.41 (m, 4H,  $\text{CH}_2$ ), 1.35 (m, 24H), 1.27 (m, 42H), 1.16 (d,  $J=7.5$  Hz, 18H).  $^{13}\text{C}$  NMR (101 MHz,  $\text{C}_6\text{D}_6$ )  $\delta$  165.46 (Ar), 157.04 (Ar),

152.93 (Ar), 144.27 (Ar), 141.30 (Ar), 140.60 (Ar), 139.50 (Ar), 135.33 (Ar), 134.84 (Ar), 132.23 (Ar), 131.40 (Ar), 130.15 (Ar), 129.46 (Ar), 129.33 (Ar), 126.15 (Ar), 125.79 (Ar), 125.70 (Ar), 124.75 (Ar), 122.71 (Ar), 121.58 (Ar), 119.86 (Ar), 67.61 (CH<sub>2</sub>), 64.79 (CH<sub>2</sub>), 64.07 (CH<sub>2</sub>), 63.87 (CH<sub>2</sub>), 60.00 (CH<sub>2</sub>), 51.37 (CH<sub>2</sub>), 34.32 (C(CH<sub>3</sub>)<sub>3</sub>), 34.16 (C(CH<sub>3</sub>)<sub>3</sub>), 31.93 (C(CH<sub>3</sub>)<sub>3</sub>), 31.88 (C(CH<sub>3</sub>)<sub>3</sub>), 22.75, 21.45, 20.33, 20.24, 19.83, 19.54, 14.31, 13.11 (SiCH(CH<sub>3</sub>)<sub>2</sub>). Anal. Calcd C<sub>108</sub>H<sub>154</sub>N<sub>4</sub>O<sub>4</sub>Si<sub>2</sub>Zr<sub>2</sub>: C, 71.63; H, 8.57, N, 3.09. Found: C, 72.01; H, 8.74; N, 3.12.

**Preparation of 2.17.** To a solution of **2.16** (1.21 g, 2.965 mmol, 1.25 equiv.) and NEtPr<sub>2</sub> (0.52 mL, 3.0 mmol, 1.25 equiv.) in THF (45 mL), **2.7** (0.927 g, 2.38 mmol, 1 equiv.) in THF (50 mL) was added over the course of several minutes. The reaction was stirred 3 h, warming, then volatiles were removed under reduced pressure. The residue was dissolved in DCM and washed with K<sub>2</sub>CO<sub>3</sub> (2x), water, and brine, then dried with MgSO<sub>4</sub>, filtered and evaporated. Purification by column chromatography (5:1 EtOAc:Hexanes (v/v)) and lyophilization from benzene afforded the proligand as a white solid (1.1 g, 1.5 mmol, 65%). <sup>1</sup>H NMR (400 MHz, CDCl<sub>3</sub>) δ 9.08 (bs, 2H, OH), 7.31 (d, *J*=2.4 Hz, 1H, Ar-*H*), 7.08 (d, *J*=2.5 Hz, 1H, Ar-*H*), 7.03 (d, *J*=2.4 Hz, 1H, Ar-*H*), 6.94 (d, *J*=2.5 Hz, 1H, Ar-*H*), 3.74 (s, 2H, CH<sub>2</sub>), 3.69 (s, 2H, CH<sub>2</sub>), 2.62 (m, 2H, CH<sub>2</sub>), 2.53 (m, 2H, CH<sub>2</sub>), 2.32 (s, 3H, ArCH<sub>3</sub>), 2.28 (s, 6H, ArCH<sub>3</sub>), 2.20 (s, 6H, ArCH<sub>3</sub>), 1.97 (s, 6H, N(CH<sub>3</sub>)<sub>2</sub>), 1.48 (sept, *J*=7.59 Hz, 3H, CH(CH<sub>3</sub>)<sub>2</sub>), 1.30 (s, 9H, C(CH<sub>3</sub>)<sub>3</sub>), 1.28 (s, 9H, C(CH<sub>3</sub>)<sub>3</sub>), 1.05 (d, *J*=7.5 Hz, 18H, CH(CH<sub>3</sub>)<sub>2</sub>). <sup>13</sup>C NMR (101 MHz, CDCl<sub>3</sub>) δ 160.27 (Ar), 151.71 (Ar), 141.40 (Ar), 140.32 (Ar), 136.72 (Ar), 133.88 (Ar), 133.82 (Ar), 132.84 (Ar), 132.16 (Ar), 129.81 (Ar), 127.73 (Ar), 126.34 (Ar), 121.65 (Ar), 120.69 (Ar), 120.29 (Ar), 58.16 (CH<sub>2</sub>), 56.95 (CH<sub>2</sub>), 55.99 (CH<sub>2</sub>), 49.66 (CH<sub>2</sub>), 45.36 (N(CH<sub>3</sub>)<sub>2</sub>), 34.16 (C(CH<sub>3</sub>)<sub>3</sub>), 34.07 (C(CH<sub>3</sub>)<sub>3</sub>), 31.86 (C(CH<sub>3</sub>)<sub>3</sub>), 19.27 (SiCH(CH<sub>3</sub>)<sub>2</sub>), 18.27 (ArCH<sub>3</sub>), 17.13 (ArCH<sub>3</sub>), 16.85 (ArCH<sub>3</sub>), 11.96 (SiCH(CH<sub>3</sub>)<sub>2</sub>). HRMS (FAB+) calcd for C<sub>46</sub>H<sub>75</sub>N<sub>2</sub>O<sub>2</sub>Si (M+H)<sup>+</sup>: 715.5598. Found: 715.5579.

**Preparation of 2.20.** Proligand **2.17** (137 mg, 0.191 mmol, 1.0 equiv.) in toluene (3 mL) was added to a stirring solution of  $\text{ZrBn}_4$  (87.3 mg, 0.192 mmol, 1.0 equiv.) in toluene (2 mL). The reaction was stirred 3 h, in the dark, then volatiles removed *in vacuo* to afford a yellow solid. This was washed with 6 mL each of pentane and diethyl ether to afford the desired product (145 mg, 0.147 mmol, 76.7%). X-ray quality crystals were grown by slow evaporation of benzene at room temperature.  $^1\text{H}$  NMR (500 MHz,  $\text{C}_6\text{D}_6$ )  $\delta$  7.72 (s, 1H, Ar-*H*), 7.31 (s, 1H, Ar-*H*), 7.24 (t,  $J=7.2$  Hz, 2H, Ar-*H*), 7.07 (d,  $J=6.6$  Hz, 2H, Ar-*H*), 7.01-6.6.95 (m, 5H, Ar-*H*), 6.85 (t,  $J=7.2$  Hz, 2H, Ar-*H*), 6.64 (t,  $J=7.2$  Hz, 1H, Ar-*H*), 3.82 (d,  $J=13.5$  Hz, 1H,  $\text{CH}_2$ ), 3.59 (d,  $J=13.5$  Hz, 1H,  $\text{CH}_2$ ), 2.66 (d,  $J=13.5$  Hz, 1H,  $\text{CH}_2$ ), 2.62 (s, 3H,  $\text{ArCH}_3$ ), 2.61 (d, 1H,  $\text{CH}_2$ ), 2.45 (s, 3H,  $\text{ArCH}_3$ ), 2.43 (d, 1H,  $\text{CH}_2$ ), 2.39 (d,  $J=10.1$  Hz, 1H,  $\text{CH}_2$ ), 2.30 (s, 6H,  $\text{ArCH}_3$ ), 2.26 (d,  $J=9.8$  Hz, 1H,  $\text{CH}_2$ ), 2.19 (d,  $J=9.8$  Hz, 1H,  $\text{CH}_2$ ), 2.14-2.07 (m, 7H), 1.90 (br m, 1H), 1.51-1.41 (m, 16H), 1.36-1.33 (m, 27H), 1.25 (br m, 1H).  $^{13}\text{C}$  NMR (126 MHz,  $\text{C}_6\text{D}_6$ )  $\delta$  165.19 (Ar), 156.80 (Ar), 151.20 (Ar), 145.79 (Ar), 141.54 (Ar), 140.75 (Ar), 137.11 (Ar), 135.45 (Ar), 133.96 (Ar), 133.73 (Ar), 132.85 (Ar), 132.34 (Ar), 130.79 (Ar), 130.67 (Ar), 129.02 (Ar), 128.76 (Ar), 127.30 (Ar), 127.10 (Ar), 126.91 (Ar), 126.60 (Ar), 125.47 (Ar), 125.35 (Ar), 124.78 (Ar), 122.36 (Ar), 122.00 (Ar), 120.18 (Ar), 67.38 ( $\text{CH}_2$ ), 66.03 ( $\text{CH}_2$ ), 64.98 ( $\text{CH}_2$ ), 64.43 ( $\text{CH}_2$ ), 60.08 ( $\text{CH}_2$ ), 51.30 ( $\text{CH}_2$ ), 47.14 ( $\text{CH}_2$ ), 34.24 ( $\text{C}(\text{CH}_3)_3$ ), 34.19 ( $\text{C}(\text{CH}_3)_3$ ), 31.88 ( $\text{C}(\text{CH}_3)_3$ ), 20.33, 19.84, 19.40, 17.40, 16.98, 13.22 ( $\text{SiCH}(\text{CH}_3)_2$ ). Anal. Calcd  $\text{C}_{60}\text{H}_{86}\text{N}_2\text{O}_2\text{SiZr}$ : C, 73.04; H, 8.79; N, 2.84. Found: C, 73.22; H, 8.96; N, 3.14.

**Synthesis of compound 2.2anth.** The teraryl compounds was synthesized via a Negishi coupling using the same general procedure as for the synthesis of **2.2**, *vide supra*. In the glove box, 2-bromo-4-*tert*-butylanisole (**2.1**) (19.72 g, 81.10 mmol, 1 equiv.) and 220 mL of THF were combined in a Schlenk tube and frozen in the cold well.  $t\text{BuLi}$  (100 mL, 170 mmol, 1.7 M in pentane, 2.1 equiv.) was added to the top of the frozen solution and the resulting

solution allowed to stir, warming, for 1 h. ZnCl<sub>2</sub> (7.76 g, 56.9 mmol, 0.7 equiv.) was added in several portions to the solution with an additional 80 mL THF and the reaction stirred 1 h. 9,10-dibromoanthracene (12.402 g, 36.91 mmol, 0.45 equiv.), Pd(PPh<sub>3</sub>)<sub>4</sub> (0.9412 g, 0.8145 mmol, 0.01 equiv.), and 80 mL THF were added at room temperature. The Schlenk tube was sealed, brought out of the glovebox and heated to 70 °C for 7 days. The vessel was cooled to room temperature and quenched by addition of water. The resulting chunky suspension was filtered over silica with excess dichloromethane and volatiles removed under reduced pressure. The residue was taken up in fresh dichloromethane and washed with water and brine, dried with MgSO<sub>4</sub>, filtered, and evaporated to give a yellow solid. Precipitation from methanol afforded the desired product as a mixture of *syn* and *anti* atropisomers (10.89 g, 21.66 mmol, 59 %). <sup>1</sup>H NMR (300 MHz, CDCl<sub>3</sub>) δ 7.66 (m, 4H, anth-*H*), 7.54 (dd, *J*=8.4, 2.5 Hz, 2H Ar-*H*), 7.39 (d, *J*=2.5 Hz, 2H, Ar-*H*), 7.31 (m, 4H, anth-*H*), 7.09 (d, *J*=8.7 Hz, 2H Ar-*H*), 3.64-3.49 (6H, OCH<sub>3</sub>), 1.35-1.34 (18H, C(CH<sub>3</sub>)<sub>3</sub>). HRMS (FAB+) calcd for C<sub>36</sub>H<sub>38</sub>O<sub>2</sub>: 502.2872. Found: 502.2889.

**Synthesis of compound 2.3anth.** An oven-dried 1 L Schlenk was assembled hot under flowing nitrogen and evacuated until cool to the touch. **2.2anth** (3.606 g, 7.17 mmol, 1 equiv.) was added under positive N<sub>2</sub> flow and 180 mL dry DCM by cannula addition. The yellow solution was cooled to 0 °C with an ice-water bath and boron tribromide (3.5 mL, 36.3 mmol, 5 equiv.) added by syringe over the course of several minutes. The resulting brown solution was stirred, warming, for 21 h then quenched by slow addition of water with rapid stirring. Organics were washed with water (2x) and brine, then dried with MgSO<sub>4</sub>, filtered, and evaporated. The crude mixture of atropisomers was purified by column chromatography in 5 hexanes: 1 EtOAc : 1/2 DCM (v/v/v) to afford the *anti* atropisomer (*R*<sub>F</sub> ~ 0.5) further purified



by precipitation from methanol (0.758 g, 1.59 mmol, 22 %) and *syn* atropisomer ( $R_F \sim 0.15$ , 1.25 g, 2.64 mmol, 37 %). HRMS (FAB+) calcd for  $C_{34}H_{34}O_2$ : 474.2559. Found: 474.2544.

*Anti Atropisomer*:  $^1H$  NMR (400 MHz,  $CDCl_3$ )  $\delta$  7.80-7.77 (m, 4H, anthH), 7.54-7.52 (dd,  $J = 2.1$  Hz,  $J = 8.8$  Hz, 2H, ArH), 7.46-7.44 (m, 4 H, anthH), 7.35 (d,  $J = 2.1$  Hz, 2H, ArH), 7.13 (d,  $J = 8.5$  Hz, 2H, ArH), 4.48 (s, 2H, OH), 1.38 (s, 9H,  $C(CH_3)_3$ ).  $^{13}C$  NMR (101 MHz,  $CDCl_3$ )  $\delta$  151.59, 143.77, 132.20, 130.96, 129.19, 126.92, 126.82, 126.45, 123.47, 34.47 ( $C(CH_3)_3$ ), 31.81 ( $C(CH_3)_3$ ).

*Syn Atropisomer*:  $^1H$  NMR (500 MHz,  $CDCl_3$ )  $\delta$  7.81-7.79 (m, 4H, anthH), 7.55-7.53 (dd,  $J = 2.4$  Hz,  $J = 8.6$  Hz, 4H, ArH), 7.48-7.46 (m, 4H, anthH), 7.33 (d,  $J = 2.4$  Hz, 2H, ArH), 7.15 (d,  $J = 8.6$  Hz, 2H, ArH), 4.55 (s, 2H, OH), 1.38 (s, 9H,  $C(CH_3)_3$ ).  $^{13}C$  NMR (126 MHz,  $CDCl_3$ )  $\delta$  151.44, 143.65, 132.26, 130.79, 129.22, 126.78, 126.69, 126.30, 123.35, 115.24, 34.32 ( $C(CH_3)_3$ ), 31.65 ( $C(CH_3)_3$ ).

**Synthesis of compound 2.4anth.** A Schlenk flask was charged with a stirbar, **2.3anth** (3.734 g, 7.867 mmol, 1 equiv.), paraformaldehyde (0.994 g, 33.1 mmol, 4.2 equiv.), 24 mL glacial acetic acid, and 12 mL benzene. Anhydrous HBr (g) was bubbled through the resulting suspension, with rapid stirring, for 15 min. (Note: excess HBr (g) was bubbled through water and 1 M NaOH to neutralize.) The resulting brown solution was stirred 4 h, then diluted with hexanes and dichloromethane (ca. 2:1 v/v) and washed with water (2x) and brine, dried with  $MgSO_4$ , filtered, and evaporated. Precipitation from hexanes afforded the desired product as an emerald green solid (3.38 g, 5.11 mmol, 65 %).  $^1H$  NMR (400 MHz,  $CDCl_3$ )  $\delta$  7.76-7.73 (m, 4 H, anthH), 7.56 (d, 2 H, ArH), 7.48-7.46 (m, 4 H, anthH), 7.30 (d, 2 H, ArH), 4.85 (bs, 2 H, OH), 4.74 (s, 4 H,  $CH_2Br$ ), 1.36 (s, 18 H,  $C(CH_3)_3$ ).  $^{13}C\{^1H\}$  NMR (101 MHz,  $CDCl_3$ )  $\delta$  149.79, 143.74, 131.76, 130.75, 130.08, 128.03, 126.61, 126.53, 124.11, 123.96, 34.35, 31.55, 29.87. HRMS (FAB+) calcd for  $C_{36}H_{36}Br_2O_2$ : 660.1062. Found: 660.1069.

**Preparation of 2.9.** To a solution of **2.7** (1.539 g, 3.785 mmol, 2.5 equiv.),  $\text{NEt}^t\text{Pr}_2$  (0.658 mL, 3.78 mmol, 2.5 equiv.) in THF (75 mL) at 0 °C, **2.4anth** (1.008 g, 1.523 mmol, 1 equiv.) in THF (40 mL) was added over the course of several minutes. The resulting red solution was stirred 3 h, warming, then volatiles were removed under reduced pressure. The residue was dissolved in DCM and washed with  $\text{K}_2\text{CO}_3$  (2x), water, and brine, dried with  $\text{MgSO}_4$ , filtered, and evaporated. Purification by column chromatography (3:2:1 EtOAc:Hexanes:Benzene (v/v/v)) afforded the desired proligand as a tan solid (1.16 g, 0.886 mmol, 58%).  $^1\text{H}$  NMR (400 MHz,  $\text{CDCl}_3$ )  $\delta$  9.73 (br s, 4H, OH), 7.71-7.69 (m, 4H, anth-*H*), 7.36 (d,  $J=2.8$  Hz, 2H, Ar-*H*), 7.35 (d,  $J=2.8$  Hz, 2H, Ar-*H*), 7.32-7.30 (m, 4H, anth-*H*), 7.26 (d,  $J=2.3$  Hz, 2H, Ar-*H*), 7.08 (d,  $J=2.8$  Hz, 2H, Ar-*H*), 3.89 (s, 4H, Ar- $\text{CH}_2$ ), 3.83 (s, 4H, Ar- $\text{CH}_2$ ), 2.74 (m, 4H,  $\text{CH}_2$ ), 2.59 (m, 4H,  $\text{CH}_2$ ), 2.13 (s, 12H,  $\text{N}(\text{CH}_3)_2$ ), 1.42 (m, 6H,  $\text{SiCH}(\text{CH}_3)_2$ ), 1.35 (s, 18H,  $\text{C}(\text{CH}_3)_3$ ), 1.33 (s, 18H,  $\text{C}(\text{CH}_3)_3$ ), 1.00 (d,  $J=7.5$  Hz, 36 H,  $\text{SiCH}(\text{CH}_3)_2$ ).  $^{13}\text{C}$  NMR (101 MHz,  $\text{CDCl}_3$ )  $\delta$  160.51 (Ar), 152.66 (Ar), 141.79 (Ar), 140.25 (Ar), 134.17 (Ar), 133.87 (Ar), 130.61 (Ar), 129.80 (Ar), 127.85 (Ar), 127.32 (Ar), 127.27 (Ar), 125.82 (Ar), 124.96 (Ar), 122.41 (Ar), 121.03 (Ar), 120.31 (Ar), 57.72 ( $\text{CH}_2$ ), 56.82 ( $\text{CH}_2$ ), 55.47 ( $\text{CH}_2$ ), 49.60 ( $\text{CH}_2$ ), 45.27 ( $\text{N}(\text{CH}_3)_2$ ), 34.34 ( $\text{C}(\text{CH}_3)_3$ ), 34.09 ( $\text{C}(\text{CH}_3)_3$ ), 31.89 ( $\text{C}(\text{CH}_3)_3$ ), 19.16 ( $\text{SiCH}(\text{CH}_3)_2$ ), 11.90 ( $\text{SiCH}(\text{CH}_3)_2$ ). HRMS (FAB+) calcd for  $\text{C}_{84}\text{H}_{127}\text{N}_4\text{O}_4\text{Si}_2$ : 1311.94. Found: 1311.9396.

**Preparation of 2.12.** A 20 mL scintillation vial was charged in the dark with a stirbar,  $\text{ZrBn}_4$  (113 mg, 0.248 mmol, 2 equiv.), and 3 mL toluene, and the solution was frozen in the glovebox cold well. A separate vial was charged with **anthH<sub>4</sub><sup>SiiPr<sub>3</sub></sup>-NMe<sub>2</sub>** (163 mg, 0.124 mmol, 1 equiv.) dissolved in toluene (4 mL) and the solution frozen in the cold well. The thawing proligand solution was added to the top of the thawing  $\text{ZrBn}_4$  solution and the stirred, in the dark, warming, for 3 h. Volatiles were removed and the resulting yellow solid recrystallized by

pentane/benzene layering at room temperature to give the  $C_2$  symmetric complex as a yellow, crystalline solid (116 mg, 0.0626 mmol, 51%). X-ray quality crystals were grown by toluene/hexanes layering at -35 °C.  $^1\text{H}$  NMR (400 MHz,  $\text{C}_6\text{D}_6$ )  $\delta$  8.84 (d,  $J=8.5$  Hz, 2H, anthH), 8.12 (d,  $J=9.1$  Hz, 2H, anthH), 7.70-7.63 (m, 4H, Ar-H), 7.59 (t,  $J=7.1$  Hz, 2 H, Ar-H) 7.41 (t,  $J=7.1$  Hz, 2H, Ar-H), 7.25 (d,  $J=2.3$  Hz, 2H, Ar-H), 7.12 (d,  $J=2.3$  Hz, 2H, Ar-H), 6.99 (m, 10H), 6.83 (br m, 4H), 6.70 (m, 4H), 6.43 (br m, 2H), 4.07 (d,  $J=13.6$  Hz, 2H,  $\text{CH}_2$ ), 3.75 (d,  $J=12.4$  Hz, 2H,  $\text{CH}_2$ ), 2.75 (d,  $J=12.4$  Hz, 2H,  $\text{CH}_2$ ), 2.70 (d,  $J=13.2$  Hz, 2H,  $\text{CH}_2$ ), 2.39 (br m, 2H), 2.04-1.91 (m, 10H), 1.80 (br m, 2H), 1.67 (d,  $J=10.2$  Hz, 4H,  $\text{CH}_2$ ), 1.60 (br m, 2H) 1.46 (d,  $J=7.52$  Hz, 18H), 1.36 (s, 18H), 1.31 (m, 42H) 1.19 (br s, 6H), 1.08 (br m, 2H).  $^{13}\text{C}\{^1\text{H}\}$  NMR (101 MHz,  $\text{C}_6\text{D}_6$ )  $\delta$  165.50 (Ar), 157.91 (Ar), 153.07 (Ar), 143.63 (Ar), 141.53 (Ar), 140.60 (Ar), 136.22 (Ar), 135.40 (Ar), 133.09 (Ar), 131.69 (Ar), 131.12 (Ar), 130.29 (Ar), 129.88 (Ar), 129.34 (Ar), 128.60 (Ar), 127.23 (Ar), 126.67 (Ar), 126.33 (Ar), 126.25 (Ar), 125.71 (Ar), 125.58 (Ar), 124.71 (Ar), 122.41 (Ar), 121.59 (Ar), 119.85 (Ar), 68.12 ( $\text{CH}_2$ ), 64.86 ( $\text{CH}_2$ ), 63.92 ( $\text{CH}_2$ ), 63.73 ( $\text{CH}_2$ ), 60.15 ( $\text{CH}_2$ ), 51.37, 34.36 ( $\text{C}(\text{CH}_3)_3$ ), 34.19 ( $\text{C}(\text{CH}_3)_3$ ), 31.90 ( $\text{C}(\text{CH}_3)_3$ ), 31.83, 22.75, 20.25, 19.76, 14.31, 13.02. Anal. Calcd  $\text{C}_{112}\text{H}_{150}\text{N}_4\text{O}_4\text{Si}_2\text{Zr}_2$ : C, 72.52; H, 8.15; N, 3.02. Found: C, 72.18; H, 8.35; N, 3.05.

**Synthesis of compound 2.14anth.** In the glove box, **2.13** (4.592 g, 16.81 mmol, 1 equiv.) and 30 mL THF were combined in a Schlenk tube and frozen in the cold well.  $^t\text{BuLi}$  (21.0 mL, 35.7 mmol, 1.7 M in pentane, 2.1 equiv.) was added to the top of the frozen solution and the resulting solution allowed to stir, warming, for 30 min.  $\text{ZnCl}_2$  (1.708 g, 12.53 mmol, 0.7 equiv.) was added in several portions to the solution with an additional 20 mL THF and the reaction stirred 1 h. 9-bromo-10-methylanthracene (3.671 g, 13.54 mmol, 0.8 equiv.),  $\text{Pd}(\text{PPh}_3)_4$  (0.251 g, 0.217 mmol, 0.01 equiv.), and 20 mL THF were added at room temperature. The Schlenk tube was sealed, brought out of the glovebox and heated to 70 °C

for 36 h. The reaction was cooled to room temperature and quenched by addition of water. The resulting chunky suspension was filtered over silica with excess dichloromethane and volatiles removed under reduced pressure. The residue was taken up in fresh dichloromethane and washed with water and brine, dried with  $\text{MgSO}_4$ , filtered, and evaporated to give a yellow solid. Precipitation from methanol afforded the desired product as a yellow solid in ca. 85 % NMR purity (3.38 g, 8.78 mmol, 65 %).  $^1\text{H}$  NMR (300 MHz,  $\text{CDCl}_3$ )  $\delta$  8.35 (d,  $J=8.7$  Hz, 2H, anthH), 7.66 (d,  $J=8.6$  Hz, 2H, anthH), 7.52-7.48 (m, 3H, ArH), 7.37-7.28 (m, 6H, ArH), 4.87 (s, 2H,  $\text{OCH}_2\text{OCH}_3$ ), 3.18 (s, 3H, anth $\text{CH}_3$ ), 3.03 (s, 3H,  $\text{OCH}_2\text{OCH}_3$ ), 1.33 (s,  $\text{C}(\text{CH}_3)_3$ ).  $^{13}\text{C}$  NMR (101 MHz,  $\text{CDCl}_3$ )  $\delta$  153.22, 144.74, 132.98, 130.29, 130.15, 129.82, 128.16, 127.71, 125.73, 124.94, 124.73, 124.65, 114.61, 94.22, 55.76, 34.31, 31.58. HRMS (FAB+) calcd for  $\text{C}_{27}\text{H}_{29}\text{O}_2$  (M+H) $^+$ : 385.2168. Found: 385.2155.

**Synthesis of compound 2.15anth.** A round bottom was charged with a stirbar, **2.14anth** (2.97 g, 7.72 mmol, 1 equiv.), 62 mL MeOH, and concentrated HCl (10 mL, 14 equiv.) and heated to 65 °C for 8 h. The resulting suspension was concentrated then taken up in DCM and washed with water (2x) and brine, dried with  $\text{MgSO}_4$ , filtered, and evaporated. Purification by column chromatography in 10 % benzene in hexanes afforded the desired product as an off-white solid (1.43 g, 4.21 mmol, 55 %).

**Synthesis of compound 2.16anth.** A Schlenk flask was charged with a stirbar, **2.15anth** (1.78 g, 5.23 mmol, 1 equiv.), paraformaldehyde (0.20 g, 6.5 mmol, 1.25 equiv.), 24 mL glacial acetic acid, and 12 mL benzene. Anhydrous HBr (g) was bubbled through the resulting suspension, with rapid stirring, for 15 min. (Note: excess HBr (g) was bubbled through water and 1 M NaOH to neutralize.) The resulting brown solution was stirred 4 h, then diluted with hexanes and dichloromethane and washed with water (2x) and brine, dried with  $\text{MgSO}_4$ , filtered, and evaporated to afford the crude product as an emerald green solid

(2.15 g, 4.96 mmol, 95 %) which was used for subsequent reactions without further purification.

**Preparation of 2.18.** To a solution of **2.16**anth (2.384 g, 5.861 mmol, 1.25 equiv.) and NEtPr<sub>2</sub> (1.02 mL, 5.86 mmol, 1.25 equiv.) in THF (150 mL) at 0 °C, **2.7** (2.035 g, 4.695 mmol, 1 equiv.) in THF (100 mL) was added over the course of several minutes. The resulting red solution was stirred 3 h, warming, then volatiles were removed under reduced pressure. The residue was taken up in DCM and washed with K<sub>2</sub>CO<sub>3</sub> (2x), water, and brine, then dried with MgSO<sub>4</sub>, filtered, and evaporated. Purification by column chromatography (3:1 EtOAc:Hexanes (v/v)) and lyophilization from benzene afforded the desired proligand as a tan solid (1.233 g, 1.624 mmol, 35%). <sup>1</sup>H NMR (500 MHz, CDCl<sub>3</sub>) δ 9.81 (br s, 2H, OH), 8.36 (d, *J*=8.7 Hz, 2H, anth-*H*), 7.66 (d, *J*=8.7 Hz, 2H, anth-*H*), 7.50 (dd, 2H, anth-*H*), 7.31 (m, 4H, anth-*H* and Ar-*H*), 7.20 (d, *J*=2.4 Hz, 1H, Ar-*H*), 7.06 (d, *J*=2.5 Hz, 1H, Ar-*H*), 3.84 (s, 2H, ArCH<sub>2</sub>), 3.76 (s, 2H, ArCH<sub>2</sub>), 3.19 (s, 3H, anthCH<sub>3</sub>), 2.70 (m, 2H, CH<sub>2</sub>), 2.55 (m, 2H, CH<sub>2</sub>), 2.07 (s, 6H, N(CH<sub>3</sub>)<sub>2</sub>), 1.37 (m, 3H, SiCH(CH<sub>3</sub>)<sub>2</sub>), 1.33 (s, 9H, C(CH<sub>3</sub>)<sub>3</sub>), 1.31 (s, 9H, C(CH<sub>3</sub>)<sub>3</sub>), 0.93 (d, 18H, *J*=7.5 Hz, SiCH(CH<sub>3</sub>)<sub>2</sub>). <sup>13</sup>C NMR (126 MHz, CDCl<sub>3</sub>) δ 160.29 (Ar), 153.04 (Ar), 141.54 (Ar), 140.20 (Ar), 134.00 (Ar), 133.37 (Ar), 130.49 (Ar), 130.09 (Ar), 129.84 (Ar), 129.76 (Ar), 128.54 (Ar), 128.13 (Ar), 128.03 (Ar), 126.99 (Ar), 126.01 (Ar), 124.96 (Ar), 124.77 (Ar), 124.57 (Ar), 122.22 (Ar), 121.31 (Ar), 120.19 (Ar), 57.28 (CH<sub>2</sub>), 56.74 (CH<sub>2</sub>), 56.26 (CH<sub>2</sub>), 49.44 (CH<sub>2</sub>), 45.16 (N(CH<sub>3</sub>)<sub>2</sub>), 34.28 (C(CH<sub>3</sub>)<sub>3</sub>), 34.06 (C(CH<sub>3</sub>)<sub>3</sub>), 31.89 (C(CH<sub>3</sub>)<sub>3</sub>), 19.09 (SiCH(CH<sub>3</sub>)<sub>2</sub>), 14.41 (anthCH<sub>3</sub>), 11.85 (SiCH(CH<sub>3</sub>)<sub>2</sub>). HRMS (FAB+) calcd for C<sub>50</sub>H<sub>71</sub>SiN<sub>2</sub>O<sub>2</sub> (M+H)<sup>+</sup>: 759.5285. Found: 759.5264.

**Preparation of 2.21.** Proligand **2.18** (200.0 mg, 0.2634 mmol, 1 equiv.) in 4 mL toluene was added to the top of a stirred solution of ZrBn<sub>4</sub> (119.9 mg, 0.2631 mmol, 1 equiv.) in 3 mL toluene and stirred 3 h, dark. Volatiles were removed *in vacuo* and the resulting yellow solid

washed with pentane and ether to afford the desired complex (140 mg, 0.136 mmol, 52%).  $^1\text{H}$  NMR (500 MHz,  $\text{C}_6\text{D}_6$ )  $\delta$  8.44 (d,  $J=9.1$  Hz, 1H, anth-*H*), 8.41 (d,  $J=9.1$  Hz, 1H, anth-*H*), 8.33 (d,  $J=9.1$  Hz, 1H, anth-*H*), 8.00 (d,  $J=9.0$  Hz, 1H, anth-*H*), 7.69 (d,  $J=2.4$  Hz, 1H, Ar-*H*), 7.57 (d,  $J=2.2$  Hz, 1H, Ar-*H*), 7.51 (m, 2H, anth-*H*), 7.38 (m, 1H, anth-*H*), 7.22 (m, 2H, Ar-*H*), 7.12 (d,  $J=2.2$  Hz, 1H, Ar-*H*), 6.97-6.93 (m, 4H, Ar-*H*), 6.89-6.83 (m, 3H, Ar-*H*), 6.70 (m, 1H, anth-*H*), 6.13 (d,  $J=6.9$  Hz, 2H, Ar-*H*), 4.01 (d,  $J=13.3$  Hz, 1H,  $\text{CH}_2$ ), 3.46 (d,  $J=13.3$  Hz, 1H,  $\text{CH}_2$ ), 2.99 (s, 3H, anth $\text{CH}_3$ ), 2.70 (2d,  $J=13.3$  Hz, 2H,  $\text{CH}_2$ ), 2.30 (br m, 1H,  $\text{CH}_2$ ), 2.11 (d,  $J=10.2$  Hz, 1H,  $\text{CH}_2$ ), 2.00-1.89 (m, 5H), 1.53 (m, 1H,  $\text{CH}_2$ ), 1.49 (d,  $J=9.3$  Hz, 1H,  $\text{CH}_2$ ), 1.46 (d,  $J=9.3$  Hz, 1H,  $\text{CH}_2$ ), 1.41-1.36 (m, 18 H), 1.32-1.26 (m, 25H).  $^{13}\text{C}$  NMR (126 MHz,  $\text{C}_6\text{D}_6$ )  $\delta$  165.30 (Ar), 157.86 (Ar), 151.74 (Ar), 143.57 (Ar), 141.82 (Ar), 140.66 (Ar), 135.41 (Ar), 134.20 (Ar), 131.49 (Ar), 131.41 (Ar), 130.95 (Ar), 130.75 (Ar), 130.58 (Ar), 129.01 (Ar), 126.96 (Ar), 126.77 (Ar), 126.50 (Ar), 126.21 (Ar), 125.98 (Ar), 125.91 (Ar), 125.79 (Ar), 125.37 (Ar), 124.77 (Ar), 124.68 (Ar), 124.08 (Ar), 122.64 (Ar), 121.86 (Ar), 120.00 (Ar), 66.14 ( $\text{CH}_2$ ), 65.07 ( $\text{CH}_2$ ), 64.61 ( $\text{CH}_2$ ), 64.19 ( $\text{CH}_2$ ), 60.09 ( $\text{CH}_2$ ), 51.64, 47.47, 34.33, 34.18, 31.86, 20.19, 19.70, 14.31, 13.06. Anal. Calcd  $\text{C}_{64}\text{H}_{82}\text{N}_2\text{O}_2\text{SiZr}$ : C, 74.58; H, 8.02; N, 2.72. Found: C, 74.25; H, 8.17; N, 2.64.

**Synthesis of 2.19.** To a solution of **2.7** (1.173 g, 2.844 mmol, 1 equiv.) and  $\text{NEt}^i\text{Pr}_2$  (0.51 mL, 2.9 mmol, 1.25 equiv.) in THF (86 mL) at 0 °C, **2.16**<sup>*t*</sup>Bu (0.577 g, 1.93 mmol, 1 equiv.) in THF (38 mL) was added in 2 mL portions. The reaction was stirred, warming over 3 h then volatiles removed under reduced pressure. The residue was taken up in DCM and washed with  $\text{K}_2\text{CO}_3$  (2x) and brine. The combined organics were dried with  $\text{MgSO}_4$ , filtered, and evaporated to afford the crude product which was further purified by column chromatography in 10:1 Hexanes:EtOAc (v/v) (1.021 g, 1.633 mmol, 85%).  $^1\text{H}$  NMR (500 MHz,  $\text{CDCl}_3$ )  $\delta$  10.36 (br s, 1H, OH), 9.43 (br s, 1H OH), 7.38 (d, 1H,

ArH), 7.21 (d, 1H, ArH), 7.06 (d, 1H, ArH), 6.90 (d, 1H, ArH), 3.73 (s, 2H, ArCH<sub>2</sub>), 3.57 (s, 2H, ArCH<sub>2</sub>), 2.60 (br m, 4H, CH<sub>2</sub>), 2.32 (s, 6H, N(CH<sub>3</sub>)<sub>2</sub>), 1.53 (sep, 3H, CH(CH<sub>3</sub>)<sub>2</sub>), 1.37 (s, 9H, C(CH<sub>3</sub>)<sub>3</sub>), 1.32 (s, 9H, C(CH<sub>3</sub>)<sub>3</sub>), 1.30 (s, 9H, C(CH<sub>3</sub>)<sub>3</sub>), 1.15 (d, 18H, CH(CH<sub>3</sub>)<sub>2</sub>). <sup>13</sup>C NMR (126 MHz, CDCl<sub>3</sub>) δ 160.29, 153.32, 140.50, 139.85, 135.83, 134.29, 128.61, 124.45, 123.26, 121.68, 121.38, 120.14, 58.09, 56.14, 56.06, 49.23, 44.93, 35.00, 34.25, 33.97, 31.85, 30.49, 29.61, 19.27, 11.96. HRMS (FAB+) calcd for C<sub>39</sub>H<sub>69</sub>O<sub>2</sub>N<sub>2</sub>Si (M+H)<sup>+</sup>: 625.5128. Found: 625.5107.

**Synthesis of 2.22.** A 20 mL scintillation vial was charged with a stirbar, zirconium tetrabenzyl (62.0 mg, 0.136 mmol, 1.0 equiv.), and toluene (1.5 mL). The proligand **2.19** (84.7 mg, 0.136 mmol, 1.0 equiv.) in toluene (2) was added over several minutes then the reaction stirred for 3 hours in the dark. Volatiles were removed *en vacuo* and the residue fractionated between pentane (6 mL) and ether (6 mL). The desired complex was isolated in as a bright yellow solid from the ether fraction (68.8 mg, 0.0767 mmol, 56 %). <sup>1</sup>H NMR (500 MHz, C<sub>6</sub>D<sub>6</sub>) δ 7.76 (d, 1H, ArH), 7.67 (d, 2H, ArH), 7.61 (d, 1H, ArH), 7.39 (t, 2H, ArH), 7.09 (d, 1H, ArH), 7.03 (t, 1H, ArH), 6.98 (d, 2H, ArH), 6.91 (d, 1H, ArH), 6.74 (t, 2H, ArH), 6.56 (t, 1H, ArH), 3.83 (d, 1H, ArCH<sub>2</sub>), 3.04 (d, 1H, ArCH<sub>2</sub>), 2.84 (d, 1H, ArCH<sub>2</sub>), 2.78 (d, 1H, ArCH<sub>2</sub>), 2.60 (d, 1H, ArCH<sub>2</sub>), 2.58 – 2.51 (m, 2H, ArCH<sub>2</sub>), 2.47 (d, 1H, ArCH<sub>2</sub>), 2.19 (sep, 3H, CH(CH<sub>3</sub>)<sub>3</sub>), 1.83 (s, 9H), 1.54 (m, 13H), 1.47 (s, 4H), 1.42 – 1.34 (m, 29H). <sup>13</sup>C{<sup>1</sup>H} NMR (126 MHz, C<sub>6</sub>D<sub>6</sub>) δ 164.71, 157.51, 148.85, 147.33, 140.93, 140.57, 136.21, 134.99, 126.87, 125.44, 124.49, 124.36, 124.28, 121.92, 121.76, 120.05, 68.83, 66.25, 64.92, 64.35, 59.72, 50.67, 36.54, 35.34, 34.03, 33.81, 31.52, 30.46, 19.95, 19.43, 12.92. Anal. Calcd C<sub>53</sub>H<sub>80</sub>N<sub>2</sub>O<sub>2</sub>SiZr: C, 71.00; H, 8.99; N, 3.12. Found: C, 70.92; H, 9.18; N, 3.20.

**General procedure for 1-hexene polymerization.** In the glovebox, a Schlenk tube was charged with a stirbar, 1-hexene (2.5 mL, 20.0 mmol, 5000 equiv.), 1.5 mL PhCl, and Zr catalyst (4.0  $\mu$ mol, 1 equiv.) in 0.5 mL PhCl.  $[\text{CPh}_3][\text{B}(\text{C}_6\text{F}_5)_4]$  (3.7 mg, 4.0  $\mu$ mol) in 0.5 mL PhCl was added and the reaction stirred 10 min then quenched by addition of 0.5 mL MeOH in 5 mL hexanes. In the case of dried MAO and the anilinium activator, a Schlenk tube was charged with a stirbar, 1-hexene (2.5 mL, 20.0 mmol, 5000 equiv.), 2.0 mL PhCl, and dried MAO (58.0 mg, 1.00 mmol, 250 equiv.) or  $[\text{HNMe}_2\text{Ph}][\text{B}(\text{C}_6\text{F}_5)_4]$  (3.2 mg, 4.0  $\mu$ mol), then the Zr catalyst (4.0  $\mu$ mol, 1 equiv.) in 0.5 mL PhCl was added and the reaction stirred 10 min. before quench by addition of 0.5 mL MeOH in 5 mL hexanes. (Note: MAO was purchased from Albemarle and volatiles were removed first at room temperature and then under high vacuum at 110 °C for 12 h.) Volatiles were removed under reduced pressure and the resulting highly viscous oil was dried in a vacuum oven at 150 °C for 10 h.  $^{13}\text{C}\{^1\text{H}\}$  NMR were acquired in  $\text{CDCl}_3$  on a 500 MHz instrument and samples were prepared using ca. 50 mg of isolated polymer. Integration of the  $\text{C}_3$  signal was used to determine the % *mmmm* where the region of  $\delta$  35.1 – 34.58 was assigned to the *mmmm* pentad and the region of  $\delta$  34.58 – 33.1 was assigned to the remaining pentads<sup>17</sup>.

**General procedure for ethylene and propylene homo- and copolymerizations.** Ethylene and propylene homopolymerizations were carried out in a 250 mL Büchi glass autoclave using an Imtech (Netherlands) laboratory-scale reactor system. The reactor was heated to 120 °C and was purged several times with Ar to remove air and moisture. It was then cooled to 60 °C under Ar and charged with 85 mL toluene, 2.5 mL (10.0 mmol, 1000 equiv.) MAO and 0.01 mmol Zr catalyst in 2 mL toluene. The reactor was pressurized to 5 bar with ethylene or propylene and maintained at that pressure for 1 h. For ethylene-propylene copolymerizations the pressure was maintained at 5 bar using an ethylene-propylene feed with



a ratio of 2:3 flow ratio. Gas consumption was measured by a mass flow controller (Brooks Instrument). After 1 h the reactor was degassed and quenched by addition of 30 mL 5% HCl/MeOH. The polymer was isolated by filtration, washed with fresh methanol and dried under high vacuum.

**General procedure for the copolymerization of ethylene with 1-hexene and 1-tetradecene.** The polymerizations were carried out in a 250 mL Büchi glass autoclave using an Imtech (Netherlands) laboratory-scale reactor system. The reactor was prepared in the same manner as for homopolymerizations, however, it was charged with 65 mL toluene, 20 mL comonomer, 2.5 mL MAO (10.0 mmol, 1000 equiv.), and 0.01 mmol Zr catalyst in 2 mL toluene and run at 3 bar ethylene pressure.

**GPC Analysis.** Gel permeation chromatographic analyses of ethylene and propylene homo- and copolymers were performed at 160 °C using a PL-GPC 220 (Agilent Technologies) equipped with two PLgel Olexis 300 x 7.5 mm columns. BHT (0.0125 wt%) was added to 1,2,4-trichlorobenzene to prevent polymer sample degradation. A sample solution of 5 mg/1.5 mL (w/v) was prepared at 140 °C in the prepared solvent and 100 µL was injected into the GPC columns. Chromatogram data was analyzed using the Cirrus software, which was calibrated using polystyrene standards. The polystyrene-based calibration curve was converted into the universal one using the Mark-Houwink constants of polystyrene ( $K = 0.000121 \text{ dL/g}$  and  $\alpha = 0.707$ ) and polyethylene ( $K = 0.000406 \text{ dL/g}$  and  $\alpha = 0.725$ )<sup>17</sup>.

**Differential Scanning Calorimetry Analysis.** Differential scanning calorimetric (DSC) analysis was performed using a DSC Q2000 (TA Instruments). The temperature and heat flow of the apparatus were calibrated with an indium standard. Polymer samples were first equilibrated at 25 °C, followed by heating from 25 °C to 200 °C at a rate of 10 °C/min under N<sub>2</sub> flow (5 mL/min). This temperature was maintained for 5 min then samples were

cooled to 25 °C at a rate of 10 °C/min. This temperature was maintained for 5 min and then samples were reheated to 200 °C at a rate of 10 °C/min. The melting temperature ( $T_m$ ) was determined from the second heating scan. The percent crystallinity was calculated from  $\Delta H_f$  (J/g)/ $\Delta H_{std}$  (J/g), where  $\Delta H_{std}$  is the heat of fusion for a perfectly crystalline polyethylene; this equals to 290.0 J/g<sup>18</sup>.

**Polymer NMR Characterization.** NMR spectra of ethylene- $\alpha$ -olefin copolymers and propylene homopolymers were acquired in  $C_2D_2Cl_4$  on a Varian Inova 500 at 130 °C following a 10 min temperature equilibration period.  $^{13}C$  NMR spectra were integrated and the percent incorporation calculated based on literature assignments.<sup>19,20</sup>

**Crystal Refinement Details.** Crystals were mounted on a glass fiber or MiTeGen loop using Paratone oil, then placed on the diffractometer under a nitrogen stream. Diffractometer manipulations, including data collection, integration, and scaling were performed using the Bruker APEXII software.<sup>28</sup> Absorption corrections were applied using SADABS or TWINABS (**2.12**).<sup>29</sup> Space groups were determined on the basis of systematic absences and intensity statistics and the structures were solved in the Olex 2 software interface<sup>30</sup> by intrinsic phasing using XT (incorporated into SHELXTL)<sup>31</sup> and refined by full-matrix least squares on  $F^2$ . All non-hydrogen atoms were refined using anisotropic displacement parameters. Hydrogen atoms were placed in the idealized positions and refined using a riding model. Graphical representation of structures with 50% probability thermal ellipsoids were generated using Diamond 3 visualization software.<sup>32</sup> **2.20** had disorder associated with one tert-butyl group and the ethylene diamine group and both sets of disorder were both modeled in two parts. **2.11** was treated as a racemic twin and electron density corresponding to co-crystallized solvent was observed in the lattice. As these could not be satisfactorily modeled, the SQUEEZE

protocol contained with the program PLATON<sup>33</sup> was used to generate a bulk solvent correction to the observed intensities. Both *tert*-butyl groups, the ethylene dimethylamine group, and one benzyl group were modeled in two parts and restraints were used to bring the displacement parameters of these groups to acceptable sizes. **2.12** was integrated as a 50-50 twin and the co-crystallized toluene molecules were modeled in two parts and constrained to bring the displacement parameters to acceptable sizes. The disordered benzyl group was modeled in two parts and restraints were used to bring displacement parameters to acceptable sizes.

**Table 2.5.** Crystal and refinement data for **2.11**, **2.12**, and **2.20**

	<b>2.20</b>	<b>2.11</b>	<b>2.12</b>
CCDC Number	1529995	1529994	1529996
Empirical formula	C <sub>69</sub> H <sub>95</sub> N <sub>2</sub> O <sub>2</sub> SiZr	C <sub>108</sub> H <sub>154</sub> N <sub>4</sub> O <sub>4</sub> Si <sub>2</sub> Zr <sub>2</sub>	C <sub>126</sub> H <sub>166</sub> N <sub>4</sub> O <sub>4</sub> Si <sub>2</sub> Zr <sub>2</sub>
Formula weight	1103.77	1810.96	2039.26
T (K)	100.01	99.98	100
a, Å	9.0866(14)	15.1120(6)	15.3649(10)
b, Å	11.0615(17)	22.3907(10)	18.5121(12)
c, Å	32.200(5)	34.1289(16)	22.6331(15)
α, °	86.076(3)	90	75.488(4)
β, °	89.449(4)	90	73.031(4)
γ, °	77.974(3)	90	73.114(4)
Volume, Å <sup>3</sup>	3158.0(8)	11548.1(9)	5794.4(7)
Z	2	4	2
Crystal system	triclinic	orthorhombic	triclinic
Space group	P-1	I222	P-1
d <sub>calc</sub> , g/cm <sup>3</sup>	1.161	1.042	1.160
θ range, °	3.774 to 73.662	2.360 to 79.497	2.85 to 50.802
μ, mm <sup>-1</sup>	0.237	2.018	0.252
Abs. Correction	Semi-empirical	Semi-empirical	Semi-empirical
GOF	1.042	1.053	1.033
R <sub>1</sub> , <sup>a</sup> wR <sub>2</sub> <sup>b</sup> [I>2	0.0446, 0.1021	0.0455, 0.1055	0.0470, 0.0992
σ(I)]			
Radiation Type	Mo Kα	Cu Kα	Mo Kα

$$^a R1 = \sum ||F_o| - |F_c|| / \sum |F_o|, ^b wR2 = [\sum [w(F_o^2 - F_c^2)^2] / \sum [w(F_o^2)^2]^{1/2}.$$

## REFERENCES

1. Delferro, M.; Marks, T. J. *Chem. Rev.* **2011**, *111*, 2450-2485.
2. Li, L.; Metz, M. V.; Li, H.; Chen, M.-C.; Marks, T. J.; Liable-Sands, L.; Rheingold, A. L. *J. Am. Chem. Soc.* **2002**, *124*, 12725-12741.
3. Salata, M. R.; Marks, T. J. *J. Am. Chem. Soc.* **2008**, *130*, 12-13.
4. Gao, Y.; Mouat, A. R.; Motta, A.; Macchioni, A.; Zuccaccia, C.; Delferro, M.; Marks, T. J. *ACS Catal.* **2015**, *5*, 5272-5282.
5. Takeuchi, D.; Chiba, Y.; Takano, S.; Osakada, K. *Angew. Chem. Int. Ed. Engl.* **2013**, *52*, 12536-12540.
6. (a) Takano, S.; Takeuchi, D.; Osakada, K.; Akamatsu, N.; Shishido, A. *Angew. Chem. Int. Ed. Engl.* **2014**, *53*, 9246-9250; (b) Takano, S.; Takeuchi, D.; Osakada, K. *Chem. Eur. J.* **2015**, *21*, 16209-16218.
7. (a) Radlauer, M.; Day, M. W.; Agapie, T. *Organometallics* **2012**, *31*, 2231-2243; (b) Radlauer, M. R.; Day, M. W.; Agapie, T. *J. Am. Chem. Soc.* **2012**, *134*, 1478-1481; (c) Radlauer, M. R.; Buckley, A. K.; Henling, L. M.; Agapie, T. *J. Am. Chem. Soc.* **2013**, *135*, 3784-3787.
8. (a) Coates, G. W. *Chem. Rev.* **2000**, *100*, 1223-1252; (b) Brintzinger, H. H.; Fischer, D.; Mülhaupt, R.; Rieger, B.; Waymouth, R. M. *Angew. Chem. Int. Ed. Engl.* **1995**, *34*, 1143-1170.
9. (a) Gibson, V. C.; Spitzmesser, S. K. *Chem. Rev.* **2003**, *103*, 283-315; (b) Britovsek, G. J. P.; Gibson, V. C.; Wass, D. F. *Angew. Chem. Int. Ed. Engl.* **1999**, *38*, 428-447; (c) Resconi, L.; Cavallo, L.; Fait, A.; Piemontesi, F. *Chem. Rev.* **2000**, *100*, 1253-1346.
10. Wei, J.; Hwang, W.; Zhang, W.; Sita, L. R. *J. Am. Chem. Soc.* **2013**, *135*, 2132-2135.
11. (a) Lee, D.-H.; Yoon, K.-B.; Lee, E.-H.; Noh, S.-K.; Byun, G.-G.; Lee, C.-S. *Macromol. Rapid Comm.* **1995**, *16*, 265-268; (b) Noh, S. K.; Byun, G.-G.; Lee, C.-S.; Lee, D.; Yoon, K.-B.; Kang, K. S. *J. Organomet. Chem.* **1996**, *518*, 1-6; (c) Noh, S. K.; Kim, S.; Yang, Y.; Lyoo, W. S.; Lee, D.-H. *Eur. Polym. J.* **2004**, *40*, 227-235; (d) Noh, S. K.; Jung, W.; Oh, H.; Lee, Y. R.; Lyoo, W. S. *J. Organomet. Chem.* **2006**, *691*, 5000-5006; (e) Linh, N. T. B.; Huyen, N. T. D.; Noh, S. K.; Lyoo, W. S.; Lee, D.-H.; Kim, Y. *J. Organomet. Chem.* **2009**, *694*, 3438-3443.
12. Radlauer, M. R.; Agapie, T. *Organometallics* **2014**, *33*, 3247-3250.
13. (a) Groysman, S.; Tshuva, E. Y.; Reshef, D.; Gendler, S.; Goldberg, I.; Kol, M.; Goldschmidt, Z.; Shuster, M.; Lidor, G. *Isr. J. of Chem.* **2002**, *42*, 373-381; (b) Tshuva, E. Y.; Groysman, S.; Goldberg, I.; Kol, M.; Goldschmidt, Z. *Organometallics* **2002**, *21*, 662-670; (c) Tshuva, E. Y.; Goldberg, I.; Kol, M.; Weitman, H.; Goldschmidt, Z. *Chem. Commun.* **2000**, 379-380; (d) Tshuva, E. Y.; Goldberg, I.; Kol, M.; Goldschmidt, Z. *Organometallics* **2001**, *20*, 3017-3028; (e) Groysman, S.; Goldberg, I.; Kol, M.; Genizi, E.; Goldschmidt, Z. *Inorg. Chim. Acta.* **2003**, *345*, 137-144; (f) Groysman, S.; Goldberg, I.; Kol, M.; Genizi, E.; Goldschmidt, Z. *Organometallics* **2003**, *22*, 3013-3015; (g) Switzer, J. M.; Travia, N. E.; Steelman, D. K.; Medvedev, G. A.; Thomson, K. T.; Delgass, W. N.; Abu-Omar, M. M.; Caruthers, J. M. *Macromolecules* **2012**, *45*, 4978-4988; (h) Steelman, D. K.; Xiong, S.; Pletcher, P. D.; Smith, E.; Switzer, J. M.; Medvedev, G. A.; Delgass, W. N.; Caruthers, J. M.; Abu-Omar, M. M. *J. Am. Chem. Soc.* **2013**, *135*, 6280-6288; (i) Steelman, D. K.; Pletcher, P. D.; Switzer, J. M.; Xiong, S.; Medvedev, G. A.; Delgass, W. N.; Caruthers, J. M.; Abu-Omar, M. M. *Organometallics* **2013**, *32*, 4862-4867; (j)

- Steelman, D. K.; Xiong, S.; Medvedev, G. A.; Delgass, W. N.; Caruthers, J. M.; Abu-Omar, M. M. *ACS Catal.* **2014**, *4*, 2186-2190; (k) Pletcher, P. D.; Switzer, J. M.; Steelman, D. K.; Medvedev, G. A.; Delgass, W. N.; Caruthers, J. M.; Abu-Omar, M. M. *ACS Catal.* **2016**, *6*, 5138-5145; (l) Reybuck, S. E.; Lincoln, A. L.; Ma, S.; Waymouth, R. M. *Macromolecules* **2005**, *38*, 2552-2558.
14. (a) Busico, V.; Cipullo, R.; Ronca, S.; Budzelaar, P. H. M. *Macromol. Rapid Commun.* **2001**, *22*, 1405-1410; (b) Cohen, A.; Kopilov, J.; Goldberg, I.; Kol, M. *Organometallics* **2009**, *28*, 1391-1405; (c) Gendler, S.; Zelikoff, A. L.; Kopilov, J.; Goldberg, I.; Kol, M. *J Am Chem Soc* **2008**, *130*, 2144-5; (d) Segal, S.; Goldberg, I.; Kol, M. *Organometallics* **2005**, *24*, 200-202.
15. (a) Golisz, S. R.; Bercaw, J. E. *Macromolecules* **2009**, *42*, 8751-8762; (b) Agapie, T.; Henling, L. M.; DiPasquale, A. G.; Rheingold, A. L.; Bercaw, J. E. *Organometallics* **2008**, *27*, 6245-6256; (c) Kirillov, E.; Roisnel, T.; Razavi, A.; Carpentier, J.-F. *Organometallics* **2009**, *28*, 5036-5051.
16. Pangborn, A. B.; Giardello, M. A.; Grubbs, R. H.; Rosen, R. K.; Timmers, F. J. *Organometallics* **1996**, *15*, 1518-1520.
17. Atiqullah, M.; Moman, A. A.; Akhtar, M. N.; Al-Muallem, H. A.; Abu-Raqabah, A. H.; Ahmed, N. *J. Appl. Polym. Sci.* **2007**, *106*, 3149-3157.
18. Dias, P.; Lin, Y. J.; Poon, B.; Chen, H. Y.; Hiltner, A.; Baer, E. *Polymer* **2008**, *49*, 2937-2946.
19. (a) Carman, C. J.; Harrington, R. A.; Wilkes, C. E. *Macromolecules* **1977**, *10*, 536-544; (b) Cheng, H. N. *Macromolecules* **1984**, *17*, 1950-1955; (c) Cheng, H. N.; Smith, D. A. *Macromolecules* **1986**, *19*, 2065-2072; (d) Randall, J. C. *Macromolecules* **1978**, *11*, 33-36; (e) Randall, J. C.; Hsieh, E. T. *Macromolecules* **1982**, *15*, 1584-1586; (f) Tritto, I.; Fan, Z.-Q.; Locatelli, P.; Sacchi, M. C.; Camurati, I.; Galimberti, M. *Macromolecules* **1995**, *28*, 3342-3350.
20. (a) Hsieh, E. T.; Randall, J. C. *Macromolecules* **1982**, *15*, 1402-1406; (b) Cheng, H. N. *Polym. Bull.* **1991**, *26*, 325-332; (c) Galland, G. B.; Mauler, R. S.; de Menezes, S. C.; Quijada, R. *Polym. Bull.* **1995**, *34*, 599-604; (d) Quijada, R.; Dupont, J.; Miranda, M. S. L.; Scipioni, R. B.; Galland, G. B. *Macromol. Chem. Phys.* **1995**, *196*, 3991-4000.
21. Yeori, A.; Goldberg, I.; Shuster, M.; Kol, M. *J. Am. Chem. Soc.* **2006**, *128*, 13062-13063.
22. Sworen, J. C.; Smith, J. A.; Wagener, K. B.; Baugh, L. S.; Rucker, S. P. *J. Am. Chem. Soc.* **2003**, *125*, 2228-2240.
23. Zysman-Colman, E.; Arias, K.; Siegel, J.S. *Can.J. Chem.* **2009**, *87*, 440-447.
24. Christensen, P.R.; Patrick, B.O.; Caron, E.; Wolf, M.O. *Angew. Chem. Int. Ed.* **2013**, *52*, 12946-12950.
25. Appiah, W.O.; DeGreeff, A.D.; Razidlo, G.L.; Spessard, S.J.; Pink, M.; Young, V.G.; Hofmeister, G.E. *Inorg. Chem.* **2002**, *41*, 3656-3667.
26. Baldwin, D.; Gates, P.S., Process for preparing pyrogallol. Google Patents: 1979.
27. Thadani, A.N.; Huang, Y; Rawal, V.H. *Org. Lett.* **2007**, *9*, 3873-3876.
28. APEX2, Version 2 User Manual, M86-E01078, Bruker Analytical X-ray Systems, Madison, WI, June 2006.
29. Sheldrick, G.M. "SADABS (version 2008/l): Program for Absorption Correction for Data from Area Detector Frames", University of Göttingen, 2008.
30. Dolomanov, O.V.; Bourhis, L.J.; Gildea, R.J.; Howard, J.A.K.; Puschmann, H. J. *Appl. Cryst.* **2009**, *42*, 339.
31. Sheldrick, G.M. (2008). *Acta Cryst.* A64, 112-122.

32. Brandenburg, K. (1999), DIAMOND. Crystal Impact GdR, Bonn, Germany.
33. Spek, A.L. "PLATON – A Multipurpose Crystallographic Tool, Utrecht University", Utrecht, the Netherlands, 2006.

## **CHAPTER 3**

EARLY METAL DI(PYRIDYL) PYRROLIDE COMPLEXES WITH SECOND COORDINATION  
SPHERE ARENE-PI INTERACTIONS: SUBSTRATE BINDING AND ETHYLENE  
POLYMERIZATION



**ABSTRACT**

Early metal complexes supported by hemilabile, monoanionic di(pyridyl)pyrrolide ligands substituted with mesityl and anthracenyl groups were synthesized in order to probe the use of  $\pi$ - $\pi$  interactions as a means of allosteric control in coordination chemistry, substrate activation, and olefin polymerization. Yttrium alkyl, indolide, and amide complexes were prepared and structurally characterized; close contacts between the anthracenyl substituents and Y-bound ligands are observed in the solid state. Titanium, zirconium, and hafnium tris(dimethylamido) complexes were synthesized and their ethylene polymerization activity tested. In the solid state structure of one of the Ti tris(dimethylamido) complexes, coordination of Ti to only one of the pyridine donors is observed.

## INTRODUCTION

The use of secondary coordination sphere interactions in transition metal ancillary ligand design has recently emerged as a powerful strategy to modulate the behavior of the resulting complexes and catalysts.<sup>1</sup> Incorporation of hydrogen bond donor groups has been reported to support metal oxo and hydroxo (**3.A**),<sup>1a, 1b, 2</sup> nitrite activation,<sup>3</sup> CO<sub>2</sub> reduction,<sup>4</sup> and other reactivity.<sup>5</sup> Ligands appended with Lewis acidic moieties have also been reported to promote hydrazine bonding at Fe,<sup>6</sup> reductive CO coupling (**3.B**),<sup>7</sup> selective alkyne hydrogenation,<sup>8</sup> and other small molecule activation.<sup>9</sup> Lewis base incorporation into the secondary-coordination sphere of Fe complexes for N<sub>2</sub> reduction,<sup>10</sup> Ni catalysts for proton reduction (**3.C**),<sup>11</sup> and Co water oxidation catalysts<sup>12</sup> has reported to change catalyst selectivity activity. Finally, use of the combination of pendant Lewis acids and Lewis bases has been reported as a strategy for stabilization of hydrazine binding at V (**3.D**).<sup>13</sup>

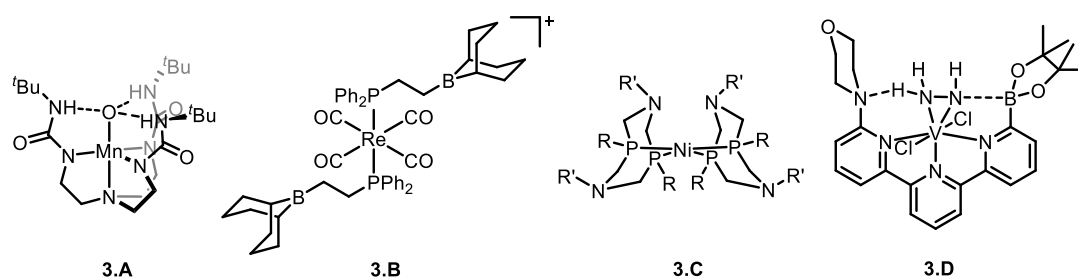


**Figure 3.1.** Examples of ligands incorporating secondary coordination sphere effects.

One type of potential interaction which has been under-explored in the literature is the use of  $\pi$ - $\pi$  interactions through incorporation of pendant  $\pi$  systems into the ancillary ligands.<sup>14</sup> Terpyridine (terpy) ligands are an example of a ligand framework in which incorporation of such motifs can lead to  $\pi$ - $\pi$  interactions with additional ligands (Figure 3.2). Lehn and coworkers have demonstrated that incorporation of pyrene groups into

the terpy ligand results in formation, upon metal binding, of heteroligated Zn complex **3.E** which displays average distances of 3.50 Å between the pyrene units and the other terpy ligand<sup>15</sup> and homoligated Cu complex **3.F** displaying average distances of 3.50 Å between the pyrene units and the plane of the terpy backbone.<sup>16</sup> Chan and coworkers have also demonstrated that incorporation of both 2,6-dimethoxyphenyl, **3.G**, and anthracenyl, **3.H**, groups on to the terpy backbone can be used to selectively prepare the heteroligated complexes as a consequence of the favorable electronics of  $\pi$ -stacking in these cases.<sup>17</sup> Despite these and other<sup>18</sup> examples of arene-appended terpy ligands displaying favorable  $\pi$ - $\pi$  interactions in the solid state, monoligated complexes, in the absence of additional ligands bearing extended  $\pi$ -systems, do not display parallel aryl substituents in the solid state<sup>19</sup> as a consequence of the central six-membered pyridine donor.

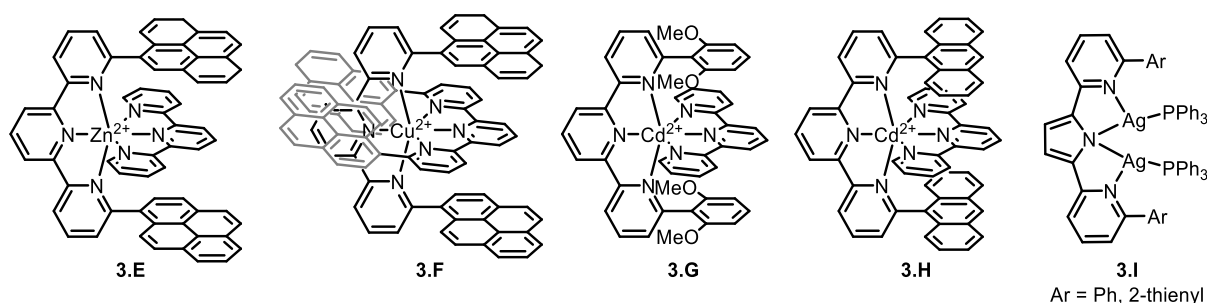


**Figure 3.2.** Examples of terpyridine-supported complexes displaying  $\pi$ - $\pi$  interactions in the solid state

The use of di(pyridyl) ligands bearing a central five-membered substituent was hypothesized to enhance the ability of flanking aryl substituents to interact with incoming substrates in directed X-H bond activation and olefin polymerization (Figure 3.3). The di(pyridyl) pyrrolide (DPP) backbone, in particular, was thought to be suitable for

supported early transition metal complexes as a consequence of its monoanionic charge. Furthermore, Zr complexes of the related bis(imino) pyrrolide ligand have been previously shown to be competent for ethylene polymerization.<sup>20</sup> Unsubstituted (dpp) ligands have received attention in the literature as ligands for Ag,<sup>21</sup> Cu,<sup>21-22</sup> Fe,<sup>23</sup> Co,<sup>24</sup> Ru,<sup>25</sup> and Pd,<sup>25a, 26</sup> however, only those bearing phenyl and 2-thienyl substituents, **3.I** (Figure 3.3)<sup>27</sup> have been reported where the DPP substituents could interact with the  $\pi$ -systems of incoming substrates. Such interactions are not observed between the phenyl and 2-thienyl substituents and the in the solid-state structures of **3.I**.

Herein we report a series of Al, Y, Ti, Zr, and Hf complexes supported by arene-appended di(pyridyl)pyrrolide ligands which display C-H- $\pi$ , Cl- $\pi$ , and  $\pi$ - $\pi$  interactions in the solid state. Furthermore, the reactivity of the Ti, Zr, and Hf complexes in ethylene polymerization upon activation with AlMe<sub>3</sub> and [CPh<sub>3</sub>][B(C<sub>6</sub>F<sub>5</sub>)<sub>4</sub>] is reported.

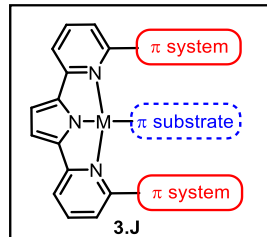
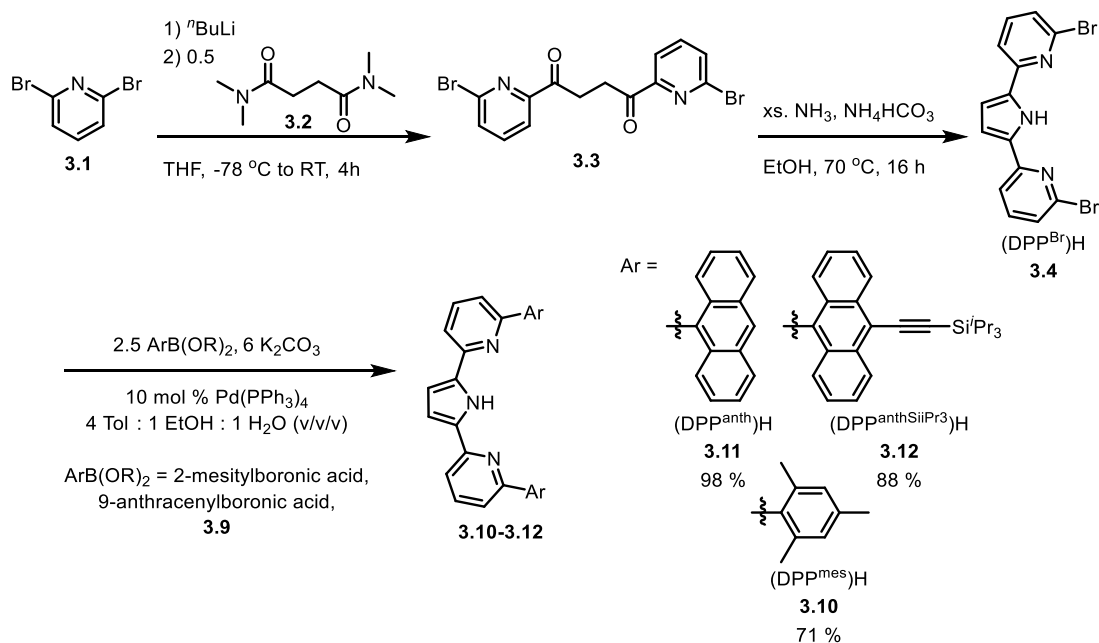


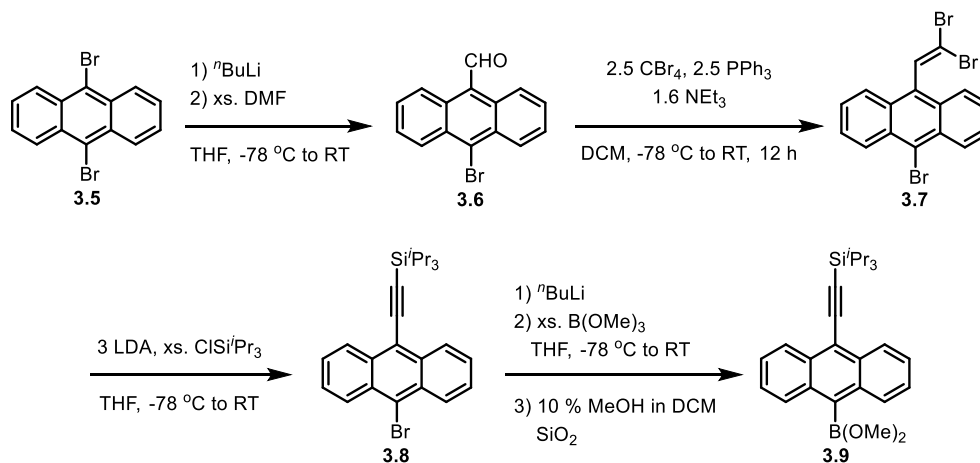
**Figure 3.3.** Di(pyridyl)pyrrolide ligands bearing flanking aryl groups for  $\pi$ - $\pi$  interaction with substrates

## RESULTS AND DISCUSSION

Aryl-substituted dipyridyl pyrrole proligands were synthesized in three steps from 2,6-dibromopyridine as shown in Scheme 3.1. Initial lithiation of 2,6-dibromopyridine (**3.1**) followed by quench with N,N,N',N'-tetramethylsuccinamide (**3.2**) affords the diketone **3.3**, which can be cyclized in the presence of aqueous ammonia to afford the dipyridyl pyrrole backbone, (DPP<sup>Br</sup>)H (**3.4**).<sup>28</sup> The 10-tri(*iso*-propyl)silylethynyl-substituted 9-bromoanthracene (**3.8**) was prepared by the Corey-Fuchs reaction of 9-bromo,10-anthracenecarboxaldehyde as previously reported by Argouarch and coworkers (Scheme 3.2).<sup>29</sup> Lithiation of **3.8**, quench with trimethylborate, and acidic workup affords the boronic acid which was converted to methyl ester **3.9** upon purification by column chromatography. 2-mesitylboronic acid and 9-anthracenylboronic acid were synthesized according to the literature.<sup>30</sup> Suzuki coupling of **3.4** with the corresponding boronic acid or boronic ester affords the aryl-substituted proligands **3.10**, **3.11**, and **3.12** which were isolated in good yields following purification by column chromatography and/or precipitation. The syntheses of **3.11** and **3.12** were initially developed by Dr. Gyeongshin Choi, however, further optimization was performed to allow them to be isolated in higher yields and purity.

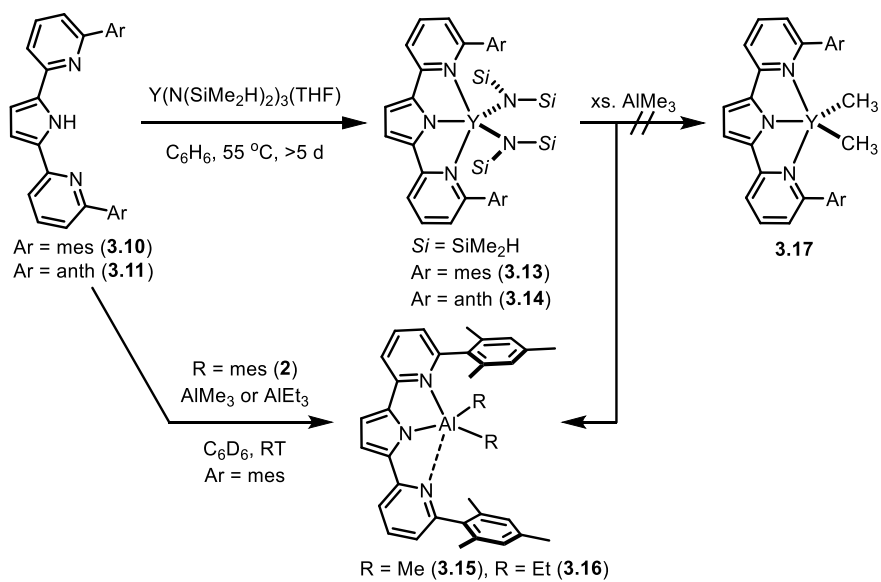


**Scheme 3.1.** Preparation of aryl-substituted di(pyridyl) pyrrole proligands through Suzuki coupling of the corresponding aryl boronic acid or ester with the previously-reported  $(\text{DPP}^{\text{Br}_2})\text{H}$ .<sup>28</sup>



**Scheme 3.2.** Preparation of tri-*iso*-propylsilyl ethynyl substituted anthracene boronic ester from the corresponding aryl bromide, prepared according to the synthesis of Argouarch and coworkers.<sup>29</sup>

Yttrium bis(tetramethyldisilylazide) complexes were prepared by reaction of the protonated pyrrole proligands with  $\text{Y}(\text{N}(\text{SiMe}_2\text{H})_2)_3(\text{THF})$  in  $\text{C}_6\text{H}_6$  at elevated temperatures (Scheme 3.3). *In situ* monitoring of these reactions indicated interaction of the proligands with the Y precursor upon mixing at room temperature; however, release of  $\text{HN}(\text{SiMe}_2\text{H})_2$  was not observed except upon heating. The NMR spectra of **3.13** and **3.14** both feature a single set of pyridine DPP and  $\text{N}(\text{SiMe}_2\text{H})_2$  resonances, consistent with fast exchange of the  $\text{SiMe}_2\text{H}$  groups. Such exchange could occur through direct rotation about the  $\text{Y}-\text{N}(\text{SiMe}_2\text{H})_2$  bond or upon dissociation of a pyridine donor. In comparison with **3.13**, **3.14** features an upfield-shifted Si-H resonance by 3.7 ppm and an upfield-shifted Si- $\text{CH}_3$  resonance by 0.48 ppm, consistent with increased shielding by the more extended  $\pi$ -system of the anthracenyl substituent.<sup>31</sup> X-Ray quality crystals of **3.14** were obtained by slow cooling of a saturated benzene solution (Figure 3.4). Crystals with two unit cells were observed from the same crystallization, however, initial solutions indicated formation of similar trigonal bipyramidal  $C_{2v}$  complexes ( $\tau_5 = 0.01$  to  $0.05$ ).<sup>32</sup> Two molecules of **3.14** are observed in the asymmetric unit of the higher-quality structure; in both Y is located near equidistant to the pyridine donors, with  $\text{Y}-\text{N}(\text{Py})$  distances in the range of 2.643(4) to 2.706(3) Å and  $\text{Y}-\text{N}(\text{pyrrole})$  distances in the range of 2.245(3) to 2.266(3) Å. Angles of 33.4 and 31.4 ° are observed between the anthracenyl groups; such distortion is likely a consequence of the size of the tetramethyldisilylazide groups.



**Scheme 3.3.** Preparation of bis(tetramethyldisilylazide)yttrium complexes supported by the dipyrrolylpyrrole ligand and subsequent DPP transmetalation upon treatment with  $AlR_3$ .



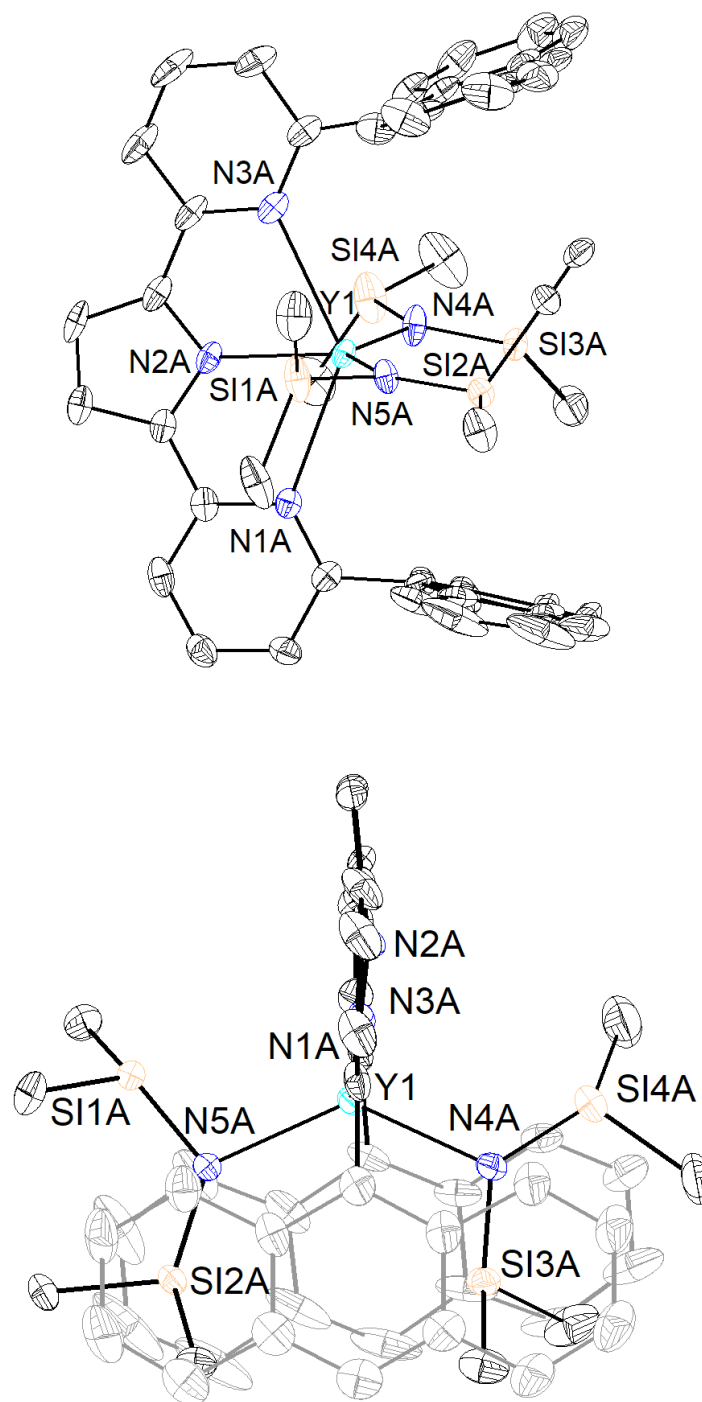


**Figure 3.4.** Solid-state structure of **3.14**. Hydrogen atoms and solvent of crystallization are omitted for clarity. The major populations of the disordered tetramethyldisilylazide groups are shown for clarity.

While treatment of **3.13** with  $\text{PhSiH}_3$  did not result in any reaction by NMR, treatment with  $\text{AlMe}_3$  or  $\text{AlEt}_3$  lead to formation of a new metal-alkyl containing species. The product of the reaction of **3.13** with  $\text{AlEt}_3$  was identified as the four-coordinate diethylaluminum complex **3.16** ( $\tau_4 = 0.88$ ; Figure 3.5)<sup>33</sup> by X-ray crystallography and independent synthesis. A distance of 2.8848(18) Å from Al(1) to N(3) of the free pyridine is observed, which is within the sum of van der Waals radii (3.91 Å).<sup>34</sup> Comparison of the  $^1\text{H}$  NMR spectra of the products **4** with  $\text{AlMe}_3$  and  $\text{AlEt}_3$  with the products of the reactions of **2** with  $\text{AlMe}_3$  and  $\text{AlEt}_3$  indicate formation of the same species in both reactions (Figures F3.13 and F3.14). Such ancillary ligand transmetalation from Y to Al has been observed in a number of other systems including in iminopyrrolide complexes.<sup>35</sup>

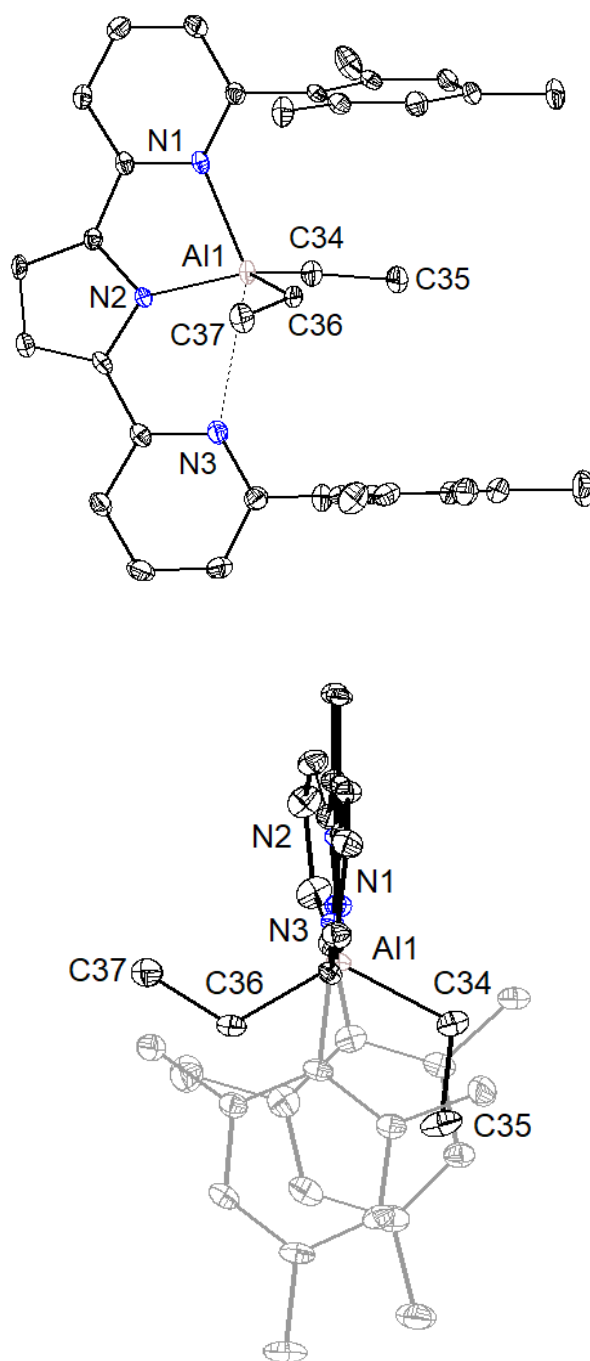
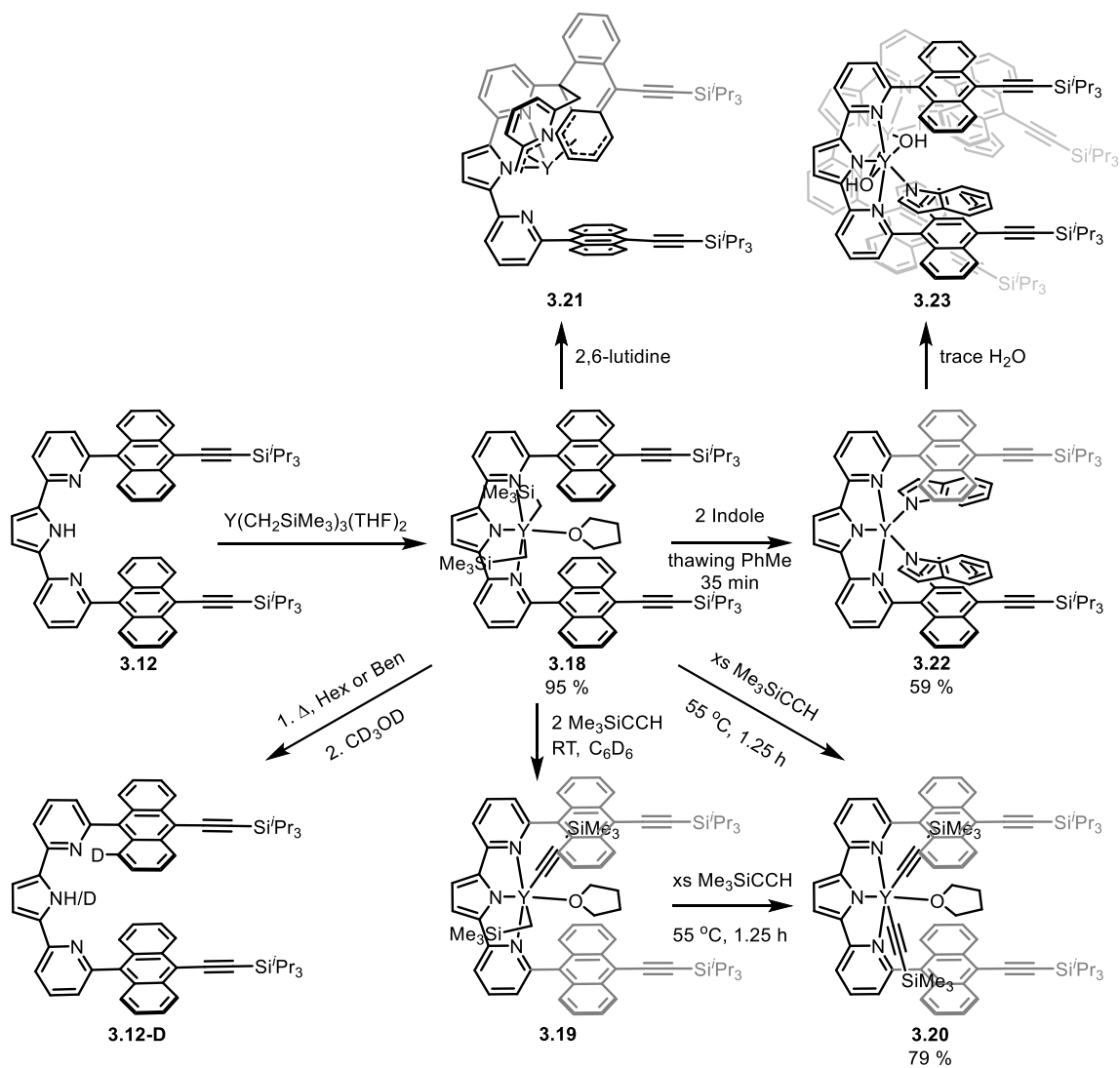


**Figure 3.5.** Solid-state structure of **3.16**. Hydrogen atoms are omitted for clarity.

Reaction of **3.12** with  $\text{Y}(\text{CH}_2\text{SiMe}_3)_3(\text{THF})_2$  in thawing hexanes over 40 minutes affords a red-brown species with NMR features consistent with  $C_{2v}$   $\text{Y}(\text{CH}_2\text{SiMe}_3)_2(\text{THF})$  complex **3.18**. An upfield-shifted doublet is observed in the  $^1\text{H}$  NMR at -2.33 ppm ( $^2J_{\text{YH}} = 2.4$  Hz) which is assigned to the four methylene protons of the  $\text{CH}_2\text{SiMe}_3$  groups; the  $\text{CH}_2\text{SiMe}_3$  resonance is observed at 29.41 ppm ( $^1J_{\text{YC}} = 31.0$  Hz) in the  $^{13}\text{C}$  NMR. The bound THF has  $^1\text{H}$  resonances between 1.35 and 1.16 ppm and broad  $^{13}\text{C}$  resonances at 71.19 and 24.50 ppm. X-ray quality crystals were grown by slow evaporation of a pentane solution of the complex at -35 °C (Figure 3.6). The DPP ligand binds meridionally with a short Y-N(pyrrolide) distance of 2.2585(22) Å and two long Y-N(pyr) distances of 2.5914(24) and 2.5626(22) Å. The two  $\text{CH}_2\text{SiMe}_3$  groups are located *trans* to one another and the coordination sphere is filled with a THF bound between the two anthracenyl substituents. Distances of 3.64 and 3.46 Å are observed between the oxygen of the bound THF and the planes of the two anthracenyl substituents, consistent with C-H- $\pi$  interactions between the THF and the ligand substituents.



**Scheme 3.4.** Synthesis and reactivity of (dialkyl)yttrium complex **3.18**.

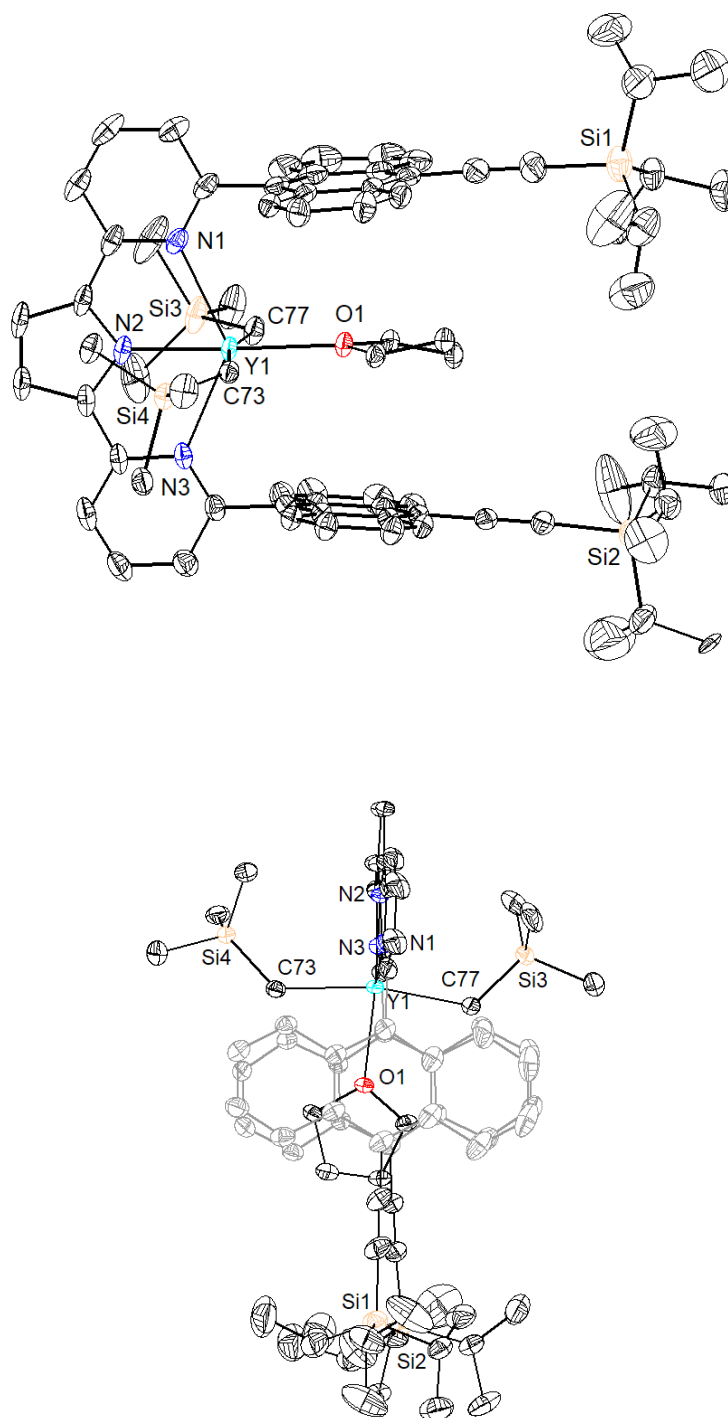


**Figure 3.6.** Solid-state structure of **3.18**. Hydrogen atoms are omitted for clarity.

Reaction of **3.18** with a variety of aromatic substrates including phenanthrene, 2,3,4,5,6-pentafluorophenyltoluene, and 1-methylnaphthalene was attempted; however, the same mixture of Y-containing products was observed from each of these reactions due to facile fast ligand activation. While heating **3.18** to 70°C for 72 h in non-coordinating solvents results in loss of all Y(CH<sub>2</sub>SiMe<sub>3</sub>) resonances and release of two equivalents of SiMe<sub>4</sub>, over shorter periods of time a species is formed with concomitant release of THF and one equivalent of SiMe<sub>4</sub> (Figure F3.21). This initially formed species features a set of two doublets of doublets centered at -2.07 and -2.53 ppm (<sup>1</sup>J<sub>HH</sub> = 11.6 Hz, <sup>2</sup>J<sub>YH</sub> = 3.3 Hz) corresponding to a species bearing a single CH<sub>2</sub>SiMe<sub>3</sub> group with loss of symmetry between the two pyridine donors. While structural characterization of this complex could not be obtained, CD<sub>3</sub>OD quench of this species lead to incorporation of deuterium into one of the anthracenyl ligand substituents (**3.12-D**, Scheme 3, Figure F3.22), indicating cyclometallation at one of these positions leads to formation of this initial decomposition product. No decomposition of **3.18** was observed upon heating in either THF or CD<sub>3</sub>CN; no reaction was observed between this initial decomposition product and ethynyltrimethylsilane.

Reaction of **3.18** with two equivalents of trimethylsilylacetylene at room temperature in C<sub>6</sub>D<sub>6</sub> affords a new C<sub>s</sub> symmetric compound with <sup>1</sup>H NMR features consistent with a mono-acetylide (**3.19**). In the presence of excess trimethylsilylacetylene no further conversion is observed at room temperature, however, upon heating to 55 °C for 1.25 h a new C<sub>2v</sub> symmetric species is generated with NMR features consistent with **3.20**, which could be isolated in 79 % yield on a 30 mg scale. In comparison with the starting material, **3.20** features an upfield-shifted pyrrole resonance at 6.96 ppm in the <sup>1</sup>H NMR and broad resonances at 1.48 and 1.00 ppm corresponding to the bound THF

group. The trimethylsilyl resonance of the bound acetylide is shifted to 0.04 ppm from 0.11 ppm in the free alkyne, while the  $^{13}\text{C}$  resonances of the  $\text{C}\equiv\text{C}-\text{SiMe}_3$  unit are observed as doublets at 171.37 ppm ( $^1J_{\text{YC}} = 48.83$  Hz) and 108.38 ppm ( $^2J_{\text{YC}} = 8.42$  Hz). Alkyne oligomerization was attempted using this complex in the presence of  $[\text{HNMe}_2\text{Ph}][\text{B}(\text{C}_6\text{F}_5)_4]$ , however, no activity was observed.

Directed C-H activation of substrates such as anisole and pyridine derivatives by **3.18** was targeted, however, reactivity based on  $^1\text{H}$  NMR monitoring was sluggish and multiple products typically observed. One insight into decomposition products of initially-observed species was obtained from X-Ray diffraction of a product of the reaction with 2,6-lutidine (**3.21**, Figure 3.7). While **3.21** was not characterized except by X-ray crystallography, attack of the 2,6-lutidine at the 9-position of one of the anthracenyl substituents is observed in its solid-state structure, with coordination of the functionalized anthracenyl moiety to Y. Based on electron counting the complex is assigned as a  $\eta^3$ -2,6-lutidine allyl complex with a delocalized anionic charge in the bound anthracene substituent. It is unclear exactly how this complex is formed, whether through formation of an initial bis(2,6-lutidine) complex or through some other intermediate, though the crude  $^1\text{H}$  NMR of this and related reactions would suggest formation of the former.



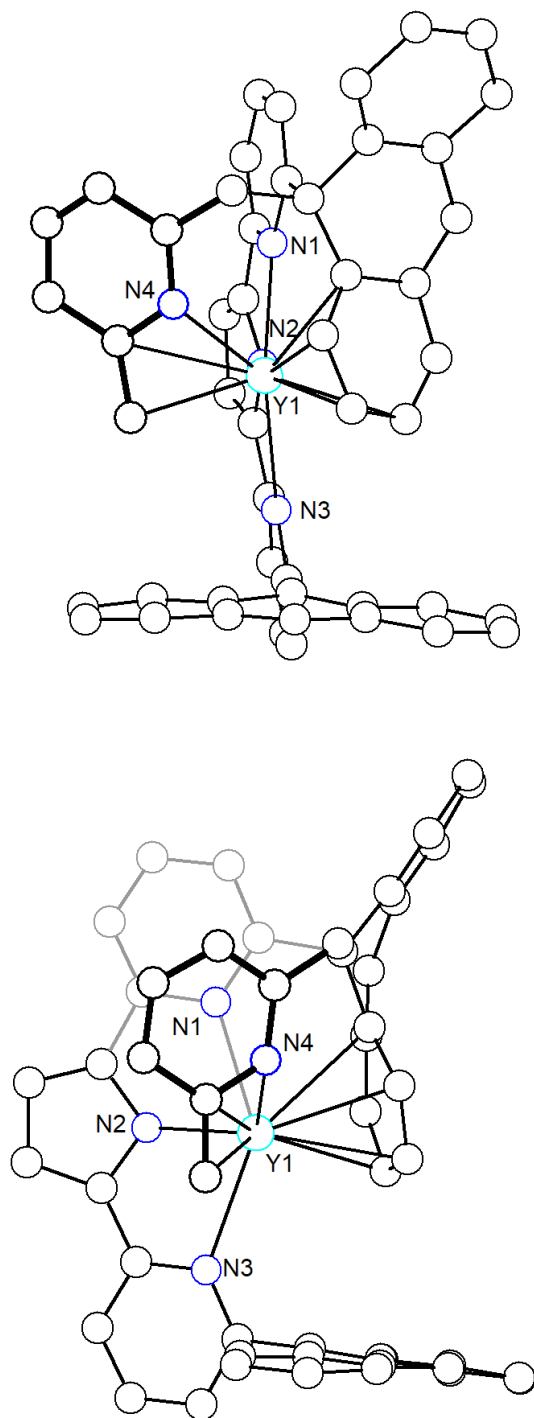


**Figure 3.7.** Preliminary solid-state structure of **3.21**. Hydrogen atoms and the tri(*iso*-propyl)ethynyl substituents are omitted for clarity.

**3.18** reacts with two equivalents of indole to release THF and two equivalents of SiMe<sub>4</sub> and afford the bis(indolide) complex **3.22**, which was confirmed by X-ray crystallography (Figure 3.8). The NMR features of this complex are broadened in comparison with **3.18** and **3.20**. This broadness could be a consequence of the interaction of the indolide substrates with the extended  $\pi$  systems of the anthracenyl substituents. In the solid state this distorted square pyramidal complex ( $\tau_5 = 0.07$ ) displays distances between 3.3 and 3.4 Å between the indolide ligands and the plane of the anthracenyl substituents, consistent with  $\pi$ - $\pi$  interaction. The six-membered rings of the indolide ligands are positioned away from the Y center and towards the anthracenyl substituents, suggesting that formation of the  $\pi$ - $\pi$  interactions is favored in comparison with formation of less sterically-congested complexes. Solid-state characterization of a water decomposition product of **3.22** was also obtained, though not otherwise characterized (**3.23**, Figure 3.9). Two Y centers with  $\mu_2$ -hydroxide are observed in this structure; as in the structure of **3.22**, distances consistent with  $\pi$ - $\pi$  interactions are observed between the nitrogens of the bound indolide groups and the planes of the anthracenyl substituents (3.45 to 3.68 Å).

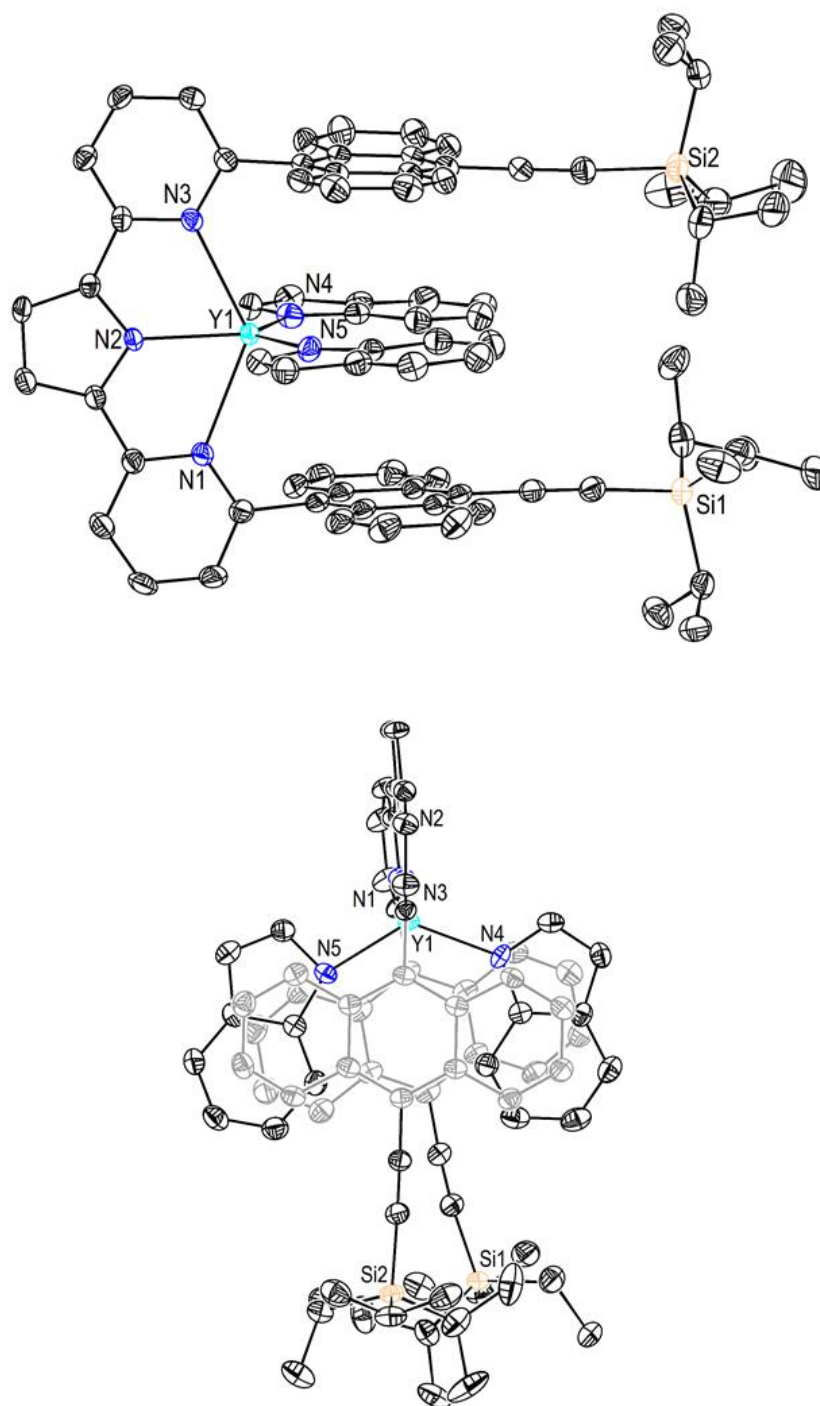


**Figure 3.8.** Preliminary solid-state structure of **3.22**. Hydrogen atoms are omitted for clarity.

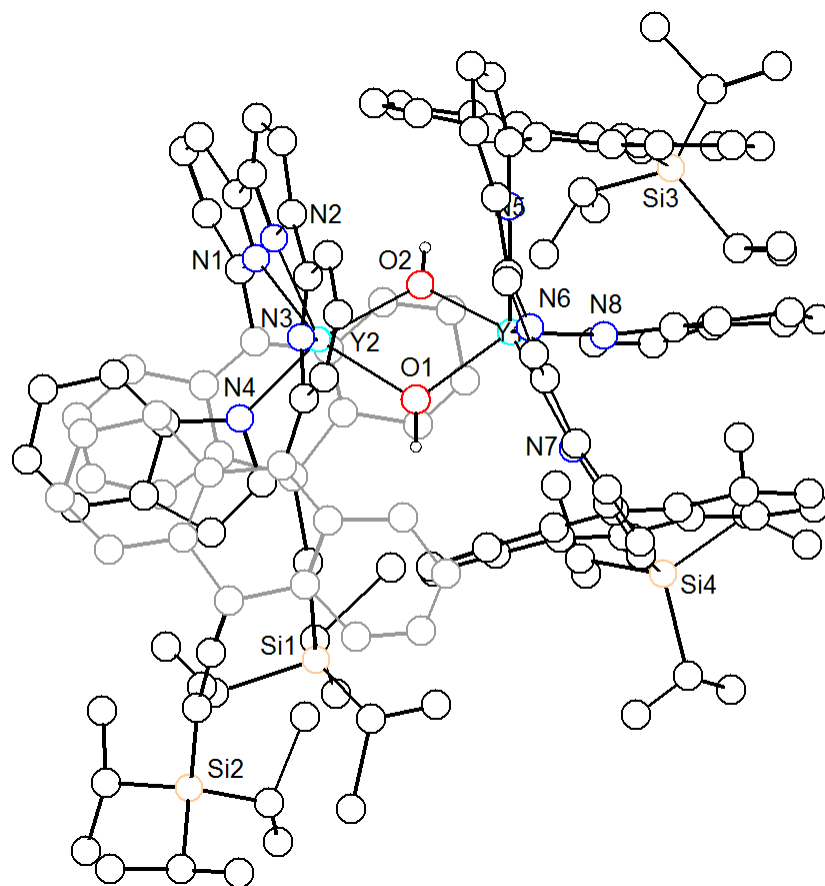


**Figure 3.9.** Solid-state structure of the water decomposition product of **3.22**, **3.23**. Hydrogen atoms are omitted for clarity.

While protonolysis of Zr tetrabenzyl and tetra(neosilyl) precursors was attempted, these reactions did not proceed readily nor cleanly, so other complexes were targeted. Dr. Gyeongshin Choi found that reaction of the DPP proligands with  $\text{ZrCl}_4$  upon *in situ* ligand deprotonation with KHMDS afforded complexes with exceedingly low solubility, leading to poor reproducibility of the syntheses. Dr. Choi was able to grow crystals suitable for X-Ray diffraction of the six-coordinate complex zirconium trichloride complex **3.24** (Figure 3.10) from this route. This complex features two long Zr-Py distances of 2.3921(13) and 2.3684(13) Å with a relatively short Zr-pyrrolide distance of 2.1478(10) Å. The three Cl

ligands are located at similar distances from Zr(1), in the range of 2.4006(6) to 2.4273(6) Å. The chloride ligand *trans* to the pyrrolide donor is located between the two anthracenyl ligand substituents with distances of 3.19 and 3.23 Å between the chloride and the planes of the anthracene groups. These distances are within the sum of the van der Waals radii (3.4 Å) and are consistent with halogen- $\pi$  interactions.<sup>36</sup> Work on the development of a reliable syntheses of Zr and Ti trichloride complexes supported by the DPP ligands are ongoing.

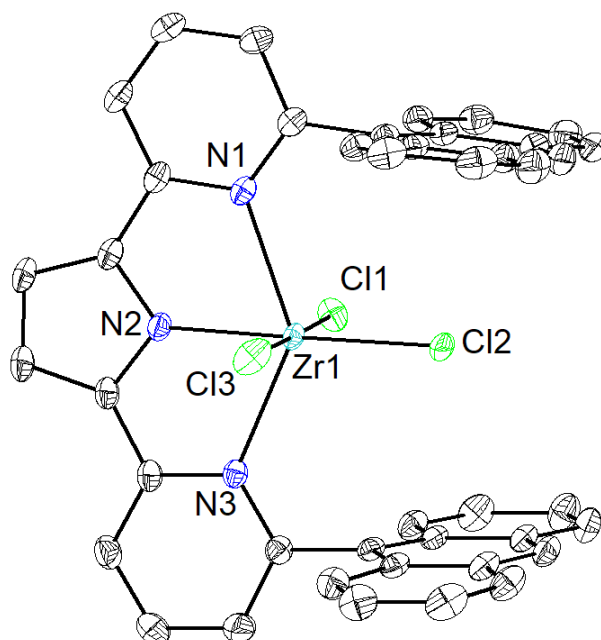
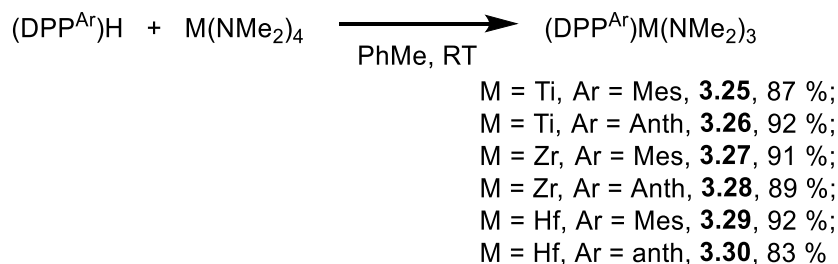


**Figure 3.10.** Solid-state structure of **3.24**. Hydrogen atoms are omitted for clarity.

Due to the low solubility of this and other targeted chloride complexes, more soluble complexes was targeted. Reaction of  $M(\text{NMe}_2)_4$  ( $M = \text{Ti}, \text{Zr}, \text{Hf}$ ) precursors with the pyrrole proligands in toluene at room temperature affords the corresponding tris(dimethylamido) complexes in good yields (Scheme 3.5). While reactions between ( $\text{DPP}^{\text{mes}}$ )H (**3.10**) and  $\text{Zr}(\text{NMe}_2)_4$  or  $\text{Hf}(\text{NMe}_2)_4$  proceed upon mixing, reaction of this

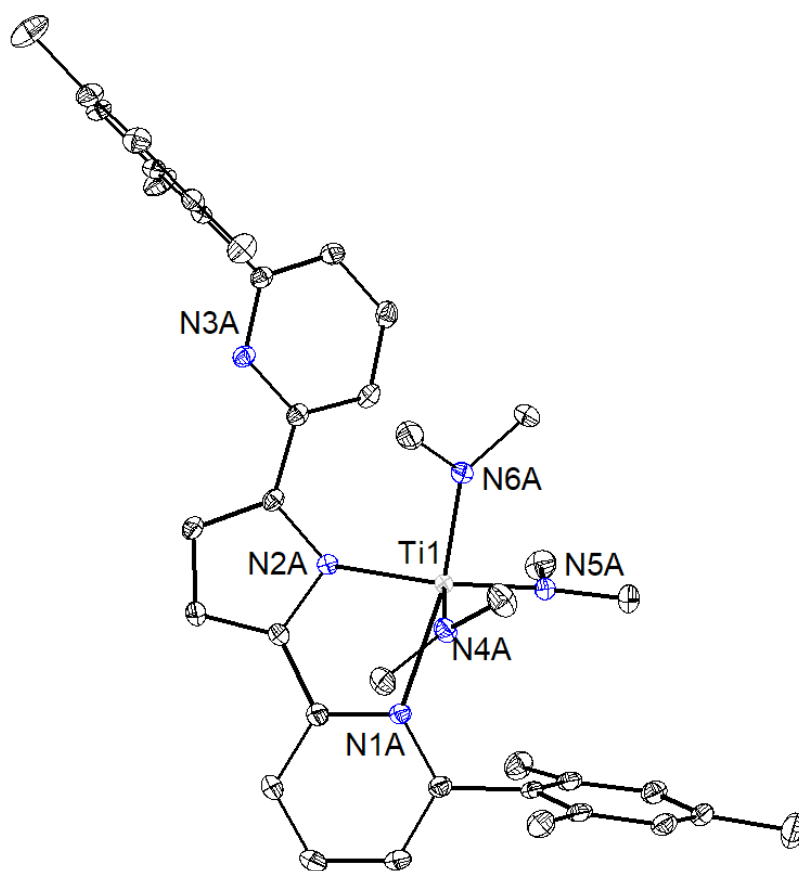
proligand with  $\text{Ti}(\text{NMe}_2)_4$  initially affords, by NMR, a species with inequivalent pyridine and mesityl resonances that converts over two days at room temperature, with loss of  $\text{HNMe}_2$ , to a species with a single set of pyridine and mesityl resonances. Reactions with  $(\text{DPP}^{\text{anth}})\text{H}$  (**3.11**) were all performed over at least two days due to the low solubility of the proligand in compatible solvents. All tris(dimethylamido) complexes, as isolated, feature a single dimethylamido resonance with equivalent pyridines and equivalent aromatic ligand substituents by  $^1\text{H}$  and  $^{13}\text{C}$  NMR, consistent with fast exchange between free and bound pyridine groups on the NMR time scale at room temperature. Upfield-shifted  $\text{NMe}_2$  resonances are also observed for the complexes bearing anthracene substituents as compared with complexes bearing mesityl substituents ( $\Delta\delta_{\text{NMe}}(\text{Ti}) = 0.38$ ;  $\Delta\delta_{\text{NMe}}(\text{Zr}) = 0.48$ ;  $\Delta\delta_{\text{NMe}}(\text{Hf}) = 0.47$ ) consistent with increased shielding by the more extended anthracenyl  $\pi$  system (*vide infra*).



**Scheme 3.5.** Synthesis of tris(dimethylamido) Ti, Zr, and Hf complexes

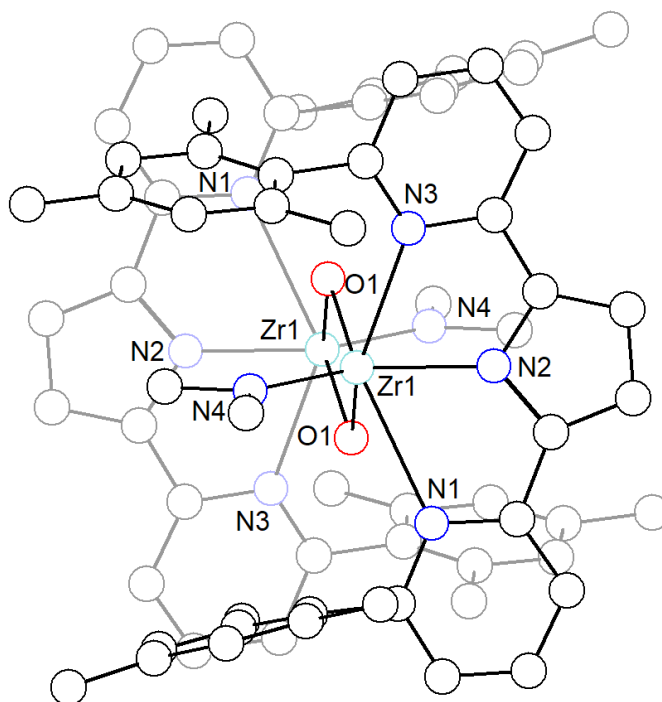
Crystals suitable for X-Ray diffraction could only be grown for **3.25** (Figure 3.11). This crystallizes with two molecules in the asymmetric unit; however, both feature five-coordinate Ti centers with distorted trigonal bipyramidal geometry. Consistent with other structures, both Ti centers are located closer to the pyrrolide N as compared with the pyridine N (2.1070(10) and 2.1054(11) Å vs. 2.3658(11) and 2.3792(11) Å). While the nitrogens of equatorial dimethylamido donors are located 1.8864(11) to 1.9143(12) Å

from Ti, the axial dimethylamido donors, located trans to the bound pyridine arms, show slight lengthening of the Ti-N bond to 1.9358(11) and 1.9327(11) Å. The dissociated pyridine arm is rotated away from the Ti center with a Ti-N distances of 5.0 to 5.1 Å and an angle of 28° between the plane of the unbound pyridine and the bound pyrrolide and pyridine. The Ti centers are both located out of the plane of the bound pyrrolide and pyridine donors by 0.87 Å. A similar metal geometry was observed by X-ray crystallography by Bochmann and coworkers in their related Zr tris(dimethylamido) complex supported by the bis(imino) pyrrolide ligand.<sup>20</sup>



**Figure 3.11.** Solid-state structure of **3.25**. Hydrogen atoms are omitted for clarity. One of two molecules in the asymmetric unit is shown for clarity.

Coordination of Zr to all three donors of the DPP ligand is observed in the X-ray crystal structure of **3.31** (Figure 3.12). This complex was formed in the presence of adventitious water during attempted crystallization of **3.27** and not otherwise characterized. The trigonal prismatic Zr centers lie near equidistant to the two pyridine donors (2.594(4) and 2.771(3) Å) with a shorter Zr-N(2) pyrrolide distance of 2.186(4) Å. The dimethylamido ligand is located *trans* to the pyrrolide with distances of 3.60 and 3.54 Å between N(4) and the planes of the mesityl substituents. As in the solid-state structure of **3.25**, Zr sits out of the plane of the DPP backbone, albeit by 1.3 Å.





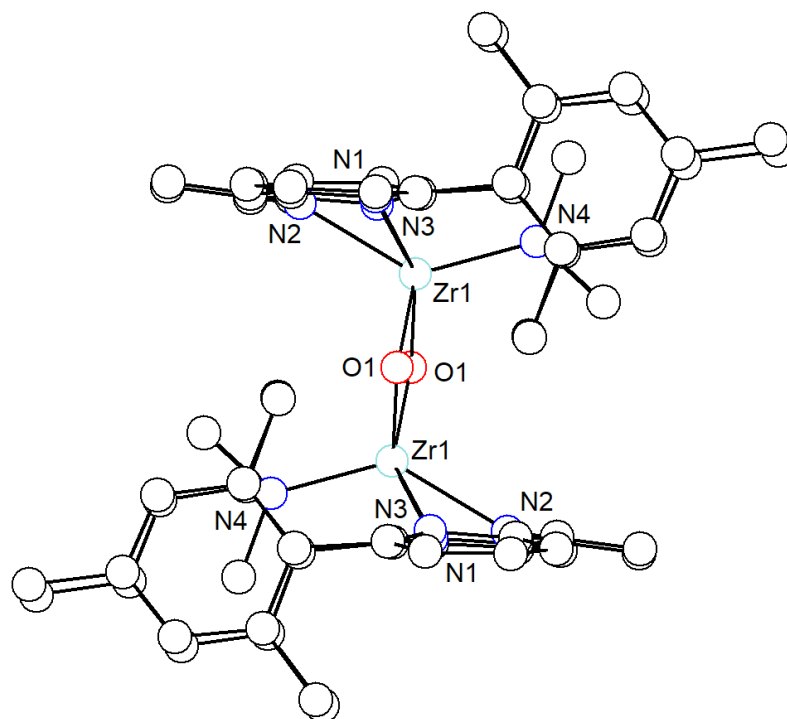


**Figure 3.12.** Solid-state structure of **3.31**. Hydrogen atoms and solvent of crystallization omitted for clarity.

Based on the crystallographically-characterized complexes supported by the aryl-substituted DPP ligands, coordination of small and/or flat ligands to metal centers supported by these ancillary ligands leads to the formation of interactions with the DPP mesityl and anthracenyl substituents. Distances in the range of 3.3 to 3.6 Å are observed between ligands and the aryl substituents, within the sum of the van der Waals radii. As demonstrated in the solid-state structure of **3.14**, coordination of the larger tetramethyldisilylazide ligands leads to significant distortion of the anthracenyl substituents away from coplanarity. As a consequence of the large bite angle of the DPP ligand ready ligand activation can occur in the case of Y and, with the Ti, Zr, and Hf tris(dimethylamido) complexes, exchange of free and bound pyridine arms is rapid at room temperature, though coordination to only two donors is favored in the solid state

structure of **3.25**. This may indicate that the use of these arene-substituted DPP ligands with larger metals could lead to compounds more competent for intermolecular substrate activation by disfavoring pyridine dissociation. From the structure of **3.22**, interaction of substrates bearing extended aromatic substituents with the flanking anthracene substituents is favored, however, competition with formation of lower coordinate number species and facile ligand activation limits applicability in the current series of complexes.

The tris(dimethylamido) complexes **3.25**, **3.26**, **3.27**, **3.28**, and **3.29** were evaluated for their activity in the homopolymerization and in the copolymerization of ethylene and 1-hexene. In initial small-scale reactions with **3.27**, no activity was observed in toluene using MMAO-12 as an activator and cocatalyst (Table 3.1, Entry 1); however, some activity upon switching the solvent to chlorobenzene ( $100 \text{ g mmol}_M^{-1} \text{ h}^{-1}$ , Table 3.1, Entry 2). The best activity from **3.27** was obtained in chlorobenzene, using a mixture of  $\text{AlMe}_3$  and  $[\text{CPh}_3][\text{B}(\text{C}_6\text{F}_5)_4]$  as an activator and cocatalyst ( $740 \text{ g mmol}_M^{-1} \text{ h}^{-1}$ , Table 3.1, Entry 3). To eliminate the possibility of mass transfer limitations upon the activity of **3.27** using  $\text{AlMe}_3/[\text{CPh}_3][\text{B}(\text{C}_6\text{F}_5)_4]$ , catalysis was also run for 10 min; under those conditions similar activity was observed ( $460 \text{ g mmol}_M^{-1} \text{ h}^{-1}$ , Table 3.1, Entry 4).

The activity of the other complexes was tested using the optimal conditions determined for **3.27**, in chlorobenzene with  $\text{AlMe}_3$  and  $[\text{CPh}_3][\text{B}(\text{C}_6\text{F}_5)_4]$  activators. No differences were observed between the mesityl- and anthracenyl-substituted complexes; however, the activity did vary depending on the nature of the metal. The highest activities were observed for the Ti complexes **3.25** and **3.26** (up to  $3600 \text{ g mmol}_M^{-1} \text{ h}^{-1}$ , Table 3.1, Entries 9-12), with an order of magnitude drop in activity for the Zr complexes **3.27** and **3.28** and no observed activity from Hf complex **3.29**. Through the assistance of the group of Dr. M. Naseem Akhtar at King Fahd University of Petroleum and Minerals, GPC

analysis was performed which showed very broad, multimodal molecular weight distributions, with higher overall  $M_w$  values from **3.25** and **3.26**. As loss of stirring was observed over the course of 1 min using either **3.25** or **3.26**, ethylene polymerization trials were also performed at one tenth the original concentration, using 0.4  $\mu\text{mol}$  precatalyst (Table 3.1, Entries 10 and 12). Similar activities were observed under these conditions ( $3000 \text{ g mmol}_M^{-1} \text{ h}^{-1}$ ); however, the resulting polymers displayed larger  $M_w$  values by GPC (917 vs. 271 kDa for **3.25** and 1069 vs. 286 kDa for **3.26**).

**Table 3.1.** Ethylene polymerization by (DPP<sup>Ar</sup>)M(NMe<sub>2</sub>)<sub>3</sub> precatalysts<sup>a</sup>

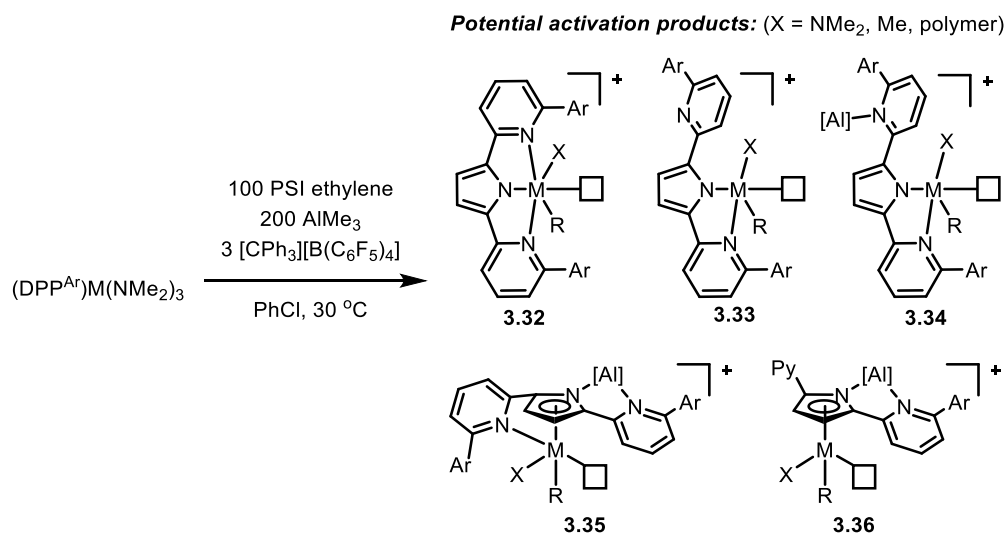
	<b>M</b>	<b>Ar</b>	<b>Activator</b>	<b>Time</b>	<b>Yield</b>	<b>Activity</b>	<b>T<sub>M</sub></b>	<b>M<sub>w</sub><sup>b</sup></b>	<b>PDI<sup>b</sup></b>
				(min)	(g)	(g mmol <sup>-1</sup> h <sup>-1</sup> )	(°C)	(kDa)	
1	Zr	Mes	MMAO-12	30	0.06	30	n.d.	n.d. <sup>c</sup>	n.d.
2	Zr	Mes	MMAO-12	30	0.2	100	n.d.	185	155
3	Zr	Mes	AlMe <sub>3</sub> / [CPh <sub>3</sub> ][B(C <sub>6</sub> F <sub>5</sub> ) <sub>4</sub> ]	30	1.47	740	124.2	94	126
4	Zr	Mes	AlMe <sub>3</sub> / [CPh <sub>3</sub> ][B(C <sub>6</sub> F <sub>5</sub> ) <sub>4</sub> ]	10	0.31	460	124.7	141	188
6	Zr	Anth	AlMe <sub>3</sub> / [CPh <sub>3</sub> ][B(C <sub>6</sub> F <sub>5</sub> ) <sub>4</sub> ]	10	0.08	120	125.6	81	93
7	Zr	Anth	AlMe <sub>3</sub> / [CPh <sub>3</sub> ][B(C <sub>6</sub> F <sub>5</sub> ) <sub>4</sub> ]	30	0.72	360	n.d.	110	145
8	Hf	Mes	AlMe <sub>3</sub> / [CPh <sub>3</sub> ][B(C <sub>6</sub> F <sub>5</sub> ) <sub>4</sub> ]	30	0.006	0	n.d.	n.d.	n.d.
9	Ti	Mes	AlMe <sub>3</sub> / [CPh <sub>3</sub> ][B(C <sub>6</sub> F <sub>5</sub> ) <sub>4</sub> ]	1	0.24	3600	n.d.	271	121
10	Ti	Mes	AlMe <sub>3</sub> / [CPh <sub>3</sub> ][B(C <sub>6</sub> F <sub>5</sub> ) <sub>4</sub> ]	8	0.17	3000	134.8	917	143
11	Ti	Anth	AlMe <sub>3</sub> / [CPh <sub>3</sub> ][B(C <sub>6</sub> F <sub>5</sub> ) <sub>4</sub> ]	1	0.22	3400	134.1	286	130
12	Ti	Anth	AlMe <sub>3</sub> / [CPh <sub>3</sub> ][B(C <sub>6</sub> F <sub>5</sub> ) <sub>4</sub> ]	10	0.12	3000	133.5	1069	91

<sup>a</sup> Polymerization conditions: 4.0 μmol precatalyst in 10 mL total reaction volume in the presence of either 1000 equiv. MMAO-12 (7 wt% in PhMe) or 200 equiv. AlMe<sub>3</sub> and 3

equiv.  $[\text{CPh}_3][\text{B}(\text{C}_6\text{F}_5)_4]$  at 30 °C and 100 PSI of ethylene. <sup>b</sup>Measured by GPC. <sup>c</sup>n.d. = Not determined.

Very broad, multimodal molecular weight distributions were observed by GPC for complexes **3.25**, **3.26**, **3.27**, and **3.28** using either MMAO-12 or  $\text{AlMe}_3/[\text{CPh}_3][\text{B}(\text{C}_6\text{F}_5)_4]$ . NMR analysis of the ethylene homopolymers from **3.27** and **3.28** showed no evidence of branching, though methyl-terminated chains could be clearly observed. Resonances corresponding to terminal olefins were observed by  $^1\text{H}$  NMR, consistent with some chain termination by  $\beta$ -hydride elimination. Integration of the olefinic and methyl signals shows a relative ratio of 1:9.40 indicating that the majority of polymer chains are methyl terminated at both ends. This suggests that chain transfer to Al may be the dominant mode of chain termination, potentially leading to the observed broadened molecular weight distributions.<sup>37,38</sup>

Another possible explanation for the broadened molecular weight distributions is the formation of a variety of species competent for ethylene oligomerization and polymerization under catalysis conditions (Scheme 3.6). Six potential active species can be proposed based on the DPP binding mode, degree of metal alkylation, and aluminum coordination of potential free pyridine arms (**3.32**, **3.33**, and **3.34**). Furthermore, migration of the titanium or zirconium centers from pyrrolide N-coordination to the pyrrolide  $\pi$ -system, as has been observed in other early metal pyrrolide systems,<sup>39</sup> could provide access to additional species (**3.35** and **3.36**).



**Scheme 3.6.** Potential products of activation of (DPP<sup>Ar</sup>)M(NMe<sub>2</sub>)<sub>3</sub> precatalysts.

Ethylene-1-hexene copolymerizations were also run using complexes **3.25**, **3.26**, **3.27**, and **3.28** in the presence of AlMe<sub>3</sub>/[CPh<sub>3</sub>][B(C<sub>6</sub>F<sub>5</sub>)<sub>4</sub>] and 1000 equiv. of the  $\alpha$ -olefin comonomer (Table 3.2). Activities were similar to those observed in ethylene homopolymerization, with Ti complexes **3.25** and **3.26** exhibiting higher activities in comparison to Zr complexes **3.27** and **3.28**. Broad molecular weight distributions, resembling those observed in ethylene homopolymerization trials, were observed from all catalysts. Butyl branches were observed by <sup>13</sup>C NMR and the T<sub>M</sub> values were observed to drop by DSC in the materials resulting from ethylene-1-hexene copolymerization, consistent with comonomer incorporation.<sup>40</sup> 1-hexene incorporation was greater for the Ti precatalysts based on integration of the <sup>13</sup>C spectra and the larger drops in T<sub>M</sub> values.

**Table 3.2.** Ethylene-1-hexene copolymerization trials by (DPP<sup>Ar</sup>)M(NMe<sub>2</sub>)<sub>3</sub> precatalysts<sup>a</sup>

	<b>M</b>	<b>Ar</b>	<b>Time</b>	<b>Yield</b>	<b>Activity</b>	<b>T<sub>M</sub><sup>b</sup></b>	<b>M<sub>w</sub><sup>c</sup></b>	<b>PDI<sup>c</sup></b>	<b>% I<sup>d</sup></b>
			(min)	(g)	(g mmol <sub>M</sub> <sup>-1</sup> h <sup>-1</sup> )	(°C)	(kDa)		
1	Zr	Mes	10	0.45	680	122.4	84	107	1.32
2	Zr	Anth	30	0.30	150	125.7	221	207	0.95
3	Ti	Mes	1	0.39	5900	121.3	197	73	2.20
4	Ti	Anth	2	0.30	2300	121.4	530	204	1.62

<sup>a</sup>Polymerization conditions: 4.0 μmol precatalyst, 100 PSI ethylene, 10 mL PhCl with 200 equiv. AlMe<sub>3</sub>, 3 equiv. [CPh<sub>3</sub>][B(C<sub>6</sub>F<sub>5</sub>)<sub>4</sub>], 1000 equiv. 1-hexene. <sup>b</sup>Measured by DSC. <sup>c</sup>Measured by GPC. <sup>d</sup>Determined by integration of the <sup>13</sup>C NMR spectra.

The behaviors of **3.25**, **3.27**, and **3.28** were also evaluated by Dr. M. Naseem Akhtar and coworkers at larger scales, elevated temperatures (60 and 80 °C), 5 bar ethylene pressure, and using MAO as a cocatalyst. Lower activities were observed under these conditions, which could result from the lower solubility of ethylene under these conditions. Ethylene polymerization from **3.25** and MAO was also run in the presence of BHT (0.5 equiv. relative to MAO) as a free AlMe<sub>3</sub> scavenger (Table 3.3, Entry 3).<sup>41</sup> In comparison with ethylene polymerization using **16** under otherwise identical conditions (Table 3.3, Entry 2), a substantially higher molecular weight and lower PDI is observed (M<sub>w</sub> of 1000 kDa and PDI of 4.3 vs. M<sub>w</sub> of 155 and PDI of 15). These results are

consistent with the proposal that chain transfer to aluminum is the dominant mode of chain termination.

**Table 3.3.** Large-scale ethylene and ethylene-1-hexene copolymerizations by **3.25**<sup>a</sup>

	Additive	Temp	Yield	Activity	T <sub>M</sub>	M <sub>w</sub>	PDI
		(°C)	(g)	(g mmol <sub>M</sub> <sup>-1</sup> h <sup>-1</sup> )	(°C)	(kDa)	
1	--	60	2.1	210	137.6	317	31
2	--	80	4.9	490	134.3	155	15
3	BHT	80	1.1	110	135.8	1000	4.3
4	1-hexene	60	3.5	350	119.0	156	14
5	1-hexene	80	4.4	440	118.5	79	11

<sup>a</sup>Polymerization conditions: 10 μmol precatalyst in 100 mL PhMe in the presence of 1000 equiv. MAO, 0 or 20 mL 1-hexene, and 0 or 500 equiv. BHT at 60 or 80 °C and 5 bar ethylene pressure over 60 min.

Based on the trials performed with (DPP<sup>Ar</sup>)M(NMe<sub>2</sub>)<sub>3</sub> precatalysts in the presence of AlR<sub>3</sub>/[CPh<sub>3</sub>][B(C<sub>6</sub>F<sub>5</sub>)<sub>4</sub>], minimal changes in polymerization behavior are observed as a consequence of the aryl substituent, however, substantial differences in activity are observed depending on the metal. The lack of effect from the aryl substituents could indicate that interaction between the 1-hexene and ethylene monomers and the mesityl and anthracenyl substituents does not substantially alter catalyst behavior; alternatively, this could indicate that these groups are not positioned so as to interact with the incoming monomers in the active catalyst(s). The differences in activity between the Ti, Zr, and Hf complexes could be indicative that different species are formed upon activation of these



complexes; with the smaller Ti it may be that a more active species that produces higher molecular weight products, whereas with the larger metals, formation of less active species is favored.

## CONCLUSIONS

In conclusion, a series of early metal alkyl, amide, indolide, and acetylide complexes supported by mesityl- and anthracenyl-substituted di(pyridyl)pyrrolide ligands were synthesized and the effects of the extended  $\pi$ -substituents on their NMR and structural features examined. As a consequence of the anthracenyl substituents, significantly upfield shifted NMR resonances are observed for the amide resonances on Y, Ti, Zr, and Hf complexes. The anthracenyl substituents are observed to have close contacts with indolide, THF, chloride, and tetramethyldisilylazide substituents and long metal-pyridine distances where coordination of both pyridine donors is favored. In the structurally-characterized tris(dimethylamido)titanium complex, however, dissociation of one pyridine is observed in the solid state to accommodate a closer metal-pyridine distance. The ethylene polymerization behavior of the tris(dimethylamido) group IV complexes was tested and Ti and Zr complexes were found to be competent for ethylene polymerization when activated with  $\text{AlMe}_3$  and  $[\text{CPh}_3][\text{B}(\text{C}_6\text{F}_5)_4]$ , though the resulting polymers displayed very broad molecular weight distributions, which is proposed to result from both chain transfer to Al and the formation of multiple species under these activation conditions.

## EXPERIMENTAL SECTION

### *General Comments*

All air- and water-sensitive compounds were manipulated under N<sub>2</sub> using standard Schlenk or glovebox techniques. Solvents for air- and moisture-sensitive reactions were dried by the method of Grubbs.<sup>42</sup> 2,6-lutidine, quinoline, trimethylsilylacetylene, allylbenzene, chlorobenzene, and 1-hexene were stirred over CaH<sub>2</sub> for upwards of 72 h, vacuum transferred or distilled, and run over activated alumina plugs prior to use. Indole was sublimed under vacuum prior to use. **3.4**,<sup>28</sup> 2-mesitylboronic acid,<sup>30a</sup> 9-anthracenylboronic acid,<sup>30b</sup> **3.8**,<sup>29</sup> Zr(NMe<sub>2</sub>)<sub>4</sub>,<sup>43</sup> Hf(NMe<sub>2</sub>)<sub>4</sub>,<sup>44</sup> Y(CH<sub>3</sub>SiMe<sub>3</sub>)<sub>3</sub>(THF)<sub>2</sub>,<sup>45</sup> and Y(N(SiMe<sub>2</sub>H)<sub>3</sub>(THF)<sub>2</sub><sup>46</sup> were prepared according to literature procedures. [CPh<sub>3</sub>][B(C<sub>6</sub>F<sub>5</sub>)<sub>4</sub>] was purchased from Strem and used without further purification. AlMe<sub>3</sub> was purchased from Sigma Aldrich and used without further purification. Deuterated solvents were purchased from Cambridge Isotopes Lab, Inc.; CDCl<sub>3</sub> was used without further purification; C<sub>6</sub>D<sub>6</sub> was distilled from purple Na/benzophenone ketyl and stored over 4 Å molecular sieves prior to use. <sup>1</sup>H and <sup>13</sup>C spectra were recorded on Varian INOVA-400, Bruker Cryoprobe 400, and Bruker 400 spectrometers. <sup>1</sup>H and <sup>13</sup>C chemical shifts are reported relative to residual solvent resonances. Elemental analysis was performed on a Perkin-Elmer 2400 CHNS/O Analyzer and samples were taken from representative batches prepared in an N<sub>2</sub>-filled glovebox, unless otherwise noted.

**Preparation of 3.9.** A Schlenk flask was charged with **3.8** (4.6167 g, 10.55 mmol) and THF (400 mL) and cooled to -78 °C with a dry-ice/acetone bath. <sup>n</sup>BuLi (4.2 mL, 10.5 mmol) was added over the course of several minutes then B(OMe)<sub>3</sub> (3.5 mL, 31.4 mmol) was added in one portion after 1 h. The reaction was allowed to come to room temperature over 8 h then quenched by addition of 2 N HCl. Volatiles were removed under reduced pressure and the residue taken up in DCM and washed with water (2x) and

brine, dried with  $\text{MgSO}_4$ , filtered, and evaporated. Purification by column chromatography with an initial eluent of 10 % EtOAc in Hexanes allowed separation of the major impurities and the desired material was eluted with 10 % MeOH in DCM to afford a mixture of the dimethyl borate, methyl borate, and boronic acid which was used for the next Suzuki coupling without further purification (3.273 g, 77 %).  $^1\text{H}$  NMR (400 MHz,  $\text{CDCl}_3$ )  $\delta$  8.66 (m, 2H, anth), 7.86 (m, 2H, anth), 7.60-7.50 (m, 4H, anth), 3.61 (s, 6H,  $\text{B}(\text{OCH}_3)_2$ ), 1.27 (m, 21H,  $\text{Si}^i\text{Pr}_3$ ).  $^{13}\text{C}$  NMR (101 MHz,  $\text{CDCl}_3$ )  $\delta$  134.16, 133.01, 132.46, 128.65, 127.63, 126.65, 126.14, 118.64, 103.53 ( $-\text{C}\equiv\text{C}-$ ), 103.42 ( $-\text{C}\equiv\text{C}-$ ), 52.96 ( $\text{B}(\text{OCH}_3)_2$ ), 19.05 ( $\text{Si}(\text{CH}(\text{CH}_3)_2)_3$ ), 11.66 ( $\text{Si}(\text{CH}(\text{CH}_3)_2)_3$ ). HRMS (FAB+) for  $\text{C}_{27}\text{H}_{35}\text{O}_2\text{BSi}$ : 430.2499. Found: 430.2501.

**Preparation of 3.10.** A Schlenk tube was charged with **3.4** (0.9217 g, 2.432 mmol), 2-mesitylboronic acid (1.0188 g, 6.212 mmol),  $\text{K}_2\text{CO}_3$  (2.2078 g, 15.975 mmol), toluene (24 mL), ethanol (6 mL), and water (6 mL) and then degassed by three freeze-pump thaw cycles at  $-78^\circ\text{C}$ . The flask was backfilled with  $\text{N}_2$  then  $\text{Pd}(\text{PPh}_3)_4$  (0.147 g, 0.127 mmol) was added against strong  $\text{N}_2$  counterflow and the flask heated to  $70^\circ\text{C}$  overnight. Aqueous and organic layers were separated and the aqueous layer extracted twice with DCM. The combined organic layers were washed with water and brine then dried with  $\text{MgSO}_4$ , filtered, and evaporated. Column chromatography in 10:1 hexanes:EtOAc(v/v) afforded the desired compound as a pale yellow (0.7873 g, 1.720 mmol, 71 % yield).  $^1\text{H}$  NMR (400 MHz,  $\text{CDCl}_3$ ,  $25^\circ\text{C}$ )  $\delta$  10.43 (s, 1H, NH), 7.69 (t,  $J = 7.7$  Hz, 2H, Py), 7.55 (dd,  $J = 8.0, 1.1$  Hz, 2H, Py), 6.99 – 6.95 (m, 10H, mes and Py), 6.86 (d,  $J = 2.6$  Hz, 2H, pyrr), 2.36 (s, 6H, mes $\text{CH}_3$ ), 2.07 (s, 12H, mes $\text{CH}_3$ ).  $^{13}\text{C}$  NMR (101 MHz,  $\text{CDCl}_3$ ,  $25^\circ\text{C}$ )  $\delta$  159.5 (py), 150.1 (pyrr), 138.3 (mes), 137.5 (mes), 136.5 (Py), 136.1 (mes), 133.7 (Py),

128.3 (mes), 121.8 (Py), 116.4 (Py), 109.2 (pyrr), 21.3 (mesCH<sub>3</sub>), 20.39 (mesCH<sub>3</sub>). HRMS (FAB+) for C<sub>32</sub>H<sub>32</sub>N<sub>3</sub> (M+H): 458.2596. Found: 458.2609.

**Preparation of 3.11.** A Schlenk tube was charged with **3.4** (1.034 g, 2.729 mmol), 9-anthracenylboronic acid (1.514 g, 6.820 mmol), K<sub>2</sub>CO<sub>3</sub> (2.620 g, 18.95 mmol), toluene (54 mL), ethanol (14 mL), and water (14 mL) then degassed by three freeze-pump-thaw cycles at -78 °C. The flask was backfilled with N<sub>2</sub> then Pd(PPh<sub>3</sub>)<sub>4</sub> (0.335 g, 0.290 mmol) was added against strong N<sub>2</sub> counterflow. The flask was sealed and heated to 70 °C for 15 h. Upon cooling to room temperature, the reaction was filtered and a yellow solid collected. This was subsequently washed with methanol then dried under vacuum to afford the desired compound (1.530 g, 2.667 mmol, 98 % yield). <sup>1</sup>H NMR (400 MHz, DMSO-*d*<sub>6</sub>, 25 °C) δ 11.02 (s, 1H, NH), 8.65 (s, 2H, CH of anthracene), 8.11 (d, *J* = 8.4 Hz, 4H), 8.04 (dd, *J* = 8.1, 1.2 Hz, 2H, CH of py), 7.99 (t, *J* = 7.7 Hz, 2H, CH of py), 7.57–7.53 (m, 4H, CH of anthracene), 7.47 (ddd, *J* = 8.2, 6.6, 1.2 Hz, 4H, CH of anthracene), 7.36 (ddd, *J* = 8.8, 6.5, 1.3 Hz, 4H, CH of anthracene), 7.31 (dd, *J* = 7.2, 1.1 Hz, 2H, CH of py), 6.99 (d, *J* = 2.3 Hz, 2H, CH of pyrrole). <sup>13</sup>C NMR (101 MHz, DMSO-*d*<sub>6</sub>, 25 °C) δ 157.0, 150.5, 137.8 (CH of py), 135.5, 135.4, 135.0, 134.1, 133.5, 131.3, 129.8, 129.7, 129.0 (anth), 128.8, 127.6 (anth), 127.23, 126.5 (anth), 126.1 (anth), 125.8 (anth), 124.5 (Py), 118.1 (Py), 111.2 (pyrr). HRMS (FAB+) for C<sub>42</sub>H<sub>28</sub>N<sub>3</sub>: 574.2283. Found: 574.2279.

**Preparation of 3.12.** A Schlenk tube was charged with **3.4** (0.5170 g, 1.364 mmol, 1 equiv.), K<sub>2</sub>CO<sub>3</sub> (1.1641 g, 8.422 mmol, 6.2 equiv.), **3.9** (1.377 g, 3.42 mmol 2.5 equiv.), toluene (35 mL, 10 mL/mmol), ethanol (8 mL, 2.5 mL/mmol), and water (8 mL, 2.5 mL/mmol). This was degassed by three freeze-pump-thaw cycles then Pd(PPh<sub>3</sub>)<sub>4</sub> (0.203 g, 0.176 mmol, 0.129 equiv.) was added against strong N<sub>2</sub> counterflow. The flask was sealed, heated to 70 °C for 9 h, then cooled to room temperature and diluted with DCM

and water. The organic phase was separated and washed with water and brine then dried with  $\text{MgSO}_4$ , filtered and volatiles removed under reduced pressure. The crude reaction was dry-loaded with  $\text{SiO}_2$  and purified by column chromatography in 10 % benzene, 20 % DCM in hexanes to afford the desired product as a bright yellow solid (1.1 g, 1.2 mmol, 88 % yield).  $^1\text{H}$  NMR (500 MHz,  $\text{CDCl}_3$ )  $\delta$  10.24 (s, 1H, NH), 8.6 (d,  $J$  = 8.8 Hz, 4H), 7.79 (t,  $J$  = 7.9 Hz, 2H), 7.71 (d,  $J$  = 7.9 Hz, 2H), 7.53 (d,  $J$  = 8.7 Hz, 4H), 7.46 (t,  $J$  = 7.5 Hz, 4H), 7.24 (t,  $J$  = 7.4 Hz, 4H), 7.13 (d,  $J$  = 7.1 Hz, 2H), 6.95 (d,  $J$  = 1.9 Hz, 2H, pyrr), 1.34-1.25 (m, 42H,  $\text{Si}^i\text{Pr}_3$ ).  $^{13}\text{C}$  NMR ( $\text{CDCl}_3$ , 101 MHz)  $\delta$  157.51 (Py), 150.41 (Py), 136.57 (Py), 133.68 (pyrr), 132.66 (anth), 129.59 (anth), 127.04 (anth), 126.86 (anth), 126.41 (anth), 125.86 (anth), 124.10 (Py), 118.58 (anth), 117.42 (Py), 109.89 (pyrr), 108.59 (anth), 103.60 ( $-\text{C}\equiv\text{C}-$ ), 103.18 ( $-\text{C}\equiv\text{C}-$ ), 19.05 ( $\text{SiCH}(\text{CH}_3)_2$ ), 11.65 ( $\text{SiCH}(\text{CH}_3)_2$ ). HRMS (FAB+) for  $\text{C}_{64}\text{H}_{66}\text{N}_3\text{Si}_2$  ( $\text{M}+\text{H}$ )-H<sub>2</sub>: 932.4795. Found: 932.4796.

**Preparation of 3.13.** A Schlenk tube was charged in the glovebox with  $\text{Y}(\text{N}(\text{SiMe}_2\text{H})_2)_3(\text{THF})_2$  (0.2902 g, 0.4605 mmol), **3.10** (0.2105 g, 0.4599 mmol, 1 equiv.) and benzene (9 mL) then sealed and heated to 75 °C for 5 days. Volatiles were removed under reduced pressure then the resulting solids triturated with hexanes and solids collected by filtration to afford the desired compound as a bright yellow solid (0.1483 g, 0.1830 mmol, 40 % yield).  $^1\text{H}$  NMR ( $\text{C}_6\text{D}_6$ , 400 MHz): 7.27 (dd,  $J$  = 1.2, 8.1 Hz, 2H, Py), 6.98 (t,  $J$  = 7.8 Hz, 2H, Py), 6.90 (s, 2H, pyrr), 6.86 (s, 4H, mes), 6.29 (dd,  $J$  = 1.2, 7.5 Hz, Py), 4.34 (sept,  $J$  = 2.9 Hz, 4H,  $\text{SiH}(\text{CH}_3)_2$ ), 2.21 (s, 12H, mes $\text{CH}_3$ ), 2.16 (s, 6H, mes $\text{CH}_3$ ), 0.11 (d,  $J$  = 3.0 Hz, 24H,  $\text{SiH}(\text{CH}_3)_2$ ).  $^{13}\text{C}$  NMR ( $\text{C}_6\text{D}_6$ , 101 MHz)  $\delta$  161.69 (Py), 157.12 (Py), 141.73 (pyrr), 138.58 (Py), 138.11 (mes), 137.40 (mes), 136.37 (mes), 129.65 (mes), 122.39 (Py), 118.07 (Py), 112.16 (pyrr), 22.20 (mes $\text{CH}_3$ ), 21.15 (mes $\text{CH}_3$ ), 3.78 ( $\text{SiH}(\text{CH}_3)_2$ ). Satisfactory analysis could not be obtained for this complex.

**Preparation of 3.14.** A J-Young tube was charged in the glovebox with  $\text{Y}(\text{N}(\text{SiMe}_2\text{H})_2)_3(\text{THF})_2$  (16.8 mg, 0.0267 mmol), **3.11** (14.8 mg, 0.0258 mmol) and  $\text{C}_6\text{D}_6$  (0.5 mL) then sealed and heated to 75 °C for 5 days. Volatiles were removed *in vacuo*. Recrystallization from benzene-pentane at room temperature afforded the desired compound as a yellow-orange solid (12.3 mg, 0.0133 mmol, 52 % yield). Note that this compound was isolated with a small amount (ca. 12 % by  $^1\text{H}$  NMR integration) of another  $\text{N}(\text{SiHMe}_2)_2$  containing-species from which it could not be separated. X-Ray quality crystals were grown by slow cooling of the crude reaction mixture in a J-Young tube.  $^1\text{H}$  NMR ( $\text{C}_6\text{D}_6$ , 400 MHz)  $\delta$  8.15 (s, 2H, anth), 7.78-7.73 (m, 8H, anth), 7.44 (dd,  $J$  = 8.1, 1.2 Hz, 2H, Py), 7.22-7.13 (m, 12H, anth), 7.08 (s, 2H, pyrr), 6.95 (dd,  $J$  = 8.1, 7.6 Hz, 2H, Py), 6.25 (dd,  $J$  = 7.4, 1.2 Hz, 2H), 3.73.74 (sept,  $J$  = 2.7 Hz, 4H,  $\text{N}(\text{SiH}(\text{CH}_3)_2)_2$ ), -0.48 (d,  $J$  = 2.9 Hz, 24 H,  $\text{N}(\text{SiH}(\text{CH}_3)_2)_2$ ).  $^{13}\text{C}$  NMR ( $\text{C}_6\text{D}_6$ , 101 MHz)  $\delta$  160.03 (Py), 157.13 (Py), 141.89 (pyrr), 138.29 (Py), 134.47 (anth), 132.14 (anth), 131.66 (anth), 129.12 (anth), 129.04 (anth), 127.55 (anth), 126.68 (anth), 125.61 (anth), 125.13 (Py), 118.82 (Py), 112.63 (pyrr), 2.92 ( $\text{SiH}(\text{CH}_3)_2$ ). Satisfactory analysis could not be obtained for this complex.

**Preparation of 3.16.** *Method A:* A J-Young tube was charged with **3.10** (19.2 mg, 0.0420 mmol) and  $\text{AlEt}_3$  (5.8  $\mu\text{mol}$ , 0.0423 mmol) in  $\text{C}_6\text{D}_6$  (0.5 mL), then sealed and inverted. Gas evolution was observed upon mixing and yellow crystals were observed upon standing (quantitative yield by NMR). *Method B:*  $\text{AlEt}_3$  (67  $\mu\text{L}$ , 0.49 mmol) was added to a thawing solution of **3.13** (39.7 mg, 0.0490 mmol) in PhMe (2 mL) and stirred 30 min, warming. Volatiles were removed under reduced pressure and the resulting yellow oil triturated with pentane and filtered over Celite. Extraction of the remaining yellow solids with benzene afforded the desired complex as a yellow solid (22.2 mg, 0.0410 mmol, 84 %). X-ray quality crystals were grown by vapor diffusion of pentane into a toluene

solution of the complex in toluene at -35 °C. Elemental analysis was performed on material prepared by method A.  $^1\text{H}$  NMR ( $\text{C}_6\text{D}_6$ , 400 MHz)  $\delta$  7.19 (dd,  $J = 8.0, 1.1$  Hz, 2H, Py), 7.05 – 6.98 (m, 4H, Py and pyrr), 6.70 (s, 4H, mes), 6.41 (dd,  $J = 7.4, 1.1$  Hz, 2H, Py), 2.07 (s, 12H, mes $\text{CH}_3$ ), 1.94 (s, 6H, mes $\text{CH}_3$ ), 0.79 (t,  $J = 8.1$  Hz, 6H,  $\text{AlCH}_2\text{CH}_3$ ), 0.00 (q,  $J = 8.1$  Hz, 4H,  $\text{AlCH}_2\text{CH}_3$ ).  $^{13}\text{C}$  NMR ( $\text{C}_6\text{D}_6$ , 101 MHz)  $\delta$  159.89 (Py), 153.22 (Py), 139.73 (pyrr), 138.18 (Py), 138.05 (mes), 136.64 (mes), 136.23 (mes), 128.44 (mes), 121.42 (Py), 116.49 (Py), 111.81 (pyrr), 21.06 (mes $\text{CH}_3$ ), 20.53 (mes $\text{CH}_3$ ), 9.55 ( $\text{AlCH}_2\text{CH}_3$ ), -0.64 ( $\text{AlCH}_2\text{CH}_3$ ). Anal calcd. for  $\text{C}_{36}\text{H}_{40}\text{N}_3\text{Al}$ : C, 79.82; H, 7.44; N, 7.76. Found: C, 79.98; H, 7.51; N, 7.81.

**Preparation of 3.18.** A vial was charged with  $\text{Y}(\text{CH}_2\text{SiMe}_3)_3(\text{THF})_2$  (83.2 mg, 0.168 mmol, 1.2 equiv.), a stirbar and 2 mL hexanes and frozen in the glovebox cold well. A separate vial was charged with **3.12** (132.0 mg, 0.1413 mmol, 1 equiv.) and 3 mL hexanes and frozen then the thawing solution of **3.12** was added thawing to the top of the stirred Y solution. This was stirred 40 min, warming then filtered over Celite and volatiles removed to afford the product as a red-brown microcrystalline solid (170.6 mg, 0.1345 mmol, 95 % yield). X-Ray quality crystals were grown by slow evaporation of pentane solution of the compound into toluene at -35 °C.  $^1\text{H}$  NMR ( $\text{C}_6\text{D}_6$ , 400 MHz)  $\delta$  8.67 (d,  $J = 8.5$  Hz, 4H, anth), 7.79 (d,  $J = 8.6$  Hz, 4H, anth), 7.49 (dd,  $J = 8.2, 1.1$  Hz, 2H, Py), 7.24 – 7.17 (m, 6H), 7.15 – 7.07 (m, 6H), 6.35 (dd,  $J = 7.3, 1.1$  Hz, 2H, Py), 1.43 – 1.20 (m, 53H, THF,  $\text{Si}^i\text{Pr}_3$ ), 0.02 (s, 18H), -2.31 (d,  $^2J_{\text{YH}} = 2.1$  Hz, 4H,  $\text{CH}_2\text{SiMe}_3$ ).  $^{13}\text{C}$  NMR ( $\text{C}_6\text{D}_6$ , 101 MHz)  $\delta$  157.87 (Py), 156.52 (Py), 141.25 (pyrr), 138.69, 134.21 (Py), 132.85 (anth), 130.18 (anth), 128.86, 126.81, 125.94 (anth), 122.16 (Py), 119.35, 118.86 (Py), 112.20 (pyrr), 104.14 ( $-\text{C}\equiv\text{C}-$ ), 103.74 ( $-\text{C}\equiv\text{C}-$ ), 71.19 (THF), 29.41 (d,  $^1J_{\text{YC}} = 31.0$  Hz,



$\text{CH}_2\text{SiMe}_3$ ), 24.50 (THF), 19.15 ( $\text{SiCH}(\text{CH}_3)_2$ ), 11.83 ( $\text{SiCH}(\text{CH}_3)_2$ ), 4.32 ( $\text{SiCH}_3$ ).

Satisfactory analysis could not be obtained for this complex.

**Preparation of 3.20.** A Schlenk tube was charged with a stirbar, **3.18** (34.5 mg, 0.0272 mmol), trimethylsilylacetylene (25  $\mu\text{L}$ , 0.180 mmol), and benzene (4 mL) in the glovebox. This was sealed, brought out of the glovebox, and heated to 55  $^\circ\text{C}$  for 75 min then cooled to room temperature and brought back into the glovebox where volatiles were removed *in vacuo*. The crude reaction mixture was fractionated over Celite between pentane and benzene and removal of volatiles from the benzene fraction afforded the product as an orange solid (27.2 mg, 0.0211 mmol, 79 %).  $^1\text{H}$  NMR ( $\text{C}_6\text{D}_6$ , 400 MHz)  $\delta$  8.76 (m, 4H, anth), 8.01 (m, 4H, anth), 7.40 (m, 4H, anth), 7.28 (m, 4H, anth), 7.19 (dd,  $J$  = 0.95, 8.13 Hz, 2H, Py), 6.96 (s, 2H, pyrr), 6.91 (dd,  $J$  = 7.48, 0.69 Hz, 2H, Py), 6.25 (dd,  $J$  = 0.98, 7.34 Hz, 2H, Py), 1.48 (br m, 4H, THF), 1.30 (m, 42H,  $\text{Si}^i\text{Pr}_3$ ), 1.00 (br m, 4H, THF), 0.04 (s, 18H,  $\text{SiMe}_3$ ).  $^{13}\text{C}$  NMR ( $\text{C}_6\text{D}_6$ , 101 MHz)  $\delta$  171.37 (d,  $J_{\text{YC}}$  = 48.83 Hz,  $\text{Y}-\text{C}\equiv\text{CSiMe}_3$ ), 157.02 (Py), 156.42 (Py), 140.91 (pyrr), 138.42 (Py), 133.94 (anth), 132.84 (anth), 130.37 (anth), 129.28 (anth), 127.66 (anth), 127.55 (anth), 125.90 (anth), 122.50 (Py), 119.49 (anth), 118.53 (Py), 111.84 (pyrr), 108.28 (d,  $J_{\text{YC}}$  = 8.42 Hz,  $\text{Y}-\text{C}\equiv\text{C}-\text{SiMe}_3$ ), 104.02 ( $-\text{C}\equiv\text{C}-\text{Si}^i\text{Pr}_3$ ), 103.98 ( $-\text{C}\equiv\text{C}-\text{Si}^i\text{Pr}_3$ ), 72.17 (THF), 24.54 (THF), 19.13 ( $\text{Si}(\text{CH}(\text{CH}_3)_2)_3$ ), 11.84 ( $\text{Si}(\text{CH}(\text{CH}_3)_2)_3$ ), 1.69 ( $\text{SiMe}_3$ ). Satisfactory analysis could not be obtained for this complex.

**Preparation of 3.22.** A solution of indole (15.9 mg, 0.136 mmol) in toluene (2 mL) was added dropwise, thawing, to a thawing solution of **3.18** (86.4 mg, 0.0681 mmol) in toluene (2 mL). The solution was stirred 35 min, warming, then volatiles were removed under reduced pressure. The resulting orange solids were washed with pentane and ether, then extracted with benzene to afford the desired complex as a yellow-orange solid (50.8

mg, 0.0405 mmol, 59 %). X-ray quality crystals were grown by slow evaporation of a pentane solution of the complex into toluene at -35 °C.  $^1\text{H}$  NMR ( $\text{C}_6\text{D}_6$ , 400 MHz)  $\delta$  8.47 (br m, 4H, anth), 7.43 (d,  $J$  = 6.5 Hz, 2H, Ind), 7.12 (dd,  $J$  = 8.1, 0.8 Hz, 2H, Py), 7.07 (s, 2H, pyrr), 7.05 (t,  $J$  = 7.4 Hz, 2H, Ind), 6.89 – 6.76 (m, 8H, anth, Py, Ind), 6.46 (m, 4H, anth), 6.33 – 6.22 (m, 4H, anth), 5.98 (dd,  $J$  = 7.4, 1.0 Hz, 2H, Py), 5.81 (br s, 2H, Ind), 5.13 (br s, 2H, Ind), 1.43 (m, 42 H).  $^{13}\text{C}$  NMR ( $\text{C}_6\text{D}_6$ , 101 MHz)  $\delta$  158.62 (Py), 156.23 (Py), 143.01, 141.61 (pyrr), 139.94 (Py), 132.19, 130.80, 129.71, 129.33, 126.34, 126.08, 123.76, 123.37, 120.53, 119.74, 119.48, 118.09, 117.86, 112.58 (pyrr), 104.66 ( $-\text{C}\equiv\text{C}-$ ), 103.63 ( $-\text{C}\equiv\text{C}-$ ), 102.38, 19.29 ( $\text{SiCH}(\text{CH}_3)_2$ ), 12.03 ( $\text{SiCH}(\text{CH}_3)_2$ ). Anal calcd. for  $\text{C}_{80}\text{H}_{78}\text{N}_5\text{Si}_2\text{Y}$ : C, 76.59; H, 6.27; N, 5.58. Found: C, 76.12; H, 6.39; N, 5.79.

**Preparation of 3.24.**  $\text{Ti}(\text{NMe}_2)_4$  (0.03 mL, 0.13 mmol) was added at once to a solution of **3.10** (57.7 mg, 0.126 mmol) in 3 mL toluene and stirred for 2.5 days. Volatiles were removed and the resulting red-orange solids washed with pentane then extracted with benzene to afford the product as a red-orange powder (70.0 mg, 0.110 mmol, 87 % yield). Crystals suitable for X-ray diffraction were grown by vapor diffusion of pentane into a toluene solution of the compound.  $^1\text{H}$  NMR ( $\text{C}_6\text{D}_6$ , 400 MHz)  $\delta$  7.33 (dd, 2H), 7.24 (s, pyrr-*H*, 2H), 7.13 (apparent t, 2H), 6.82 (s, mes-*H*, 4H), 6.52 (dd, Py-*H*, 2H), 2.77 (s,  $\text{N}(\text{CH}_3)_2$ , 18H), 2.16 (s, mes- $\text{CH}_3$ , 6H), 2.01 (s, mes- $\text{CH}_3$ , 12 H).  $^{13}\text{C}$  NMR ( $\text{C}_6\text{D}_6$ , 101 MHz)  $\delta$  159.34 (Py), 155.72 (Py), 144.43 (Pyrr), 138.48 (mes), 136.54 (mes), 136.27 (Py), 135.78 (mes), 128.21 (mes), 120.54 (Py), 117.48 (Py), 113.39 (Pyrr), 45.19 ( $\text{N}(\text{CH}_3)_2$ ), 20.75 (mes- $\text{CH}_3$ ), 20.18 (mes- $\text{CH}_3$ ). Anal calcd. for  $\text{C}_{38}\text{H}_{48}\text{N}_6\text{Ti}$ : C, 71.68; H, 7.60; N, 13.20. Found: C, 71.4; H, 7.50; N, 13.04.

**Preparation of 3.25.**  $\text{Ti}(\text{NMe}_2)_4$  (0.13 mL, 0.55 mmol) was added at once to a suspension of **3.11** (325.8 mg, 0.568 mmol) in 6 mL toluene and stirred for 2 days.

Volatiles were removed and the resulting orange solids triturated with pentane then collected by filtration and washed with fresh pentane to afford the product as an orange powder (381.2 mg, 0.506 mmol, 92 % yield).  $^1\text{H}$  NMR ( $\text{C}_6\text{D}_6$ , 400 MHz)  $\delta$  8.18 (s, 2H, anth), 7.82-7.79 (m, 8H, anth), 7.42 (dd,  $J$  = 8.1, 1.0 Hz, 2H, Py), 7.26 (s, 2H, pyrr), 7.24-7.20 (m, 4H, anth), 7.15-7.10 (m, 6H, anth, Py), 6.71 (dd,  $J$  = 7., 1.0 Hz, Py), 2.39 (s, 18H,  $\text{N}(\text{CH}_3)_2$ ).  $^{13}\text{C}$  NMR ( $\text{C}_6\text{D}_6$ , 101 MHz)  $\delta$  157.67 (Py), 156.41 (Py), 145.06 (pyrr), 136.54 (anth), 136.50 (Py), 131.91 (anth), 130.60 (anth), 128.52 (anth), 127.47 (anth), 125.52 (anth), 125.34 (anth), 123.04 (Py), 118.62 (Py), 116.40 (anth), 114.27 (pyrr), 45.16 ( $\text{N}(\text{CH}_3)_2$ ). Satisfactory analysis could not be obtained for this complex.

**Preparation of 3.26.** A solution of **3.10** (63.2 mg, 0.138 mmol) in 3 mL toluene was added at once to a solution of  $\text{Zr}(\text{NMe}_2)_4$  (40.2 mL, 0.150 mmol) in 2 mL toluene and stirred for 30 min. Volatiles were removed and the resulting yellow solids triturated with pentane then collected on a frit and washed with fresh pentane to afford the product as a yellow powder (85.0 mg, 0.125 mmol, 91 % yield).  $^1\text{H}$  NMR ( $\text{C}_6\text{D}_6$ , 400 MHz)  $\delta$  7.33 (d,  $J$  = 7.9 Hz, 2H, Py), 7.19 (s, 2H, pyrr), 7.14 (dd,  $J$  = 7.6 Hz, 2H, Py), 6.81 (s, 4H, mes), 6.55 (dd,  $J$  = 7.4 Hz, 2H, Py), 2.60 (s, 18H,  $\text{N}(\text{CH}_3)_2$ ), 2.14 (s, 18H, mes $\text{CH}_3$ ).  $^{13}\text{C}$  ( $\text{C}_6\text{D}_6$ , 101 MHz)  $\delta$  159.59 (Py), 155.47 (Py), 143.95 (pyrr), 138.02 (mes), 137.17 (mes), 137.03 (Py), 136.41 (mes), 128.70 (mes), 121.08 (Py), 117.56 (Py), 114.44 (pyrr), 41.96 ( $\text{N}(\text{CH}_3)_2$ ), 21.11 (mes $\text{CH}_3$ ), 20.58 (mes $\text{CH}_3$ ). Anal calcd. for  $\text{C}_{38}\text{H}_{48}\text{N}_6\text{Zr}$ : C, 67.11; H, 7.11; N, 12.36. Found: C, 66.73; H, 6.93; N, 12.07.

**Preparation of 3.27.** A suspension of **3.11** (320.5 mg, 0.559 mmol) in 5 mL toluene was added at once to a solution of  $\text{Zr}(\text{NMe}_2)_4$  (150.5 mg, 0.5626 mmol, 1 equiv.) in 2 mL toluene and stirred for 2 days. Volatiles were removed and the resulting yellow solids triturated with pentane, collected by filtration, and washed with fresh pentane to

afford the product as a yellow powder (398.10 mg, 0.500 mmol, 89 % yield).  $^1\text{H}$  NMR ( $\text{C}_6\text{D}_6$ , 400 MHz)  $\delta$  8.14 (s, 2H, anth), 7.85 (m, 4H, anth), 7.77 (m, 4H, anth), 7.44 (dd, 2H, Py), 7.23 (s, 2H, pyrr), 7.22-7.14, 7.10, 6.75 (dd, Py), 2.12 (s, 18H,  $\text{N}(\text{CH}_3)_2$ ).  $^{13}\text{C}$  NMR ( $\text{C}_6\text{D}_6$ , 101 MHz)  $\delta$  157.65 (Py), 155.87 (Py), 144.08 (pyrr), 137.02 (Py), 135.59 (anth), 131.85 (anth), 130.69 (anth), 128.53 (anth), 127.93 (anth), 127.24 (anth), 125.65 (anth), 125.28 (anth), 123.21 (Py), 118.28 (Py), 114.88 (pyrr), 41.51 ( $\text{N}(\text{CH}_3)_2$ ). Satisfactory analysis could not be obtained for this complex.

**Preparation of 3.28.** A solution of **3.10** (52.1, 0.114 mmol) in 1.5 mL toluene was added at once to a solution of  $\text{Hf}(\text{NMe}_2)_4$  (45.2 mg, 0.127 mmol) in 2 mL toluene and stirred for 30 min. Volatiles were removed and the resulting yellow solids washed with pentane then extracted with benzene to afford the product as a yellow powder (80.5 mg, 0.105 mmol, 92 % yield).  $^1\text{H}$  NMR ( $\text{C}_6\text{D}_6$ , 400 MHz)  $\delta$  7.32 (d,  $J = 8.0$  Hz, 2H, Py), 7.16 (s, 2H, pyrr), 7.13 (apparent t,  $J = 7.94$  Hz, 2H, Py), 6.82 (s, 4H, mes), 6.56 (d,  $J = 7.4$  Hz, 2H, Py), 2.63 (s, 18H,  $\text{NMe}_2$ ), 2.15 (s, 18H, mes $\text{CH}_3$ ).  $^{13}\text{C}$  ( $\text{C}_6\text{D}_6$ , 101 MHz)  $\delta$  159.82 (Py), 155.21 (Py), 144.27 (pyrr), 137.98 (mes), 137.19 (mes), 137.13 (Py), 136.38 (mes), 128.73 (mes), 128.59 (mes), 121.39 (Py), 117.62 (Py), 114.86 (pyrr), 41.62 ( $\text{NCH}_3$ ), 21.11 (mes $\text{CH}_3$ ), 20.58 (mes $\text{CH}_3$ ). Anal calcd. for  $\text{C}_{38}\text{H}_{48}\text{N}_6\text{Hf}$ : C, 59.48; H, 6.31; N, 10.95. Found: C, 59.93; H, 6.30; N, 10.47.

**Preparation of 3.29.** A solution of **3.11** (48.1 mg, 0.0838 mmol) in 2 mL toluene was added at once to a solution of  $\text{Hf}(\text{NMe}_2)_4$  (34.0 mg, 0.0959 mmol) in 1.5 mL toluene and stirred for 2 days. Volatiles were removed and the resulting yellow solids washed with pentane then extracted with benzene to afford the product as a yellow powder (61.1 mg, 0.0692 mmol, 83 % yield).  $^1\text{H}$  NMR ( $\text{C}_6\text{D}_6$ , 400 MHz)  $\delta$  8.15 (s, 2H, anth), 7.85 (m, 4H, anth), 7.78 (m, 4H, anth), 7.42 (d,  $J = 7.9$  Hz, 2H, Py), 7.22-7.18 (m, 6H, anth and pyrr),

7.18-7.06 (m, 6H, anth, Py), 6.75 (d,  $J = 7.2$  Hz, 2H, Py), 2.16 (s, 18H,  $N(CH_3)_2$ ).  $^{13}C$  NMR ( $C_6D_6$ , 101 MHz)  $\delta$  157.85 (Py), 155.60 (Py), 144.47 (pyrr), 137.11 (Py), 135.54 (anth), 131.86 (anth), 130.69 (anth), 128.46 (anth), 127.98 (anth), 127.21 (anth), 125.66 (anth), 125.28 (anth), 123.50 (Py), 118.34 (Py), 115.32 (pyrr), 41.18 ( $N(CH_3)_2$ ). Satisfactory analysis could not be obtained for this complex.

#### *General Polymerization Procedure.*

In the glovebox a Fisher-Porter bottle was charged with PhCl (7 mL), 1-hexene (0 or 0.50 mL, 0 or 4.0 mmol, 0 or 1000 equiv.)  $AlMe_3$  (0.08 mL, 0.8 mmol, 200 equiv.), and  $[CPh_3][B(C_6F_5)_4]$  (2 mL of a 33.3 mg in 6 mL PhCl stock solution, 3 equiv.) and sealed. A syringe was charged with the desired precatalyst (0.004 mmol in 1 mL PhCl, 1 equiv.) and sealed. Both were brought out of the glovebox and the Fisher-Porter charged with 40 PSI ethylene, the precatalyst solution injected, and the pressure rapidly increased to 100 PSI. After the desired reaction time, ethylene flow was stopped, pressure vented, and the reaction quenched by slow addition of a 10 % HCl in MeOH solution (v/v). Solids were triturated in at least 50 mL of 10% HCl in MeOH for several hours then collected by filtration, washed with additional fresh 10% HCl in MeOH, and dried under vacuum.

#### *GPC Analysis.*

Gel permeation chromatographic (GPC) analysis of polymers was at 160 °C PL-GPC 220 (Agilent Technologies) equipped with two PLgel Olexis 300 x 7.5 mm columns. BHT (0.0125 wt%) was added to 1,2,4-trichlorobenzene to prevent polymer sample degradation. Sample solutions of 2.5-3.0 mg/1.5 mL were prepared at 140 °C and 100  $\mu$ L were injected into the GPC. Data was analyzed using the Cirrus software package and the

GPC was calibrated using polystyrene standards. The polystyrene calibration curve was converted into the universal using the Mark-Houwink constants of polystyrene ( $K = 0.000406 \text{ dL/g}$  and  $\alpha = 0.725$ ).<sup>47</sup> GPC analysis of polymers was performed by the group of Dr. M. Naseem Akhtar at King Fahd University of Petroleum.

#### *DSC Analysis.*

Differential scanning calorimetric (DSC) analysis was performed using a DSC Q2000 (TA Instruments). The temperature and heat flow of the instrument were calibrated with an indium standard. Polymer samples were first equilibrated at 25 °C, followed by heating to 200 °C at a rate of 10 °C/min under N<sub>2</sub> flow (50 mL/min). The temperature was maintained at 200 °C for 5 min, then the samples were cooled to 25 °C at a rate of 10 °C/min. The temperature was maintained at 25 °C for 5 min then samples were reheated to 200 °C at a rate of 100 °C/min. The melting temperature ( $T_M$ ) for each sample was determined from the second heating scan. The percent crystallinity was calculated from  $\Delta H_f(\text{J/g})/\Delta H(\text{J/g})$ , where  $\Delta H_{\text{std}}$  is the heat of fusion for a perfectly crystalline polyethylene (290.0 J/g).<sup>48</sup> DSC analysis of polymers was performed by the group of Dr. M. Naseem Akhtar at King Fahd University of Petroleum

*Complete Polymerization Tables*

**Table 3.4.** Complete small-scale ethylene polymerization results.

	<b>M</b>	<b>Ar</b>	<b>Time</b>	<b>Yield</b>	<b>Activity</b>	<b>M<sub>w</sub><sup>a</sup></b>	<b>PDI<sup>b</sup></b>	<b>T<sub>m</sub><sup>c</sup></b>	<b>χ<sub>c</sub><sup>d</sup></b>
			min	g	g mmol <sub>m</sub> <sup>-1</sup> h <sup>-1</sup>	kDa		°C	%
1 <sup>e</sup>	Zr	Mes	30	0.06	--	n.d. <sup>f</sup>	n.d.		
2 <sup>g</sup>	Zr	Mes	30	0.20	100	185	155		
3	Zr	Mes	30	1.47	740	94	126	124.2	65.3
4	Zr	Mes	10	0.49	730	93	130		
5	Zr	Mes	10	0.31	460	65	87	124.7	71.1
6	Zr	Mes	10	0.31	460	141	188		
7	Zr	Anth	10	0.08	120	81	93	126.4	72.5
8	Zr	Anth	30	0.72	360	110	145	125.6	74.5
9	Zr	Anth	30	0.82	410	191	260		
10	Hf	Mes	30	0.006	--	n.d.	n.d.		
11 <sup>h</sup>	Ti	Mes	3.5	0.33	1400	355	143		
12	Ti	Mes	1	0.23	3400	293	130		
13	Ti	Mes	1	0.24	3600	271	141	134.5	75.4
14 <sup>i</sup>	Ti	Mes	8	0.17	3000	917	143	134.8	58.1
15	Ti	Anth	1	0.23	3400	255	112	135.6	72.7
16	Ti	Anth	1	0.22	3400	286	130	134.1	68.8
17 <sup>i</sup>	Ti	Anth	10	0.12	3000	1069	91	133.5	56.3

Conditions: 100 PSI, 10 mL PhCl, 200 equiv. AlMe<sub>3</sub>, 3 equiv. [CPh<sub>3</sub>][B(C<sub>6</sub>F<sub>5</sub>)<sub>4</sub>]. <sup>a</sup>From

GPC analysis; <sup>b</sup>From GPC analysis where PDI = M<sub>w</sub>/M<sub>N</sub>; <sup>c</sup>Melting temperature

determined by DSC; <sup>d</sup>Percent crystallinity determined by DSC; <sup>e</sup>1000 equiv. of MMAO

and PhMe was used in place of the AlMe<sub>3</sub>/[CPh<sub>3</sub>][B(C<sub>6</sub>F<sub>5</sub>)<sub>4</sub>] activator mixture and PhCl;

<sup>f</sup>Not determined; <sup>g</sup>1000 equiv. of MMAO was used in place of the AlMe<sub>3</sub>/[CPh<sub>3</sub>][B(C<sub>6</sub>F<sub>5</sub>)<sub>4</sub>]

activator mixture; <sup>h</sup>Stirring lost over the course of the reaction due to high viscosity; <sup>i</sup>0.4

μmol precatalyst loading.

**Table 3.5.** Complete ethylene-1-hexene copolymerization results.

	<b>M</b>	<b>Ar</b>	<b>Time</b>	<b>Yield</b>	<b>Activity</b>	<b>M<sub>w</sub><sup>a</sup></b>	<b>PDI<sup>b</sup></b>	<b>% I<sup>c</sup></b>	<b>T<sub>M</sub><sup>d</sup></b>	<b>χ<sub>c</sub><sup>e</sup></b>
			min	g	g mmol <sub>M</sub> <sup>-1</sup> h <sup>-1</sup>	kDa			°C	%
1	Zr	Mes	10	0.75	1100	2.5	4.1	n.d.	119.9	50.09
2	Zr	Mes	10	0.45	680	84.1	107.0	1.3	122.4	61.18
3	Zr	Anth	10	0.14	200	63.0	74.0	1.0	123.3	58.58
4	Zr	Anth	30	0.30	150	221	207.1	n.d.	125.7	64.1
5	Zr	Anth	30	1.18	590	117	149.9	n.d.	122.6	52.88
6	Ti	Mes	1	0.33	5000	272	136.8	n.d.	120.0	31.55
7	Ti	Mes	1	0.39	5900	197	73.4	2.2	121.3	32.73
8	Ti	Anth	2	0.30	2300	530	204.2	n.d.	121.4	33.82
9	Ti	Anth	1	0.27	4000	323	109.5	1.6	120.3	32.66

Conditions: 100 PSI, 10 mL PhCl, 200 equiv. AlMe<sub>3</sub>, 3 equiv. [CPh<sub>3</sub>][B(C<sub>6</sub>F<sub>5</sub>)<sub>4</sub>], 1000

equiv. 1-hexene. <sup>a</sup>From GPC analysis; <sup>b</sup>From GPC analysis where PDI = M<sub>w</sub>/M<sub>N</sub>;

<sup>c</sup>Insertion mol% as determined by integration of the <sup>13</sup>C NMR; <sup>d</sup>Melting temperature

determined by DSC; <sup>e</sup>Percent crystallinity determined by DSC.



*Crystallographic Information*

Refinement Details: Crystals were mounted on a glass fiber or MiTeGen loop using Paratone oil, then placed on the diffractometer under a nitrogen stream. Diffractometer manipulations, including data collection, integration, and scaling were performed using the Bruker APEXII software<sup>8</sup>. Absorption corrections were applied using SADABS or TWINABS.<sup>38</sup> Space groups were determined on the basis of systematic absences and intensity statistics and the structures were solved in the Olex 2 software interface<sup>39</sup> by intrinsic phasing using XT (incorporated into SHELXTL)<sup>40</sup> and refined by full-matrix least squares on  $F^2$ . All non-hydrogen atoms were refined using anisotropic displacement parameters, except as noted. Hydrogen atoms were placed in the idealized positions and refined using a riding model. Graphical representation of structures with 50% probability thermal ellipsoids were generated using Diamond 3 visualization software.<sup>41</sup> As the quality of the data sets collected for **3.14**, **3.19**, **3.20**, and **3.30** were poor and/or twinned, only isotropic refinement was performed. Disordered solvents of crystallization were observed in the difference maps of **3.18** and **3.23**; these were removed using the solvent mask tool in Olex 2<sup>49</sup> as they could not be satisfactorily modeled.

**Table 3.6.** Crystal and refinement data for **3.14** and **3.16**

	<b>3.14, cell 1</b>	<b>3.14, cell 2</b>	<b>3.16</b>
CCDC Number	1901334		1901318
Empirical formula	C <sub>53</sub> H <sub>57</sub> N <sub>5</sub> Si <sub>4</sub> Y	C <sub>56</sub> H <sub>61</sub> N <sub>5</sub> Si <sub>4</sub> Y	C <sub>36</sub> H <sub>40</sub> AlN <sub>3</sub>
Formula weight	965.30	1005.38	541.69
T (K)	100	100	100
a, Å	12.8334(15)	12.6269(15)	10.0846(7)
b, Å	18.935(2)	13.2018(15)	10.7246(7)
c, Å	21.972(2)	16.826(2)	14.7495(11)
α, °	66.153(4)	70.060(4)	88.535(3)
β, °	86.673(4)	83.034(4)	85.525(3)
γ, °	89.451(4)	76.338(4)	72.732(3)
Volume, Å <sup>3</sup>	4874.6(10)	2559.51	1518.66(19)
Z	4	2	2
Crystal system	Triclinic	Triclinic	Triclinic
Space group	P -1	P1	P -1
θ range, °	2.347 to 25.702	2.573 to 29.513	2.419 to 27.463
μ, mm <sup>-1</sup>	1.336	1.27	0.096
Abs. Correction	Multi-scan	Multi-scan	Multi-scan
GOF	1.124	1.161	1.046
R <sub>1</sub> , <sup>a</sup> wR <sub>2</sub> <sup>b</sup> [I>2 σ(I)]	0.0497, 0.1431	0.2324, 0.5416	0.0622, 0.1750
Radiation Type	Mo Kα	Mo Kα	Mo Kα

$$^a R_1 = \sum ||F_o| - |F_c|| / \sum |F_o|, ^b wR_2 = [\sum [w(F_o^2 - F_c^2)^2] / \sum [w(F_o^2)^2]^{1/2}.$$

**Table 3.7.** Crystal and refinement data for **3.18**, **3.19**, and **3.20**

	<b>3.18</b>	<b>3.22</b>	<b>3.23</b>
CCDC Number	1900723	1900722	
Empirical formula	C <sub>76</sub> H <sub>96</sub> N <sub>3</sub> OSi <sub>4</sub> Y	C <sub>80</sub> H <sub>78</sub> N <sub>5</sub> Si <sub>2</sub> Y	C <sub>144</sub> H <sub>147</sub> N <sub>8</sub> O <sub>2</sub> Si <sub>4</sub> Y <sub>2</sub>
Formula weight	1268.83	1254.57	2311.89
T (K)	100	100	100
a, Å	11.597(5)	12.1287(7)	12.8103(7)
b, Å	16.582(7)	22.4625(13)	18.0605(9)
c, Å	21.396(5)	24.6736(14)	28.0359(12)
α, °	96.041(6)	90	90.114(3)
β, °	104.761(6)	90.137(3)	97.937(2)
γ, °	94.927(7)	90	99.127(3)
Volume, Å <sup>3</sup>	3929(3)	6722.1(7)	6341.0(5)
Z	2	4	2
Crystal system	Triclinic	Monoclinic	Triclinic
Space group	P -1	P 2 <sub>1</sub> /n	P -1
<i>d</i> <sub>calc</sub> , g/cm <sup>3</sup>	1.072	1.240	1.211
θ range, °	2.297 to 27.387	3.936 to 79.873	3.982 to 51.487
μ, mm <sup>-1</sup>	0.845	1.925	2.003
Abs. Correction	Multi-scan	Multi-scan	Multi-scan
GOF	1.042	1.023	3.051
R <sub>1</sub> , <sup>a</sup> wR <sub>2</sub> <sup>b</sup> [I>2 σ(I)]	0.0532, 0.1554	0.0421, 0.1080	0.1443, 0.3878
Radiation Type	Mo Kα	Cu Kα	Cu Kα

$$^a R1 = \sum ||F_o| - |F_c|| / \sum |F_o|. \quad ^b wR2 = [\sum [w(F_o^2 - F_c^2)^2] / \sum [w(F_o^2)^2]^{1/2}.$$

**Table 3.8.** Crystal and refinement data for **3.23**, **3.24**, and **3.30**

	<b>3.24</b>	<b>3.25</b>	<b>3.31</b>
CCDC Number	1900724	1900725	
Empirical formula	C <sub>42</sub> H <sub>26</sub> Cl <sub>3</sub> N <sub>3</sub> Zr	C <sub>38</sub> H <sub>48</sub> N <sub>6</sub> Ti	C <sub>92</sub> H <sub>96</sub> N <sub>8</sub> O <sub>2</sub> Zr <sub>2</sub>
Formula weight	770.23	636.72	1528.21
T (K)	100	293	100
a, Å	13.1280(6)	13.9896(10)	12.3976(17)
b, Å	20.0709(9)	14.8633(11)	13.131(2)
c, Å	16.0162(7)	17.6638(12)	14.230(2)
α, °	90	73.735(3)	74.605(4)
β, °	110.871(2)	87.623(3)	83.230(5)
γ, °	90	88.398(3)	62.106(4)
Volume, Å <sup>3</sup>	3943.22	3522.3(4)	1973.9(5)
Z	4	4	1
Crystal system	Monoclinic	Triclinic	Triclinic
Space group	P 2 <sub>1</sub> /c	P -1	P -1
<i>d</i> <sub>calc</sub> , g/cm <sup>3</sup>	1.297	1.201	1.286
θ range, °	2.439 to 27.4795	2.403 to 27.487	2.155 to 27.022
μ, mm <sup>-1</sup>	0.513	2.310	0.318
Abs. Correction	Multi-scan	Multi-scan	Multi-scan
GOF	1.040	1.049	0.755
R <sub>1</sub> , <sup>a</sup> wR <sub>2</sub> <sup>b</sup> [I>2 σ(I)]	0.0247, 0.0686	0.0336, 0.0901	0.0464, 0.0784
Radiation Type	Mo Kα	Mo Kα	Mo Kα

$$^a R1 = \sum ||F_o| - |F_c|| / \sum |F_o|. \quad ^b wR2 = [\sum [w(F_o^2 - F_c^2)^2] / \sum [w(F_o^2)^2]^{1/2}.$$

## REFERENCES

1. (a) Shook, R. L.; Borovik, A. S. *Inorg. Chem.* **2010**, *49* (8), 3646-3660; (b) Cook, S. A.; Borovik, A. S. *Acc. Chem. Res.* **2015**, *48* (8), 2407-2414; (c) Moore, C. M.; Szymczak, N. K., Appended Functionality in Pincer Ligands. In *Pincer and Pincer-Type Complexes*, Wiley-VCH: 2014; (d) Hale, L. V. A.; Szymczak, N. K. *ACS Catalysis* **2018**, *8*, 6446-6461.
2. (a) Shirin, Z.; Hammes, B. S.; Young, V. G.; Borovik, A. S. *J. Am. Chem. Soc.* **2000**, *122*, 1836-1837; (b) MacBeth, C. E.; Gupta, R.; Mitchell-Koch, K. R.; Young, V. G., Jr.; Lushington, G. H.; Thompson, W. H.; Hendrich, M. P.; Borovik, A. S. *J. Am. Chem. Soc.* **2004**, *126* (8), 2556-2567; (c) Borovik, A. S. *Acc. Chem. Res.* **2005**, *38* (1), 54-61; (d) Shook, R. L.; Peterson, S. M.; Greaves, J.; Moore, C.; Rheingold, A. L.; Borovik, A. S. *J. Am. Chem. Soc.* **2011**, *133* (15), 5810-5817; (e) Han, Z.; Horak, K. T.; Lee, H. B.; Agapie, T. *J. Am. Chem. Soc.* **2017**, *139* (27), 9108-9111; (f) Wallen, C. M.; Palatinus, L.; Bacsa, J.; Scarborough, C. C. *Angew. Chem. Int. Ed.* **2016**, *55* (39), 11902-11906; (g) Wallen, C. M.; Bacsa, J.; Scarborough, C. C. *Inorg. Chem.* **2018**, *57* (9), 4841-4848; (h) Dahl, E. W.; Kiernicki, J. J.; Zeller, M.; Szymczak, N. K. *J. Am. Chem. Soc.* **2018**, *140* (32), 10075-10079; (i) Dahl, E. W.; Dong, H. T.; Szymczak, N. K. *Chem. Commun.* **2018**, *54* (8), 892-895.
3. Moore, C. M.; Szymczak, N. K. *Chem. Sci.* **2015**, *6* (6), 3373-3377.
4. (a) Franco, F.; Cometto, C.; Ferrero Vallana, F.; Sordello, F.; Priola, E.; Minero, C.; Nervi, C.; Gobetto, R. *Chem. Commun.* **2014**, *50* (93), 14670-14673; (b) Franco, F.; Cometto, C.; Nencini, L.; Barolo, C.; Sordello, F.; Minero, C.; Fiedler, J.; Robert, M.; Gobetto, R.; Nervi, C. *Chem. Eur. J.* **2017**, *23* (20), 4782-4793.
5. (a) Moore, C. M.; Szymczak, N. K. *Dalton Trans.* **2012**, *41* (26), 7886-7889; (b) Geri, J. B.; Szymczak, N. K. *J. Am. Chem. Soc.* **2015**, *137* (40), 12808-12814; (c) Dahl, E. W.; Szymczak, N. K. *Angew. Chem. Int. Ed.* **2016**, *55* (9), 3101-3105.
6. (a) Kiernicki, J. J.; Zeller, M.; Szymczak, N. K. *J. Am. Chem. Soc.* **2017**, *139* (50), 18194-18197; (b) Kiernicki, J. J.; Zeller, M.; Szymczak, N. K. *Inorg. Chem.* **2019**.
7. (a) Miller, A. J.; Labinger, J. A.; Bercaw, J. E. *J. Am. Chem. Soc.* **2008**, *130* (36), 11874-11875; (b) Miller, A. J. M.; Labinger, J. A.; Bercaw, J. E. *Organometallics* **2010**, *29*, 4499-4516.
8. Tseng, K. N.; Kampf, J. W.; Szymczak, N. K. *J. Am. Chem. Soc.* **2016**, *138* (33), 10378-10381.
9. Ostapowicz, T. G.; Merkens, C.; Holscher, M.; Klankermayer, J.; Leitner, W. *J. Am. Chem. Soc.* **2013**, *135* (6), 2104-2107.
10. Creutz, S. E.; Peters, J. C. *Chem. Sci.* **2017**, *8* (3), 2321-2328.
11. Rakowski DuBois, M.; DuBois, D. L. *Acc. Chem. Res.* **2009**, *42* (12), 1974-1982.
12. (a) Yang, J. F. K. K. J. W. Z. J. Y. *J. Coord. Chem.* **2015**, *69*, 11-13; (b) Khosrowabadi Kotyk, J. F.; Hanna, C. M.; Combs, R. L.; Ziller, J. W.; Yang, J. Y. *Chem. Sci.* **2018**, *9* (10), 2750-2755.
13. Tutusaus, O.; Ni, C.; Szymczak, N. K. *J. Am. Chem. Soc.* **2013**, *135* (9), 3403-3406.
14. (a) He, L.; Ma, D.; Duan, L.; Wei, Y.; Qiao, J.; Zhang, D.; Dong, G.; Wang, L.; Qiu, Y. *Inorg. Chem.* **2012**, *51* (8), 4502-4510; (b) Mashita, T.; Tsushima, S.; Takao, K. *Dalton Trans.* **2018**, *47* (37), 13072-13080; (c) Qu, Z. Z.; Gao, T. B.; Wen, J.; Rui, K.; Ma, H.; Cao, D. K. *Dalton Trans.* **2018**, *47* (29), 9779-9786; (d) Pandey, I. K.; Natarajan, M.; Faujdar, H.; Hussain, F.; Stein, M.; Kaur-Ghumaan, S. *Dalton Trans.* **2018**, *47* (14), 4941-4949; (e) Blindauer, C. A.; Griesser, R.; Holy, A.; Operschall, B. P.; Sigel, A.; Song, B.; Sigel, H. *J. Coord. Chem.* **2018**, *71*, 11-13; (f) Congrave, D. G.; Hsu, Y. T.; Batsanov, A. S.; Beeby, A.; Bryce, M. R. *Dalton Trans.* **2018**, *47* (6), 2086-2098; (g) Namanga, J. E.;

- Gerlitzki, N.; Smetana, V.; Mudring, A. V. *ACS Appl. Mater. Interfaces* **2018**, *10* (13), 11026-11036; (h) Shih, W.-C.; Chiang, Y.-T.; Wang, Q.; Wu, M.-C.; Yap, G. P. A.; Zhao, L.; Ong, T.-G. *Organometallics* **2017**, *36*, 4287-4297; (i) Congrave, D. G.; Hsu, Y.-t.; Batsanov, A. S.; Beeby, A.; Bryce, M. R. *Organometallics* **2017**, *36*, 981-993; (j) Martinez, C. R.; Iverson, B. L. *Chem. Sci.* **2012**, *3*, 2191-2201; (k) Meyer, E. A.; Castellano, R. K.; Diederich, F. *Angew. Chem. Int. Ed.* **2003**, *42*, 1210-1250; (l) Kobayashi, M.; Hayakawa, N.; Matsuo, T.; Li, B.; Fukunaga, T.; Hashizume, D.; Fueno, H.; Tanaka, K.; Tamao, K. *J. Am. Chem. Soc.* **2016**, *138* (3), 758-761; (m) Wang, Z.; Yang, H.; He, P.; He, Y.; Zhao, J.; Tang, H. *Dalton Trans.* **2016**, *45* (7), 2839-2844; (n) Schneider, G. E.; Pertegás, A.; Constable, E. C.; Housecroft, C. E.; Hostettler, N.; Morris, C. D.; Zampese, J. A.; Bolink, H. J.; Junquera-Hernández, J. M.; Ortí, E.; Sessolob, M. *J. Mat. Chem. C* **2014**, *2*, 7047-7055; (o) Li, P.; Shan, G. G.; Cao, H. T.; Zhu, D. X.; Su, Z. M.; Jitchati, R.; Bryce, M. R. *Eur. J. Inorg. Chem.* **2014**, *2014*, 2376-2382; (p) Costa, R. D.; Casillas, R.; Cano, J. *J. Phys. Chem. C* **2013**, *117*, 8545-8555; (q) Fraser, M. G.; van der Salm, H.; Cameron, S. A.; Blackman, A. G.; Gordon, K. C. *Inorg. Chem.* **2013**, *52* (6), 2980-92.
15. Barboiu, M.; Prodi, L.; Montalti, M.; Kyritsakas, N.; Lehn, J.-M. *Chem. Eur. J.* **2004**, *10*, 2953-2959.
16. Barboiu, M.; Legrand, Y.-M.; Prodi, L.; Montalti, M.; Zaccheroni, N.; Vaughan, G.; Lee, A. v. d.; Petit, E.; Lehn, J.-M. *Eur. J. Inorg. Chem.* **2009**, 2621-2628.
17. (a) Wang, S.-Y.; Fu, J.-H.; Liang, Y.-P.; He, Y.-J.; Chen, Y.-S.; Chan, Y.-T. *J. Am. Chem. Soc.* **2016**, *138*, 3651-3654; (b) He, Y.-J.; Tu, T.-H.; Su, M.-K.; Yang, C.-W.; Kong, K. V.; Chan, Y.-T. *J. Am. Chem. Soc.* **2017**, *139*, 4218-4224.
18. (a) Brauchli, S. Y.; Constable, E. C.; Harris, K.; Haussinger, D.; Housecroft, C. E.; Rosel, P. J.; Zampese, J. A. *Dalton Trans.* **2010**, *39* (44), 10739-10748; (b) Pelascini, F.; Wesolek, M.; Peruch, F.; Cian, A. D.; Kyritsakas, N.; Lutz, P. J.; Kress, J. *Polyhedron* **2004**, *23* (18), 3193-3199.
19. (a) Onoda, A.; Kawakita, K.; Okamura, T.-A.; Yamamoto, H.; Ueyama, N. *Acta Crystallogr., Sect. E: Struct. Rep. Online* **2003**, *59*, m266; (b) Constable, E. C.; Edwards, A. J.; Haire, G. R.; Hannon, M. J.; Raithby, P. R. *Polyhedron* **1998**, *17* (2-3), 243-253; (c) Onoda, A.; Kawakita, K.; Okamura, T.; Yamamoto, H.; Ueyama, N. *Acta Crystallogr., Sect. E: Struct. Rep. Online* **2003**, *59*, m291; (d) Kamata, K.; Suzuki, A.; Nakai, Y.; Nakazawa, H. *Organometallics* **2012**, *31* (10), 3825-3828.
20. Dawson, D. M.; Walker, D. A.; Thornton-Pett, M.; Bochmann, M. *J.C.S. Dalton Trans.* **2000**, (4), 459-466.
21. (a) Hu, X.-H.; Liang, Y.; Li, C.; Yi, X.-Y. *Dalton Trans.* **2014**, *43* (6), 2458-2464; (b) Wang, Y.-P.; Hu, X.-H.; Wang, Y.-F.; Pan, J.; Yi, X.-Y. *Polyhedron* **2015**, *102*, 782-787.
22. (a) Tabatchnik-Rebillon, A.; Aube, C.; Bakkali, H.; Delaunay, T.; Manh, G. T.; Blot, V.; Thobie-Gautier, C.; Renault, E.; Souldard, M.; Planchat, A.; Le Questel, J.-Y.; Le Guevel, R.; Guguen-Guillouzo, C.; Kauffmann, B.; Ferrand, Y.; Huc, I.; Urgin, K.; Condon, S.; Leonel, E.; Evain, M.; Lebreton, J.; Jacquemin, D.; Pipelier, M.; Dubreuil, D. *Chem. - Eur. J.* **2010**, *16* (39), 11876-11889, S11876/1-S11876/17; (b) Balewski, L.; Saczewski, F.; Bednarski, P. J.; Gdaniec, M.; Borys, E.; Makowska, A. *Molecules* **2014**, *19* (10), 17026-17051; (c) Samanta, S. K.; Rana, A.; Schmittel, M. *Dalton Trans.* **2014**, *43* (25), 9438-47; (d) Wang, Y.-P.; Xiao, J.-J.; Hu, X.-H.; Yi, X.-Y. *Inorg. Chim. Acta* **2015**, *435*, 125-130; (e) Min, R.; Hu, X.-h.; Yi, X.-y.; Zhang, S.-c. *J. Cent. South Univ. (Engl. Ed.)* **2015**, *22* (5), 1619-1625; (f) Fang, W.-Z.; Wang, Y.-P.; Wang, Y.-F.; Zhang, S.-C.; Yi, X.-Y. *RSC Adv.* **2015**, *5* (12), 8996-9001.

23. (a) Alam, M. S.; Stocker, M.; Gieb, K.; Mueller, P.; Haryono, M.; Student, K.; Grohmann, A. *Angew. Chem. Int. Ed.* **2010**, *49* (6), 1159-1163; (b) Frazier, B. A.; Williams, V. A.; Wolczanski, P. T.; Bart, S. C.; Meyer, K.; Cundari, T. R.; Lobkovsky, E. B. *Inorg. Chem.* **2013**, *52* (6), 3295-3312; (c) Bowman, D. N.; Bondarev, A.; Mukherjee, S.; Jakubikova, E. *Inorg. Chem.* **2015**, *54* (17), 8786-8793.
24. (a) Yan, L.; Seminario, J. M. *J. Phys. Chem. A* **2005**, *109* (30), 6628-6633; (b) Liu, Y.; Liang, H.; Chen, Z.; Qin, Q.; Xu, Q.; Jiang, Y. Method for synthesis of cobalt(II) metal complex using oxoisoaporphines derivative as ligand for use in preparation of anti-tumor drug. CN104370908A, 2015; (c) Qin, Q.-P.; Qin, J.-L.; Meng, T.; Lin, W.-H.; Zhang, C.-H.; Wei, Z.-Z.; Chen, J.-N.; Liu, Y.-C.; Liang, H.; Chen, Z.-F. *Eur. J. Med. Chem.* **2016**, *124*, 380-392; (d) McPherson, J. N.; Hogue, R. W.; Akogun, F. S.; Bondi, L.; Luis, E. T.; Price, J. R.; Garden, A. L.; Brooker, S.; Colbran, S. B. *Inorg. Chem.* **2019**, Article ASAP.
25. (a) McSkimming, A.; Diachenko, V.; London, R.; Olrich, K.; Onie, C. J.; Bhadhbade, M. M.; Bucknall, M. P.; Read, R. W.; Colbran, S. B. *Chem. - Eur. J.* **2014**, *20* (36), 11445-11456; (b) Nomura, K.; Sato, H.; Kobayashi, K. Photoelectric conversion element, dye-sensitized solar cell, metal complex dye, and dye solution made by dissolving metal complex dye. WO2014050578A1, 2014; (c) Nomura, K.; Sato, H.; Kobayashi, K.; Watanabe, K. Photoelectric conversion element and dye-sensitized solar cell. WO2014050528A1, 2014; (d) Zhong, Y.-Q.; Xiao, H.-Q.; Yi, X.-Y. *Dalton Trans.* **2016**, *45* (45), 18113-18119.
26. Imler, G. H.; Lu, Z.; Kistler, K. A.; Carroll, P. J.; Wayland, B. B.; Zdilla, M. J. *Inorg. Chem.* **2012**, *51* (19), 10122-10128.
27. Chen, J.-J.; Gan, Z.-L.; Huang, Q.; Yi, X.-Y. *Inorg. Chim. Acta* **2017**, *466*, 93-99.
28. Zhang, Z.; Lim, J. M.; Ishida, M.; Roznyatovskiy, V. V.; Lynch, V. M.; Gong, H. Y.; Yang, X.; Kim, D.; Sessler, J. L. *J. Am. Chem. Soc.* **2012**, *134* (9), 4076-9.
29. Argouarch, G.; de Montigny, F.; Lapinte, C. *Synthesis* **2006**, (2), 293-298.
30. (a) Usui, K.; Tanoue, K.; Yamamoto, K.; Shimizu, T.; Suemune, H. *Org. Lett.* **2014**, *16* (17), 4662-4665; (b) Natarajan, P.; Schmittl, M. *Inorg. Chem.* **2013**, *52* (15), 8579-8590.
31. Wannere, C. S.; Schleyer, P. V. *Org. Lett.* **2003**, *5* (5), 605-608.
32. Addison, A. W.; Rao, T. N.; Reedijk, J.; van Rijn, J.; Verschoor, G. C. *J. Chem. Soc., Dalton Trans.* **1984**, (7), 1349-1356.
33. Yang, L.; Powell, D. R.; Houser, R. P. *Dalton Trans.* **2007**, (9), 955-964.
34. WebElements.com (accessed November 26, 2018).
35. Kaneko, H.; Dietrich, H. M.; Schädle, C.; Maichle-Mössmer, C.; Tsurugi, H.; Törnroos, K. W.; Mashima, K.; Anwender, R. *Organometallics* **2013**, *32*, 1199-1208.
36. Imai, Y. N.; Inoue, Y.; Nakanishi, I.; Kitaura, K. *Protein Sci.* **2008**, *17* (7), 1129-1137.
37. Britovsek, G. J. P.; Bruce, M.; Gibson, V. C.; Kimberley, B. S.; Maddox, P. J.; Mastroianni, S.; McTavish, S. J.; Redshaw, C.; Solan, G. A.; Strömberg, S.; White, A. J. P.; Williams, D. J. *J. Am. Chem. Soc.* **1999**, *121*, 8728-8740.
38. (a) Nakazawa, H.; Ikai, S.; Imaoka, K.; Kai, Y.; Yano, T. *J. Mol. Cat. A* **1998**, *132*, 33-41; (b) Scollard, J. D.; McConville, D. H.; Vittal, J. J.; Payne, N. C. *J. Mol. Cat. A* **1998**, *128* (1-3), 201-214; (c) Murtuza, S.; Jr., O. L. C.; Jordan, R. F. *Organometallics* **2002**, *21* (9), 1882-1890; (d) Amin, S. B.; Marks, T. J. *Angew. Chem. Int. Ed.* **2008**, *47* (11), 2006-2025; (e) Chan, M. C. W.; Tam, K.-H.; Zhu, N.; Chiu, P.; Matsui, S. *Organometallics* **2006**, *25* (3), 785-792; (f) Saito, J.; Tohi, Y.; Matsukawa, N.; Mitani, M.; Fujita, T. *Macromolecules* **2005**, *38* (12), 4955-4957; (g) Michiue, K.; Jordan, R. F. *Macromolecules* **2003**, *36* (26), 9707-9709; (h) Tohi, Y.; Mako, H.; Matsui, S.; Onda, M.; Fujita, T. *Macromolecules* **2003**, *36* (3), 523-

- 525; (i) Obenauf, J.; Kretschmer, W. P.; Kempe, R. *Eur. J. Inorg. Chem.* **2014**, 2014 (9), 1446-1453; (j) Lee, J.; Kim, Y. *J. Industrial Eng. Chem.* **2012**, 18 (1), 429-432; (k) Park, S.-J.; Han, Y.-G.; Kim, S.-K.; Lee, J.-S.; Kim, H.-K.; Do, Y.-K. *Bull. Korean Chem. Soc.* **2005**, 26 (5), 713-714; (l) Resconi, L.; Piemontesi, F.; Franciscano, G.; Abis, L.; Fiorani, T. *J. Am. Chem. Soc.* **1992**, 114 (3), 1025-1032; (m) Mogstad, A. L.; Waymouth, R. M. *Macromolecules* **1992**, 25 (2282-2284); (n) Rieger, B.; Reinmuth, A.; Röhl, W.; Brintzinger, H. H. *J. Mol. Cat.* **1993**, 82 (1), 67-73; (o) Leino, R.; Luttikhedde, H. J. G.; Lehmus, P.; Wilén, C.-E.; Sjöholm, R.; Lehtonen, A.; Seppälä, J. V.; Näsman, J. H. *Macromolecules* **1997**, 30 (12), 3477-3483; (p) Valente, A.; Mortreux, A.; Visseaux, M.; Zinck, P. *Chem. Rev.* **2013**, 113 (5), 3836-3857; (q) Byun, D.-J.; Shin, D.-K.; Kim, S. Y. *Polym. Bull.* **1999**, 42, 301-307; (r) Byun, D.-J.; Shin, D.-K.; Kim, S. Y. *Macromol. Rapid. Commun.* **1999**, 20 (8), 419-422; (s) Byun, D.-J.; Kim, S. Y. *Macromolecules* **2000**, 33 (6), 1921-1923; (t) Barsties, E.; Schaible, S.; Prosenc, M.-H.; Rief, U.; Röhl, W.; Weynand, O.; Dorer, B.; Brintzinger, H.-H. *J. Organomet. Chem.* **1996**, 520 (1-2), 63-68; (u) Przybyla, C.; Fink, G. *Acta Polymerica* **1999**, 50 (2-3), 77-83.
39. (a) Kulangara, S. V.; Jabri, A.; Yang, Y.; Korobkov, I.; Gambarotta, S.; Duchateau, R. *Organometallics* **2012**, 31 (6085-6094); (b) Dias, A. R.; Ferreira, A. P.; Veiros, L. F. *Organometallics* **2003**, 22 (24), 5114-5125; (c) Dias, A. R.; Veiros, L. F. *J. Organomet. Chem.* **2005**, 690 (7), 1840-1844; (d) Heys, P. N.; Odedra, R.; Kingsley, A.; Davies, H. O. Hafnium and zirconium pyrrolyl-based organometallic precursors and their use for preparing dielectric thin films. WO2009155520A1, 2009; (e) Hsu, J.-W.; Lin, Y.-C.; Hsiao, C.-S.; Datta, A.; Lin, C.-H.; Huang, J.-H.; Tsai, J.-C.; Hsu, W.-C. *Dalton Trans.* **2012**, 41 (25), 7700-7707; (f) Huang, J.-H.; Kuo, P.-C.; Lee, G.-H.; Peng, S.-M. *J. Chin. Chem. Soc.* **2000**, 47 (6), 1191-1195; (g) Kaushik, N. K.; Bhushan, B.; Sodhi, G. S. *Indian J. Chem., Sect. A* **1981**, 20A (6), 625-6; (h) Sodhi, G. S.; Kaushik, N. K. *Bull. Soc. Chim. Fr.* **1982**, (1-2, Pt. 1), 45-8; (i) Sodhi, G. S.; Kumar, S.; Kaushik, N. K. *Acta Chim. Hung.* **1983**, 114 (3-4), 329-35; (j) Sharma, A. K.; Kaushik, N. K. *Acta Chim. Hung.* **1984**, 116 (4), 361-365; (k) Zhao, W.; Xu, X.; Yi, J.; Jing, X.; Chen, W. Olefin polymerization catalysts of Group IV metal complexes with pyrrole ring-containing ligands. CN1317500A, 2001.
40. Sworen, J. C.; Smith, J. A.; Wagener, K. B.; Baugh, L. S.; Rucker, S. P. *J. Am. Chem. Soc.* **2003**, 125 (8), 2228-2240.
41. Busico, V.; Cipullo, R.; Cutillo, F.; Friederichs, N.; Ronca, S.; Wang, B. *J. Am. Chem. Soc.* **2003**, 125 (41), 12402-12403.
42. Pangborn, A. B.; Giardello, M. A.; Grubbs, R. H.; Rosen, R. K.; Timmers, F. J. *Organometallics* **1996**, 15 (5), 1518-1520.
43. (a) Bradley, D. C.; Thomas, I. M. *J. Chem. Soc.* **1960**, 0 (0), 3857-3861; (b) Chisholm, M. H.; Hammond, C. E.; Huffman, J. C. *Polyhedron* **1988**, 7 (24), 2515-2520; (c) Diamond, G. M.; Rodewald, S.; Jordan, R. F. *Organometallics* **1995**, 14 (1), 5-7.
44. (a) Chandra, G.; Lappert, M. F. *Journal of the Chemical Society A: Inorganic, Physical, Theoretical* **1968**; (b) Diamond, G. M.; Jordan, R. F.; Petersen, J. L. *Organometallics* **1996**, 15 (19), 4030-4037.
45. (a) Estler, F.; Eickerling, G.; Herdtweck, E.; Anwender, R. *Organometallics* **2003**, 22 (6), 1212-1222; (b) Arndt, S.; Voth, P.; Spaniol, T. P.; Okuda, J. *Organometallics* **2000**, 19 (23), 4690-4700; (c) Lappert, M. F.; Pearce, R. *Journal of the Chemical Society, Chemical Communications* **1973**, (4).
46. (a) Anwender, R.; Runte, O.; Eppinger, J.; Gerstberger, G.; Herdtweck, E.; Spiegler, M. *Journal of the Chemical Society, Dalton Transactions* **1998**, (5), 847-858; (b)



- Herrmann, W. A.; Anwender, R.; Munck, F. C.; Scherer, W.; Dufaud, V.; Huber, N. W.; Artus, G. R. J. *Zeitschrift für Naturforschung B* **1994**, *49* (12), 1789-1797.
47. Atiqullah, M.; Moman, A. A.; Akhtar, M. N.; Al-Muallem, H. A.; Abu-Raqabah, A. H.; Ahmed, N. *Journal of Applied Polymer Science* **2007**, *106* (5), 3149-3157.
48. Dias, P.; Lin, Y. J.; Poon, B.; Chen, H. Y.; Hiltner, A.; Baer, E. *Polymer* **2008**, *49* (12), 2937-2946.
49. (a) Dolomanov, O. V.; Bourhis, L. J.; Gildea, R. J.; Howard, J. A. K.; Puschmann, H. J. *Appl. Crystallogr.* **2009**, *42* (2), 339-341; (b) Spek, A. L. *Acta Cryst.* **2009**, *D65*, 148-155.

## APPENDIX A

TACTICITY CONTROL IN 1-HEXENE POLYMERIZATION BY AMINE BIS(PHENOLATE)  
ZIRCONIUM CATALYSTS WITH BULKY SILYL SUBSTITUENTS

**ABSTRACT**

Towards gaining insight into tacticity control in  $C_1$  symmetric monozirconium amine bis(phenolate) Kol type-catalysts, a series of catalysts bearing bulky *ortho* triarylsilyl and trialkylsilyl substituents were prepared and tested in 1-hexene homopolymerization. While catalysts bearing tri(*iso*-propyl)silyl substituents did not exhibit any tacticity control, the catalyst bearing a triphenylsilyl substituent produced poly-1-hexene with 53 % *mmmm* and moderate activity of  $0.557 \text{ g mmol}_{\text{Zr}}^{-1} \text{ h}^{-1}$ . Replacement of the triphenylsilyl substituent with diphenyl(*tert*-butyl)silyl or diphenyl(methyl)silyl resulted in significant loss of tacticity control to 21 and 15 % *mmmm*, respectively, albeit with improved activities of 1.03 and  $2.58 \text{ kg mmol}_{\text{Zr}}^{-1} \text{ h}^{-1}$ . These results suggest that the use of bulky substituents extending away from the catalyst center could aid in tacticity control. Future directions for improvement of tacticity control by this class of  $C_1$  symmetric Zr amine(bisphenolate) catalyst could include use of tris(2,6-dimethylphenyl)silyl substituents, exploration of the role of the other *ortho* substituent, and changing catalyst electronics through modification of the *para* substituents.

## INTRODUCTION

Isotactic polypropylene is an important plastic produced on billion tons annual scale through a mixture of heterogeneous and homogeneous catalysis.<sup>1</sup> While metallocene catalysts have dominated the field of prochiral  $\alpha$ -olefin polymerization, the use of non-metallocene catalysts for prochiral  $\alpha$ -olefin polymerization has emerged as a complementary approach towards the synthesis of isotactic polypropylene.<sup>2</sup>

One class of ligands for  $\alpha$ -olefin polymerization that has received some attention are the Kol-type amine bis(phenolate) ligands shown in Figure A.1.  $C_s$  symmetric catalyst **A.1** is highly active for 1-hexene polymerization ( $15.5 \text{ kg mmol}_{\text{Zr}}^{-1} \text{ h}^{-1}$ ), though producing only atactic polymer.<sup>3-5</sup> Activity is nearly lost upon removal of one donor (**A.2**,  $0.023 \text{ kg mmol}_{\text{Zr}}^{-1} \text{ h}^{-1}$ ). In contrast, while  $C_2$  symmetric catalyst **A.3** produces highly isotactic poly-1-hexene ( $>95 \%$ ), it exhibits low activity ( $0.018 \text{ kg mmol}_{\text{Zr}}^{-1} \text{ h}^{-1}$ ).<sup>6-7</sup> The related  $C_1$  symmetric catalyst **A.4** shows the best of both worlds compared with catalysts **A.1**, **A.2**, and **A.3**, producing moderately ( $54 \%$ ) isotactic poly-1-hexene with moderate ( $1.3 \text{ kg mmol}_{\text{Zr}}^{-1} \text{ h}^{-1}$ ) activity.<sup>8</sup>

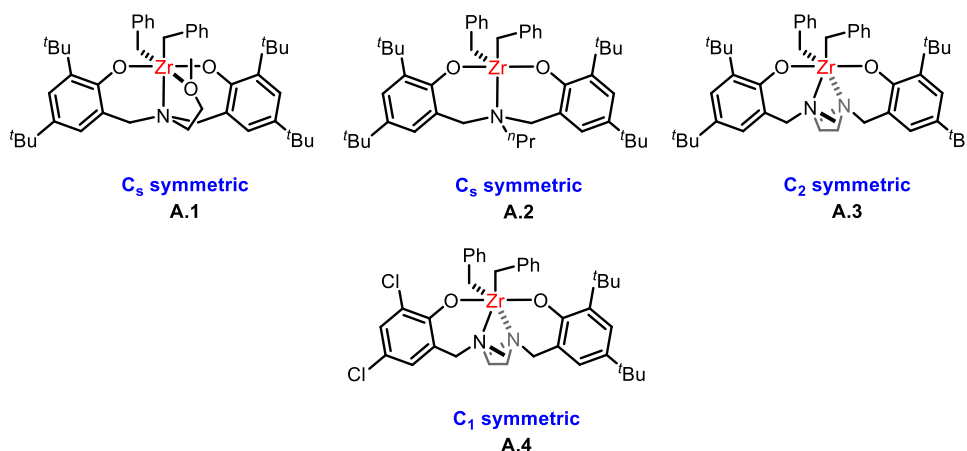
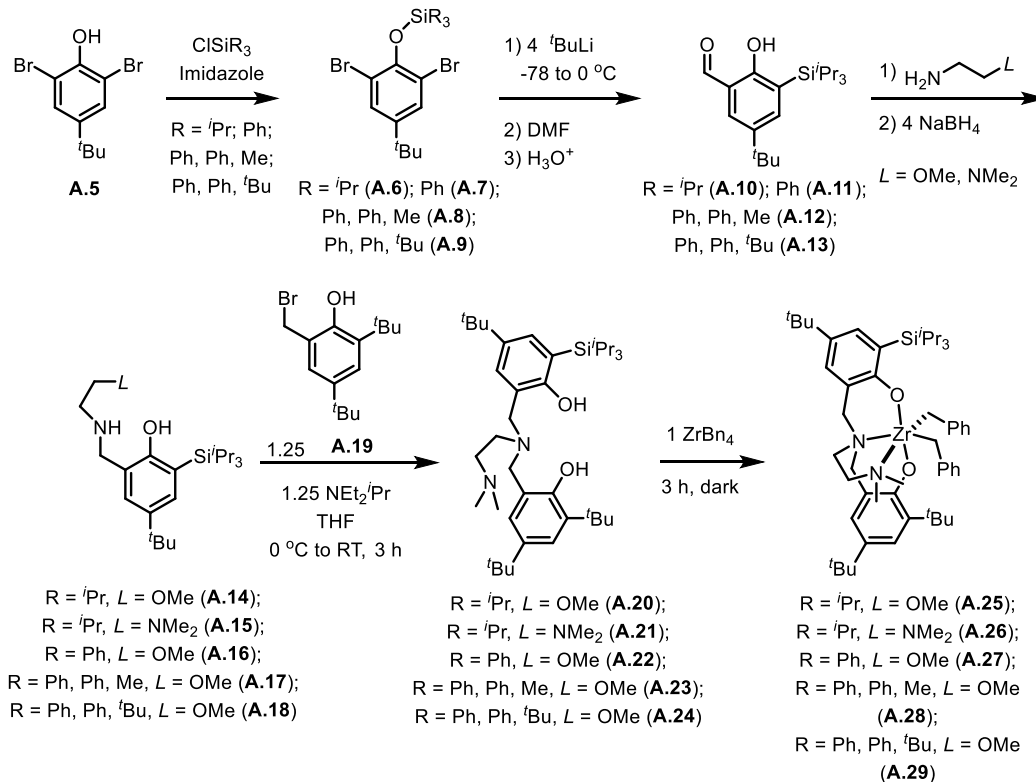


**Figure A.1.** Kol-type amine bis(phenolate) Zr catalysts for 1-hexene polymerization

In conjunction with our studies on dizirconium amine bis(phenolate) catalysts bearing bulky trialkylsilyl substituents, a series of  $C_1$  symmetric monozirconium catalysts were also prepared. While single isomers of the dizirconium catalysts could not be isolated, the corresponding monozirconium catalysts could be isolated and these catalysts were tested for 1-hexene and ethylene homopolymerization.

## RESULTS

The silyl-substituted amine bisphenolate catalysts were synthesized analogously to reported  $C_1$  symmetric catalysts. Starting from 2,6-dibromo-4-*tert*-butylphenol (**A.5**), reaction with the desired chlorosilane affords the corresponding silyl-aryl ether (**A.6-A.9**). Formation of the corresponding salicylaldehydes was accomplished through *retro*-Brook reagent of these species via reaction with four equivalents of *tert*-butyllithium and subsequent quench with DMF to give **A.10-A.13**. Reductive amination of **A.10-A.13** with either N,N-dimethylethylenediamine or 2-methoxyethylamine afforded 2° amines **A.14-A.18** and subsequent reaction with benzyl bromide **A.19** in the presence of Hünig's base affords the desired proligands **A.20-A.24** following isolation by column chromatography. Metalation can be accomplished via protonolysis with 1 equivalent of  $ZrBn_4$  in toluene and the desired precatalysts **A.25-A.29** isolated in moderate to good yields.



**Scheme A.1.** Synthesis of silyl-substituted amine bis(phenolate) proligands and their corresponding Zr benzyl complexes.

This series of precatalysts was tested for 1-hexene polymerization activity in the presence of  $[\text{CPh}_3][\text{B}(\text{C}_6\text{F}_5)_4]$  as an activator. The two catalysts bearing the tri(*iso*-propyl)silyl substituents (**A.25** and **A.26**) show similar tacticity control (8-9 % *mmmm*) as compared with the literature  $C_s$  symmetric *tert*-butyl substituted catalysts, however, their activity is much lower ( $0.225 \text{ kg mmol}_{\text{Zr}}^{-1} \text{ h}^{-1}$  for **A.25** and  $0.654 \text{ kg mmol}_{\text{Zr}}^{-1} \text{ h}^{-1}$  for **A.26**). The catalyst **A.27** bearing the triphenylsilyl substituent, however, shows substantially higher tacticity control, producing poly-1-hexene with 53 % *mmmm*, albeit with only moderate activity ( $0.557 \text{ kg mmol}_{\text{Zr}}^{-1} \text{ h}^{-1}$ ).

To probe the causes of this increased tacticity control in 1-hxene polymerization the catalysts **A.28** and **A.29**. Replacement of one of the phenyl rings with the smaller

methyl substituent results in a substantial increase in catalytic activity to  $2.58 \text{ kg mmol}_{\text{Zr}}^{-1} \text{ h}^{-1}$ , however, the tacticity control substantially decreases and the resulting polymer is only 15 % *mmmm*. Replacement of one of the phenyl with the bulkier *tert*-butyl substituent results in a moderate increase in activity ( $1.03 \text{ kg mmol}_{\text{Zr}}^{-1} \text{ h}^{-1}$ ), however, the polymer shows only 21 % *mmmm*, similar to that observed with **A.28**.

**Table A.1.** 1-hexene polymerization by monozirconium amine bis(phenolate) complexes<sup>a</sup>

Entry	Catalyst	Yield <sup>b</sup>	Activity <sup>c</sup>	% <i>mmmm</i> <sup>d</sup>
1	<b>A.1</b>	1.69	2.54	5
2	<b>A.25</b>	0.150	0.225	8
3	<b>A.26</b>	0.436	0.654	9
4	<b>A.27</b>	0.371	0.557	53
5	<b>A.28</b>	1.72	2.58	15
6	<b>A.29</b>	0.686	1.03	21

<sup>a</sup>Polymerizations were run with 4.0  $\mu\text{mol}$  precatalyst, 1.0 equiv.  $[\text{CPh}_3][\text{B}(\text{C}_6\text{F}_5)_4]$ , and 1000 equiv. 1-hexene in 2.5 mL PhCl at room temperature over 10 min; <sup>b</sup>Yield of polymer in grams; <sup>c</sup>Activity defined as kg of polymer per mmol of Zr per hour; <sup>d</sup>Determined by integration of the methylene signal in the  $^{13}\text{C}$  NMR spectrum.

Catalysts **A.26**, **A.28**, and **A.29** were also tested for ethylene polymerization activity in the presence of 250 equiv. of dried MAO as an activator and scavenger. All



catalysts tested under these conditions show similar activities to each other and in comparison with the literature **A.1** catalyst (1.99 to 2.70 kg mmol<sub>Zr</sub><sup>-1</sup> h<sup>-1</sup>), indicating that these bulky substituents have little to no effect when polymerizing the smaller ethylene monomer.

**Table A.2.** Ethylene polymerization by monozirconium amine bis(phenolate) complexes<sup>a</sup>

Entry	Complex	Yield <sup>b</sup>	Activity <sup>c</sup>
1	<b>A.1</b>	2.25	2.70
2	<b>A.26</b>	2.02	2.42
3	<b>A.28</b>	1.66	1.99
4	<b>A.29</b>	1.83	2.20

<sup>a</sup>Polymerizations were run with 4.0 μmol precatalyst and 250 equiv. dried MAO in 2.5 mL PhMe at 25 °C, 100 PSI ethylene over 10 min; <sup>b</sup>Yield of polymer in grams; <sup>c</sup>Activity defined as kg of polymer per mmol Zr per hour.

## DISCUSSION

While tacticity and activity effects in propylene polymerization by these catalysts could be of some interest, given that catalysts demonstrating higher tacticity control in poly-1-hexene polymerization could show similar effects with the more industrially-relevant propylene monomer, such as experiments were also not performed. Insight into the mechanism of tacticity control in this system could also be obtained from analysis of the stereoerrors errors by  $^{13}\text{C}$  NMR.

A number of approaches to further develop this class of amine bis(phenolate) Zr catalysts and improve their tacticity control and activities. The differences in tacticity control between the catalyst bearing the triphenylsilyl substituent and those bearing diphenyl(alkyl)silyl substituents suggests that improved tacticity control could be achieved through increasing the size of the aryl substituents at silicon. Improved catalyst activity could likely be achieved through incorporation of electron-withdrawing substituents at the *para* positions at the two phenoxide donors, as has been previously-observed with the dizirconium amine(bisphenolate) catalysts.<sup>9</sup> It is also possible that through reducing the size of the *ortho* substituent at the other phenoxide donor, improved tacticity control could be observed.

## CONCLUSIONS

In conclusion, a series of  $C_1$ -symmetric amine bis(phenolate) Zr bis(benzyl) complexes bearing bulky tri(*iso*-propyl)silyl, triphenylsilyl, diphenyl(methyl)silyl, and diphenyl(*tert*-butyl)silyl substituents were synthesized and tested for 1-hexene and ethylene polymerization. While no substituent effects were observed in ethylene polymerization, the poly-1-hexene produced by the triphenylsilyl-substituted complex was 53 % *mmm*. Both diphenyl(*tert*-butyl)silyl- and diphenyl(methyl)silyl-substituted complexes showed substantially less tacticity control, indicating that further improvements to this system could likely be derived from further increasing the size of the aryl substituents at silicon.

## EXPERIMENTAL SECTION

*General Notes.* All air- and water-sensitive compounds were manipulated under N<sub>2</sub> or Ar using standard Schlenk or glovebox techniques. Solvents for air- and moisture-sensitive reactions were dried by the method of Grubbs.<sup>10</sup> Chlorobenzene and 1-hexene for polymerization with stoichiometric activators were refluxed over CaH<sub>2</sub> for greater than 72 h, vacuum transferred, and run over activated alumina plugs prior to use. [CPh<sub>3</sub>][B(C<sub>6</sub>F<sub>5</sub>)<sub>4</sub>] was purchased from Strem and used without further purification. 2,6-dibromo-4-*tert*-butylphenol (**A.5**) and **A.19** were prepared according to literature procedures. Deuterated solvents were purchased from Cambridge Isotopes Lab, Inc.; CDCl<sub>3</sub> and 1,1,2,2-tetrachloroethane-d<sub>2</sub> were used without further purification; C<sub>6</sub>D<sub>6</sub> was distilled from purple Na/benzophenone ketyl and filtered over activated alumina prior to use. <sup>1</sup>H and <sup>13</sup>C spectra were recorded on Varian Mercury 300, Varian INOVA-300, 400, or 500 spectrometers or Bruker Cryoprobe 400. <sup>1</sup>H and <sup>13</sup>C chemical shifts are reported relative to residual solvent resonances.

**General synthesis of (2,6-dibromo-4-*tert*butylphenoxy)silanes.** An oven-dried Schlenk tube was charged with 2,6-dibromo-4-*tert*butylphenol (1 equiv.), imidazole (4 equiv.), DCM (1 mL/mmol, **2a**) or THF (1-2 mL/mmol, **2b-d**), and chlorosilane (1.5 equiv.), sealed and heated to reflux for 16 h. Volatiles were removed under reduced pressure and the residue taken up in DCM and washed with water (2x), 0.2 N HCl, and brine. The organics were dried with MgSO<sub>4</sub>, filtered, and volatiles removed under vacuum.

*(2,6-dibromo-4-*tert*-butylphenoxy)triisopropylsilane, A.6.* **A.6** was isolated in quantitative yield as a white solid without further purification. Spectra matched those previously reported<sup>11</sup>.

(2,6-dibromo-4-*tert*butylphenoxy)triphenylsilane, **A.7**. **A.7** was isolated in 78.3 % yield as a white solid following recrystallization from benzene/ethanol (1:3 v/v) at -35 °C. <sup>1</sup>H NMR (300 MHz, CDCl<sub>3</sub>) δ 7.73 (m, 6H), 7.43 (t, 3H), 7.39 – 7.31 (m, 8H), 1.22 (s, 9H). HRMS (FAB+) Calcd. for C<sub>28</sub>H<sub>26</sub>SiOBr<sub>2</sub>: 566.0099. Found: 566.0115.

(2,6-dibromo-4-*tert*butylphenoxy)diphenylmethylsilane, **A.8**. **A.8** was isolated in 26 % yield as a clear, viscous oil following column chromatography (4 % benzene in hexane, R<sub>f</sub> = 0.3). **A.8** could not be completely separated from tetraphenyldimethyldisiloxane (ca. 40 % by <sup>1</sup>H integration) under those conditions but was moved forward without further purification.

(2,6-dibromo-4-*tert*butylphenoxy)diphenyl*tert*butylsilane, **A.9**. **A.9** was isolated in 65.6 % yield as a white solid following column chromatography (hexane, R<sub>f</sub> = 0.4). <sup>1</sup>H NMR (300 MHz, CDCl<sub>3</sub>) δ 7.77 (m, 4H), 7.46 – 7.31 (m, 8H), 7.27 (m, 3H), 1.24 (s, 9H), 1.14 (s, 9H). HRMS (FAB+) calcd. for C<sub>26</sub>H<sub>29</sub>SiOBr<sub>2</sub>: 545.0334. Found: 545.0354.

**General synthesis of 2-hydroxybenzaldehydes.** An oven-dried Schlenk flask was charged with **2** (1 equiv.), Et<sub>2</sub>O (2 mL/mmol, **A.10**) or THF (2 mL/mmol, **A.11**, **A.12**, **A.13**), and cooled to -78 °C. <sup>t</sup>BuLi (1.7 M in pentanes, 4.5 equiv.) was added dropwise over the course of several minutes. The reaction was stirred at -78 °C for 30 minutes then allowed to warm to room temperature over 60 minutes and stirred for an additional 30 minutes. Upon cooling the reaction to -78 °C, DMF (6 equiv.) was added at once and the reaction allowed to come to room temperature. NH<sub>4</sub>Cl (aq.) was added after 1h to quench and the reaction transferred to a separatory funnel with Et<sub>2</sub>O. The aqueous fraction was removed and organics washed with water (2x), 0.2 N HCl, and brine. Combined organics

were dried with MgSO<sub>4</sub>, filtered, and volatiles removed *en vacuo* to give the crude product which was further purified by column chromatography.

*2-hydroxy,3-triisopropylsilyl,5-tertbutylbenzaldehyde*, **A.10**. **A.10** was isolated in 81 % yield (30.6 mmol scale) following purification by column chromatography (20 % benzene in hexanes). Spectra matched those previously reported<sup>11</sup>.

*2-hydroxy,3-triphenylsilyl,5-tertbutylbenzaldehyde*, **A.11**. **A.11** was isolated in 79 % yield (15 mmol scale) following purification by column chromatography (40 % benzene in hexanes, R<sub>f</sub> = 0.2). <sup>1</sup>H NMR (300 MHz, CDCl<sub>3</sub>) δ 11.28 (s, 1H), 9.92 (s, 1H), 7.66 – 7.61 (m, 6H), 7.60 (d, *J* = 2.6 Hz, 1H), 7.54 (d, *J* = 2.6 Hz, 1H), 7.47 – 7.35 (m, 10H), 1.18 (s, 9H). HRMS (FAB+) calcd. for C<sub>29</sub>H<sub>29</sub>O<sub>2</sub>Si: 437.1937. Found: 437.1937.

*2-hydroxy,3-diphenylmethylsilyl,5-tertbutylbenzaldehyde*, **A.12**. **A.12** was isolated in 39.8 % yield following purification by column chromatography (30 % benzene in hexanes, R<sub>f</sub> = 0.5). <sup>1</sup>H NMR (500 MHz, CDCl<sub>3</sub>) δ 11.19 (s, 1H), 9.89 (s, 1H), 7.56 – 7.53 (m, 5H), 7.47 (d, 1H), 7.41 (m, 2H), 7.39 (m, 2H), 7.37 (m, 3H), 7.36 (m, 1H), 1.21 (s, 9H), 0.93 (s, 3H). <sup>13</sup>C NMR (126 MHz, CDCl<sub>3</sub>) δ 197.05, 164.65, 142.95, 142.27, 135.93, 135.27, 131.98, 129.53, 128.47, 127.93, 124.37, 119.27, 34.20, 31.29, -3.27. HRMS (FAB+) calcd. for C<sub>24</sub>H<sub>26</sub>O<sub>2</sub>Si: 374.1702. Found: 374.1709.

*2-hydroxy,3-diphenyltertbutylsilyl,5-tertbutylbenzaldehyde*, **A.13**. **A.13** was isolated in 82.7 % yield following purification by column chromatography (30 % benzene in hexanes, R<sub>f</sub> = 0.4). <sup>1</sup>H NMR (500 MHz, CDCl<sub>3</sub>) δ 11.48 (s, 1H), 9.93 (s, 1H), 7.59 (m, 4H), 7.56 (dd, 1H), 7.47 (dd, 1H), 7.43 (m, 2H), 7.39 – 7.35 (m, 4H), 1.25 (s, 9H), 1.17 (s, 9H). <sup>13</sup>C NMR (126 MHz, CDCl<sub>3</sub>) δ 197.15, 164.56, 145.10, 142.13, 136.33, 135.07, 131.91, 129.28, 128.47, 127.74, 123.67, 119.22, 34.17, 31.20, 29.69, 18.68. HRMS (FAB+) calcd. for C<sub>27</sub>H<sub>33</sub>O<sub>2</sub>Si: 417.2250. Found: 417.2260.

**Preparation of compounds A.14-A.18.** To solution of **A.10-A.13** (1 equiv.) in methanol (4 mL/mmol) 2-methoxyethylamine or N,N-dimethylethylenediamine (1.1 equiv.) was added and the reaction heated to 65 °C for 8 to 13 h. Complete consumption of the aldehyde starting material was confirmed by  $^1\text{H}$  NMR, then volatiles removed *en vacuo*. The residue was taken up in methanol (4 mL/mmol)<sup>12</sup> and  $\text{NaBH}_4$  (4 equiv.) was added in several portions, then the reaction stirred 4 h. The resulting colourless solution was concentrated and HCl (2N) added to quench. 1 M NaOH was added in small portions to bring to pH~7 then the reaction was transferred to a separatory funnel and extracted twice with DCM. Combined organics were washed with water then dried with  $\text{MgSO}_4$ , filtered, and evaporated. All compounds were used without further purification.

**A.14.**  $^1\text{H}$  NMR (500 MHz,  $\text{CDCl}_3$ )  $\delta$  7.31 (d, 1H, ArH), 6.97 (d, 1H, ArH), 3.96 (s, 2H, ArCH<sub>2</sub>), 3.51 (t, 2H, CH<sub>2</sub>CH<sub>2</sub>), 3.36 (s, 3H, OCH<sub>3</sub>), 2.80 (t, 2H, CH<sub>2</sub>CH<sub>2</sub>), 1.51 (sep, 3H, CH(CH<sub>3</sub>)<sub>2</sub>), 1.29 (s, 9H, C(CH<sub>3</sub>)<sub>3</sub>), 1.10 (d, 18H, CH(CH<sub>3</sub>)<sub>2</sub>).  $^{13}\text{C}$  NMR (126 MHz,  $\text{CDCl}_3$ )  $\delta$  161.27, 140.28, 133.29, 126.42, 120.64, 120.61, 58.99, 53.11, 47.83, 34.03, 31.79, 19.13, 11.95.

**A.15.**  $^1\text{H}$  NMR (300 MHz, Chloroform-*d*)  $\delta$  7.30 (d, 1H, ArH), 6.97 (d, 1H, ArH), 3.95 (s, 2H, ArCH<sub>2</sub>), 2.70 (t, 2H, CH<sub>2</sub>CH<sub>2</sub>), 2.43 (t, 2H, CH<sub>2</sub>CH<sub>2</sub>), 2.23 (s, 6H, N(CH<sub>3</sub>)<sub>2</sub>), 1.50 (sep, 3H, CH(CH<sub>3</sub>)<sub>2</sub>), 1.27 (s, 9H, C(CH<sub>3</sub>)<sub>3</sub>), 1.09 (d, 21H, CH(CH<sub>3</sub>)<sub>2</sub>).

**A.16** was isolated in 90.8 % yield as a pale yellow solid.  $^1\text{H}$  NMR (300 MHz,  $\text{CDCl}_3$ )  $\delta$  7.65 (m, 6H, ArH), 7.44 – 7.32 (m, 10H, ArH), 7.09 (d, 2H, ArH), 4.03 (s, 2H, ArCH<sub>2</sub>), 3.46 (t, 2H, CH<sub>2</sub>CH<sub>2</sub>), 3.33 (s, 3H, OCH<sub>3</sub>), 2.80 (t, 2H, CH<sub>2</sub>CH<sub>2</sub>), 1.13 (s, 9H, C(CH<sub>3</sub>)<sub>3</sub>).

**A.17** was isolated in 97.7% yield.  $^1\text{H}$  NMR (500 MHz,  $\text{CDCl}_3$ )  $\delta$  7.52 – 7.48 (m, 4H, ArH), 7.29 (m, 6H, ArH), 6.99 (s, 2H, ArH), 3.41 (t, 2H, CH<sub>2</sub>CH<sub>2</sub>), 3.28 (s, 3H, OCH<sub>3</sub>), 2.75 (t, 2H, CH<sub>2</sub>CH<sub>2</sub>), 1.10 (s, 9H, C(CH<sub>3</sub>)<sub>3</sub>), 0.84 (s, 3H, SiCH<sub>3</sub>).  $^{13}\text{C}$  NMR (126 MHz,  $\text{CDCl}_3$ )  $\delta$

161.42, 140.95, 137.48, 135.36, 133.43, 129.02, 127.66, 121.17, 120.86, 58.97, 52.94, 48.05, 34.07, 31.64, -2.84. HRMS (FAB+) calcd. for  $C_{27}H_{36}O_2SiN$ : 434.2515. Found: 434.2536.

**A.18** was isolated in 91.4 % yield as a yellow viscous oil.  $^1H$  NMR (500 MHz,  $CDCl_3$ )  $\delta$  7.61-7.59 (m, 4H, ArH), 7.40 – 7.31 (m, 6H, ArH), 7.08 (d, 1H, ArH), 7.05 (d, 1H, ArH), 4.02 (s, 2H, ArCH<sub>2</sub>), 3.49 (t, 2H, CH<sub>2</sub>CH<sub>2</sub>), 3.35 (s, 3H, OCH<sub>3</sub>), 2.82 (t, 2H, CH<sub>2</sub>CH<sub>2</sub>), 1.22 (s, 9H, C(CH<sub>3</sub>)<sub>3</sub>), 1.13 (s, 9H, C(CH<sub>3</sub>)<sub>3</sub>).  $^{13}C$  NMR (126 MHz,  $CDCl_3$ )  $\delta$  161.02, 140.68, 136.46, 136.41, 135.38, 128.78, 127.44, 120.64, 120.45, 71.06, 58.98, 52.93, 47.83, 34.04, 31.60, 29.84, 18.67. HRMS (FAB+) calcd. for  $C_{30}H_{42}NSiO_2$ : 476.2985. Found: 476.2977.

**General preparation of compounds A.20-A.24.** To a solution of **A.19** (1.25 equiv.) and NEt<sup>*t*</sup>Pr<sub>2</sub> (1.25 equiv.) in THF (30 mL/mmol) at 0 °C, **A.14-A.18** (1 equiv.) in THF (20 mL/mmol) was added in 2 mL portions. The reaction was stirred, warming over 3 h then volatiles removed under reduced pressure. The residue was taken up in DCM and washed with K<sub>2</sub>CO<sub>3</sub> (2x) and brine. The combined organics were dried with MgSO<sub>4</sub>, filtered, and evaporated to afford the crude product which was further purified by column chromatography (details below). All ligands were dried extensively under vacuum then lyophilized from dry benzene prior to metalation.

*Proligand A.20.* Purification by column chromatography in 10:1 Hexanes:EtOAc (v/v).  $^1H$  NMR (500 MHz, Chloroform-*d*)  $\delta$  7.37 (d, 1H, ArH), 7.23 (d, 1H, ArH), 7.05 (d, 1H, ArH), 6.91 (d, 1H, ArH), 3.80 (s, 2H, ArCH<sub>2</sub>), 3.74 (s, 2H, ArCH<sub>2</sub>), 3.56 (m, 2H, CH<sub>2</sub>CH<sub>2</sub>), 3.47 (s, 3H, OCH<sub>3</sub>), 2.76 (m, 2H, CH<sub>2</sub>CH<sub>2</sub>), 1.53 (sep, 3H, CH(CH<sub>3</sub>)<sub>2</sub>), 1.41 (s, 9H, C(CH<sub>3</sub>)<sub>3</sub>), 1.30 (s, 18H, C(CH<sub>3</sub>)<sub>3</sub>), 1.13 (d, 18H, CH(CH<sub>3</sub>)<sub>2</sub>).  $^{13}C$  NMR (126 MHz,  $cdCl_3$ )  $\delta$  159.37, 153.24, 140.82, 140.74, 136.07, 134.16, 128.50, 124.68, 123.47, 121.63, 121.11, 120.41, 71.72, 58.98, 58.36,



51.57, 35.07, 34.03, 31.84, 30.49, 29.67, 19.20, 11.91. HRMS (FAB+) calcd for  $C_{38}H_{66}O_3NSi$ : 612.4812. Found: 612.4819.

*Proligand A.21.* Purification by column chromatography in 10:1 Hexanes:EtOAc (v/v).  $^1H$  NMR (500 MHz, Chloroform-*d*)  $\delta$  7.38 (d, 1H, ArH), 7.21 (d, 1H, ArH), 7.06 (d, 1H, ArH), 6.90 (d, 1H, ArH), 3.73 (s, 2H, ArCH<sub>2</sub>), 3.57 (s, 2H, ArCH<sub>2</sub>), 2.60 (s, 4H, CH<sub>2</sub>), 2.32 (s, 6H, N(CH<sub>3</sub>)<sub>2</sub>), 1.53 (sep, 3H, CH(CH<sub>3</sub>)<sub>2</sub>), 1.37 (s, 9H, C(CH<sub>3</sub>)<sub>3</sub>), 1.32 (s, 9H, C(CH<sub>3</sub>)<sub>3</sub>), 1.30 (s, 9H, C(CH<sub>3</sub>)<sub>3</sub>), 1.15 (d, 18H, CH(CH<sub>3</sub>)<sub>2</sub>).  $^{13}C$  NMR (126 MHz, Chloroform-*d*)  $\delta$  160.29, 153.32, 140.50, 139.85, 135.83, 134.29, 128.61, 124.45, 123.26, 121.68, 121.38, 120.14, 58.09, 56.14, 56.06, 49.23, 44.93, 35.00, 34.25, 33.97, 31.85, 30.49, 29.61, 19.27, 11.96. HRMS (FAB+) calcd for  $C_{39}H_{69}O_2N_2Si$ : 625.5128. Found: 625.5107.

*Proligand A.22.* Purification by column chromatography in 15:1 Hexanes:EtOAc (v/v).  $^1H$  NMR (300 MHz, Benzene-*d*<sub>6</sub>)  $\delta$  8.91 (s, 2H, OH), 7.91 (m, 6H, ArH), 7.58 (d, *J* = 2.4 Hz, 1H, ArH), 7.52 (d, 1H, ArH), 7.31 – 7.20 (m, 9H, ArH), 6.97 (d, 1H, ArH), 3.63 (s, 2H, ArCH<sub>2</sub>), 3.57 (s, 2H, ArCH<sub>2</sub>), 2.90 (t, 2H, CH<sub>2</sub>CH<sub>2</sub>), 2.74 (s, 3H, OCH<sub>3</sub>), 2.34 (t, 2H, CH<sub>2</sub>CH<sub>2</sub>), 1.65 (s, 9H, C(CH<sub>3</sub>)<sub>3</sub>), 1.36 (s, 9H, C(CH<sub>3</sub>)<sub>3</sub>), 1.20 (s, 9H, C(CH<sub>3</sub>)<sub>3</sub>). HRMS (FAB+) calcd. for  $C_{47}H_{60}O_3SiN$ : 714.4342. Found: 714.4358.

*Proligand A.23.* Purification by column chromatography in 15:1 Hexanes:EtOAc (v/v).  $^1H$  NMR (500 MHz, Benzene-*d*<sub>6</sub>)  $\delta$  8.80 (s, 2H, OH), 7.79 – 7.74 (m, 4H, ArH), 7.51 (d, 1H, ArH), 7.48 (d, 1H, ArH), 7.23 (m, 6H, ArH), 6.95 (d, 1H, ArH), 3.57 (s, 2H, ArCH<sub>2</sub>), 3.52 (s, 2H, ArCH<sub>2</sub>), 2.91 (t, 2H, CH<sub>2</sub>CH<sub>2</sub>), 2.83 (s, 3H, OCH<sub>3</sub>), 2.31 (t, 2H, CH<sub>2</sub>CH<sub>2</sub>), 1.67 (s, 9H, C(CH<sub>3</sub>)<sub>3</sub>), 1.35 (s, 9H, C(CH<sub>3</sub>)<sub>3</sub>), 1.22 (s, 9H, C(CH<sub>3</sub>)<sub>3</sub>), 1.11 (s, 3H, SiCH<sub>3</sub>).

*Proligand A.24.* Isolated in 80.7 % yield as a white solid following purification by column chromatography in 15:1 Hexanes:EtOAc (v/v).  $^1H$  NMR (300 MHz, Chloroform-*d*)  $\delta$  8.57 (s, 2H, OH), 7.61 (m, 4H, ArH), 7.36 (m, 6H, ArH), 7.21 (d, 1H, ArH), 7.12 (d, 1H,

ArH), 7.08 (d, 1H, ArH), 6.89 (d, 1H, ArH), 3.80 (s, 2H, ArCH<sub>2</sub>), 3.75 (s, 2H, ArCH<sub>2</sub>), 3.51 (t, 2H, CH<sub>2</sub>CH<sub>2</sub>), 3.31 (s, 3H, OCH<sub>3</sub>), 2.74 (t, 2H, CH<sub>2</sub>CH<sub>2</sub>), 1.39 (s, 9H, C(CH<sub>3</sub>)<sub>3</sub>), 1.28 (s, 9H, C(CH<sub>3</sub>)<sub>3</sub>), 1.21 (s, 9H, C(CH<sub>3</sub>)<sub>3</sub>), 1.11 (s, 9H, C(CH<sub>3</sub>)<sub>3</sub>). HRMS (FAB+) calcd. for C<sub>45</sub>H<sub>64</sub>SiO<sub>3</sub>N: 694.4656. Found: 694.4678.

### General synthesis of mononuclear Zr complexes.

A 20 mL scintillation vial was charged with a stirbar, zirconium tetrabenzyl (1.0 equiv.), and toluene (10 mL/mmol). The proligand (1.0 equiv.) in toluene (15 mL/mmol) was added over several minutes then the reaction stirred for 3 hours in the dark. Volatiles were removed *en vacuo* and the residue fractionated between pentane (6 mL), ether (6 mL), and benzene.

*Precatalyst A.25.* Isolated in 63.5 % yield as a bright yellow solid from the ether fraction. <sup>1</sup>H NMR (500 MHz, Benzene-*d*<sub>6</sub>) δ 7.77 (d, 1H, ArH), 7.70 (d, 2H, ArH), 7.61 (d, 1H, ArH), 7.39 (t, 2H, ArH), 7.06 (d, 1H, ArH), 7.03 (t, 1H, ArH), 6.95 (d, 2H, ArH), 6.89 (d, 1H, ArH), 6.75 (t, 2H, ArH), 6.58 (t, 1H, ArH), 3.67 (d, 1H, ArCH<sub>2</sub>), 3.33 (d, 1H, ArCH<sub>2</sub>), 2.80 (d, 1H, ArCH<sub>2</sub>), 2.72 (dd, 2H, ArCH<sub>2</sub>), 2.61 (d, 1H, ArCH<sub>2</sub>), 2.57 (d, 1H, ArCH<sub>2</sub>), 2.53 (s, 3H, OCH<sub>3</sub>), 2.50 (d, 1H, ArCH<sub>2</sub>), 2.25 (m, 1H), 2.18 (sep, 3 H, CH(CH<sub>3</sub>)<sub>2</sub>), 1.92 (m, 1H), 1.84 (m, 10H), 1.53 (d, 9H), 1.40 (m, 18H), 1.36 (s, 9H).

*Precatalyst A.25.* Isolated in 52.9 % yield as a bright yellow solid from the ether fraction. <sup>1</sup>H NMR (500 MHz, Benzene-*d*<sub>6</sub>) δ 7.76 (d, 1H, ArH), 7.67 (d, 2H, ArH), 7.61 (d, 1H, ArH), 7.39 (t, 2H, ArH), 7.09 (d, 1H, ArH), 7.03 (t, 1H, ArH), 6.98 (d, 2H, ArH), 6.91 (d, 1H, ArH), 6.74 (t, 2H, ArH), 6.56 (t, 1H, ArH), 3.83 (d, 1H, ArCH<sub>2</sub>), 3.04 (d, 1H, ArCH<sub>2</sub>), 2.84 (d, 1H, ArCH<sub>2</sub>), 2.78 (d, 1H, ArCH<sub>2</sub>), 2.60 (d, 1H, ArCH<sub>2</sub>), 2.58 – 2.51 (m, 2H, ArCH<sub>2</sub>), 2.47 (d, 1H, ArCH<sub>2</sub>), 2.19 (sep, 3H, CH(CH<sub>3</sub>)<sub>3</sub>), 1.83 (s, 9H), 1.54 (m, 13H), 1.47 (s, 4H), 1.42 – 1.34 (m,

29H).  $^{13}\text{C}$  NMR (126 MHz, Benzene- $d_6$ )  $\delta$  164.71, 157.51, 148.85, 147.33, 140.93, 140.57, 136.21, 134.99, 126.87, 125.44, 124.49, 124.36, 124.28, 121.92, 121.76, 120.05, 68.83, 66.25, 64.92, 64.35, 59.72, 50.67, 36.54, 35.34, 34.03, 33.81, 31.52, 30.46, 19.95, 19.43, 12.92.

*Precatalyst A.25.* Isolated in 63.5 % yield as a yellow solid from the benzene fraction.

$^1\text{H}$  NMR (500 MHz, Benzene- $d_6$ )  $\delta$  8.03 (m, 7H), 7.60 (d, 1H, ArH), 7.57 (s, 1H, ArH), 7.25 (m, 11H, ArH), 6.99 (m, 6H, ArH), 6.95 – 6.90 (m, 4H, ArH), 6.85 (t, 2H, ArH), 6.64 (t, 1H, ArH), 4.00 (d, 1H, ArCH<sub>2</sub>), 3.41 (d, 1H, ArCH<sub>2</sub>), 2.75 (d, 1H, ArCH<sub>2</sub>), 2.60 (d, 1H, ArCH<sub>2</sub>), 2.42 (d, 1H, ArCH<sub>2</sub>), 2.34 (dd, 2H, ArCH<sub>2</sub>), 2.30 (s, 3H, OCH<sub>3</sub>), 2.16 (m, 2H, ArCH<sub>2</sub>), 1.93 (m, 1H, ArCH<sub>2</sub>), 1.82 (d, 1H, ArCH<sub>2</sub>), 1.77 (s, 9H), 1.59 (d, 1H, ArCH<sub>2</sub>), 1.35 (s, 9H), 1.24 (s, 9H).

*Precatalyst A.25.* Isolated in 48.6 % yield as a yellow solid from the benzene fraction.

$^1\text{H}$  NMR (500 MHz, Benzene- $d_6$ )  $\delta$  7.84 (m, 4H, ArH), 7.57 (dd, 2H, ArH), 7.33 – 7.22 (m, 9H, ArH), 7.19 (m, 2H, ArH), 7.00 (t, 1H, ArH), 6.95 – 6.90 (m, 3H, ArH), 6.83 (t, 2H, ArH), 6.63 (t, 1H, ArH), 3.73 (d, 1H, ArCH<sub>2</sub>), 3.47 (d, 1H, ArCH<sub>2</sub>), 2.66 (d, 1H, ArCH<sub>2</sub>), 2.60 (d, 1H, ArCH<sub>2</sub>), 2.42 (dd, 2H, ArCH<sub>2</sub>), 2.37 (s, 3H, OCH<sub>3</sub>), 2.31 (d, 2H, ArCH<sub>2</sub>), 2.22 (m, 1H), 2.17 (d, 1H, ArCH<sub>2</sub>), 2.03 (m, 1H), 1.86 (m, 1H), 1.78 (s, 9H, C(CH<sub>3</sub>)<sub>3</sub>), 1.38 (s, 3H, SiCH<sub>3</sub>), 1.35 (s, 9H, C(CH<sub>3</sub>)<sub>3</sub>), 1.26 (s, 9H, C(CH<sub>3</sub>)<sub>3</sub>).  $^{13}\text{C}$  NMR (126 MHz, Benzene- $d_6$ )  $\delta$  165.53, 158.67, 150.11, 145.14, 141.63, 141.43, 138.02, 137.89, 136.92, 136.74, 136.66, 136.41, 129.94, 129.62, 129.34, 125.68, 125.20, 124.96, 124.89, 124.35, 123.18, 122.73, 120.97, 73.48, 67.43, 67.08, 65.00, 64.70, 61.70, 51.53, 35.87, 34.75, 34.58, 32.33, 30.64, -1.77, -1.87.

*Precatalyst A.25.* Isolated in 75.1 % yield as a yellow solid from the benzene fraction.

$^1\text{H}$  NMR (500 MHz, Benzene- $d_6$ )  $\delta$  8.34 (d, 1H, ArH), 8.18 (d, 2H, ArH), 7.95 (d, 2H, ArH), 7.52 (s, 1H, ArH), 7.39 (t, 2H, ArH), 7.29 (t, 1H, ArH), 7.24 (s, 1H, ArH), 7.12 (m, 5H, ArH), 6.97 (s, 1H, ArH), 6.94 (d, 2H, ArH), 6.88 (d, 1H, ArH), 6.84 (d, 4H, ArH), 6.64 (m, 1H, ArH),

3.79 (d, 1H, ArCH<sub>2</sub>), 3.26 (d, 1H, ArCH<sub>2</sub>), 2.68 (d, 1H, ArCH<sub>2</sub>), 2.57 (d, 1H, ArCH<sub>2</sub>), 2.38 (m, 1H), 2.28 (s, 3H, OCH<sub>3</sub>), 2.21 (m, 1H), 2.15 (d, 1H, ArCH<sub>2</sub>), 2.03 (m, 1H), 1.96 (d, 1H, ArCH<sub>2</sub>), 1.93 (m, 1H), 1.86 (d, 1H, ArCH<sub>2</sub>), 1.68 (d, 1H, ArCH<sub>2</sub>), 1.62 (s, 9H), 1.44 (s, 9H), 1.40 (s, 9H), 1.33 (s, 9H). <sup>13</sup>C NMR (126 MHz, Benzene-*d*<sub>6</sub>) δ 165.75, 158.58, 150.29, 145.51, 141.21, 137.39, 137.00, 136.96, 136.78, 136.55, 135.61, 129.36, 129.01, 127.52, 125.55, 122.63, 121.09, 120.76, 73.31, 69.24, 67.27, 64.94, 61.92, 51.60, 35.74, 34.78, 32.32, 30.56, 29.11, 19.48.

*General Considerations for Polymerizations.* Toluene was vacuum transferred from a purple sodium benzophenone pot onto titanocene and then freshly vacuum transferred from this second pot prior to use. Chlorobenzene was heated over calcium hydride under N<sub>2</sub> for at least 72 h, vacuum transferred, and filtered over activated, solvent-free alumina prior to use. 1-Hexene was refluxed over calcium hydride for at least 24 h, vacuum transferred, and filtered over activated, solvent-free alumina prior to use. All solvents were stored in Kontes valved Schlenk flasks in a N<sub>2</sub> atmosphere glovebox following purification.

*General Procedure for 1-Hexene Polymerization.*

A Schlenk tube was charged with 1-hexene (2.5 mL, 20.00 mmol), chlorobenzene (1.5 mL) and the Zr precatalyst (4.0 μmol, 1 equiv.) in 0.5 mL chlorobenzene. The activator, [CPh<sub>3</sub>][B(C<sub>6</sub>F<sub>5</sub>)<sub>4</sub>] (4.0 μmol, 1 equiv.), in 0.5 mL chlorobenzene was added and a timer immediately started. After 10 minutes 0.5 mL MeOH and 5 mL hexanes were added and the reaction rapidly stirred. This solution was filtered over Celite and volatiles removed. Polymers were dried under vacuum at elevated temperatures (> 100 °C) for extended periods of time (> 10 h) prior to characterization. <sup>1</sup>H and <sup>13</sup>C NMR spectra were acquired

in CDCl<sub>3</sub> on a 500 MHz spectrometer and % *mmmm* was calculated based on literature assignment.<sup>13</sup>

## REFERENCES

1. Baier, M. C.; Zuideveld, M. A.; Mecking, S. *Angew. Chem. Int. Ed.* **2014**, *53* (37), 9722-9744.
2. Gibson, V. C.; Spitzmesser, S. K. *Chem. Rev.* **2003**, *103* (1), 283-315.
3. (a) Tshuva, E. Y.; Goldberg, I.; Kol, M.; Weitman, H.; Goldschmidt, Z. *Chem. Commun.* **2000**, 379-380; (b) Tshuva, E. Y.; Groysman, S.; Goldberg, I.; Kol, M.; Goldschmidt, Z. *Organometallics* **2002**, *21*, 662-670; (c) Groysman, S.; Tshuva, E. Y.; Reshef, D.; Gendler, S.; Goldbert, I.; Kol, M.; Goldschmidt, Z.; Shuster, M.; Lidor, G. *Isr. J. Chem.* **2010**, *42*, 373-381.
4. (a) Busico, V.; Cipulla, R.; Ronca, S.; Budzelaar, P. H. M. *Macromol. Rapid. Commun.* **2001**, *22*, 1405; (b) Tshuva, E. Y.; Goldberg, I.; Kol, M. *J. Am. Chem. Soc.* **2000**, *122*, 10706-10707.
5. Cohen, A.; Kopilov, J.; Goldberg, I.; Kol, M. *Organometallics* **2009**, *28*, 1391-1405.
6. Radlauer, M. R.; Agapie, T. *Organometallics* **2014**, *33* (13), 3247-3250.
7. Pangborn, A. B.; Giardello, M. A.; Grubbs, R. H.; Rosen, R. K.; Timmers, F. J. *Organometallics* **1996**, *15* (5), 1518-1520.
8. Thadani, A. N.; Huang, Y.; Rawal, V. H. *Org. Lett.* **2007**, *9* (20), 3873-3876.
9. For A.11, a 1:1 MeOH:DCM (v/v, 8 mL/mmol) solvent system was used due to the low solubility of the starting material in MeOH.
10. Asakura, T.; Demura, M.; Nishiyama, Y. *Macromolecules* **1991**, *24* (9), 2334-2340.

## **APPENDIX B**

### PREPARATION OF BIMETALLIC AMINE BIS(PHENOLATE) ZR COMPLEXES

**ABSTRACT**

Binucleating amine bis(phenolate) proligands supported by central 9,10-anthracenyldiyl and *meta*-terphenyl linkers were prepared to test the tacticity control of their corresponding dizirconium complexes in 1-hexene polymerization. While separate  $C_s$  and  $C_2$  isomers could be isolated for a select few (Chapter 2), separation of the metalation isomers was not achieved for the rest. Solid-state structures were obtained for a number of these metal complexes, this appendix describes the synthesis of these binucleating proligands and their corresponding zirconium complexes.



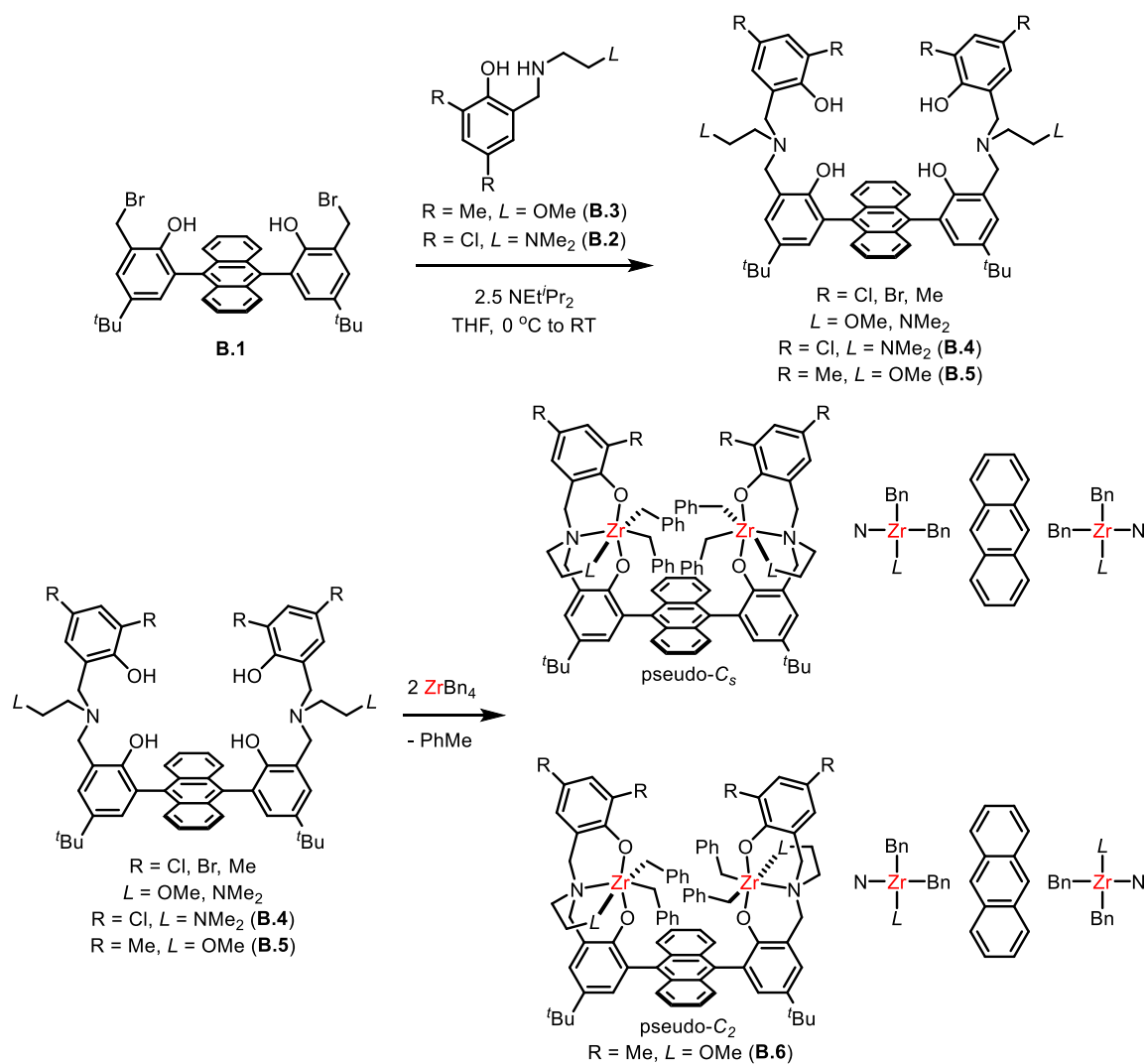
## INTRODUCTION

In conjunction with the studies on the tri(*iso*-propyl)silyl-substituted dizirconium amine bis(phenolate) catalysts presented in Chapter 2, a wide range of other binucleating proligands based on 9,10-anthracenyldiyl and *meta*-terphenyl linkers were synthesized. Previous work had demonstrated effects of both linkers (Chapter 2) and phenolate substituents<sup>1</sup> on the tacticity control of the dizirconium complexes in a limited number of cases; expansion of the series would help to better elucidate the relationships between precatalyst structure, tacticity control, and catalyst activity and allow access to industrially-relevant catalysts in the dizirconium amine bis(phenolate) system.

To that end, catalysts were targeted featuring central arene motifs other than those previously-prepared by Dr. Madalyn Radlauer but bearing small and electron-withdrawing substituents. While metalation isomers could not be separated in the vast majority of cases or could not be reliably separated, crystals suitable for X-ray diffraction could be grown of the dizirconium complexes in a limited number of cases. Those structures and the synthesis of their corresponding proligands is presented herein.

## RESULTS

All binucleating proligands based on the central 9,10-anthracenyldiyl linker were prepared according to the methods described in Chapter 2 of this thesis. Reactions of these proligands with two equivalents of tetrabenzylzirconium afforded a mixture of  $C_s$  and  $C_2$  isomers, as previously-observed with other binucleating amine bis(phenolate) proligands. Crystals suitable for X-ray diffraction could be grown of the  $C_2$  symmetric isomer of anth $Zr_2^{Me_4}$ -OMe (**B.6**, Figure 2.6), though this complex could not be reliably separated from the corresponding  $C_s$  isomer by crystallization or fractionation, this structure could not be fully isotropically modeled, and the complex was not otherwise characterized except in mixtures by  $^1H$  NMR. In the solid state structure of this complex a distance of 7.66 Å is observed between the two Zr centers, which is longer by 0.3 Å in comparison with the  $C_s$  previously-reported tetramethylphenyl-linked complex.



**Scheme B.1.** Preparation of the mixture of  $C_s$  and  $C_2$  isomers of 9,10-anthracenyldiyl linked dizirconium complexes.

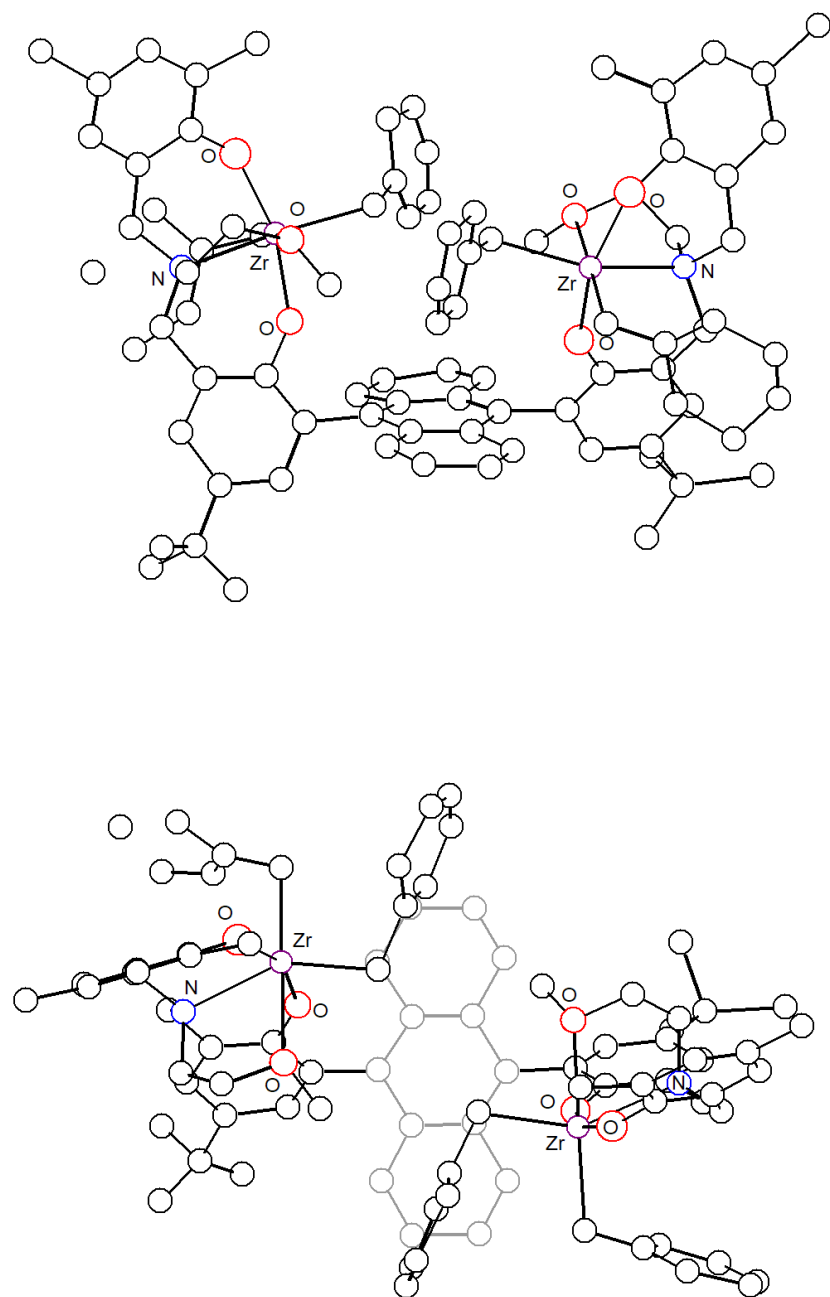
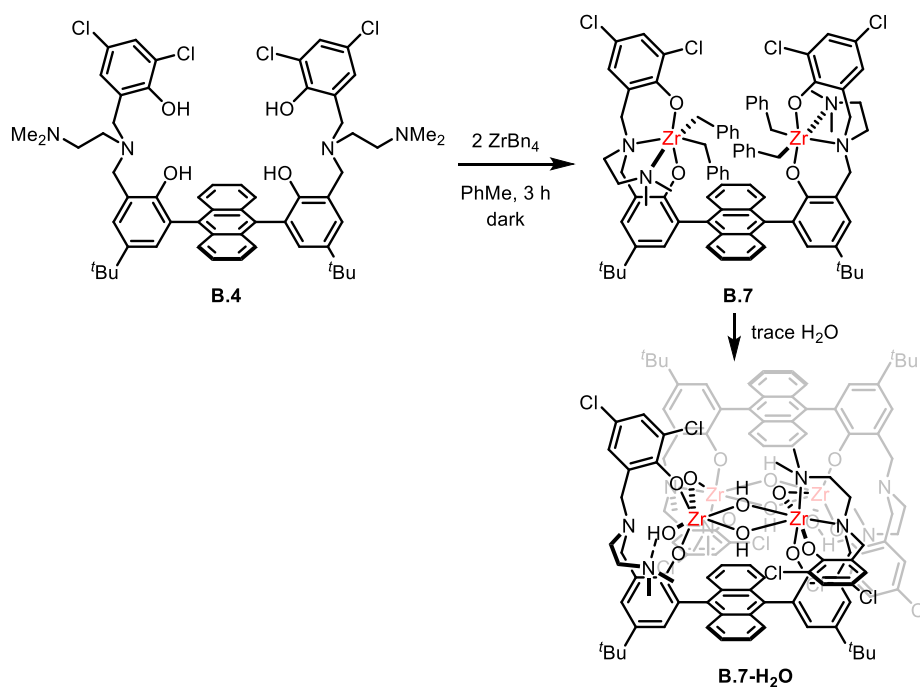


**Figure B.1.** Solid-state structure of **B.6**. Hydrogen atoms are omitted for clarity and only the better-quality of the two molecules in the asymmetric unit is shown for clarity.

Crystals suitable for X-ray diffraction of the Zr benzyl complexes could not be obtained for any of the other ligands described above; however, crystals of a water decomposition product (**B.7**) of the reaction of **B.4** with two equivalents of  $\text{ZrBn}_4$  were obtained (Scheme B.2). This complex was generated upon reaction with adventitious water in the glovebox and not otherwise characterized. Bridging oxides and hydrogens are observed between all Zr centers and, in contrast with other structurally-characterized dizirconium amine bis(phenolate) complexes, coordination to the central tertiary amine is not observed for all Zr centers.



**Scheme B.2.** Synthesis of water decomposition product **B.7-H<sub>2</sub>O**.

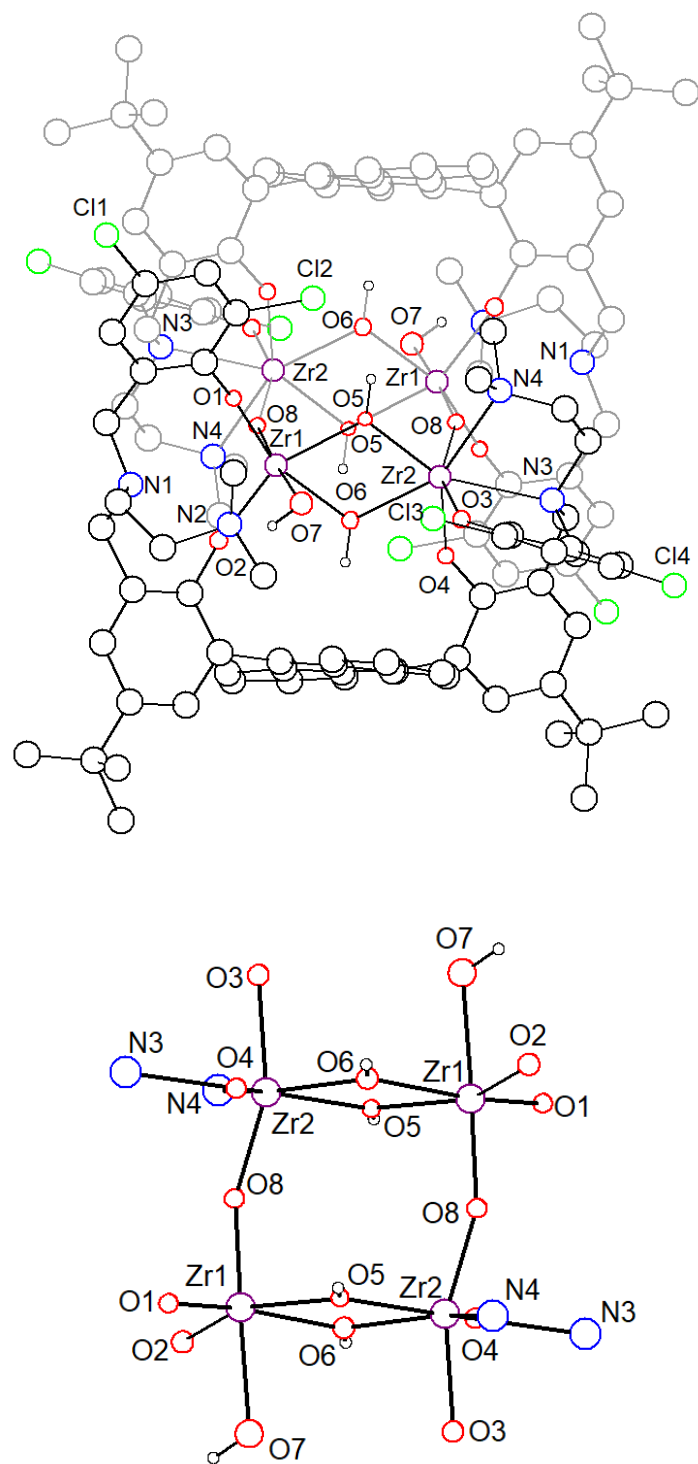
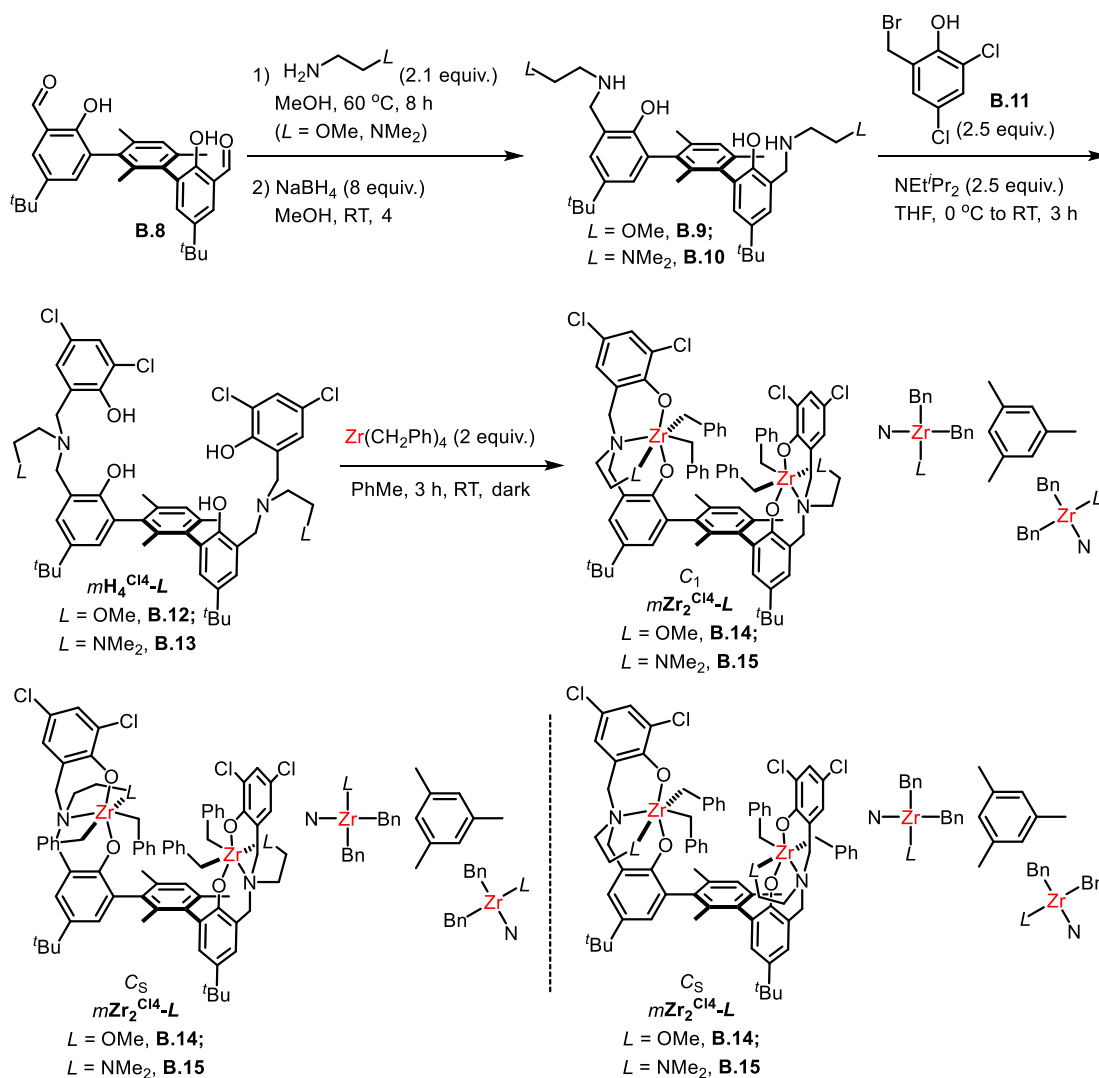


**Figure B.2.** Solid-state structure of **B.7-H<sub>2</sub>O**. Hydrogen atoms are omitted for clarity.

The ligands are omitted from the bottom structure for clarity.

*Meta*-terphenyl linked proligands and their corresponding dizirconium complexes were targeted, though an alternative strategy was taken for their synthesis (Scheme B.3) due to complications when an analogous route to the *para*-teraryl proligands was taken. Two-step reductive amination of **B.8** with either 2-methoxyethylamine or N,N-dimethylethylenediamine leads to formation of secondary amines **B.9** and **B.10** respectively. Reaction of these species with **B.11** affords proligands  $m\text{H}_4^{\text{Cl}_4}\text{-OMe}$  (**B.12**) and  $m\text{H}_4^{\text{Cl}_4}\text{-NMe}_2$  (**B.13**). Treatment of these proligands with two equivalents of zirconium tetrabenzyl affords a mixture of three metalation isomers: one  $C_1$  symmetric isomer and two  $C_s$  symmetric isomers.



**Scheme B.3.** Synthesis of *meta*-terphenyl-supported dizirconium complexes and their corresponding proligands.

The symmetry of the metalation isomers could be established using <sup>1</sup>H NMR spectroscopy. *Para*-terphenyl-derived bimetallic zirconium complexes display two characteristic doublets downfield of 3 ppm (top spectrum, Figure B.3); with the C<sub>1</sub> symmetric isomer, the number of signals in this region is expected to increase to four as the two Zr centers are no longer symmetry related. The two C<sub>s</sub> symmetric isomers should each give rise to a set of two doublets in this region as the two Zr centers in each isomer



are still related by symmetry. While all of these species are observed in the crude reaction mixtures from **B.14** and **B.15**, the isomers of **B.15** could be separated and species with  $^1\text{H}$  NMR features consistent with  $C_1$  and  $C_s$  symmetry isolated in moderate purity. The  $C_s$  isomers could likely be distinguished based on comparison of their NOESY spectra; such experiments were not performed.

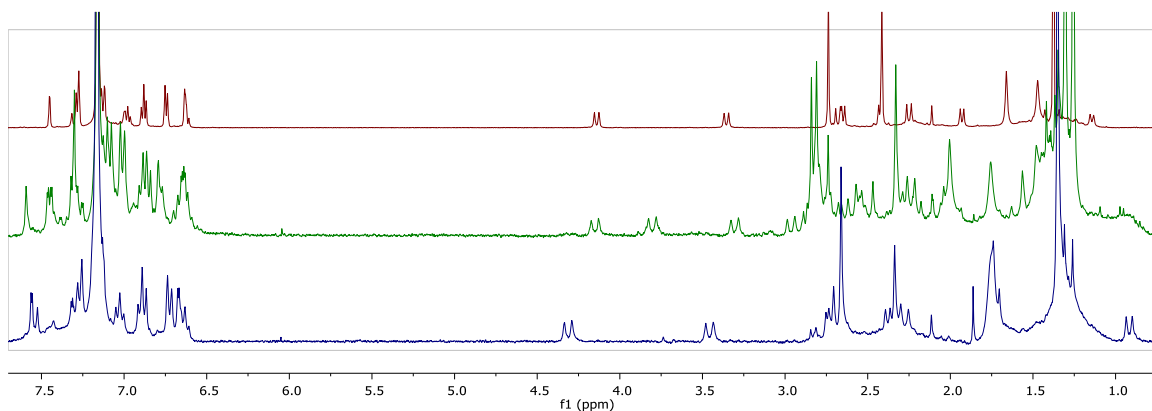


**Figure B.3.**  $^1\text{H}$  NMR spectra of (top to bottom) a  $C_2$  symmetric *para*-terphenyl supported dizirconium complex, the  $C_1$  isomer of **B.15**, and a  $C_s$  isomer of **B.15**.

One of the  $C_s$  symmetric complexes of **B.15** (spectrum 3, Figure B.3) was crystallographically characterized (Figure B.4). While the quality of the crystal was only sufficient to determine connectivity, this confirms the identity of the Zr complex as the  $C_s$  symmetric isomer with two  $\text{NMe}_2$  moieties positioned towards one another. The Zr-Zr distance in this complex is 8.03 Å, elongated from 7.62 Å in the parent  $\text{Zr}_2^{\text{Cl}_4}\text{-NMe}_2$  complex.<sup>7a</sup> In comparison with the other structurally-characterized  $C_s$  symmetric bimetallic complex,  $\text{Zr}_2^{\text{Me}_4}\text{-OMe}$ , the distance between the two *L* groups is greatly shortened from an O-O distance of 7.65 Å in the *para*-terphenyl complex to an N-N distance of 5.81 Å in the *meta*-terphenyl complex. Isolation of individual metalation isomers of **B.14** was not successful; furthermore, methods for clean isolation of single metalation isomers

of **B.15** could not be developed. Examination of the activity and stereoselectivity of these systems, through 1-hexene and propylene polymerization experiments, could provide insight into mechanisms of tacticity control in dizirconium catalysts.

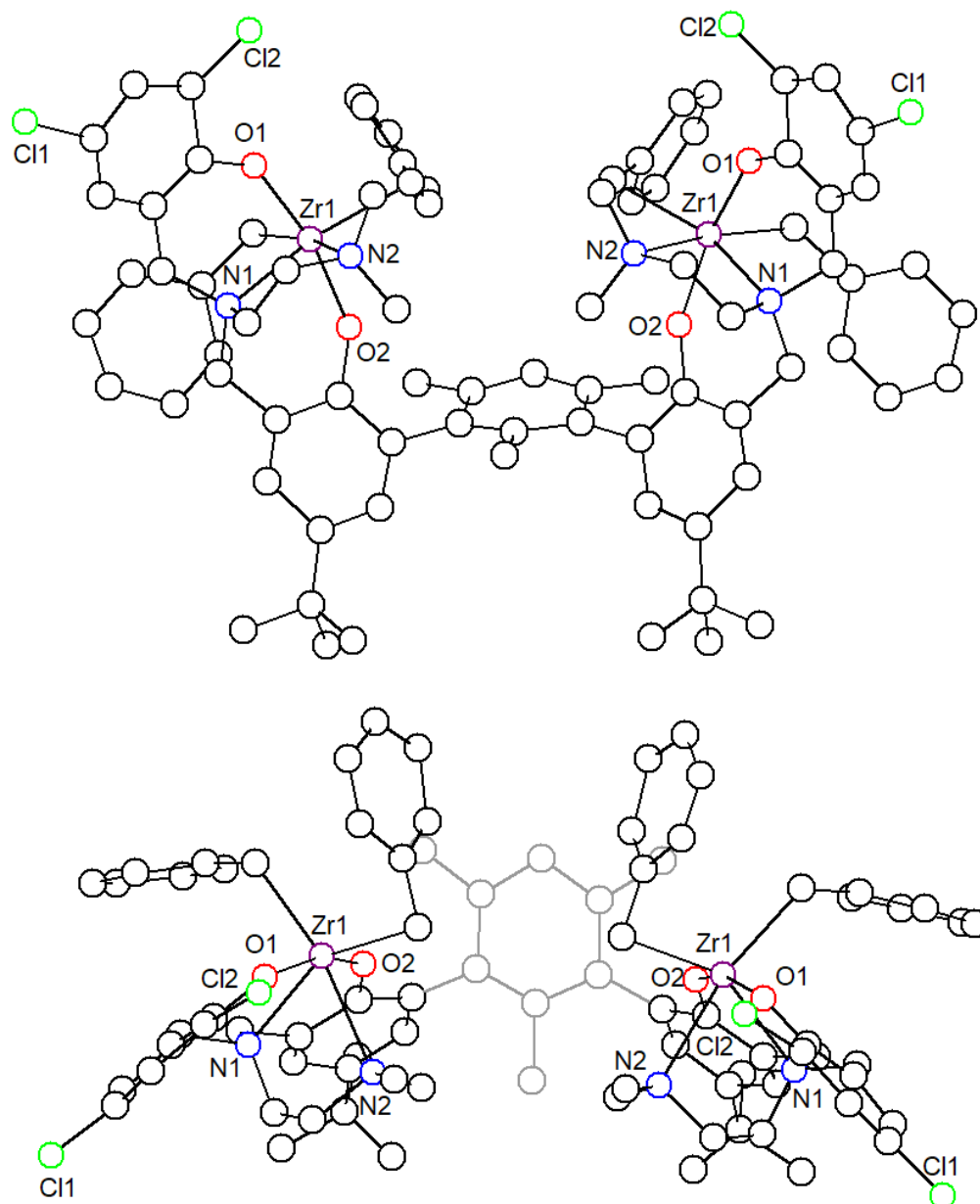


**Figure B.4.** Solid-state structure of one of the  $C_s$  isomers of **B.15**. The disordered pentane of crystallization and hydrogen atoms are omitted for clarity.

## DISCUSSION

This work on the expansion of the series of dizirconium amine bis(phenolate) precatalysts to these their activity and tacticity control in prochiral  $\alpha$ -olefin polymerization demonstrates one of the fundamental challenges with this ligand framework: that metalation isomers are generated and must be separated. The example of  $\text{anthZr}_2^{\text{SiPr}_3}\text{-NMe}_2$  demonstrates that, in at least that case, a majority of a single isomer can be generated directly from reaction with  $\text{ZrBn}_4$ . It is likely possible that a more expansive search of the chemical space using this ligand system could allow access to a more broad series of dizirconium precatalysts. Given the time invested in the studies presented in this thesis (Chapter 2, Appendices A and B) and the relatively few number of dizirconium complexes for which single isomers could be isolated, such a search was not undertaken. It is worth noting, however, that the ligand  $\text{H}_4^{\text{SiPr}_3}\text{-NEt}_2$  was prepared to test whether increasing the size could improve the relative ratios of  $C_s$  and  $C_2$  isomers and no changes were observed in the crude reaction mixtures in comparison with  $\text{H}_4^{\text{SiPr}_3}\text{-NMe}_2$ .

## CONCLUSIONS

In conclusion, a series of binucleating amine bis(phenolate) ligands based on central 9,10-anthracenyldiyl and *meta* terphenyl teraryl linkages and their corresponding dizirconium complexes were prepared. Crystals suitable for X-ray diffraction were obtained for a select few compounds and those structures were described in addition to a structure of a water decomposition product obtained on one of these ligands.

## EXPERIMENTAL SECTION

*General Notes.* All air- and water-sensitive compounds were manipulated under N<sub>2</sub> or Ar using standard Schlenk or glovebox techniques. Solvents for air- and moisture-sensitive reactions were dried by the method of Grubbs.<sup>10</sup> Chlorobenzene and 1-hexene for polymerization with stoichiometric activators were refluxed over CaH<sub>2</sub> for greater than 72 h, vacuum transferred, and run over activated alumina plugs prior to use. **B.1** and ZrBn<sub>4</sub> were prepared as described in Chapter 2 of this thesis. **B.2**,<sup>1</sup> **B.3**,<sup>1</sup> **B.8**,<sup>2</sup> and **B.11**<sup>3</sup> were prepared as previously described in the literature. Deuterated solvents were purchased from Cambridge Isotopes Lab, Inc.; CDCl<sub>3</sub> and 1,1,2,2-tetrachloroethane-d<sub>2</sub> were used without further purification; C<sub>6</sub>D<sub>6</sub> was distilled from purple Na/benzophenone ketyl and filtered over activated alumina prior to use. <sup>1</sup>H and <sup>13</sup>C spectra were recorded on Varian Mercury 300 or Varian INOVA-400 spectrometers. <sup>1</sup>H and <sup>13</sup>C chemical shifts are reported relative to residual solvent resonances.

**Preparation of B.4, B.7, and B.7-H<sub>2</sub>O.** A solution of **B.1** (161.6 mg, 0.245 mmol) in THF (9 mL) was added to a stirred solution of **B.2** (165 mg, 0.627 mmol) and NEt<sup>*i*</sup>Pr<sub>2</sub> (0.11 mL, 0.63 mmol) in THF (15 mL) at 0 °C. The reaction was stirred, warming, for 6 h, then an additional portion of **B.2** (48.8 mg, 0.185 mmol) and NEt<sup>*i*</sup>Pr<sub>2</sub> (0.1 mL, 0.6 mmol) were added and the reaction stirred until complete consumption of **B.1** was observed. Volatiles were removed under reduced pressure and the crude reaction mixture taken up in DCM and washed with K<sub>2</sub>CO<sub>3</sub>, water, and brine. Purification by column chromatography afforded **B.4**, which was dried under vacuum and lyophilized from benzene prior to metalation. A solution of **B.4** (52.7 mg, 0.0514 mmol) in toluene (2 mL) was added to a solution of ZrBn<sub>4</sub> (46.2 mg, 0.101 mmol) in toluene (1 mL) and stirred 3 h, dark. Volatiles were removed and the crude reaction mixture extracted with pentane,

ether, and benzene. X-ray quality crystals of **B.7-H<sub>2</sub>O** were grown upon standing of the pentane solution at room temperature. <sup>1</sup>H NMR (**B.4**, C<sub>6</sub>D<sub>6</sub>, 500 MHz) δ 10.08 (s, 4H, OH), 8.19 – 8.12 (m, 4H, anth), 7.39 (m, 4H, anth), 7.34 (d, *J* = 2.5 Hz, 2H, Ar), 7.29 (d, *J* = 2.5 Hz, 2H, Ar), 7.18 (d, *J* = 2.5 Hz, 2H, Ar), 6.72 (d, *J* = 2.5 Hz, 2H, Ar), 3.34 (s, 4H, ArCH<sub>2</sub>), 3.21 (s, 4H, ArCH<sub>2</sub>), 2.03 (t, *J* = 5.9 Hz, 4H, CH<sub>2</sub>), 1.78 (t, *J* = 5.9 Hz, 4H, CH<sub>2</sub>), 1.52 (s, 12H, NCH<sub>3</sub>), 1.35 (s, 18H, <sup>t</sup>Bu).

**Preparation of B.5.** A solution of **B.1** (1.1604 g, 1.757 mmol) in THF (40 mL) was added portionwise to a solution of **B.3** (0.981 mmol, 4.69 mmol) and NEt<sup>t</sup>Pr<sub>2</sub> (0.77 mmol, 4.4 mmol) in THF (100 mL) at 0 °C. The resulting solution was stirred, warming, for 3 h, then volatiles were removed under reduced pressure. The crude reaction mixture was taken up in DCM and washed with K<sub>2</sub>CO<sub>3</sub>, water, and brine, dried with MgSO<sub>4</sub>, filtered, and evaporated. Purification by column chromatography afforded the desired compound as a white solid (1.286 g, 1.402 mmol, 80 % yield). <sup>1</sup>H NMR (CDCl<sub>3</sub>, 300 MHz) δ 7.73 (m, 4H, anth), 7.49 – 7.30 (m, 6H, anth, Ar), 7.24 (d, *J* = 1.8 Hz, 2H, Ar), 6.87 (s, 2H, Ar), 6.74 (s, 2H, Ar), 3.95 (s, 4H, ArCH<sub>2</sub>), 3.88 (s, 4H, ArCH<sub>2</sub>), 3.61 (t, *J* = 5.3 Hz, 4H, CH<sub>2</sub>), 3.31 (s, 6H, OCH<sub>3</sub>), 2.84 (t, *J* = 5.5 Hz, 4H, ArCH<sub>2</sub>), 2.22 (s, 6H, ArCH<sub>3</sub>), 2.19 (s, 6H, ArCH<sub>3</sub>), 1.32 (s, 18H, <sup>t</sup>Bu).

**Preparation of B.6.** A solution of **B.5** (214.5 mg, 0.2339 mmol) in toluene (7 mL) was added to a solution of ZrBn<sub>4</sub> (212.7 mg, 0.4667 mmol) in toluene (4 mL) and stirred 2 h, dark. Volatiles were removed under reduced pressure, then resulting yellow solids washed with ether and extracted with benzene. X-ray quality crystals were grown from benzene/hexanes diffusion at room temperature.

**Preparation of B.9.** 2-methoxyethylamine (0.10 mL, 1.2 mmol) and **B.8** (237.2 mg, 0.4976 mmol) were combined in methanol (4 mL) and heated to 60 °C overnight.

Volatiles were removed under reduced pressure and the residue taken up in fresh methanol (4 mL). NaBH<sub>4</sub> (180.5 mg, 4.771 mmol) was added at once and the resulting solution stirred 8 h at room temperature. Volatiles were removed, the residue suspended in 2 M HCl, then the pH brought to 7-8 by addition of 1 M NaOH. The suspension was extracted thrice with DCM and the organics dried with MgSO<sub>4</sub>, filtered, and evaporated to afford the desired compound (273 mg, 0.462 mmol, 93 %). <sup>1</sup>H NMR (CDCl<sub>3</sub>, 500 MHz) δ 7.10 (s, 1H, central Ar), 7.07 (d, *J* = 2.4 Hz, 2H, Ar), 6.99 (d, *J* = 2.4 Hz, 2H, Ar), 4.08 (d, *J* = 13.6 Hz, 2H, ArCH<sub>2</sub>), 3.99 (d, *J* = 13.7 Hz, 2H, ArCH<sub>2</sub>), 3.51 (t, *J* = 5.0 Hz, 4H, CH<sub>2</sub>), 3.36 (s, 6H, OCH<sub>3</sub>), 2.83 (t, *J* = 5.0 Hz, 4H, CH<sub>2</sub>), 2.08 (s, 6H, ArCH<sub>3</sub>), 1.82 (s, 3H, ArCH<sub>3</sub>), 1.30 (s, 18H, <sup>t</sup>Bu). <sup>13</sup>C NMR (126 MHz, CDCl<sub>3</sub>) δ 152.57, 141.44, 136.24, 136.03, 135.71, 128.58, 128.18, 127.34, 123.96, 121.71, 71.22, 58.94, 52.88, 48.09, 34.17 (<sup>t</sup>Bu), 31.78 (<sup>t</sup>Bu), 20.79 (ArCH<sub>3</sub>), 18.35 (ArCH<sub>3</sub>).

**Preparation of B.10.** Using the method described for the preparation of **B.9**, **B.10** (243.8 mg, 0.5115 mmol) and N,N-dimethylethylenediamine (0.12 mL, 1.1 mmol) were combined and then NaBH<sub>4</sub> (157.9 mg, 4.174 mmol) added to afford the desired product (309 mg, 0.501 mmol, 98 %). <sup>1</sup>H NMR (500 MHz, CDCl<sub>3</sub>) δ 7.09 (s, 1H, central Ar), 7.05 (d, *J* = 2.4 Hz, 2H, Ar), 6.99 (d, *J* = 2.3 Hz, 2H, Ar), 4.08 (d, *J* = 13.6 Hz, 2H, ArCH<sub>2</sub>), 3.98 (d, *J* = 13.6 Hz, 2H, ArCH<sub>2</sub>), 2.72 (t, *J* = 6.0 Hz, 4H, CH<sub>2</sub>), 2.43 (t, *J* = 5.9 Hz, 4H, CH<sub>2</sub>), 2.21 (s, 12H, N(CH<sub>3</sub>)<sub>2</sub>), 2.07 (s, 6H, ArCH<sub>3</sub>), 1.80 (s, 3H, ArCH<sub>3</sub>), 1.29 (s, 18H, <sup>t</sup>Bu). <sup>13</sup>C NMR (126 MHz, CDCl<sub>3</sub>) δ 152.61, 141.37, 136.27, 136.07, 135.75, 128.57, 128.13, 127.27, 123.94, 121.85, 58.30 (CH<sub>2</sub>), 52.96 (ArCH<sub>2</sub>), 45.96 (CH<sub>2</sub>), 45.55 (N(CH<sub>3</sub>)<sub>2</sub>), 34.16 (<sup>t</sup>Bu), 31.79 (<sup>t</sup>Bu), 20.78 (ArCH<sub>3</sub>), 18.34 (ArCH<sub>3</sub>).

**Preparation of B.12.** A solution of **B.11** (317.4 mg, 1.240 mmol) in THF (15 mL) was added to a solution of **B.10** (298.8 mg, 0.4738 mmol) and NEt<sub>3</sub> (0.17 mL, 1.2

mmol) in THF (28 mL) at 0 °C and stirred 3h, warming. Volatiles were removed under reduced pressure and the resulting solids taken up in DCM and hexanes, washed with brine and K<sub>2</sub>CO<sub>3</sub>, dried with MgSO<sub>4</sub>, filtered, and evaporated. Purification by column chromatography (10 % MeOH in DCM) afforded the desired compound (94.7 mg, 0.0979 mmol, 21 %). <sup>1</sup>H NMR (300 MHz, CDCl<sub>3</sub>) δ 7.24 (d, *J* = 2.5 Hz, 2H, Ar), 7.10 (s, 1H, central Ar), 7.02 (s, 4H, Ar), 6.95 (d, *J* = 2.5 Hz, 2H, Ar), 3.70 (s, 4H, ArCH<sub>2</sub>), 3.66 (s, 4H, ArCH<sub>2</sub>), 2.66 (t, *J* = 5.7 Hz, 4H, CH<sub>2</sub>), 2.56 (t, *J* = 5.3 Hz, 4H, CH<sub>2</sub>), 2.22 (s, 12H, N(CH<sub>3</sub>)<sub>2</sub>), 2.02 (s, 6H, ArCH<sub>3</sub>), 1.66 (s, 3H, ArCH<sub>3</sub>), 1.26 (s, 18H, <sup>t</sup>Bu).

**Preparation of B.14.** A solution of **B.12** (51.2 mg, 0.0529 mmol) in toluene (1.5 mL) was added to a solution of ZrBn<sub>4</sub> (48.3 mg, 0.106 mmol) and stirred 3 h, dark. Volatiles were removed under reduced pressure and the crude reaction mixture fractionated between hexanes, ether, and benzene. X-ray quality crystals of one of the C<sub>s</sub> isomers were obtained by diffusion of pentane into a toluene solution of the benzene fraction at -35 °C.

**Crystallographic Information.** Crystals were mounted on a glass fiber or MiTeGen loop using Paratone oil, then placed on the diffractometer under a nitrogen stream. Diffractometer manipulations, including data collection, integration, and scaling were performed using the Bruker APEXII software.<sup>4</sup> Absorption corrections were applied using SADABS or TWINABS.<sup>5</sup> Space groups were determined on the basis of systematic absences and intensity statistics and the structures were solved in the Olex 2 software interface<sup>6</sup> by intrinsic phasing using XT (incorporated into SHELXTL)<sup>7</sup> and refined by full-matrix least squares on F<sup>2</sup>. Hydrogen atoms were placed in the idealized positions and refined using a riding model. Graphical representation of structures were generated using Diamond 3 visualization software.<sup>8</sup> Due to partial data collections and poor-quality



crystals, only isotropic refinements were performed for all structures. A second molecule of the dizirconium complex is believed to be located in the asymmetric unit of **C.8**; however, due to significant disorder, this could not be satisfactorily modeled.

**Table B.1.** Crystal and refinement data for **B.6**, **B.7**, and **B.14**

	<b>B.6</b>	<b>B.7</b>	<b>B.14</b>
CCDC Number			
Empirical formula	<sup>c</sup>	C <sub>116</sub> H <sub>130</sub> Cl <sub>8</sub> N <sub>8</sub> O <sub>16</sub> Zr <sub>4</sub>	C <sub>81</sub> H <sub>92</sub> Cl <sub>4</sub> N <sub>4</sub> O <sub>4</sub> Zr <sub>2</sub>
Formula weight	<sup>c</sup>	2540.75	1509.83
T (K)	100	100	100
a, Å	16.5204(9)	13.6427(13)	24.302(7)
b, Å	21.4923(12)	16.440(3)	25.361(9)
c, Å	29.3423(19)	17.997(2)	15.150(6)
α, °	90	64.978(5)	90
β, °	100.434(4)	87.227(6)	90
γ, °	90	72.335(6)	90
Volume, Å <sup>3</sup>	10246.0(10)	3470.1(8)	9337(5)
Z	4	1	4
Crystal system	Monoclinic	Triclinic	Orthorhombic
Space group	P 2 <sub>1</sub>	P -1	Pnma
d <sub>calc</sub> , g/cm <sup>3</sup>	<sup>c</sup>	1.216	1.074
θ range, °	2.563 to 70.184	2.279 to 33.083	2.262 to 28.700
μ, mm <sup>-1</sup>	0.99	0.501	0.38
Abs. Correction	Multi-scan	None	None
GOF	2.121	1.083	1.022
R <sub>1</sub> , <sup>a</sup> wR <sub>2</sub> <sup>b</sup> [I>2 σ(I)]	0.2734, 0.6228	0.0715, 0.1744	0.1504, 0.4054
Radiation Type	Cu Kα	Mo Kα	Mo Kα

<sup>a</sup>  $R_1 = \sum ||F_o| - |F_c|| / \sum |F_o|$ . <sup>b</sup>  $wR_2 = [\sum [w(F_o^2 - F_c^2)^2] / \sum [w(F_o^2)^2]]^{1/2}$ . <sup>c</sup> Electron density peaks consistent with another molecule, likely a second molecule of the dizirconium complex, were observed but could not be fully modeled

## REFERENCES

1. Radlauer, M. R.; Agapie, T. *Organometallics* **2014**, *33* (13), 3247-3250.
2. Radlauer, M. R.; Buckley, A. K.; Henling, L. M.; Agapie, T. *J. Am. Chem. Soc.* **2013**, *135* (10), 3784-3787.
3. Gendler, S.; Zelikoff, A. L.; Kopilov, J.; Goldberg, I.; Kol, M. *J. Am. Chem. Soc.* **2008**, *130* (7), 2144-2145.
4. APEX2, Version 2 User Manual, M86-E01078, Bruker Analytical X-ray Systems, Madison, WI, June 2006.
5. Sheldrick, G.M. "SADABS (version 2008/1): Program for Absorption Correction for Data from Area Detector Frames", University of Gottingen, 2008.
6. Dolomanov, O. V.; Bourhis, L. J.; Gildea, R. J.; Howard, J. A. K.; Puschmann, H. *J. Appl. Crystallogr.* **2009**, *42* (2), 339-341.
7. Sheldrick, G. M. *Acta Cryst.* **2008**, *A64*, 112-122.
8. Brandenburg, K. (1999), DIAMOND. Crystal Impact GdR, Bonn, Germany.

## **APPENDIX C**

### **COORDINATION CHEMISTRY AND INTRAMOLECULAR $\pi$ - $\pi$ INTERACTIONS IN DI(PYRIDYL) NHC IRON COMPLEXES**

**ABSTRACT**

A series of mono- and bisligated Fe complexes supported by mesityl and 9-anthracenyl-substituted di(pyridyl) pyrrolide and di(pyridyl) N-heterocyclic carbene (NHC) ligands were synthesized and structurally-characterized. In the solid state the bisligated complexes display  $\pi$ - $\pi$  interactions between the mesityl and anthracenyl substituents and the backbone of the other ligand with long Fe-Py and short Fe-pyrrolide and Fe-NHC distances. The bisligated complexes were investigated electrochemically; stoichiometric reduction of one of the di(pyridyl) NHC complexes with  $\text{Cp}_2\text{Co}$  or  $\text{Cp}^*_2\text{Co}$  was found to lead to formation of a neutral complex with dissociation of two pyridine arms. Preliminary Mössbauer studies were performed on both oxidized and reduced complexes, however, the oxidation states of the compounds could not be assigned from these studies as multiple species were observed.

## INTRODUCTION

Linear iron complexes supported by two strong *trans* ligands have received attention in the literature as single-molecule magnets and for their small molecule reactivity.<sup>1</sup> The magnetism of Fe(II) and Fe(I) complexes supported by amide (**C.A**),<sup>2</sup> alkyl (**C.B**),<sup>2d, 3</sup> anilide (**C.C**),<sup>2c</sup> and phenolate (**C.D**)<sup>2c</sup> ligands have all been investigated and computational studies of their properties have indicated contributions to the overall Fe electronic structure from the symmetry of the supporting ligands, favoring those with local *pseudo*  $C_{2v}$  and  $C_{3v}$  symmetry.<sup>4</sup>

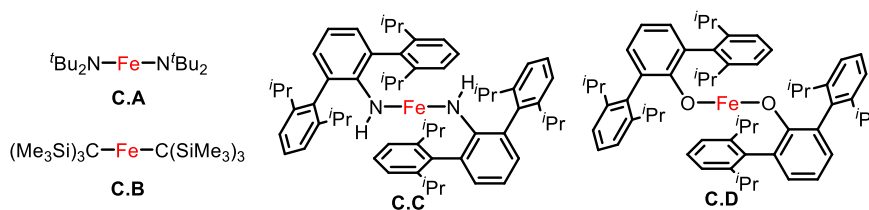
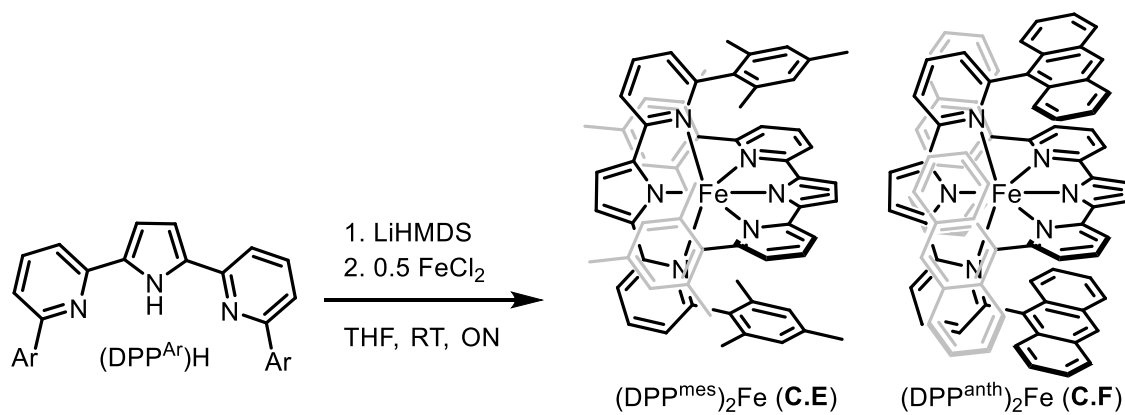
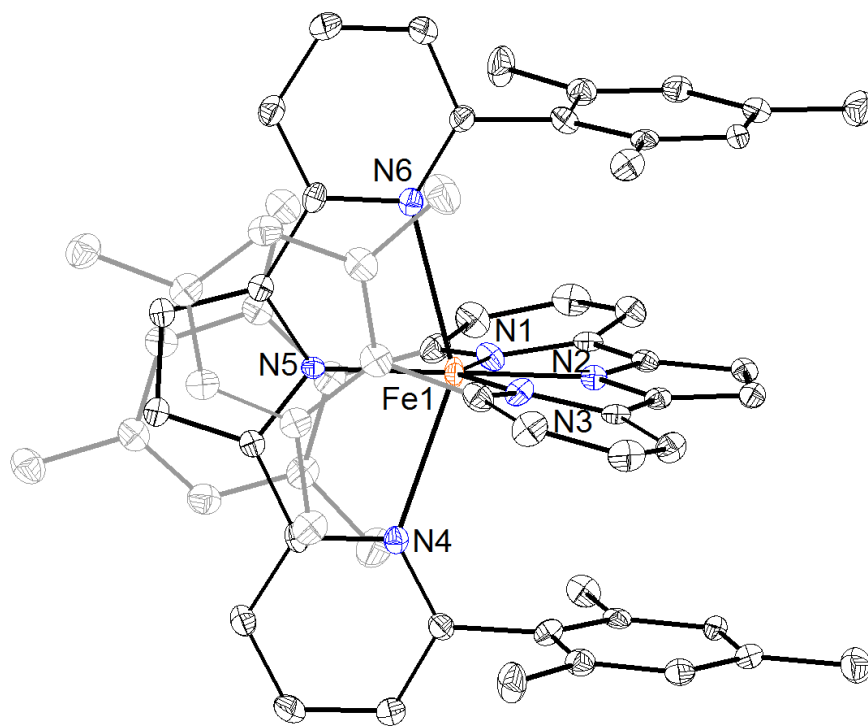


**Figure C.1.** Examples of two-coordinate Fe complexes.

Initial work by Dr. Gyeongshin Choi demonstrated that the homologated DPP Fe(II) complexes could be prepared by salt metathesis of the lithium salts of the mesityl- and anthracenyl-substituted DPP proligands with  $\text{FeCl}_2$  in THF at room temperature (Scheme C.1). The resulting red complexes were crystallographically characterized and exhibit long Fe-N(Py) distances of 2.46 and 2.47 Å with shorter Fe-N(pyrrolide) distances of 1.94 and 1.95 Å for complexes **C.E** and **C.F** respectively. Distances of 3.30 to 3.41 Å are observed between the planes of the mesityl substituents of **C.E** and the centroids of the pyrrolide donor on the other ligands. Distances of 3.34 to 3.43 Å are observed between the centroid of the pyrrolide donors and the plane of the anthracene substituents in **C.F**. N(pyr)-Fe-N(pyr') angles of 180 ° are observed for both complexes.



**Scheme C.1.** Preparation of homologated Fe(II) di(pyridyl) pyrrolide complexes as developed by Dr. Gyeongshin Choi.



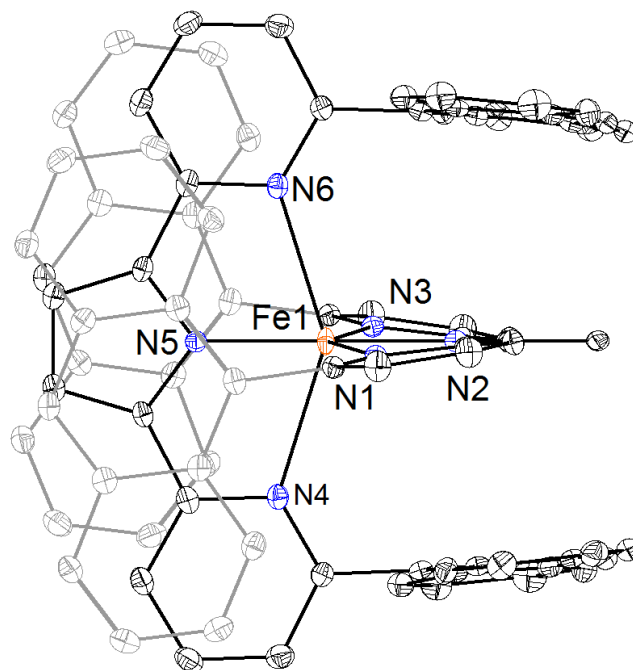


**Figure C.2.** Solid state structures of **C.E** (top) and **C.F** (bottom). Hydrogen atoms are omitted for clarity. Images generated by Jessica Sampson.

It was hypothesized that these ligands and the related di(pyridyl) NHC ligands could support homoligated Fe complexes which could act as single molecule magnets. In such complexes, if *pseudo*-two-coordinate structures are generated, the long, weak Fe-N(Py) interactions could help to prevent Fe coordination to additional donors, prevent distortion away from linearity, and improve the overall stability of organometallic single-molecule magnets towards water and oxygen. Furthermore, by substituting the pyridine donors with mesityl or 9-anthracenyl substituents,  $\pi$ - $\pi$  interactions between these substituents and the backbone of the other ligand could help to stabilize the reduced complexes.

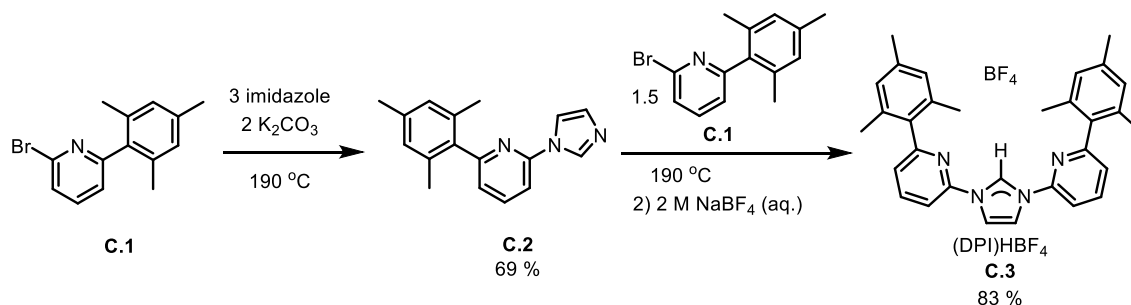
Herein is described work on the synthesis of mono- and bisligated di(pyridyl) NHC Fe complexes, their electrochemistry, and the preparation of a reduced bisligated



di(pyridyl) NHC Fe complex which shows dissociation of two pyridine arms in the solid state.

## RESULTS

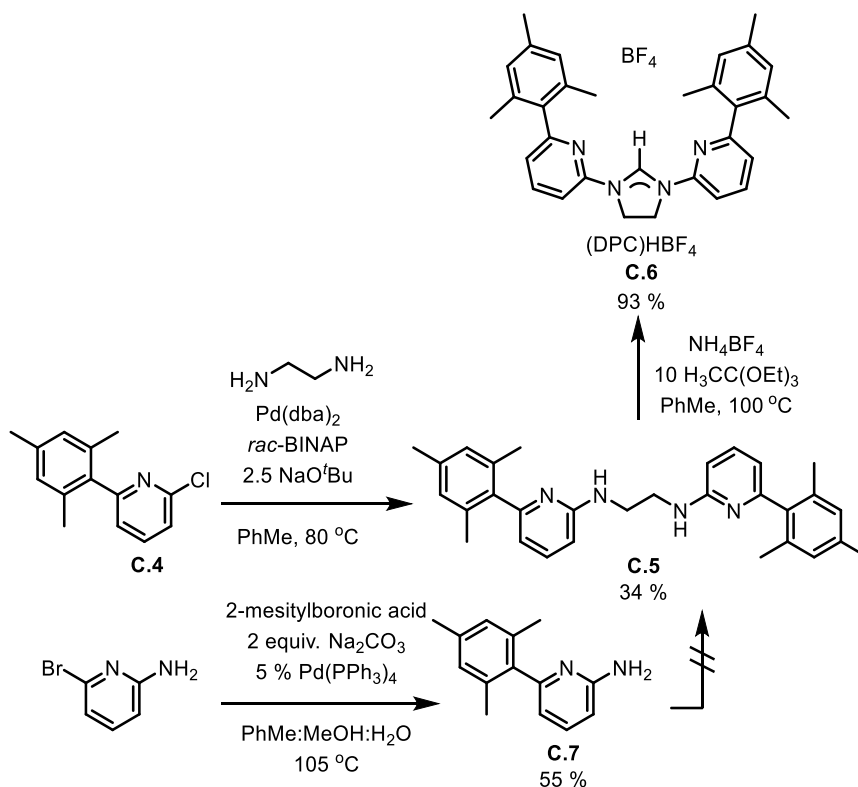
Dipyridyl imidazolium proligands were prepared according to the method reported by Kühn and coworkers (Scheme C.2).<sup>5</sup> Neat reaction of substituted 2-bromo-6-mesitylpyridine **C.1** with excess imidazole in the presence of  $K_2CO_3$  at elevated temperature results in formation of the corresponding N-substituted imidazole **C.2**. Subsequent reaction with a second equivalent of the substituted pyridine affords the imidazolium proligand, **C.3**, which was isolated as the tetrafluoroborate salt (DPI)HBF<sub>4</sub> by anion exchange with aqueous 2M NaBF<sub>4</sub>. Synthesis of **C.3** directly from **C.1** without isolation of **C.2** was not pursued due to poor conversion of **C.1** in initial tests.



**Scheme C.2.** Synthesis of di(pyridyl) NHC proligand **C.3**.

The imidazolinium-derived ligand (DPC)HBF<sub>4</sub> (**C.6**) was prepared as shown in Scheme C.3. Pd-catalyzed Buchwald-Hartwig coupling of either 2-chloro-6-mesitylpyridine (**C.4**) with ethylenediamine to afford the N,N'-diamine substituted product **C.5** in 34 % yield from the 2-chloro pyridine (lower yields were obtained from 2-bromo-6-mesitylpyridine). Efforts to identify the causes of the low yield of this reaction or to find better Pd-catalyzed conditions were unsuccessful. Use of 2-amino-6-mesitylpyridine (**C.7**) as the ligand precursor was also investigated, however, this was found not to react with 1,2-dibromoethane and reaction with oxalyl chloride only afforded the

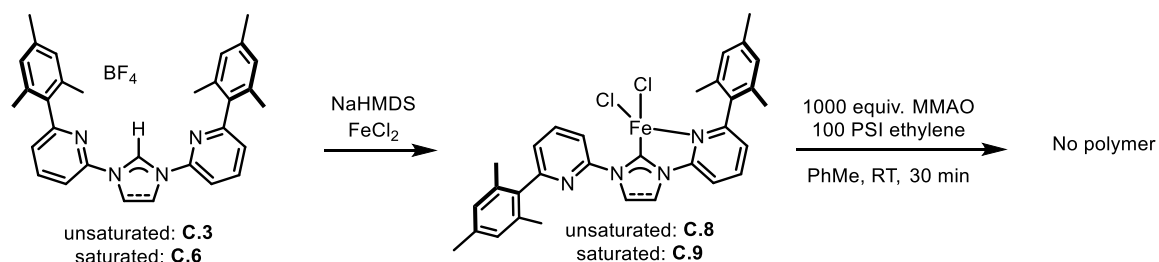
corresponding amide in low yields, so this route was not pursued. Cyclization of **C.5** with triethylorthoformate in the presence of stoichiometric  $\text{NH}_4\text{BF}_4$  affords the imidazoline salt  $(\text{DPC})\text{HBF}_4$ , **C.6**, following precipitation with dry ether.



**Scheme C.3.** Routes pursued for the synthesis of  $(\text{DPC})\text{HBF}_4$  (**C.6**).

Monoligated  $\text{FeCl}_2$  complexes of the DPI and DPC ligands could be generated by reaction of the  $\text{HBF}_4$  salts with 1:1 mixtures of  $\text{FeCl}_2$  and  $\text{NaHMDS}$  (Scheme C.4), per previous reports by Byers and coworkers on the synthesis of bis(imino)carbene-ligated Fe complexes.<sup>6</sup> Paramagnetically-shifted  $^1\text{H}$  NMR features are observed for both complexes and crystals suitable for X-Ray diffraction were grown from benzene and feature *pseudo*-tetrahedral four-coordinate Fe centers coordinated in an  $\kappa^2$  fashion to the NHC and one pyridine arm (Figures C.3 and C.4). Similar Fe-Cl bond lengths, in the

range of 2.24 to 2.26 Å, are observed in both structures, with Fe-C(1) and Fe-N(1) distances of 2.1188(16) and 2.1261(13) Å for **4.7** and 2.1024(23) and 2.1502(17) Å for **4.6**. The other ligand pyridine arms are rotated away from the Fe center leading to long Fe-N(4) distances of 5.066 and 5.096 Å for **4.7** and **4.6** respectively. The complexes were tested as precatalysts for ethylene polymerization in the presence of MMAO, however, no activity was observed.



**Scheme C.4.** Synthesis of mono-ligated Fe(II) dichloride complexes **C.8** and **C.9**.

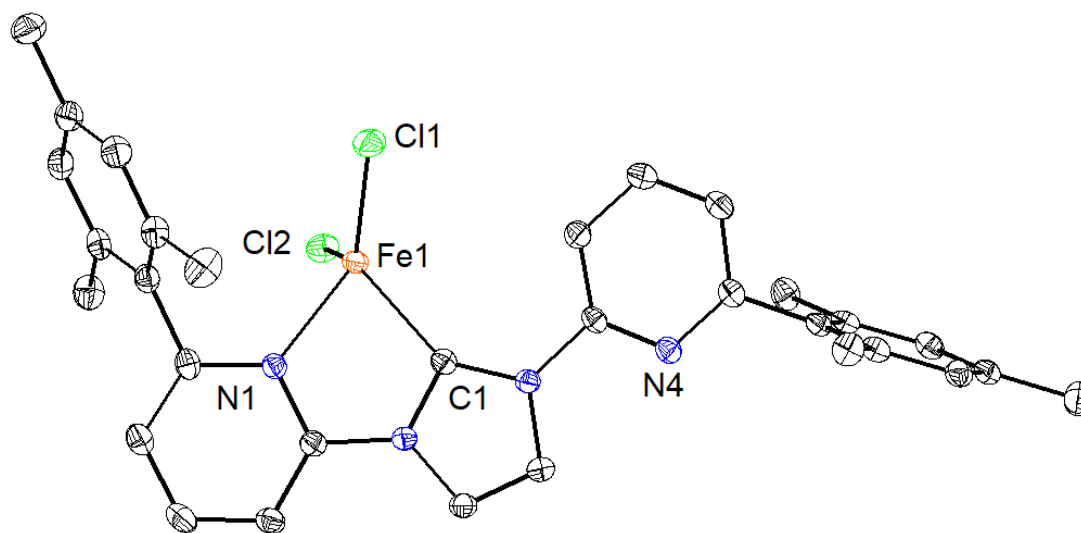


**Figure C.3.** Solid-state structure of **C.8**. Hydrogen atoms are omitted for clarity.

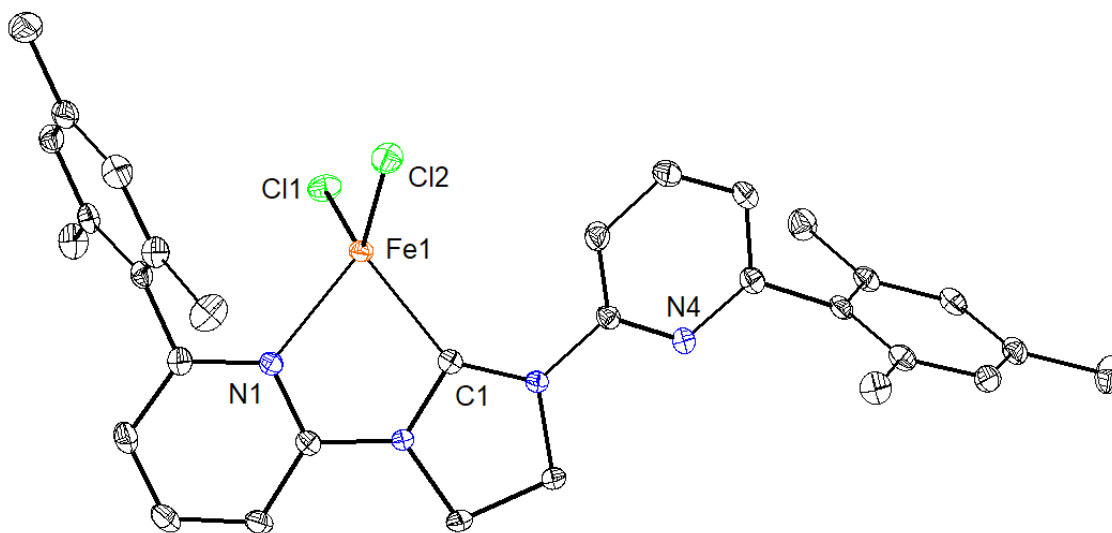
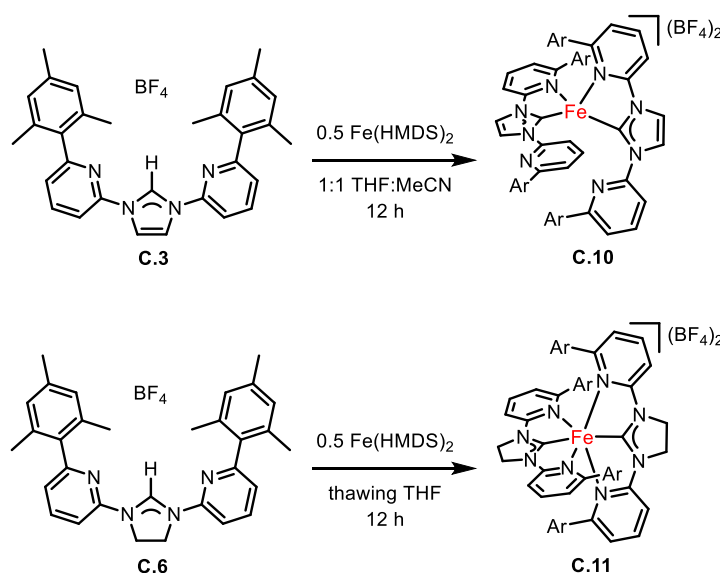


**Figure C.4.** Solid-state structure of **C.9**. Hydrogen atoms are omitted for clarity.

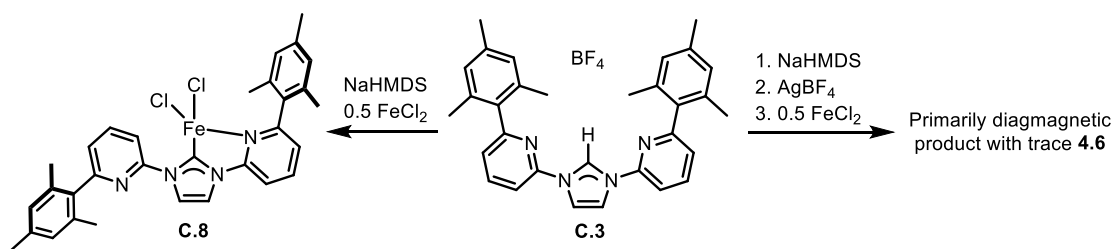
Homo-ligated dipyridyl imidazoline and imidazolidine Fe complexes were initially synthesized by reaction of two equivalents of the  $\text{HBF}_4$  salts of the proligands with one equivalent of  $\text{Fe}(\text{N}(\text{SiMe}_3)_2)_2$  in THF at room temperature (Scheme C.5). Filtration of the crude reaction mixture and extraction of the resulting yellow-brown solids with acetonitrile afforded the crude compounds which could be further purified by recrystallization from acetonitrile-ether, though unreacted proligand could not be removed by this protocol due to similar solubility. Furthermore, decomposition of **C.10** to the corresponding proligand **C.3** was observed under crystallization conditions.



**Scheme C.5.** Synthesis of homoligated DPC and DPI Fe complexes from the corresponding protonated proligands.

As a result of the similar solubility of **C.3** and **C.10**, decomposition of **C.10** under crystallization conditions, and the typically low conversion of **C.3** to **C.10** when reactions were run in THF, other routes to **C.10** were explored (Scheme C.6). Use of  $\text{CD}_3\text{CN}$  as the reaction solvent results in formation of the desired compound, however, unreacted **C.3** is observed even after 17h at room temperature, likely due to background reactivity of the  $\text{Fe(HMDS)}_2$  with acetonitrile. Performing the reaction in a 1:1 mixture of acetonitrile and THF with a slight subcess of proligand, however, allowed for complete proligand consumption, though decomposition to the proligand **C.3** is still observed upon crystallization. In contrast, reaction of two equivalents of **C.3** with two equivalents of NaHMDS in THF followed by addition of this mixture to a suspension of  $\text{FeCl}_2$  results in formation of a THF-soluble species with sharp, paramagnetically-shifted  $^1\text{H}$  NMR inconsistent with formation of the desired homoligated complex but consistent with formation of **C.8**. Reaction of an *in situ* generated Ag(I) complex with  $\text{FeCl}_2$  resulted in a

crude reaction mixture that contained only trace paramagnetically-shifted peaks with resonances more consistent with formation of **C.8**.



**Scheme C.6.** Other routes explored for the synthesis of **C.10**.

Crystals suitable for X-Ray diffraction were grown of **C.10** and **C.11** via slow vapor diffusion of ether into acetonitrile (Figures 4.5 and 4.6). In the solid state **C.11** features a six-coordinate Fe center coordinated to all donors of the two tridentate ligands. Short Fe-C distances of 1.8466(1) and 1.8432(1) Å are observed with a C(1A)-Fe-C(1B) angle of 178 °. Shorter Fe-N(Py) distances of 2.21 to 2.24 Å are observed in comparison with the corresponding DPP-ligated complex. Distances in the range of 3.4 to 3.5 Å are observed between the centroids of the mesityl substituents and the plane of the other ligand, within the sum of the van der Waals radii.<sup>7</sup> In contrast with **C.11**, a distorted trigonal pyramidal four-coordinate Fe center is observed in the X-ray structure of **C.10** with a calculated  $\tau_4$  value of 0.83 with coordination to both NHC donors, one pyridine donor of each ligand, a long Fe-N interaction with a pyridine donor of one ligand, and rotation of the final pyridine arm away from Fe. Fe-C distances of 2.0041(1) and 2.0422(1) Å are observed with Fe-N distances of 2.1456(2) and 2.1277(1) Å to the bound donors. Distances of 3.40 and 3.47 Å are observed between the mesityl substituents and the plane of the other ligand.

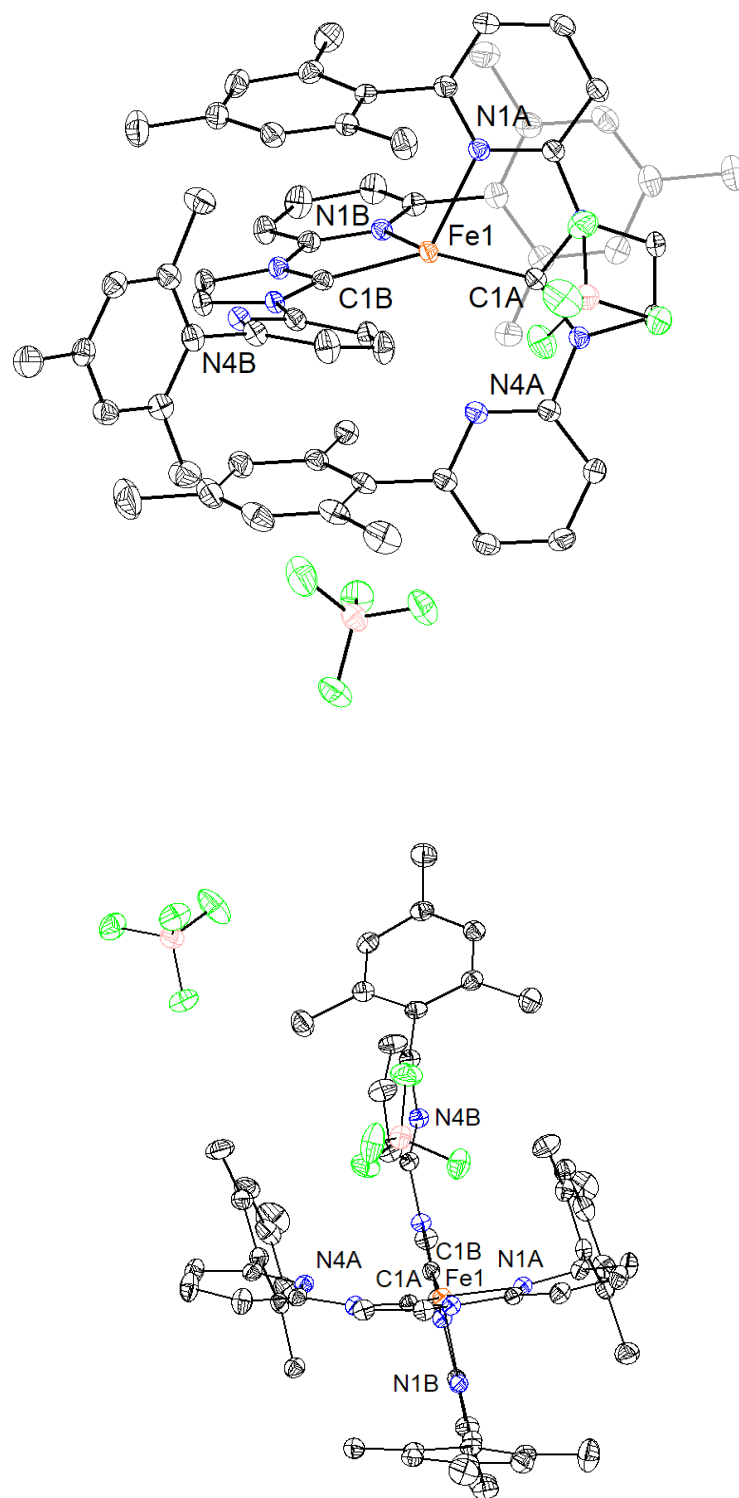


**Figure C.5.** Solid-state structure of **C.10**. Hydrogen atoms, BF<sub>4</sub> counteranions, and solvents of crystallization are omitted for clarity.



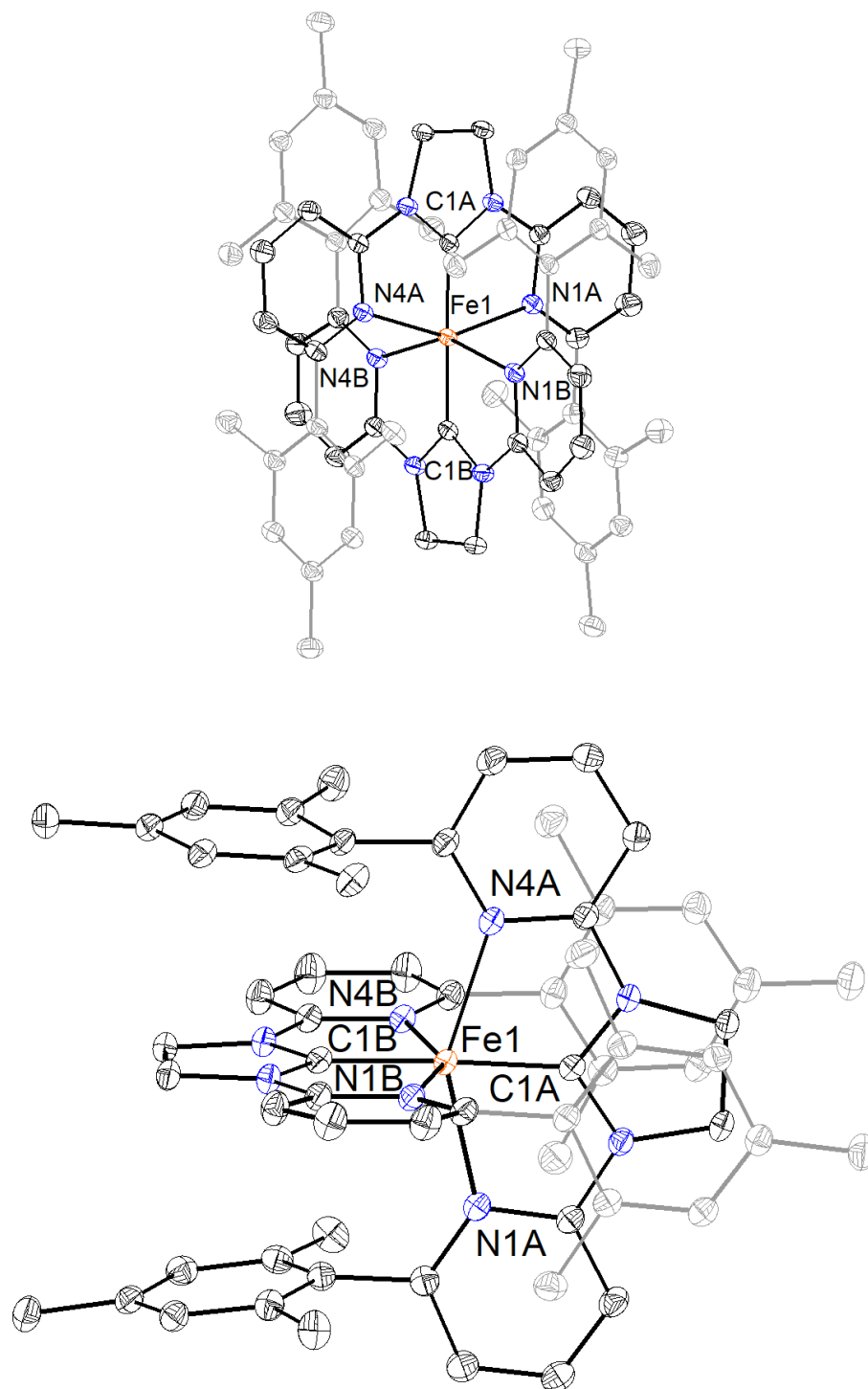


**Figure C.6.** Solid-state structure of **C.11**. Hydrogen atoms, BF<sub>4</sub> counteranions, and solvents of crystallization are omitted for clarity.

Cyclic voltammetry studies of **C.10** and **C.11** in acetonitrile were performed in order to assess its available reduced states (Figures C.7 and C.8). **C.11** shows a quasi-reversible oxidation with an  $E_{1/2}$  of 1.3 V vs.  $\text{Fc}/\text{Fc}^+$ , one irreversible reduction at -1 V, and an additional reduction event at -1.5 V. **C.10** shows a reversible oxidation with an  $E_{1/2}$  of -1.19 V and a reversible reduction with an  $E_{1/2}$  of -2.48 V. An additional irreversible reduction is observed with a maximum current at -1.86 V, scanning oxidatively. Following this reduction, additional events are observed near -0.5 V.

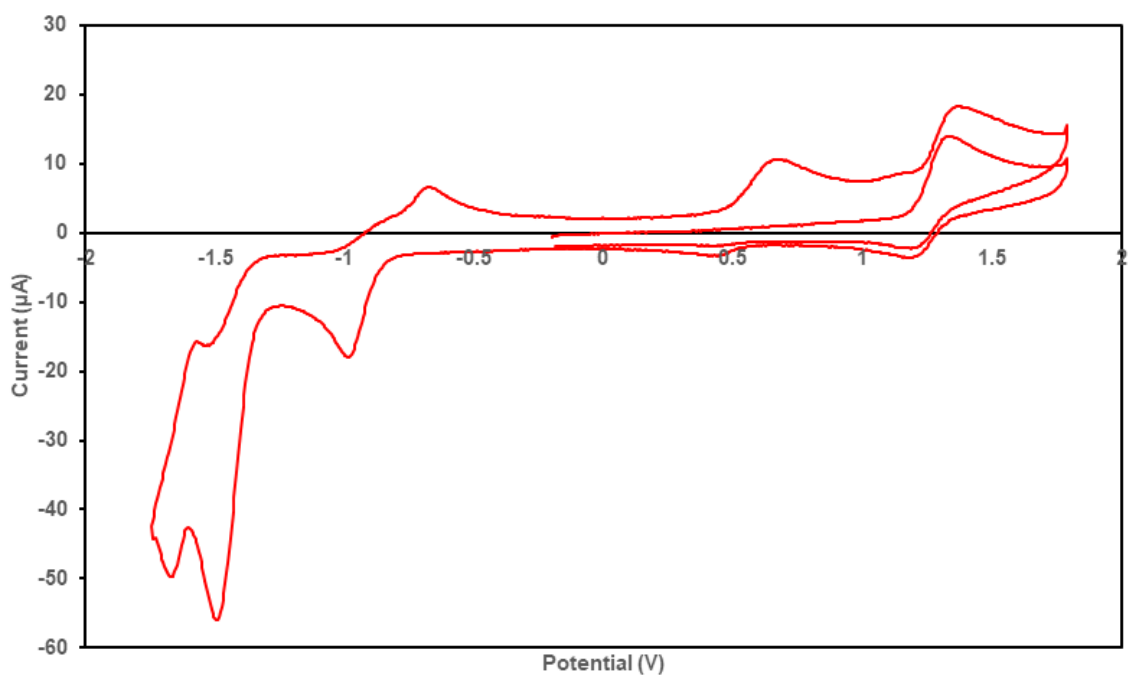


**Figure C.7.** CV of **C.11** in acetonitrile. Conditions: 0.2 mM substrate, 0.1 M  $\text{TBAPF}_6$ , 100 mV/s.

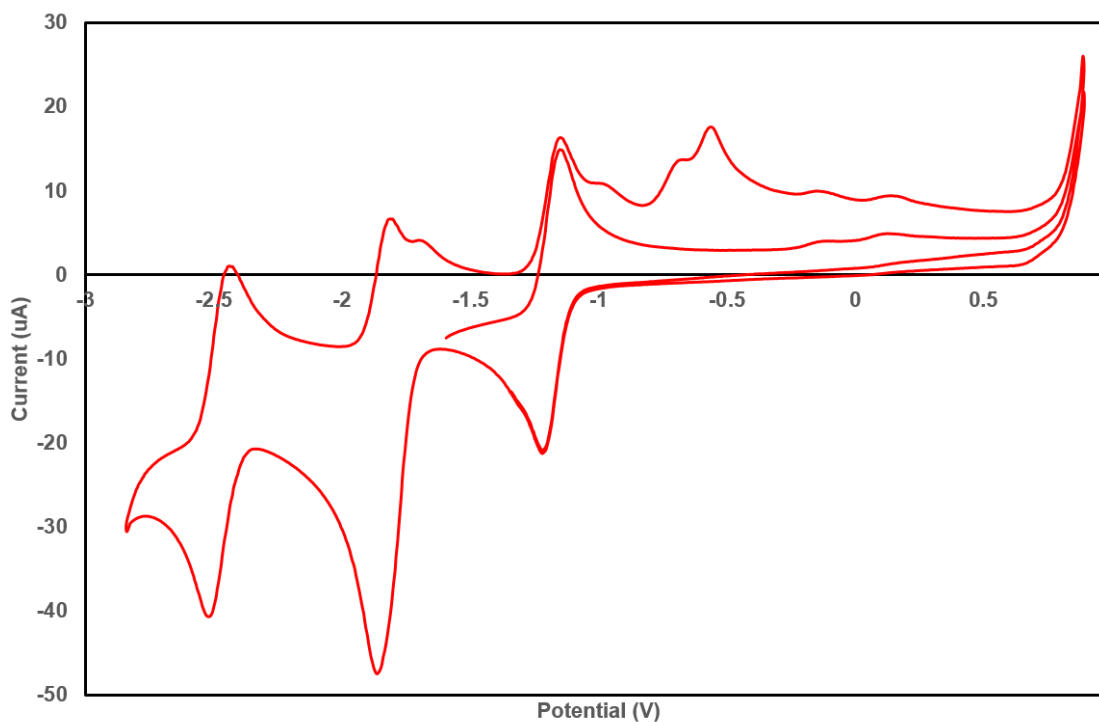
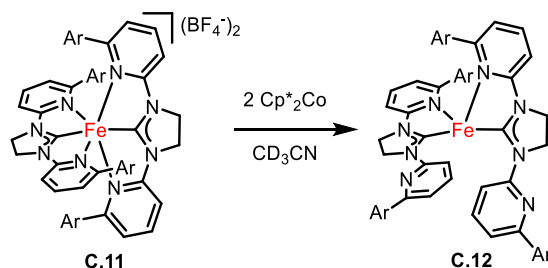


**Figure C.8.** CV of **C.10** in acetonitrile. Conditions: 0.2 mM substrate, 0.1 M TBAPF<sub>6</sub>, 100 mV/s.

Stoichiometric reduction studies were performed to access the first reduced species from **C.11**. By <sup>1</sup>H NMR, treatment of **C.11** with one equivalent of Cp\*<sub>2</sub>Co results in partial conversion to a new species with a larger number of paramagnetically-shifted <sup>1</sup>H NMR resonances. Full conversion is observed upon treatment with two equivalents of the reductant, which was identified crystallographically as the neutral complex **C.12** (Scheme C.7 and Figure 4.6). While the structure is of somewhat low quality, **C.12** features a four-coordinate trigonal pyramidal Fe center with a  $\tau_4$  value of 0.82. Fe(1) is coordinated to two carbene donors with an C(1A)-Fe(1)-C(1B) angle of 153° and two pyridine donors with an N(1A)-Fe(1)-N(1B) angle of 114°. Both free pyridine groups are rotated away from the Fe center and no close Fe-N contacts are observed, unlike in the solid-state

structure of **C.10**. Some elongation of the C-C bonds in the pyridine donors is observed, suggesting that this reduction occurs, at least in part, on the ligand. Distances of 3.39 and 3.49 Å are observed between the centroids of the mesityl substituents and the plane of the other ligand backbone. Initial Mössbauer studies were performed on both **C.11** and **C.12** with help from Chris Reed and Matt Chalkley, however, multiple signals were observed for both compounds as prepared. For **C.11** a crystalline sample was re-dissolved and volatiles removed prior to spectrum acquisition, so isomerization between the crystallographically-characterized 6-coordinate species and a 5- or 4-coordinate species in solution is a possible explanation for the multiple signals. For **C.12** it was hypothesized that sample oxidation occurred during preparation.



**Scheme C.7.** Stoichiometric reduction of **C.11** in CD<sub>3</sub>CN

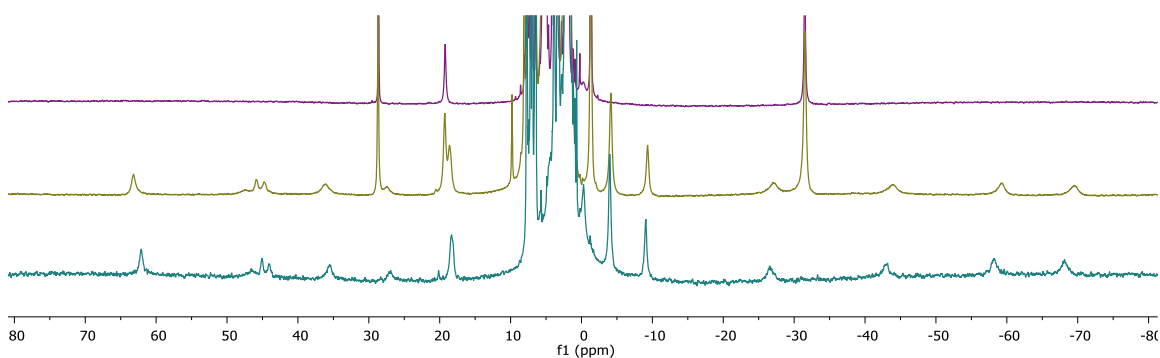


**Figure C.9.** Reduction of **C.11** with (top to bottom) 0 equiv. Cp\*<sub>2</sub>Co, 1 equiv. Cp\*<sub>2</sub>Co, and 2 equiv. Cp\*<sub>2</sub>Co.

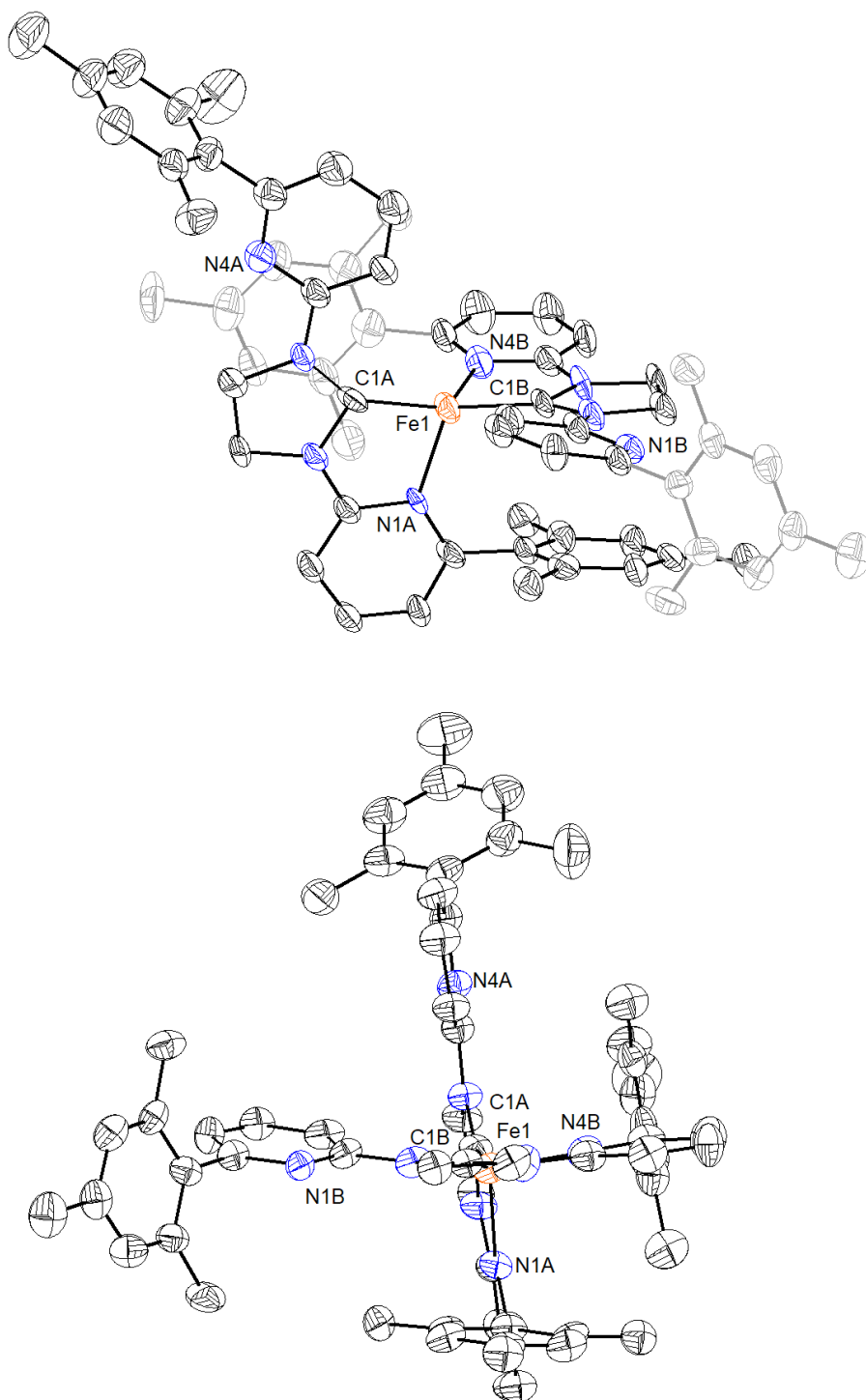


**Figure C.10.** Solid-state structure of **C.12**. Hydrogen atoms are omitted for clarity.

## DISCUSSION

Based on the structurally-characterized DPI and DPC Fe complexes, binding of both pyridine donors and formation of multiple sets of  $\pi$ - $\pi$  interactions is not favored over closer interaction of the Fe centers with a single pyridine donor. This effect is observed in the X-ray crystal structures of **C.6**, **C.7**, **C.8**, and **C.10**. In contrast, when binding of both pyridine arms is favored, as in the structure of **C.9**, shorter Fe-N(Py) distances are observed in comparison with the corresponding DPP-ligated complex. Whether these shorter distances are a consequence of increased flexibility in the DPC ligand compared with the DPP ligand or some other phenomenon is unclear at this point. Given that such close Fe-N(Py) distances are observed crystallographically, in addition to ligand hemilability upon minor ligand modification, this does not seem to be a promising platform to pursue for preparation of Fe single molecule magnets. The hemilability of the ligand, however, could be an advantage in the development of the chemistry of monoligated DPI and DPC complexes.

## CONCLUSIONS

In conclusion, a series of di(pyridyl) NHC (DPI and DPC) supported Fe complexes were synthesized and structurally-characterized. Hemilability of the DPI and DPC ligands are observed in the solid-state structures of the complexes, with either  $\kappa_2$  or  $\kappa_3$  coordination modes observed depending on the other Fe ligands, whether the NHC backbone is saturated or unsaturated, and the overall complex charge. In the homoligated complexes, distances consistent with  $\pi$ - $\pi$  interactions are observed between the mesityl substituents and the backbone of the other DPI or DPC ligand. The formation of such interactions, however, does not lead to binding of all ligand donors.

## EXPERIMENTAL SECTION

*General Comments.* All air- and water-sensitive compounds were manipulated under N<sub>2</sub> using standard Schlenk or glovebox techniques. Solvents for air- and moisture-sensitive reactions were dried by the method of Grubbs<sup>8</sup>. 2,4,6-trimethylphenylboronic acid<sup>9</sup> was prepared according to literature reports. Dipyrindyl pyrrole proligands were prepared as described in Chapter 3 of this thesis. Deuterated solvents were purchased from Cambridge Isotopes Lab, Inc.; CDCl<sub>3</sub> was used without further purification; C<sub>6</sub>D<sub>6</sub> was distilled from purple Na/benzophenone ketyl and stored over 4 Å molecular sieves; CD<sub>3</sub>CN was distilled from CaH<sub>2</sub>. <sup>1</sup>H and <sup>13</sup>C spectra were recorded on Varian Mercury 300, Varian INOVA-300, 400, or 500 spectrometers or Bruker Cryoprobe 400. <sup>1</sup>H and <sup>13</sup>C chemical shifts are reported relative to residual solvent resonances. Elemental analysis was performed on a Perkin-Elmer 2400 CHNS/O Analyser and samples were taken from representative batches prepared in an N<sub>2</sub>-filled glovebox, unless otherwise noted.

**Preparation of C.E.** A solution of LiHMDS (16.3 mg, 0.0974 mmol) in THF (2 mL) was added to a solution of DPP<sup>mes</sup>H (54.7 mg, 0.120 mmol) and stirred 15 min at room temperature. The resulting bright yellow solution was transferred to the top of a suspension of FeCl<sub>2</sub> (7.6 mg, 0.060 mmol) in THF (2 mL) and stirred overnight. Volatiles were removed under reduced pressure. The desired compound was isolated by extraction of the crude reaction mixture with hexanes (48.1 mg, 0.0496 mmol, 83 %). Anal calcd. for C<sub>64</sub>H<sub>60</sub>FeN<sub>6</sub>: C, 79.32; H, 6.24; N, 8.67. Found: C, 79.81; H, 6.23; N, 8.59.

**Preparation of C.1.** A Schlenk tube was charged with 2,6-dibromopyridine (22.2686 g, 94.004 mmol), 2-mesitylboronic acid (10.1720 g, 62.021 mmol), K<sub>2</sub>CO<sub>3</sub> (26.6162 g, 192.592 mmol), toluene (620 mL), ethanol (155 mL), and water (155 mL). The flask was degassed by three freeze-pump-thaw cycles at -78 °C, then Pd(PPh<sub>3</sub>)<sub>4</sub> (1.4245 g,



1.2327 mmol) was added against N<sub>2</sub> counterflow. The flask was heated to 70 °C for 9 h under N<sub>2</sub>. Upon cooling to room temperature the crude reaction mixture was diluted with DCM and water and separated; the combined organics layers were washed with water and brine, dried with MgSO<sub>4</sub>, filtered, and evaporated. Purification by column chromatography (5 % EtOAc in hexanes) afforded the desired product as a colorless, viscous oil (14.716 g, 53.284 mmol, 86 %). Spectral features were consistent with those previously reported.<sup>10</sup>

**Preparation of C.2.** A Schlenk tube was charged with K<sub>2</sub>CO<sub>3</sub> (2.135 g, 15.45 mmol, 2.1 equiv.), imidazole (1.6739 g, 24.59 mmol, 3.3 equiv.), and **C.1** (2.073 g, 7.507 mmol, 1 equiv.) in DCM. Volatiles were removed and the resulting mixture dried for several hours under vacuum. The flask was backfilled with N<sub>2</sub> and then the flask was vigorously stirred and heated to 180 °C through use of a heating mantel and Lab Armor beads. The flask was then cooled to room temperature and the reaction suspended in DCM. This suspension was washed with water and brine, dried with MgSO<sub>4</sub>, filtered, and evaporated. Purification by column chromatography (5:1 EtOAc:Hexanes (v/v)) afforded the desired compound as a white solid (1.358 g, 5.157 mmol, 69 % yield). <sup>1</sup>H NMR (CDCl<sub>3</sub>, 400 MHz) δ 8.42 (s, 1H, Imid), 7.89 (dd, *J* = 7.9, 0.4 Hz, 1H, Py), 7.69 (s, 1H), 7.33 (dd, *J* = 8.1, 0.6 Hz, 1H, Py), 7.19 (s, 1H, Imid), 7.17 (dd, *J* = 7.6, 0.7 Hz, 1H, Py), 6.97 (s, 2H, Mes), 2.35 (s, 3H, mesCH<sub>3</sub>), 2.08 (s, 6H, mesCH<sub>3</sub>). <sup>13</sup>C NMR (CDCl<sub>3</sub>, 101 MHz) δ 159.95 (Py), 148.95 (Py), 139.29 (Py), 138.24 (mes), 136.84 (mes), 135.90 (mes), 135.20 (Imid), 130.53 (Imid), 128.71 (mes), 123.36 (Py), 116.43 (Imid), 110.14 (Py), 21.32 (mes), 20.46 (mes). HRMS (FAB+) calcd. for C<sub>17</sub>H<sub>18</sub>N<sub>3</sub> (M+H<sup>+</sup>) 264.1501. Found: 264.1505.

**Synthesis of C.3.** A Schlenk tube was charged with a solution of 2-mesityl-6-bromopyridine (2.040 g, 7.387 mmol) and **C.2** (1.358 g, 5.157 mmol) in DCM. Volatiles were removed and the resulting mixture dried under high vacuum for several hours. The flask was refilled with N<sub>2</sub> and then stirred and heated to 190 °C for 12 h through use of a heating mantel and Lab Armor beads. Upon cooling to room temperature the brown solids were taken up in DCM, washed twice with 2 M NaBF<sub>4</sub>, dried with MgSO<sub>4</sub>, filtered and evaporated. The resulting solids were triturated with Et<sub>2</sub>O then collected by filtration, washed with fresh Et<sub>2</sub>O, and dried under vacuum at 100 °C overnight to afford the desired compound as a light brown solid (2.346 g, 4.293 mmol, 83 % yield). <sup>1</sup>H NMR (400 MHz, CDCl<sub>3</sub>) δ 10.46 (t, *J* = 1.6 Hz, 1H, imid), 8.49 (d, *J* = 1.6 Hz, 2H, imid), 8.27 (dd, *J* = 8.2, 0.6 Hz, 2H, Py), 8.19 (dd, *J* = 8.4, 7.5 Hz, 2H, Py), 7.45 (dd, *J* = 7.5, 0.6 Hz, 2H, Py), 6.98 (s, 4H, mes), 2.35 (s, 6H, mesCH<sub>3</sub>), 2.04 (s, 12H, mesCH<sub>3</sub>). <sup>13</sup>C NMR (101 MHz, CDCl<sub>3</sub>) δ 160.42 (Py), 145.61 (Py), 141.43 (Py), 138.78 (mes), 135.78 (mes), 135.75 (mes), 131.16 (NCN), 128.72 (mes), 127.19 (Py), 120.31 (Imid), 112.70 (Py), 21.25 (mesCH<sub>3</sub>), 20.39 (mesCH<sub>3</sub>). HRMS (FAB+) calcd for C<sub>31</sub>H<sub>31</sub>N<sub>4</sub>: 459.2549. Found: 459.2557.

**Preparation of C.4.** A Schlenk tube was charged with 2,6-dichloropyridine (15.357 g, 103.8 mmol), 2-mesitylboronic acid (11.3597 g, 69.262 mmol), K<sub>2</sub>CO<sub>3</sub> (28.731 g, 207.89 mmol), toluene (660 mL), ethanol (170 mL), and water (170 mL) then degassed by three freeze-pump-thaw cycles. Pd(PPh<sub>3</sub>)<sub>4</sub> (2.4976 g, 2.1614 mmol) was added against N<sub>2</sub> flow then the flask sealed and heated to 70 °C for 16 h. Upon cooling to room temperature the crude reaction was diluted with DCM and water, separated, and the organic layer washed with water and brine, dried with MgSO<sub>4</sub>, filtered and evaporated. Column chromatography (5 % EtOAc in Hexanes) afforded the desired compound as a colorless oil (13.137 g, 82 %). Note: 2-chloro-6-mesitylpyridine was isolated with 7 % 2,6-

dimesitylpyridine and 20 % 2,6-dichloropyridine and used as-is.  $^1\text{H}$  NMR ( $\text{CDCl}_3$ , 300 MHz)  $\delta$  7.71 (t,  $J$  = 7.7 Hz, 1H, Py), 7.29 (dd,  $J$  = 8.0, 0.8 Hz, 1H, Py), 7.15 (dd,  $J$  = 7.5, 0.8 Hz, 1H, Py), 6.91 (s, 2H, mes), 2.31 (s, 3H, mes $\text{CH}_3$ ), 2.03 (s, 6H, mes $\text{CH}_3$ ).

**Preparation of C.5.** In the glovebox a Schlenk tube was charged with  $\text{Pd}(\text{dba})_2$  (0.2106 g, 0.3663 mmol), *rac*-BINAP (0.393 g, 0.631 mmol), and  $\text{NaO}^t\text{Bu}$  (2.1049 g, 21.903 mmol) then sealed. On the Schlenk line **C.4** (4.2553 g, 18.364 mmol), ethylenediamine (0.53 mL, 7.9 mmol), and toluene (80 mL) were added by syringe. The flask was sealed and heated to 80 °C for 16 h. Upon cooling to room temperature the crude reaction mixture was filtered through Celite with DCM then volatiles were removed from the filtrate under reduced pressure. Purification by column chromatography afforded the desired product as a pale yellow solid (1.20 g, 2.66 mmol, 34 %).  $^1\text{H}$  NMR ( $\text{CDCl}_3$ , 500 MHz)  $\delta$  7.36 (t,  $J$  = 7.8 Hz, 2H, Py), 6.91 (s, 4H, mes), 6.47 (d,  $J$  = 7.2 Hz, 2H, Py), 6.30 (d,  $J$  = 8.3 Hz, 2H, Py), 5.09 (s, 2H, NH), 3.50 (d,  $J$  = 4.8 Hz, 4H,  $\text{CH}_2$ ), 2.32 (s, 6H, mes $\text{CH}_3$ ), 2.08 (s, 12H, mes $\text{CH}_3$ ).  $^{13}\text{C}$  NMR ( $\text{CDCl}_3$ , 500 MHz)  $\delta$  158.68, 158.23, 138.50, 137.59, 137.03, 135.83, 128.27, 113.75, 104.91, 42.35 ( $\text{CH}_2$ ), 21.22 (mes $\text{CH}_3$ ), 20.30 (mes $\text{CH}_3$ ). HRMS (FAB+) calcd for  $\text{C}_{30}\text{H}_{35}\text{N}_4$ : 451.2962. Found: 451.2851.

**Preparation of C.6.** An oven-dried Schlenk tube was charged with **C.5** (0.514 g, 1.14 mmol) and  $\text{NH}_4\text{BF}_4$  (0.126 g, 1.20 mmol), then sealed with a septum and triethyl orthoformate (1.9 mL, 11 mmol) and toluene (1.4 mL) added by syringe. The flask was heated to 70 °C under  $\text{N}_2$  for 9 h, then cooled to room temperature, diluted with additional toluene (6 mL) and heated to 100 °C for an additional 9 h. Upon cooling to room temperature dry ether (30 mL) was added by syringe, then solids collected by filtration, washed with hexanes, and dried under vacuum to afford the desired compound as a tan solid (0.567 g, 1.02 mmol, 93%).  $^1\text{H}$  NMR ( $\text{CD}_3\text{CN}$ , 400 MHz)  $\delta$  9.77 (s, 1H), 8.05 (dd,  $J$

= 8.2, 7.7 Hz, 2H), 7.32 (ddd,  $J$  = 7.6, 4.8, 0.6 Hz, 5H), 6.97 – 6.94 (m, 4H), 4.64 (s, 4H), 1.97 (s, 12H).  $^{13}\text{C}$  NMR ( $\text{CD}_3\text{CN}$ , 101 MHz)  $\delta$  160.56 (Py), 151.89 (NCN), 148.47 (Py), 141.13 (Py), 139.18 (mes), 137.35 (mes), 136.50 (mes), 129.20 (mes), 125.24 (Py), 110.88 (Py), 48.72 ( $\text{CH}_2$ ), 21.13 (mes $\text{CH}_3$ ), 20.23 (mes $\text{CH}_3$ ). HRMS (FAB+) calcd for  $\text{C}_{31}\text{H}_{33}\text{N}_4$ : 461.2705. Found: 461.2708.

**Preparation of C.7.** A Schlenk tube was charged with 2-bromo-6-amino pyridine (0.6894 g, 3.985 mmol), 2-mesitylboronic acid (0.6424 g, 3.917 mmol),  $\text{Na}_2\text{CO}_3$  (0.8332 g, 7.861 mmol), PhMe (19 mL), methanol (2 mL), and water (4.7 mL), then degassed by three freeze-pump-thaw cycles.  $\text{Pd}(\text{PPh}_3)_4$  (0.2429 g, 0.210 mmol) was added against  $\text{N}_2$  counterflow, then the flask was sealed and heated to 105 °C overnight. Upon cooling to room temperature the crude reaction mixture was diluted with DCM and water, then the organic layer was separated, washed with water and brine, dried with  $\text{MgSO}_4$ , filtered, and evaporated. Volatiles were removed under reduced pressure; the desired product was isolated as a white crystalline solid column chromatography in 30 % ethyl acetate in hexanes (0.459 g, 2.16 mmol, 55 %).  $^1\text{H}$  NMR ( $\text{CDCl}_3$ , 500 MHz)  $\delta$  7.49 (dd,  $J$  = 8.1, 7.4 Hz, 1H, Py), 6.90 (s, 2H, mes), 6.57 (dd,  $J$  = 7.3, 0.7 Hz, 1H, Py), 6.45 (dd,  $J$  = 8.2, 0.7 Hz, 1H, Py), 4.47 (s, 2H,  $\text{NH}_2$ ), 2.30 (s, 3H, mes $\text{CH}_3$ ), 2.07 (s, 6H, mes $\text{CH}_3$ ).  $^{13}\text{C}$  NMR ( $\text{CDCl}_3$ , 126 MHz)  $\delta$  158.52 (Py), 158.26 (Py), 138.12, 137.94, 137.24, 135.70, 128.32, 114.89 (Py), 106.40 (Py), 21.21 (mes $\text{CH}_3$ ), 20.18 (mes $\text{CH}_3$ ). HRMS (FAB+) calcd. For  $\text{C}_{14}\text{H}_{17}\text{N}_2$ : 213.1392. Found: 213.1386.

**Preparation of C.8.** A solution of NaHMDS (27.0 mg, 0.147 mmol) in THF (1 mL) was added to a suspension of **C.3** (73.2 mg, 0.134 mmol) and stirred 10 min. The resulting dark solution was transferred to the top of a suspension of  $\text{FeCl}_2$  (18.1 mg, 0.143 mmol) in THF (1 mL) and stirred 10 h. Volatiles were removed under reduced pressure,

then the solids washed with hexanes and ether and extracted with benzene and THF to afford the desired complex as a yellow solid (73.8 mg, 0.126 mmol, 94 %). X-ray quality crystals were grown from benzene.  $^1\text{H}$  NMR ( $\text{CD}_3\text{CN}$ , 400 MHz)  $\delta$  38.92 (s), 29.16 (s), 5.16 (s), 2.63 (s), -6.82 (s), -11.43 (s).

**Preparation of C.9.** A thawing solution of NaHMDS (33.8 mg, 0.184 mmol) in THF (3 mL) was added to the top of  $\text{FeCl}_2$  (25.2 mg, 0.199 mmol) and stirred 20 min, warming. A thawing suspension of **C.6** (80.2 mg, 0.146 mmol) was added to the top and the resulting suspension stirred 9 h, warming. Volatiles were removed under reduced pressure and the resulting yellow solids were washed with hexanes and ether then extracted with benzene to afford the desired compound as a yellow solid (52.8 mg, 0.0899 mmol, 62 % yield). X-ray quality crystals were grown by vapor diffusion of pentane into a toluene solution of the compound at  $-35\text{ }^\circ\text{C}$ .  $^1\text{H}$  NMR (400 MHz,  $\text{C}_6\text{D}_6$ )  $\delta$  32.21 (br s), 12.03 (s), 5.24 (s), 2.18 (s), -5.06 (br s).

**Preparation of C.10.** In the glovebox a solution of  $\text{Fe}(\text{HMDS})$  (42.6 mg, 0.113 mmol) in THF (2 mL) was added to a stirred solution of **C.3** (120.1 mg, 0.2198 mmol) in acetonitrile (2 mL). The dark brown solution was stirred 15 h at room temperature, then volatiles were removed. The resulting brown-tan solids were triturated and evaporated with THF, then washed extensively with fresh THF. Extraction with acetonitrile afforded the desired complex as a brown-tan solid (116.5 mg, 0.1029 mmol, 94 % yield). X-ray quality crystals were grown by vapor transfer of ether into an acetonitrile solution of the complex.  $^1\text{H}$  NMR (400 MHz,  $\text{CD}_3\text{CN}$ )  $\delta$  54.82 (br s), 47.14 (br s), 34.55 (br s), 4.00 (s), 2.43 (s), 1.69 (s).  $^{19}\text{F}$  NMR (376 MHz,  $\text{CD}_3\text{CN}$ )  $\delta$  -150.18.

**Preparation of C.11.** In the glovebox a solution of  $\text{Fe}(\text{HMDS})_2$  (76.3 mg, 0.2026 mmol) in THF (3 mL) was added to a suspension of **C.6** (216.3 mg, 0.3944 mmol) in THF

(4 mL) and stirred overnight at room temperature. Volatiles were removed under reduced pressure. The resulting solids washed with THF and then extracted with acetonitrile to afford the desired complex as a tan solid (143.2 mg, 0.1244 mmol, 61 %). X-ray quality crystals were grown by vapor diffusion of ether into an acetonitrile solution of the complex at -35 °C.  $^1\text{H}$  NMR (300 MHz,  $\text{CD}_3\text{CN}$ )  $\delta$  28.84 (s), 19.32 (br s), 7.70 (s), 7.39 (s), 6.99 (s), 6.53 (s), 5.47 (br s), 4.91 (s), 4.13 (s), 3.52 (s), 3.33 (s), 2.33 (s), -1.37 (s), -31.87 (br s).  $^{19}\text{F}$  NMR (282 MHz,  $\text{CD}_3\text{CN}$ )  $\delta$  -145.62.

**Preparation of C.12.** A J-Young tube was charged with **C.11** (19.5 mg, 0.0169 mmol),  $\text{Cp}^*\text{Co}$  (11.2 mg, 0.0340 mmol), and  $\text{CD}_3\text{CN}$  (0.5 mL), then sealed and inverted. Upon confirmation of complete consumption of the starting Fe complex by  $^1\text{H}$  NMR, the tube was returned to the glovebox, the dark solution transferred to a vial, and volatiles removed. The solids were extracted with hexanes to afford the desired complex as a black solid (12.6 mg, 0.0129 mmol, 76 %). X-ray quality crystals were grown by slow evaporation of a saturated pentane solution of the complex into toluene at -35 °C.  $^1\text{H}$  NMR (400 MHz,  $\text{CD}_3\text{CN}$ )  $\delta$  62.10 (s), 46.62 (s), 45.06 (s), 43.99 (s), 35.54 (s), 26.91 (s), 18.34 (s), 7.70 (s), 6.93 (s), 6.46 (s), 3.32 (s), 2.32 (s), -3.99 (s), -9.07 (s), -26.85 (s), -43.18 (s), -58.18 (s), -67.92 (s).

**Electrochemical Measurements.** CVs were recorded with a Pine Instrument Company AFCBPi biopotentiostat with the AfterMath software package. Measurements were performed in a three component cell, consisting of a glassy carbon working electrode ( $\phi = 3.0$  mm), a Pt wire counterelectrode, and a Ag wire reference electrode in dry solvent in an  $\text{N}_2$  filled glovebox. The ferrocene/ferrocenium couple was used as an internal reference.

**Crystallographic Information.** Crystals were mounted on a glass fiber or MiTeGen loop using Paratone oil, then placed on the diffractometer under a nitrogen stream. Diffractometer manipulations, including data collection, integration, and scaling were performed using the Bruker APEXII software.<sup>11</sup> Absorption corrections were applied using SADABS or TWINABS.<sup>12</sup> Space groups were determined on the basis of systematic absences and intensity statistics and the structures were solved in the Olex 2 software interface<sup>13</sup> by intrinsic phasing using XT (incorporated into SHELXTL)<sup>14</sup> and refined by full-matrix least squares on  $F^2$ . Hydrogen atoms were placed in the idealized positions and refined using a riding model. Graphical representation of structures with 50% probability thermal ellipsoids were generated using Diamond 3 visualization software.<sup>15</sup> Non-hydrogen atoms were refined using anisotropic displacement parameters. Disordered solvents of crystallization in **C.12** could not be satisfactorily modeled and were removed using the solvent mask implementation in Olex 2.

**Table C.1.** Crystal and refinement data for complexes **C.8**, **C.9**, and **C.10**

	<b>C.8</b>	<b>C.9</b>	<b>C.10</b>
CCDC Number			
Empirical formula	C <sub>31</sub> H <sub>32</sub> Cl <sub>2</sub> FeN <sub>4</sub>	C <sub>31</sub> H <sub>30</sub> Cl <sub>2</sub> FeN <sub>4</sub>	C <sub>62</sub> H <sub>60</sub> B <sub>2</sub> N <sub>8</sub> F <sub>8</sub> Fe
Formula weight	587.37	585.35	1187.70
T (K)	100	100	100
<i>a</i> , Å	8.1523(3)	8.0795(7)	11.5136(11)
<i>b</i> , Å	14.2525(5)	14.3422(6)	15.0306(14)
<i>c</i> , Å	49.2956(17)	49.031(3)	17.1792(17)
$\alpha$ , deg	90	90	93.072(4)
$\beta$ , deg	90	90	90.582(4)
$\gamma$ , deg	90	90	98.729(4)
Volume, Å <sup>3</sup>	5727.7(4)	5681.7(6)	2933.8(5)
Z	8	8	2
Crystal system	Orthorhombic	Orthorhombic	Triclinic
Space group	Pbca	Pbca	P-1
$\theta$ range, deg	2.477 to 27.490	3.604 to 78.853	2.373 to 27.488
$\mu$ , mm <sup>-1</sup>	0.740	6.192	0.332
Abs. Correction	Multi-scan	Multi-scan	Multi-scan
GOF	1.114	1.125	1.042
$R_1$ , <sup>a</sup> $wR_2$ <sup>b</sup> [ $I > 2\sigma(I)$ ]	0.0317, 0.0739	0.0404, 0.0920	0.0317, 0.0934
Radiation Type	Mo K $\alpha$	Cu K $\alpha$	Mo K $\alpha$

$$^a R_1 = \sum ||F_o| - |F_c|| / \sum |F_o|, \quad ^b wR_2 = [\sum [w(F_o^2 - F_c^2)^2] / \sum [w(F_o^2)^2]]^{1/2}.$$



**Table C.2.** Crystal and refinement data for complexes **C.11** and **C.12**.

	<b>C.11</b>	<b>C.12</b>
CCDC Number		
Empirical formula	C <sub>67</sub> H <sub>71.5</sub> B <sub>2</sub> F <sub>8</sub> FeN <sub>10.5</sub>	C <sub>62</sub> H <sub>64</sub> FeN <sub>8</sub>
Formula weight	1150.68	977.06
T (K)	100	100
<i>a</i> , Å	13.6681(8)	39.358(4)
<i>b</i> , Å	21.9036(15)	15.4018(18)
<i>c</i> , Å	20.6471(15)	21.678(2)
$\alpha$ , deg	90	90
$\beta$ , deg	94.058(2)	107.184(7)
$\gamma$ , deg	90	90
Volume, Å <sup>3</sup>	6165.8(7)	12554(2)
Z	4	8
Crystal system	Monoclinic	Monoclinic
Space group	P 2 <sub>1</sub> /n	C 2/c
$\theta$ range, deg	2.385 to 27.482	2.354 to 78.923
$\mu$ , mm <sup>-1</sup>	0.320	2.230
Abs. Correction	Multi-scan	Multi-scan
GOF	1.002	1.065
$R_1$ , <sup>a</sup> $wR_2$ <sup>b</sup> [I > 2 $\sigma$ (I)]	0.0486, 0.1409	0.1243, 0.3316
Radiation Type	Mo K $\alpha$	Cu K $\alpha$

$$^a R_1 = \sum ||F_o| - |F_c|| / \sum |F_o|, \quad ^b wR_2 = [\sum [w(F_o^2 - F_c^2)^2] / \sum [w(F_o^2)^2]]^{1/2}.$$

## REFERENCES

1. (a) Layfield, R. A. *Organometallics* **2014**, *33* (5), 1084-1099; (b) Craig, G. A.; Murrie, M. *Chem. Soc. Rev.* **2015**, *44* (8), 2135-2147; (c) Power, P. P. *Chem. Rev.* **2012**, *112* (6), 3482-3507.
2. (a) Reiff, W. M.; Schulz, C. E.; Whangbo, M. H.; Seo, J. I.; Lee, Y. S.; Potratz, G. R.; Spicer, C. W.; Girolami, G. S. *J. Am. Chem. Soc.* **2009**, *131* (2), 404-405; (b) Lin, C. Y.; Fettingner, J. C.; Grandjean, F.; Long, G. J.; Power, P. P. *Inorg. Chem.* **2014**, *53* (17), 9400-9406; (c) Zadrozny, J. M.; Atanasov, M.; Bryan, A. M.; Lin, C.-Y.; Rekker, B. D.; Power, P. P.; Neese, F.; Long, J. R. *Chem. Sci.* **2013**, *4* (1), 125-138; (d) Bryan, A. M.; Lin, C.-Y.; Sorai, M.; Miyazaki, Y.; Hoyt, H. M.; Hablutzel, A.; LaPointe, A.; Reiff, W. M.; Power, P. P.; Schulz, C. E. *Inorg. Chem.* **2014**, *53* (22), 12100-12107; (e) Chilton, N. F.; Lei, H.; Bryan, A. M.; Grandjean, F.; Long, G. J.; Power, P. P. *Dalton Trans.* **2015**, *44* (24), 11202-11211; (f) Pratt, J.; Bryan, A. M.; Faust, M.; Boynton, J. N.; Vasko, P.; Rekker, B. D.; Mansikkamaki, A.; Fettingner, J. C.; Tuononen, H. M.; Power, P. P. *Inorg. Chem.* **2018**, *57* (11), 6491-6502.
3. (a) Hall, K.; Murphy, V.; Lapointe, A. M.; Van Beek, J. A. M.; Diamond, G. M. Combinatorial synthesis and analysis of metal-ligand compositions using soluble metal precursors for polymerization catalysts. US20020034829A1, 2002; (b) LaPointe, A. M. *Inorg. Chim. Acta* **2003**, *345*, 359-362; (c) Reiff, W. M.; LaPointe, A. M.; Witten, E. H. *J. Am. Chem. Soc.* **2004**, *126* (33), 10206-10207.
4. Atanasov, M.; Zadrozny, J. M.; Long, J. R.; Neese, F. *Chem. Sci.* **2013**, *4* (1), 139-156.
5. (a) Raba, A.; Anneser, M. R.; Jantke, D.; Cokoja, M.; Herrmann, W. A.; Kuhn, F. E. *Tet. Lett.* **2013**, *54* (26), 3384-3387; (b) Riener, K.; Bitzer, M. J.; Pothig, A.; Raba, A.; Cokoja, M.; Herrmann, W. A.; Kuhn, F. E. *Inorg. Chem.* **2014**, *53* (24), 12767-12777.
6. Kaplan, H. Z.; Li, B.; Byers, J. A. *Organometallics* **2012**, *31*, 7343-7350.
7. WebElements.com (accessed November 26, 2018).
8. Pangborn, A. B.; Giardello, M. A.; Grubbs, R. H.; Rosen, R. K.; Timmers, F. J. *Organometallics* **1996**, *15* (5), 1518-1520.
9. Dorkó, É.; Kótai, B.; Földes, T.; Gyömöre, Á.; Pápai, I.; Soós, T. *Journal of Organometallic Chemistry* **2017**, *847*, 258-262.
10. Labonne, A.; Kribber, T.; Hintermann, L. *Organic Letters* **2006**, *8* (25), 5853-5856.
11. APEX2, Version 2 User Manual, M86-E01078, Bruker Analytical X-ray Systems, Madison, WI, June 2006.
12. Sheldrick, G.M. "SADABS (version 2008/1): Program for Absorption Correction for Data from Area Detector Frames", University of Gottingen, 2008.
13. Dolomanov, O. V.; Bourhis, L. J.; Gildea, R. J.; Howard, J. A. K.; Puschmann, H. *J. Appl. Crystallogr.* **2009**, *42* (2), 339-341.
14. Sheldrick, G. M. *Acta Cryst.* **2008**, *A64*, 112-122.
15. Brandenburg, K. (1999), DIAMOND. Crystal Impact GdR, Bonn, Germany.

## APPENDIX D

### SYNTHESIS AND ELECTROCHEMISTRY OF DI(PYRIDYL) NHC AND DI(PYRIDYL) PYRROLIDE CU(I) AND CU(II) COMPLEXES

**ABSTRACT**

A series of homo- and heteroleptic di(pyridyl) pyrrolide (DPP) and di(pyridyl) NHC (DPI) Cu complexes were prepared, structurally characterized, and the electrochemical behavior studied. While a bis(DPP) Cu(I) could not be isolated, the corresponding Cu(II) complex and a bis(DPP) dicopper(I) complex were prepared by salt metathesis and structurally characterized. Reaction of the *in situ* generated Na salt of the DPP proligand with (phenanthroline)CuCl resulted in formation of the corresponding heteroligated complex, which was characterized in solution by NMR and in the solid state by X-ray crystallography. A bis(DPI) Cu(I) complex and a bis(DPI) dicopper(I) complex were prepared by reaction of the proligand with Cu(I) precursors in the presence of NaHMDS and structurally characterized. Four coordinate Cu(I) centers were observed for all complexes and, in the case of the monocopper(I) complexes, rotation of at least one of the free pyridine arms away from the Cu center is observed. The electrochemical behavior of all complexes was studied by cyclic voltammetry; furthermore, stoichiometric oxidation studies were performed with the heteroligated DPP-phenanthroline complex. Binding of both pyridine arms upon one electron oxidation is observed by X-ray crystallography; both six-coordinate, acetonitrile-bound and five-coordinate, solvent free species were observed.

## INTRODUCTION

Emissive Cu(I) complexes have received significant attention in the literature as lower-cost alternatives to Ir and Ru photosensitizers for solar energy conversion.<sup>1</sup> A variety of ligand scaffolds have been reported to supported emissive Cu(I) complexes with relatively long lifetimes including phosphines,<sup>2</sup> carbenes,<sup>3</sup> phenanthroline,<sup>4</sup> and heteroleptic phosphine-phenanthroline complexes.<sup>5</sup>

Ligands bearing bulky groups have been demonstrated by Schmittl and coworkers to allow selective access to heteroleptic Cu(I) phenanthroline complexes using the so-called HETPHEN approach.<sup>6</sup> Bulky aromatic groups, such as mesityl and anthracenyl moieties, are typically favored and the resulting heteroleptic complexes show intramolecular  $\pi$ - $\pi$  interactions between the aromatic groups and the other phenanthroline ligand in the solid state.<sup>4j, 7</sup> Gordon and coworkers have reported a series homoleptic and heteroleptic Cu(I) complexes supported by mesityl-substituted bipyridine ligands (**D.A**) that display  $\pi$ - $\pi$  interactions in the solid state,<sup>7b</sup> however, due to the bidentate nature of the bipyridine ligand, one mesityl substituent is pulled out of interaction with the other ligand. The lifetimes of these complexes are short ( $\tau < 5$  ns), which is attributed the flexibility of the bipyridine-based ligand. Odobel and coworkers have reported a series complexes including **D.B** (Figure D.1) which display  $\pi$ - $\pi$  interactions between one of the mesityl substituents and the other phenanthroline-derived ligand in the solid state.<sup>7a</sup> These complexes have longer lifetimes in comparison with **D.A**, with  $\tau$  values of up to 50 ns for **D.B**. Mulfort and coworkers have reported complexes **D.C** and **D.D**, which have  $\tau$  values of 74 and 68 ns, respectively, for their long-lived excited states.<sup>7e, 7g</sup> The use of heteroleptic Cu(I) complexes employing the

HETPHEN approach in dye-sensitized solar cells has been reported by Odobel and coworkers (**D.E**, Figure D.1).<sup>7c, 7h</sup>

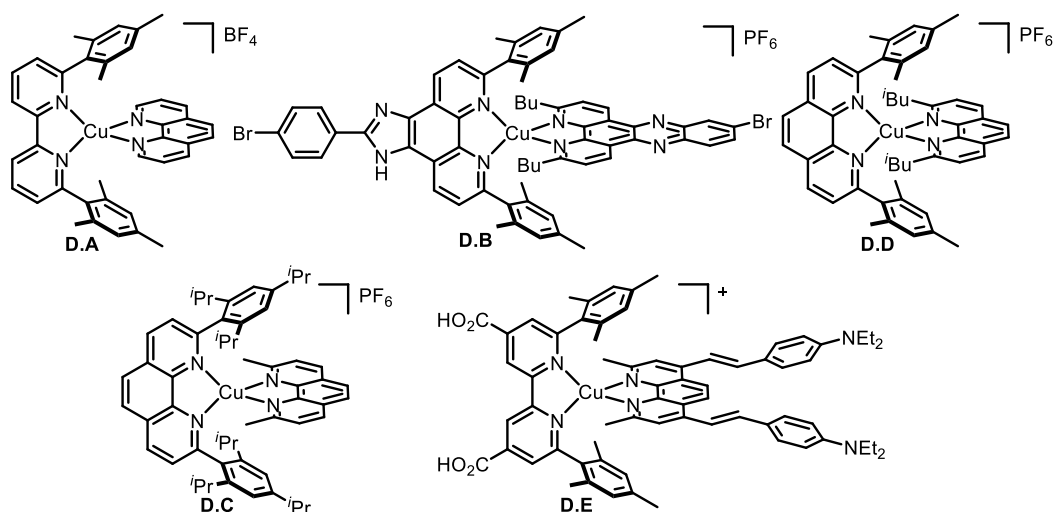


**Figure D.1.** Examples of heteroleptic Cu(I) phenanthroline complexes exhibiting intramolecular  $\pi$ - $\pi$  interactions in the solid state.

Based on previous work on the use of the hemilabile, mesityl-substituted di(pyridyl) pyrrolide (DPP) and di(pyridyl) NHC (DPI) ligands, it was hypothesized that Cu(I) complexes bearing these ligands could potentially show long excited state lifetimes through stabilizing  $\pi$ - $\pi$  interactions. Such interactions could disfavor Cu planarization, a process which is proposed to lead to short excited state lifetimes in Cu(I) bis(phenanthroline).<sup>4a, 4b</sup> If Cu(I) prefers to bind to the DPI or DPP ligands in a bidentate fashion, as has been previously observed in the [(DPI)<sub>2</sub>Fe][BF<sub>4</sub>]<sub>2</sub> (Appendix C) complex, then binding of the free pyridine arm(s) upon formation of the excited state could also potentially prolong the lifetime of the excited state.

A handful of DPP and DPI Cu(I) complexes have been reported in the literature (Figure D.2). The electrochemical synthesis of DPI-supported tricopper complex **D.F**

has been reported by Chen and coworkers,<sup>8</sup> while their use in monoarylation of anilines has been reported by Scholz and coworkers.<sup>9</sup> Cu(II) complexes supported by di(pyridyl) pyrrolide ligands have been reported for self-assembly on gold surfaces,<sup>10</sup> magnetism,<sup>11</sup> and DNA cleavage.<sup>12</sup> The structures and syntheses of a number of halide- and phosphine-bound Cu(I) di(pyridyl) pyrrolide complexes have also been reported (Figure D.2). Yi and coworkers have reported heterobimetallic complex **D.G**, halide-bridged dicopper complex **D.H**, and heteroleptic phosphine-di(pyridyl) pyrrolide complex **D.I**.<sup>13</sup> Based on comparison of the UV-Vis spectra of these complexes with their corresponding proligands bands near 400 nm to the MLCT features for complexes **D.H** and **D.I**.

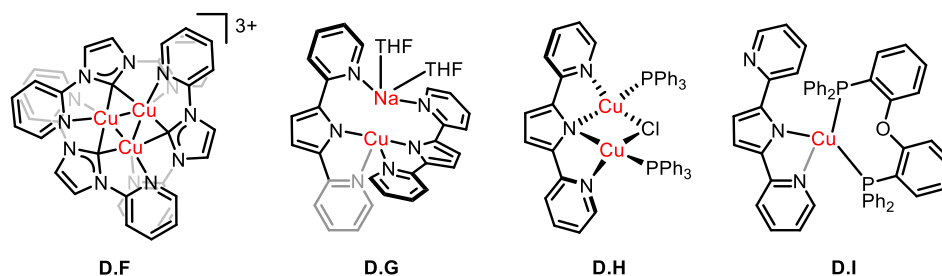


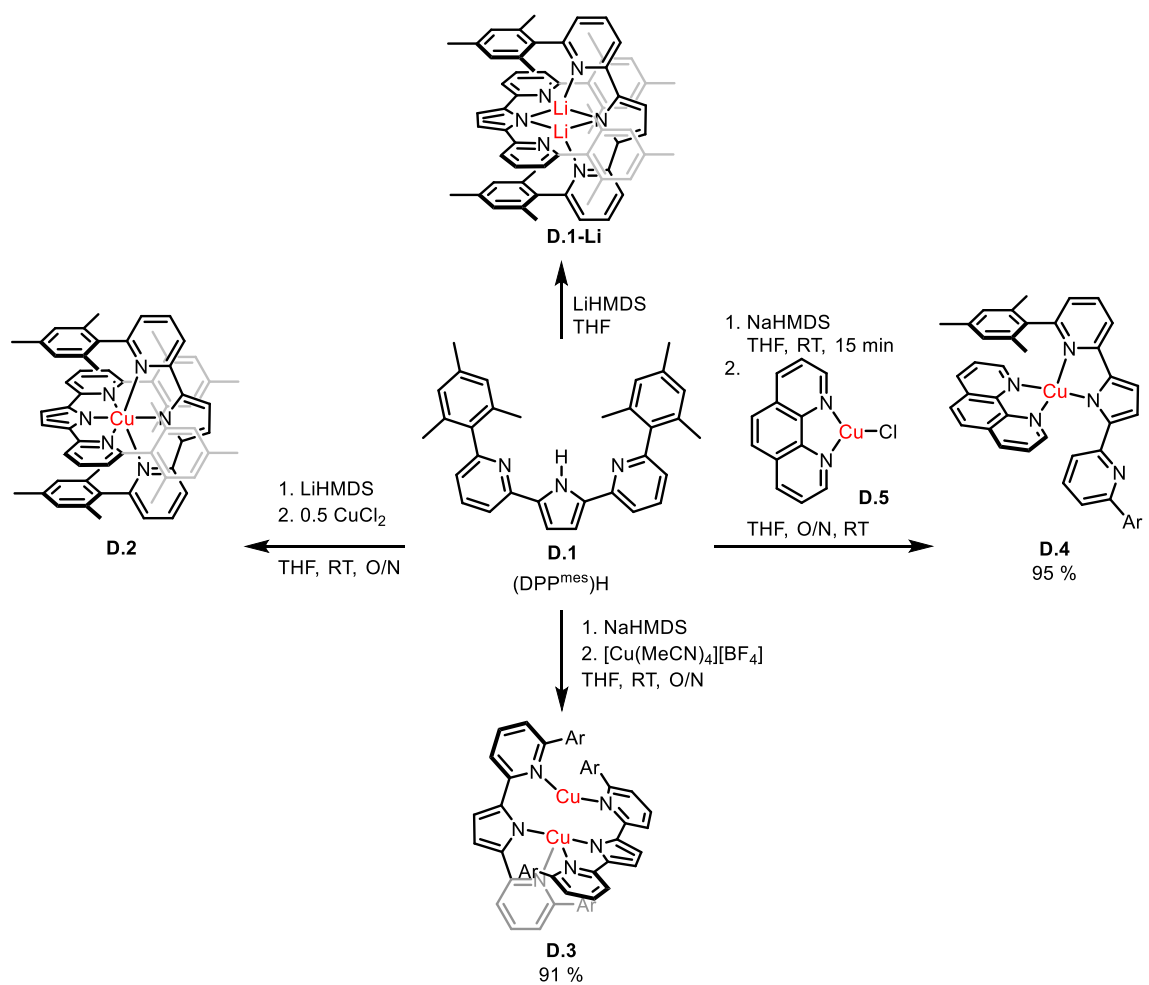
**Figure D.2.** Examples of DPP and DPI Cu(I) complexes.

## RESULTS

The mesityl-substituted di(pyridyl) pyrrolide (DPP) was prepared by Suzuki coupling of 2-mesityl boronic acid with the dibromide-substituted di(pyridyl) pyrrole backbone, as described in Chapter 3. Di(pyridyl) NHC (DPI) prolignands bearing unsaturated backbones were prepared from 2-mesityl-6-bromopyridine using the method of Kühn and coworkers,<sup>14</sup> as described in Appendix C.

DPP-ligated Cu(I) and Cu(II) complexes were prepared by salt metathesis of the corresponding *in situ*-generated Li and Na salts (Scheme D.1). Reaction of the Li salt of **D.1** with CuCl<sub>2</sub> was found by Dr. Gyeongshin Choi to lead to formation of a species with broadened, paramagnetically-shifted NMR resonances, which was crystallographically characterized as the six-coordinate Cu(II) complex **D.2**. Reaction of two equivalents of the Na salt of **D.1** with two equivalents of [Cu(MeCN)<sub>4</sub>][BF<sub>4</sub>] resulted in formation of a red species with broadened <sup>1</sup>H NMR resonances and three broadened mesityl methyl peaks. This was crystallographically characterized as the dicopper(I) species **D.3**. The heteroligated complex **D.4** could be prepared by reaction of the Na salt of **D.1** with one equivalent of (phenanthroline)CuCl (**D.5**) in THF at room temperature. This brown complex features sharp NMR features with one set of pyridine and mesityl resonances, consistent with fast exchange between bound and free DPP pyridine groups. While **D.3** and **D.4** have similar absorption features in their UV-Vis spectra, **D.4** has an additional feature with a  $\lambda_{\text{max}}$  of 534 nm (Figure D.3). It is worth noting that the lithium, sodium, and potassium salts of **D.1** have similar UV-Vis features (Figure FD.33).





**Scheme D.1.** Preparation of DPP-ligated Cu(I) and Cu(II) complexes. Ar = mesityl.

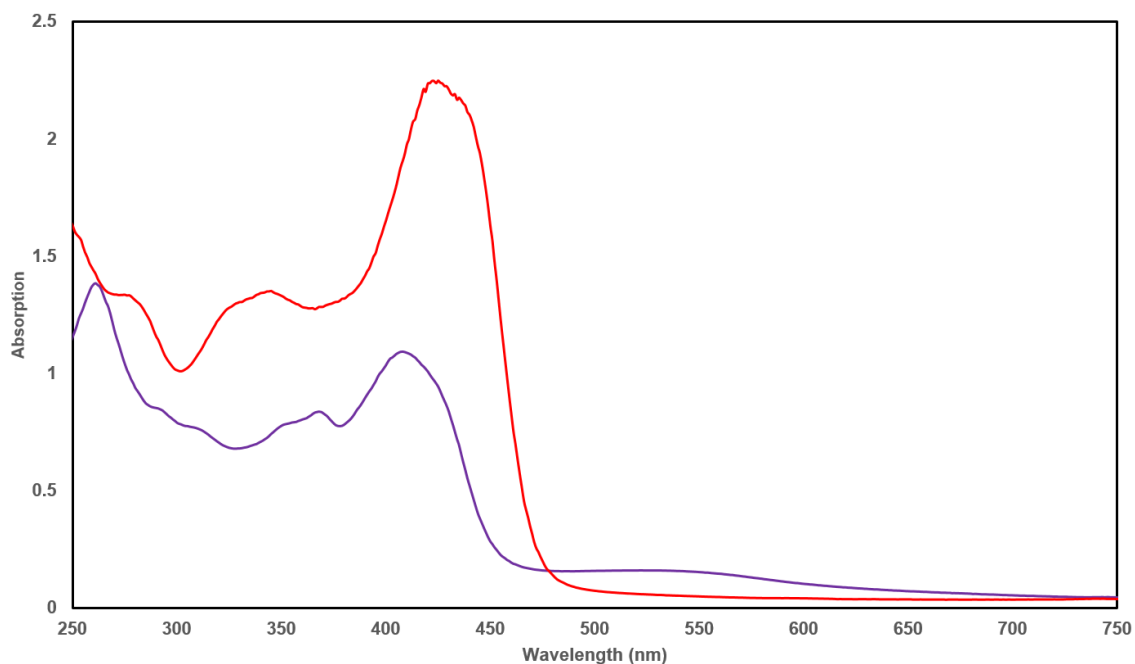


**Figure D.3.** UV-Vis spectra of **D.3** (red) and **D.4** (purple). Conditions: 25  $\mu\text{M}$  in complex in THF.

Complexes **D.2**, **D.3**, and **D.4** were crystallographically characterized (Figures D.4 through D.7); all display close contacts between the mesityl substituents and the backbones of the other ligand, consistent with intramolecular  $\pi$ - $\pi$  interactions. In the solid-state **D.2** features a six-coordinate Cu(1) center (Figure D.4) with Cu(1)-N(Py) distances of 2.40 – 2.43 Å and Cu(1)-N(pyrrolide) distances of 1.83 – 1.85 Å. Distances of 3.40 Å are observed between the centroids of the pyrrolide donors and the planes of the mesityl substituents. In the solid state **D.3** features two different Cu centers (Figure D.5): Cu(1) is coordinated to both pyrrolide donors and two pyridine donors with a distorted trigonal pyramidal geometry ( $\tau_4 = 0.63$ ); Cu(2) adopts a distorted linear geometry with a N(12)-Cu(2)-N(9) angle of 162°. The Cu(1)-Cu(2) distances are 2.51 and 2.55 Å in the two molecules in the asymmetric unit. Cu(1)-N(pyrrolide) distances of 1.95 to 1.96 Å

are observed with an average Cu(1)-N(Py) distance of 2.21 Å. The average Cu(2)-N(Py) distance is 1.95 Å. The two different coordination environments in **D.3** is in contrast with the equivalent coordination environments observed in the structure of the lithium salt of **D.1** (Figure D.6). Dimerization of the salt is observed in the solid state with a  $\mu_2$ -N(pyrrolide) motif between the two Li centers. Ryan Ribson has demonstrated that the lithium salt of the pentacene-substituted DPP also associates in solution. Such helical structures have been observed in bis(terpy) dicopper complexes,<sup>15</sup> and in bis(DPP) Cu(II) complexes.<sup>11</sup> Complex **D.4** features a four-coordinate distorted trigonal pyramidal four-coordinate Cu(1) center ( $\tau_4 = 0.81$ ) bound to the pyrrolide donor and one pyridine of the DPP ligand and both nitrogen donors of the phenanthroline ligand (Figure D.7). Similar bond distances between 1.98 and 2.08 Å are observed between Cu(1) and all bound nitrogen atoms. The free pyridine donor is rotated away from the metal center and a distance of 2.6 Å is calculated between Cu(1) and the hydrogen atom bound to the proximal pyridine group, consistent with an anagostic interaction.<sup>16</sup> A distance of 3.4 Å is calculated between the centroid of the mesityl substituent of the bound pyridine and the plane of the phenanthroline ligand, within the sum of the van der Waals radii (3.54 Å) and consistent with intramolecular  $\pi$ - $\pi$  interactions.<sup>17 17 17</sup>

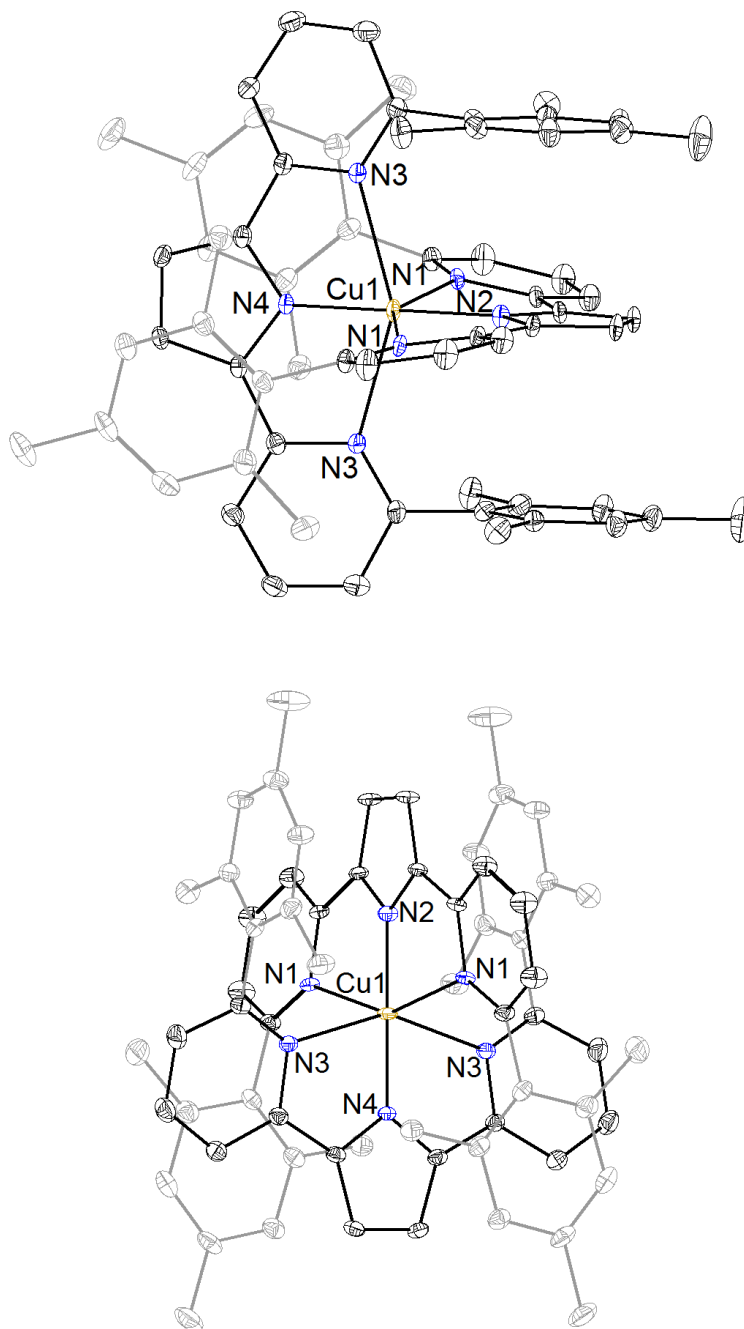


**Figure D.4.** Solid-state structure of **D.2**. Hydrogen atoms and solvents of crystallization are omitted for clarity.

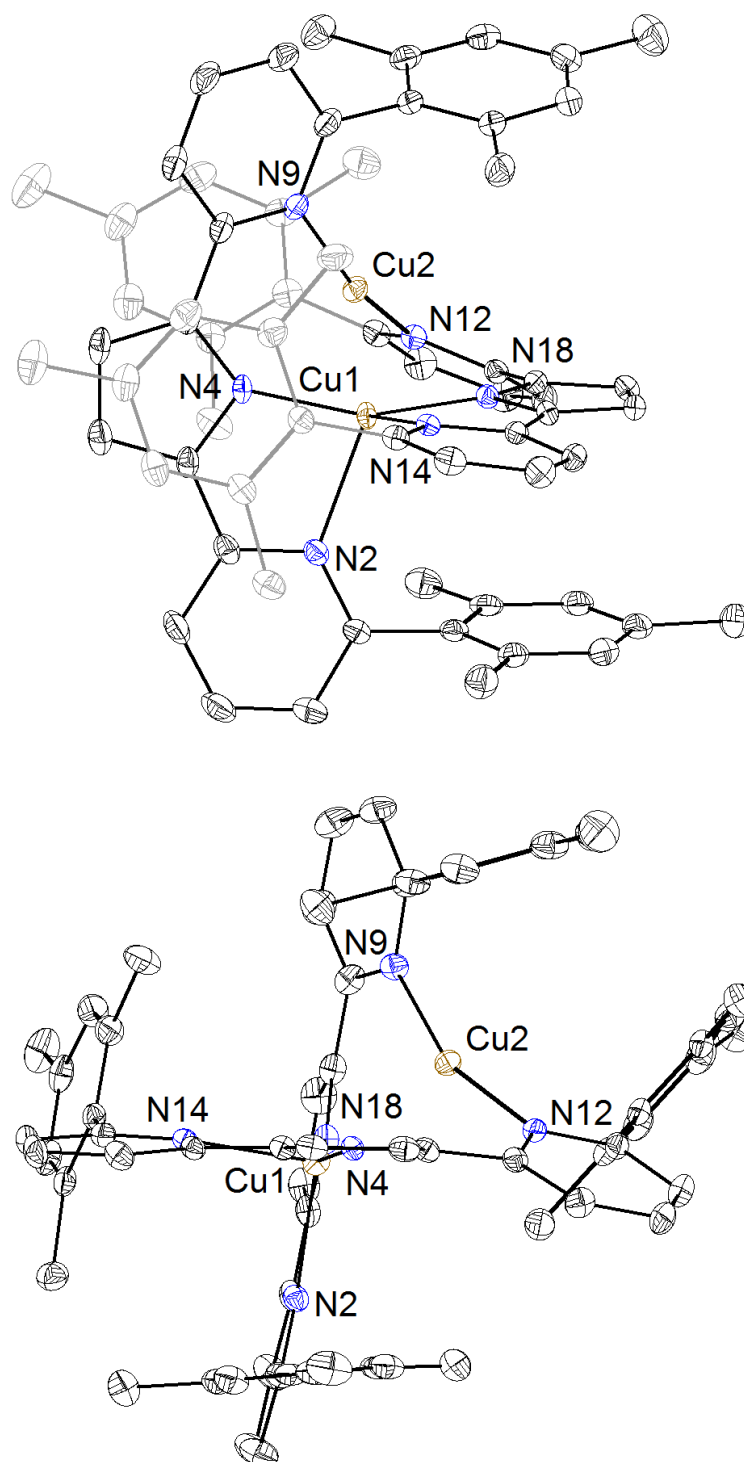


**Figure D.5.** Solid-state structure of **D.3**. Hydrogen atoms are omitted for clarity; one of two molecules in the asymmetric unit is shown for clarity.

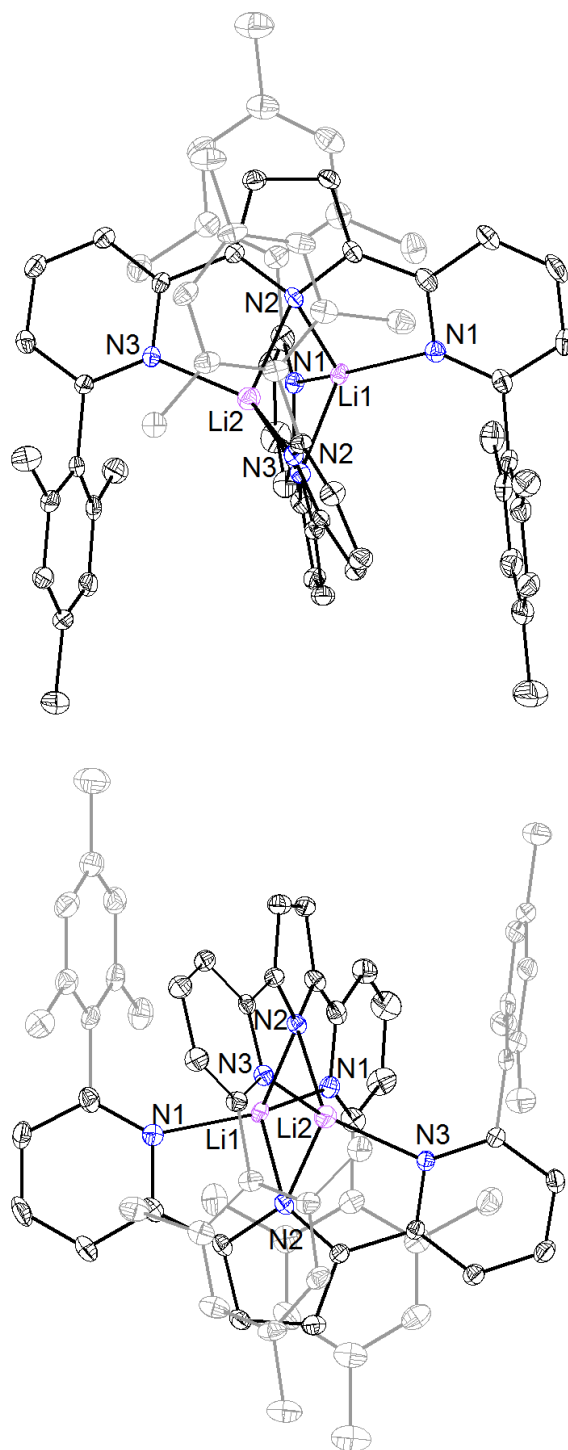


**Figure D.6.** Solid-state structure of **D.1-Li**. Hydrogen atoms are omitted for clarity.

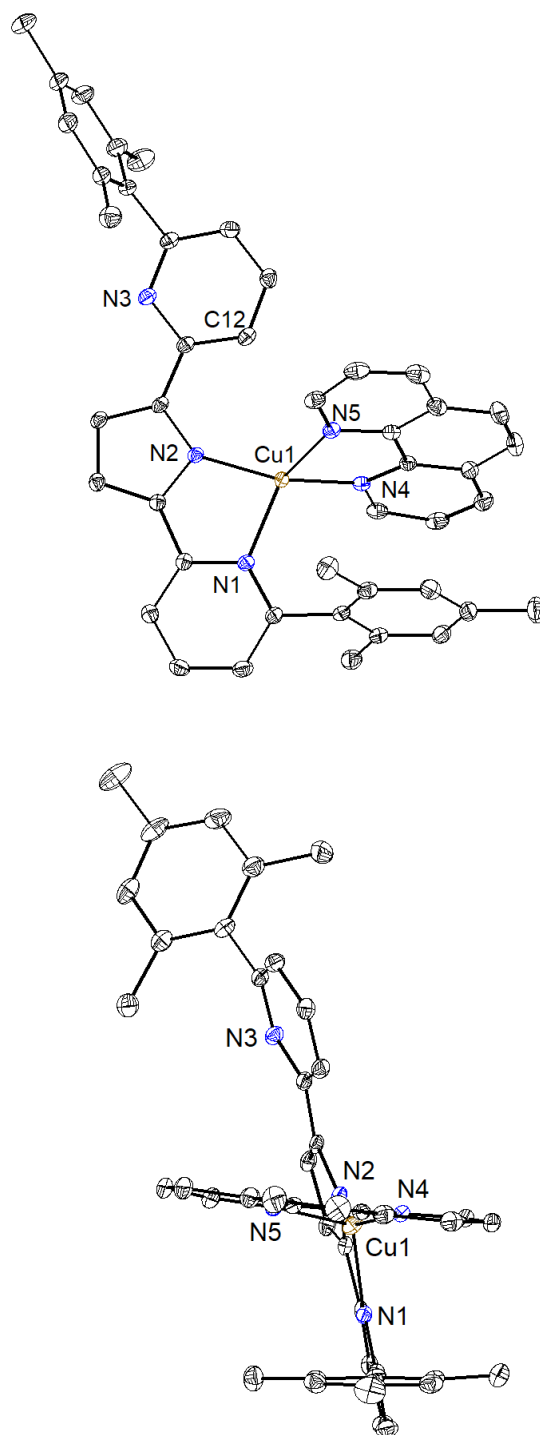
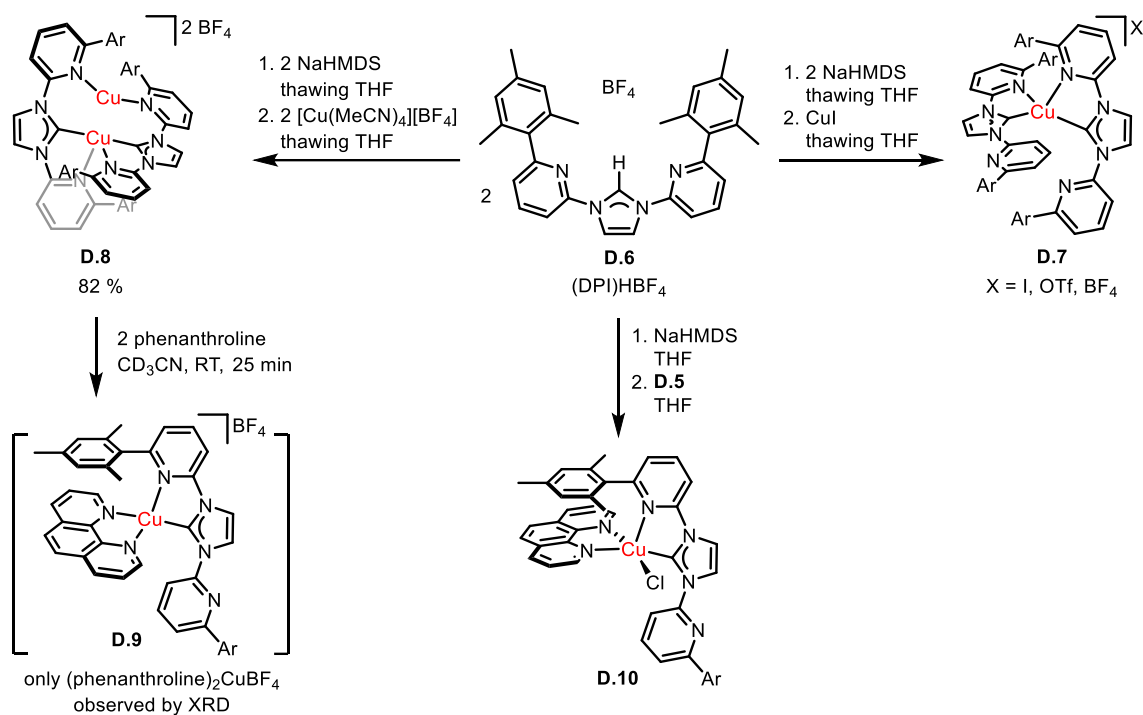


**Figure D.7.** Solid-state structure of **D.4**. Hydrogen atoms and solvent of crystallization are omitted for clarity.

An analogous series of complexes bearing the DPI ligand were also prepared (Scheme D.2), though the DPI-ligated analogue of **D.4** could not be isolated as a result of ligand scrambling. Reaction of **D.6** with one equivalent of NaHMDS in thawing THF, followed by addition to a thawing suspension of half an equivalent of CuI in THF results in formation of the bis-ligated Cu(I) complex **D.7**. Due to the cosolubility of NaI and the desired complex, this has only been isolated with a mixture of  $\text{BF}_4^-$  and  $\text{I}^-$  counteranions or, using  $[\text{Cu}(\text{MeCN})_4][\text{OTf}]$ , with a mixture of  $\text{BF}_4^-$  and  $\text{OTf}^-$  counteranions. Reaction of **D.6** with NaHMDS and  $[\text{Cu}(\text{MeCN})_4][\text{BF}_4]$  or CuCl in thawing THF led to formation of half an equivalent of the orange-red dicopper(I) complex **D.8**. Due to the similar solubilities of **D.8** and  $\text{NaBF}_4$  in THF and acetonitrile, this complex could only be isolated free of salt impurities through use of CuCl. The heteroleptic complex **D.9** was targeted both by reaction of **D.8** with two equivalents of phenanthroline and by reaction of **D.5** with **D.6** in the presence of NaO*t*Bu or NaHMDS; however, crystals of bis(phenanthroline) Cu(I) were isolated from both routes. An additional species was also isolated when **D.5** was used as the Cu precursor; based on the significant THF solubility and asymmetric NMR features of this species, it was identified as chloride-bound complex **D.10**. Reaction of this complex with excess  $\text{NaBF}_4$  led to broadening of the  $^1\text{H}$  NMR features, though a species with the expected NMR features for **D.9** was not generated; reaction with one equivalent of  $\text{AgBF}_4$  lead to formation of a mixture of species with paramagnetically broadened NMR features. The formation of the bis(phenanthroline) and **D.10** under these conditions is likely a consequence of the high ligand lability in Cu(I) complexes;<sup>18</sup> the isolation of **D.4** may be feasible, in part, as a consequence of its increased solubility in non-polar solvents.





**Scheme D.2.** Preparation of DPI-ligated Cu(I) complexes.

Complexes **D.7** and **D.8** were characterized in the solid state by X-ray diffraction (Figures D.8 through D.10) and feature similar coordination geometries to those observed in the analogous DPP-ligated complexes. A four-coordinate see-saw metal center is observed for **D.7** ( $\tau_4 = 0.75$ ), where Cu(1) is bound to both NHC donors and a single pyridine donor from each ligand. A long contact is observed between Cu(1) and N(4B) with rotation of the other free pyridine away from the metal center. Distances of 1.9223(15) and 1.9050(15) Å are observed between Cu and C(1A) and C(1B) of bound NHC donors, with distances of 2.1768(13) and 2.2493(13) Å between Cu and N(1A) and N(1B) of the bound pyridine arms. A long Cu(1)-N(4B) distance of 3.342 Å is observed between Cu and the proximal pyridine, which is within the sum of the van der Waals radii (4.04 Å).<sup>17a 17a19</sup> In the solid-state complex **D.8** features a four-coordinate see-saw Cu(1) center ( $\tau_4 = 0.55$ ) and one two-coordinate distorted linear Cu(2) center. A Cu(1)-Cu(2)

distance of 2.4885(4) Å is observed. Cu(1) is bound to two NHC donors and two pyridine donors with Cu(1)-C(1A) and Cu(1)-C(1B) distances of 1.9298(16) and 1.9311(16) Å and Cu(1)-N(1A) and Cu(1)-N(1B) distances of 2.1369(13) and 2.1375(13) Å respectively. Cu(2)-N(4A) and Cu(2)-N(4B) distances of 1.9328(13) and 1.9348(14) Å and a N(4A)-Cu(2)-N(4B) angle of 158.07(6)°. Distances of 3.5 Å between one of the mesityl substituents of each ligand and the backbone of the other ligand are observed, consistent with intramolecular  $\pi$ - $\pi$  interactions.

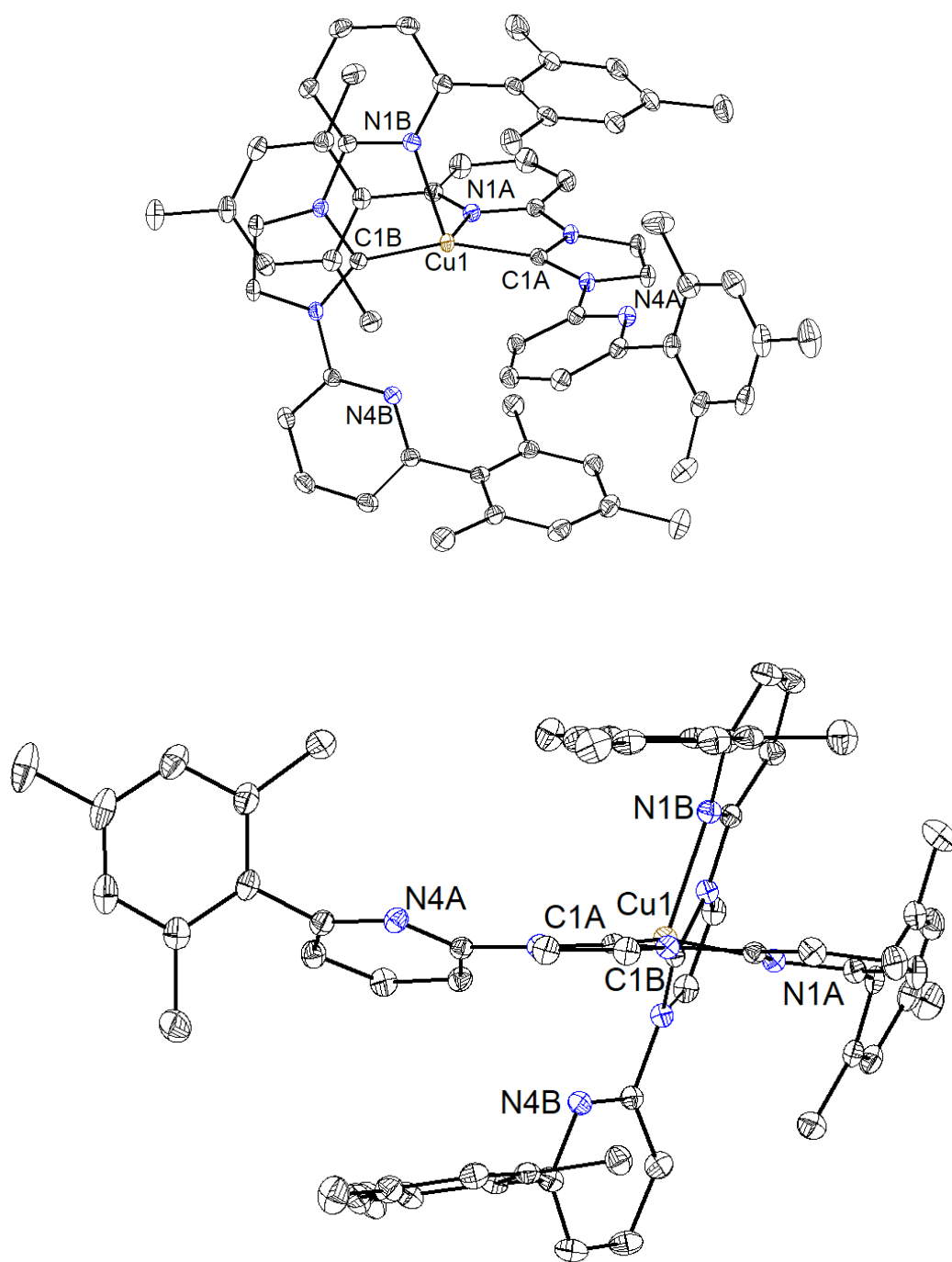


**Figure D.8.** Solid-state structure of **D.7** with iodide counteranion. Hydrogen atoms, solvent of crystallization, and iodide counteranion are omitted for clarity.

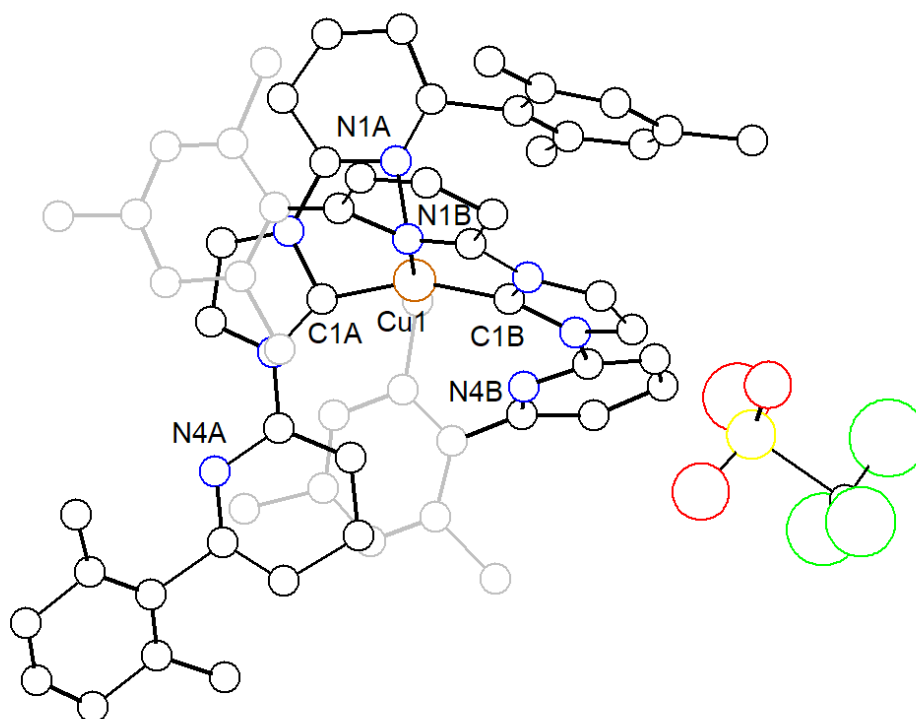


**Figure D.9.** Preliminary solid-state structure of **D.7** with triflate counteranion. Hydrogen atoms and disordered solvent of crystallization are omitted for clarity.

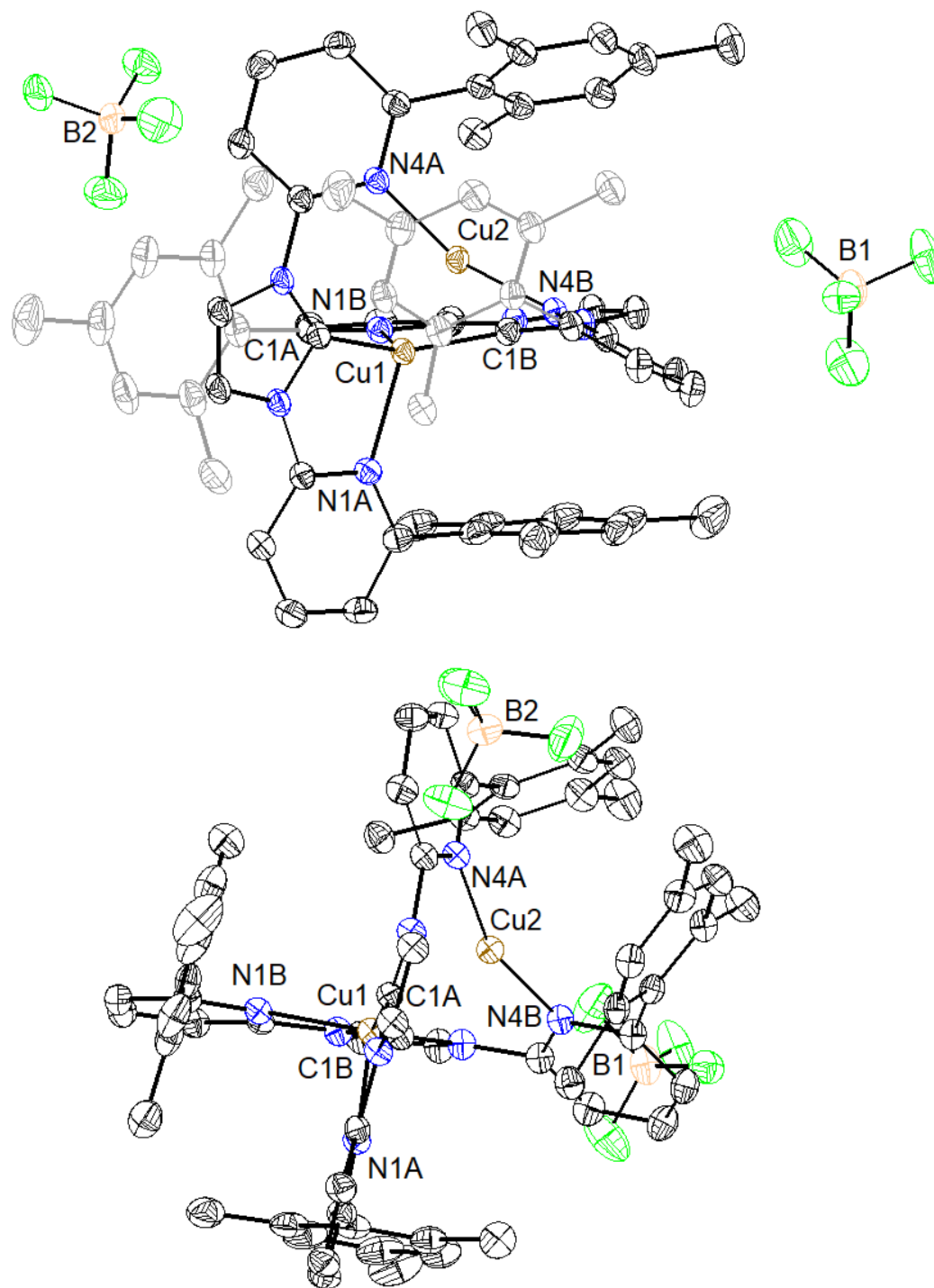


**Figure D.10.** Solid-state structure of **D.8**. Hydrogen atoms are omitted for clarity.

Cyclic voltammetry studies were on the Cu(I) complexes (Figures D.11 to D.14) in THF (DPP-ligated) or acetonitrile (DPI-ligated). **D.3** shows a reversible oxidation at -0.44 V and two additional features at 0.68 and 0.92 V vs. Fc/Fc<sup>+</sup>. Complex **D.4** features a reversible reduction at -2.43 V and a reversible oxidation at -0.64 V vs. Fc/Fc<sup>+</sup> with additional irreversible features at potentials more positive of 0 V. In the initial measurements, as **D.7** contained an equivalent of iodide, the I<sup>-</sup>/I<sub>2</sub> couple was also observed, however, an additional apparently reversible feature was also observed at +0.21 V vs. Fc/Fc<sup>+</sup> which is assigned to the one electron oxidation couple for this complex. As this peak could not be isolated, due to its proximity to the iodide couple, measurement of the Cu(I)/Cu(II) couple in **D.7** in the absence of NaI must be performed. Complex **D.8** shows three electrochemical events: a reversible oxidation at +0.23 V, a quasi-reversible oxidation at +0.81 V, and an irreversible reduction centered at -0.58 V.

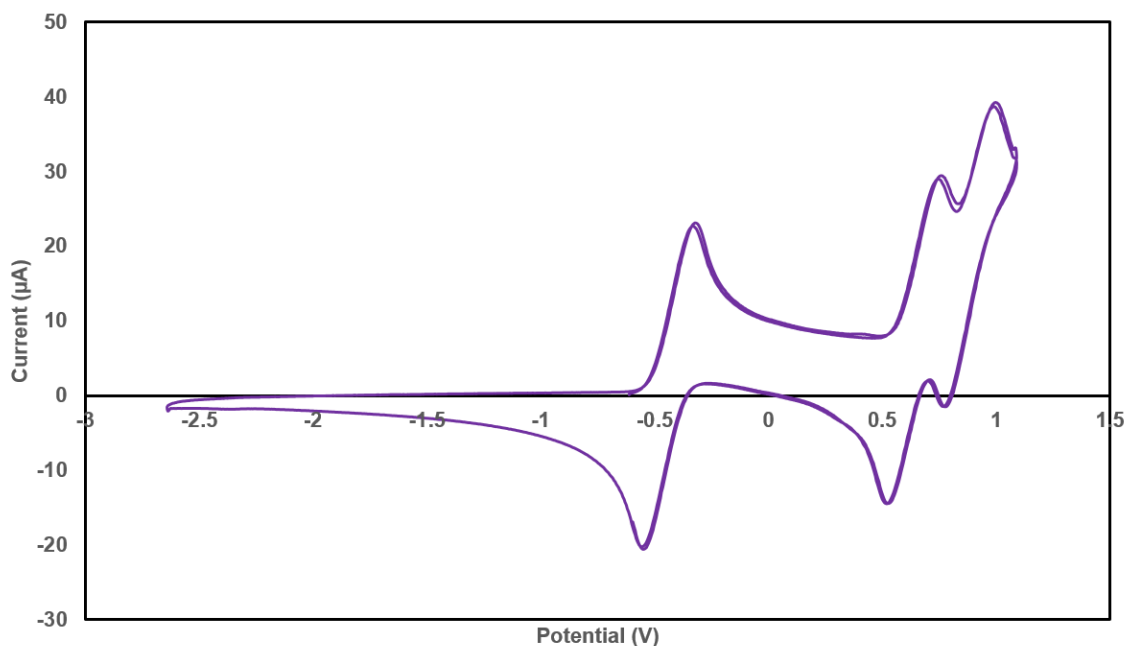


**Figure D.11.** CV of **D.3** in THF. 0.1 M TBAPF<sub>6</sub>, 0.2 mM substrate, GC working electrode, Pt counter-electrode, referenced internally to Fc/Fc<sup>+</sup>.

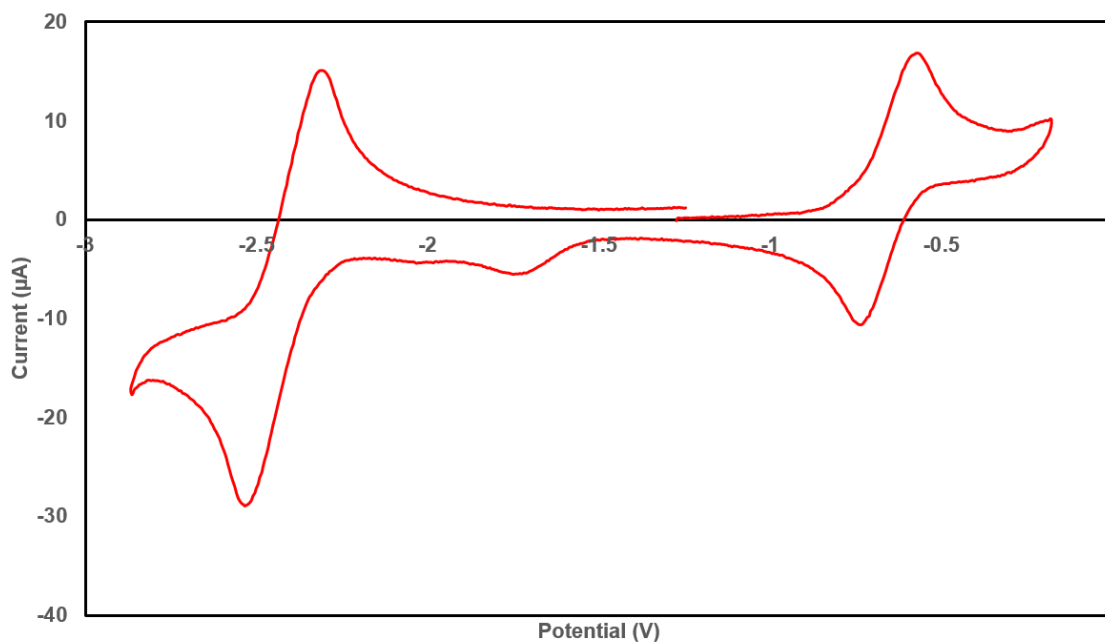


**Figure D.12.** Partial CV of **D.4** in THF. Conditions: 0.1 M TBAPF<sub>6</sub>, 0.2 mM substrate, 100 mV/s, internal reference to Fc/Fc<sup>+</sup>.

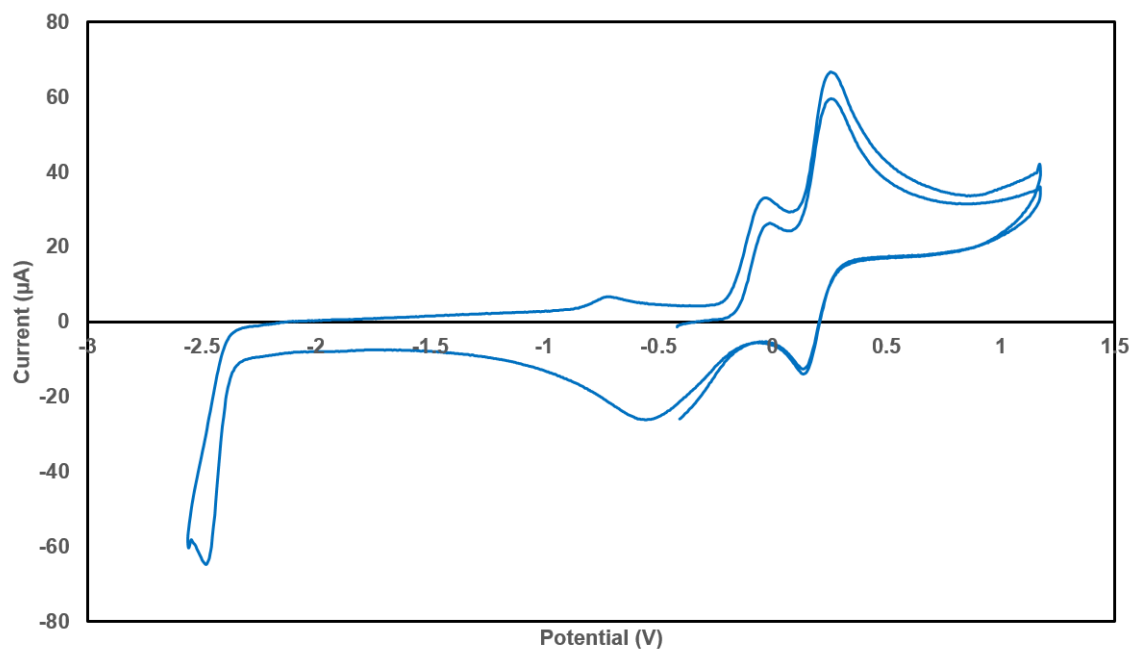


**Figure D.13.** CV of **D.7** with NaI in CH<sub>3</sub>CN. Conditions: 0.1 M TBAPF<sub>6</sub>, 0.2 mM substrate, 100 mV/s, internal reference to Fc/Fc<sup>+</sup>.

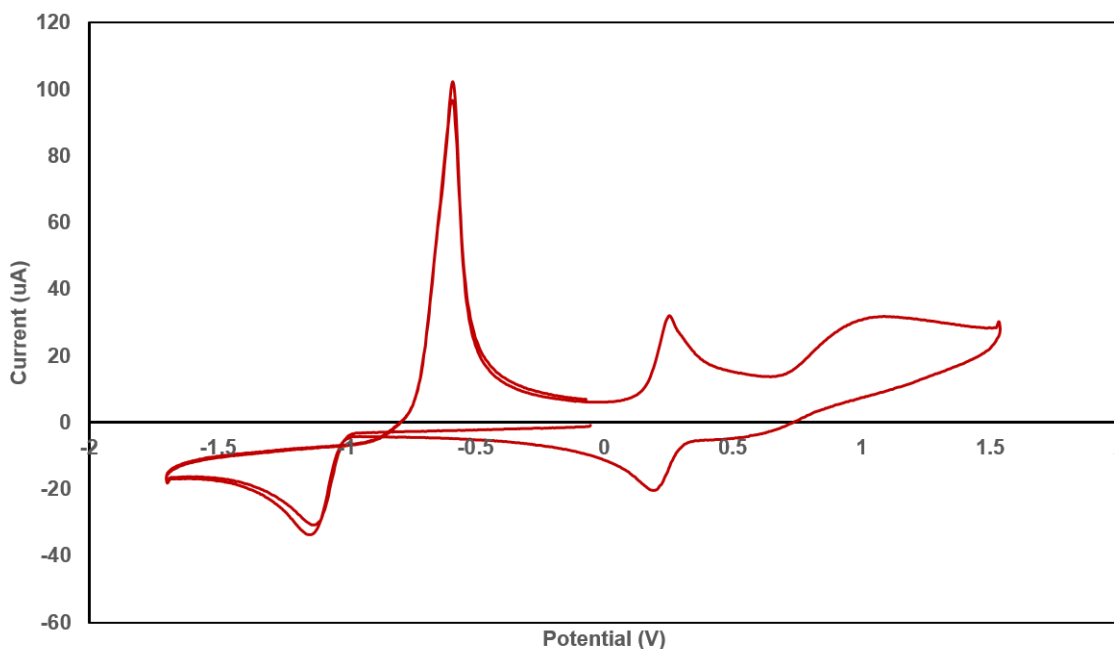
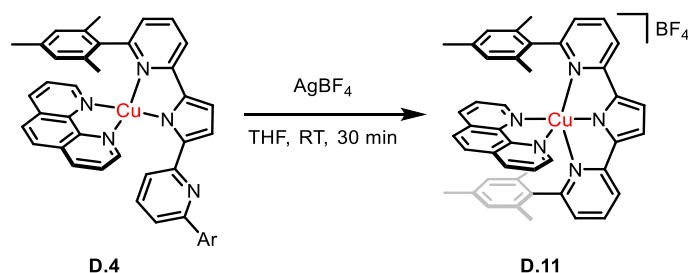


**Figure D.14.** CV of **D.8** in CH<sub>3</sub>CN. Conditions: 0.1 M TBAPF<sub>6</sub>, 0.2 mM substrate, 100 mV/s, internal reference to Fc/Fc<sup>+</sup>.

One potential role for the hemilabile pyridine donors in the monocopper complex would be to bind upon metal oxidation, preventing metal planarization by formation of higher-coordinate species. While the solid-state structure of **D.2** would provide evidence that this could occur, as solid-state characterization of the corresponding Cu(I) was not obtained, the hypothesis was more directly tested through oxidation of **D.4**. Treatment of **D.4** in THF with one equivalent of AgBF<sub>4</sub> resulted in color change from dark brown to green upon addition with extensive formation of dark precipitate. Extraction of the crude reaction mixture with acetonitrile afforded a green microcrystalline solid with paramagnetically-shifted and broadened NMR features. A mixture of green and bronze crystals were obtained from DCM/pentane solvent diffusion crystallization, corresponding to the acetonitrile-bound oxidized complex **D.11(MeCN)** (Figure D.15),



the acetonitrile-bound oxidized complex (**D.11(MeCN)**) co-crystallized with the oxidized **D.3** (Figure D.16), and the solvent-free complex **D.11** (Figure D.17). Cu is bound to both pyridine arms in all structures of **D.11**. In the co-crystallized structure (Figure D.16) two  $\text{BF}_4$  counteranions are observed; while  $\text{AgBF}_4$  could further oxidize **D.4** under the reaction conditions, this is assumed to be the oxidized form of **D.3** (**D.3+**) based on the oxidation potential of that complex observed by CV. Furthermore, a better fit for the crystallographic data was obtained by modeling the two-coordinate metal center as disordered between Cu (65 %) and Ag (35 %). **D.3** was not observed in NMRs of the isolated **D.4**, however, it is unclear whether this was generated by ligand scrambling or present in the crude at such a concentration to not be observed by NMR.



**Scheme D.3.** Oxidation of **D.4** with  $\text{AgBF}_4$  in THF.

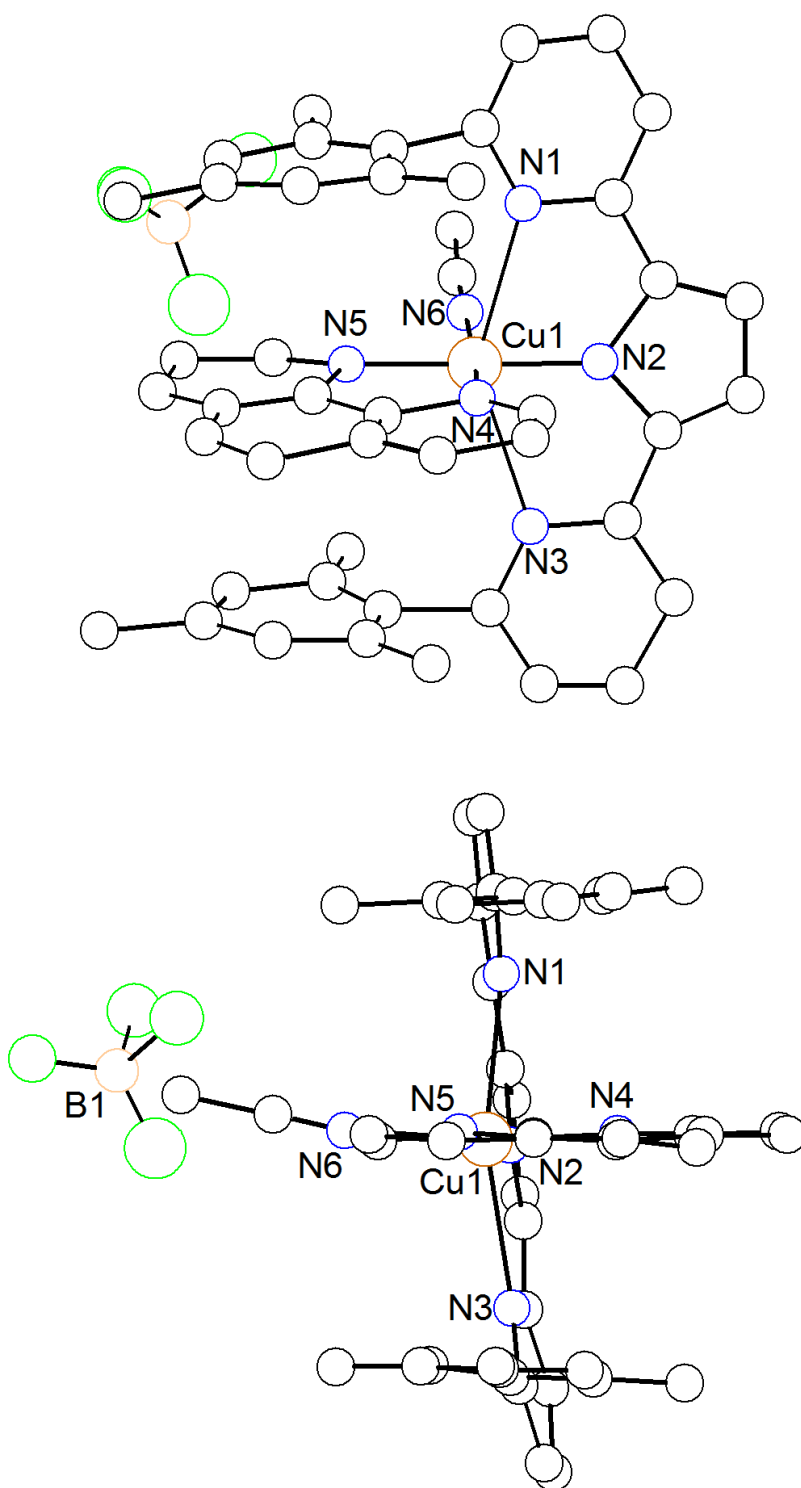


**Figure D.15.** Solid-state structure of the acetonitrile-bound **D.11(MeCN)**. Hydrogen atoms are omitted for clarity.

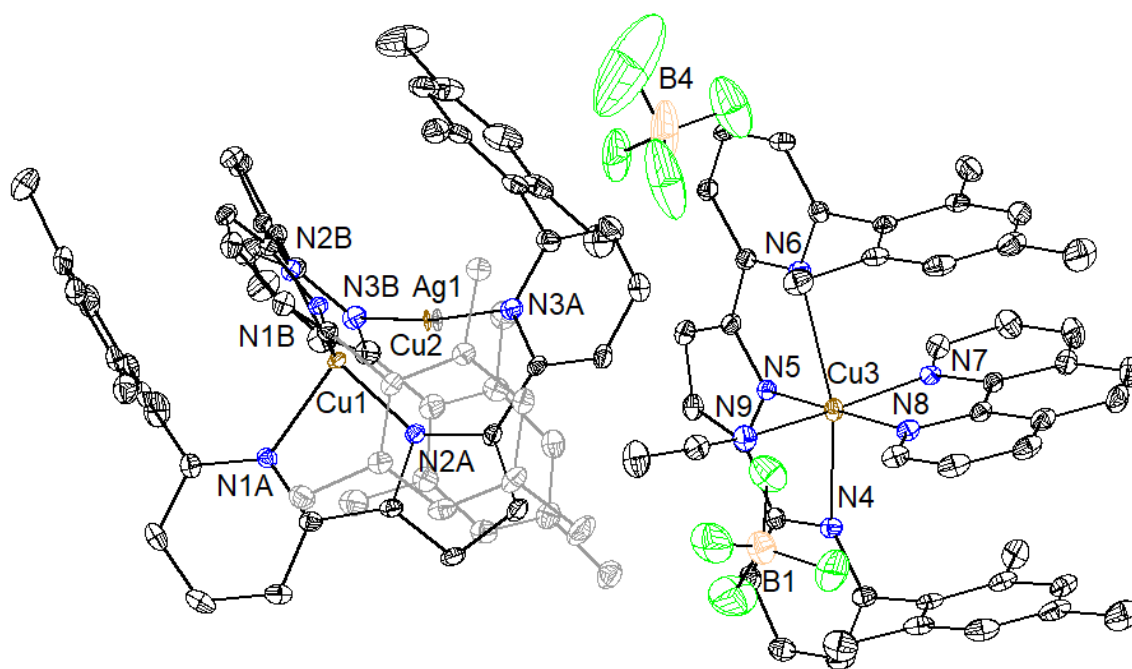


**Figure D.16.** Solid-state structure of the co-crystallized acetonitrile-bound **D.11(MeCN)** with the one-electron oxidized **D.3<sup>+</sup>**. Hydrogen atoms and solvent of crystallization are omitted for clarity.

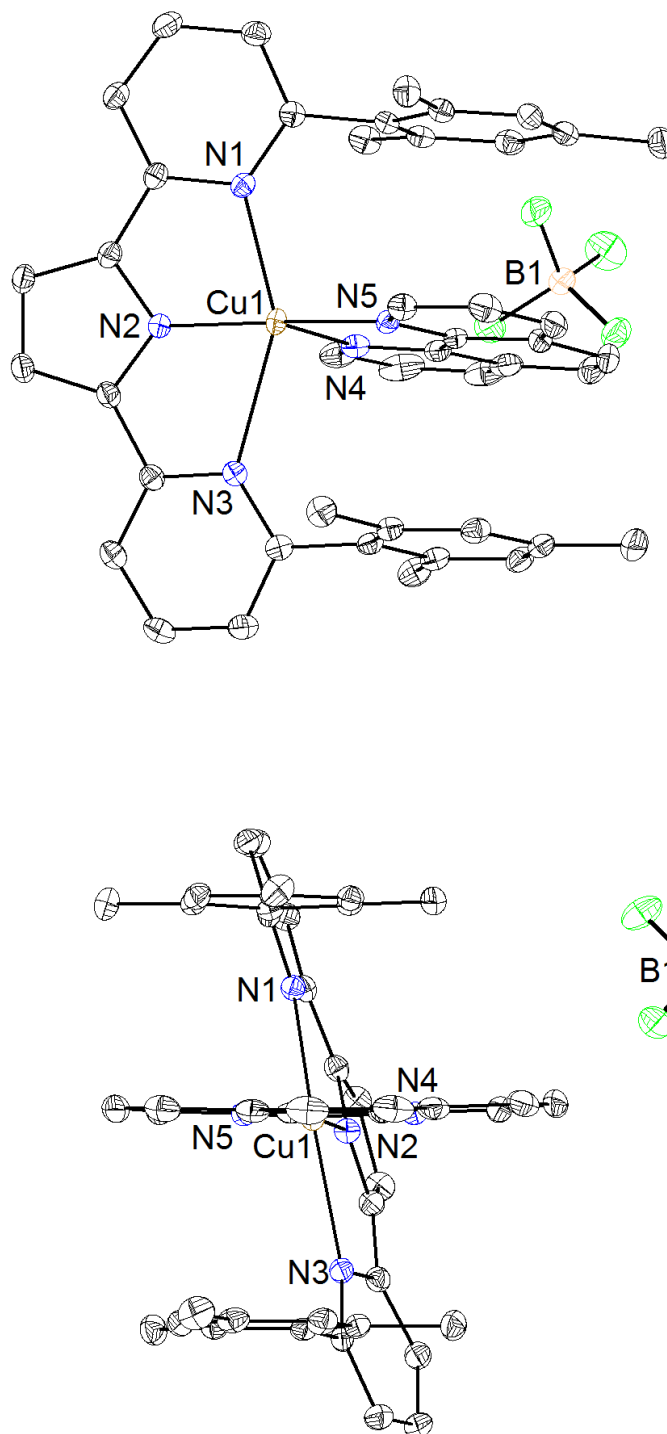


**Figure D.17.** Solid-state structure of **D.11**. Hydrogen atoms and solvent of crystallization are omitted for clarity.

Six-coordinate, distorted octahedral Cu centers are observed in both acetonitrile-bound structures of **D.11(MeCN)** while a distorted square pyramidal Cu center is observed in the solvent-free structure of **D.11**. In the acetonitrile-bound complex **D.11(MeCN)** long Cu(1)-N(Py) contacts are observed with an average distance of 3.53 Å. Cu(1)-N(2) distances of 1.81 and 1.95 Å are observed with an average distance of 3.44 Å between the centroids of the mesityl substituents and the plane of the phenanthroline ligand. In the solvent-free structure of **D.11** Cu-N(Py) distances of 2.4576(12) and 2.1936(11) Å are observed with a Cu-N(2) distance of 1.8554(12) Å. Contacts of 3.34 and 3.28 Å are observed between the mesityl groups and the plane of the phenanthroline ligand. The Cu adopts a distorted square pyramidal geometry with a  $\tau_5$  value of 0.21.

Work on measuring the emission lifetimes of these complexes is ongoing in collaboration with Ryan Ribson and Dr. Brian Sanders.

## DISCUSSION

Based on the solid-state characterization of this series of Cu(I) and Cu(II) complexes, simultaneous binding of all four pyridine donors of both the DPP and DPI ligands to a single reduced Cu center is not favored in the solid-state. The structure of these complexes in solution was not established. It is possible that there is either rapid exchange between free and bound pyridine donors on the NMR time scale or that higher coordinate number structures are adopted in solution. Either possibility would lead to sharp, symmetric NMR features and could facilitate the reversible electrochemical one-electron oxidations observed by CV through either facile binding of the additional pyridine donors or precoordination of all pyridine donors.

While distorted tetrahedral geometries in the reduced Cu complexes could likely be accommodated by the DPP and DPI ligands, see-saw and distorted trigonal pyramidal geometries are observed in their solid-state structures. Such geometries position the carbon atoms of the mesityl substituents parallel to and within the van der Waals radii of the backbone of the other ligand, consistent with  $\pi$ - $\pi$  interactions between these groups. Such interactions likely stabilize the observed geometries and could help to facilitate facile exchange between the pyridine groups or to potentially enforce higher-coordinate geometries in solution. Measurement of the rate of exchange between free and bound pyridine arms using variable temperature NMR could be used to distinguish between such potential solution-state structures; however, due to the overlap of the aromatic  $^1\text{H}$  NMR resonances of **D.4** with *d*<sub>8</sub>-PhMe and reactivity with CD<sub>2</sub>Cl<sub>2</sub>, such an experiment was not performed. Use of quantitative NOESY experiments could potentially be used to establish the average distance in solution between the mesityl groups and the DPP and DPI backbones.

From the cyclic voltammetry studies, all complexes show a reversible one-electron wave which likely corresponds to a Cu(I)/Cu(II) couple. Both **D.7** and **D.8** have similar one-electron oxidation potentials, which could indicate that the oxidation occurs on the four-coordinate Cu center. From the preliminary structure of **D.11** co-crystallized with oxidized **D.3**, minimal structural distortion is observed in the oxidized dicopper species, indicating the same may be true upon oxidation of **D.8**. In the case of the dicopper complexes, the oxidation could be born across the two copper centers leading to a mixed valent complex. Such behavior has been previously observed in the case of bis(amido) phosphine dicopper complexes reported by Peters and coworkers.<sup>2b, 2c, 20</sup> It is worth noting that it is possible that the structures of **D.3** and **D.8** observed by X-ray crystallography may not be maintained in solution and, in particular, may not be maintained in the presence of coordinating solvents.

There are a number of avenues that could be explored to potentially modify the emission lifetimes of DPI and DPP ligated complexes through modification of the electronics of the flanking aryl substituents. Preparation of DPP and DPI ligands bearing electron-withdrawing substituents (i.e. fluorinated arenes) or more extended aromatic substituents (i.e. anthracene, pentacene, or pyrene derivatives) which would form  $\pi$  donor-acceptor interactions with the other Cu ligand could prevent rotation of the free pyridine arms away from the Cu center. This could allow for faster rates of exchange between free and bound pyridine donors, potentially allowing for increased stabilization of the excited state. Use of di(pyridyl) NHC donors based upon central 6-membered rings, similar to those previously reported by Roesler and coworkers,<sup>21</sup> could potentially have a similar effect. Ligand modifications could also be leveraged for tuning of the first oxidation potential; Brooker and Colbran and coworkers have recently reported that the

Co<sup>III/II</sup> couple in bis(DPP) complex can be tuned through pyrrolide substitution with electron-donating and electron-withdrawing substituents.<sup>22</sup>



## CONCLUSIONS

In conclusion, a series of Cu complexes supported by mesityl-substituted di(pyridyl) pyrrolide (DPP) and di(pyridyl) NHC (DPI) ligands were prepared, structurally characterized, and their electrochemistry examined. Both monocopper and dicopper complexes can be supported by the DPP and DPI ligands; additionally heteroleptic DPP-phenanthroline Cu(I) and Cu(II) complexes were prepared. Distances consistent with  $\pi$ - $\pi$  interactions are observed between the mesityl substituents and the other Cu ligands. Four coordinate Cu(I) centers are observed in the solid state, while solution characterization by NMR suggests rapid exchange between free and bound pyridine groups on the NMR time scale. Reversible, one-electron oxidations are observed for the complexes by cyclic voltammetry. X-ray crystallographic characterization of the oxidized heteroleptic DPP-phenanthroline Cu(II) complex shows binding of both pyridine donors.

## EXPERIMENTAL SECTION

*General Comments.* All air- and water-sensitive compounds were manipulated under N<sub>2</sub> using standard Schlenk or glovebox techniques. Solvents for air- and moisture-sensitive reactions were dried by the method of Grubbs<sup>23</sup>. **D.1** was prepared as described in Chapter 3 of this thesis. **D.6** was prepared as described in Appendix C of this thesis. [Cu(MeCN)<sub>4</sub>][BF<sub>4</sub>] was purchased from Sigma Aldrich and used as received. All other Cu salts were purchased from Strem and used as received. Deuterated solvents were purchased from Cambridge Isotopes Lab, Inc.; CDCl<sub>3</sub> was used without further purification; C<sub>6</sub>D<sub>6</sub> was distilled from purple Na/benzophenone ketyl and stored over 4 Å molecular sieves; CD<sub>3</sub>CN was distilled from CaH<sub>2</sub>. <sup>1</sup>H and <sup>13</sup>C spectra were recorded on Varian Mercury 300, Varian INOVA-300, 400, or 500 spectrometers or Bruker Cryoprobe 400. <sup>1</sup>H and <sup>13</sup>C chemical shifts are reported relative to residual solvent resonances. Elemental analysis was performed on a Perkin-Elmer 2400 CHNS/O Analyser and samples were taken from representative batches prepared in an N<sub>2</sub>-filled glovebox, unless otherwise noted. UV-Vis spectra were acquired on a Varian Cary Bio 50 spectrophotometer in Teflon-pin sealed cuvettes.

**Preparation of D.2.** LiHMDS (55.6 mg, 0.332 mmol) in THF (2 mL) was added to a stirred solution of **D.1** (148.5 mg, 0.325 mmol) in THF (1 mL) and stirred at room temperature for 10 min. This was transferred to the top of a suspension of CuCl<sub>2</sub> (22.0 mg, 0.164 mmol) in THF (2 mL) and stirred at room temperature for 20 h. Volatiles were removed under reduced pressure and the resulting yellow-green solids washed with benzene, then extracted with DCM to afford the desired complex as a yellow-green solid. X-ray quality crystals were grown by diffusion of pentane into a DCM solution of the complex in DCM. <sup>1</sup>H NMR (CD<sub>2</sub>Cl<sub>2</sub>, 400 MHz) δ 28.09, 16.78, 11.89, 10.25, 9.41, 6.98,

6.02, 2.31, 1.50, 1.20. Anal calcd. For  $C_{64}H_{60}CuN_6$ : C, 78.70; H, 6.19; N, 8.60. Found: C, 75.73; H, 6.09; N, 8.28.

**Preparation of D.3.** A solution of NaHMDS (32.2 mg, 0.176 mmol) in THF (2 mL) was added to a solution of **D.1** (73.2 mg, 0.160 mmol) in THF (1 mL) and stirred 15 min at room temperature. The resulting yellow solution was then transferred to the top of a  $[Cu(MeCN)_4][BF_4]$  (54.1 mg, 0.172 mmol) suspension in THF (2 mL) and stirred 15 h at room temperature. Volatiles were removed under reduced pressure and the resulting orange-red solids washed extensively with hexanes. Extract with benzene afforded the desired complex as an orange-red solid (75.6 mg, 91 %). X-ray quality crystals were grown by evaporation of a pentane solution of the complex into toluene at room temperature.  $^1H$  NMR ( $C_6D_6$ , 400 MHz)  $\delta$  7.25 (dd,  $J = 8.1, 1.1$  Hz, 2H, Py), 7.02 (dd,  $J = 8.1, 7.4$  Hz, 2H, Py), 6.82 (s, 2H, pyrr), 6.60 (br s, 2H, mes), 6.58 (br s, 2H, mes), 6.37 (dd,  $J = 7.3, 1.1$  Hz, 2H, Py), 2.17 (s, 6H, mesCH<sub>3</sub>), 1.72 (br s, 6H, mesCH<sub>3</sub>), 1.64 (br s, 6H, mesCH<sub>3</sub>).  $^{13}C$  NMR ( $C_6D_6$ , 101 MHz)  $\delta$  158.34 (Py), 156.72 (Py), 141.70 (pyrr), 137.42, 136.80, 136.69, 135.75, 133.94, 128.59, 119.39 (Py), 118.65 (Py), 111.66 (pyrr), 21.35 (mesCH<sub>3</sub>), 20.78 (mesCH<sub>3</sub>), 20.43 (mesCH<sub>3</sub>).

**Preparation of D.4.** NaHMDS (20.8 mg, 0.113 mmol) in 2 mL THF was added to a stirred solution of **D.1** (49.5 mg, 0.108 mmol) in 1 mL and the resulting bright yellow solution stirred 15 min at room temperature. This solution was then transferred to the top of a rapidly stirred suspension of **D.5** (31.2 mg, 0.112 mmol) in 1 mL THF. The resulting red-brown suspension was stirred 13 h at room temperature then filtered, concentrated to 4 mL, layered with pentane, and allowed to sit at room temperature. The crystallization was filtered after 3 days, the solids washed with fresh pentane, and dried under vacuum to afford the desired compound as a dark brown, crystalline solid (71.8

mg, 95 %). X-ray quality crystals were grown by vapor diffusion of pentane into a benzene solution of the complex at room temperature.  $^1\text{H}$  NMR ( $\text{C}_6\text{D}_6$ , 400 MHz)  $\delta$  8.20 (dd,  $J$  = 4.7, 1.5 Hz, 2H, phen), 7.89 (dd,  $J$  = 8.1, 0.8 Hz, 2H, Py), 7.72 (s, 2H, pyrr), 7.36 (dd,  $J$  = 8.0, 1.5 Hz, 2H, phen), 7.05 (dd,  $J$  = 8.1, 7.4 Hz, 4H, phen, Py), 6.71 (dd,  $J$  = 8.0, 4.7 Hz, 2H, phen), 6.36 (dd,  $J$  = 7.3, 1.0 Hz, 2H, Py), 5.81 (s, 4H, mes), 1.73 (s, 6H, mesCH<sub>3</sub>), 1.65 (s, 6H, mesCH<sub>3</sub>).  $^{13}\text{C}$  NMR ( $\text{C}_6\text{D}_6$ , 101 MHz)  $\delta$  157.41 (Py), 156.84 (Py), 147.33 (phen), 143.58, 141.85, 139.01, 135.35 (Py), 134.64, 134.46, 132.80 (phen), 128.22, 126.54 (mes), 125.33 (phen), 123.86 (phen), 117.43 (Py), 115.60 (Py), 111.59 (pyrr), 20.72 (mesCH<sub>3</sub>), 19.84 (mesCH<sub>3</sub>). Anal calcd. For  $\text{C}_{44}\text{H}_{38}\text{CuN}_5 + \text{C}_6\text{H}_6$ : C, 77.14; H, 5.70; N, 9.00. Found: C, 76.93; H, 5.55; N, 8.92.

**Preparation of D.7/NaI.** NaHMDS (37.5 mg, 0.204 mmol) in THF (2 mL) was added, thawing to a suspension of **D.6** (109.0 mg, 0.1995 mmol) in THF (4 mL) and allowed to stir, warming for 30 min. This brown solution was then refrozen and added, thawing to a suspension of CuI (19.2 mg, 0.101 mmol). The resulting suspension was allowed to stir, warming for 10 h then volatiles were removed under reduced pressure. The resulting brown-orange solids were washed with benzene and THF and the desired compound obtained as an orange solid via extraction with acetonitrile (90 mg, 0.0739 mmol, 73 %). X-ray quality crystals were grown by vapor diffusion of ether into an acetonitrile solution of the complex at room temperature.  $^1\text{H}$  NMR ( $\text{CD}_3\text{CN}$ , 400 MHz)  $\delta$  8.20 (dd,  $J$  = 8.4, 0.7 Hz, 2H, Py), 7.93 – 7.80 (m, 4H, Py, imid), 7.18 (dd,  $J$  = 7.5, 0.7 Hz, 2H, Py), 6.68 (s, 4H, mes), 2.24 (s, 6H, mesCH<sub>3</sub>), 1.71 (s, 12H, mesCH<sub>3</sub>).  $^{13}\text{C}$  NMR ( $\text{CD}_3\text{CN}$ , 101 MHz)  $\delta$  183.96 (NCN), 159.45 (Py), 151.56 (Py), 140.77, 138.86, 136.96, 136.27, 128.96, 124.99, 118.91, 112.42, 21.25 (mesCH<sub>3</sub>), 20.50 (mesCH<sub>3</sub>).  $^{19}\text{F}$  NMR (376 MHz,  $\text{CD}_3\text{CN}$ )  $\delta$  -152.42, -152.48.

**Preparation of D.8.** A thawing solution of NaHMDS (46.8 mg, 0.255 mmol) in THF (2 mL) was added to the top of a suspension of **D.6** (132.2 mg, 0.242 mmol) in THF (1 mL) and stirred 15 minutes, warming. The resulting brown solution was re-frozen and then added to the top of a thawing suspension of CuCl (29.0 mg, 0.293) in THF (2 mL) and stirred, warming for 24 h. The crude reaction was filtered over Celite, and then the resulting dark red solids extracted with acetonitrile to afford the desired complex as an orange-red microcrystalline solid (120.0 mg, 0.0985 mmol, 82 %). X-ray quality crystals were grown by vapor diffusion of ether into a solution of the complex with NaBF<sub>4</sub> at room temperature; data was collected for the orange crystals. <sup>1</sup>H NMR (CD<sub>3</sub>CN, 400 MHz) δ 8.20 (d, *J* = 8.2 Hz, 2H), 7.92 – 7.82 (m, 4H), 7.18 (d, *J* = 7.5 Hz, 2H), 6.68 (s, 4H), 2.24 (s, 6H), 1.71 (s, 12H). <sup>13</sup>C NMR (CD<sub>3</sub>CN, 101 MHz) δ 183.95, 159.45, 151.56, 140.78, 138.87, 136.96, 136.28, 128.97, 124.99, 118.91, 112.42, 21.24, 20.50. <sup>19</sup>F NMR (376 MHz, CD<sub>3</sub>CN) δ -152.19, -152.25.

**Preparation of D.11.** A solution of AgBF<sub>4</sub> (8.8 mg, 0.045 mmol) in THF (1.5 mL) was added to the top of a solution of **D.4** (31.2 mg, 0.0445 mmol) in THF (1.5 mL) and stirred 1 h at room temperature. Volatiles were removed under reduced pressure and the resulting dark green solids extracted with acetonitrile to afford the acetonitrile adduct as a green solid (31.5 mg, 0.038 mmol, 85 % yield for the acetonitrile adduct). X-ray quality crystals of a mixture of the acetonitrile-bound and free complexes were grown by diffusion of pentane into a DCM solution of the complex at room temperature. <sup>1</sup>H NMR (CD<sub>3</sub>CN, 400 MHz) δ 21.16 (br s), 9.36 (br s), 7.64 (br s), 7.18 (br s), 4.48 (s), -1.33 (br s), -1.86, -2.40. <sup>19</sup>F NMR (CD<sub>3</sub>CN, 376 MHz) δ -156.21, -156.26, -156.29. Anal calcd. for C<sub>46</sub>H<sub>41</sub>BCuF<sub>4</sub>N<sub>6</sub>: C, 66.71; H, 4.99; N, 10.15. Found: C, 67.13; H, 5.02; N, 9.93.

**Electrochemical Measurements.** CVs were recorded with a Pine Instrument Company AFCBPI biopotentiostat with the AfterMath software package. Measurements were performed in a three component cell, consisting of a glassy carbon working electrode ( $\phi = 3.0$  mm), a Pt wire counterelectrode, and a Ag wire reference electrode in dry solvent in an N<sub>2</sub> filled glovebox. The ferrocene/ferrocenium couple was used as an internal reference.

**Crystallographic Information.** Crystals were mounted on a glass fiber or MiTeGen loop using Paratone oil, then placed on the diffractometer under a nitrogen stream. Diffractometer manipulations, including data collection, integration, and scaling were performed using the Bruker APEXII software.<sup>24</sup> Absorption corrections were applied using SADABS or TWINABS.<sup>25</sup> Space groups were determined on the basis of systematic absences and intensity statistics and the structures were solved in the Olex 2 software interface<sup>26</sup> by intrinsic phasing using XT (incorporated into SHELXTL)<sup>27</sup> and refined by full-matrix least squares on F<sup>2</sup>. Hydrogen atoms were placed in the idealized positions and refined using a riding model. Graphical representation of structures with 50% probability thermal ellipsoids were generated using Diamond 3 visualization software.<sup>28</sup> All non-hydrogen atoms were refined using anisotropic displacement parameters, except for **D.7/OTf** and **D.11(MeCN)**.

**Table D.1.** Crystal and refinement data for complexes **D.2**, **D.3**, and **D.4** (iodide)

	<b>D.2<sup>c</sup></b>	<b>D.3</b>	<b>D.4</b>
CCDC Number			
Empirical formula	C <sub>66</sub> H <sub>64</sub> Cl <sub>4</sub> CuN <sub>6</sub>	C <sub>64</sub> H <sub>60</sub> Cu <sub>2</sub> N <sub>6</sub>	C <sub>50</sub> H <sub>44</sub> CuN <sub>5</sub>
Formula weight	1146.58	1040.28	778.45
T (K)	100	100	100
<i>a</i> , Å	22.3246(10)	14.4717(12)	20.1297(13)
<i>b</i> , Å	22.3246(10)	18.4346(15)	9.5465(6)
<i>c</i> , Å	11.3688(6)	21.0410(15)	21.8580(18)
$\alpha$ , deg	90	93.930(2)	90
$\beta$ , deg	90	94.239(3)	108.332(3)
$\gamma$ , deg	90	112.165(3)	90
Volume, Å <sup>3</sup>	5666.1(5)	5156.0(7)	3987.2(5)
Z	4	4	4
Crystal system	Tetragonal	Triclinic	Monoclinic
Space group	P-4	P -1	P 2 <sub>1</sub> /n
$\theta$ range, deg	2.208, 34.227	2.271 to 32.347	2.388 to 27.492
$\mu$ , mm <sup>-1</sup>	0.622	0.873	0.590
Abs. Correction	Multi-scan	Multi-scan	Multi-scan
GOF	1.055	1.025	1.109
$R_1$ , <sup>a</sup> $wR_2$ <sup>b</sup> [I>2 $\sigma$ (I)]	0.0557, 0.1446	0.0502, 0.1323	0.0306, 0.0948
Radiation Type	Mo K $\alpha$	Cu K $\alpha$	Mo K $\alpha$

<sup>a</sup>  $R_1 = \sum ||F_o| - |F_c|| / \sum |F_o|$ . <sup>b</sup>  $wR_2 = [\sum [w(F_o^2 - F_c^2)^2] / \sum [w(F_o^2)^2]]^{1/2}$ . <sup>c</sup>Crystals originally grown by Dr. Gyeongshin Choi and diffracted with assistance from Larry Henling and Dr. Mike Takase; data reprocessed and refined by Jessica Sampson.

**Table 4.2.** Crystal and refinement data for complexes **D.7/I**, **D.7/OTf**<sup>c</sup>, and **D.8**

	<b>D.7/I</b>	<b>D.7/OTf</b> <sup>c</sup>	<b>D.8</b>
CCDC Number			
Empirical formula	C <sub>64</sub> H <sub>63</sub> CuN <sub>4</sub> I	C <sub>67</sub> H <sub>68</sub> CuF <sub>3</sub> N <sub>8</sub> O <sub>4</sub> S	C <sub>62</sub> H <sub>60</sub> B <sub>2</sub> Cu <sub>2</sub> F <sub>8</sub> N <sub>8</sub>
Formula weight	1148.67	6018.1(6)	1217.90
T (K)	100	100	100
<i>a</i> , Å	12.3051(7)	18.5178(2)	13.1899(7)
<i>b</i> , Å	17.7048(6)	25.2008(16)	23.3154(12)
<i>c</i> , Å	25.7363(10)	12.9079(7)	19.3361(10)
α, deg	90	90	90
β, deg	96.265(3)	92.468(2)	108.1410(10)
γ, deg	90	90	90
Volume, Å <sup>3</sup>	5573.4(4)	6018.06	5650.8(5)
Z	4	4	4
Crystal system	Monoclinic	Monoclinic	Monoclinic
Space group	P 2 <sub>1</sub> /c	C <sub>2</sub>	P 2 <sub>1</sub> /c
θ range, deg	2.302 to 27.509	2.963 to 47.661	3.064 to 79.716
μ, mm <sup>-1</sup>	0.995	1.369	1.558
Abs. Correction	Multi-scan	Multi-scan	Multi-scan
GOF	1.085	1.607	1.055
R <sub>1</sub> , <sup>a</sup> wR <sub>2</sub> <sup>b</sup> [I>2σ(I)]	0.0339, 0.0639	0.0987, 0.2970	0.0413, 0.1156
Radiation Type	Mo Kα	Cu Kα	Cu Kα

<sup>a</sup>  $R_1 = \sum ||F_o| - |F_c|| / \sum |F_o|$ . <sup>b</sup>  $wR_2 = [\sum [w(F_o^2 - F_c^2)^2] / \sum [w(F_o^2)^2]]^{1/2}$ . <sup>c</sup> Only ID collected.



**Table 4.3.** Crystal and refinement data for complexes **D.11(MeCN)**, **D.11(MeCN)/D3+**, and **D.11**

	<b>D.11(MeCN)<sup>c</sup></b>	<b>D.11(MeCN)/D3+<sup>D</sup></b>	<b>D.11</b>
CCDC Number			
		$C_{112}H_{105}Ag_{0.26}B_2$	
Empirical formula	$C_{46}H_{41}BCuF_4N_6$	$Cl_4Cu_{2.78}F_8N_{12}$	$C_{45}H_{40}BCl_2CuF_4N_5$
Formula weight	828.21	2140.62	872.07
T (K)	100	100	100
<i>a</i> , Å	11.248(7)	15.9408(9)	35.0392(12)
<i>b</i> , Å	16.241(10)	18.2424(11)	11.6512(4)
<i>c</i> , Å	21.908(12)	19.8899(15)	23.6670(7)
$\alpha$ , deg	90	104.342(3)	90
$\beta$ , deg	90	108.277(3)	126.0060(10)
$\gamma$ , deg	90	103.918(3)	90
Volume, Å <sup>3</sup>	4002(4)	4992.5(6)	7816.1(5)
Z	4	2	8
Crystal system	Orthorhombic	Triclinic	Monoclinic
Space group	P 2 <sub>1</sub> 2 <sub>1</sub> 2 <sub>1</sub>	P -1	C2/c
$\theta$ range, deg	2.390 to 18.527	2.181 to 27.479	3.116 to 79.087
$\mu$ , mm <sup>-1</sup>	0.606	0.806	2.551
Abs. Correction	Multi-scan	Multi-scan	Multi-scan
GOF	1.166	1.019	1.077
$R_1$ , <sup>a</sup> $wR_2$ <sup>b</sup>			
[I>2 $\sigma$ (I)]	0.1460, 0.3426	0.0405, 0.1026	0.0354, 0.0981
Radiation Type	Mo K $\alpha$	Mo K $\alpha$	Cu K $\alpha$

<sup>a</sup>  $R_1 = \sum ||F_o| - |F_c|| / \sum |F_o|$ . <sup>b</sup>  $wR_2 = [\sum [w(F_o^2 - F_c^2)^2] / \sum [w(F_o^2)^2]]^{1/2}$ . <sup>c</sup> Only ID collected due to rapid solvent loss under diffraction conditions. <sup>D</sup> Co-crystallized with the oxidized

**D.3.**

## REFERENCES

1. (a) Armaroli, N. *Chem. Soc. Rev.* **2001**, 30 (2), 113-124; (b) Horváth, O. *Coord. Chem. Rev.* **1994**, 135-136, 303-324; (c) Housecroft, C. E.; Constable, E. C. *Chem. Soc. Rev.* **2015**, 44 (23), 8386-8398.
2. (a) Miller, A. J.; Dempsey, J. L.; Peters, J. C. *Inorg. Chem.* **2007**, 46 (18), 7244-7246; (b) Harkins, S. B.; Mankad, N. P.; Miller, A. J.; Szilagy, R. K.; Peters, J. C. *J. Am. Chem. Soc.* **2008**, 130 (11), 3478-85; (c) Deaton, J. C.; Switalski, S. C.; Kondakov, D. Y.; Young, R. H.; Pawlik, T. D.; Giesen, D. J.; Harkins, S. B.; Miller, A. J.; Mickenberg, S. F.; Peters, J. C. *J. Am. Chem. Soc.* **2010**, 132 (27), 9499-9508.
3. (a) Hamze, R.; Jazzar, R.; Soleilhavoup, M.; Djurovich, P. I.; Bertrand, G.; Thompson, M. E. *Chem. Comm.* **2017**, 53 (64), 9008-9011; (b) Romanov, A. S.; Di, D.; Yang, L.; Fernandez-Cestau, J.; Becker, C. R.; James, C. E.; Zhu, B.; Linnolahti, M.; Credgington, D.; Bochmann, M. *Chem. Comm.* **2016**, 52 (38), 6379-6382.
4. (a) Buckner, M. T.; McMillin, D. R. *J. Chem. Soc., Chem. Comm.* **1978**, (17); (b) Blaskie, M. W.; McMillin, D. R. *Inorg. Chem.* **1980**, 19 (11), 3519-3522; (c) Dietrich-Buchecker, C. O.; Marnot, P. A.; Sauvage, J.-P.; Kirchhoff, J. R.; McMillin, D. R. *J. Chem. Soc., Chem. Comm.* **1983**, (9), 513-515; (d) Blasse, G.; Breddels, P. A.; McMillin, D. R. *Chem. Phys. Lett.* **1984**, 109 (1), 24-26; (e) McMillin, D. R.; Kirchhoff, J. R.; Goodwin, K. V. *Coord. Chem. Rev.* **1985**, 64, 83-92; (f) Ichinaga, A. K.; Kirchhoff, J. R.; McMillin, D. R.; Dietrich-Buchecker, C. O.; Marnot, P. A.; Sauvage, J. P. *Inorg. Chem.* **1987**, 26 (25), 4290-4292; (g) Gushurst, A. K. I.; McMillin, D. R.; Dietrich-Buchecker, C. O.; Sauvage, J. P. *Inorg. Chem.* **1989**, 28 (22), 4070-4072; (h) Everly, R. M.; Ziessel, R.; Suffert, J.; McMillin, D. R. *Inorg. Chem.* **1991**, 30 (3), 559-561; (i) McCusker, C. E.; Castellano, F. N. *Inorg. Chem.* **2013**, 52 (14), 8114-8120; (j) Mara, M. W.; Fransted, K. A.; Chen, L. X. *Coord. Chem. Rev.* **2015**, 282-283, 2-18.
5. Giereth, R.; Reim, I.; Frey, W.; Junge, H.; Tschierlei, S.; Karnahl, M. *Sustainable Energy & Fuels* **2019**, 3 (3), 692-700.
6. (a) Schmittel, M.; Ganz, A. *Chem. Comm.* **1997**, (11), 999-1000; (b) Schmittel, M.; Ganz, A. *Synlett* **1997**, 1997 (6), 710-712; (c) Schmittel, M.; Ganz, A.; Fenske, D.; Herderich, M. J. *Chem. Soc., Dalton Trans.* **2000**, (3), 353-359; (d) Schmittel, M.; Michel, C.; Liu, S.-X.; Schildbach, D.; Fenske, D. *Eur. J. Inorg. Chem.* **2001**, 2001 (5), 1155-1166; (e) Fraser, M. G.; van der Salm, H.; Cameron, S. A.; Barnsley, J. E.; Gordon, K. C. *Polyhedron* **2013**, 52, 623-633.
7. (a) Pellegrin, Y.; Sandroni, M.; Blart, E.; Planchat, A.; Evain, M.; Bera, N. C.; Kayanuma, M.; Sliwa, M.; Rebarz, M.; Poizat, O.; Daniel, C.; Odobel, F. *Inorg. Chem.* **2011**, 50 (22), 11309-11322; (b) Fraser, M. G.; van der Salm, H.; Cameron, S. A.; Blackman, A. G.; Gordon, K. C. *Inorg. Chem.* **2013**, 52 (6), 2980-92; (c) Sandroni, M.; Kayanuma, M.; Planchat, A.; Szuwarski, N.; Blart, E.; Pellegrin, Y.; Daniel, C.; Boujtita, M.; Odobel, F. *Dalton Trans.* **2013**, 42 (30), 10818-10827; (d) Barnsley, J. E.; Scottwell, S. O.; Elliott, A. B.; Gordon, K. C.; Crowley, J. D. *Inorg. Chem.* **2016**, 55 (16), 8184-8192; (e) Kohler, L.; Hadt, R. G.; Hayes, D.; Chen, L. X.; Mulfort, K. L. *Dalton Trans.* **2017**, 46 (38), 13088-13100; (f) Hayes, D.; Kohler, L.; Chen, L. X.; Mulfort, K. L. *J. Phys. Chem. Lett.* **2018**, 9 (8), 2070-2076; (g) Kohler, L.; Hayes, D.; Hong, J.; Carter, T. J.; Shelby, M. L.; Fransted, K. A.; Chen, L. X.; Mulfort, K. L. *Dalton Trans.* **2016**, 45 (24), 9871-9883; (h) Sandroni, M.; Favereau, L.; Planchat, A.; Akdas-Kilig, H.; Szuwarski, N.; Pellegrin, Y.; Blart, E.; Le Bozec, H.; Boujtita, M.; Odobel, F. *J. Mater. Chem. A* **2014**, 2 (26), 9944-9947.

8. (a) Liu, B.; Zhang, Y.; Xu, D.; Chen, W. *Chem. Commun.* **2011**, 47 (10), 2883-2885; (b) Liu, B.; Jin, Z.; Lv, J.; Li, X.; Zhou, H. Method for synthesizing N-heterocyclic carbene-copper complex. CN105585584A, 2016.
9. (a) Haider, J.; Kunz, K.; Scholz, U. *Adv. Synth. Catal.* **2004**, 346 (7), 717-722; (b) Kunz, K.; Scholz, U.; Gaertzen, O.; Ganzer, D.; Wesener, J. Preparation of copper carbene complexes and their use as coupling reaction catalysts. EP1437355A1, 2004; (c) Kunz, K.; Haider, J.; Ganzer, D.; Scholz, U.; Sicheneder, A. Process for the preparation of nitrodiphenylamines. EP1437341A1, 2004.
10. Ciszek, J. W.; Keane, Z. K.; Cheng, L.; Stewart, M. P.; Yu, L. H.; Natelson, D.; Tour, J. M. *J. Am. Chem. Soc.* **2006**, 128 (10), 3179-3189.
11. Fang, W.-Z.; Wang, Y.-P.; Wang, Y.-F.; Zhang, S.-C.; Yi, X.-Y. *RSC Adv.* **2015**, 5 (12), 8996-9001.
12. Min, R.; Hu, X.-h.; Yi, X.-y.; Zhang, S.-c. *J. Cent. South Univ. (Engl. Ed.)* **2015**, 22 (5), 1619-1625.
13. (a) Hu, X.-H.; Liang, Y.; Li, C.; Yi, X.-Y. *Dalton Trans.* **2014**, 43 (6), 2458-2464; (b) Wang, Y.-P.; Hu, X.-H.; Wang, Y.-F.; Pan, J.; Yi, X.-Y. *Polyhedron* **2015**, 102, 782-787; (c) Wang, Y.-P.; Xiao, J.-J.; Hu, X.-H.; Yi, X.-Y. *Inorg. Chim. Acta* **2015**, 435, 125-130.
14. (a) Raba, A.; Anneser, M. R.; Jantke, D.; Cokoja, M.; Herrmann, W. A.; Kuhn, F. E. *Tet. Lett.* **2013**, 54 (26), 3384-3387; (b) Riener, K.; Bitzer, M. J.; Pothig, A.; Raba, A.; Cokoja, M.; Herrmann, W. A.; Kuhn, F. E. *Inorg. Chem.* **2014**, 53 (24), 12767-12777.
15. (a) Yeung, C. T.; Yeung, H. L.; Tsang, C. S.; Wong, W. Y.; Kwong, H. L. *Chem. Comm.* **2007**, (48), 5203-5205; (b) Constable, E. C.; Kulke, T.; Neuburger, M.; Zehnder, M. *Chem. Comm.* **1997**, (5), 489-490; (c) Constable, E. C.; Edwards, A. J.; Hannon, M. J.; Raithby, P. R. *J. Chem. Soc., Chem. Comm.* **1994**, (17), 1991-1992; (d) Allen, J. J.; Barron, A. R. *J. Chem. Crystallogr.* **2008**, 38 (11), 879-882.
16. Brookhart, M.; Green, M. L.; Parkin, G. *Proc. Natl. Acad. Sci.* **2007**, 104 (17), 6908-6914.
17. (a) WebElements.com (accessed November 26, 2018); (b) Martinez, C. R.; Iverson, B. L. *Chem. Sci.* **2012**, 3, 2191-2201.
18. Lei, Y.; Anson, F. C. *Inorg. Chem.* **1995**, 34 (5), 1083-1089.
19. Information retrieved from WebElements.com on 26 November, 2018
20. (a) Harkins, S. B.; Peters, J. C. *J. Am. Chem. Soc.* **2004**, 126 (9), 2885-93; (b) Mankad, N. P.; Rivard, E.; Harkins, S. B.; Peters, J. C. *J. Am. Chem. Soc.* **2005**, 127 (46), 16032-16033; (c) Harkins, S. B.; Peters, J. C. *J. Am. Chem. Soc.* **2005**, 127 (7), 2030-2031; (d) Mankad, N. P.; Harkins, S. B.; Antholine, W. E.; Peters, J. C. *Inorg. Chem.* **2009**, 48 (15), 7026-7032.
21. Jiang, Y.; Gendy, C.; Roesler, R. *Organometallics* **2018**, 37 (7), 1123-1132.
22. McPherson, J. N.; Hogue, R. W.; Akogun, F. S.; Bondi, L.; Luis, E. T.; Price, J. R.; Garden, A. L.; Brooker, S.; Colbran, S. B. *Inorg. Chem.* **2019**, Article ASAP.
23. Pangborn, A. B.; Giardello, M. A.; Grubbs, R. H.; Rosen, R. K.; Timmers, F. J. *Organometallics* **1996**, 15 (5), 1518-1520.
24. APEX2, Version 2 User Manual, M86-E01078, Bruker Analytical X-ray Systems, Madison, WI, June 2006.
25. Sheldrick, G.M. "SADABS (version 2008/I): Program for Absorption Correction for Data from Area Detector Frames", University of Gottingen, 2008.
26. Dolomanov, O. V.; Bourhis, L. J.; Gildea, R. J.; Howard, J. A. K.; Puschmann, H. *J. Appl. Crystallogr.* **2009**, 42 (2), 339-341.

27. Sheldrick, G. M. *Acta Cryst.* **2008**, *A64*, 112-122.
28. Brandenburg, K. (1999), DIAMOND. Crystal Impact GdR, Bonn, Germany.

## APPENDIX E

SYNTHESIS AND ATTEMPTED METALATIONS OF  $\mu_2$ -NNX (X = N, C) LIGANDS TO  
SUPPORT POTENTIAL HETEROBIMETALLIC OLEFIN POLYMERIZATION CATALYSTS

**ABSTRACT**

Di(pyridyl) guanidine and di(pyridyl) N-heterocyclic olefin (NHO) ligands were targeted to support potential heterobimetallic Zr, Ni, and Pd catalysts with pendant Lewis acids bridged by  $\mu_2$ -N and -C groups. While several routes were used to target the di(pyridyl) guanidine proligand, this could not be prepared under those conditions. Di(pyridyl) NHO and mono(pyridyl) NHO proligands could be prepared from the corresponding ethylenediamines by reaction with triethyl orthoacetate and subsequent deprotonation of the resulting 2-methylimidazolines with strong bases. Treatment of these proligands with metal alkyl precursors showed no conversion to the desired metal-N-heterocyclic vinylene complexes. Reaction with  $\text{Pd}(\text{OAc})_2$  seemed to indicate formation of such a species by  $^1\text{H}$  NMR, though attempts to carry this forward were unsuccessful.

## INTRODUCTION

The development of transition metal catalysts for the copolymerization of ethylene and  $\alpha$ -olefins containing polar functional groups to linear, polar-functionalized polyethylene with high catalyst activity and good control over polymer molecular weight distributions and comonomer incorporation remains a great challenge in homogeneous catalysis.<sup>1</sup> In spite of the improve printability, adhesion, durability, and rheological properties of such polymers, catalyst inhibition and poisoning by polar comonomers means only a few classes of catalysts are competent for this transformation, typically based on Ni or Pd.

Incorporation of Lewis acid binding sites into the ligands of polymerization catalysts has recently emerged as a strategy to modulate their activities and to potentially attenuate the Lewis basicity of the polar comonomers. Tonks and coworkers have reported complexes which can bind alkali metals (**E.A**, Figure E.1) and  $\text{Zn}^{2+}$  (**E.B** and **E.C**).<sup>2</sup> In the case of **E.A** alkali metal binding results in ligand tautomerization; however rotation of the alkali metal center away from Ni leads to similar polymerization behavior as in the absence of the alkali metals.<sup>2b</sup> Binding of  $\text{Zn}^{2+}$  to **E.B** promotes formation of higher molecular weight products as a result of axial steric pressure, while binding of  $\text{Zn}^{2+}$  to **E.C** promotes  $\beta$ -H elimination.<sup>2a, 2c</sup> Do and coworkers have reported the use of poly(ethylene) glycol-appended Ni phenoxy-imine catalysts (**E.D**) where catalyst activity and polymer molecular weight and branch density can be controlled through application of use of alkali metal cation additives.<sup>3</sup> Do and coworkers have also more recently reported systems **E.E** and **E.F** where binding of  $\text{Zn}^{2+}$  (**E.E**) leads to enhanced catalyst lifetime and binding of alkali metals to **E.F** leads to enhanced catalyst lifetimes at elevated temperatures.<sup>4</sup>

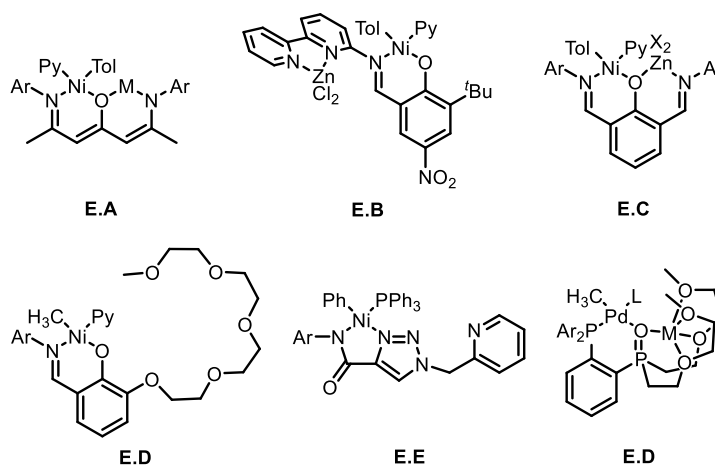


**Figure E.1.** Examples of polymerization catalysts incorporating Lewis Acid binding sites.

As early metal catalysts incorporating Lewis acid binding sites into the ancillary ligand have been comparatively underdeveloped, we proposed the use of di(pyridyl) guanidinate (**E.G**), mono(pyridyl) guanidinate (**E.H**), di(pyridyl) N-heterocyclic vinylene (**E.I**), and mono(pyridyl) N-heterocyclic vinylene (**E.J**) ligands to support either monometallic catalysts or bimetallic catalysts with  $\mu_2$ -N or  $\mu_2$ -C moieties. N-heterocyclic olefins and their deprotonated form, N-heterocyclic vinylenes, have been used as ligands for main group and transition metal chemistry as a result of their strong  $\sigma$ - and  $\pi$ -donating ability, allowing for isolation main group compounds in reduced oxidation states.<sup>5</sup> We hypothesized that these ligands might support late transition metal catalysts for olefin polymerization in conjunction with supporting weak donors such as pyridines or phosphine oxides. Guanidinate groups have found success in the literature as monodentate ligands to support highly active group IV polymerization catalysts;<sup>6</sup> however, their use in polydentate ligand scaffolds is relatively underexplored.<sup>6b, 7</sup> While guanidines typically serve as linear  $\mu_1$  groups, the presence of the chelating pyridine groups might allow the guanidinate to bridge to a second metal center. These



electronically-asymmetric ligand sets might engender similar properties on the resulting catalyst as observed with phosphine-sulfonate,<sup>8</sup> bisphosphine monoxide,<sup>9</sup> phosphine phosphonate,<sup>10</sup> and N-heterocyclic carbene phenoxide<sup>11</sup> and phosphine oxide catalysts.<sup>12</sup> Those systems feature asymmetric ligand sets leading to improved activity in polar  $\alpha$ -olefin copolymerization with the resulting polymers featuring reasonable comonomer incorporation throughout the polymer backbone and highly linear structures. Through use of the strongly-donating N-heterocyclic vinylene moiety with an additional weak donor, this desirable  $\alpha$ -olefin incorporation reactivity might be achieved.

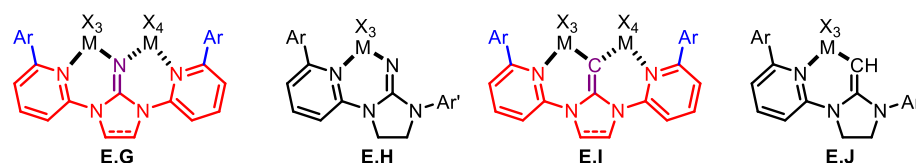
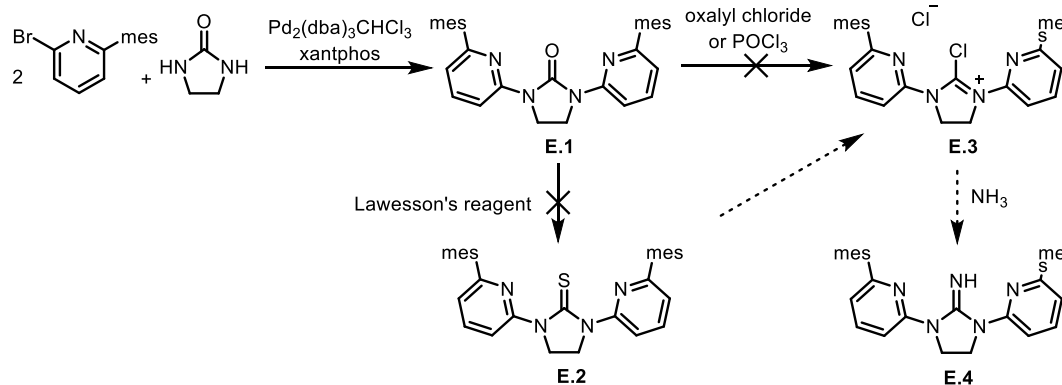


**Figure E.2.** Targeted di(pyridyl) guanidine and di(pyridyl) NHV catalysts for ethylene-polar- $\alpha$ -olefin copolymerization.

Herein is described work towards the synthesis of the di(pyridyl) guanidinate proligands, work by Diane Rafizadeh on the synthesis of di(pyridyl) urea ligated  $\text{Zn}^{2+}$  complexes, and work on the synthesis and attempted metalations of the di(pyridyl) and mono(pyridyl) N-heterocyclic vinylene proligands.

## RESULTS

The synthesis of di(pyridyl)guanidine proligands was initially approached based on the strategy of deoxygenation of the corresponding substituted di(pyridyl)urea **E.1** (Scheme E.1). Cu-catalyzed Ullman coupling of 2-imidazolidinone with halopyridines, such as 2-bromo-6-mesitylpyridine, resulted in formation of the desired di(pyridyl)ureas, however, the coupling proceeded more cleanly using Pd. In particular, the use of  $\text{Pd}_2\text{dba}_3 \bullet \text{CHCl}_3$ /xantphos with  $\text{Cs}_2\text{CO}_3$  in DMF could be used to generate **E.1** in high yields and good purity. The direct deoxygenation of **E.1** with oxalyl chloride or under Villsmeier-Haack conditions to **E.3** was attempted, however, no reaction was observed. Similarly, reaction of **E.1** with Lawesson's reagent at elevated temperatures over extended periods of time did not result in transformation to the corresponding thiourea **E.2** by  $^1\text{H}$  NMR or IR spectroscopy.



**Scheme E.1.** Attempted preparation of proligand **E.4** from di(pyridyl) urea **E.1**.

Crystals of the product of the reaction of **E.1** with Lawesson's reagent, oxalyl chloride, and  $\text{NH}_3$  were grown by slow evaporated of a methanol solution. A preliminary structure of the compound was obtained by X-Ray diffraction (Figure B.4), which confirms the overall skeleton; however the identification of X1 as oxygen is suggested by

the electron density and by the lack of observed hydrogen bonding interactions with the adjacent pyridine groups, as would likely be observed in the case of an NH substituent.

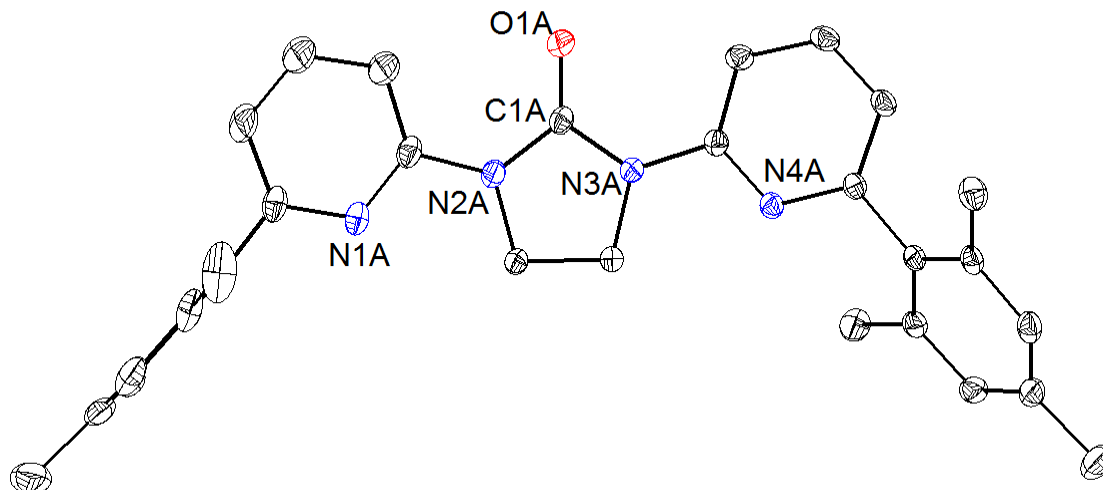
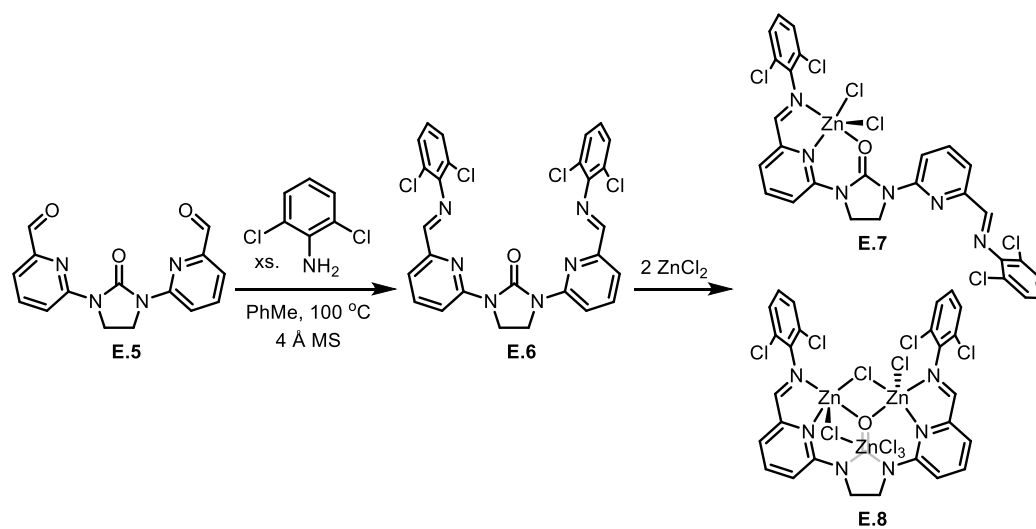


**Figure E.3.** Solid-state structure of **E.1**. Hydrogen atoms are omitted for clarity.

Using the di(pyridyl) urea framework, Diane Rafizadeh, a SURF student from Yale, prepared proligand **E.6** to support bimetallic complexes for  $\pi$ - $\pi$  interaction directed oxidation chemistry. **E.6** was prepared by condensation of 2,6-dichloroaniline with the previously-reported **E.5** at elevated temperatures in the presence of 4 Å molecular sieves. Subsequent reaction with two equivalents of  $\text{ZnCl}_2$  a mixture of two complexes: the mono(zinc) complex **E.7** and the tri(zinc) complex **E.8**, both of which could be crystallographically-characterized (Figures E.5 and E.6).



**Scheme E.2.** Preparation of Zn<sup>2+</sup> chloride complexes supported by the di(pyridyl) urea proligand **E.6** as developed by Diane Rafizadeh.

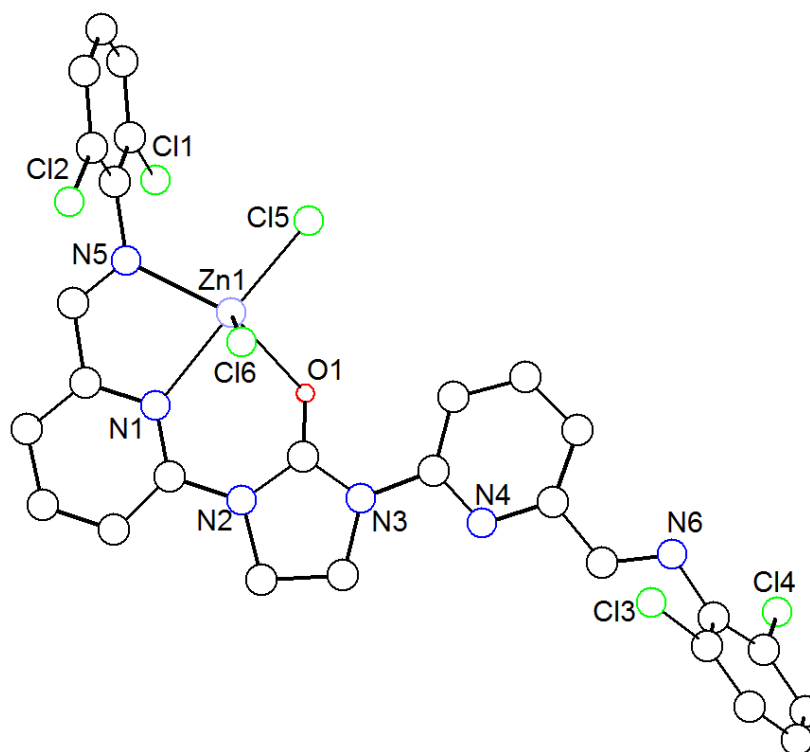


**Figure E.4.** Solid-state structure of mono(zinc) complex **E.7**. Hydrogen atoms are omitted for clarity.

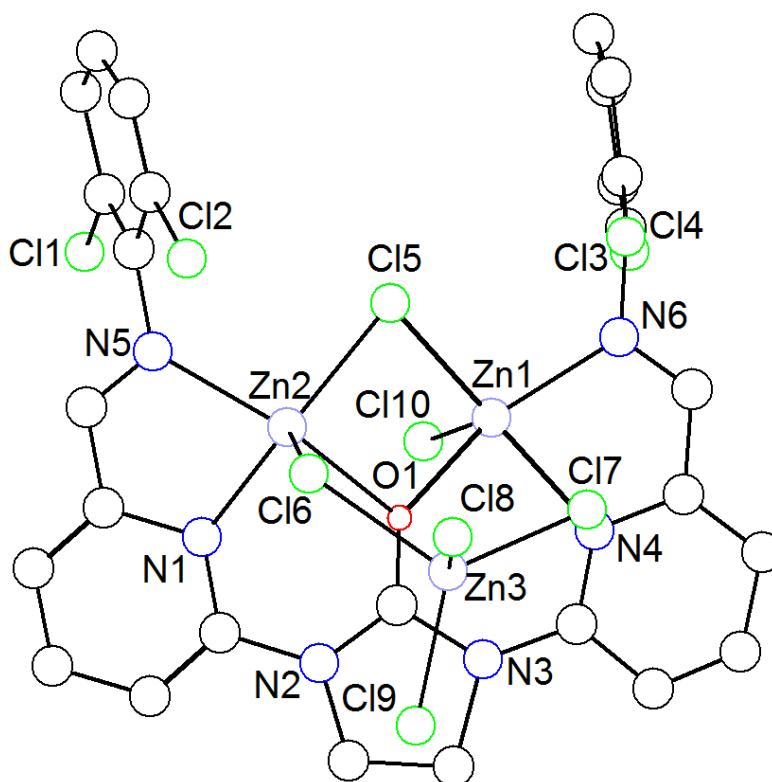
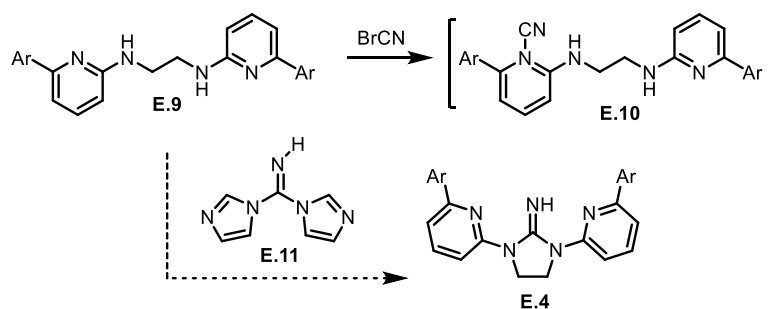


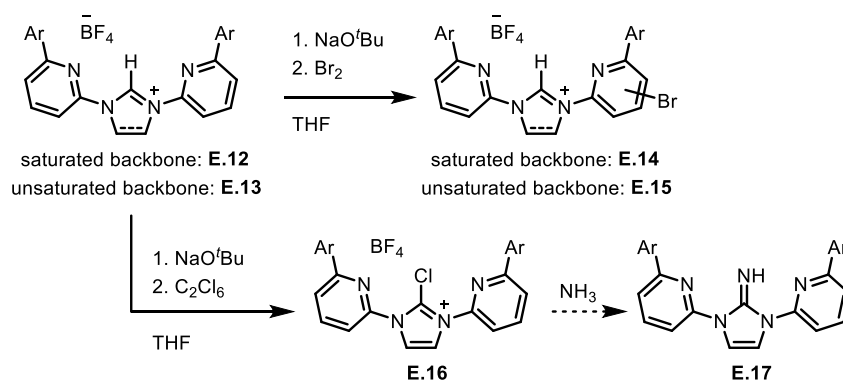
**Figure E.5.** Solid-state structure of tri(zinc) complex **E.8**. Hydrogen atoms are omitted for clarity.

Given the lack of success in this first approach, alternative strategies were sought. While ring closing of **E.9** with cyanogen bromide was attempted (Scheme E.3), a wide variety of products were observed from this reaction, likely due to competing reaction of BrCN at pyridine (**E.10**).<sup>13</sup> While use of **E.11** could potentially result in formation of **E.4**,<sup>14</sup> this reaction has not yet been attempted.



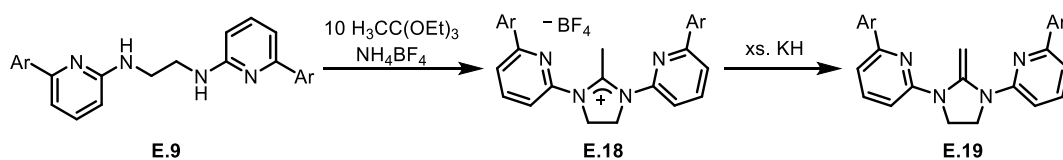
**Scheme E.3.** Potential routes to proligand **E.4** through ring closing of diamine **E.9**.

As guanidines have been generated in the literature via oxidation of the corresponding N-heterocyclic carbenes,<sup>15</sup> this strategy was then taken towards preparation of the desired proligands (Scheme E.4). Reaction of **E.12** or **E.13** with  $\text{NaO}^t\text{Bu}$  over several hours followed by low temperature addition of 1 equiv. of dried bromine resulted in formation of new species **E.14** and **E.15** with multiple sets of pyridine and mesityl resonances, likely due to oxidation of one of either the pyridine or mesityl groups. Use of the milder oxidant hexachloroethane with **E.13** under similar conditions, however, resulted in formation of a new species, **E.16** with similar NMR features to **E.13** albeit with loss of the imidazolium  $^1\text{H}$  NMR resonance. Reaction of **E.12** under identical reaction conditions produced an inseparable mixture of species. An initial attempt at conversion of **E.16** to the desired proligand **E.17** using 3 M  $\text{NH}_3$  in methanol was unsuccessful, as NMR and IR features of the product obtained from that reaction were identical to the product of **E.16** with water. Efforts are ongoing to find conditions suitable for conversion of **E.16** to **E.17**.



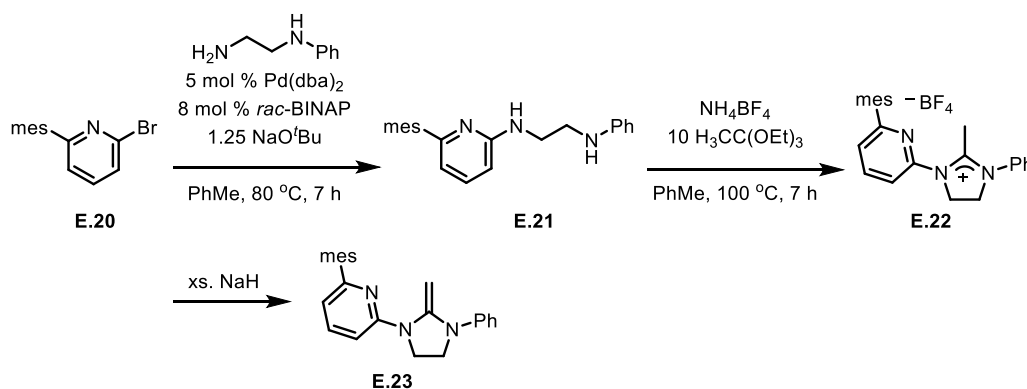
**Scheme E.4.** Routes to proligand **E.17** from the corresponding NHC precursor.

In addition to guanidine-based proligands, the related di(pyridyl) N-heterocyclic olefins (NHOs) and their corresponding Ni and Pd complexes were targeted. As alkylation of **E.12** and **E.13** with MeI or MeOTf following deprotonation resulted in a complex mixture of products, cyclization of **E.9** with triethyl orthoacetate in the presence of NH<sub>4</sub>BF<sub>4</sub> was used to generate the NHO precursor **E.18** (Scheme E.5). **E.18** could be isolated in high yields and good purity following precipitation with anhydrous ether. Deprotonation of **E.18** with KH in THF allowed isolation of NHO **E.19** as a reddish solid following extraction of the crude reaction mixture with non-polar solvents.



**Scheme E.5.** Preparation of di(pyridyl) N-heterocyclic olefin **E.19**

As initial attempts to metalate **E.19** with various Ni and Pd precursors were not promising, the mono-pyridine substituted NHO **B.15** was targeted (Scheme E.6). Pd-catalyzed cross-coupling of N-phenylethylenediamine with 2-bromo-6-mesitylpyridine, **E.20**, afforded **E.21** in good yields and subsequent cyclization with triethylorthoacetate and  $\text{NH}_4\text{BF}_4$  gave **E.22**. Deprotonation of **E.22** with NaH in THF allowed isolation of NHO **E.23** following extraction of the crude reaction mixture with non-polar solvents. In comparison with the other previously-reported NHO bearing a saturated backbone and N-aryl substituents,<sup>16</sup> **E.19** features downfield-shifted olefin resonances at 5.12 ppm, consistent with increased shielding by the hydrogen bonding interactions with the pendant pyridine groups. Analogously, and consistent with slow olefin isomerization on the NMR time scale, **E.23** features two olefin resonances in the  $^1\text{H}$  NMR as doublets ( $J = 2.5$  Hz) at 4.65 and 4.24 ppm consistent with hydrogen bonding of one of the alkenyl protons to the proximal pyridine.

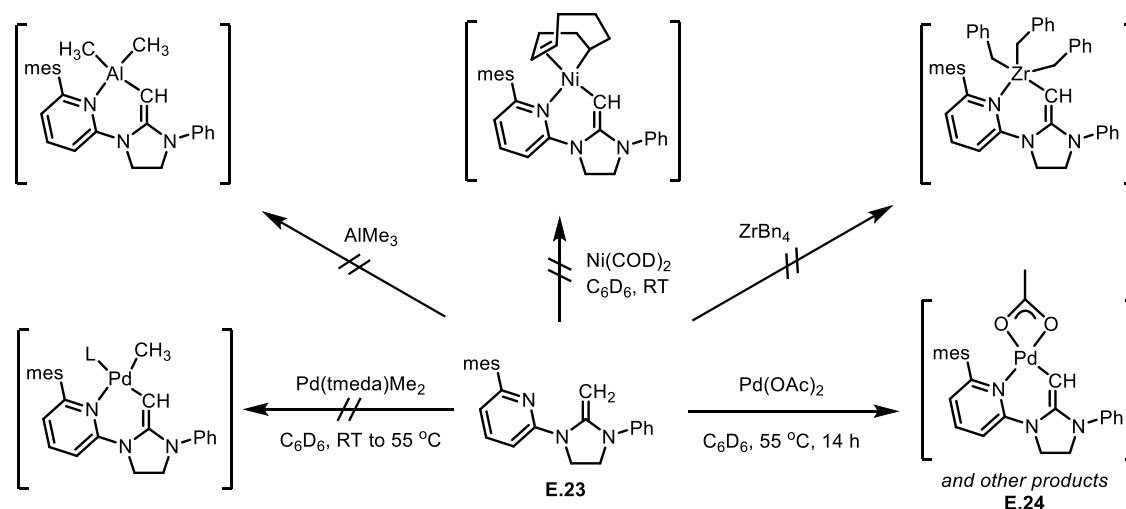


**Scheme E.6.** Preparation of monopyridyl NHO **E.23**.

A number of approaches were taken towards the synthesis of metal complexes bearing the **E.23** proligand, though no products of metalation of **E.23** with Ti, Zr, Hf,



Ni, or Pd precursors could be cleanly isolated nor crystallographically characterized. No reaction was observed between **E.23** and  $\text{Ni(COD)}_2$ ,  $\text{ZrBn}_4$ ,  $\text{M(NMe}_2)_4$  ( $\text{M} = \text{Ti, Zr, Hf}$ ),  $\text{AlMe}_3$  or  $\text{PdMe}_2(\text{tmeda})$  and the reaction of **E.23** with  $\text{PdMeCl(COD)}$  and  $\text{PdCl}_2(\text{COD})$  lead to insoluble products (Scheme E.7). The most promising result was obtained using  $\text{Pd(OAc)}_2$ , where the proposed product of this reaction is complex **E.24**. While multiple species were observed from these reactions, a major species with a singlet at 6.17 ppm was observed by  $^1\text{H}$  NMR (Figure E.6), potentially consistent with a Pd-bound N-heterocyclic vinylene. Attempts to carry this forward to a Pd-alkyl containing species by alkylation with  $\text{AlMe}_3$  were unsuccessful and lead to  $\text{Pd}^0$  formation. Similarly, addition of pyridine to the crude reaction mixture, which could serve as an additional ligand at Pd to break up potential acetate-bridged aggregates, did not result in significant improvement of the crude reaction mixtures.



**Scheme E.7.** Attempted routes towards the preparation of **E.23**-bound metal complexes

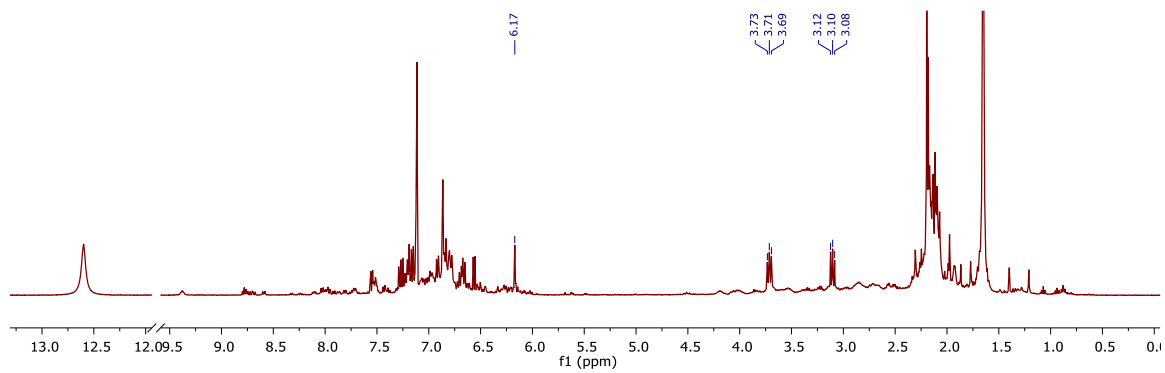


**Figure E.6.**  $^1\text{H}$  NMR of the product of **E.23** with  $\text{Pd}(\text{OAc})_2$  in  $\text{C}_6\text{D}_6$ .

## DISCUSSION

Despite the unexpected difficulty in access di(pyridyl)guanidine proligands, this remains a promising avenue for further investigation. Condensation of **E.16** with  $\text{NH}_3$  in the presence of added tertiary amines or the use of reagents such as  $\text{NaNH}_2$  could allow access to **E.17**. Additionally the use of silazanes could allow installation of the desired NH or  $\text{NSiR}_3$  group with concurrent loss of  $\text{ClSiR}_3$ . From **E.17** metalation with one or two equivalents of  $\text{MBn}_4$  ( $\text{M} = \text{Ti, Zr, Hf}$ ) is expected to afford the desired  $\text{LMBn}_3$  and  $\text{L}_2\text{MBn}_2$  precatalysts, respectively, which could be subsequently tested for olefin polymerization in the presence of absence of a variety of Lewis acids including  $\text{ZnMe}_2$  and  $\text{AlMe}_3$ .

While accessing metal-bound N-heterocyclic vinylene species may still be possible, in particular using more Lewis acidic metals such as Zr or Ti, Ni and Pd alkyl complexes may not be accessible using the current ligand platform. Such groups may not be competent for supporting late transition metal complexes more generally, particularly given more recent reports on NHO to aNHC isomerization on Pd.<sup>17</sup>

## CONCLUSIONS

In conclusion, a series of di(pyridyl) urea, di(pyridyl) guanidine, di(pyridyl) N-heterocyclic olefin, and mono(pyridyl) N-heterocyclic olefin molecules were targeted as potential ligands for heterobimetallic complexes and olefin polymerization catalysts with  $\mu_2$ -O,  $\mu_2$ -N and  $\mu_2$ -C moieties. While the di(pyridyl) guanidine proligand was targeted through a number of routes, its synthesis has not yet been achieved. The NHO-derived proligands could be synthesized from the corresponding N,N'-ethylenediamines in good overall yields; however, only promising reactivity with  $\text{Pd}(\text{OAc})_2$  was observed and attempts to carry forward this complex were unsuccessful.

## EXPERIMENTAL SECTION

### *General Comments*

All air- and water-sensitive compounds were manipulated under N<sub>2</sub> using standard Schlenk or glovebox techniques. Solvents for air- and moisture-sensitive reactions were dried by the method of Grubbs.<sup>18</sup> 2-bromo-6-mesityl pyridine was prepared as described in Chapter 3. **E.9**, **E.12**, and **E.13** were prepared as described in Appendix C. 2-imidazolidinone, hexachloroethane, and NH<sub>4</sub>BF<sub>4</sub> were purchased from Sigma Aldrich and used without further purification. Triethylorthoacetate was purchased from Sigma Aldrich and distilled from K<sub>2</sub>CO<sub>3</sub> prior to use. Pd<sub>2</sub>(dba)<sub>3</sub>•CHCl<sub>3</sub>, *rac*-BINAP, Pd(dba)<sub>2</sub>, and xantphos were purchased from Strem and used without further purification. Deuterated solvents were purchased from Cambridge Isotopes Lab, Inc.; CDCl<sub>3</sub> was used without further purification; C<sub>6</sub>D<sub>6</sub> was distilled from purple Na/benzophenone ketyl and stored over 4 Å molecular sieves prior to use; CD<sub>3</sub>CN was distilled from CaH<sub>2</sub> and stored over 4 Å molecular sieves prior to use. <sup>1</sup>H and <sup>13</sup>C spectra were recorded on Varian INOVA-400, Bruker Cryoprobe 400 spectrometers. <sup>1</sup>H and <sup>13</sup>C chemical shifts are reported relative to residual solvent resonances.

**Preparation of E.1.** An oven-dried Schlenk tube was charged under flowing N<sub>2</sub> with 2-bromo-6-mesitylpyridine (1.3398 g, 4.851 mmol), 2-imidazolidinone (0.2581 g, 2.998 mmol), and Cs<sub>2</sub>CO<sub>3</sub> (2.258 g, 6.930 mmol). The flask was then sealed, evacuated for several minutes, then refilled with N<sub>2</sub> and Pd<sub>2</sub>(dba)<sub>3</sub>•CHCl<sub>3</sub> (0.0278 g, 0.0269 mmol) and xantphos (0.0374 g, 0.0646 mmol) added against flowing N<sub>2</sub>. DMF (26 mL) was added by cannula, and the flask sealed and heated to 100 °C for 4 h. The resulting crude reaction mixture was diluted with DCM and water, separated, and the resulting aqueous layer extracted thrice with DCM. The combined organics were washed with water and brine, dried with MgSO<sub>4</sub>, filtered, evaporated, and dried under vacuum overnight. Purification by column chromatography (2 Hex : 1 EtOAc

(v/v)) afforded the desired compound as a white solid (0.847 g, 73 %).  $^1\text{H}$  NMR (400 MHz,  $\text{CDCl}_3$ )  $\delta$  8.29 (d,  $J$  = 8.47 Hz, 2H, Py), 7.74 (t,  $J$  = 8.1 Hz, 2H, Py), 6.94 (s, 4H, mes), 6.91 (d,  $J$  = 7.4 Hz, 2H, Py), 4.11 (s, 4H,  $\text{CH}_2$ ), 2.33 (s, 6H, mes $\text{CH}_3$ ), 2.07 (s, 12H, mes $\text{CH}_3$ ).  $^{13}\text{C}$  NMR (101 MHz,  $\text{CDCl}_3$ )  $\delta$  157.82 (Py), 154.87 (NCN), 151.97 (Py), 137.92, 137.65, 137.53, 135.95, 128.47, 119.33, 111.16, 41.08 ( $\text{CH}_2$ ), 21.24 (mes $\text{CH}_3$ ), 20.38 (mes $\text{CH}_3$ ).

**Preparation of E.16.** In the glovebox a Schlenk flask was charged with **E.13** (0.1846 g, 0.3378 mmol) in THF (7 mL) then NaO<sup>t</sup>Bu (0.0376 g, 0.391 mmol) was added. The resulting brown solution was stirred at room temperature for 3 h then brought on to the Schlenk line and cooled to -78 °C. 1 mL of a solution of hexachloroethane (0.241 g, 1.02 mmol) in 3 mL THF was added by syringe and the resulting solution stirred for 7 h, warming to room temperature. Volatiles were removed under reduced pressure and the resulting solids extracted with DCM and evaporated to afford the desired compound as a brown solid (0.1685 g, 0.290 mmol, 86 %).  $^1\text{H}$  NMR ( $\text{CD}_3\text{CN}$ , 400 MHz)  $\delta$  8.09 – 8.02 (m, 2H), 7.71 (s, 2H), 7.39 (dd,  $J$  = 7.7, 0.5 Hz, 2H), 7.08 – 7.03 (m, 2H), 6.94 (s, 4H), 2.41 (s, 6H), 1.32 (s, 12H).  $^{13}\text{C}$  NMR ( $\text{CD}_3\text{CN}$ , 400 MHz)  $\delta$  160.57, 146.23, 143.05, 141.74, 139.87, 136.53, 135.50, 129.13, 127.83, 121.76, 113.71, 21.35, 19.79.  $^{19}\text{F}$  NMR ( $\text{CD}_3\text{CN}$ , 376 MHz)  $\delta$  -151.84, -151.89.

**Preparation of E.18.** An oven-dried Schlenk tube was charged under flowing  $\text{N}_2$  with **E.9** (1.8066 g, 4.009 mmol) and  $\text{NH}_4\text{BF}_4$  (0.430 g, 4.101 mmol), then sealed and triethylorthoacetate (7.3 mL, 40 mmol) and anhydrous toluene (4.8 mL) were added by syringe. The flask was sealed and heated to 100 °C overnight. Upon cooling to room temperature the desired product was triturated by addition of anhydrous ether, collected by filtration, and dried under vacuum at 100 °C (1.77 g).  $^1\text{H}$  NMR ( $\text{CD}_3\text{CN}$ , 400 MHz)  $\delta$  8.06 (dd,  $J$  = 8.1, 7.9 Hz, 2H Py), 7.41 (dd,  $J$  = 8.1, 0.7 Hz, 2H, Py), 7.37 (dd,  $J$  = 7.7, 0.7

Hz, 2H, Py), 6.98 (s, 4H, mes), 4.54 (s, 4H, CH<sub>2</sub>), 2.67 (s, 3H, CH<sub>3</sub>), 2.31 (s, 6H, mesCH<sub>3</sub>), 2.01 (s, 12H, mesCH<sub>3</sub>). <sup>13</sup>C NMR (CD<sub>3</sub>CN, 400 MHz)  $\delta$  167.14, 160.64, 149.94, 140.81, 139.11, 137.40, 136.54, 129.23, 125.98, 116.86, 50.05, 21.13, 20.28, 16.78.

**Preparation of E.19.** In the glovebox a round bottom was charged with **E.18** (0.3284 g, 0.5839 mmol) in THF (30 mL). KH (0.1947 g, 4.854 mmol) was added in one portion and the resulting suspension allowed to stir open until bubbling ceased. The flask was then sealed and stirred at room temperature for 16 h. Volatiles were removed under reduced pressure and the resulting solids extracted with hexanes, filtered over Celite, and volatiles removed from the filtrate to afford the desired compound as a red solid (0.2456 g, 89 %). <sup>1</sup>H NMR (C<sub>6</sub>D<sub>6</sub>, 400 MHz)  $\delta$  7.19 (dd,  $J$  = 8.4, 7.3 Hz, 2H, Py), 7.01 (dd,  $J$  = 8.4, 0.7 Hz, 2H, Py), 6.88 (s, 4H, mes), 6.56 (dd,  $J$  = 7.3, 0.7 Hz, 2H, Py), 5.12 (s, 2H, C=CH<sub>2</sub>), 3.44 (s, 4H, CH<sub>2</sub>), 2.21 (s, 18H, mesCH<sub>3</sub>). <sup>13</sup>C NMR (C<sub>6</sub>D<sub>6</sub>, 101 MHz)  $\delta$  158.99 (Py), 154.80 (Py), 143.80 (NCN), 138.99, 137.07, 137.00, 135.86, 128.71, 116.49, 109.52, 70.18 (C=CH<sub>2</sub>), 44.70 (CH<sub>2</sub>), 21.18 (mesCH<sub>3</sub>), 20.56 (mesCH<sub>3</sub>).

**Preparation of E.21.** In the glovebox a Schlenk tube was charged with Pd(dba)<sub>2</sub> (0.125 g, 0.217 mmol), NaO<sup>t</sup>Bu (1.3437 g, 13.982 mmol), and *rac*-BINAP (0.250 g, 0.401 mmol) and toluene (30 mL) then brought out of the glovebox. On the Schlenk line 2-bromo-6-mesitylpyridine (2.9964 g, 10.853 mmol), N-phenylethylenediamine (1.41 mL, 10.8 mmol), and toluene (60 mL) were added by syringe then the flask was sealed and heated to 100 °C for 7 h. The crude reaction was filtered through Celite with DCM then volatiles were removed under reduced pressure. Purification by column chromatography (3 Hex : 1 EtOAc (v/v)) afforded the desired compound (2.925 g, 81 %). <sup>1</sup>H NMR (CDCl<sub>3</sub>, 300 MHz) 7.48 (dd,  $J$  = 8.3, 7.3 Hz, 1H, Py), 7.18 – 7.06 (m, 2H, Py), 6.92 (s, 2H, mes), 6.67 (tt,  $J$  = 7.4, 1.0 Hz, 1H, Ph), 6.60 –

6.48 (m, 3H, Ph), 6.36 (dd,  $J = 8.3, 0.6$  Hz, 1H, Py), 4.80 (br s, 1H, NH), 4.30 (br s, 1H, NH), 3.57 (q,  $J = 5.8$  Hz, 2H,  $CH_2$ ), 3.36 (m, 2H,  $CH_2$ ), 2.32 (s, 3H, mes $CH_3$ ), 2.09 (s, 6H, mes $CH_3$ ).

**Preparation of E.22.** An oven-dried Schlenk tube was charged under flowing  $N_2$  with **B.13** (1.08 g, 3.26 mmol) and  $NH_4BF_4$  (0.348 g, 3.32 mmol) then triethyl orthoacetate (6.0 mL, 33 mmol) and toluene (4.0 mL) added by syringe. The flask was sealed and heated to 95 °C for 14 h. Upon cooling to room temperature anhydrous ether was added by cannula to precipitate the desired product, which was subsequently collected by filtration and dried under vacuum at 100 °C for 16 h (1.25 g, 86 %).  $^1H$  NMR ( $CD_3CN$ , 400 MHz)  $\delta$  8.05 (dd,  $J = 8.1, 7.7$  Hz, 1H), 7.63 – 7.52 (m, 3H), 7.50 – 7.44 (m, 2H), 7.35 (dd,  $J = 8.2, 0.7$  Hz, 1H), 7.32 (dd,  $J = 7.6, 0.7$  Hz, 1H), 4.57 – 4.49 (m, 2H), 4.43 – 4.34 (m, 2H), 2.39 (s, 3H), 2.31 (s, 3H), 2.01 (s, 6H).  $^{13}C$  NMR ( $CD_3CN$ , 101 MHz)  $\delta$  167.09, 160.28, 150.46, 140.76, 139.05, 137.55, 136.73, 136.52, 131.25, 131.11, 129.23, 127.00, 125.14, 115.30, 52.82, 49.68, 21.12, 20.27, 15.73.

**Preparation of E.23.** In the glovebox a round-bottom was charged with **B.14** (0.7709 g, 1.739 mmol) in THF (40 mL). NaH (0.330 g, 13.8 mmol) was added in several portions, the flask allowed to stir uncapped for 20 min, then sealed and stirred for 13 h at room temperature. Volatiles were removed under reduced pressure and the resulting brown solids extracted with hexanes and filtered over Celite to afford the desired compound as a pale brown solid (0.5101 g, 82 %).  $^1H$  NMR (400 MHz,  $C_6D_6$ )  $\delta$  7.23 – 7.17 (m, 3H), 7.14 – 7.08 (m, 3H), 6.91 – 6.81 (m, 3H), 6.55 (dd,  $J = 7.2, 0.8$  Hz, 1H), 4.65 (d,  $J = 2.5$  Hz, 1H), 4.24 (d,  $J = 2.5$  Hz, 1H), 3.55 (t,  $J = 7.1$  Hz, 2H), 2.97 (t,  $J = 7.1$  Hz, 2H), 2.19 (s, 6H), 2.17 (s, 3H).  $^{13}C$  NMR (400 MHz,  $C_6D_6$ )  $\delta$  158.02 (Py), 154.00 (Py), 145.95 (NCN), 143.04, 138.01 (mes), 136.18, 136.00, 134.86, 128.23, 127.71, 121.87,



121.09, 115.53, 108.35 (Py), 63.10 (C=CH<sub>2</sub>), 45.65 (CH<sub>2</sub>), 44.52 (CH<sub>2</sub>), 20.18 (mesCH<sub>3</sub>), 19.56 (mesCH<sub>3</sub>).

**Crystallographic Information.** Crystals were mounted on a glass fiber or MiTeGen loop using Paratone oil, then placed on the diffractometer under a nitrogen stream. Diffractometer manipulations, including data collection, integration, and scaling were performed using the Bruker APEXII software.<sup>19</sup> Absorption corrections were applied using SADABS or TWINABS.<sup>20</sup> Space groups were determined on the basis of systematic absences and intensity statistics and the structures were solved in the Olex 2 software interface<sup>21</sup> by intrinsic phasing using XT (incorporated into SHELXTL)<sup>22</sup> and refined by full-matrix least squares on F<sup>2</sup>. Hydrogen atoms were placed in the idealized positions and refined using a riding model. Graphical representation of structures with 50% probability thermal ellipsoids were generated using Diamond 3 visualization software.<sup>23</sup> Non-hydrogen atoms were refined using anisotropic displacement parameters for **E.1**; due to the incomplete data sets collected for **E.7** and **E.8**, structures were only refined isotropically.

**Table E.1.** Crystal and refinement data for complexes **E.1**, **E.7**, and **E.8**

	<b>E.1</b>	<b>E.7<sup>c</sup></b>	<b>E.8<sup>c</sup></b>
Empirical formula	C <sub>31.62</sub> H <sub>32</sub> N <sub>4.04</sub> O	C <sub>29</sub> H <sub>21</sub> Cl <sub>6</sub> N <sub>7</sub> OZn	C <sub>27</sub> H <sub>18</sub> Cl <sub>10</sub> N <sub>6</sub> OZn <sub>3</sub>
Formula weight	484.62	761.62	993.14
T (K)	100	100	100
<i>a</i> , Å	12.0779(11)	12.7560(12)	13.482(3)
<i>b</i> , Å	34.739(3)	15.6335(14)	9.5478(15)
<i>c</i> , Å	12.6792(12)	31.019(3)	28.747(4)
$\alpha$ , deg	90	90	90
$\beta$ , deg	91.228(4)	90	98.856(3)
$\gamma$ , deg	90	90	90
Volume, Å <sup>3</sup>	5318.6(8)	6185.8(10)	3656.3(11)
Z	8	8	4
Crystal system	Monoclinic	Orthorhombic	Monoclinic
Space group	P 2 <sub>1</sub> /c	Pbca	P 2 <sub>1</sub> /c
$\theta$ range, deg	2.377 to 35.075	3.072 to 23.581	3.114 to 52.060
$\mu$ , mm <sup>-1</sup>	0.074	1.351	9.305
Abs. Correction	Multi-scan	None	None
GOF	1.059	1.126	1.085
$R_1$ , <sup>a</sup> $wR_2$ <sup>b</sup> [I > 2 $\sigma$ (I)]	0.0666, 0.1611	0.0608, 0.1859	0.1112, 0.2652
Radiation Type	Mo K $\alpha$	Mo K $\alpha$	Cu K $\alpha$

<sup>a</sup>  $R_1 = \sum ||F_o| - |F_c|| / \sum |F_o|$ . <sup>b</sup>  $wR_2 = [\sum [w(F_o^2 - F_c^2)^2] / \sum [w(F_o^2)^2]]^{1/2}$ . <sup>c</sup> Crystals grown by Diane Rafizadeh.

## REFERENCES

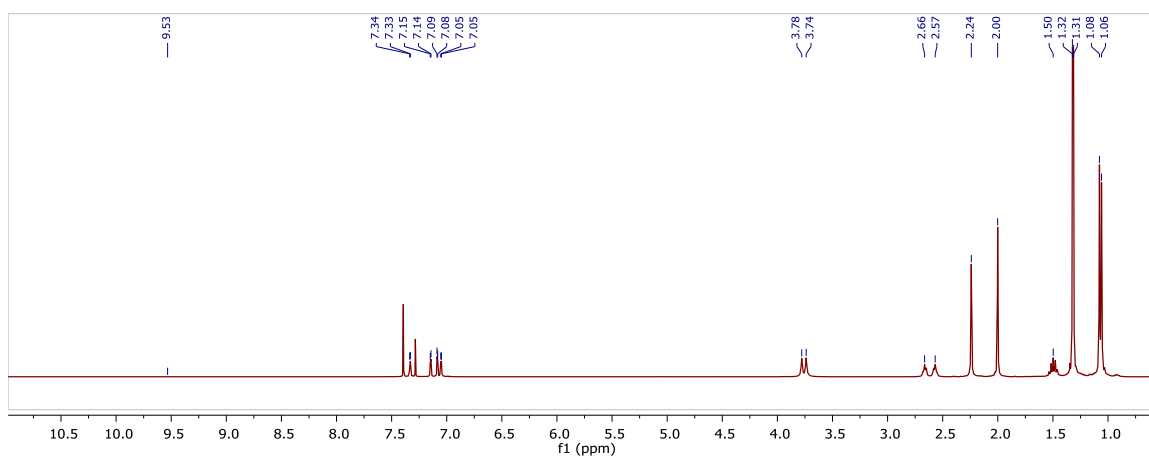
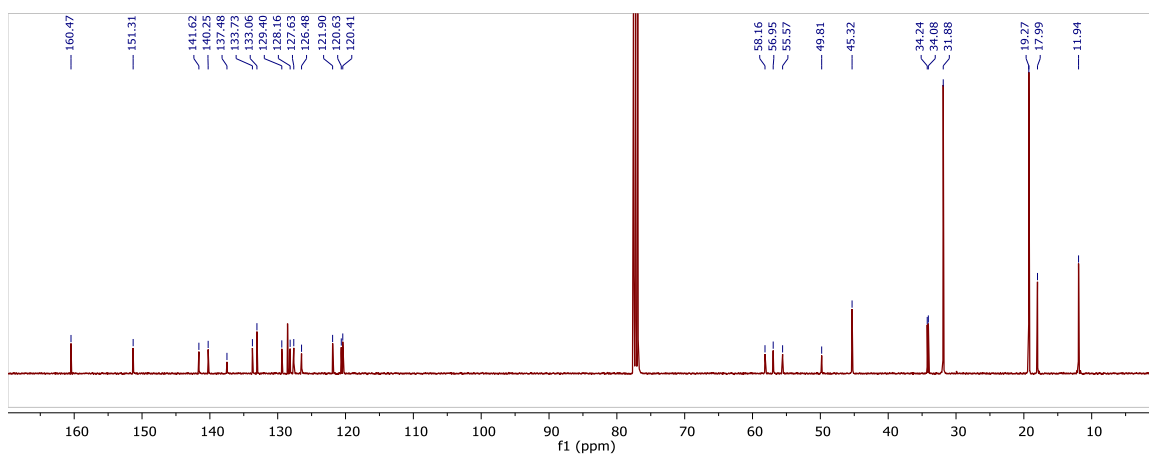
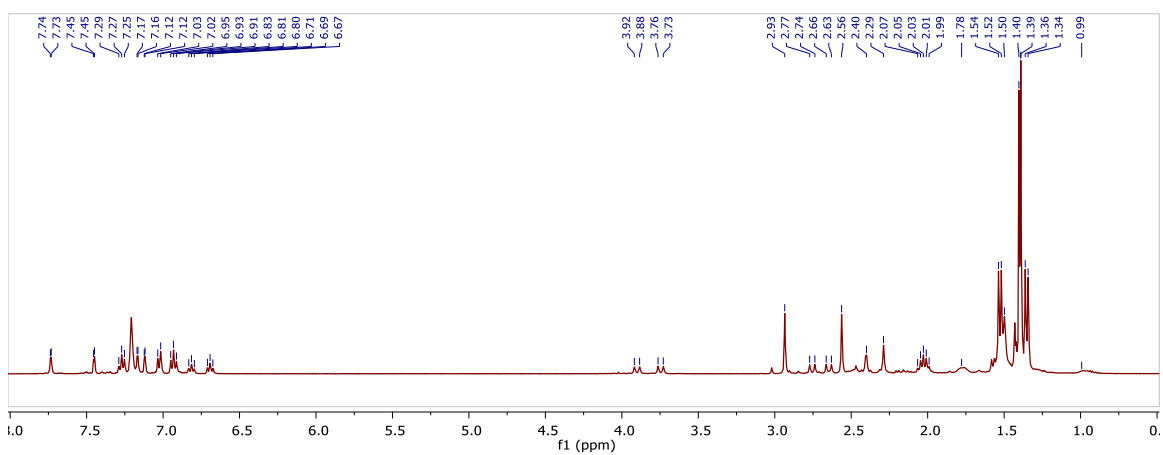
1. (a) Novak, L. S. B. B. M. *Chem. Rev.* **2000**, *100*, 1479-1494; (b) Guo, L.; Liua, W.; Chen, C. *Mater. Chem. Front.* **2017**, *1*, 2487-2494; (c) Nakamura, A.; Ito, S.; Nozaki, K. *Chem. Rev.* **2009**, *109* (11), 5215-5244.
2. (a) Smith, A. J.; Kalkman, E. D.; Gilbert, Z. W.; Tonks, I. A. *Organometallics* **2016**, *35*, 2429-2432; (b) Chiu, H.-C.; Pearce, A. J.; Dunn, P. L.; Cramer, C. J.; Tonks, I. A. *Organometallics* **2016**, *35*, 2076-2085; (c) Chiu, H. C.; Koley, A.; Dunn, P. L.; Hue, R. J.; Tonks, I. A. *Dalton Trans.* **2017**, *46* (17), 5513-5517.
3. (a) Cai, Z.; Xiao, D.; Do, L. H. *J. Am. Chem. Soc.* **2015**, *137* (49), 15501-15510; (b) Doi, Z. C. L. H. *Organometallics* **2017**, *36*, 4691-4698.
4. (a) Do, D. X. L. H. *Organometallics* **2018**, *37*, 3079-3085; (b) Do, Z. C. L. H. *Organometallics* **2018**, *37*, 3874-3882.
5. Roy, M. M. D.; Rivard, E. *Acc. Chem. Res.* **2017**, *50* (8), 2017-2025.
6. (a) Haas, I.; Hubner, C.; Kretschmer, W. P.; Kempe, R. *Chem. Eur. J.* **2013**, *19* (28), 9132-9136; (b) Klosin, J.; Fontaine, P. P.; Figueroa, R.; Pearson, D. M.; Senecal, T. D. Metal-ligand complex, olefin polymerization catalyst derived therefrom, and olefin polymerization method utilizing the catalyst. WO2015094513A1, 2015; (c) Kretschmer, W. P.; Dijkhuis, C.; Meetsma, A.; Hessen, B.; Teuben, J. H. *Chem. Commun.* **2002**, (6), 608-609; (d) Nomura, K.; Fukuda, H.; Katao, S.; Fujiki, M.; Kim, H. J.; Kim, D. H.; Zhang, S. *Dalton Trans.* **2011**, *40* (31), 7842-7849; (e) Nomura, K.; Fukuda, H.; Apisuk, W.; Trambitas, A. G.; Kitiyanan, B.; Tamm, M. *J. Mol. Cat. A: Chemical* **2012**, *363-364*, 501-511; (f) Nomura, K.; Patamma, S.; Matsuda, H.; Katao, S.; Tsutsumi, K.; Fukuda, H. *RSC Adv.* **2015**, *5* (79), 64503-64513; (g) Nomura, K.; Fukuda, H.; Matsuda, H.; Katao, S.; Patamma, S. *J. Organomet. Chem.* **2015**, *798*, 375-383.
7. (a) Balewski, L.; Saczewski, F.; Bednarski, P. J.; Gdaniec, M.; Borys, E.; Makowska, A. *Molecules* **2014**, *19* (10), 17026-17051; (b) Roquette, P.; König, C.; Hübner, O.; Wagner, A.; Kaifer, E.; Enders, M.; Himmel, H.-J. *Eur. J. Inorg. Chem.* **2010**, *2010* (30), 4770-4782.
8. Nakamura, A.; Anselment, T. M.; Claverie, J.; Goodall, B.; Jordan, R. F.; Mecking, S.; Rieger, B.; Sen, A.; van Leeuwen, P. W.; Nozaki, K. *Acc. Chem. Res.* **2013**, *46* (7), 1438-1449.
9. (a) Carrow, B. P.; Nozaki, K. *J. Am. Chem. Soc.* **2012**, *134* (21), 8802-8805; (b) Mitsushige, Y.; Yasuda, H.; Carrow, B. P.; Ito, S.; Kobayashi, M.; Tayano, T.; Watanabe, Y.; Okuno, Y.; Hayashi, S.; Kuroda, J.; Okumura, Y.; Nozaki, K. *ACS Macro Letters* **2018**, *7* (3), 305-311; (c) Chen, M.; Chen, C. *Angew. Chem. Int. Ed.* **2018**, *57* (12), 3094-3098.
10. (a) Contrella, N. D.; Sampson, J. R.; Jordan, R. F. *Organometallics* **2014**, *33* (13), 3546-3555; (b) Johnson, A. M.; Contrella, N. D.; Sampson, J. R.; Zheng, M.; Jordan, R. F. *Organometallics* **2017**, *36* (24), 4990-5002.
11. (a) Tao, W. J.; Nakano, R.; Ito, S.; Nozaki, K. *Angew. Chem. Int. Ed.* **2016**, *55* (8), 2835-2839; (b) Yasuda, H.; Nakano, R.; Ito, S.; Nozaki, K. *J. Am. Chem. Soc.* **2018**, *140* (5), 1876-1883.
12. Tao, W.; Akita, S.; Nakano, R.; Ito, S.; Hoshimoto, Y.; Ogoshi, S.; Nozaki, K. *Chem. Commun.* **2017**, *53* (17), 2630-2633.
13. Kearney, A. M.; Vanderwal, C. D. *Angew. Chem. Int. Ed. Engl.* **2006**, *45* (46), 7803-7806.
14. (a) Ma, Z.; Day, C. S.; Bierbach, U. *J. Org. Chem.* **2007**, *72* (14), 5387-5390; (b) Turockin, A.; Honeker, R.; Raven, W.; Selig, P. *J. Org. Chem.* **2016**, *81* (11), 4516-4529; (c)

- Wu, Y.-Q.; Hamilton, S. K.; Wilkinson, D. E.; Hamilton, G. S. *J. Org. Chem.* **2002**, *67*, 7553-7556.
15. (a) Kinjo, R.; Donnadieu, B.; Bertrand, G. *Angew. Chem. Int. Ed.* **2010**, *49* (34), 5930-5933; (b) Back, O.; Donnadieu, B.; Hopffgarten, M. v.; Klein, S.; Tonner, R.; Frenking, G.; Bertrand, G. *Chem. Sci.* **2011**, *2*, 858-861; (c) Tönnemann, J.; Scopelliti, R.; Severin, K. *Eur. J. Inorg. Chem.* **2014**, *2014*, 4287-4293; (d) Tang, P.; Wang, W.; Ritter, T. *J. Am. Chem. Soc.* **2011**, *133* (30), 11482-11484; (e) Fujimoto, T.; Ritter, T. *Org. Lett.* **2015**, *17* (3), 544-547.
16. Arduengo, A. J.; Davidson, F.; Dias, H. V. R.; Goerlich, J. R.; Khasnis, D.; Marshall, W. J.; Prakasha, T. K. *J. Am. Chem. Soc.* **1997**, *119*, 12742-12749.
17. Hering-Junghans, A. S. C. *Eur. J. Inorg. Chem.* **2018**, *2018*, 2584-2588.
18. Pangborn, A. B.; Giardello, M. A.; Grubbs, R. H.; Rosen, R. K.; Timmers, F. J. *Organometallics* **1996**, *15* (5), 1518-1520.
19. APEX2, Version 2 User Manual, M86-E01078, Bruker Analytical X-ray Systems, Madison, WI, June 2006.
20. Sheldrick, G.M. "SADABS (version 2008/l): Program for Absorption Correction for Data from Area Detector Frames", University of Gottingen, 2008.
21. Dolomanov, O. V.; Bourhis, L. J.; Gildea, R. J.; Howard, J. A. K.; Puschmann, H. *J. Appl. Crystallogr.* **2009**, *42* (2), 339-341.
22. Sheldrick, G. M. *Acta Cryst.* **2008**, *A64*, 112-122.
23. Brandenburg, K. (1999), DIAMOND. Crystal Impact GdR, Bonn, Germany.

## **APPENDIX F**

### SPECTRA

## CHAPTER 2

Figure F2.1. <sup>1</sup>H NMR spectrum of **2.8** in CDCl<sub>3</sub>.Figure F2.2. <sup>13</sup>C NMR spectrum of **2.8** in CDCl<sub>3</sub>.Figure F2.3. <sup>1</sup>H NMR spectrum of **2.10** in C<sub>6</sub>D<sub>6</sub>.

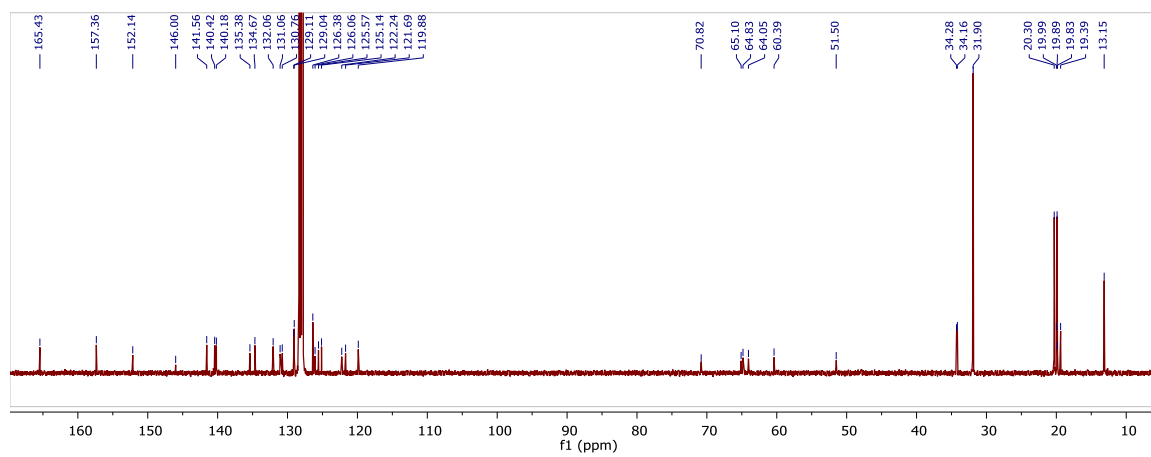


Figure F2.4. <sup>13</sup>C NMR spectrum of **2.10** in C<sub>6</sub>D<sub>6</sub>.

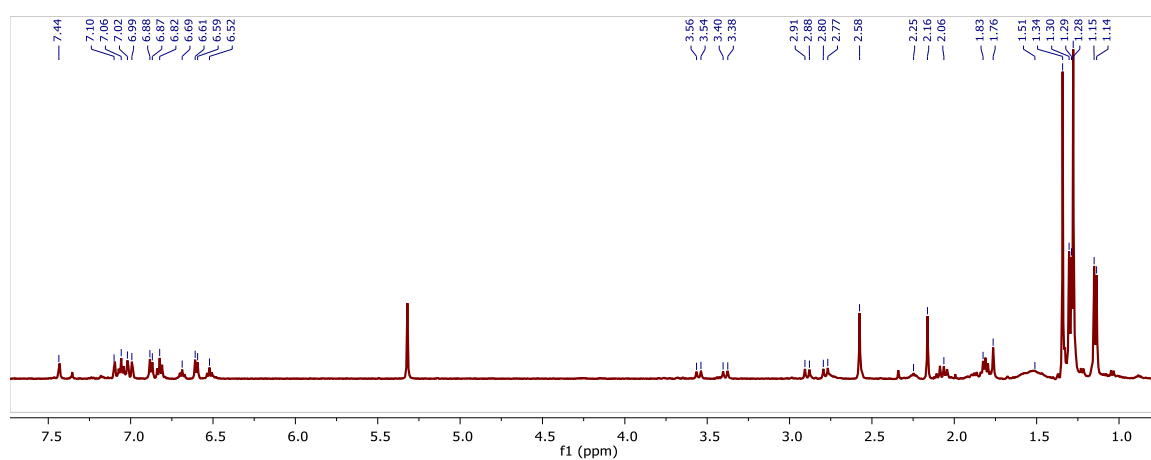


Figure F2.5. <sup>1</sup>H NMR spectrum of **2.10** in CD<sub>2</sub>Cl<sub>2</sub>.

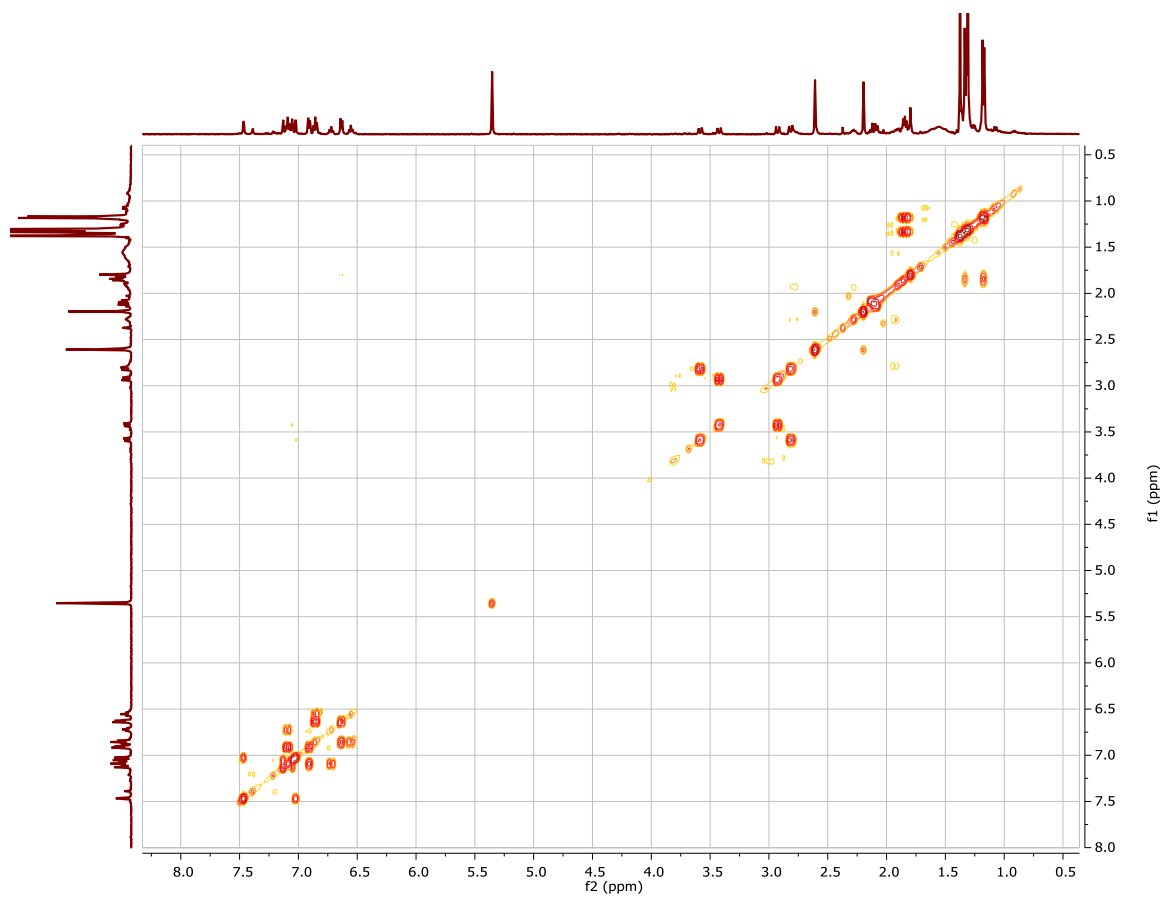


Figure F2.6. gCOSY spectrum of **2.10** in  $\text{CD}_2\text{Cl}_2$ .

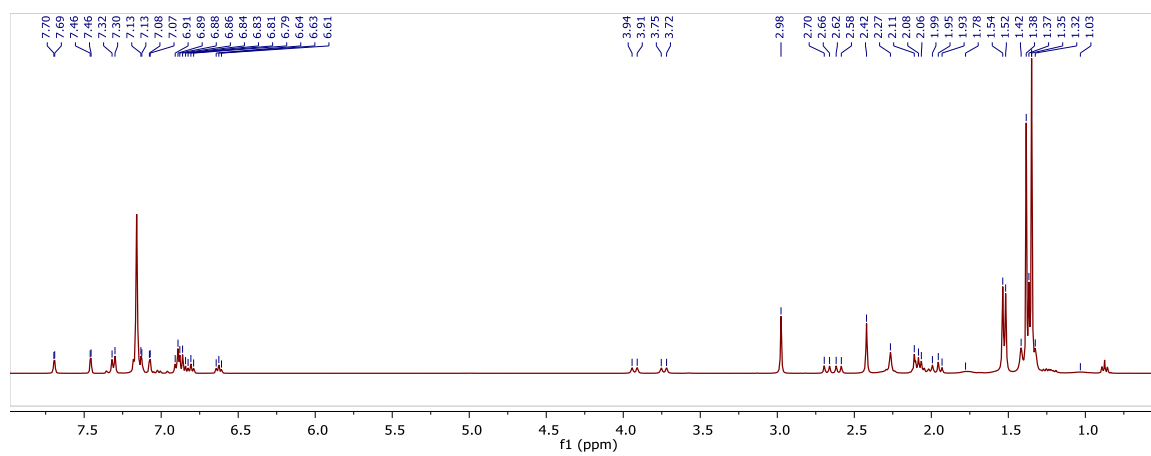
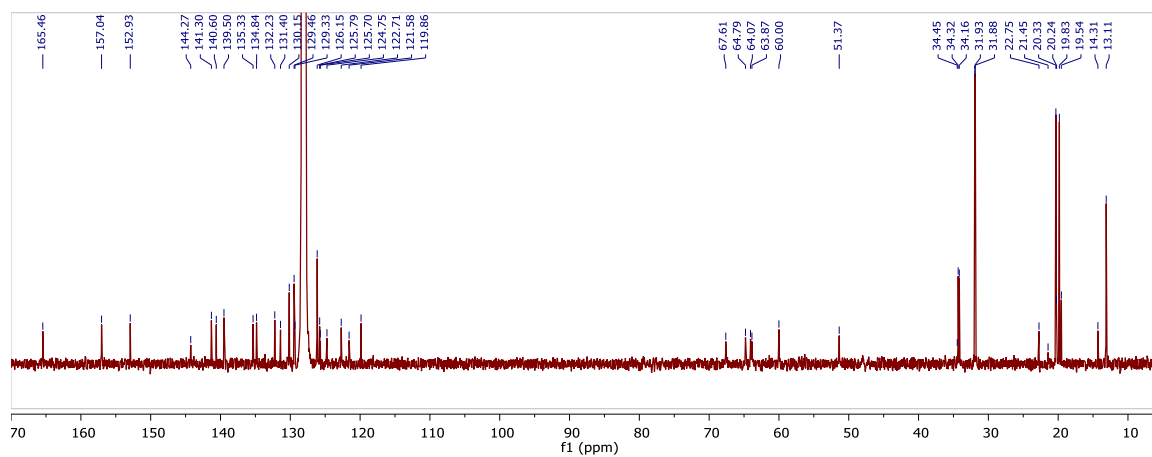
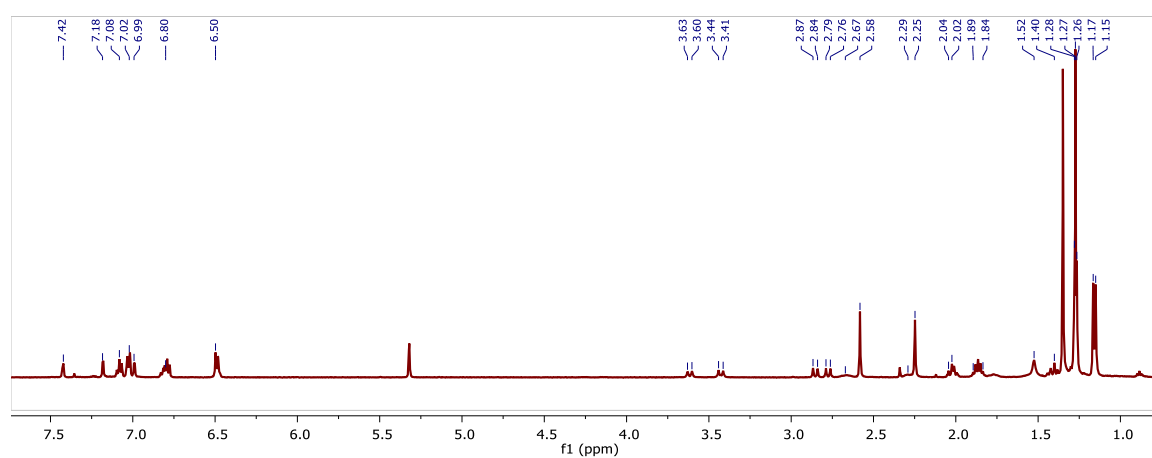


Figure F2.7.  $^1\text{H}$  NMR spectrum of **2.11** in  $\text{C}_6\text{D}_6$ .





**Figure F2.8.** <sup>13</sup>C NMR spectrum of **2.11** in C<sub>6</sub>D<sub>6</sub>.



**Figure F2.9.** <sup>1</sup>H NMR of **2.11** in CD<sub>2</sub>Cl<sub>2</sub>.

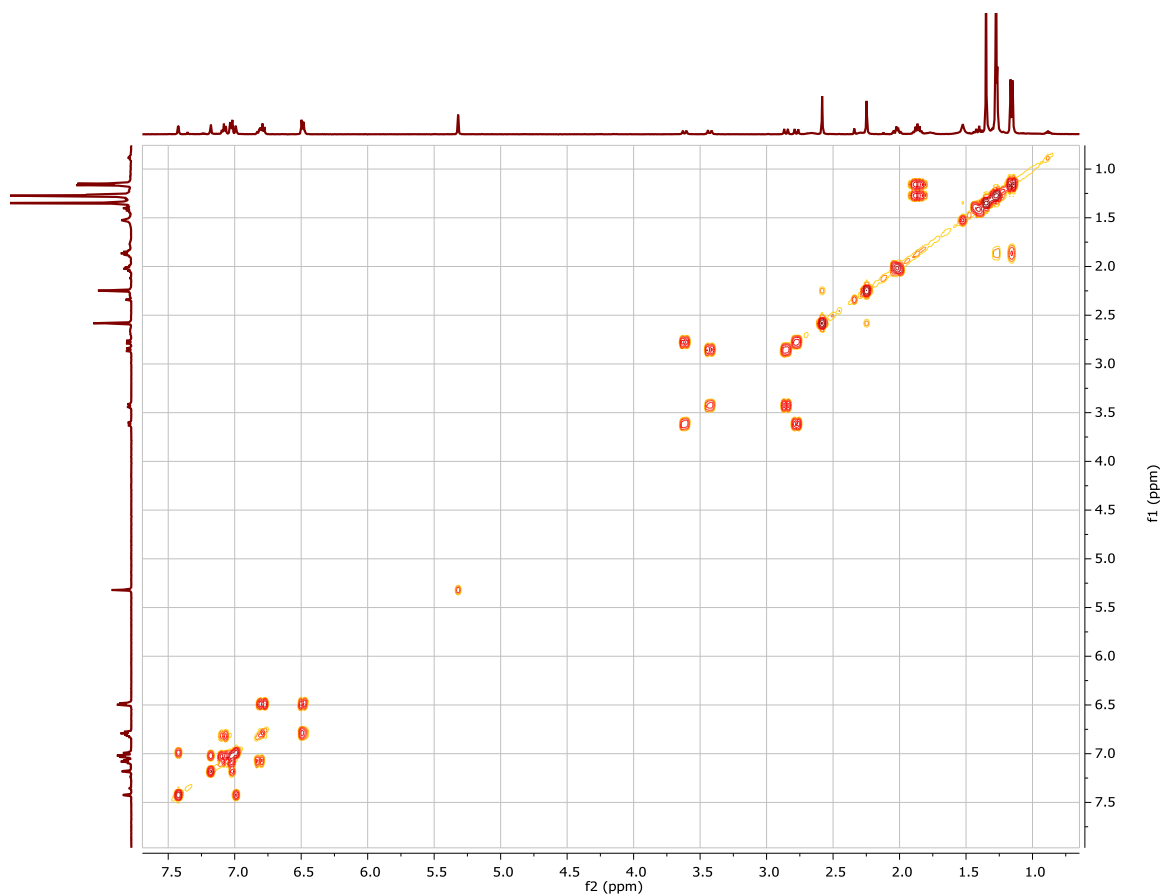


Figure F2.10. gCOSY of **2.11** in  $\text{CD}_2\text{Cl}_2$ .

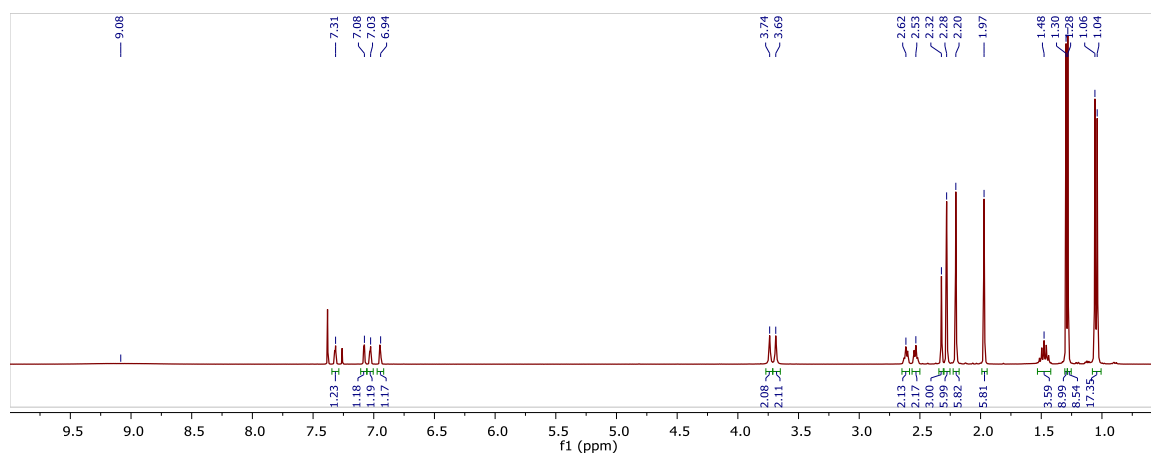


Figure F2.11.  $^1\text{H}$  NMR spectrum of **2.17** in  $\text{CDCl}_3$ .

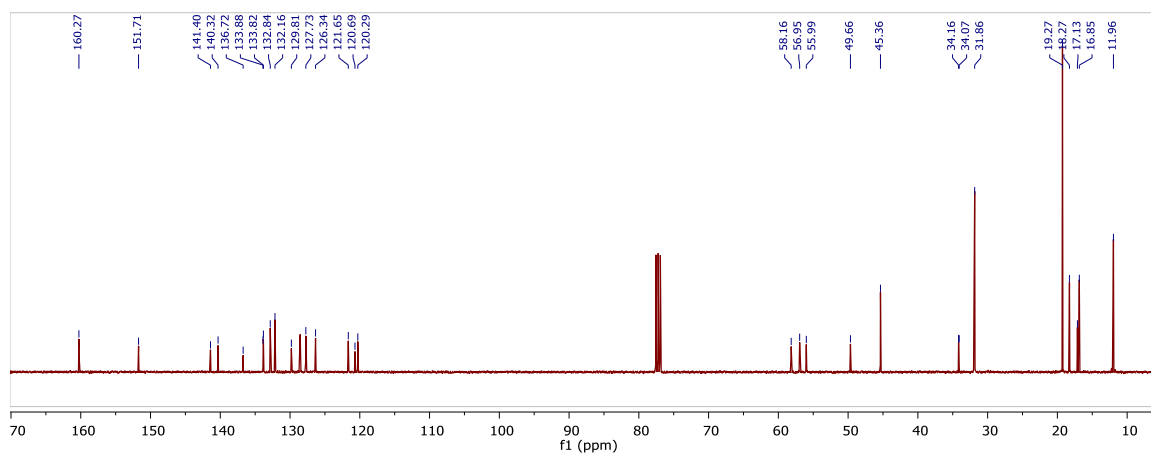


Figure F2.12. <sup>13</sup>C NMR spectrum of **2.17** in CDCl<sub>3</sub>.

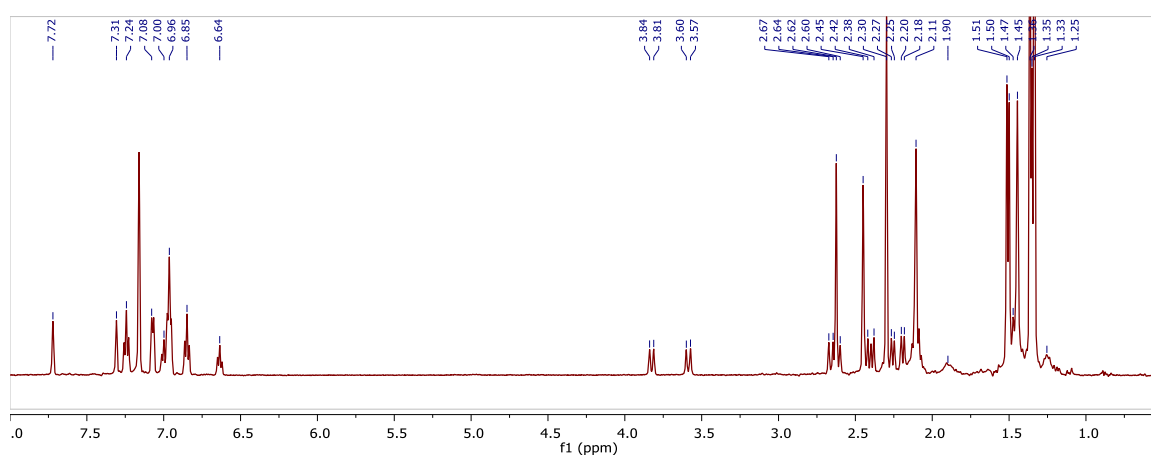


Figure F2.13. <sup>1</sup>H NMR spectrum of **2.20** in C<sub>6</sub>D<sub>6</sub>.

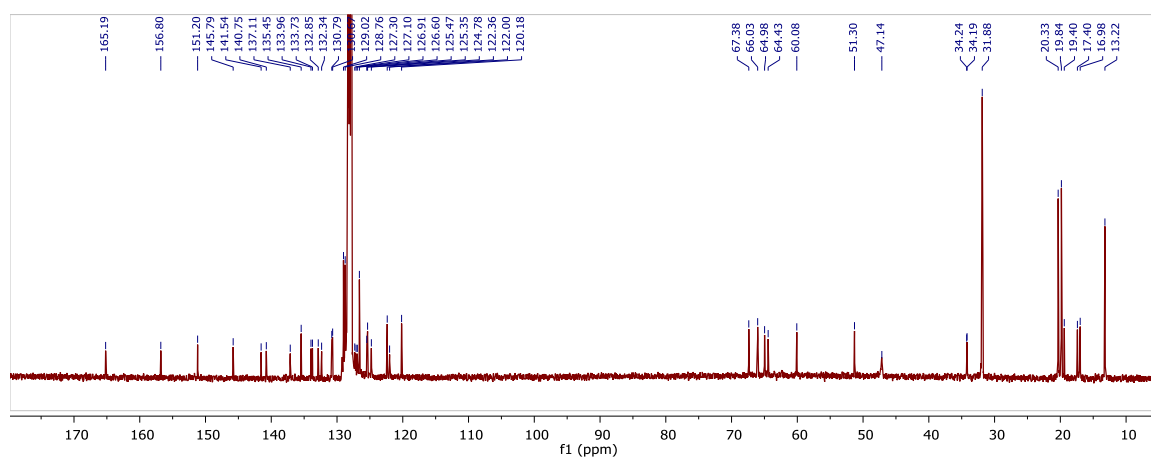


Figure F2.14. <sup>13</sup>C NMR spectrum of **2.20** in C<sub>6</sub>D<sub>6</sub>.

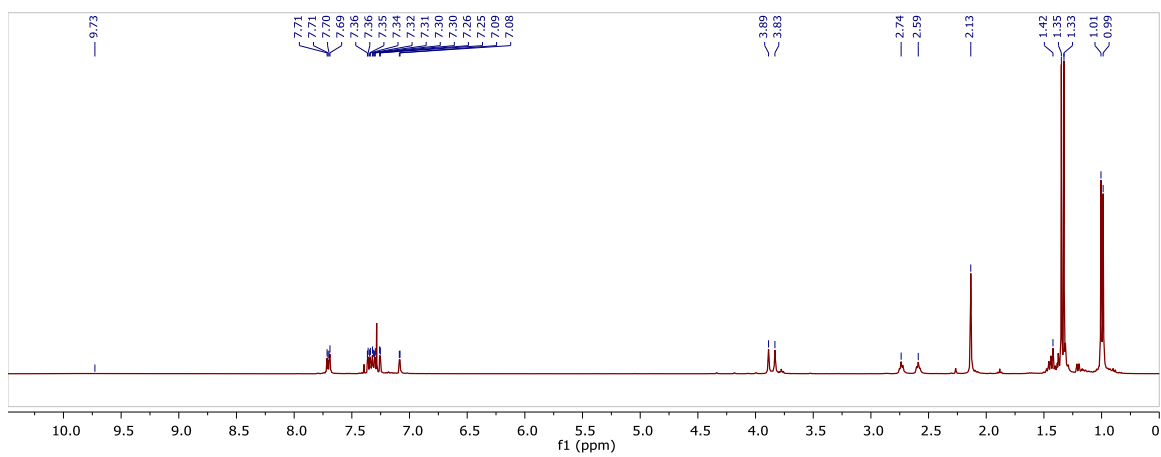


Figure F2.15. <sup>1</sup>H NMR spectrum of **anthH<sub>4</sub>SiPr<sub>3</sub>-NMe<sub>2</sub>** in CDCl<sub>3</sub>.

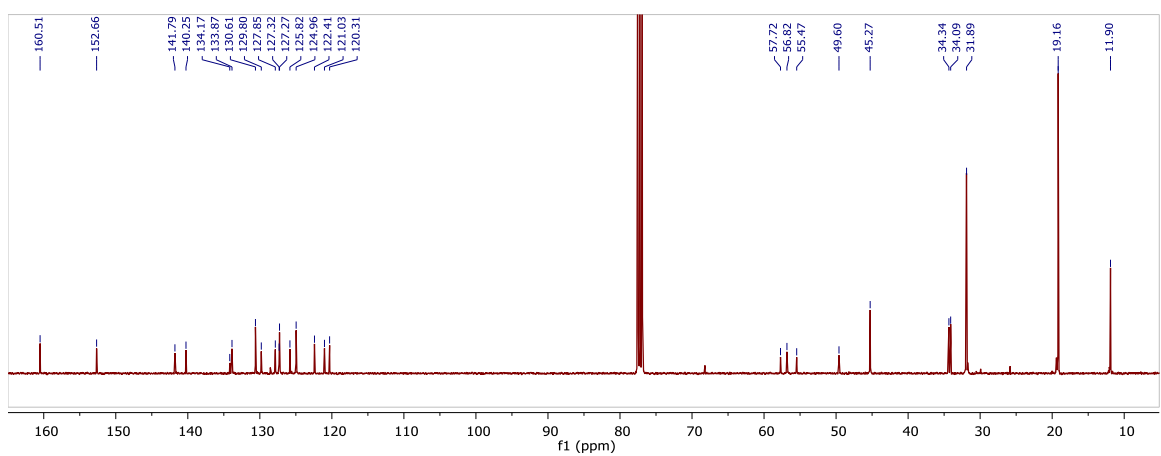


Figure F2.16. <sup>13</sup>C NMR spectrum of **2.9** in CDCl<sub>3</sub>.

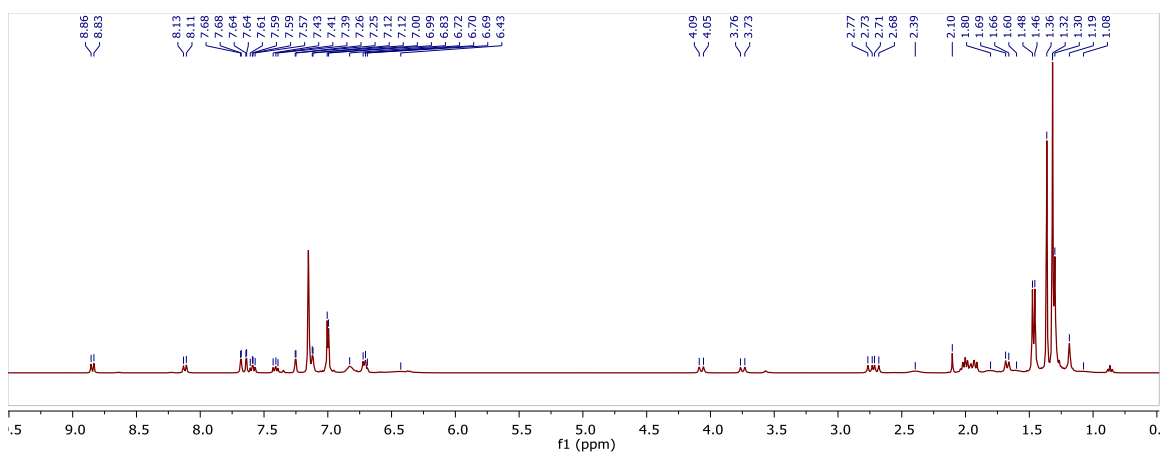


Figure F2.17. <sup>1</sup>H NMR spectrum of **2.12** in C<sub>6</sub>D<sub>6</sub>.

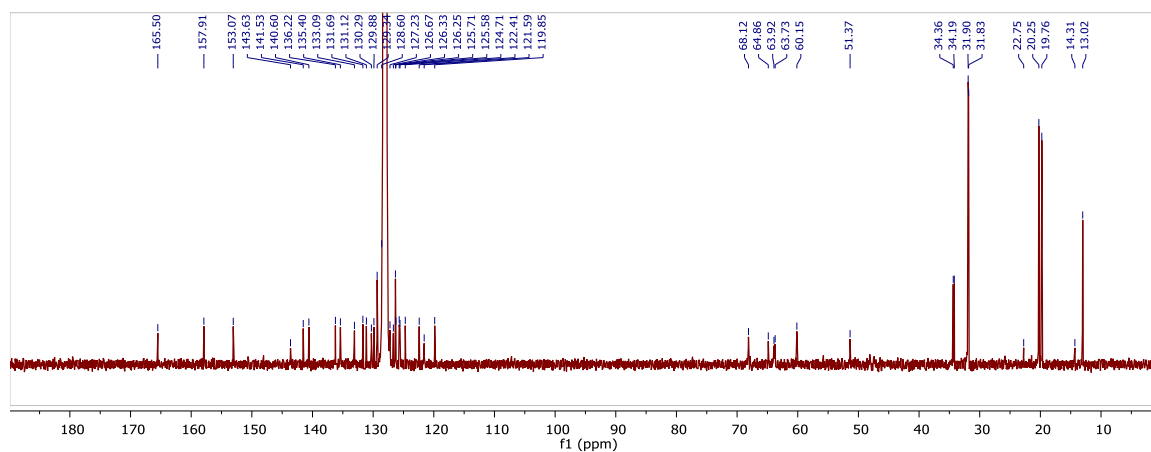


Figure F2.18. <sup>13</sup>C NMR spectrum of **2.12** in C<sub>6</sub>D<sub>6</sub>.

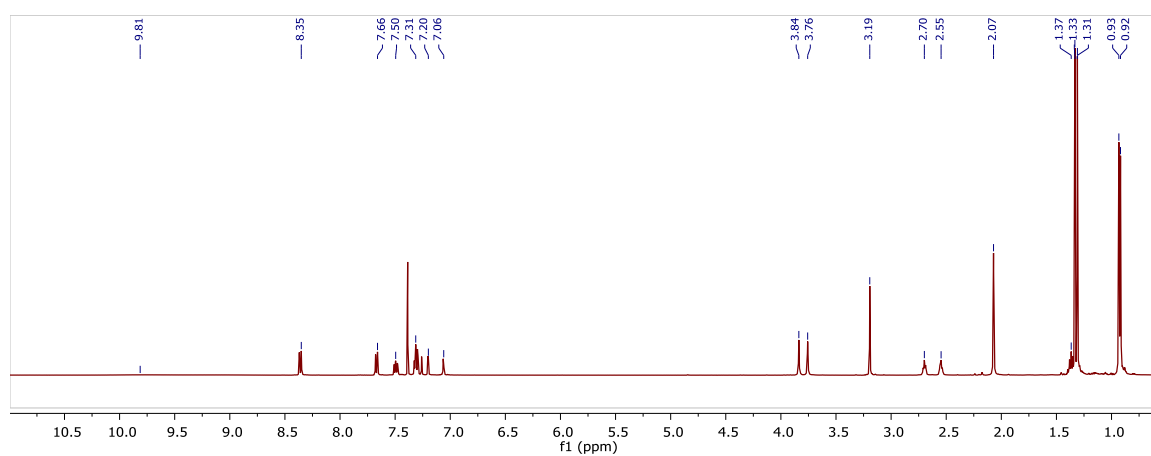


Figure F2.19. <sup>1</sup>H NMR spectrum of **2.18** in CDCl<sub>3</sub>.

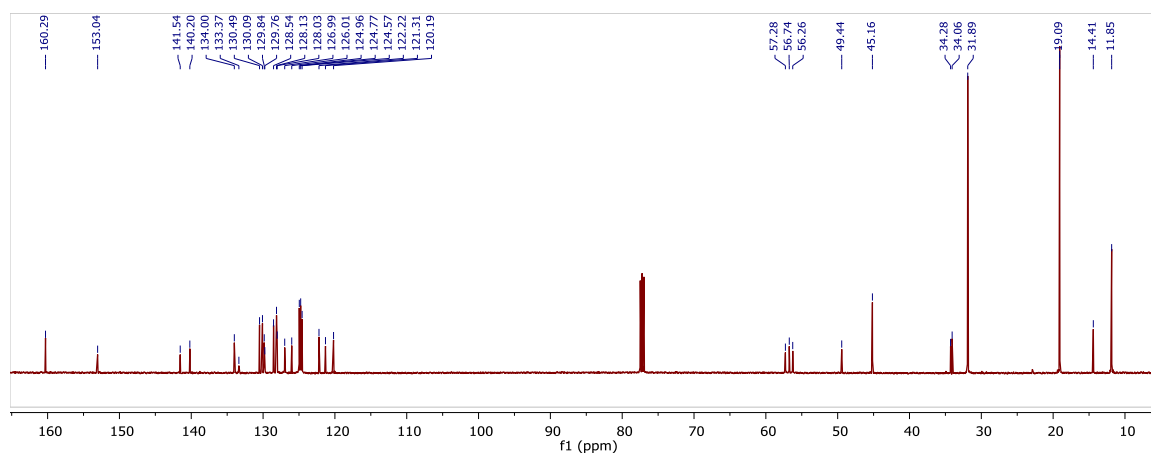


Figure F2.20. <sup>13</sup>C NMR spectrum of **2.18** in CDCl<sub>3</sub>.

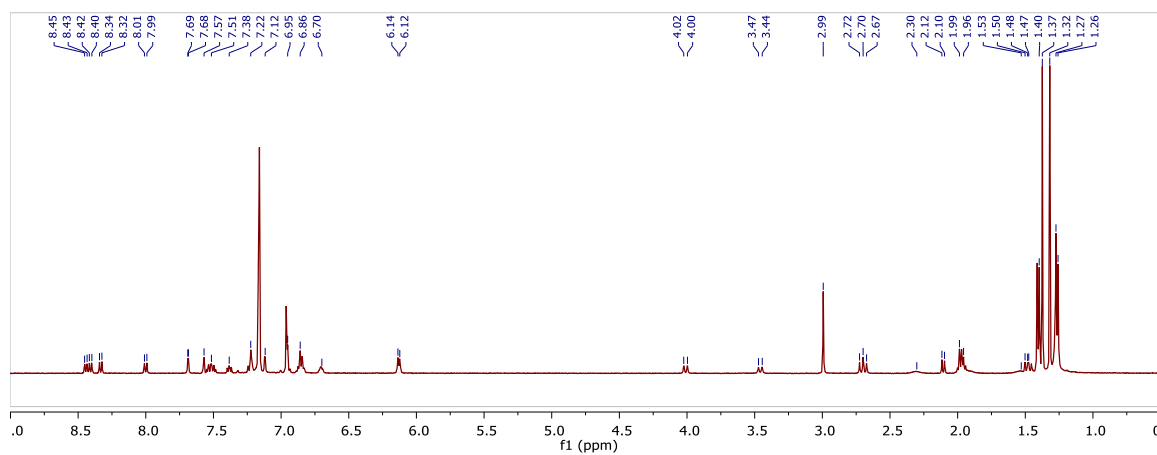


Figure F2.21. <sup>1</sup>H NMR spectrum of **2.21** in C<sub>6</sub>D<sub>6</sub>.

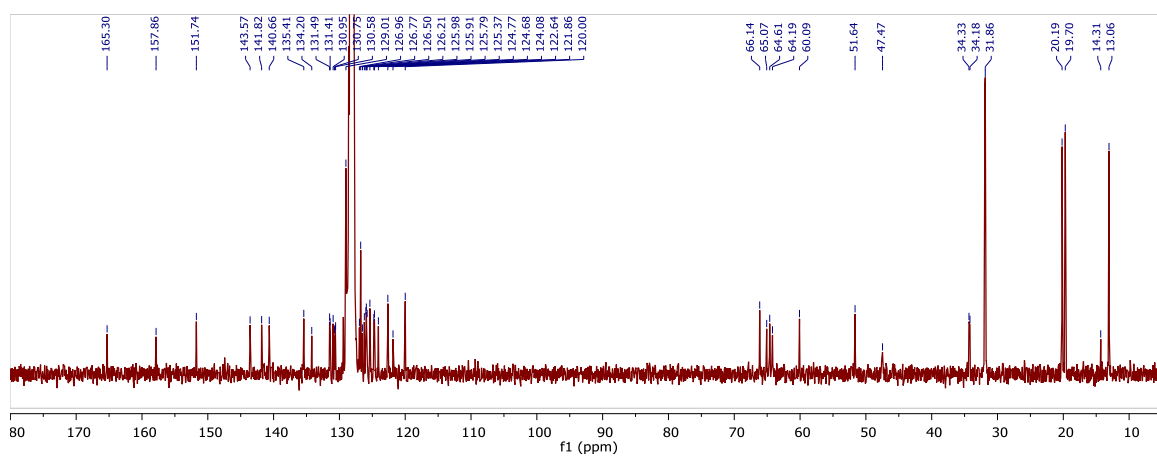
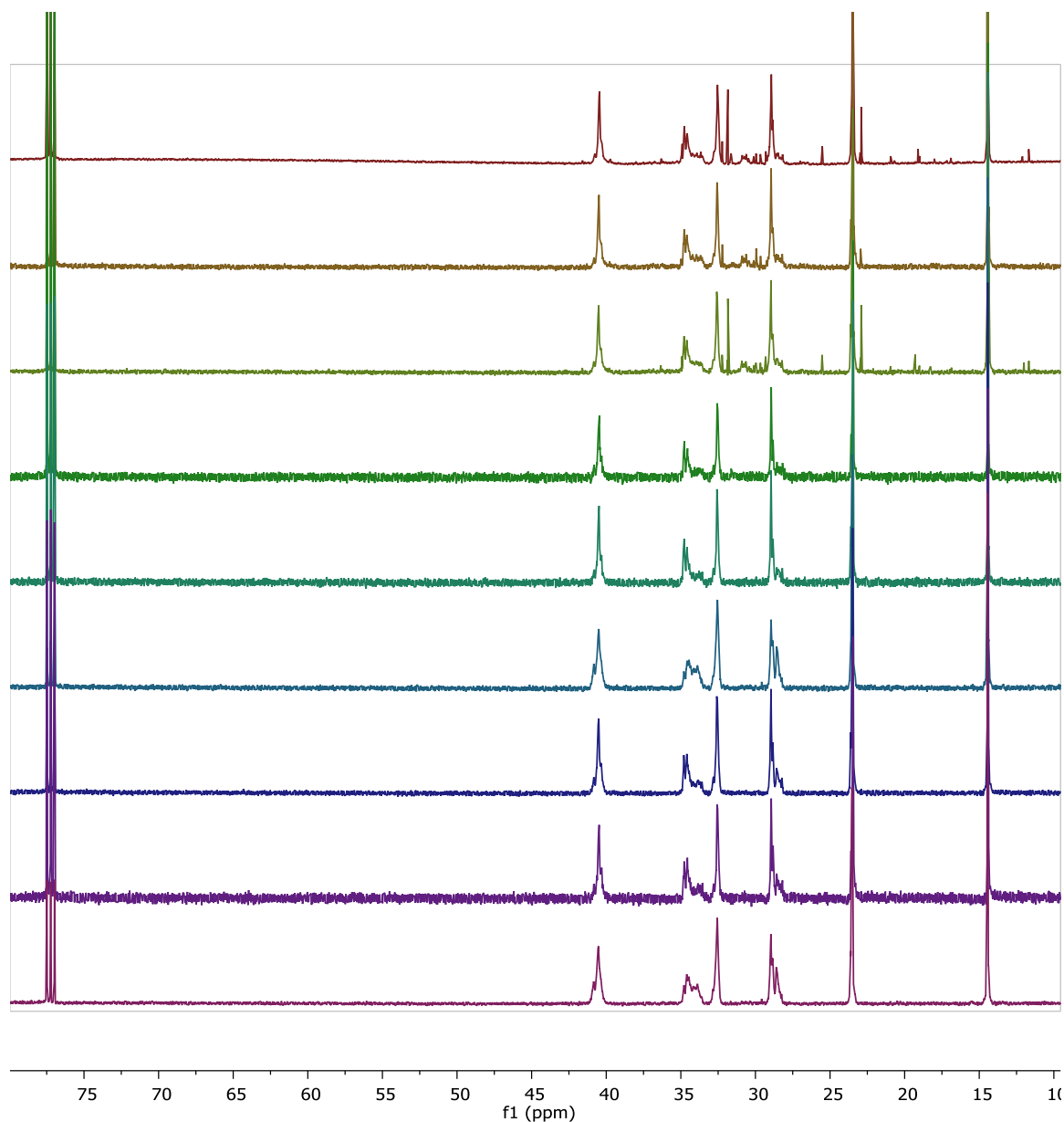
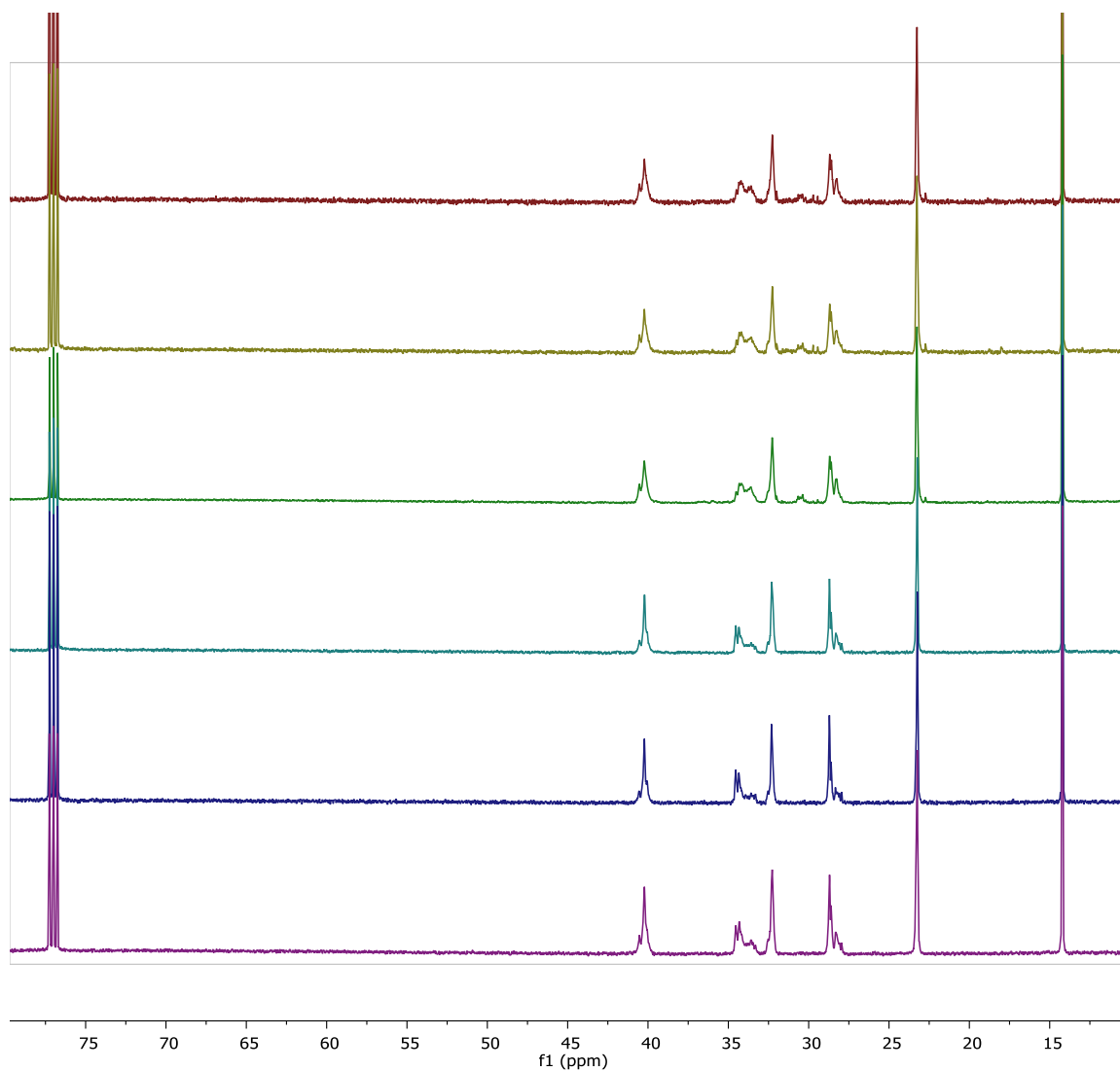


Figure F2.22. <sup>13</sup>C NMR spectrum of **2.21** in C<sub>6</sub>D<sub>6</sub>.



**Figure F2.23.**  $^{13}\text{C}$  NMR spectra in  $\text{CDCl}_3$  at  $25^\circ\text{C}$  of 1-hexene homopolymers from (top to bottom) **2.20** with  $[\text{CPh}_3][\text{B}(\text{C}_6\text{F}_5)_4]$ ,  $[\text{HNMe}_2\text{Ph}][\text{B}(\text{C}_6\text{F}_5)_4]$ , dried MAO; **2.10** with  $[\text{CPh}_3][\text{B}(\text{C}_6\text{F}_5)_4]$ ,  $[\text{HNMe}_2\text{Ph}][\text{B}(\text{C}_6\text{F}_5)_4]$ , dried MAO; and **2.11** with  $[\text{CPh}_3][\text{B}(\text{C}_6\text{F}_5)_4]$ ,  $[\text{HNMe}_2\text{Ph}][\text{B}(\text{C}_6\text{F}_5)_4]$ , dried MAO.



**Figure F2.24.**  $^{13}\text{C}$  NMR spectra in  $\text{CDCl}_3$  at  $25^\circ\text{C}$  of 1-hexene homopolymers from (top to bottom) **2.21**  $[\text{CPh}_3][\text{B}(\text{C}_6\text{F}_5)_4]$  (a),  $[\text{HNMe}_2\text{Ph}][\text{B}(\text{C}_6\text{F}_5)_4]$  (b), dried MAO (c) and **2.12**  $[\text{CPh}_3][\text{B}(\text{C}_6\text{F}_5)_4]$  (d),  $[\text{HNMe}_2\text{Ph}][\text{B}(\text{C}_6\text{F}_5)_4]$  (e), dried MAO (f).



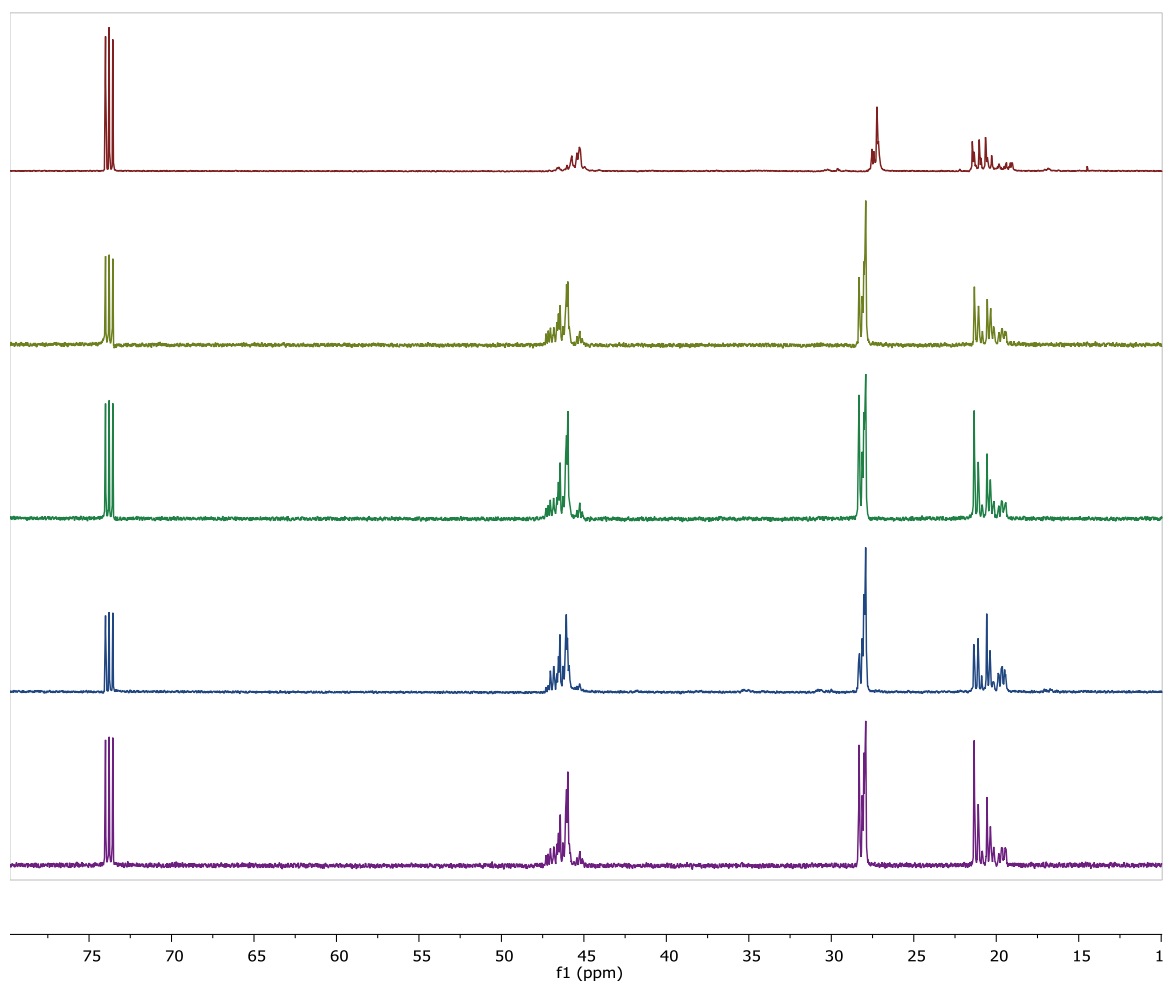


**Figure F2.25.**  $^{13}\text{C}$  NMR spectra in  $\text{C}_2\text{D}_2\text{Cl}_4$  at  $130^\circ\text{C}$  of high temperature propylene homopolymers from: (top to bottom) **2.20**, **2.10**, **2.11**, **2.21**, and **2.12**.

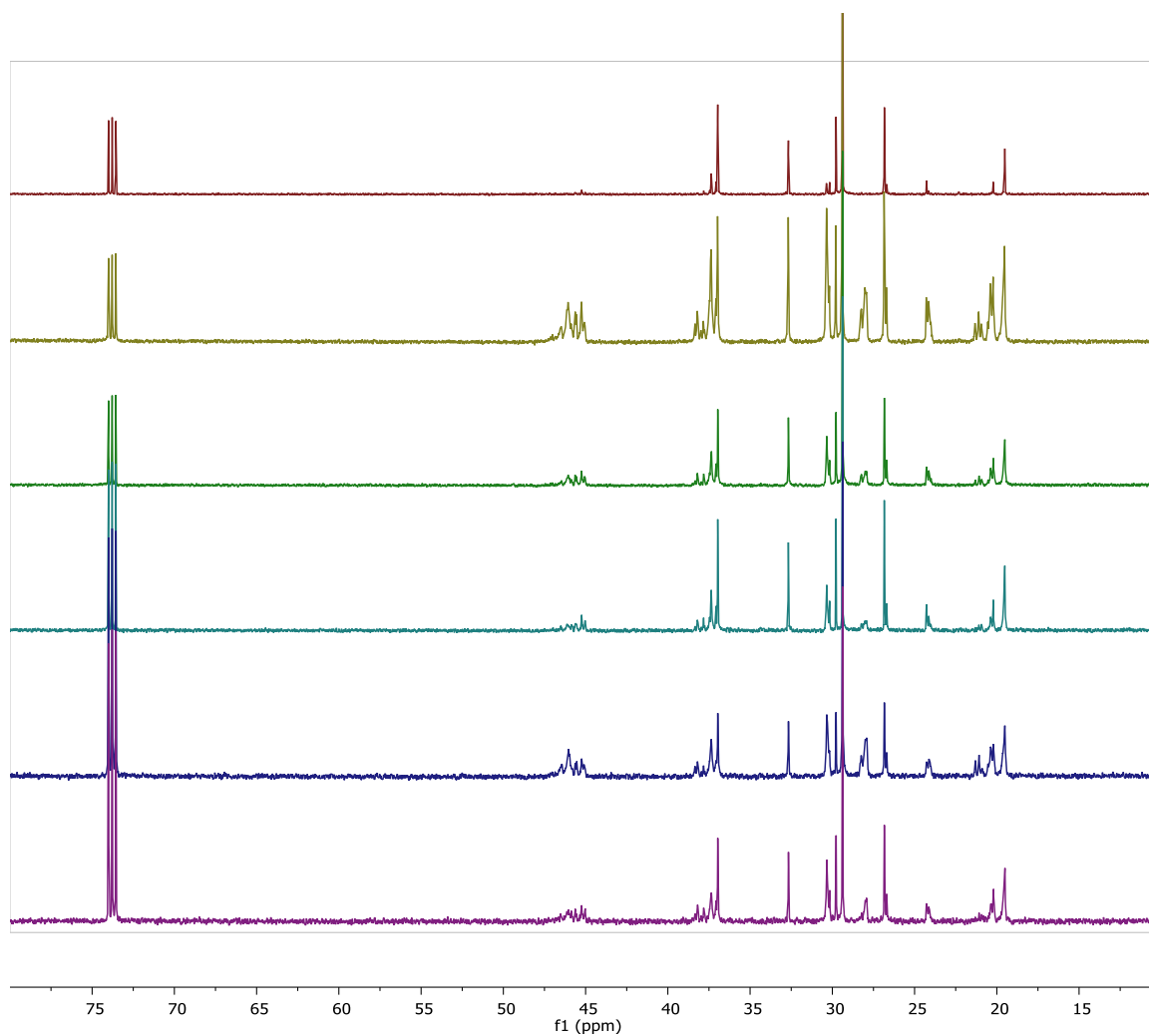


**Figure F2.26.**  $^{13}\text{C}$  NMR spectra in  $\text{C}_2\text{D}_2\text{Cl}_4$  at  $130^\circ\text{C}$  of ethylene-propylene copolymers from: (top to bottom) **2.20**, **2.10**, **2.11**, **2.21**, and **2.12**.

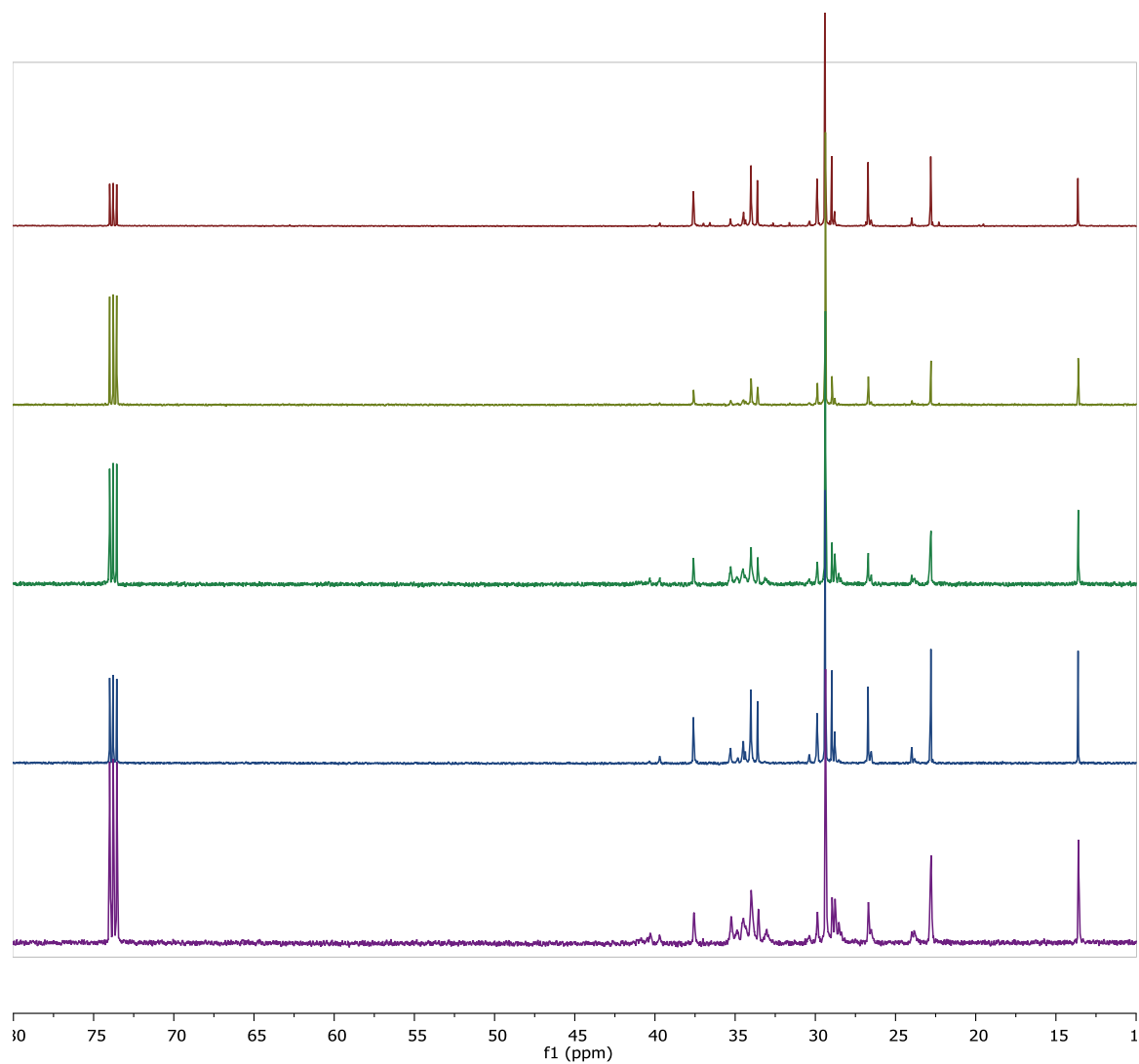


**Figure F2.27.**  $^{13}\text{C}$  NMR spectra in  $\text{C}_2\text{D}_2\text{Cl}_4$  at  $130^\circ\text{C}$  of ethylene-hexene copolymers from: (top to bottom) **2.20**, **2.10**, **2.11**, **2.21**, and **2.12**.

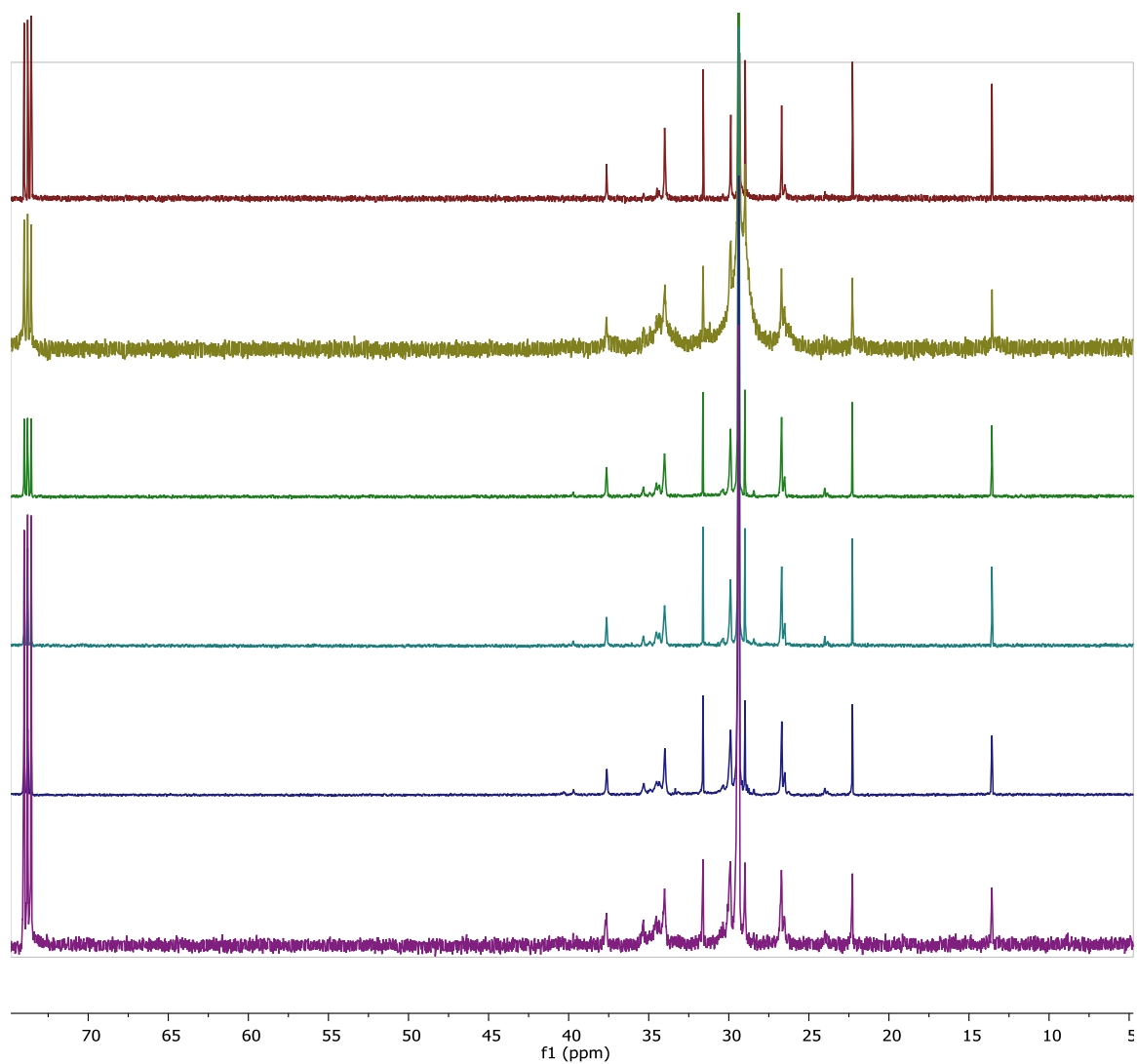


**Figure F2.28.**  $^{13}\text{C}$  NMR spectra in  $\text{C}_2\text{D}_2\text{Cl}_4$  at  $130^\circ\text{C}$  of ethylene-tetradecene copolymers from: (top to bottom) **2.20**, **2.10**, **2.11**, **2.21**, and **2.12**.

## CHAPTER 3

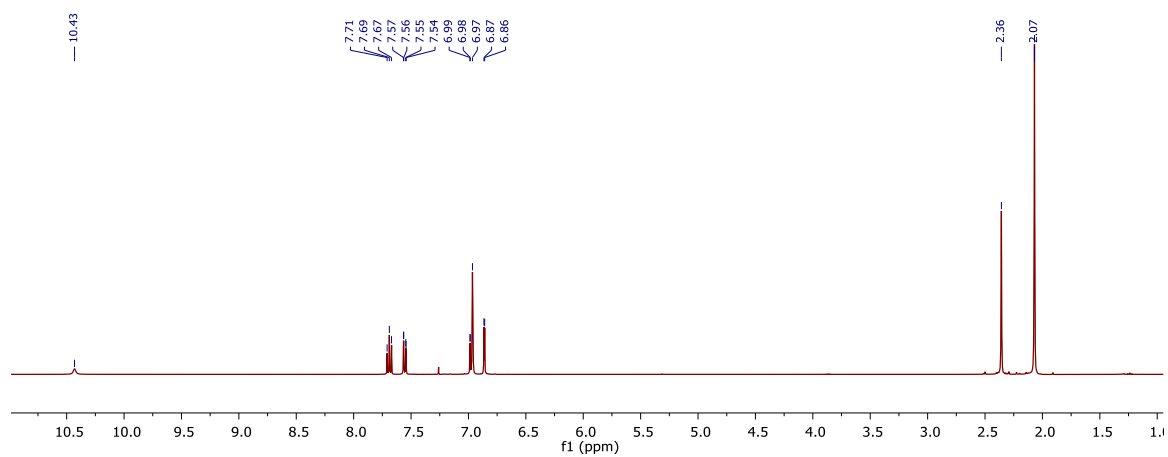


**Figure F3.1.**  $^1\text{H}$  NMR spectrum of **3.10** in  $\text{CDCl}_3$ . Acquired by Dr. Gyeongshin Choi.

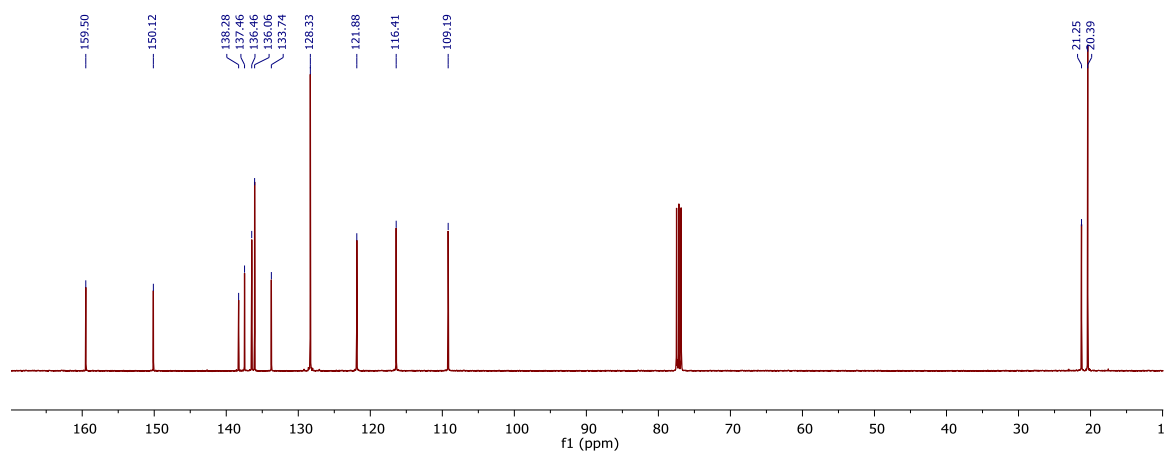


**Figure F3.2.**  $^{13}\text{C}\{^1\text{H}\}$  NMR spectrum of **3.10** in  $\text{CDCl}_3$ . Acquired by Dr. Gyeongshin Choi.

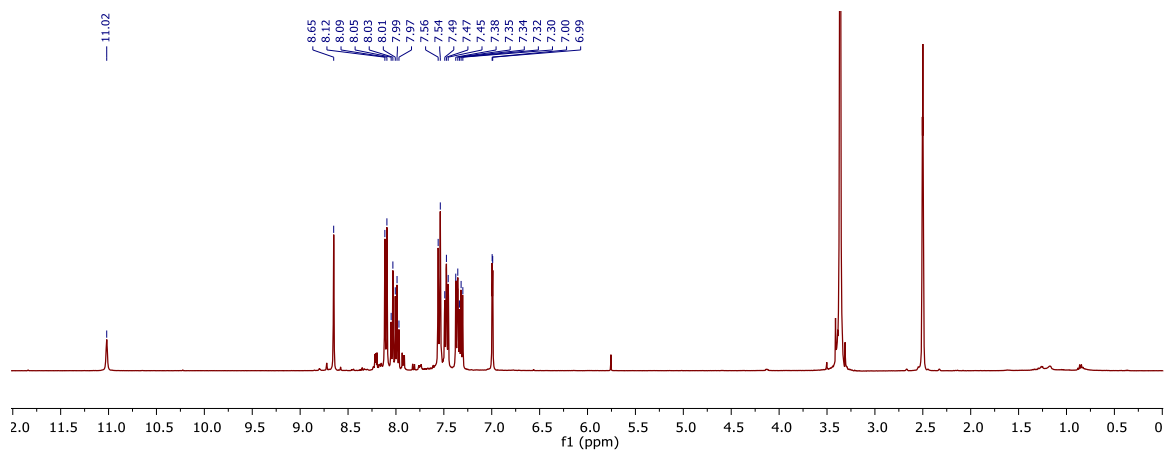


**Figure F3.3.** <sup>1</sup>H NMR spectrum of **3.11** in (CD<sub>3</sub>)<sub>2</sub>SO. Acquired by Dr. Gyeongshin Choi.

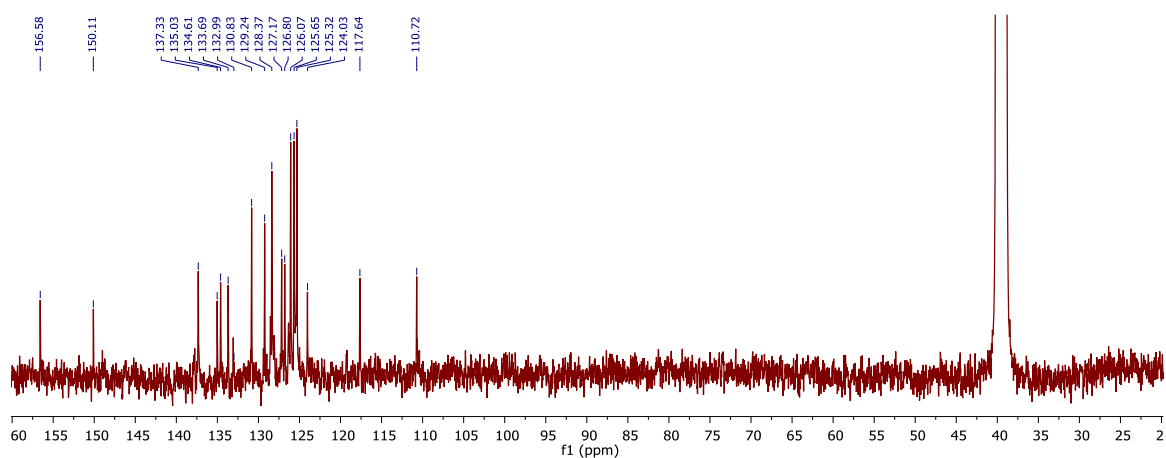


**Figure F3.4.** <sup>13</sup>C NMR spectrum of **3.11** in (CD<sub>3</sub>)<sub>2</sub>SO. Acquired by Dr. Gyeongshin Choi.

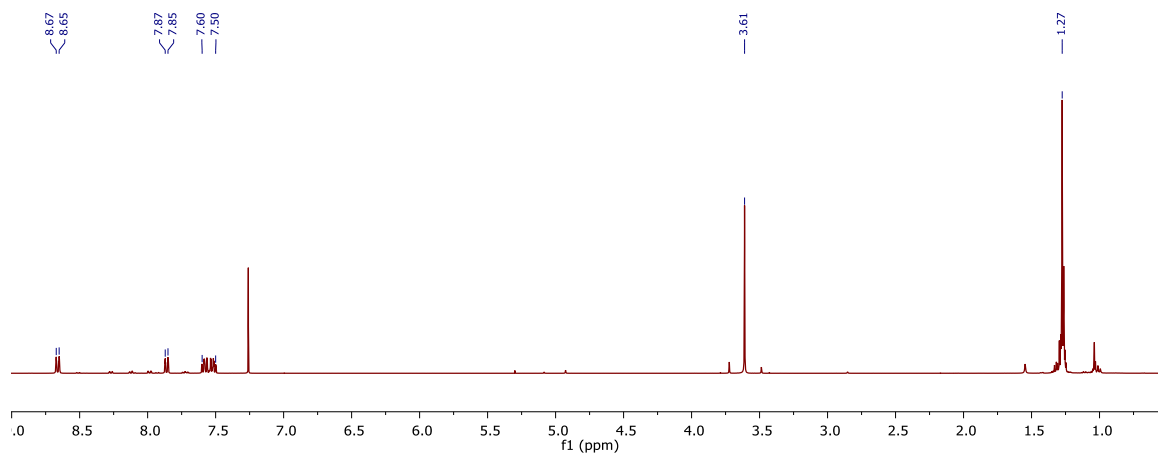


**Figure F3.5.** <sup>1</sup>H NMR spectrum of **3.9** in CDCl<sub>3</sub>.

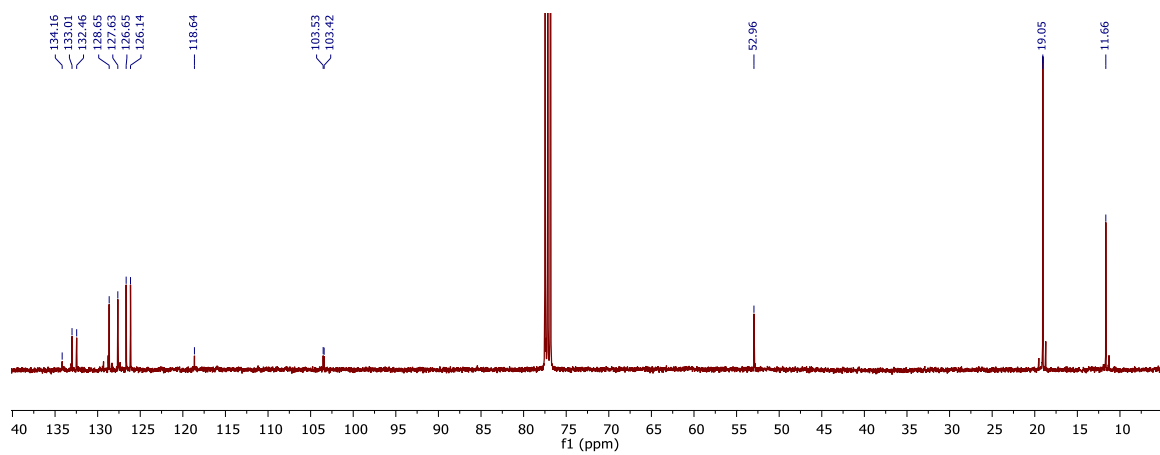


Figure F3.6. <sup>13</sup>C NMR spectrum of **3.9** in CDCl<sub>3</sub>.

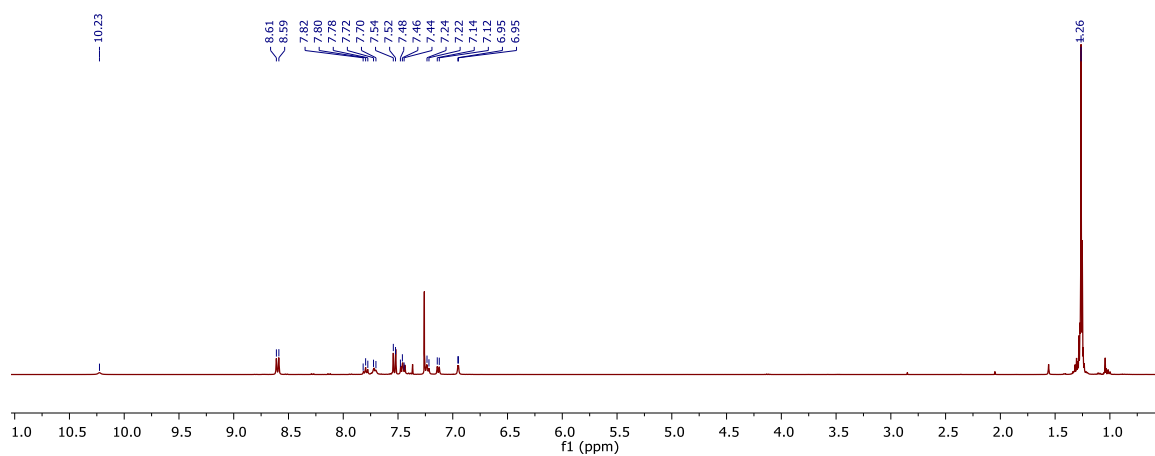


Figure F3.7. <sup>1</sup>H NMR spectrum of **3.12** in CDCl<sub>3</sub>.

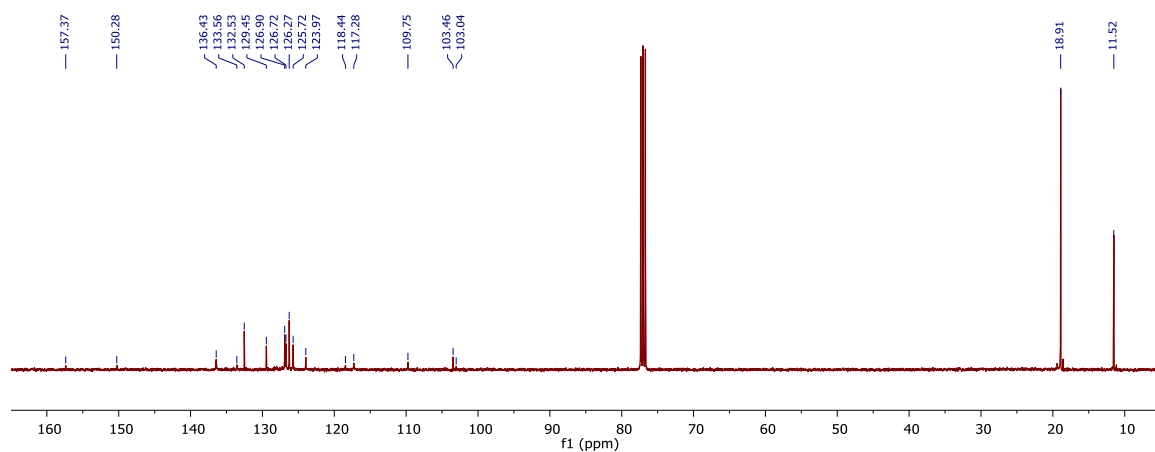


Figure F3.8. <sup>13</sup>C NMR spectrum of **3.12** in CDCl<sub>3</sub>.

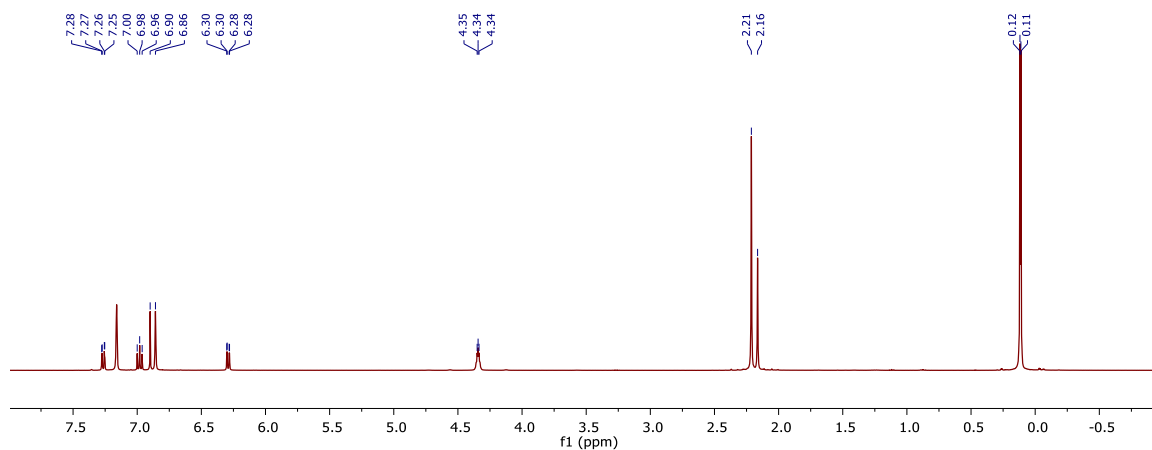


Figure F3.9.  $^1\text{H}$  NMR of **3.13** in  $\text{C}_6\text{D}_6$ .

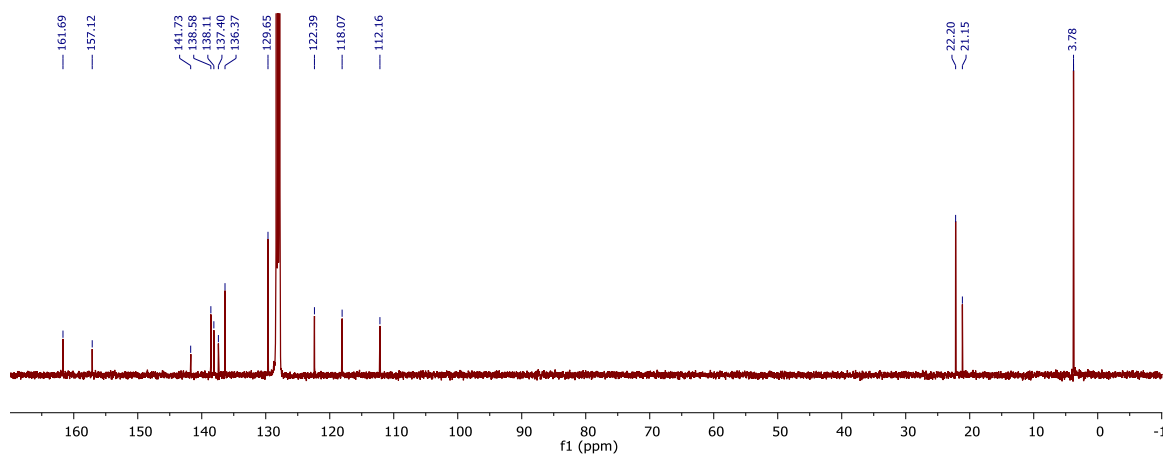


Figure F3.10.  $^{13}\text{C}$  NMR of **3.13** in  $\text{C}_6\text{D}_6$ .

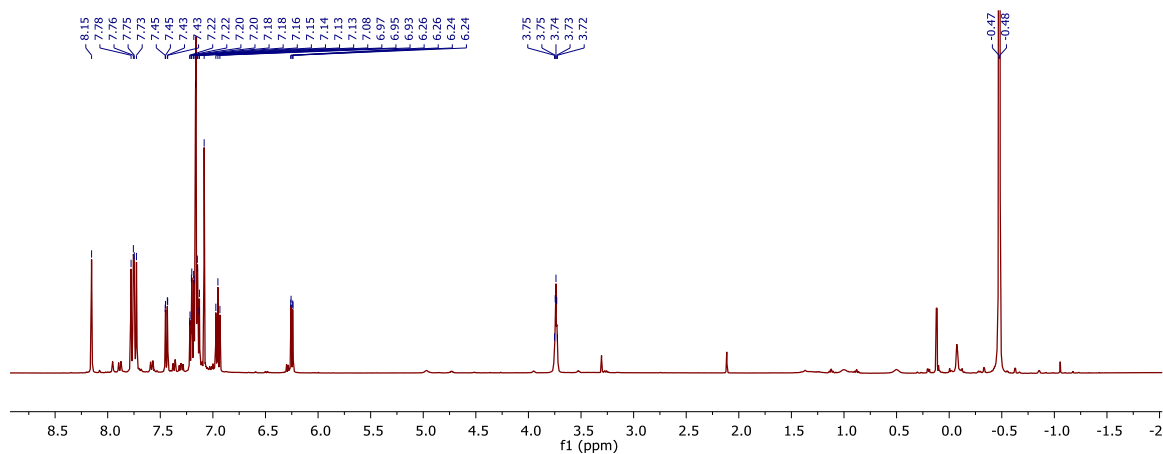
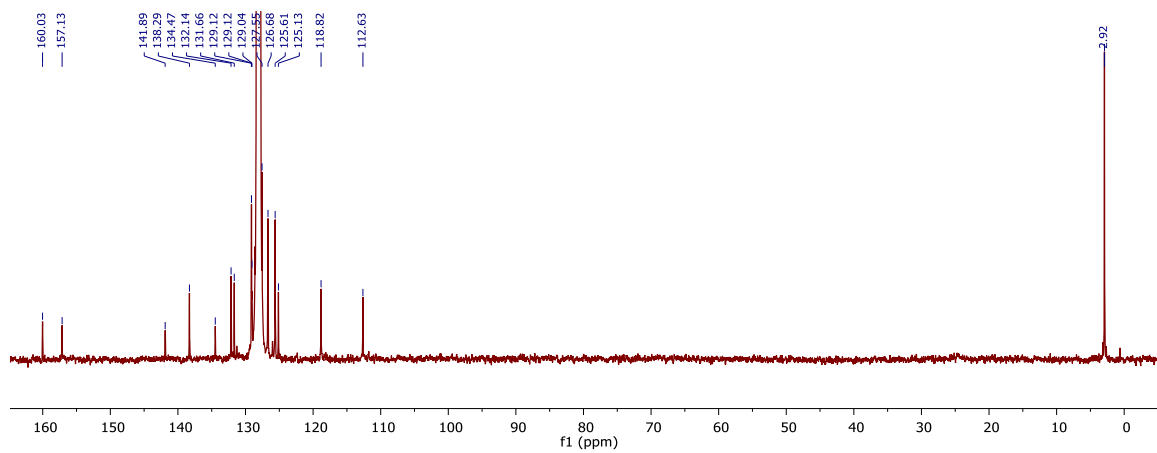
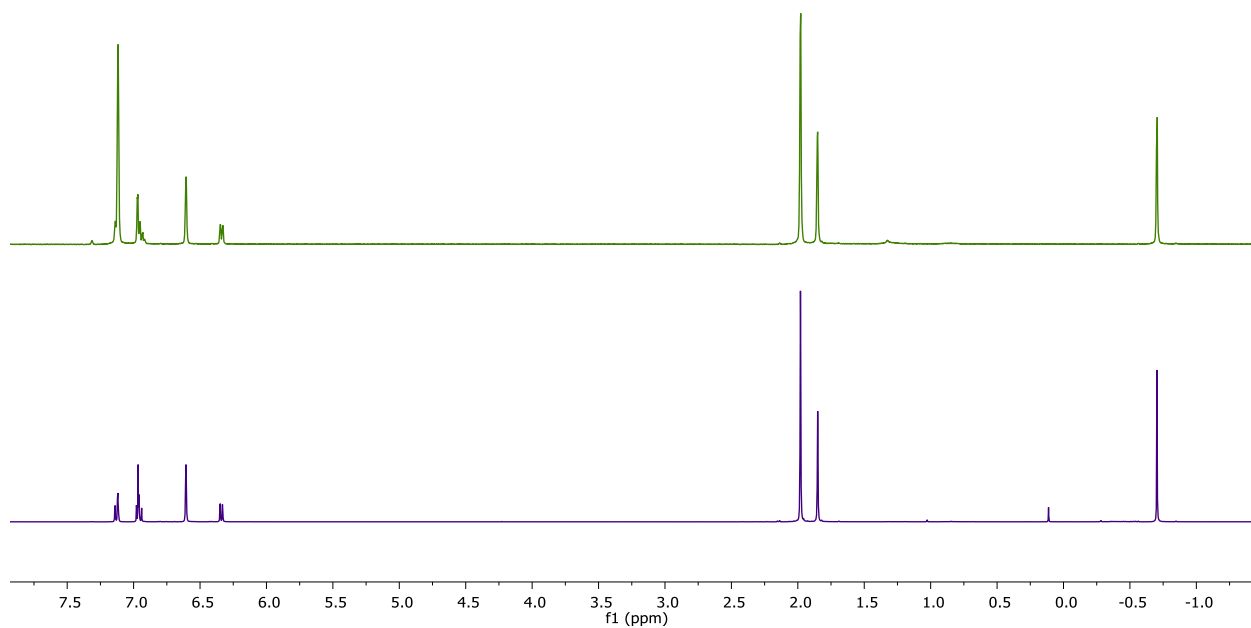


Figure F3.11.  $^1\text{H}$  NMR of **3.14** in  $\text{C}_6\text{D}_6$ .





**Figure F3.12.**  $^{13}\text{C}$  NMR of **3.14** in  $\text{C}_6\text{D}_6$ .



**Figure F3.13.** Comparison of the product of the reaction of **3.13** with  $\text{AlMe}_3$  (top, green) and the product of the reaction of  $(\text{DPP}^{\text{mes}})\text{H}$  with  $\text{AlMe}_3$  (**3.15**, bottom, blue),  $\text{C}_6\text{D}_6$ .

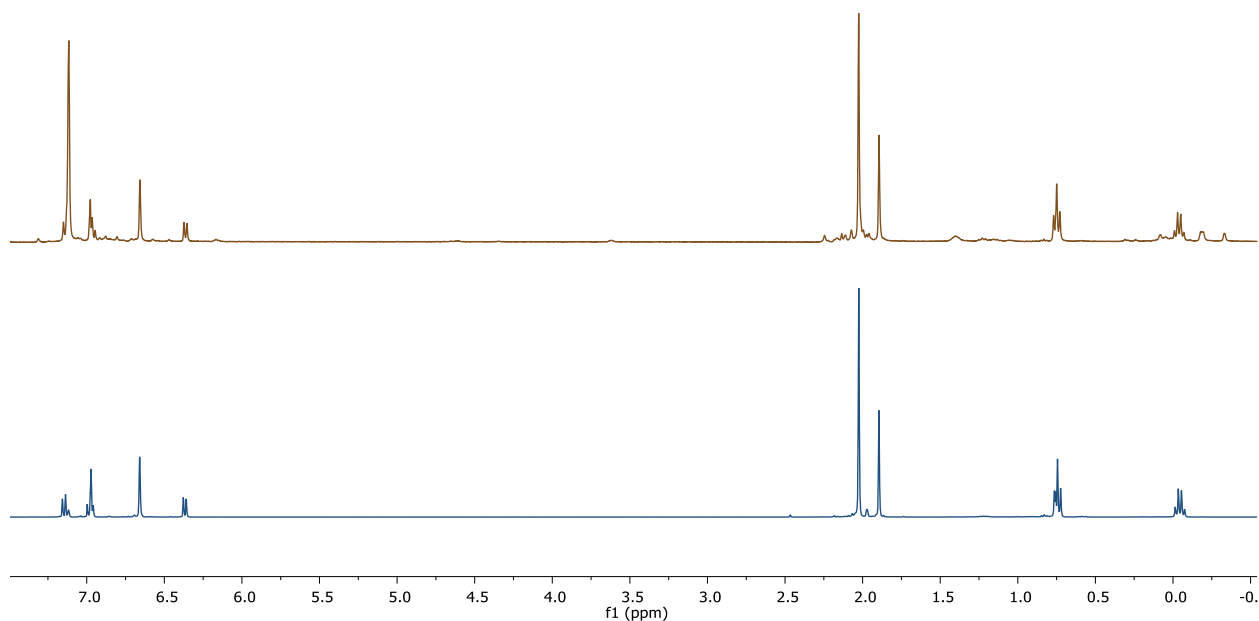


**Figure F3.14.** Comparison of the product of the reaction of **3.13** with  $\text{AlEt}_3$  and the product of the reaction of  $(\text{DPP}^{\text{mes}})\text{H}$  with  $\text{AlEt}_3$  (**3.16**),  $\text{C}_6\text{D}_6$ .

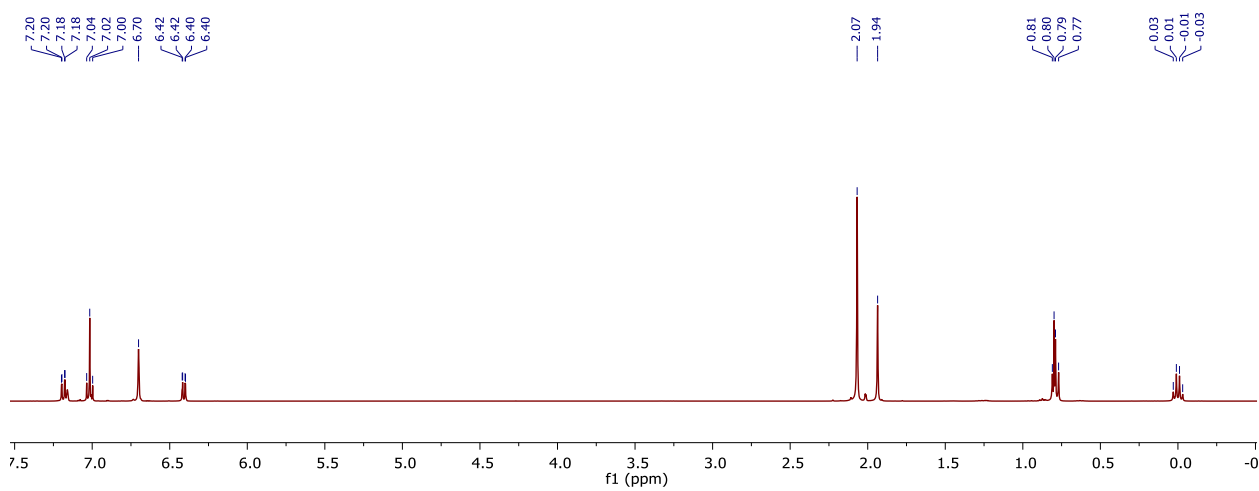


**Figure F3.15.**  $^1\text{H}$  NMR of **11** in  $\text{C}_6\text{D}_6$ . The resonance at 0.80 ppm is assigned to residual ethane.

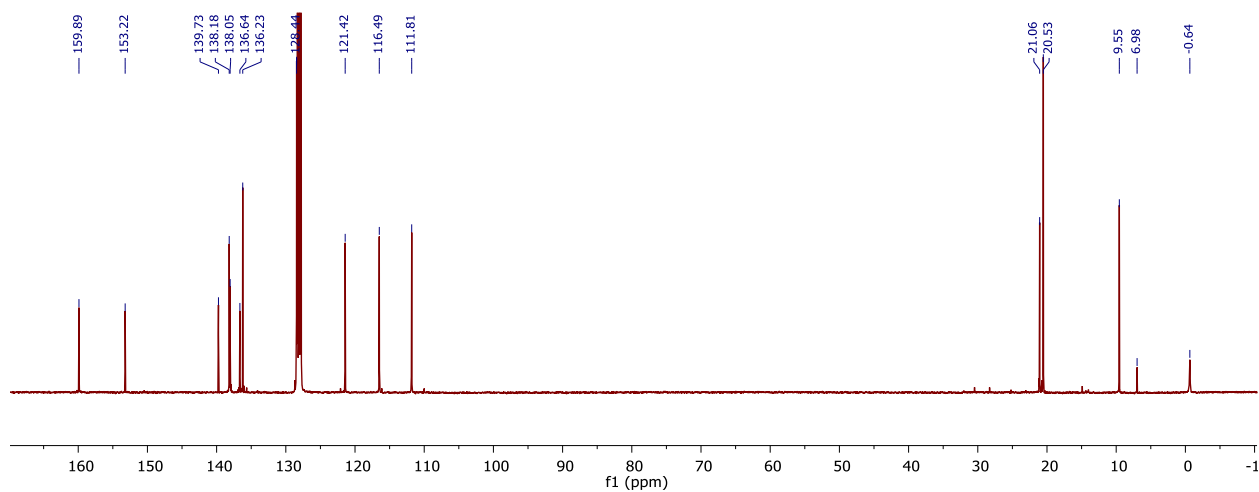


**Figure F3.16.**  $^{13}\text{C}$  NMR of **11** in  $\text{C}_6\text{D}_6$ . The resonance at 6.98 ppm assigned to residual ethane.

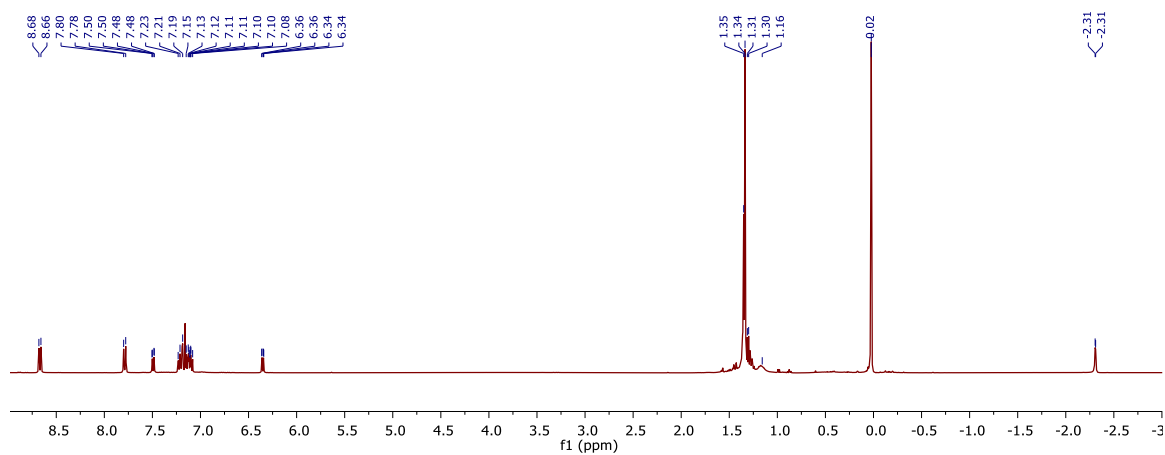


**Figure F3.17.**  $^1\text{H}$  NMR of **3.18** in  $\text{C}_6\text{D}_6$ .

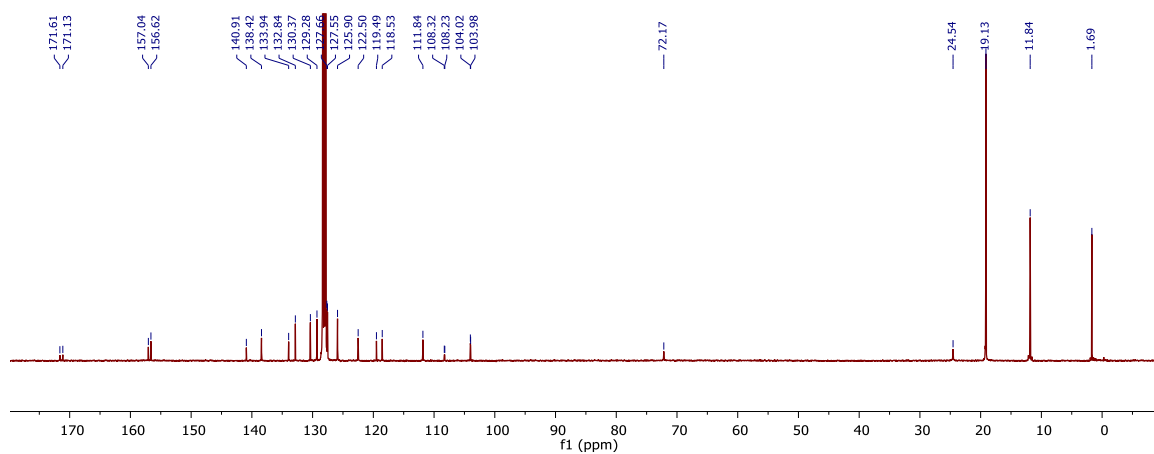


**Figure F3.18.**  $^{13}\text{C}$  NMR of **3.18** in  $\text{C}_6\text{D}_6$ .

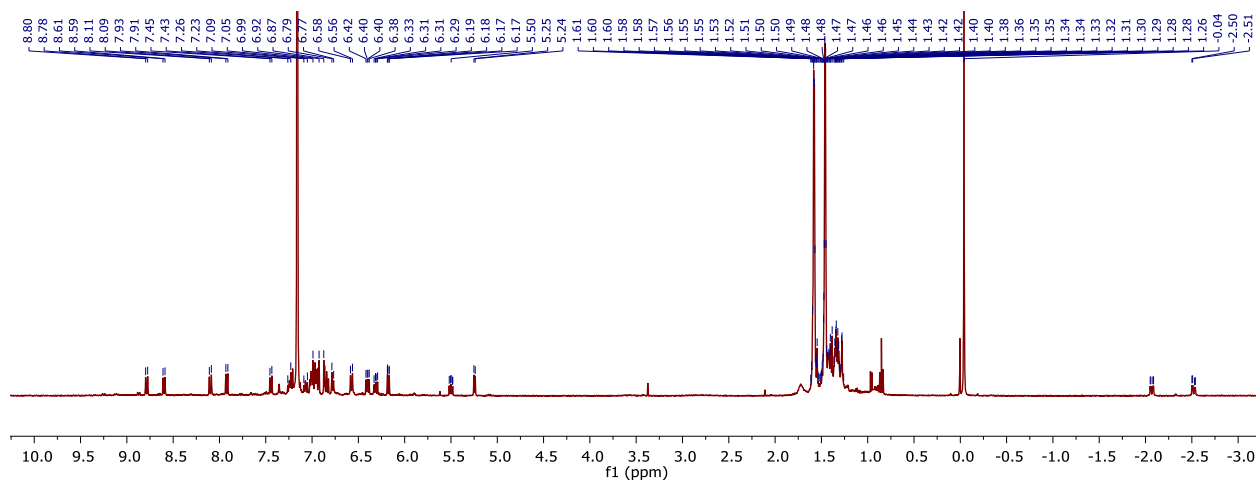


**Figure F3.19.**  $^1\text{H}$  NMR of the first decomposition product of **3.18** in  $\text{C}_6\text{D}_6$ .

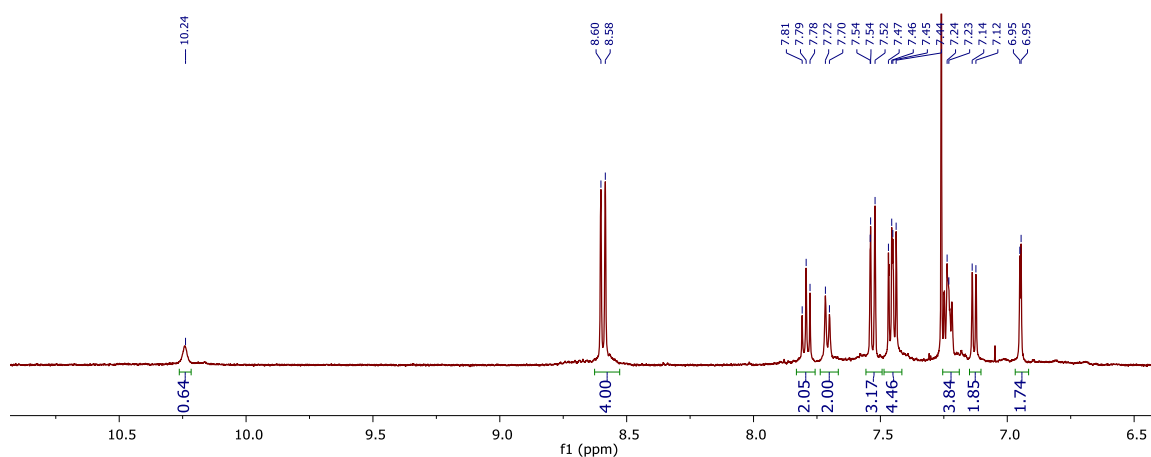


**Figure F3.20.**  $^1\text{H}$  NMR of the aromatic region of the  $\text{CD}_3\text{OD}$ -quenched first decomposition product of **3.18** in  $\text{CDCl}_3/\text{CD}_3\text{OD}$ .

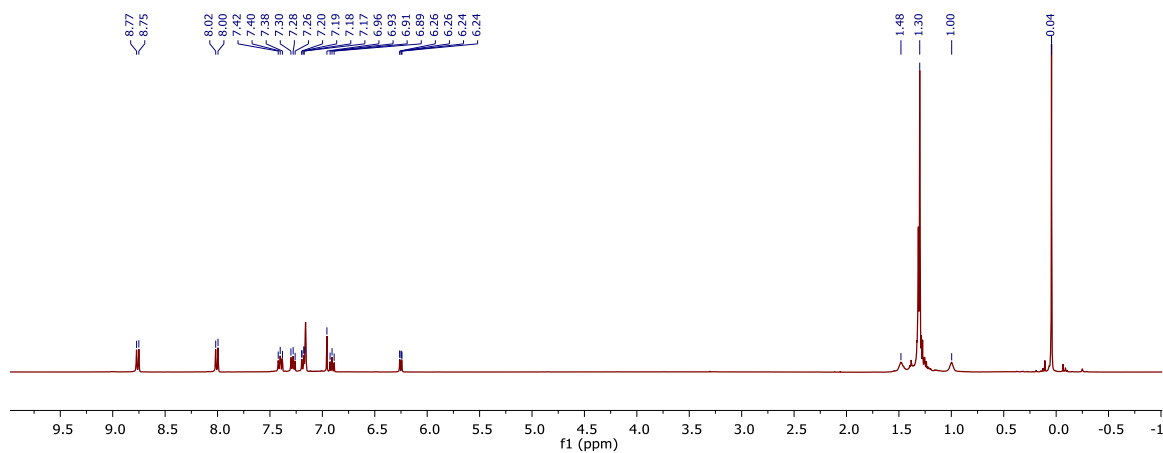


**Figure F3.21.**  $^1\text{H}$  NMR of **3.20** in  $\text{C}_6\text{D}_6$ .

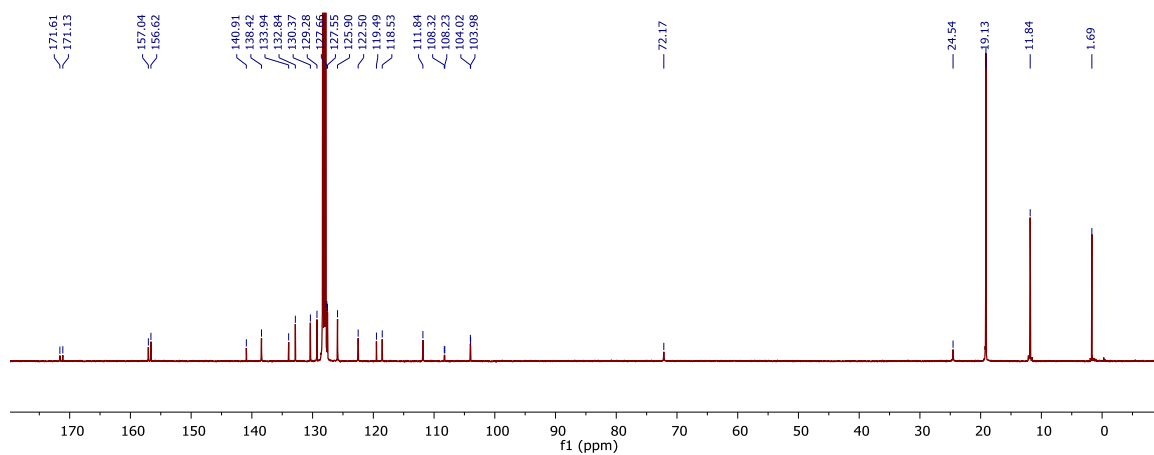


Figure F3.22.  $^{13}\text{C}$  NMR of 3.20 in  $\text{C}_6\text{D}_6$ .

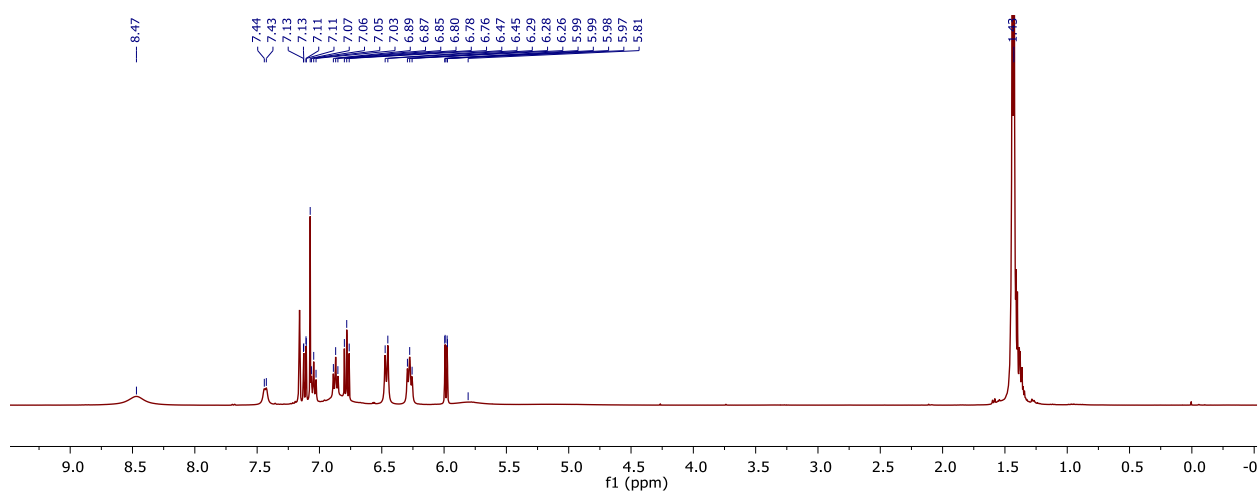


Figure F3.23.  $^1\text{H}$  NMR of 3.22 in  $\text{C}_6\text{D}_6$ .

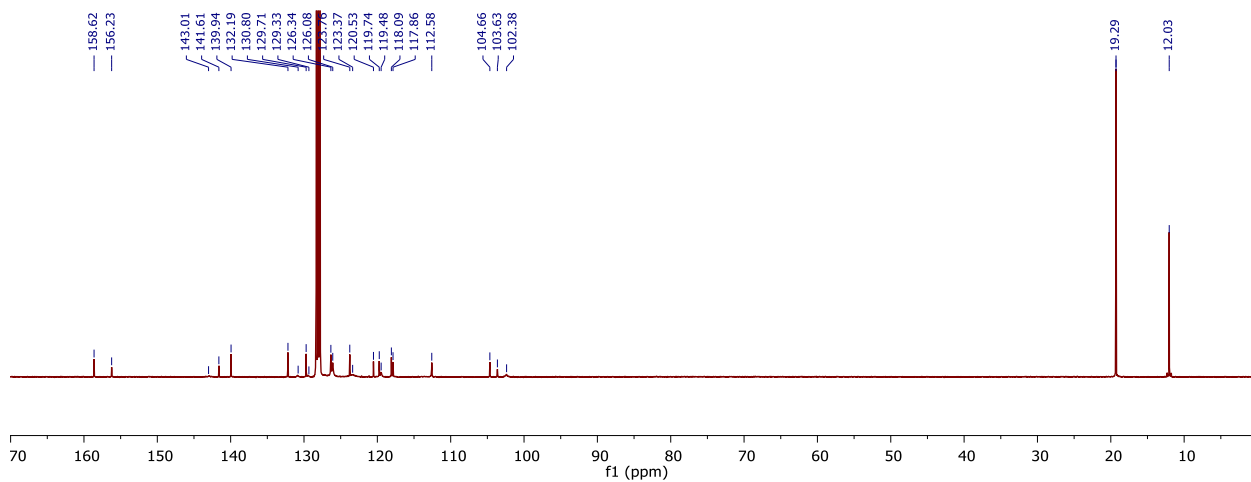


Figure F3.24.  $^{13}\text{C}$  NMR of 3.22 in  $\text{C}_6\text{D}_6$ .

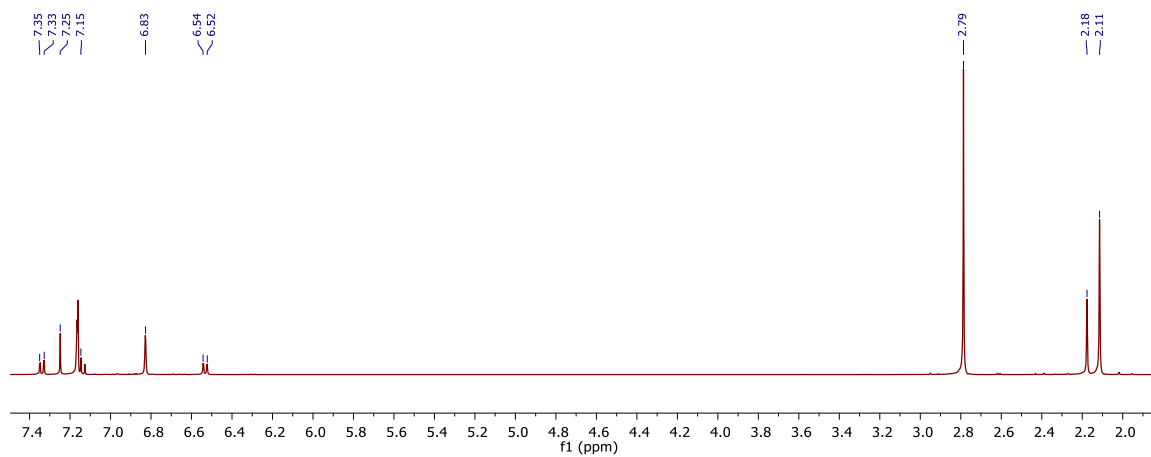


Figure F3.25.  $^1\text{H}$  NMR spectrum of **3.25** in  $\text{C}_6\text{D}_6$ .

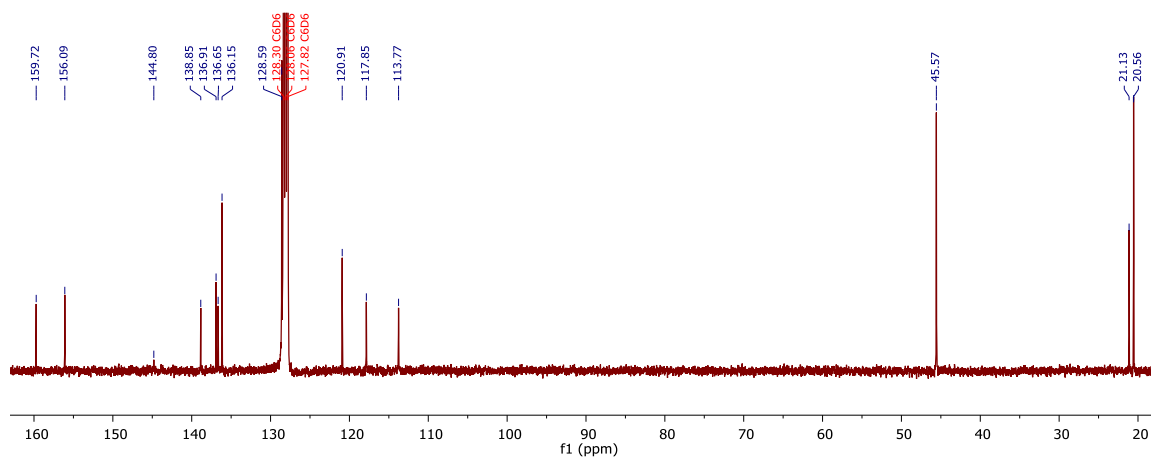


Figure F3.26.  $^{13}\text{C}$  NMR spectrum of **3.25** in  $\text{C}_6\text{D}_6$ .

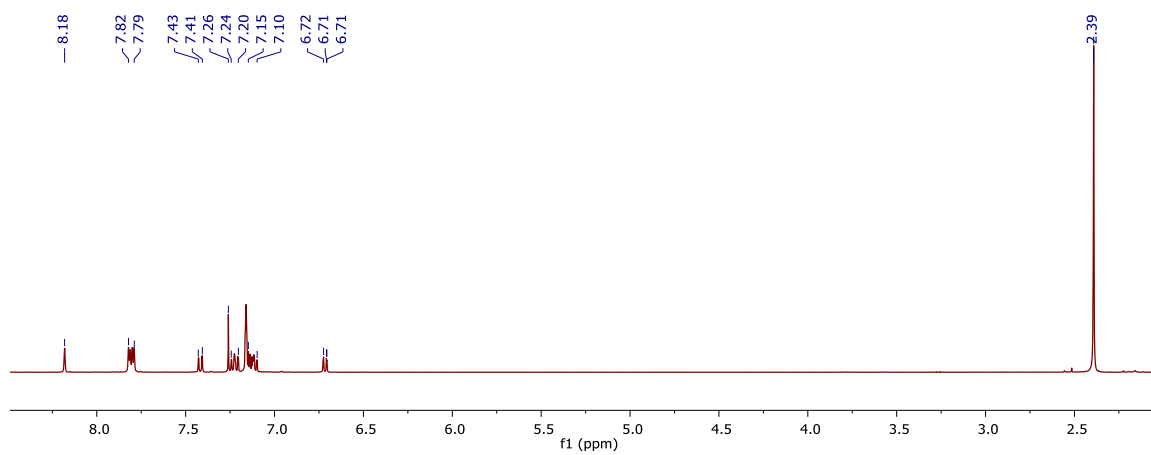


Figure F3.27.  $^1\text{H}$  NMR spectrum of **3.26** in  $\text{C}_6\text{D}_6$ .

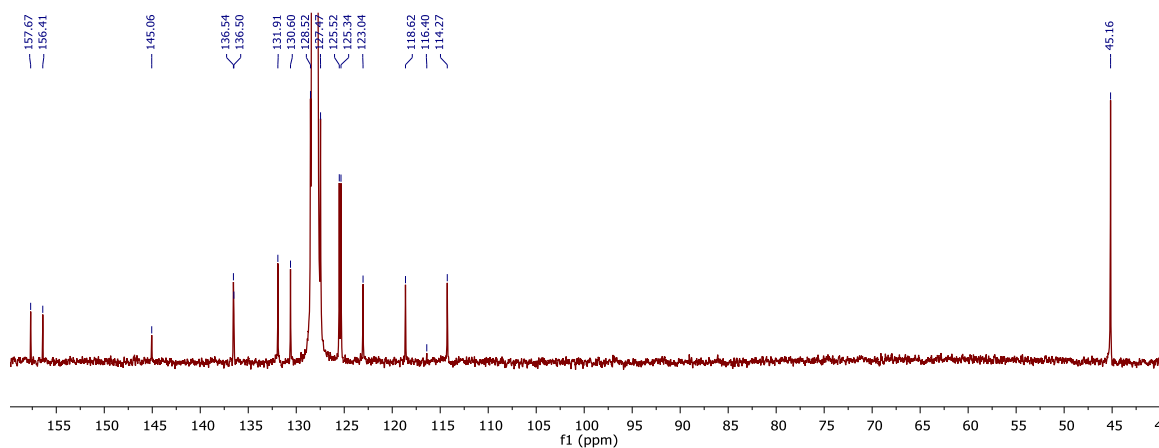


Figure F3.28. <sup>13</sup>C NMR spectrum of **3.26** in C<sub>6</sub>D<sub>6</sub>.

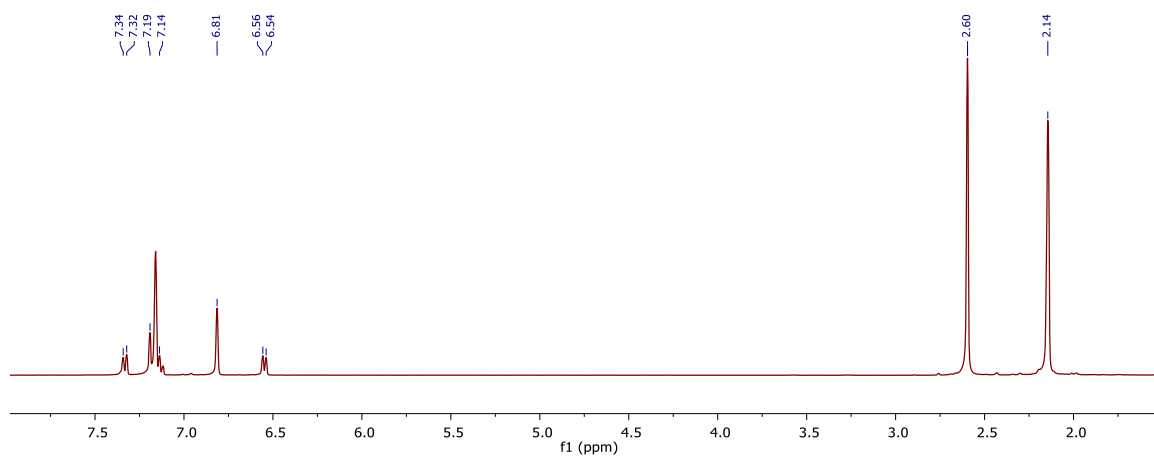


Figure F3.29. <sup>1</sup>H NMR spectrum of **3.27** in C<sub>6</sub>D<sub>6</sub>.

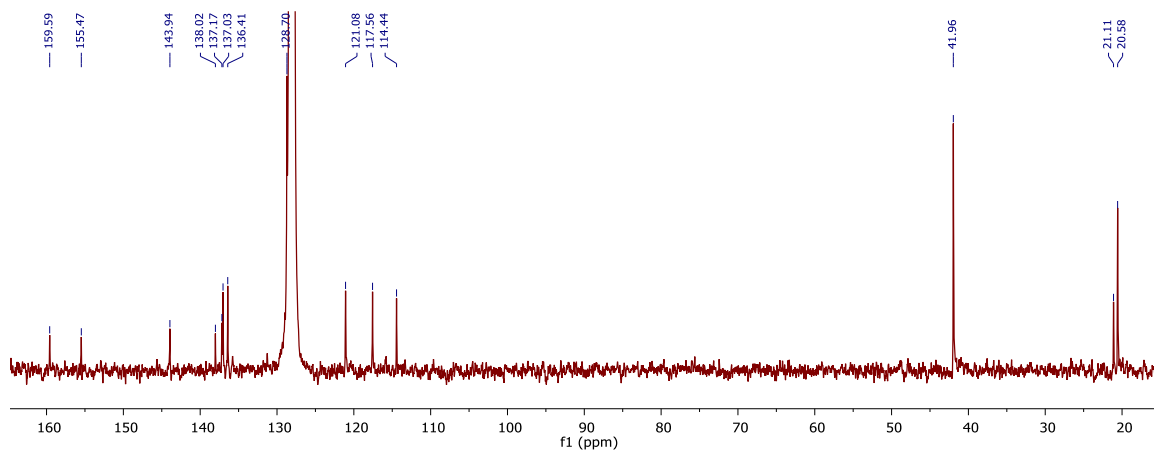


Figure F3.30. <sup>13</sup>C NMR spectrum of **3.27** in C<sub>6</sub>D<sub>6</sub>.

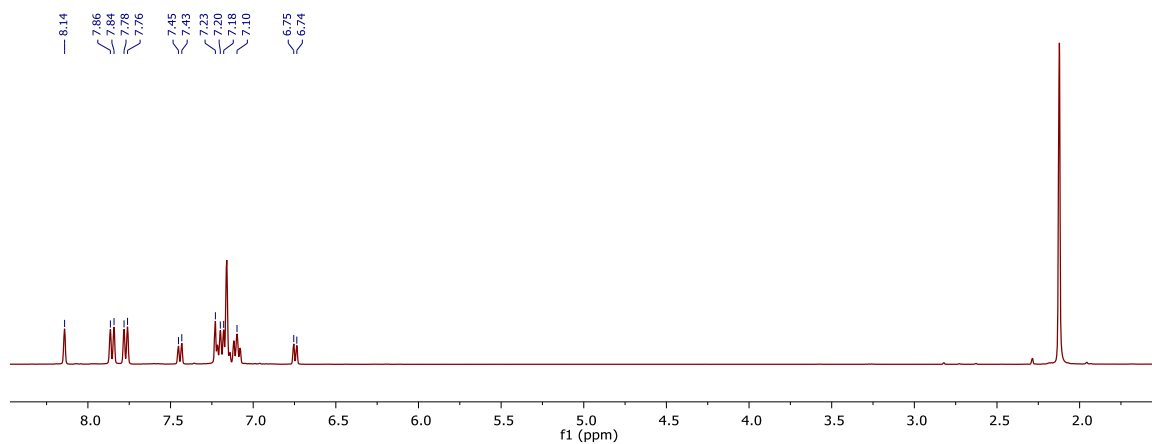


Figure F3.31.  $^1\text{H}$  NMR spectrum of **3.28** in  $\text{C}_6\text{D}_6$ .

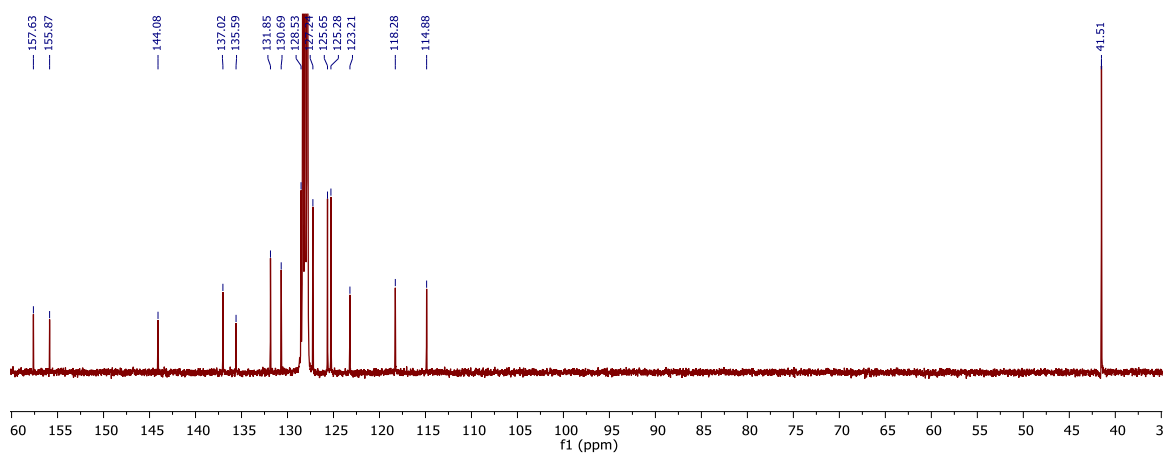


Figure F3.32.  $^{13}\text{C}$  NMR spectrum of **3.28** in  $\text{C}_6\text{D}_6$ .

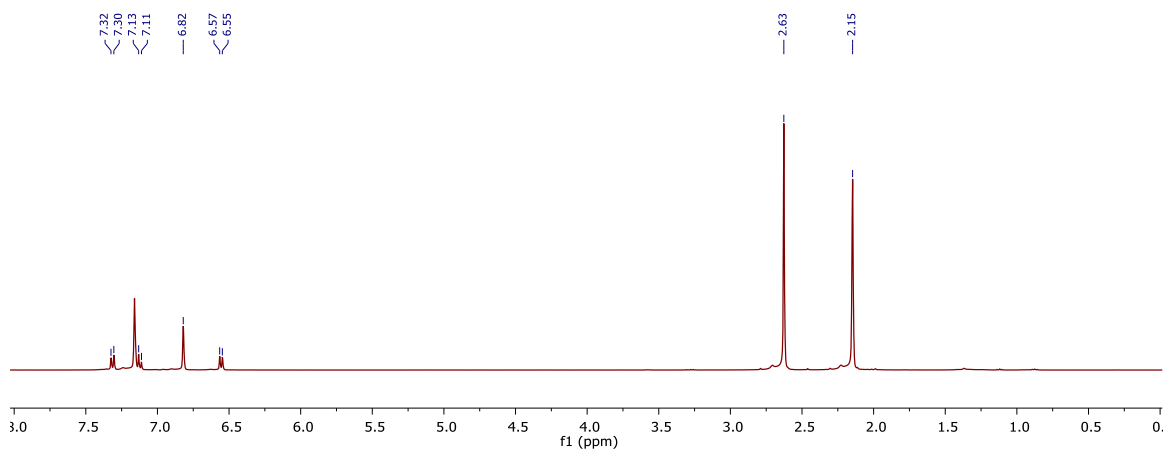


Figure F3.33.  $^1\text{H}$  NMR spectrum of **3.29** in  $\text{C}_6\text{D}_6$ .



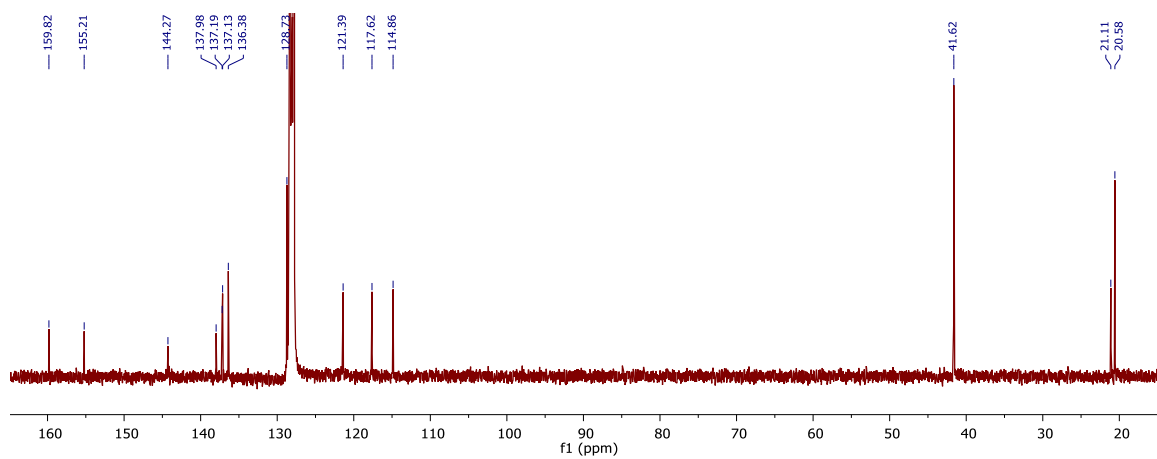


Figure F3.34.  $^{13}\text{C}$  NMR spectrum of **3.29** in  $\text{C}_6\text{D}_6$ .

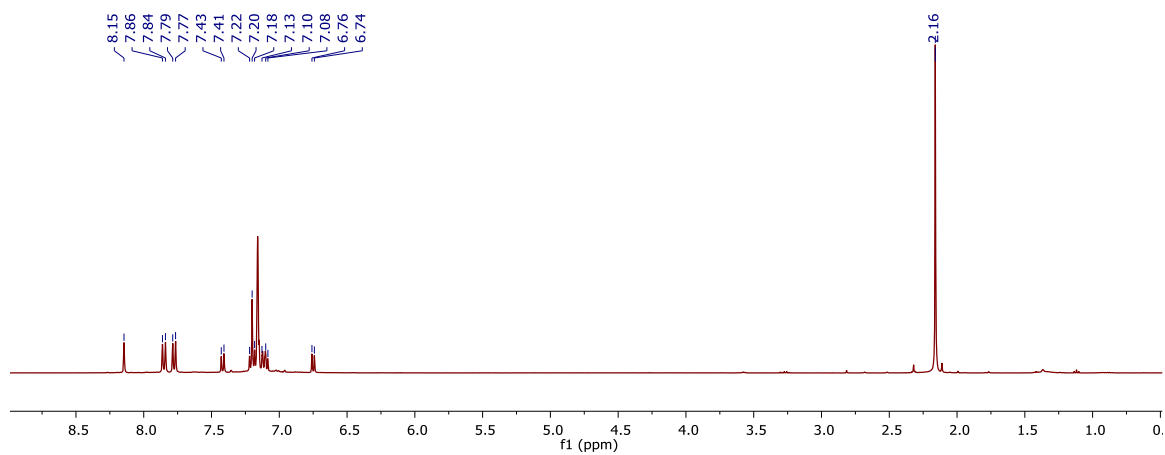


Figure F3.35.  $^1\text{H}$  NMR spectrum of **3.30** in  $\text{C}_6\text{D}_6$ .

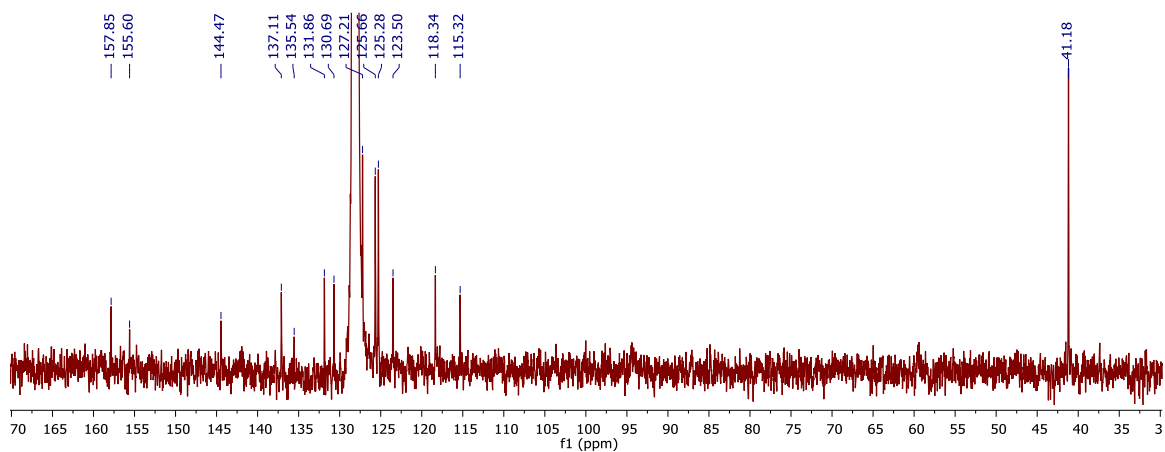
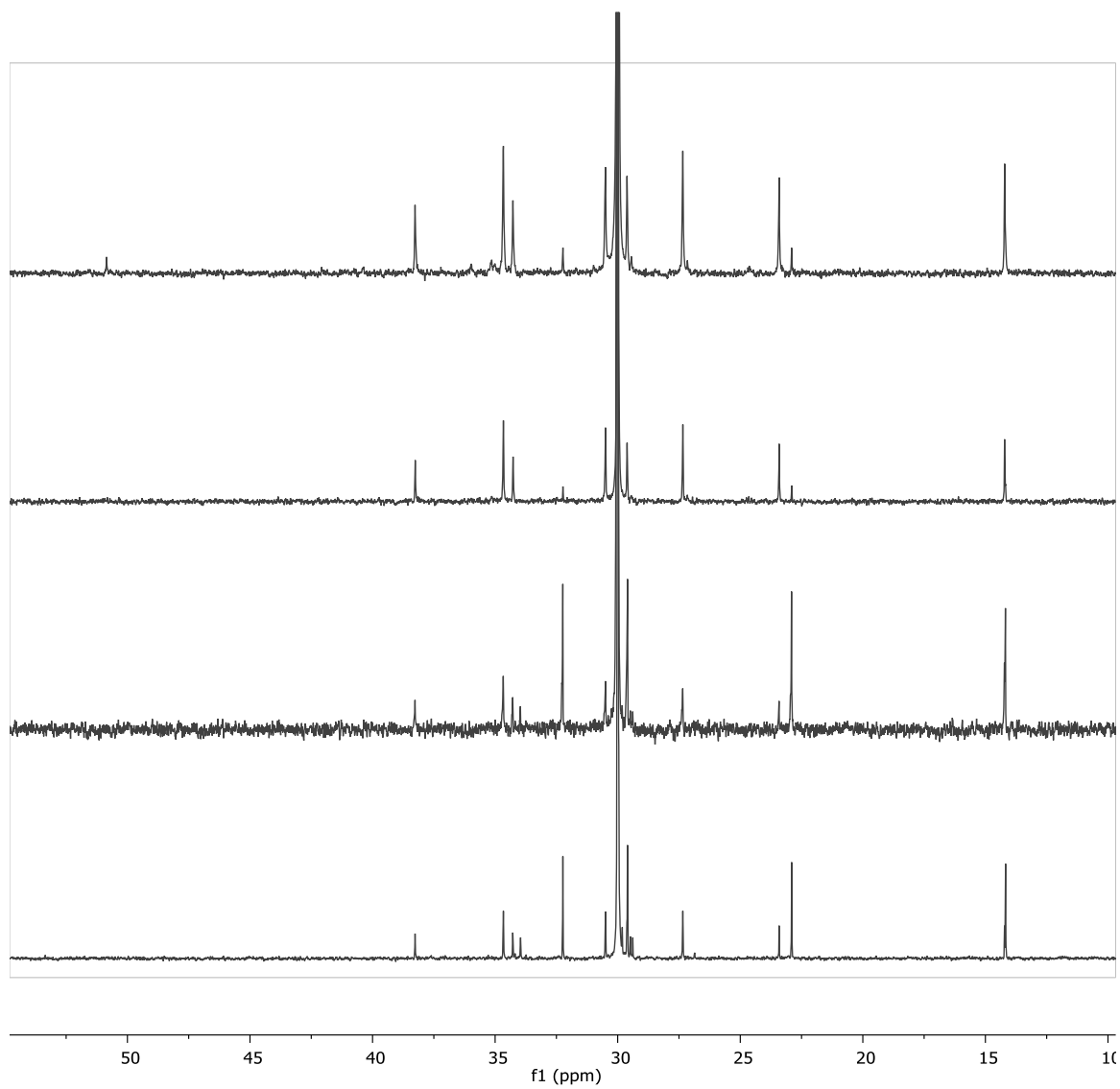
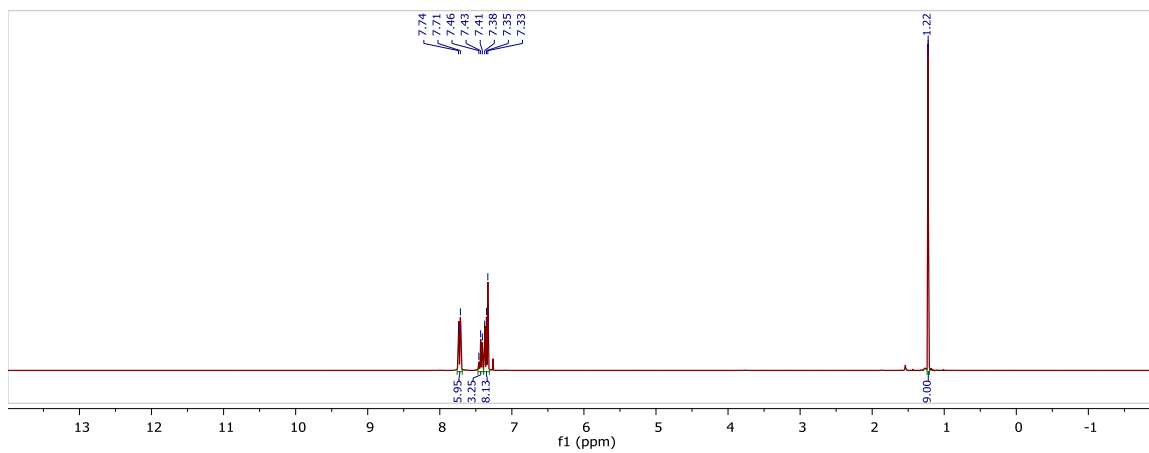
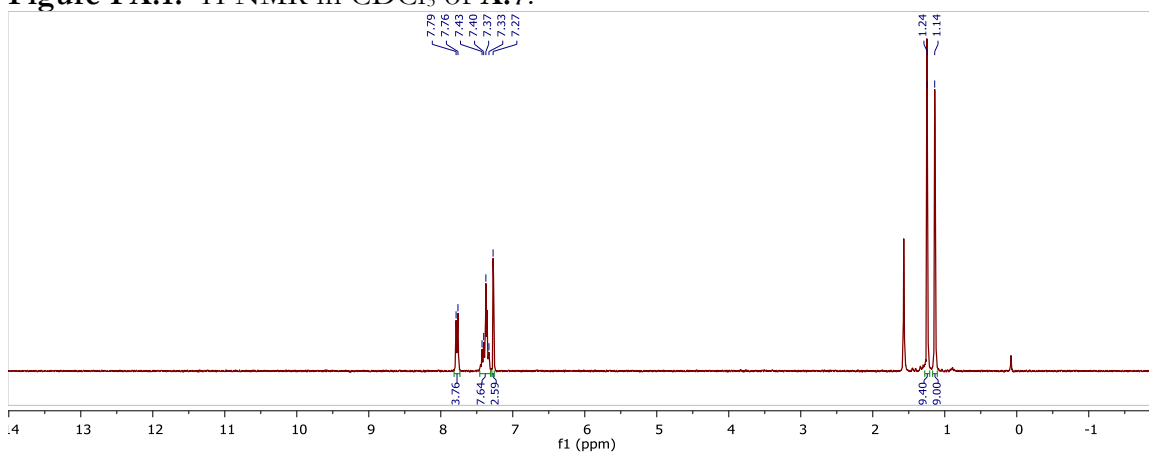
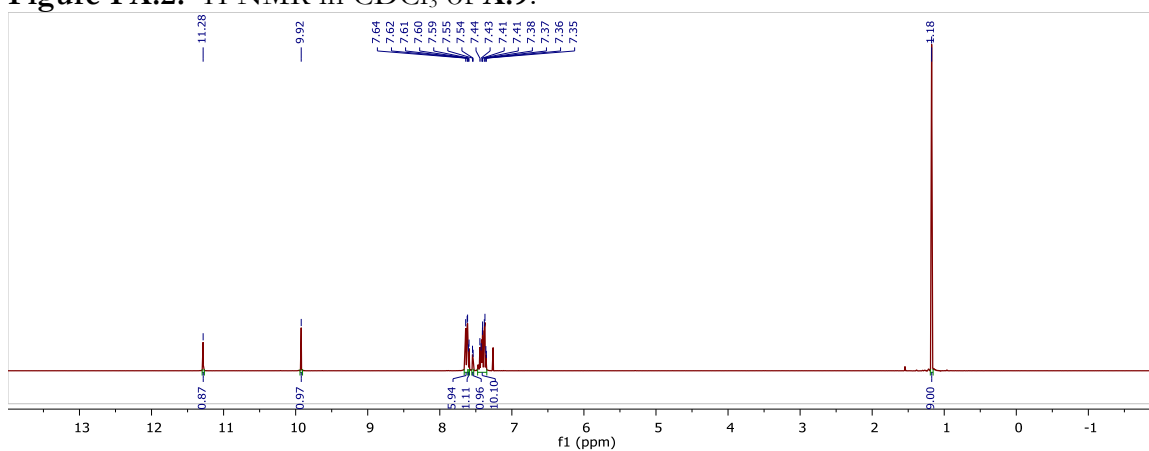


Figure F3.36.  $^{13}\text{C}$  NMR spectrum of **3.30** in  $\text{C}_6\text{D}_6$ .



**Figure S37.**  $^{13}\text{C}$  NMR spectra of ethylene-1-hexene copolymers from **3.25**, **3.26**, **3.27**, and **3.28** in  $\text{C}_2\text{D}_2\text{Cl}_4$  at 130 °C.

## APPENDIX A

Figure FA.1. <sup>1</sup>H NMR in CDCl<sub>3</sub> of A.7.Figure FA.2. <sup>1</sup>H NMR in CDCl<sub>3</sub> of A.9.Figure FA.3. <sup>1</sup>H NMR of A.11 in CDCl<sub>3</sub>.

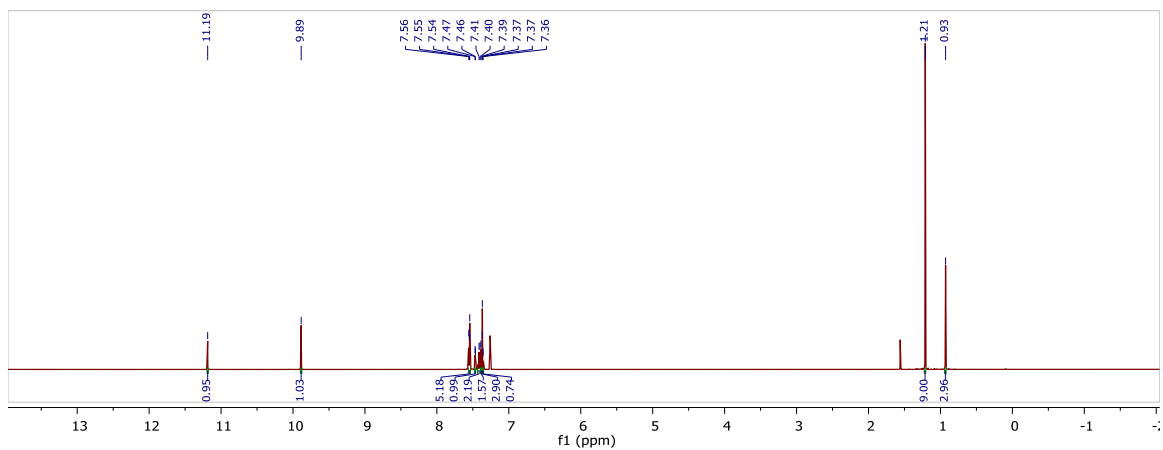


Figure FA.4. <sup>1</sup>H NMR of A.12 in CDCl<sub>3</sub>.

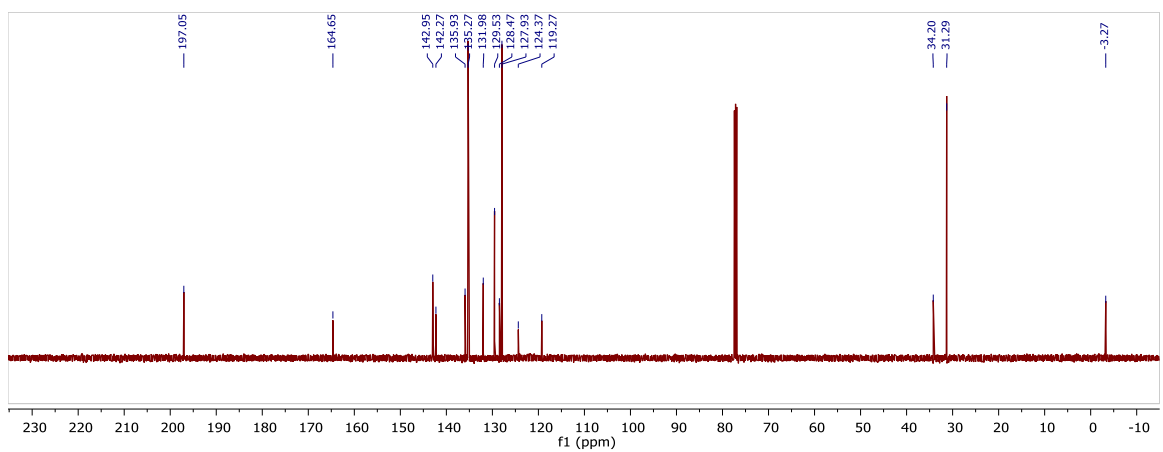


Figure FA.5. <sup>13</sup>C NMR of A.12 in CDCl<sub>3</sub>.

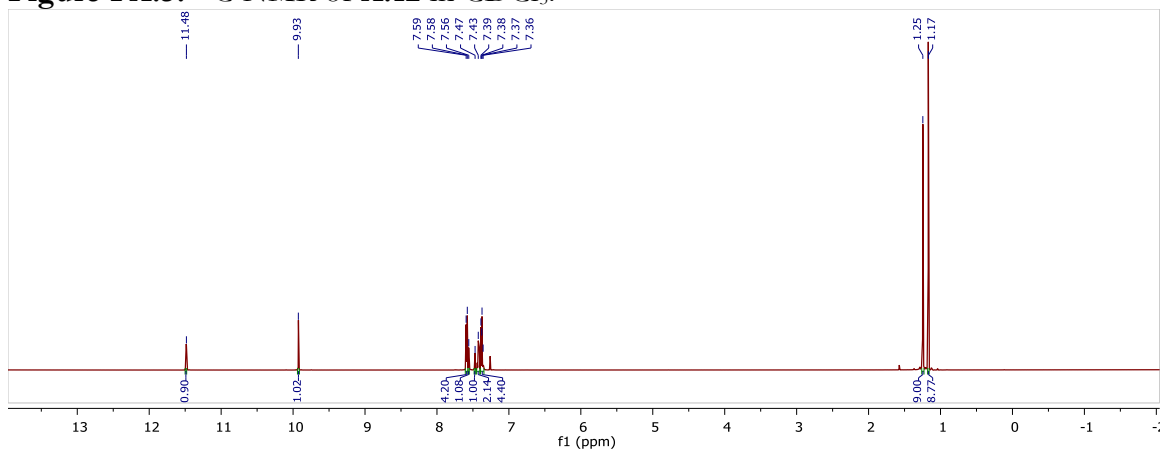


Figure FA.6. <sup>1</sup>H NMR of A.13 in CDCl<sub>3</sub>.

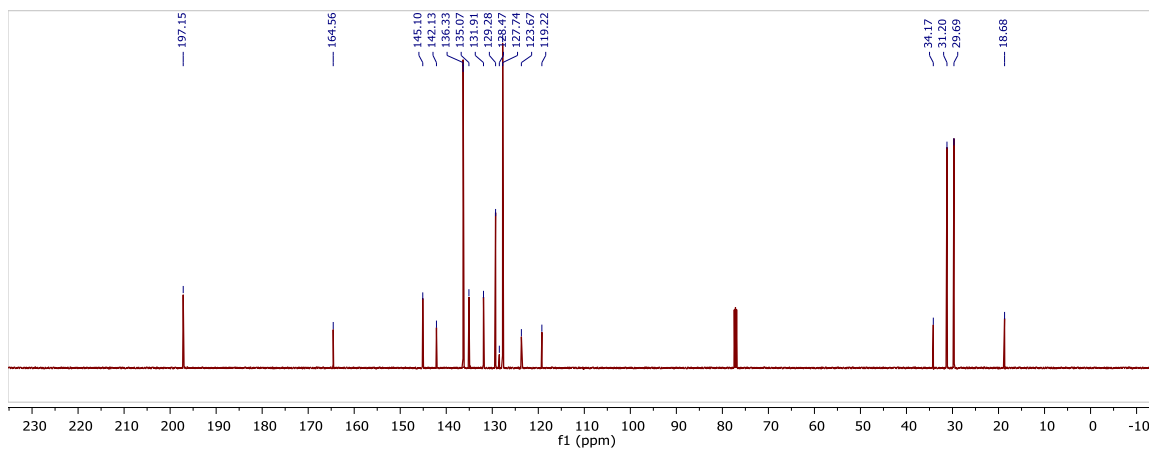


Figure FA.7. <sup>13</sup>C NMR of A.13 in CDCl<sub>3</sub>.

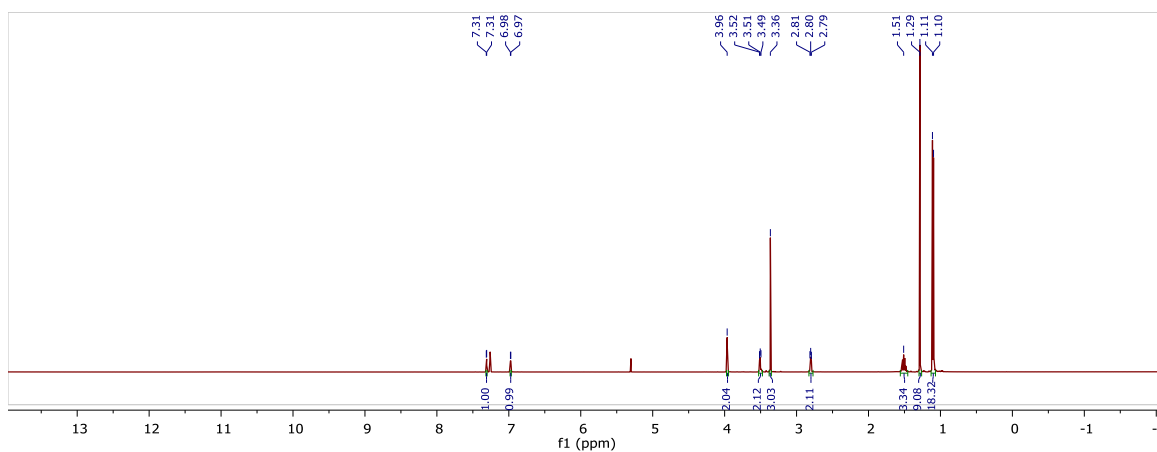


Figure FA.8. <sup>1</sup>H NMR of A.14 in CDCl<sub>3</sub>

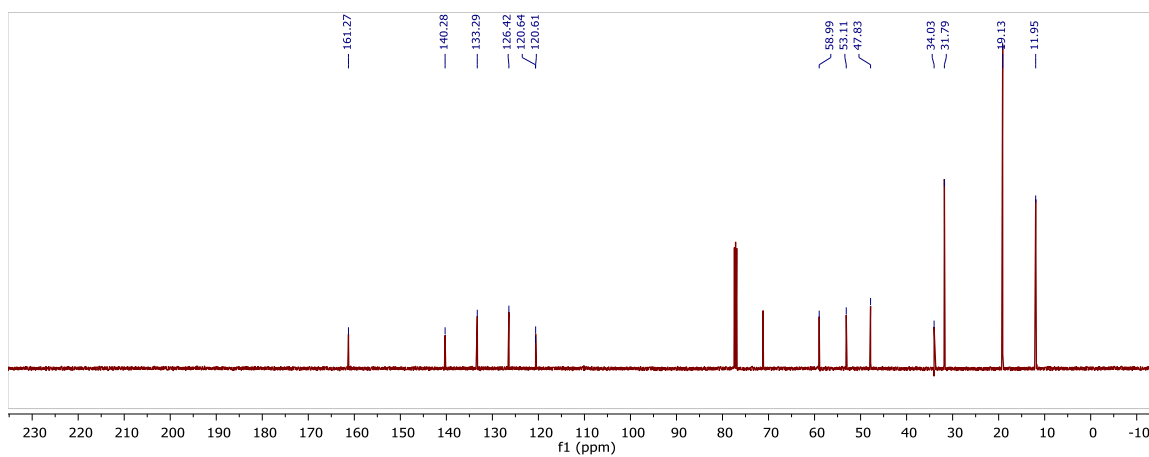


Figure FA.9. <sup>13</sup>C NMR of A.14 in CDCl<sub>3</sub>.

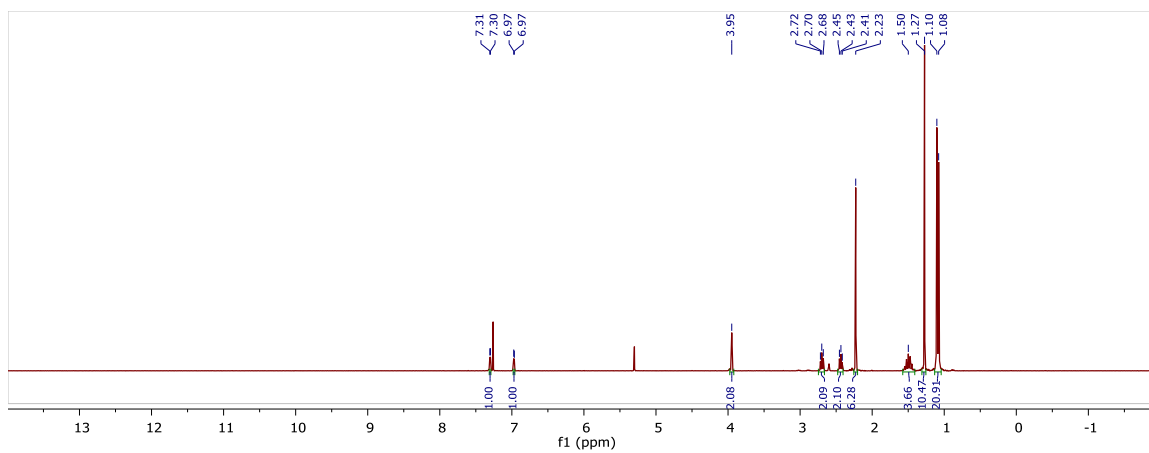


Figure FA.10. <sup>1</sup>H NMR of A.15 in CDCl<sub>3</sub>

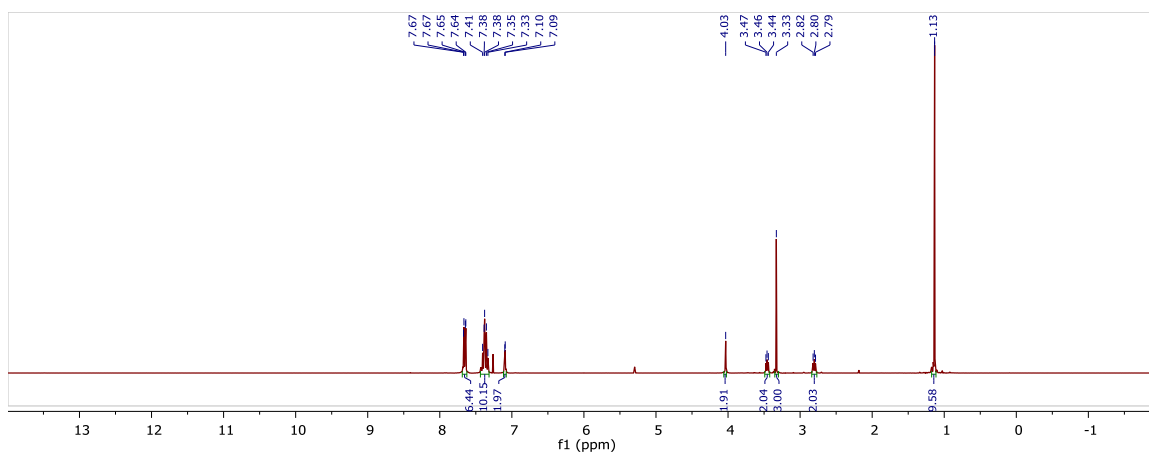


Figure FA.11. <sup>1</sup>H NMR of A.16 in CDCl<sub>3</sub>

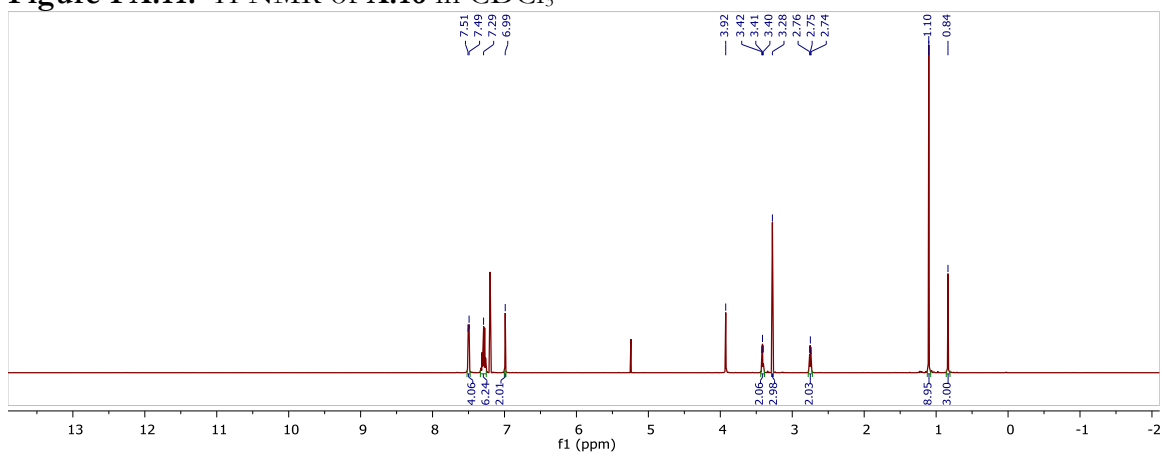


Figure FA.12. <sup>1</sup>H NMR in CDCl<sub>3</sub> of A.17

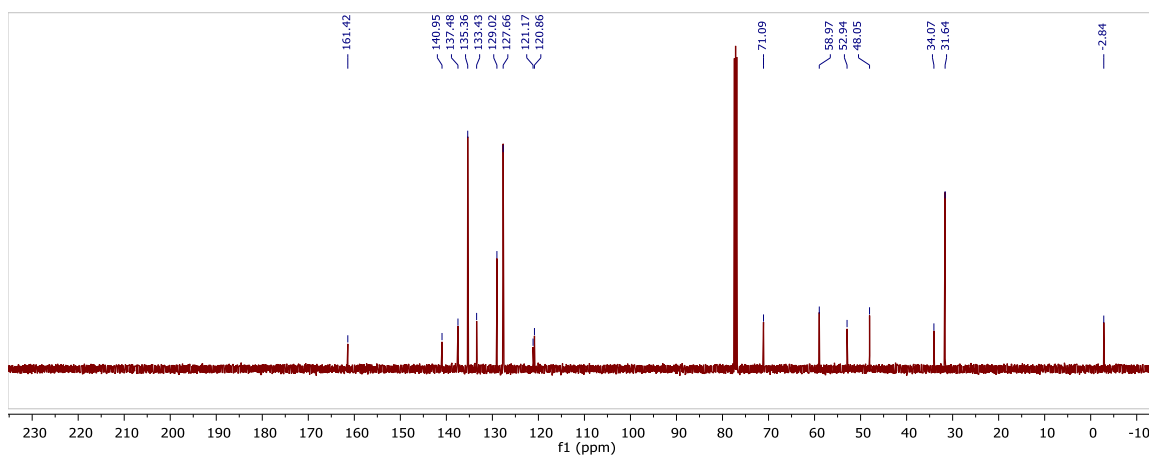


Figure FA.13.  $^{13}\text{C}$  NMR in  $\text{CDCl}_3$  of A.17

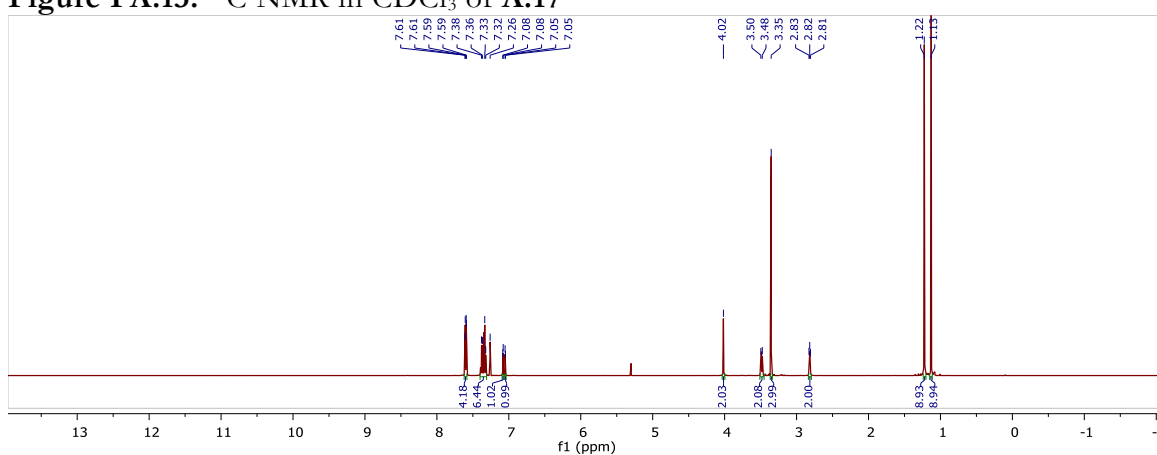


Figure FA.14.  $^1\text{H}$  NMR of A.18 in  $\text{CDCl}_3$

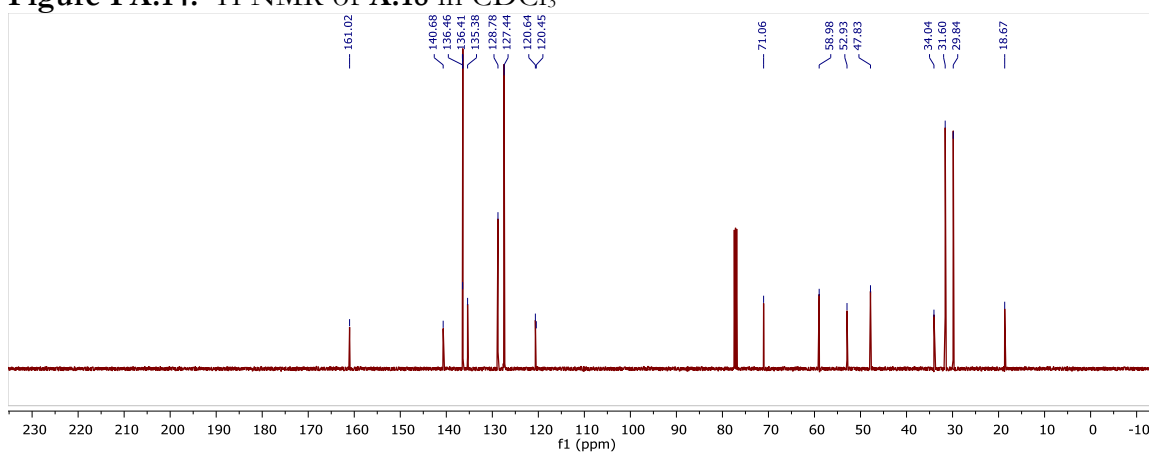


Figure FA.15.  $^{13}\text{C}$  NMR of A.18 in  $\text{CDCl}_3$

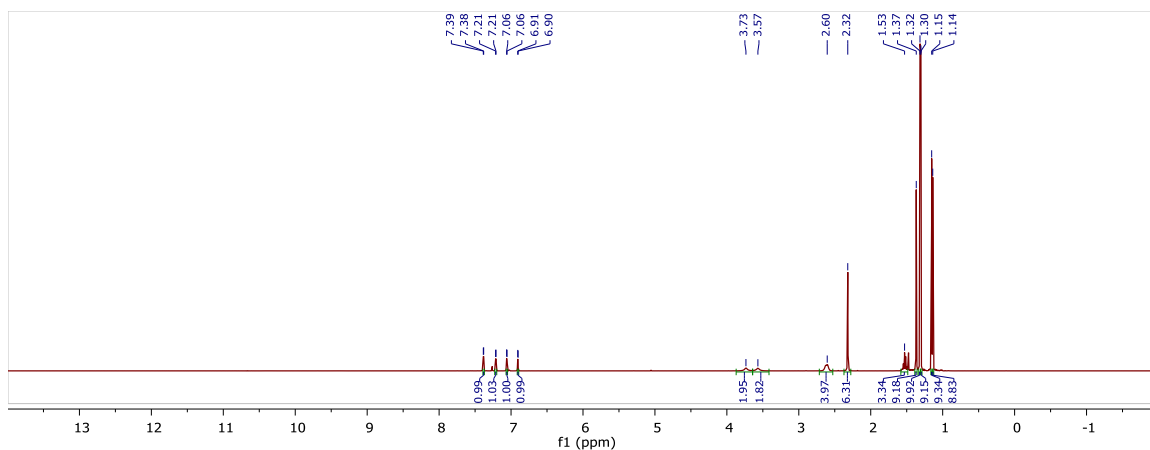


Figure FA.16. <sup>1</sup>H NMR of A.21 in CDCl<sub>3</sub>.

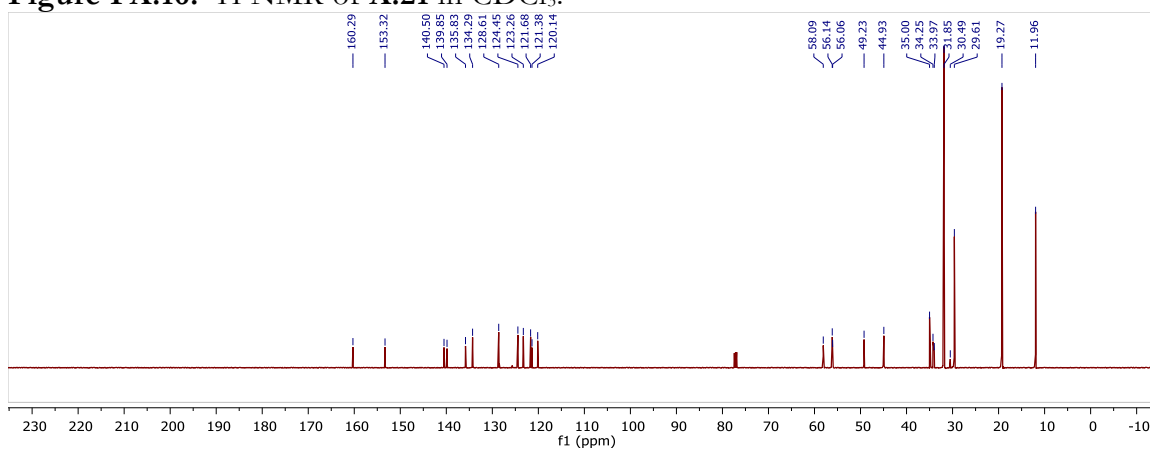


Figure FA.17. <sup>13</sup>C NMR of A.21 in CDCl<sub>3</sub>.

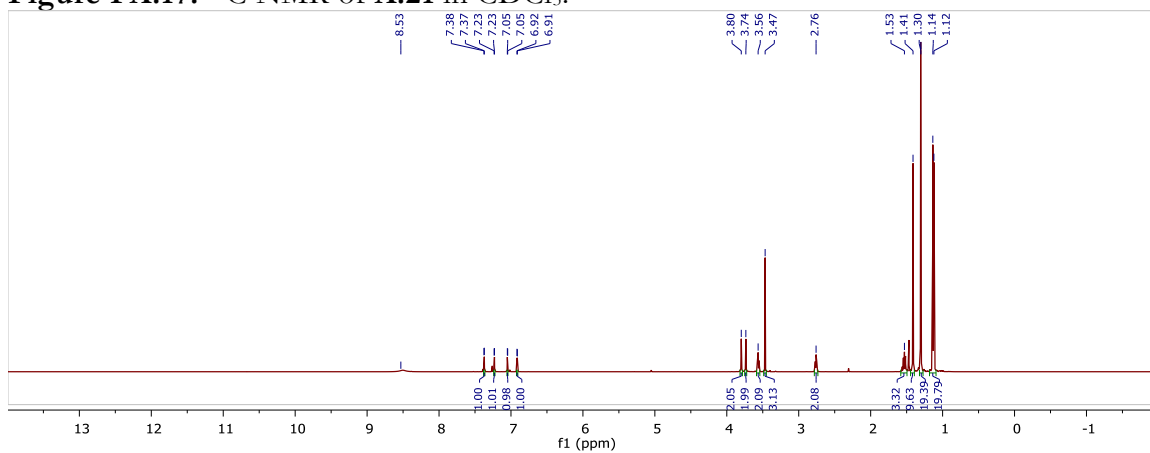
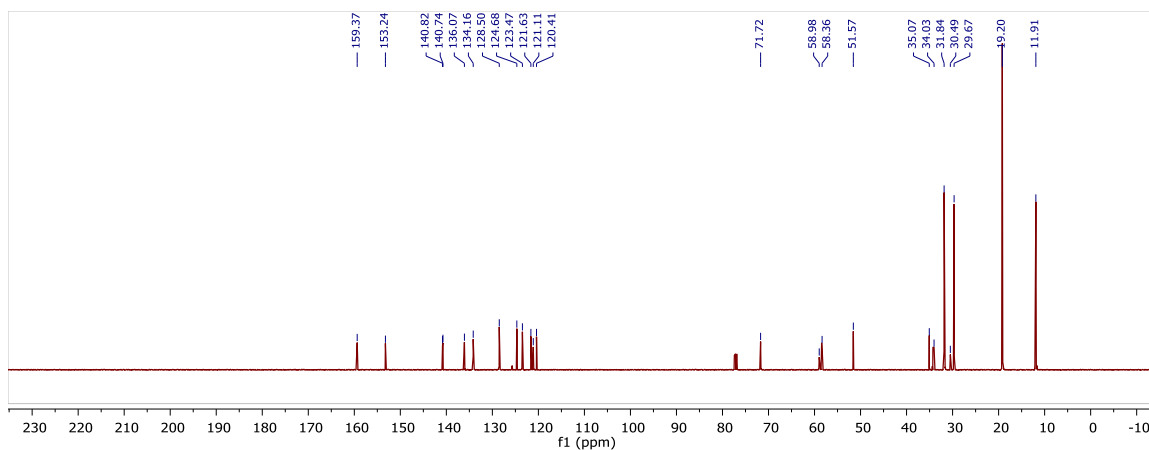
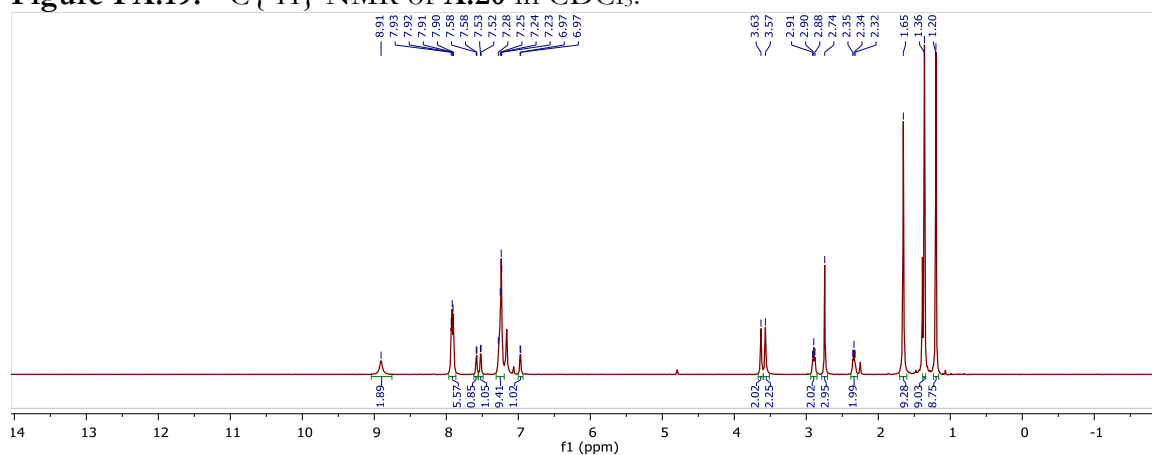


Figure FA.18. <sup>1</sup>H NMR of A.20 in CDCl<sub>3</sub>.





**Figure FA.19.**  $^{13}\text{C}\{^1\text{H}\}$  NMR of **A.20** in  $\text{CDCl}_3$ .



**Figure FA.20.**  $^1\text{H}$  NMR of **A.22** in  $\text{C}_6\text{D}_6$ .

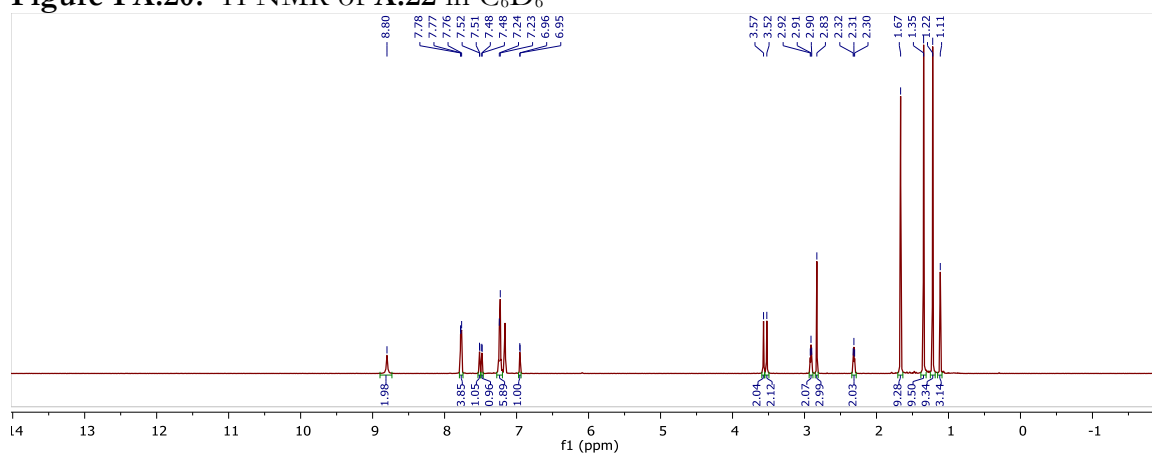


**Figure FA.21.**  $^1\text{H}$  NMR of **A.23** in  $\text{C}_6\text{D}_6$ .

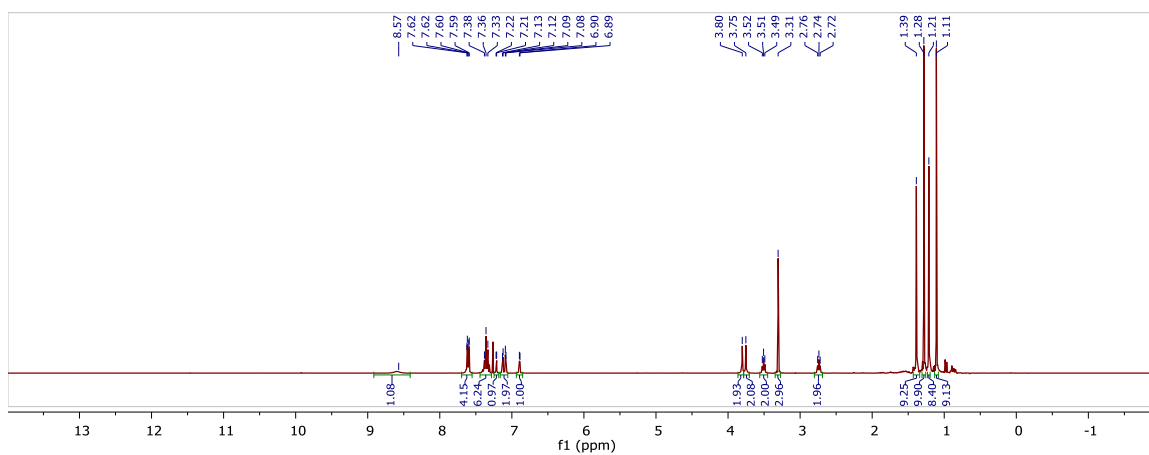


Figure FA.22. <sup>1</sup>H NMR of A.24 in CDCl<sub>3</sub>.

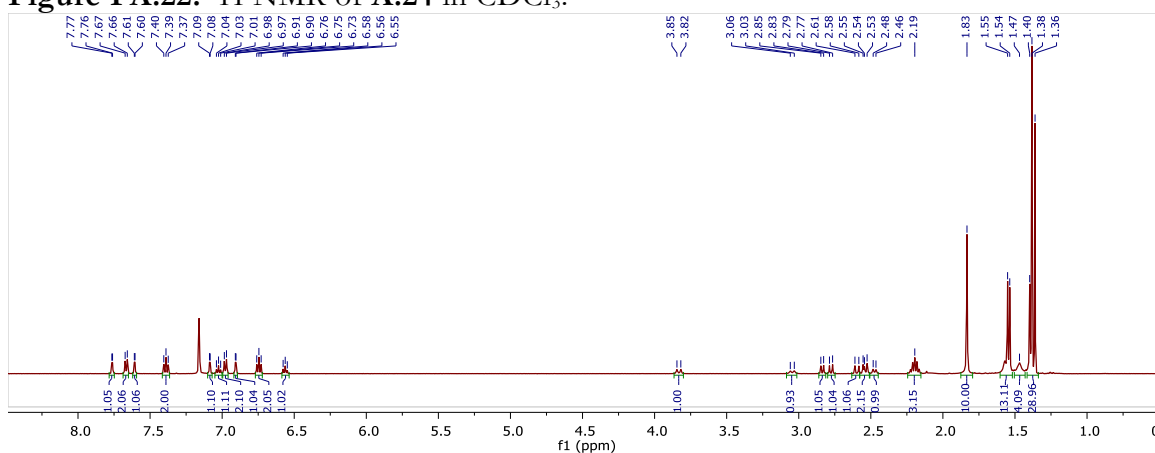


Figure FA.23. <sup>1</sup>H NMR spectrum of A.26 in C<sub>6</sub>D<sub>6</sub>.

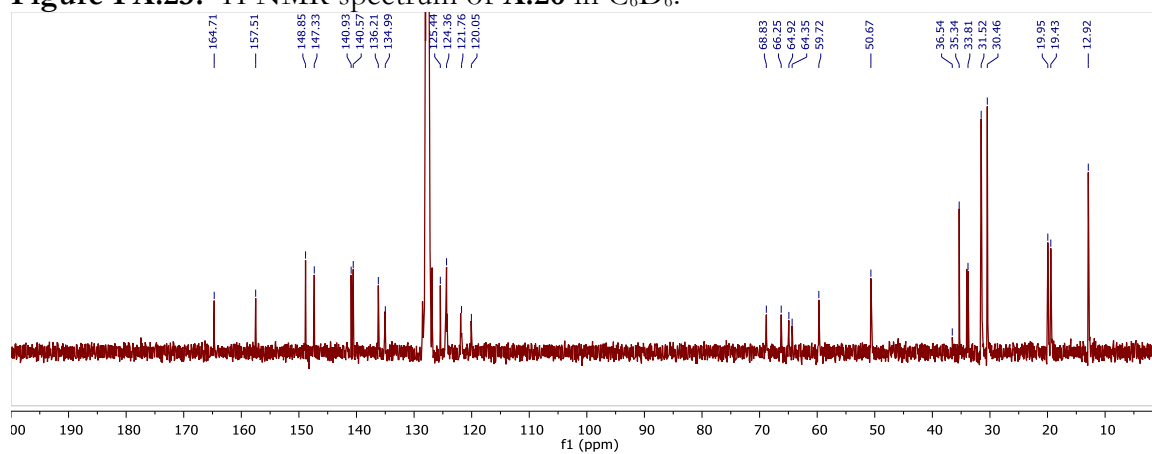


Figure FA.24. <sup>13</sup>C spectrum of A.26 in C<sub>6</sub>D<sub>6</sub>.

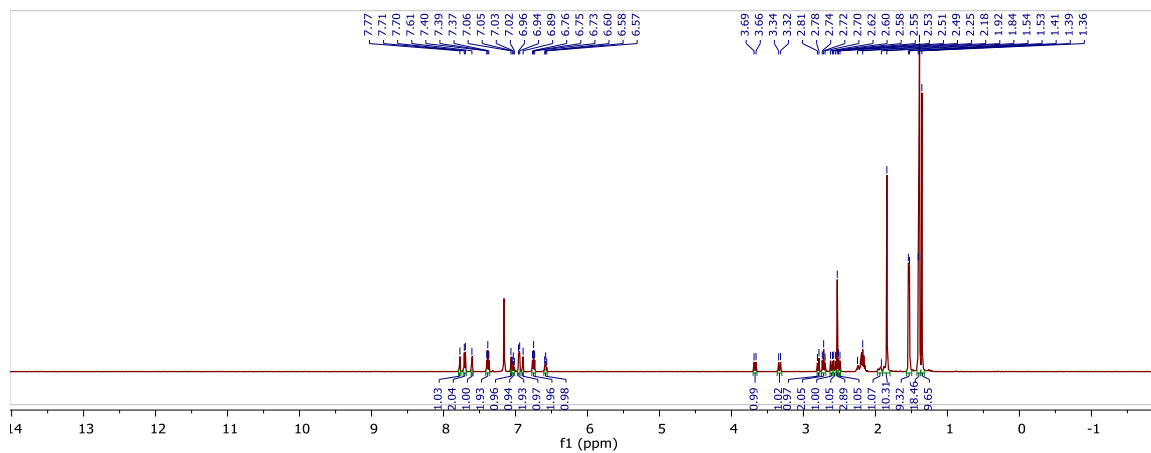


Figure FA.25. <sup>1</sup>H NMR of A.25 in C<sub>6</sub>D<sub>6</sub>.

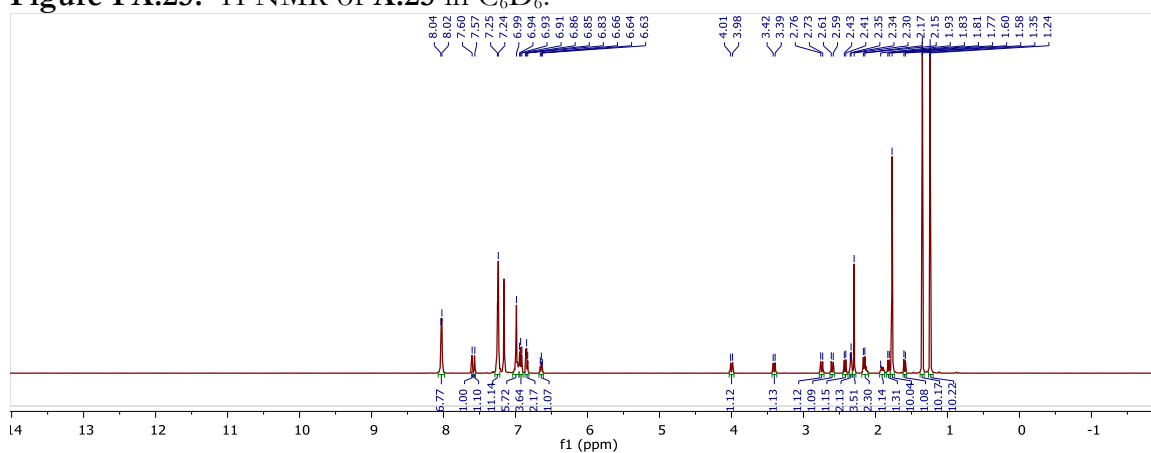


Figure FA.26. <sup>1</sup>H NMR of A.27 in C<sub>6</sub>D<sub>6</sub>.

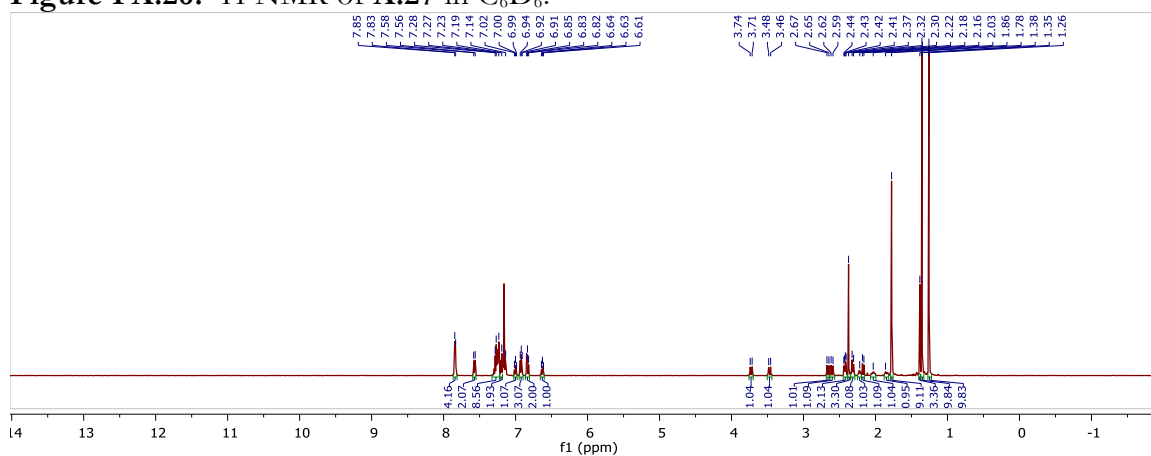


Figure FA.27. <sup>1</sup>H NMR of A.28 in C<sub>6</sub>D<sub>6</sub>.

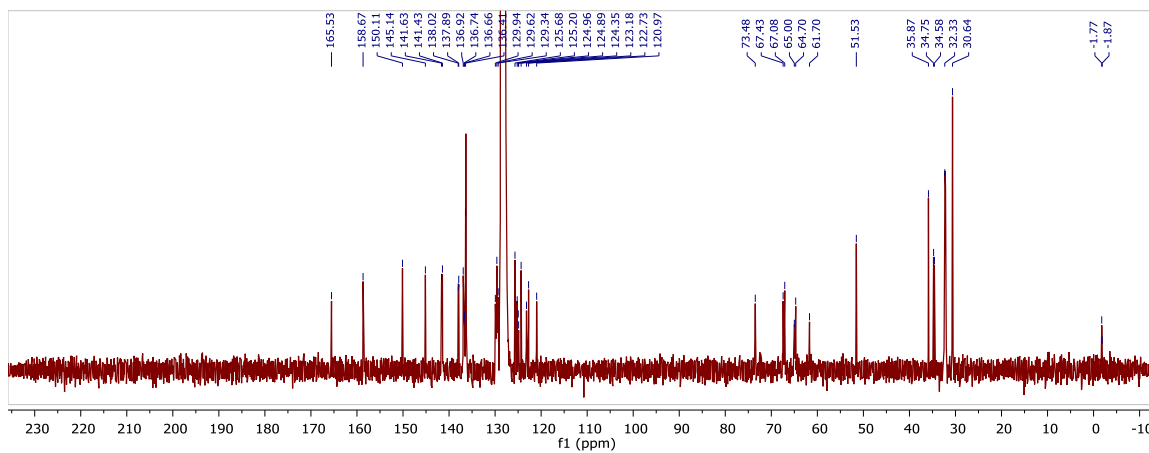


Figure FA.28.  $^{13}\text{C}$  NMR of A.28 in  $\text{C}_6\text{D}_6$ .

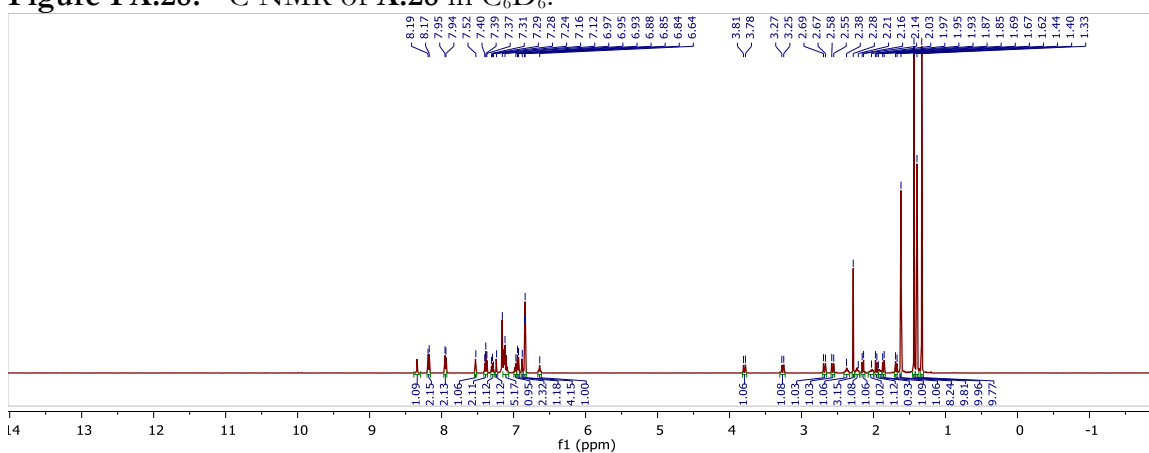


Figure FA.29.  $^1\text{H}$  NMR of A.29 in  $\text{C}_6\text{D}_6$ .

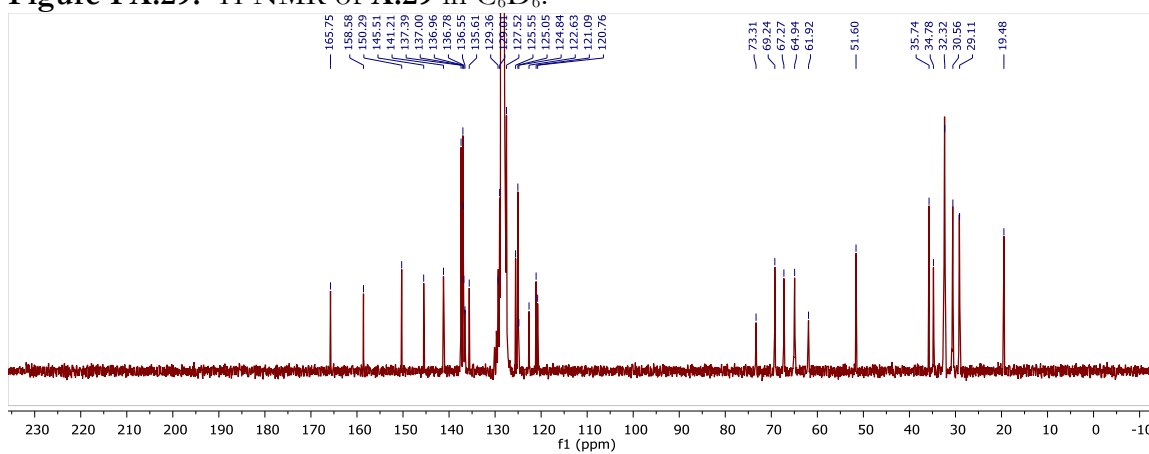
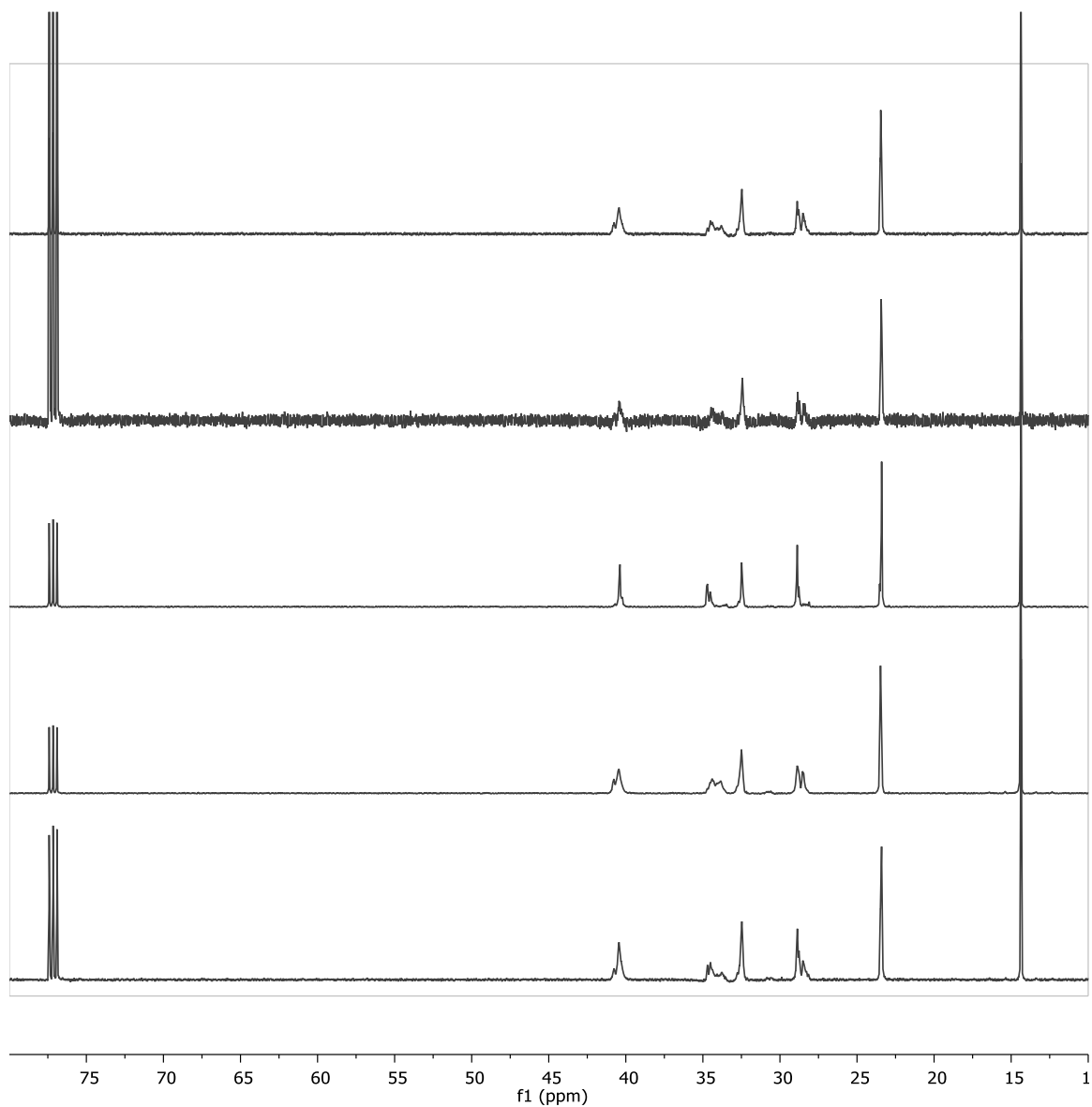
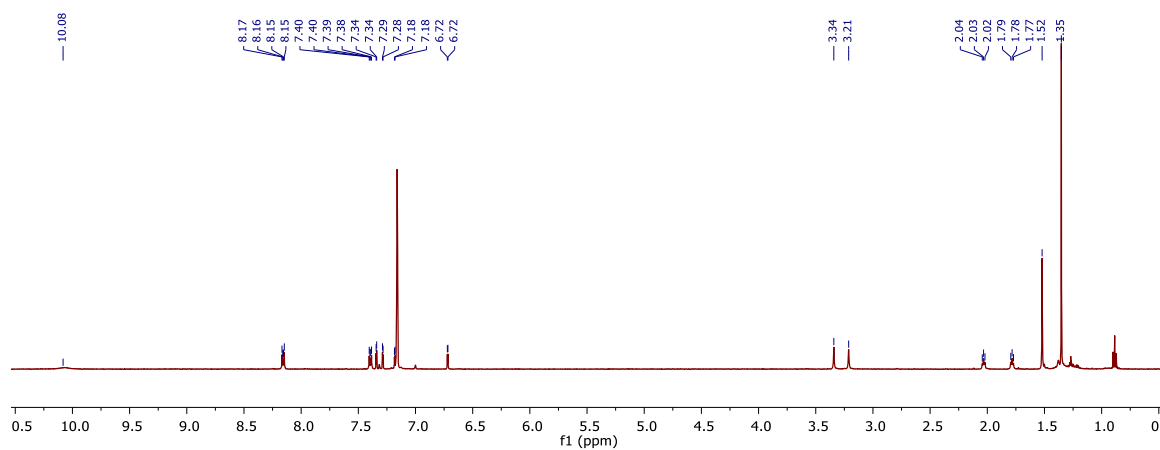
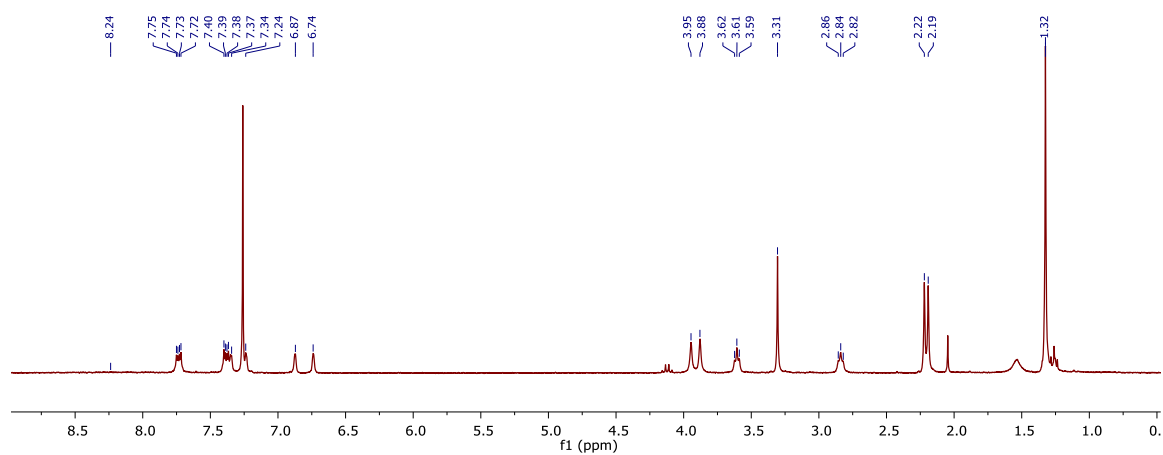
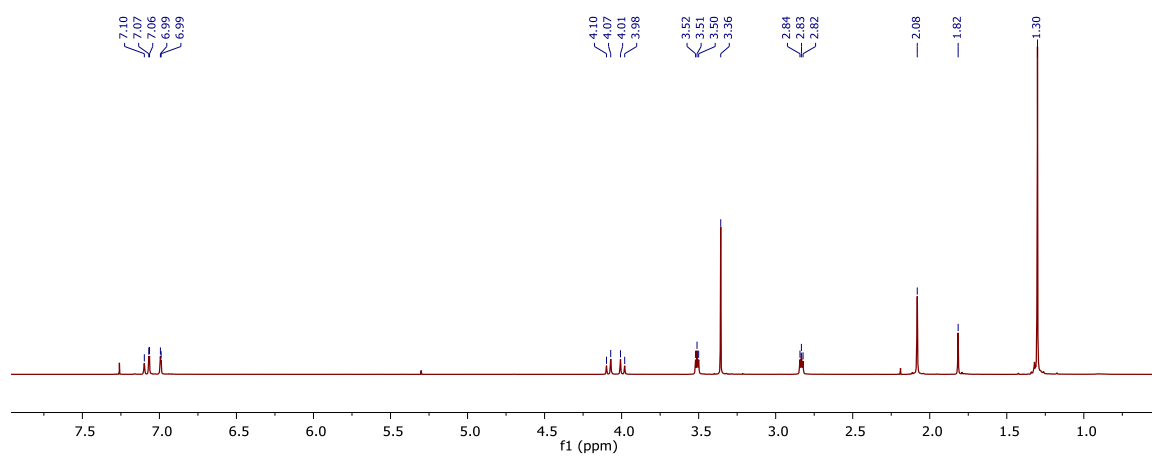


Figure FA.30.  $^{13}\text{C}$  NMR of A.29 in  $\text{C}_6\text{D}_6$ .



**Figure FA.31.**  $^{13}\text{C}$  NMR spectra of poly-1-hexene in  $\text{CDCl}_3$  from (top to bottom) **A/26**, **A.25**, **A.27**, **A.28**, and **A.29** upon activation with  $[\text{CPh}_3][\text{B}(\text{C}_6\text{F}_5)_4]$ .

## APPENDIX B

Figure FB.1. <sup>1</sup>H NMR of B.4 in C<sub>6</sub>D<sub>6</sub>.Figure FB.2. <sup>1</sup>H NMR of B.5 in CDCl<sub>3</sub>.Figure FB.3. <sup>1</sup>H NMR of B.9 in CDCl<sub>3</sub>.

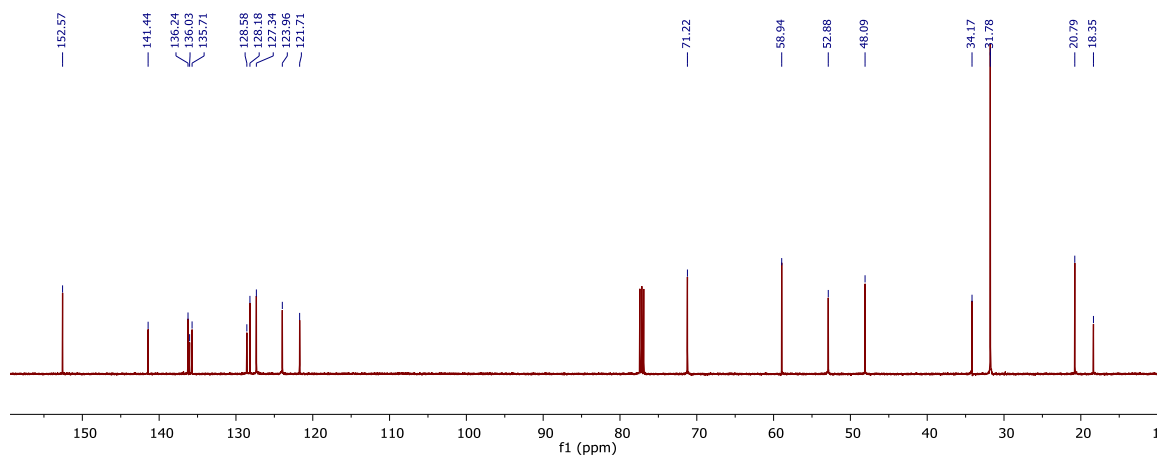


Figure FB.4. <sup>13</sup>C NMR of **B.9** in CDCl<sub>3</sub>.

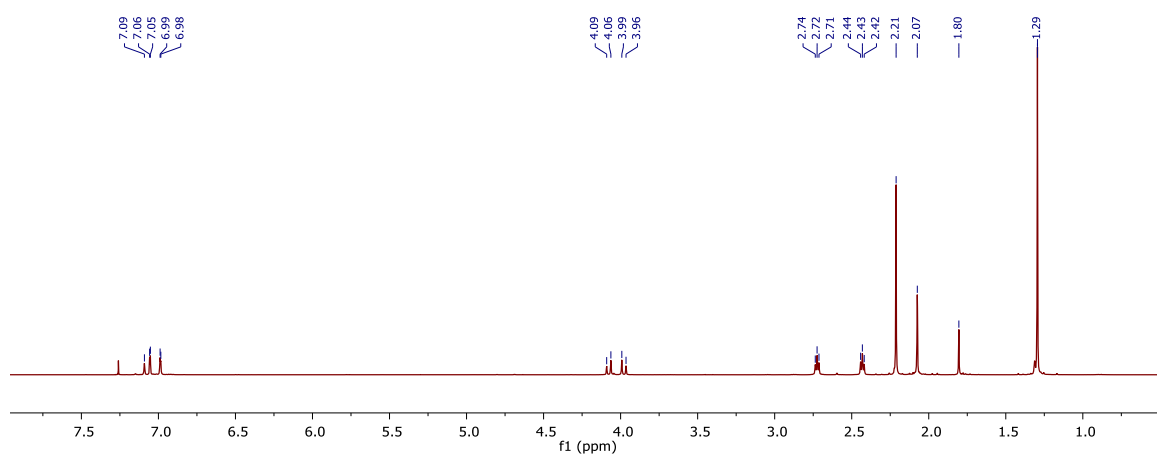


Figure FB.5. <sup>1</sup>H NMR of **B.10** in CDCl<sub>3</sub>.

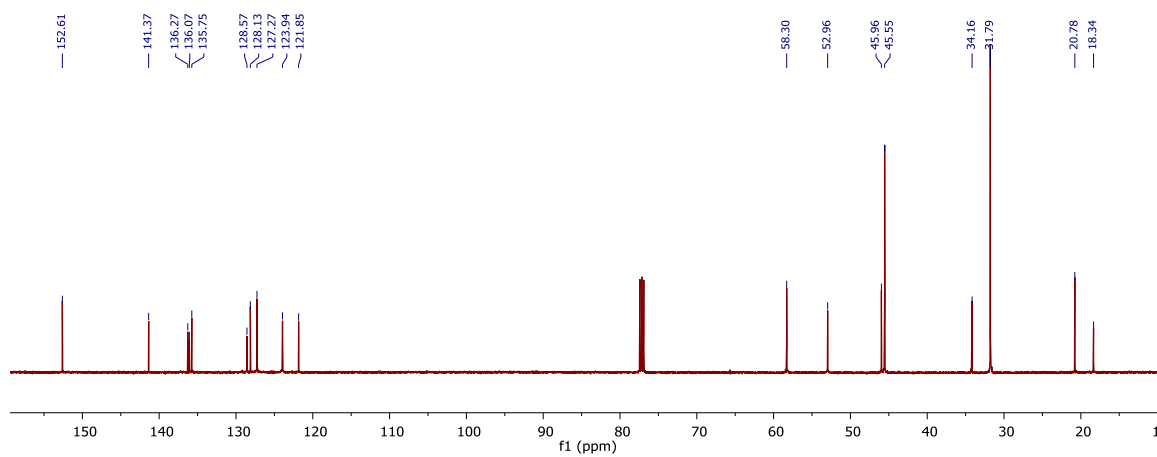
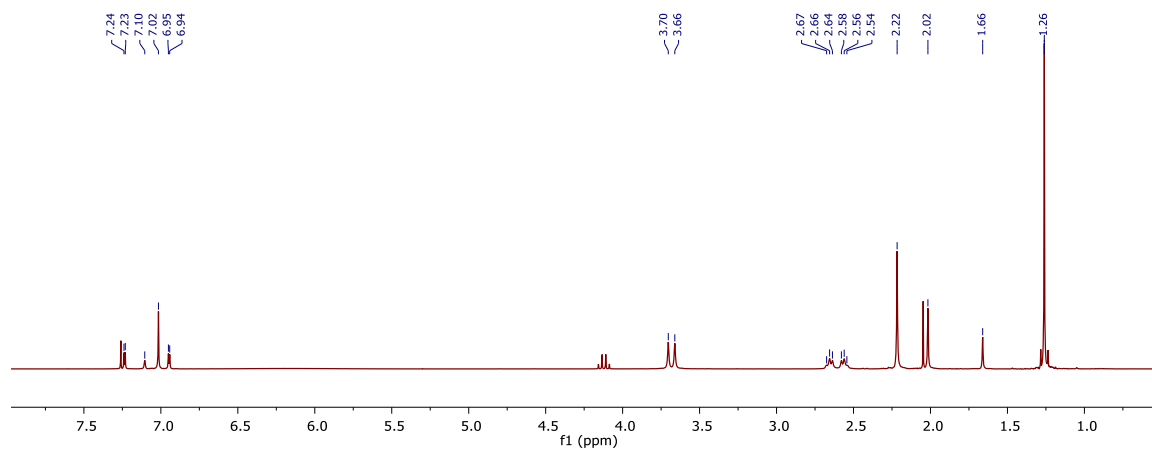


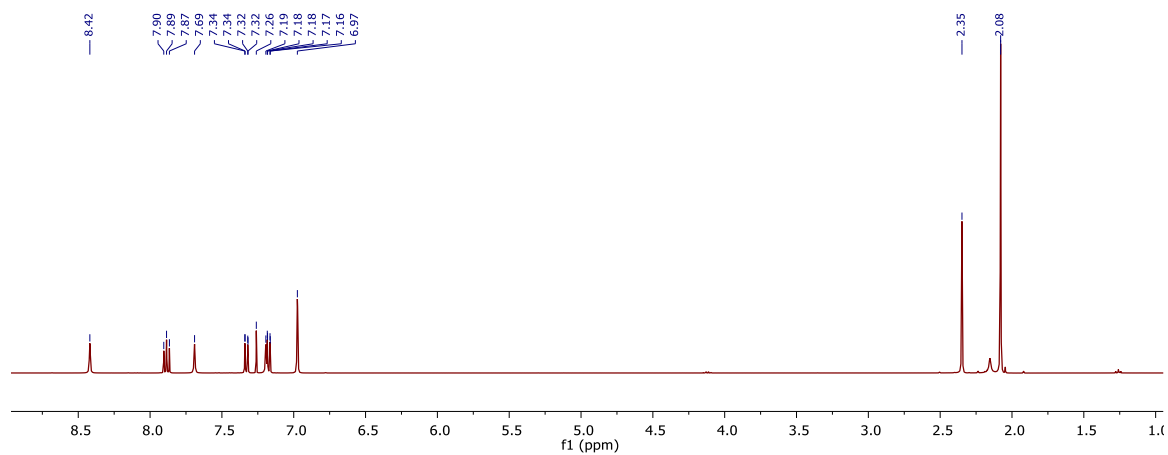
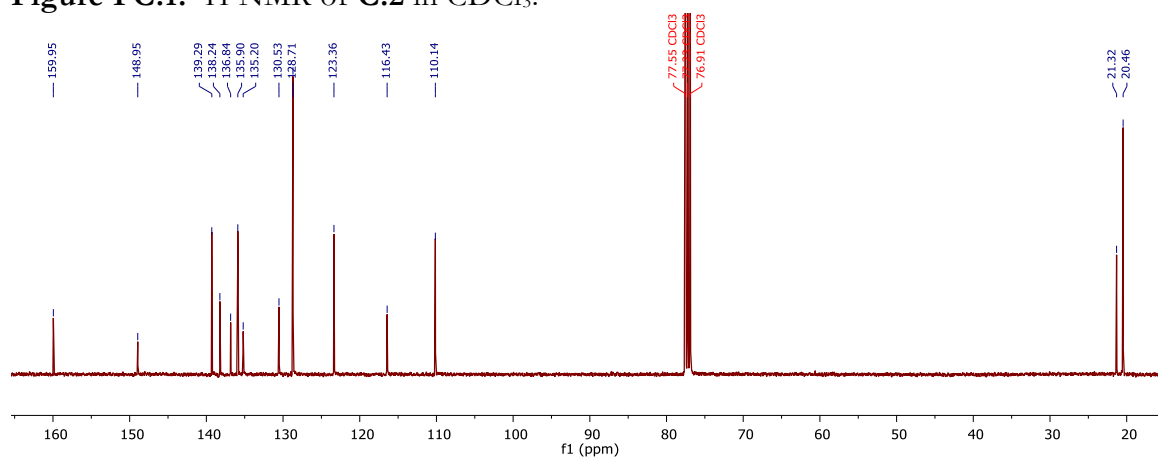
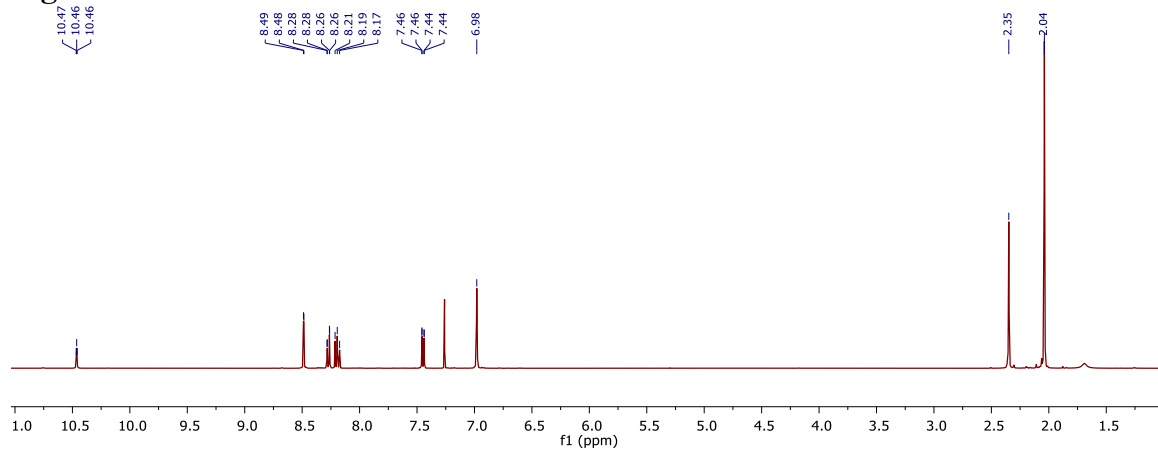
Figure FB.6. <sup>13</sup>C NMR of **B.10** in CDCl<sub>3</sub>.



**Figure FB.7.** <sup>1</sup>H NMR of **B.12** in CDCl<sub>3</sub>.



## APPENDIX C

Figure FC.1. <sup>1</sup>H NMR of **C.2** in CDCl<sub>3</sub>.Figure FC.2. <sup>13</sup>C NMR of **C.2** in CDCl<sub>3</sub>.Figure FC.3. <sup>1</sup>H NMR of **C.3** in CDCl<sub>3</sub>.

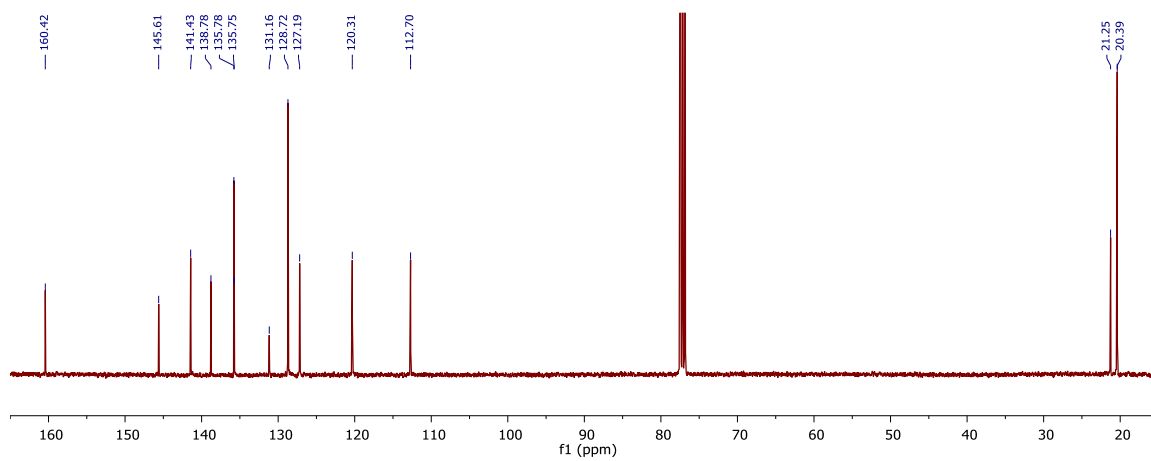


Figure FC.4.  $^{13}\text{C}$  NMR of **C.3** in  $\text{CDCl}_3$ .

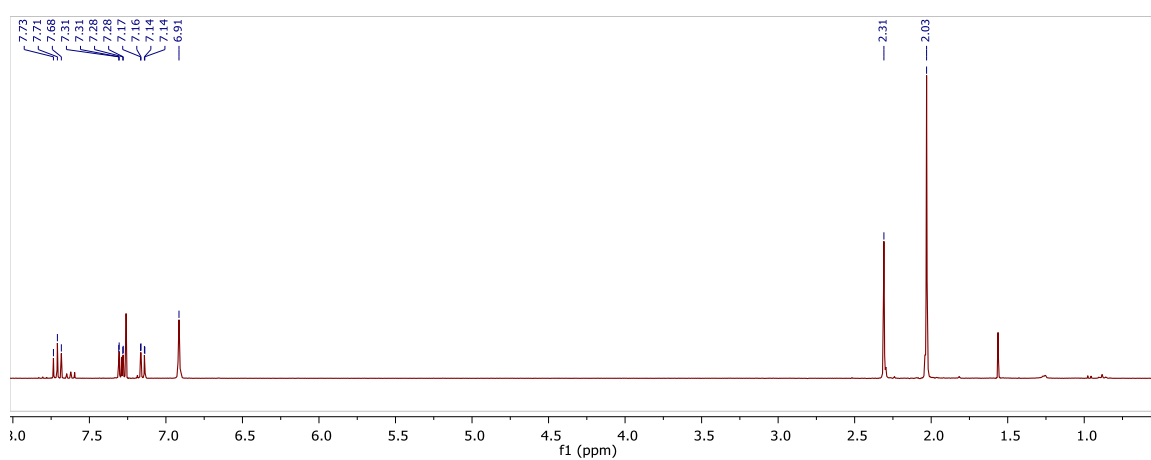


Figure FC.5.  $^1\text{H}$  NMR of **C.4** in  $\text{CDCl}_3$ .

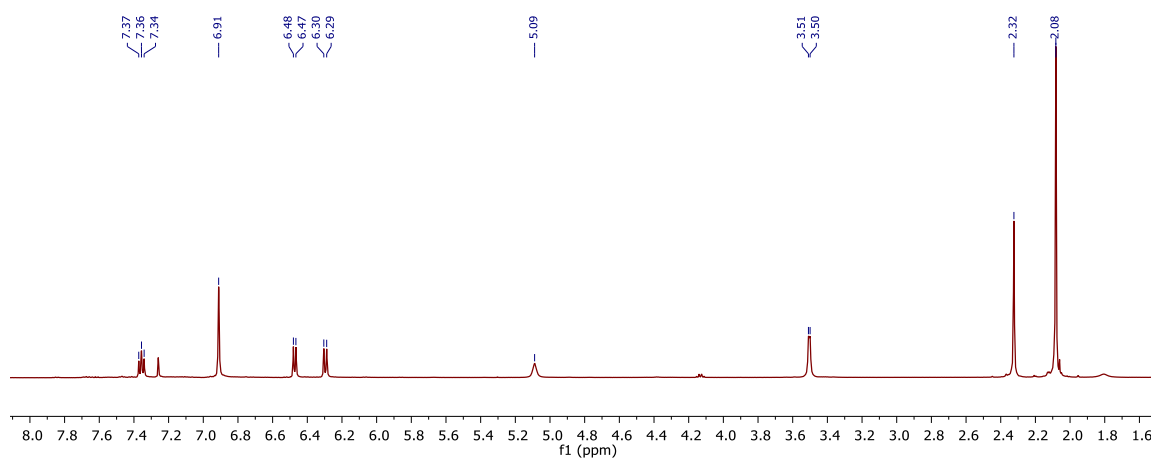


Figure FC.6.  $^1\text{H}$  NMR of **C.5** in  $\text{CDCl}_3$ .

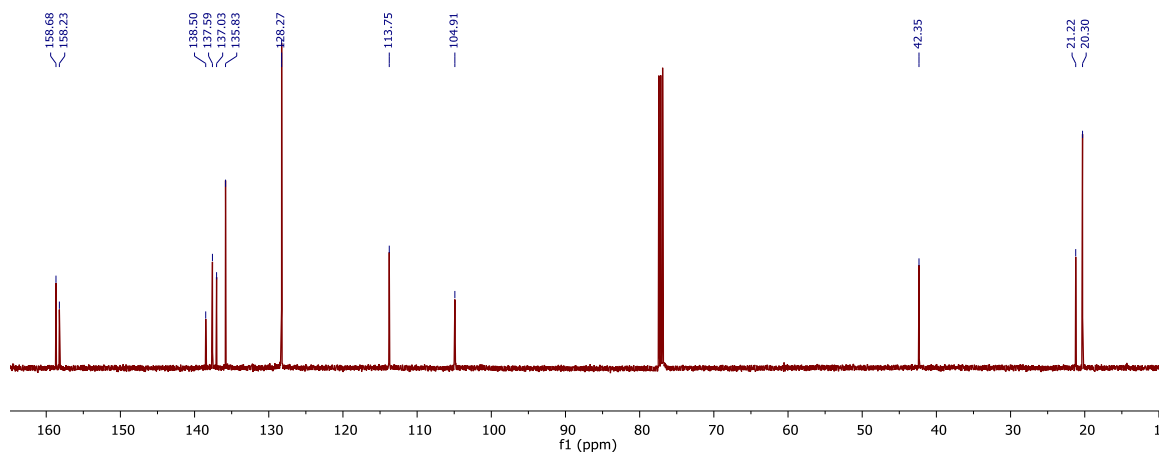


Figure FC.7. <sup>13</sup>C NMR of **C.5** in CDCl<sub>3</sub>.

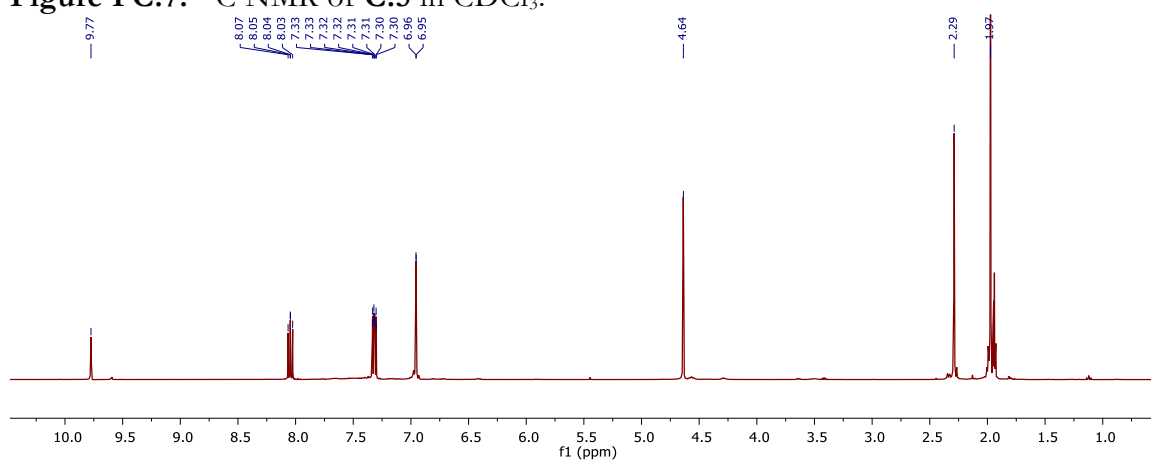


Figure FC.8. <sup>1</sup>H NMR of **C.6** in CD<sub>3</sub>CN.

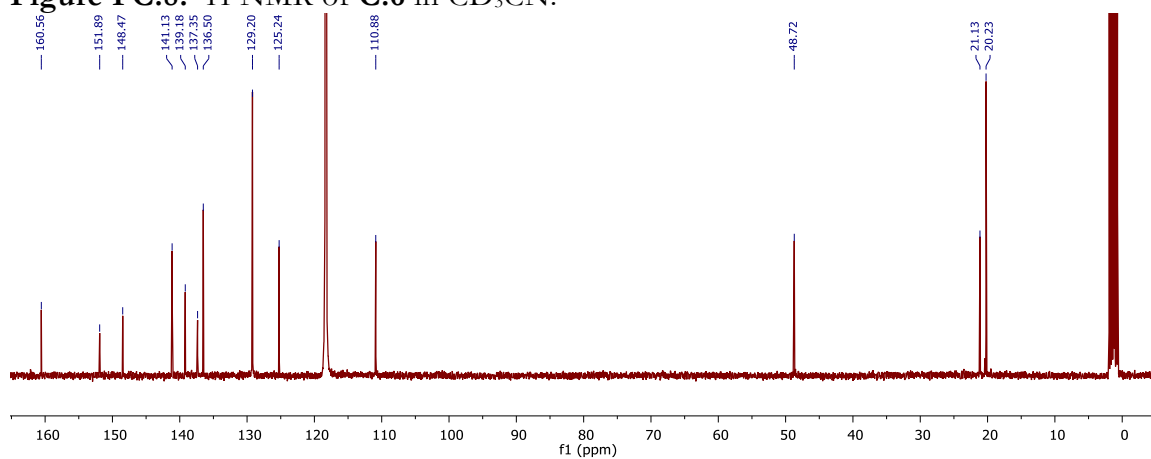


Figure FC.9. <sup>13</sup>C NMR of **C.6** in CD<sub>3</sub>CN.

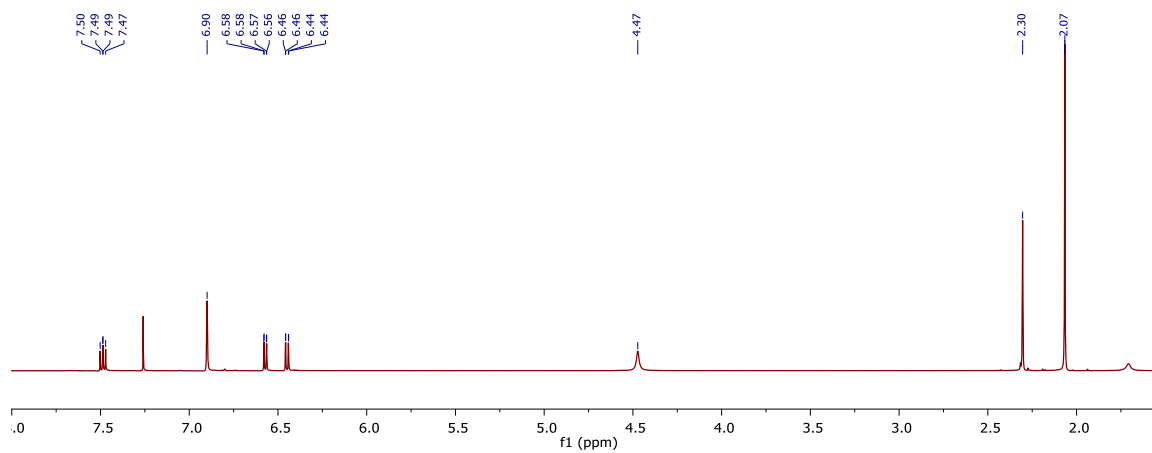


Figure FC.10. <sup>1</sup>H NMR of C.7 in CDCl<sub>3</sub>.

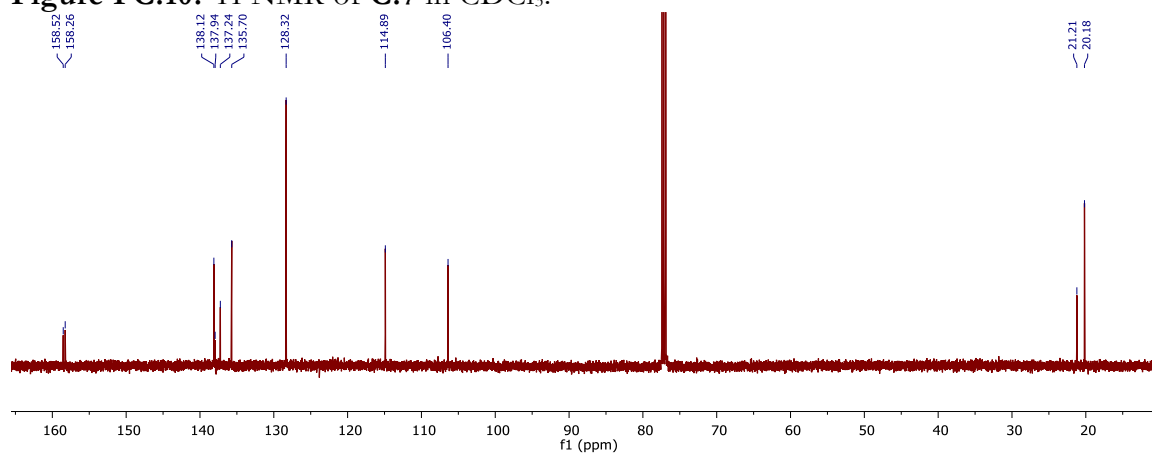


Figure FC.11. <sup>13</sup>C NMR of C.7 in CDCl<sub>3</sub>.

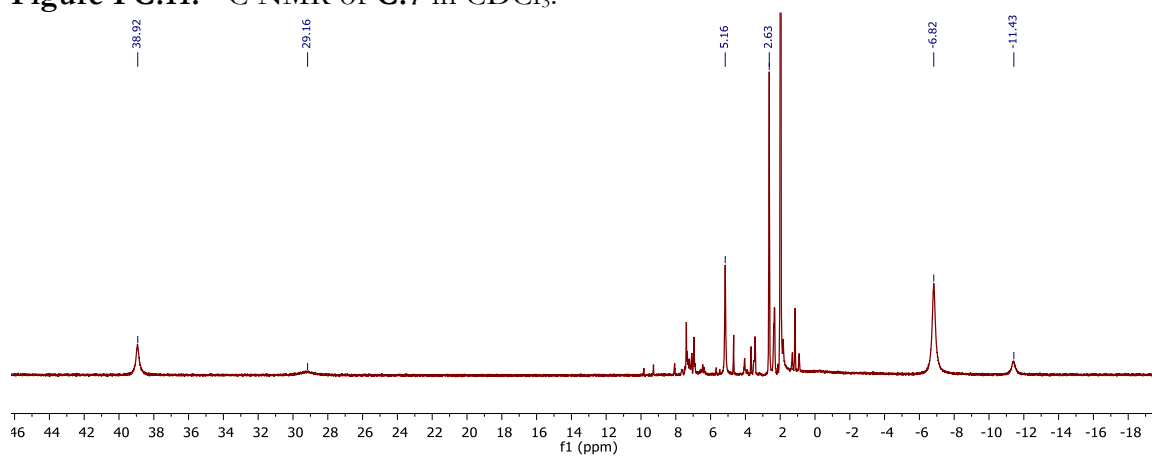
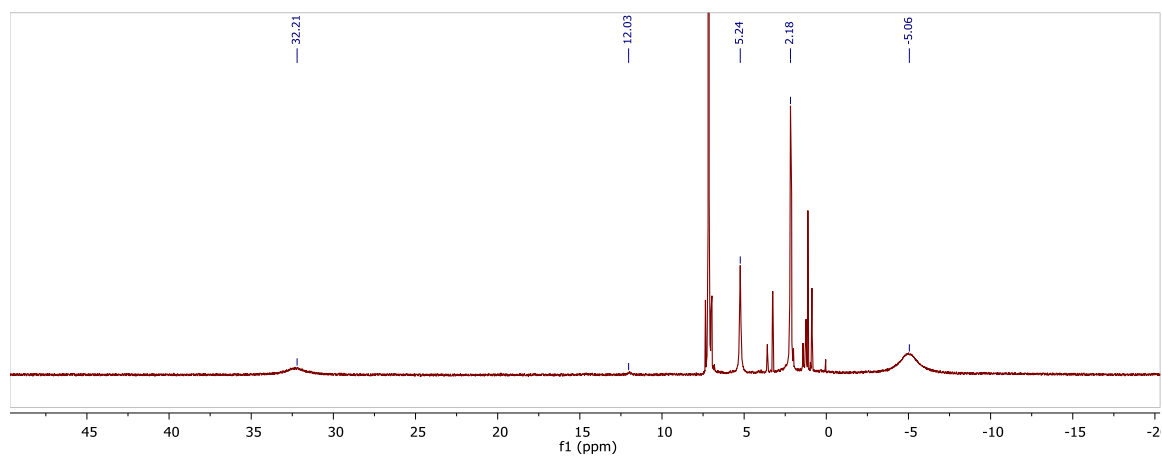
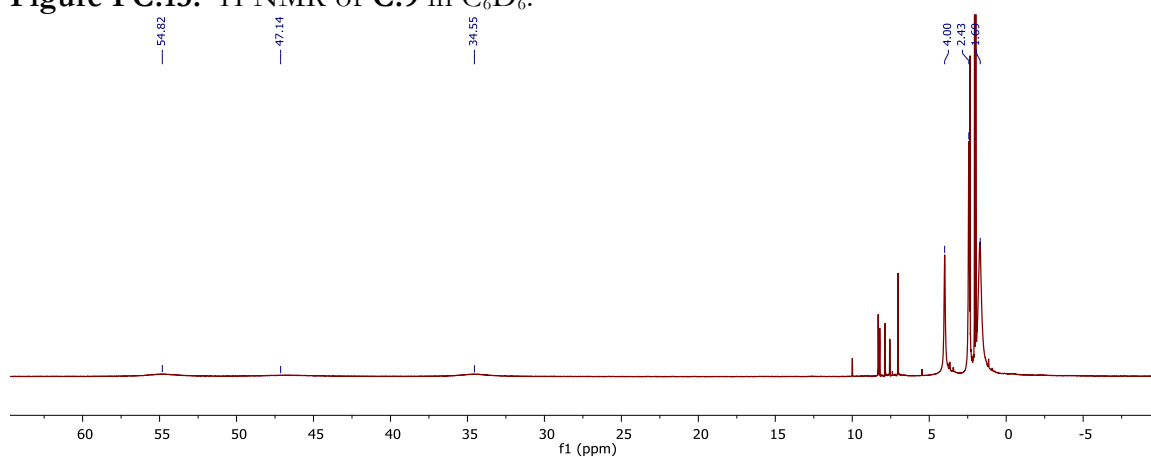


Figure FC.12. <sup>1</sup>H NMR of C.8 in CD<sub>3</sub>CN.



**Figure FC.13.**  $^1\text{H}$  NMR of **C.9** in  $\text{C}_6\text{D}_6$ .



**Figure FC.14.**  $^1\text{H}$  NMR of **C.10** in  $\text{CD}_3\text{CN}$ . The sharp resonances between 5 and 11 ppm corresponding to residual **C.3**.

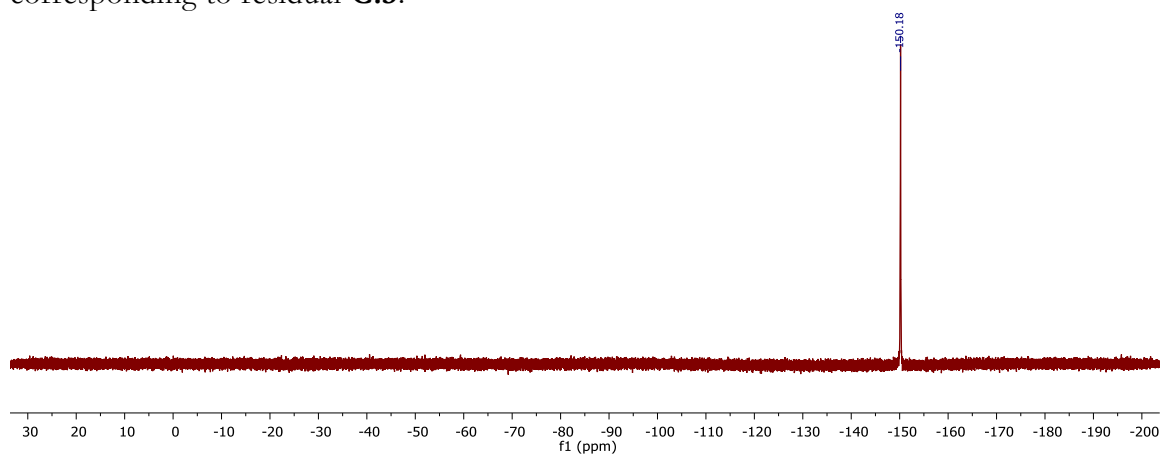


**Figure FC.15.**  $^{19}\text{F}$  NMR of **C.10** in  $\text{CD}_3\text{CN}$ .

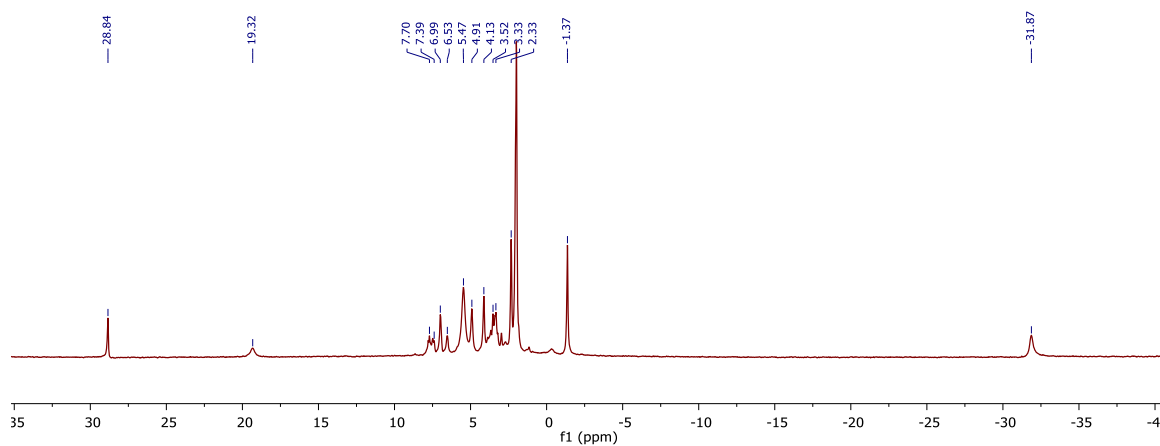


Figure FC.16. <sup>1</sup>H NMR of C.11 in CD<sub>3</sub>CN.

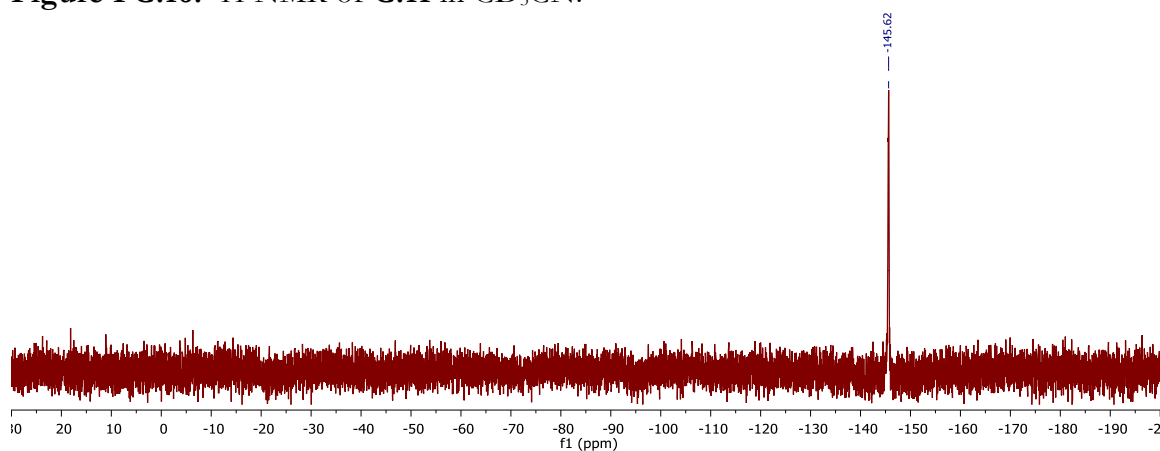


Figure FC.17. <sup>19</sup>F NMR of C.11 in CD<sub>3</sub>CN.

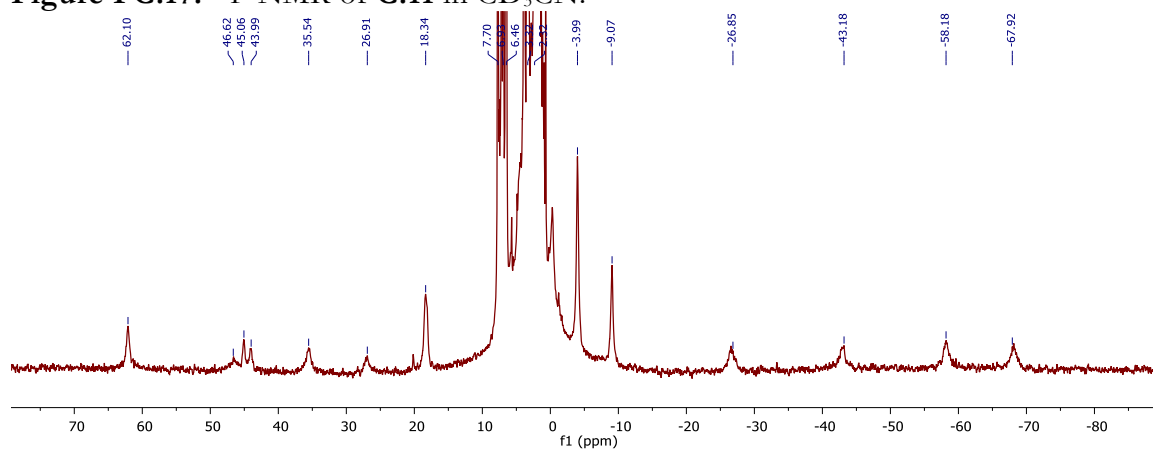
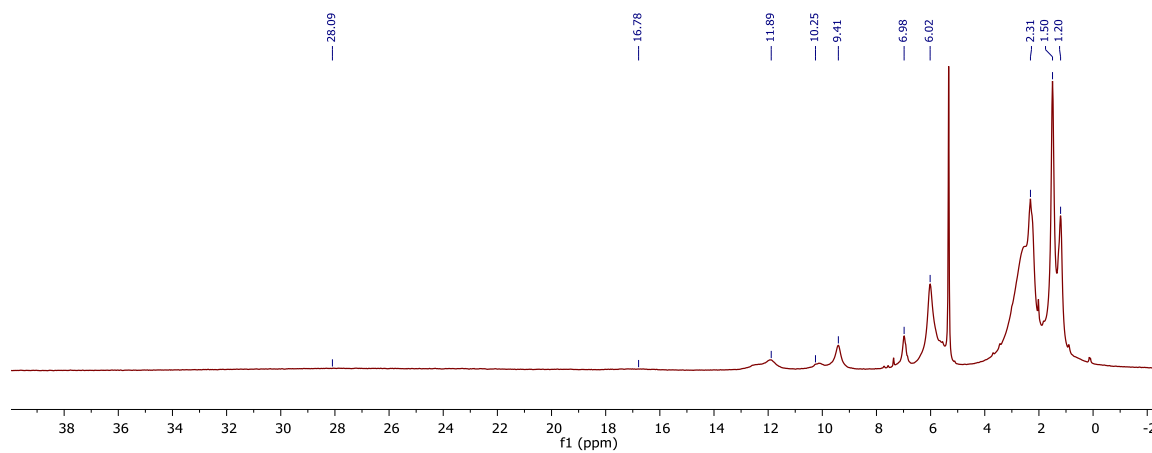
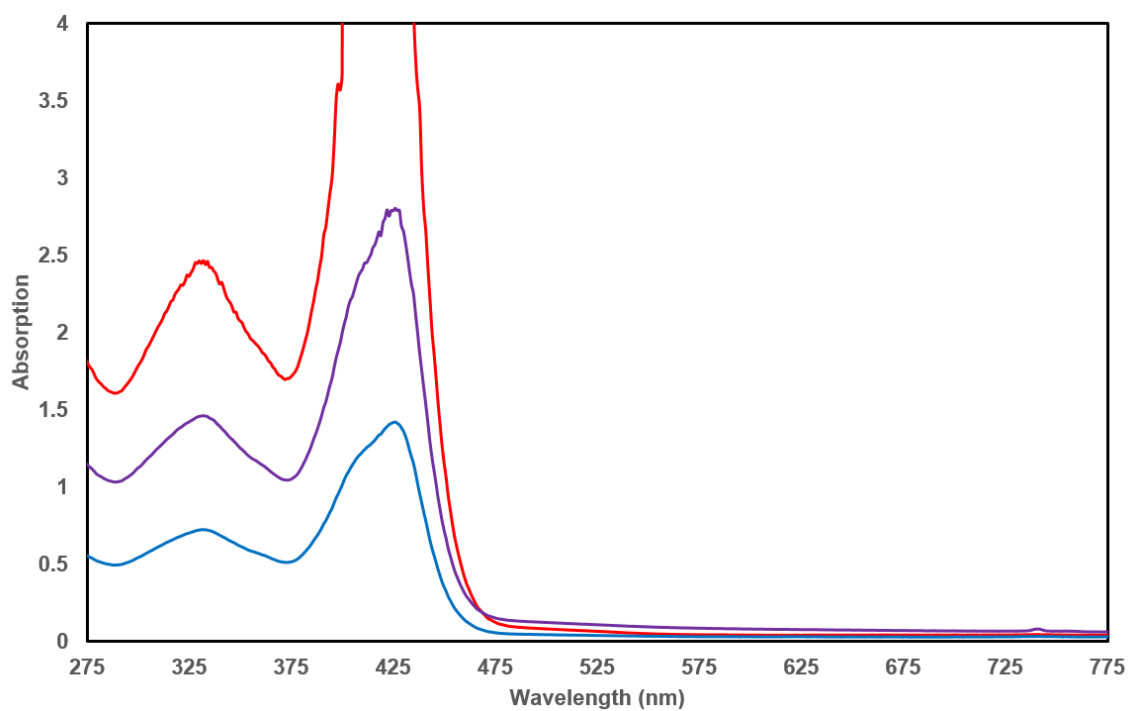


Figure FC.18. <sup>1</sup>H NMR of C.12 in CD<sub>3</sub>CN.

## APPENDIX D



**Figure FD.1.** <sup>1</sup>H NMR of **D.2** in CD<sub>2</sub>Cl<sub>2</sub>.



**Figure FD.2.** UV-Vis spectra of **D.2** in THF at 100 μM (red), 50 μM (purple), and 25 μM concentrations.

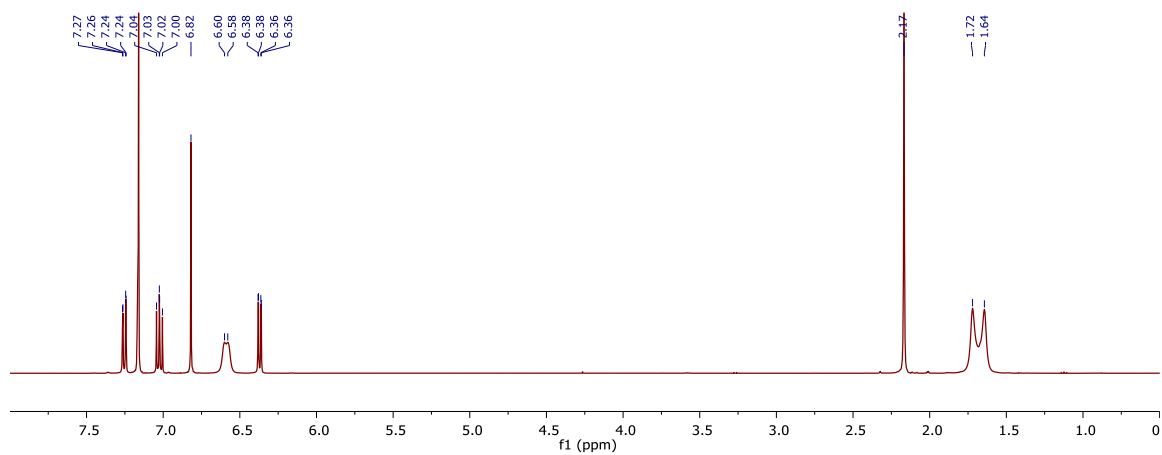


**Figure FD.3.** <sup>1</sup>H NMR of **D.3** in C<sub>6</sub>D<sub>6</sub>.

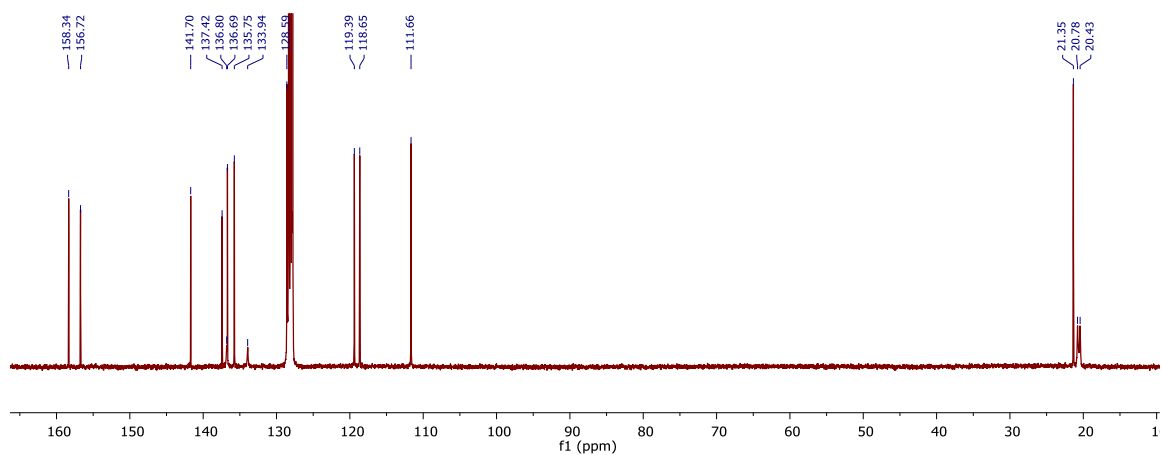


**Figure FD.4.** <sup>13</sup>C NMR of **D.3** in C<sub>6</sub>D<sub>6</sub>.



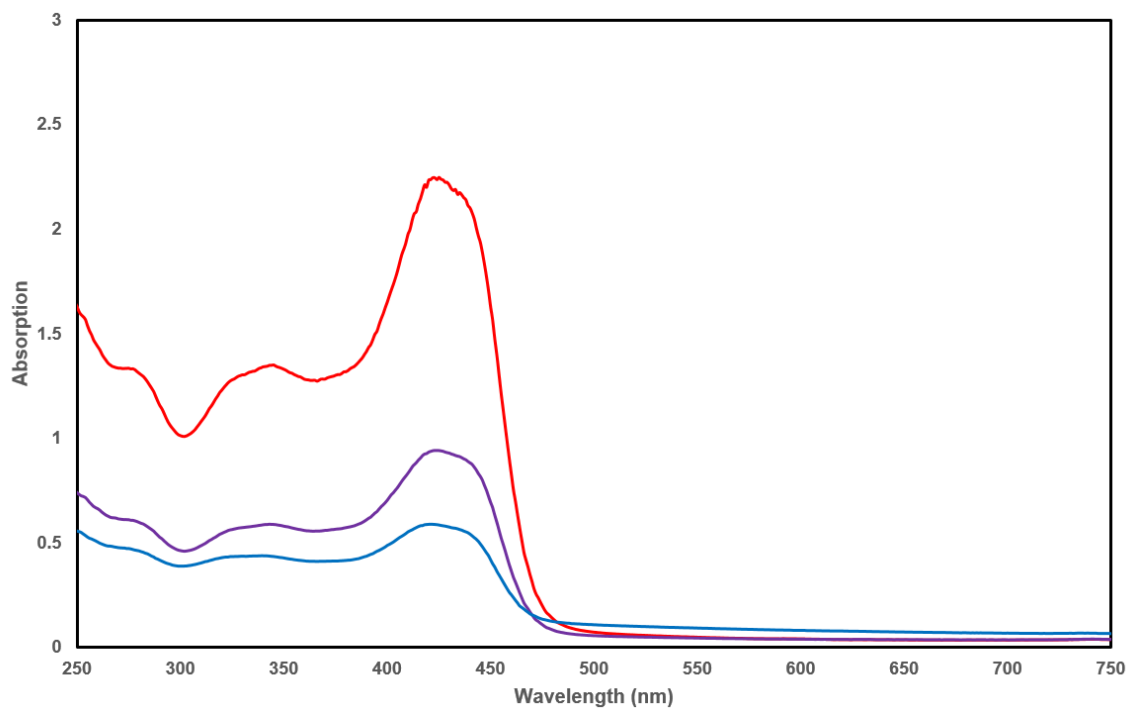


**Figure FD.5.** UV-Vis spectra of **D.3** in THF at 25  $\mu\text{M}$  (red), 10  $\mu\text{M}$  (purple), and 5  $\mu\text{M}$  (blue) concentrations.

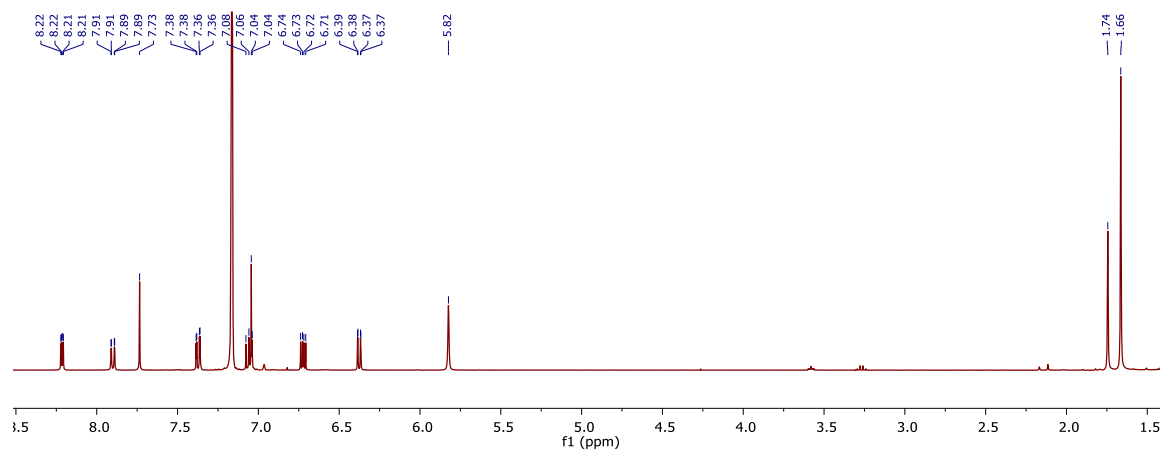


**Figure FD.6.**  $^1\text{H}$  NMR spectrum of **D.4** in  $\text{C}_6\text{D}_6$ .

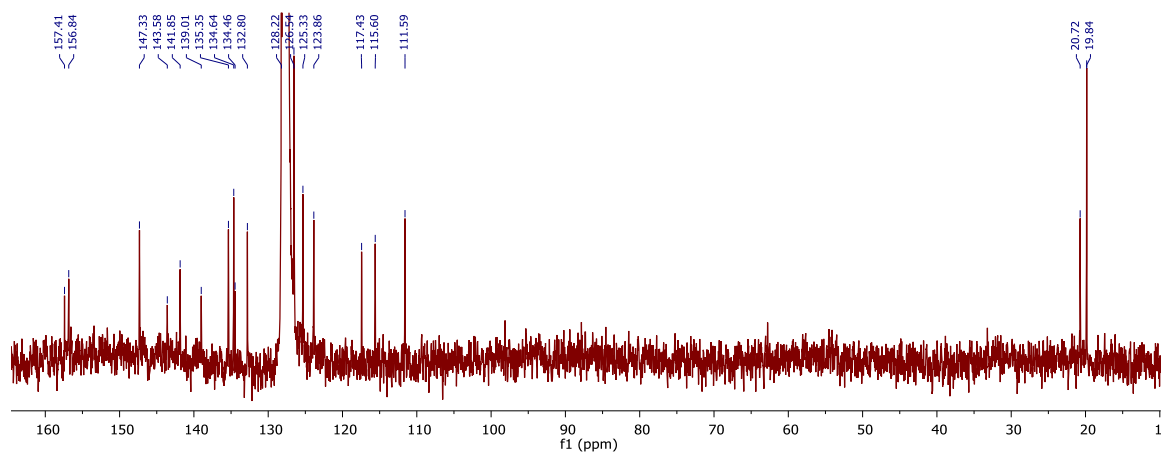


Figure FD.7.  $^{13}\text{C}$  NMR spectrum of **D.4** in  $\text{C}_6\text{D}_6$ .

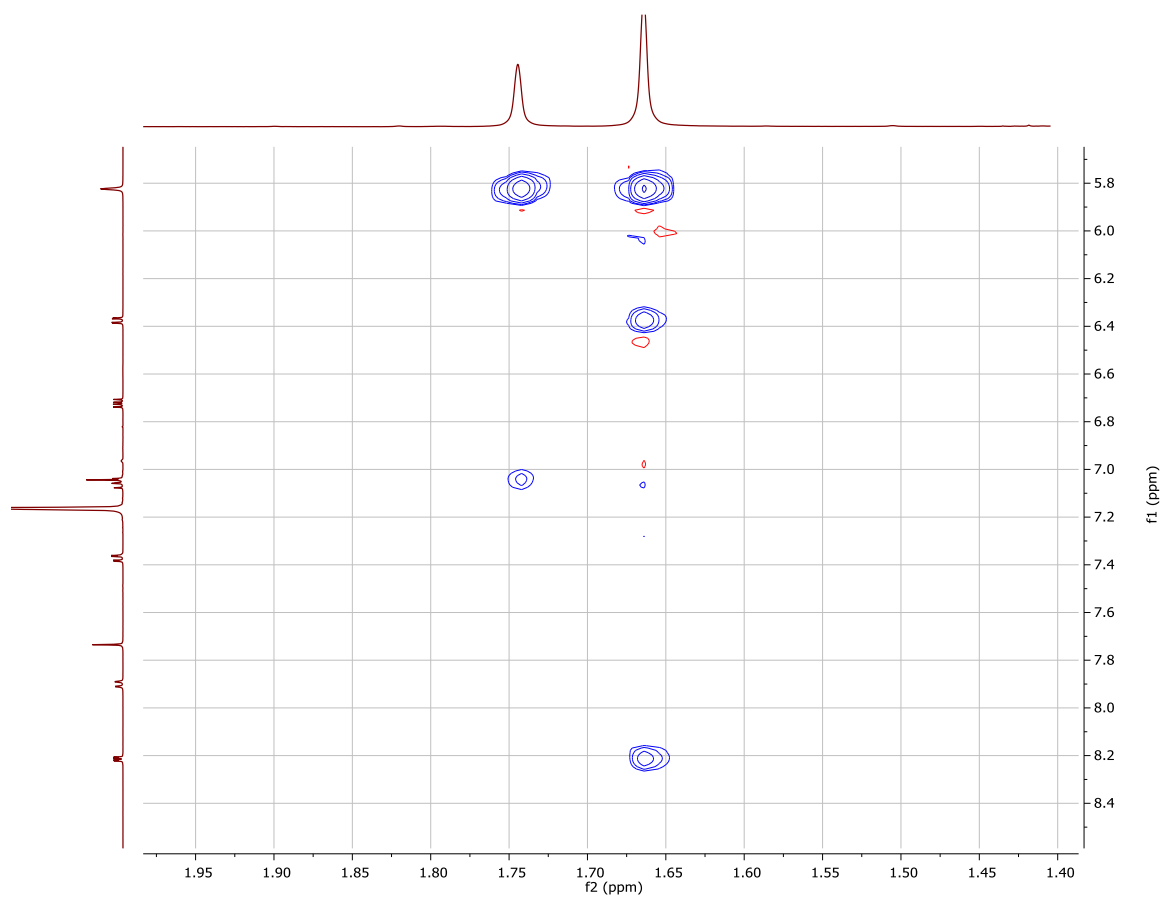
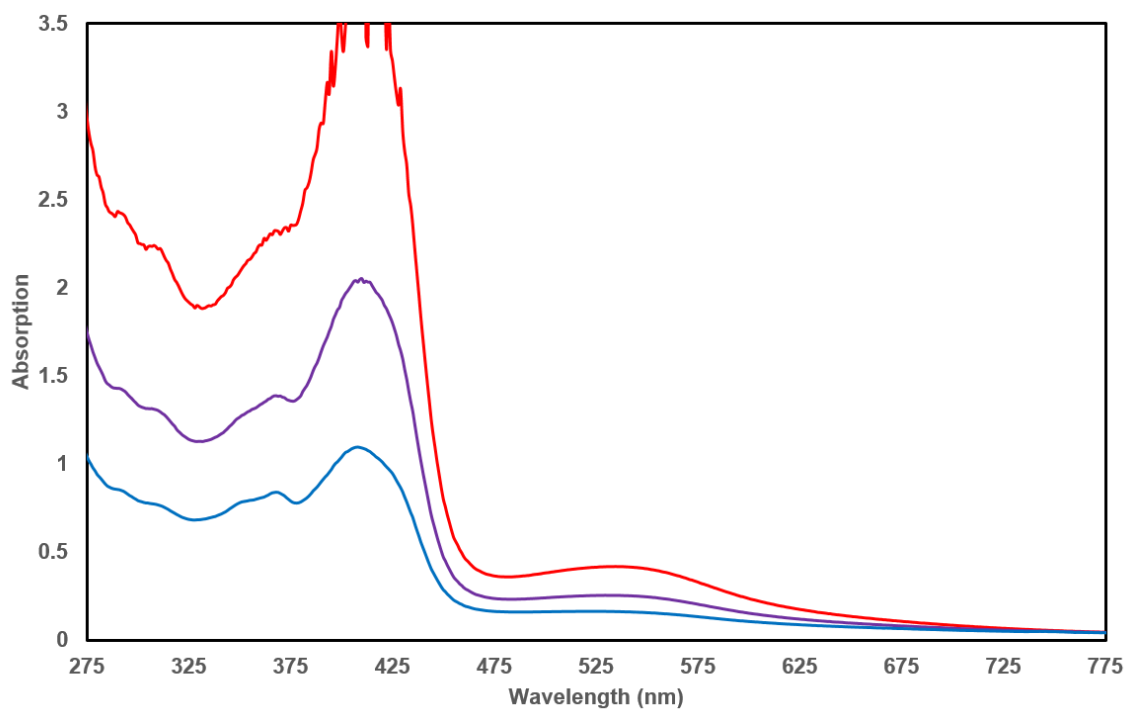
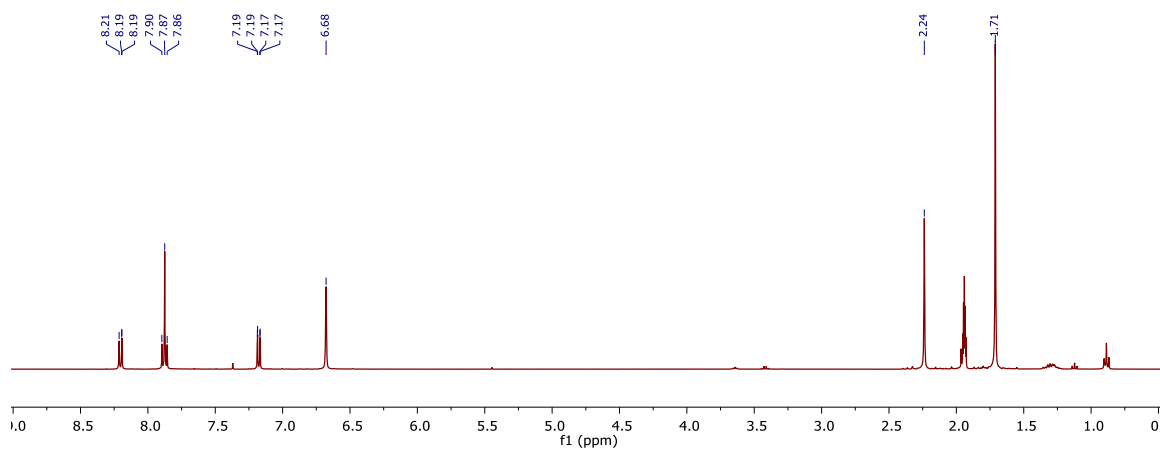


Figure FD.8. Partial  $^1\text{H}$ - $^1\text{H}$  NOESY of **D.4** in  $\text{C}_6\text{D}_6$ .



**Figure FD.9.** UV-Vis spectra of **D.4** in THF at 100  $\mu\text{M}$  (red), 50  $\mu\text{M}$  (purple), and 25  $\mu\text{M}$  (blue) concentrations.



**Figure FD.10.**  $^1\text{H}$  NMR of **D.7**/NaI in  $\text{CD}_3\text{CN}$ .

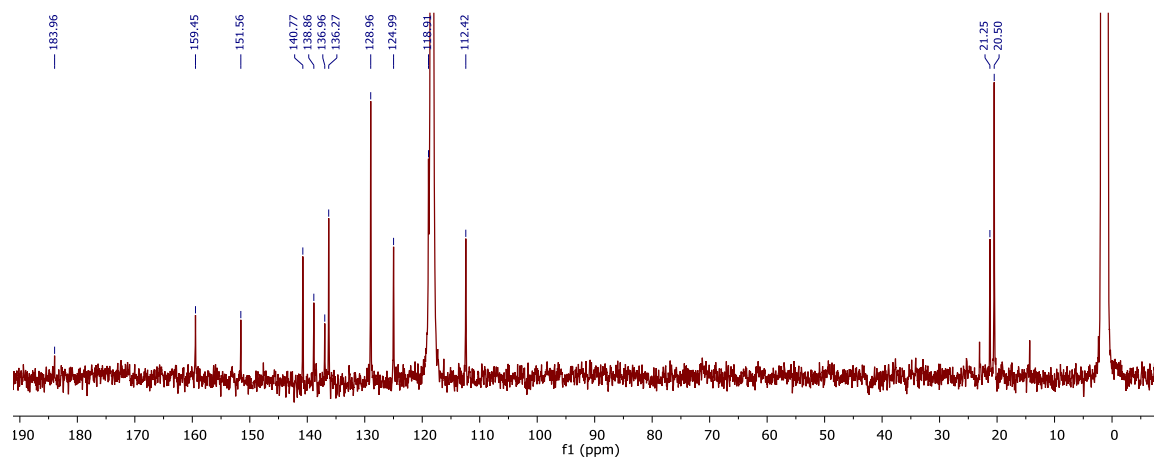


**Figure FD.11.** <sup>13</sup>C NMR of **D.7/NaI** in CD<sub>3</sub>CN.

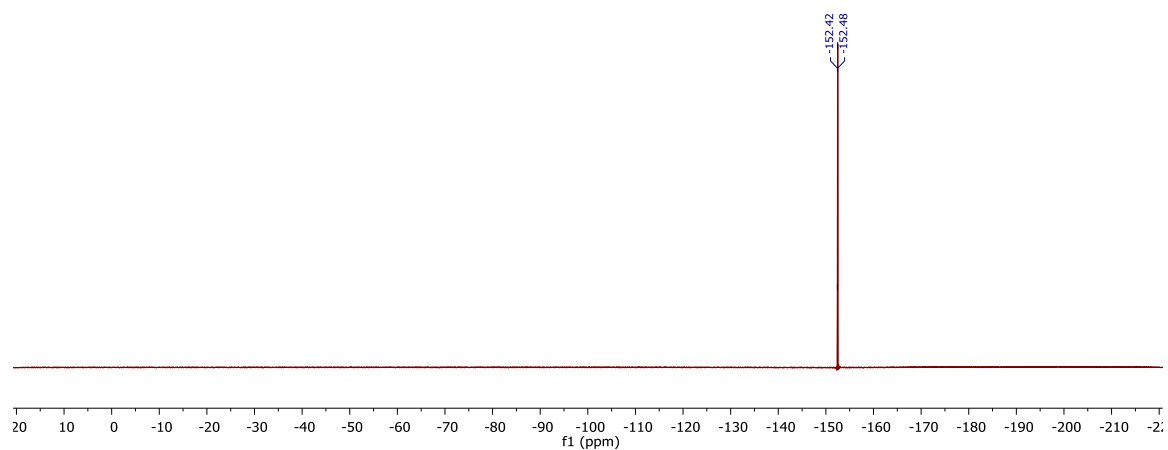


**Figure FD.12.** <sup>19</sup>F NMR of **D.7/NaI** in CD<sub>3</sub>CN.

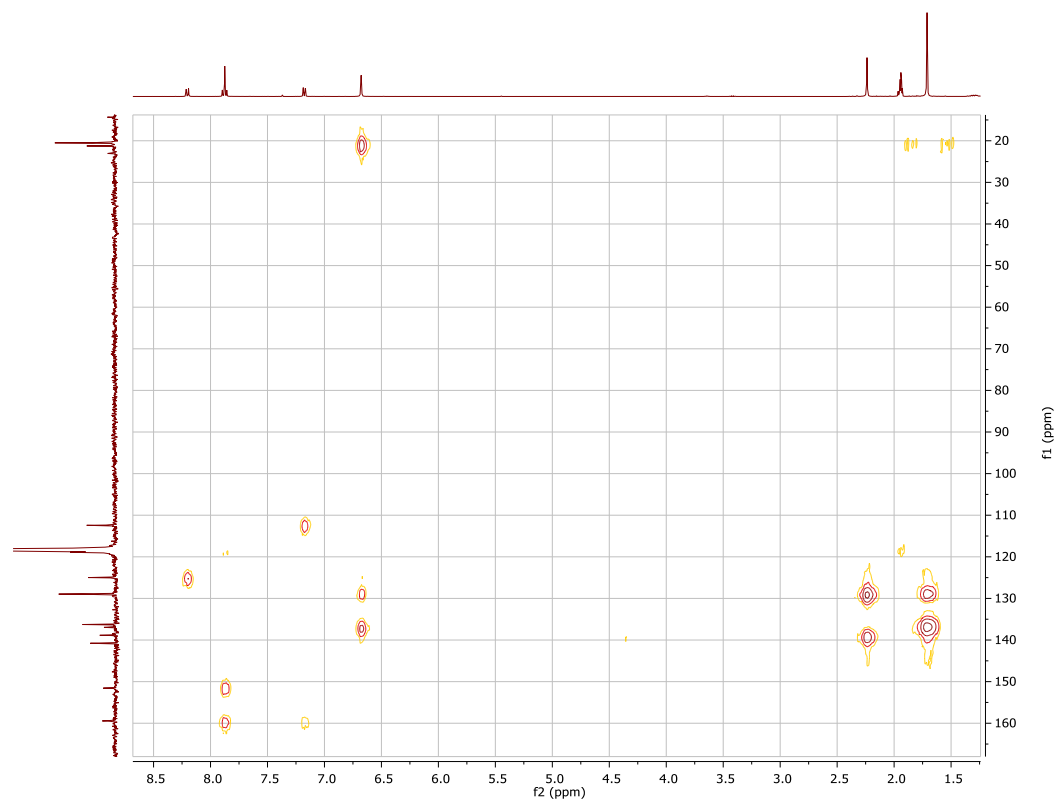


**Figure FD.13.**  $^1\text{H}$ - $^{13}\text{C}$  HMBC of **D.7**/NaI in  $\text{CD}_3\text{CN}$ .

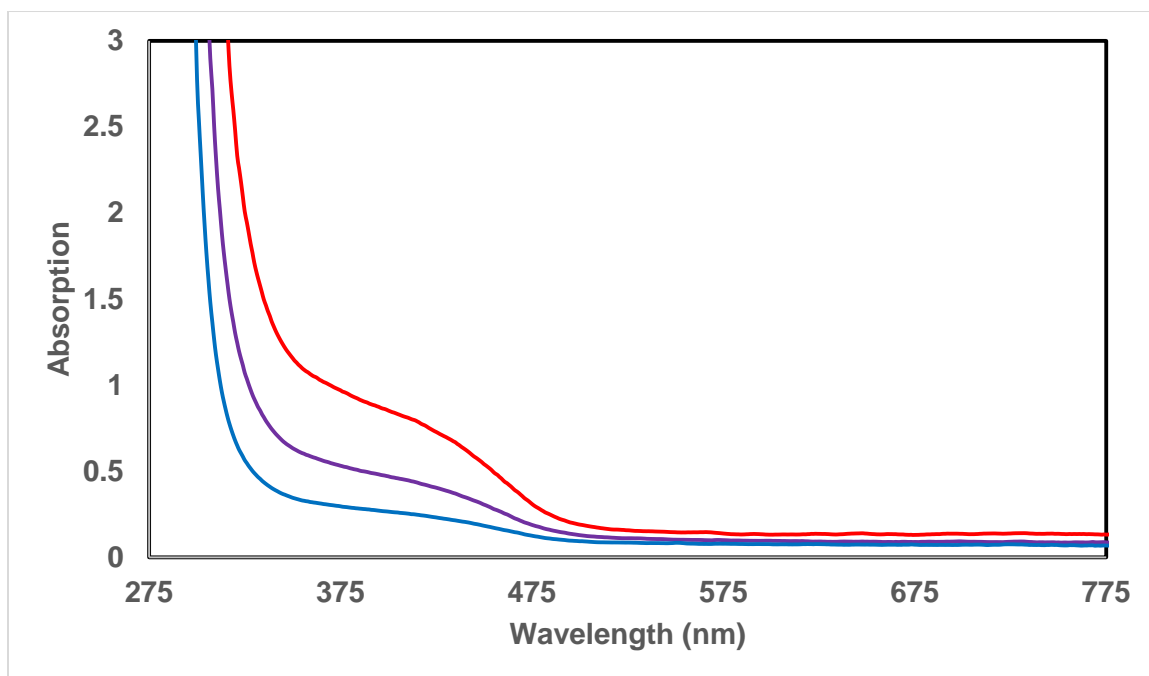


**Figure FD.14.** UV-Vis spectra of **D.7**/NaI in acetonitrile at 500  $\mu\text{M}$  (red), 250  $\mu\text{M}$  (purple), and 125  $\mu\text{M}$  (blue) concentrations.

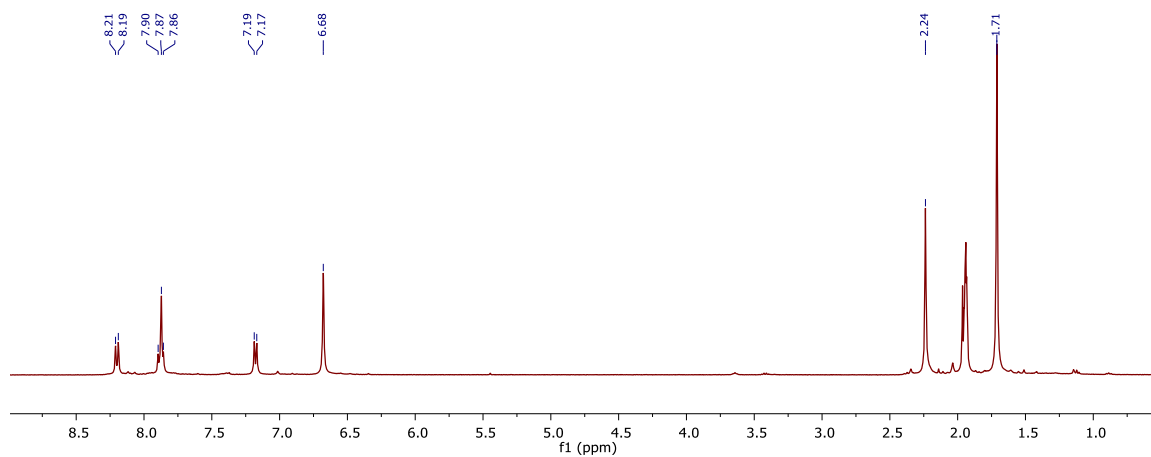


Figure FD.15. <sup>1</sup>H NMR of **D.8** in CD<sub>3</sub>CN.

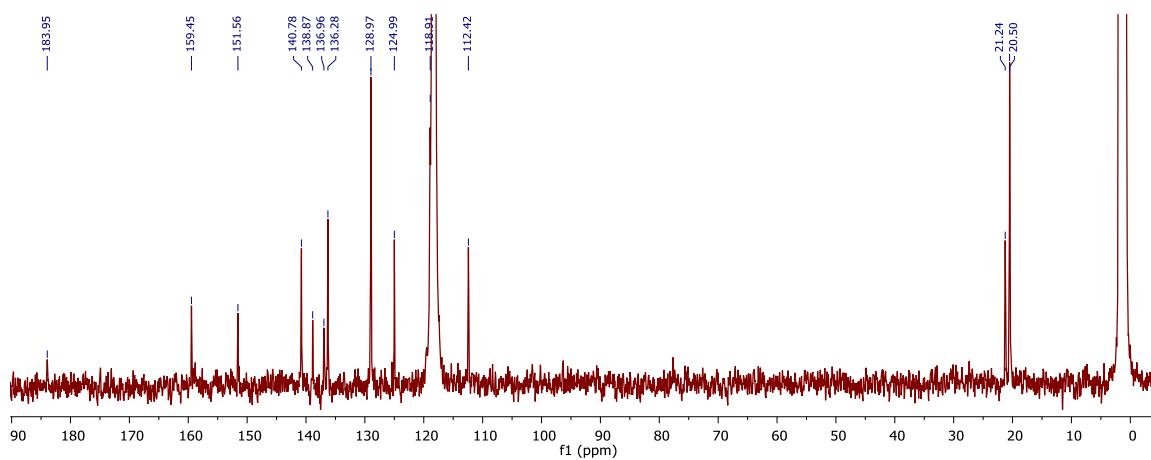


Figure FD.16. <sup>13</sup>C NMR of **D.8** in CD<sub>3</sub>CN.

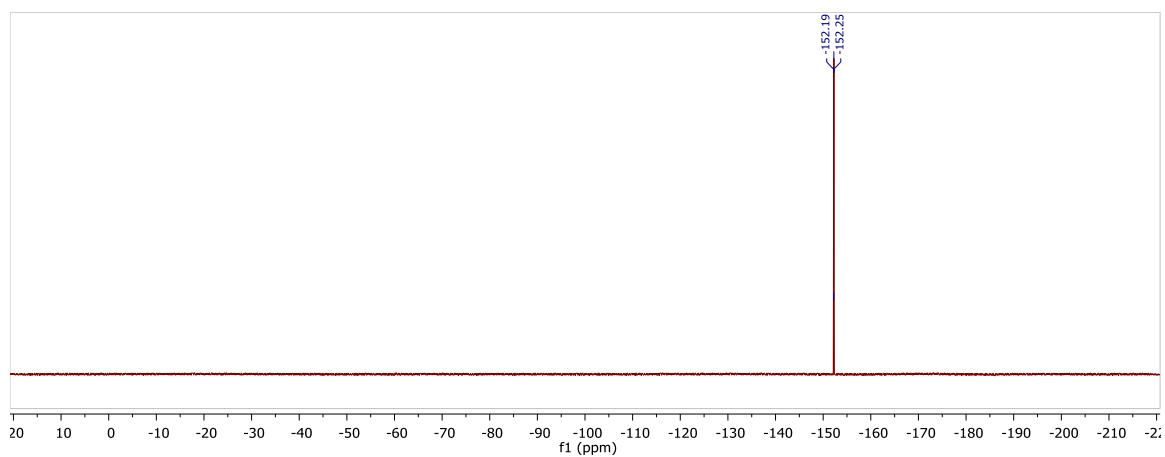
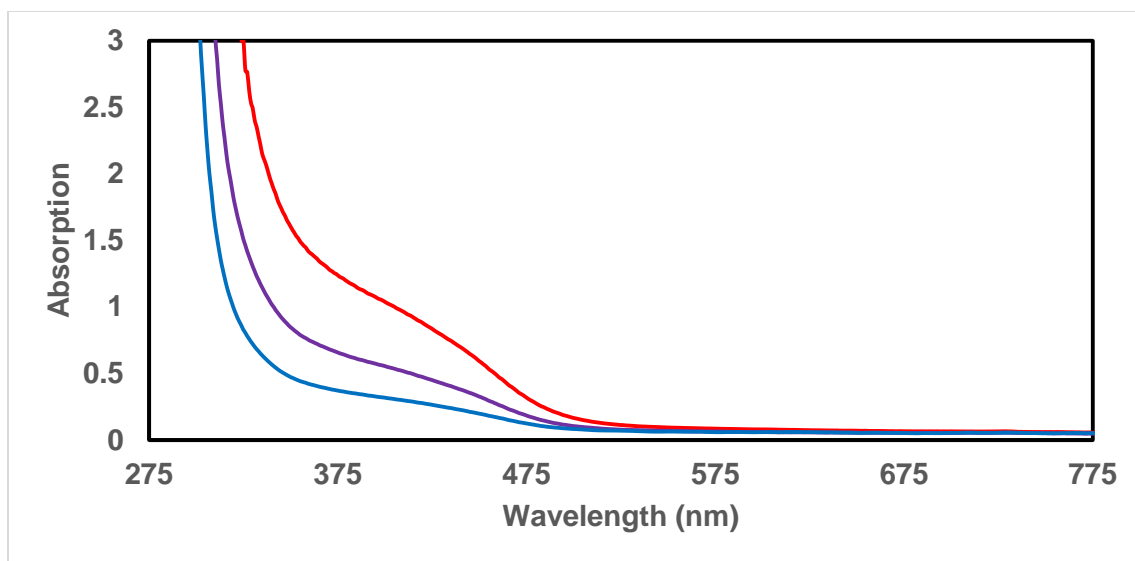
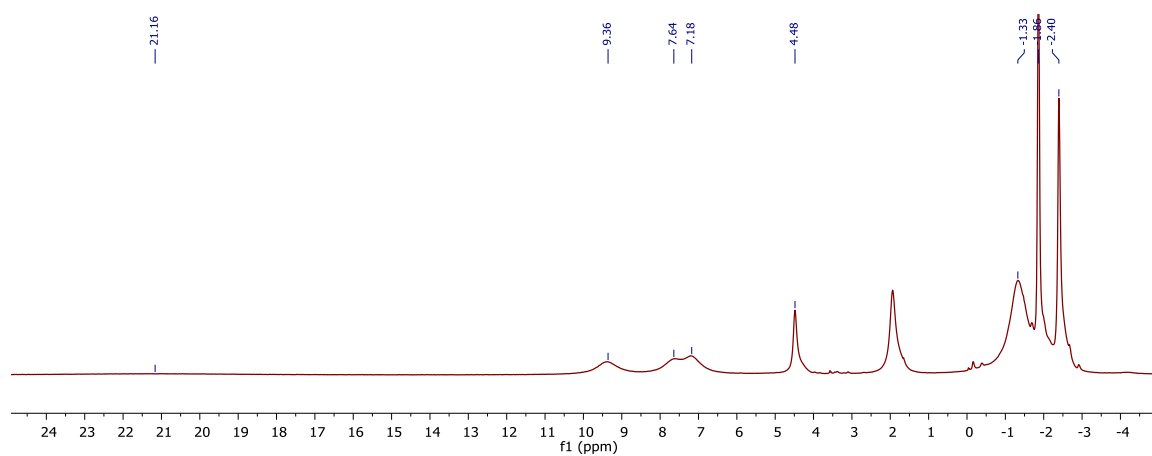


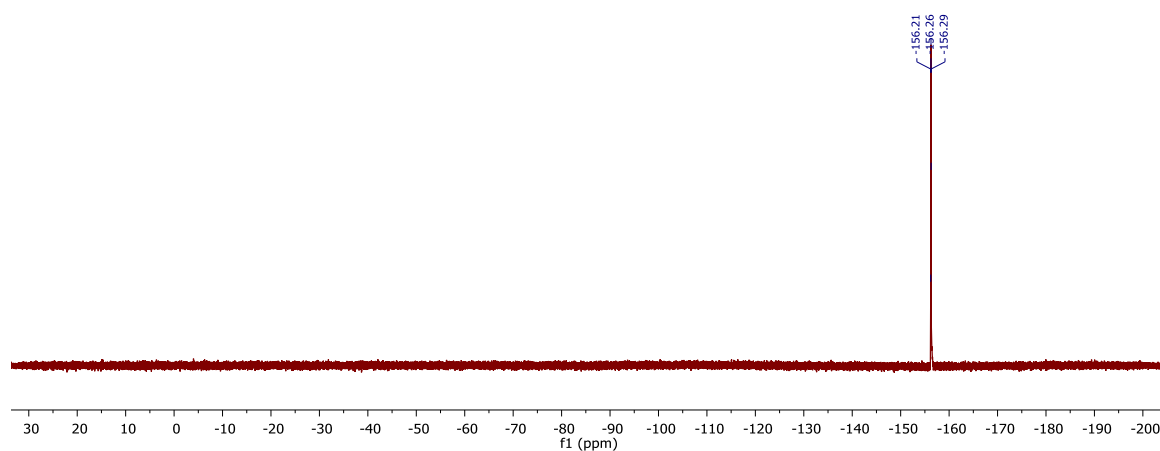
Figure FD.17. <sup>19</sup>F NMR of **D.8** in CD<sub>3</sub>CN.



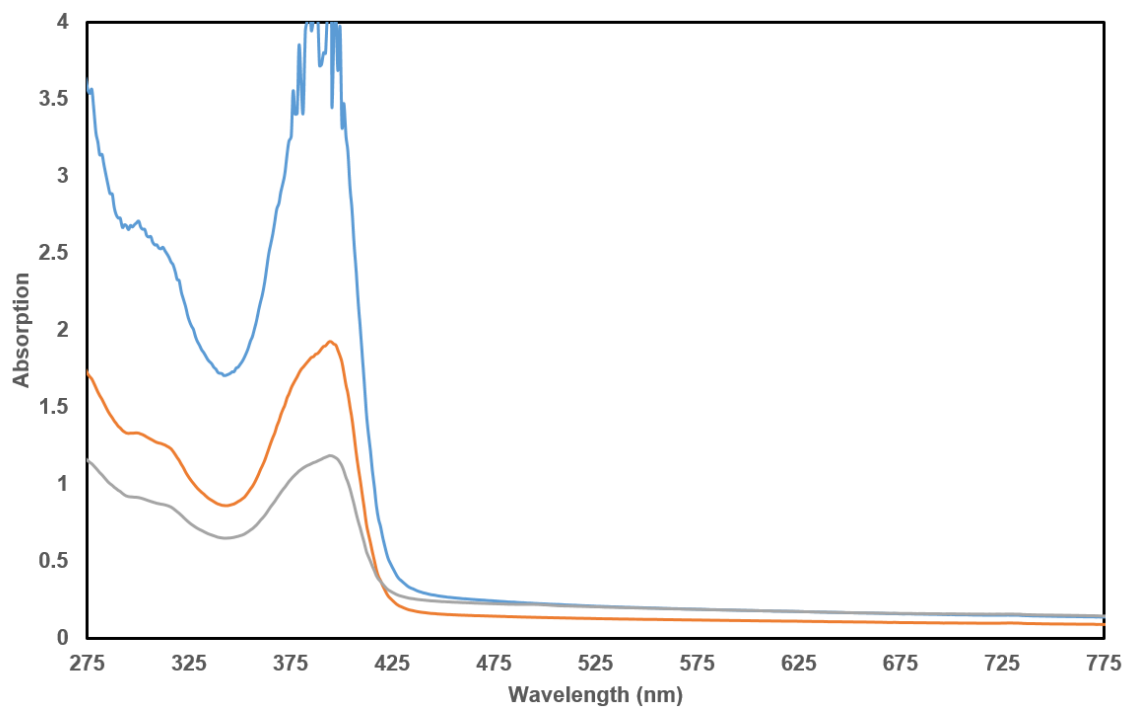
**Figure FD.18.** UV-Vis spectra of **D.8** in acetonitrile at 500  $\mu\text{M}$  (red), 250  $\mu\text{M}$  (purple), and 125  $\mu\text{M}$  (blue) concentrations.



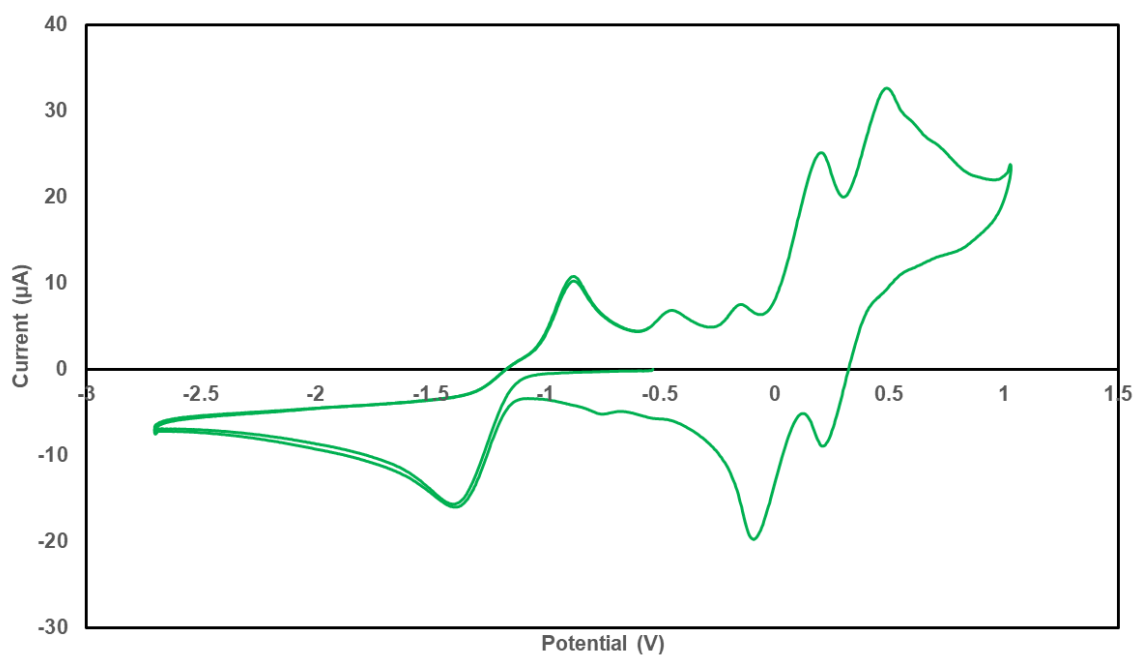
**Figure FD.19.**  $^1\text{H}$  NMR of **D.11** in  $\text{CD}_3\text{CN}$ .



**Figure FD.20.**  $^{19}\text{F}$  NMR of **D.11** in  $\text{CD}_3\text{CN}$ .

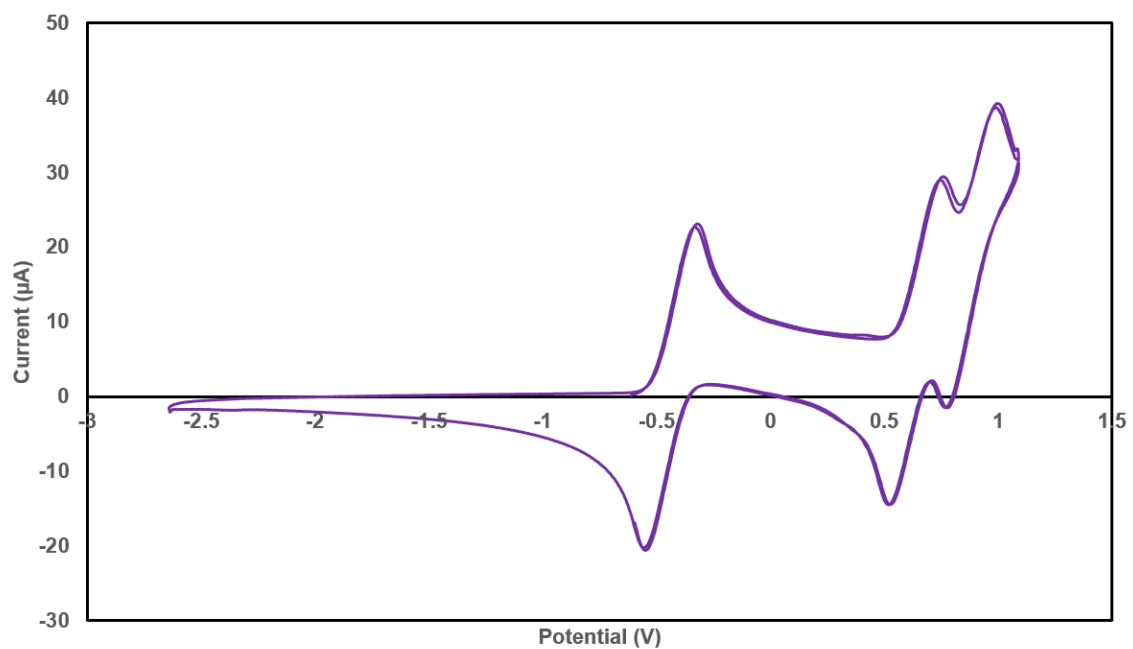


**Figure FD.21.** UV-Vis spectra of **D.11** in acetonitrile at 100  $\mu\text{M}$  (blue), 50  $\mu\text{M}$  (orange), and 25  $\mu\text{M}$  (grey).

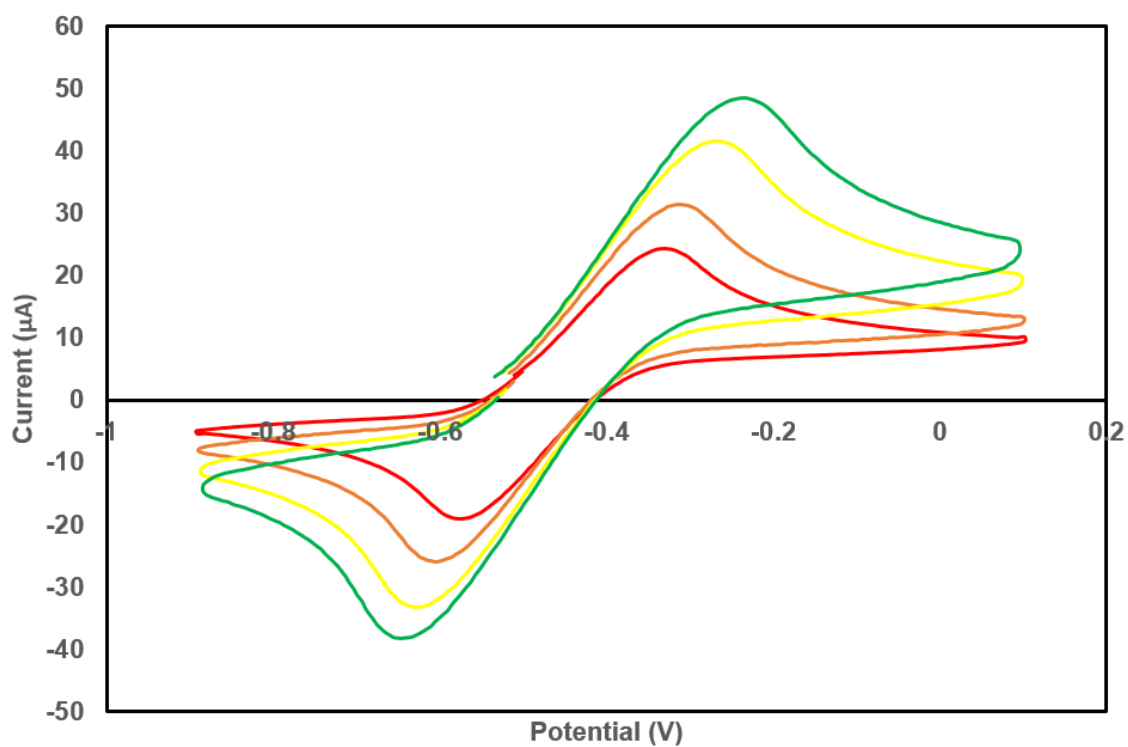


**Figure FD.22.** CV of **D.2**. Complex originally prepared by Dr. Gyeongshin Choi. Conditions: 0.1 M TBAPF<sub>6</sub>, 0.2 mM substrate in THF.

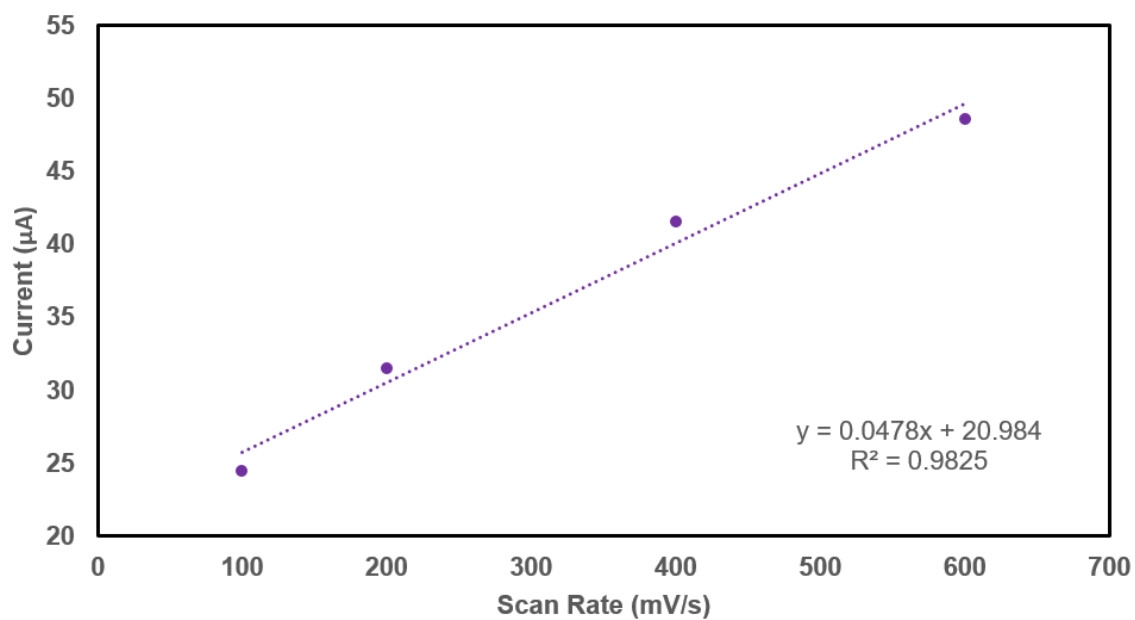




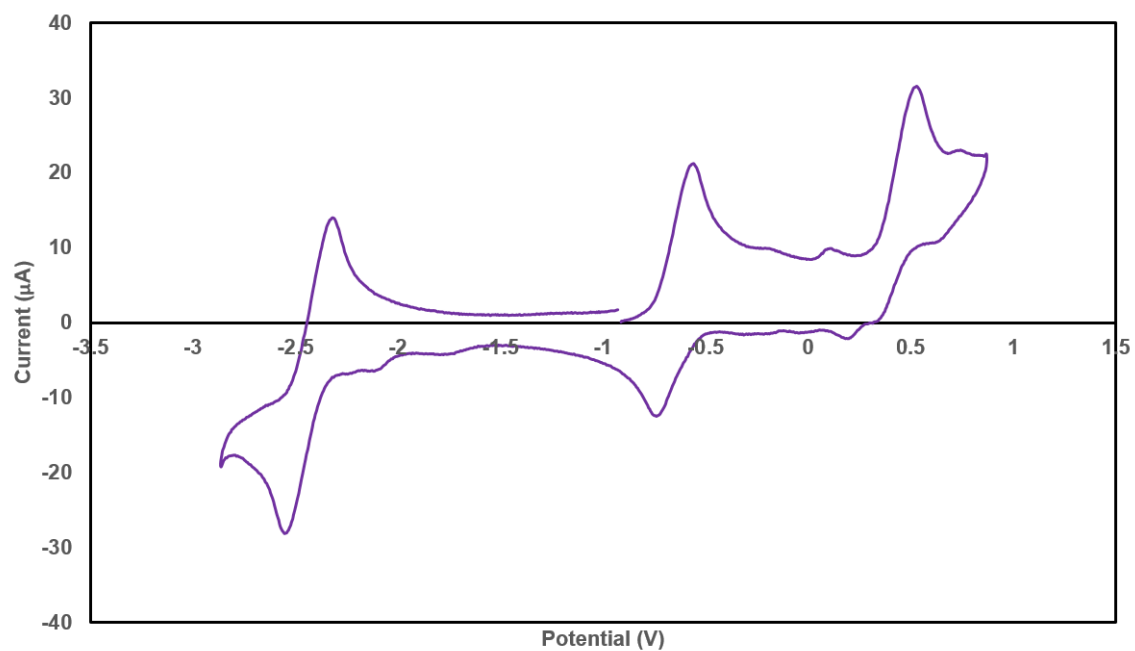
**Figure FD.23.** CV of **D.3**. Conditions: 0.1 M TBAPF<sub>6</sub>, 0.2 mM substrate in THF, 100 mV/s.



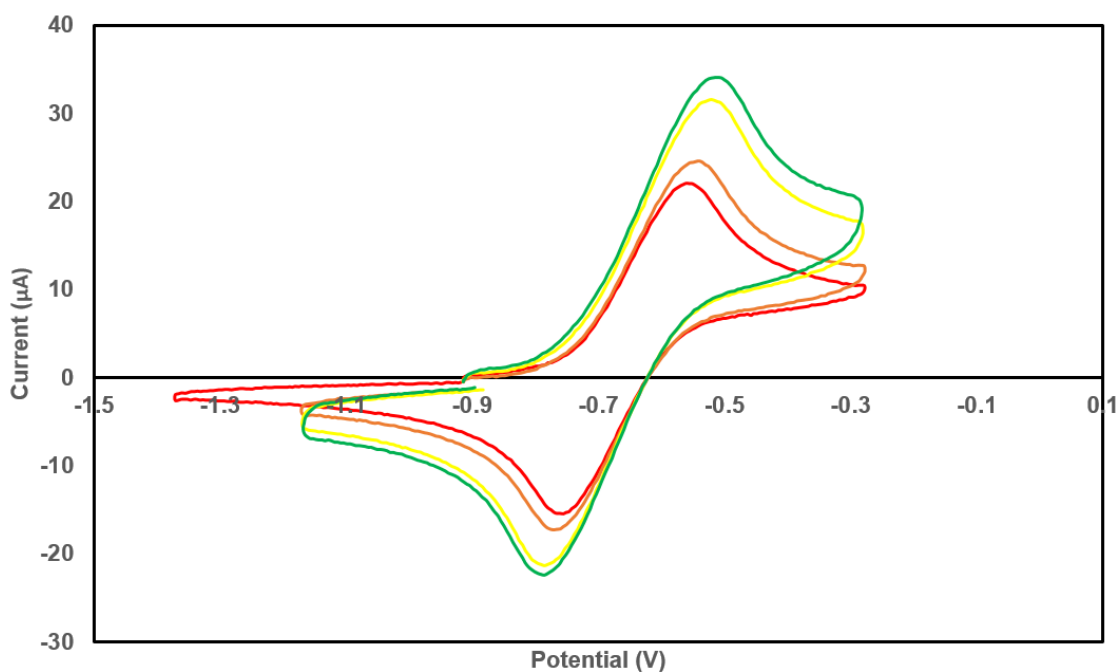
**Figure FD.24.** Isolated CV of the peak at -0.44 V from complex **D.3** with scan rates of 100 mV/s (red), 200 mV/s (orange), 400 mV/s (yellow), and 600 mV/s (green).



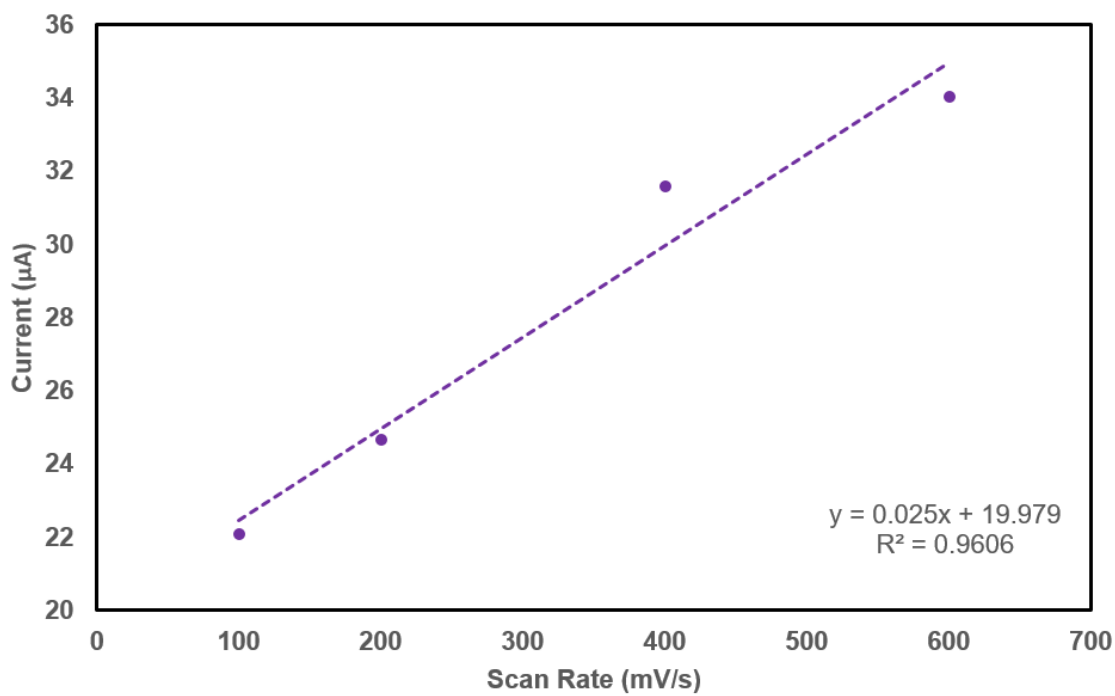
**Figure FD.25.** Current vs. scan rate plot for the feature at -0.44 V for complex **D.3**.



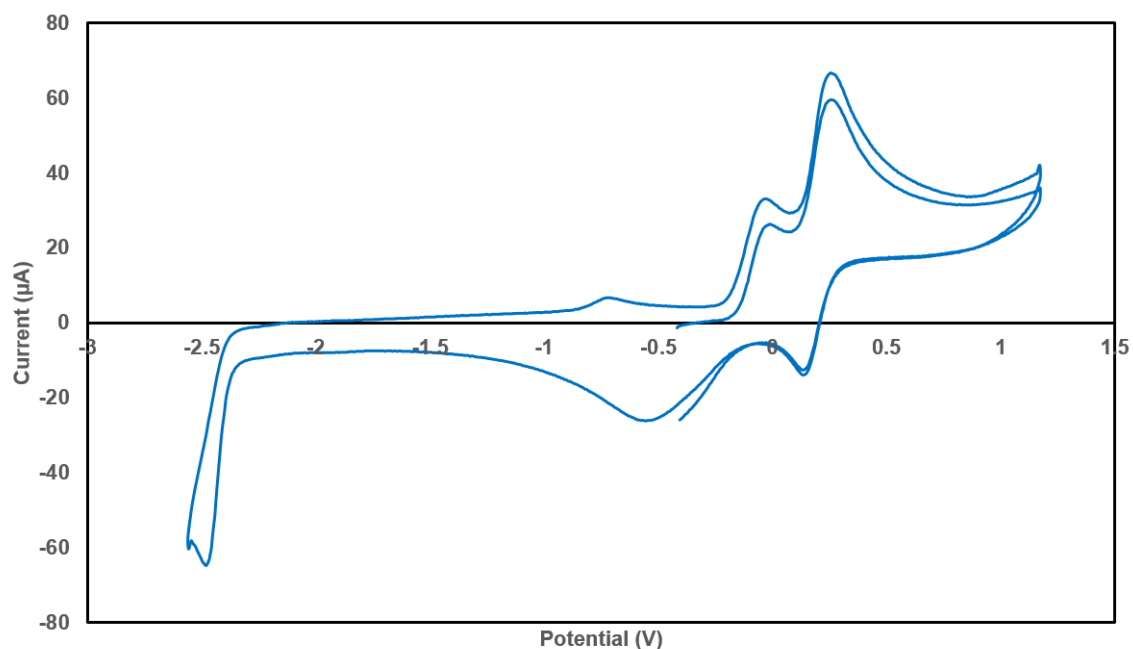
**Figure FD.26.** Full CV of **D.4**. Conditions: 0.1 M TBAPF<sub>6</sub>, 0.2 mM substrate in THF, 100 mV/s.



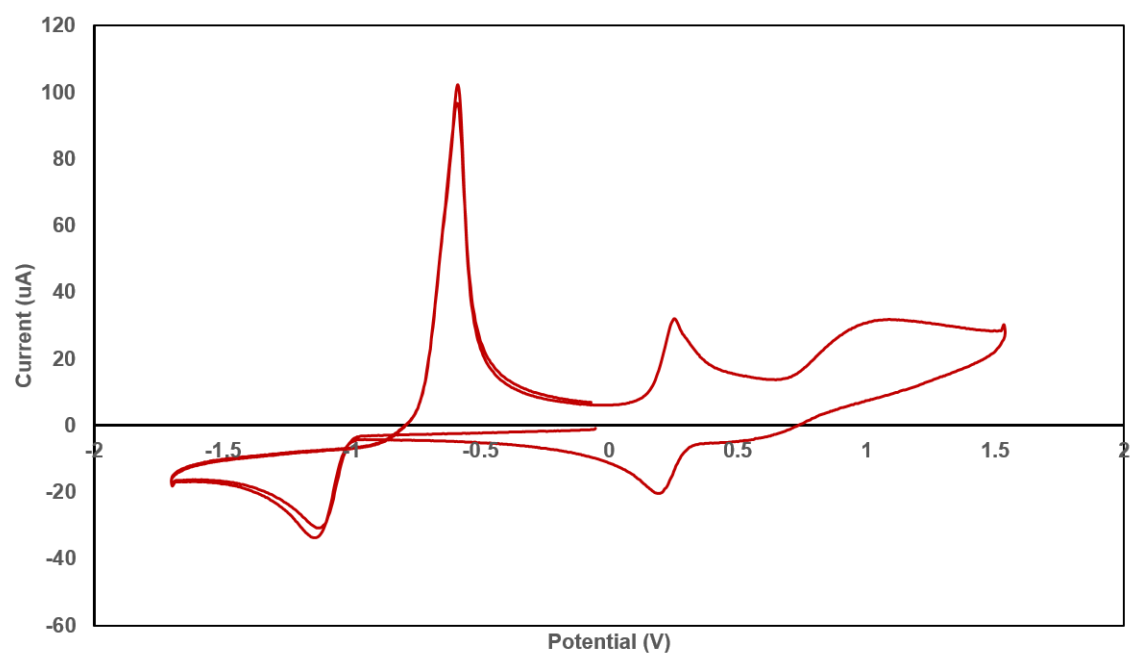
**Figure FD.27.** Isolated CV of the peak at -0.64 V from complex **D.4** at 100 mV/s (red), 200 mV/s (orange), 400 mV/s (yellow), and 600 mV/s (green).



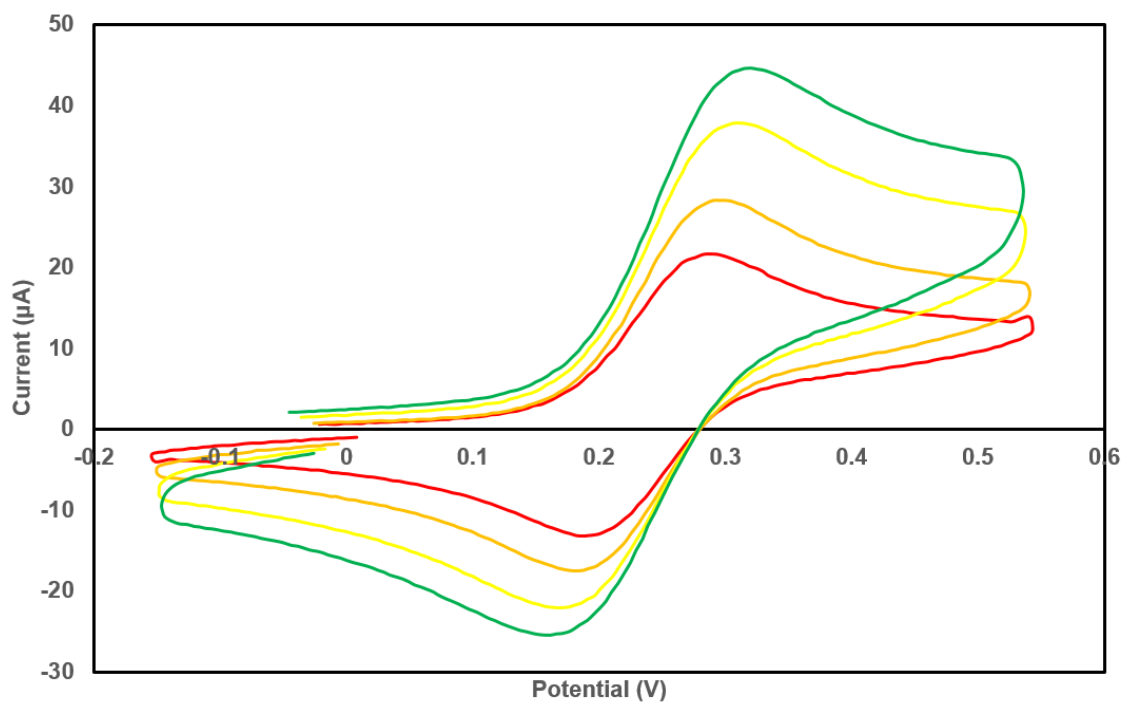
**Figure FD.28.** Current vs. scan rate plot for the feature at -0.64 V for complex **D.4**.



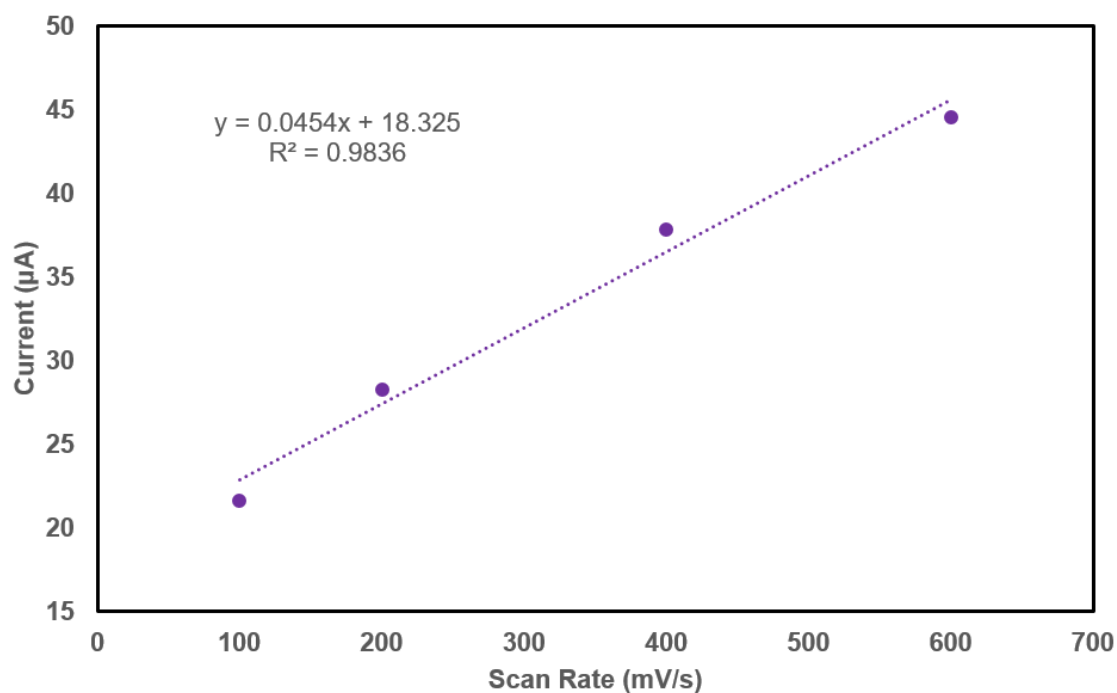
**Figure FD.29.** CV of **D.7**/NaI. Conditions: 0.1 M TBAPF<sub>6</sub>, 0.2 mM substrate in acetonitrile, 100 mV/s, internal reference to Fc/Fc<sup>+</sup>.



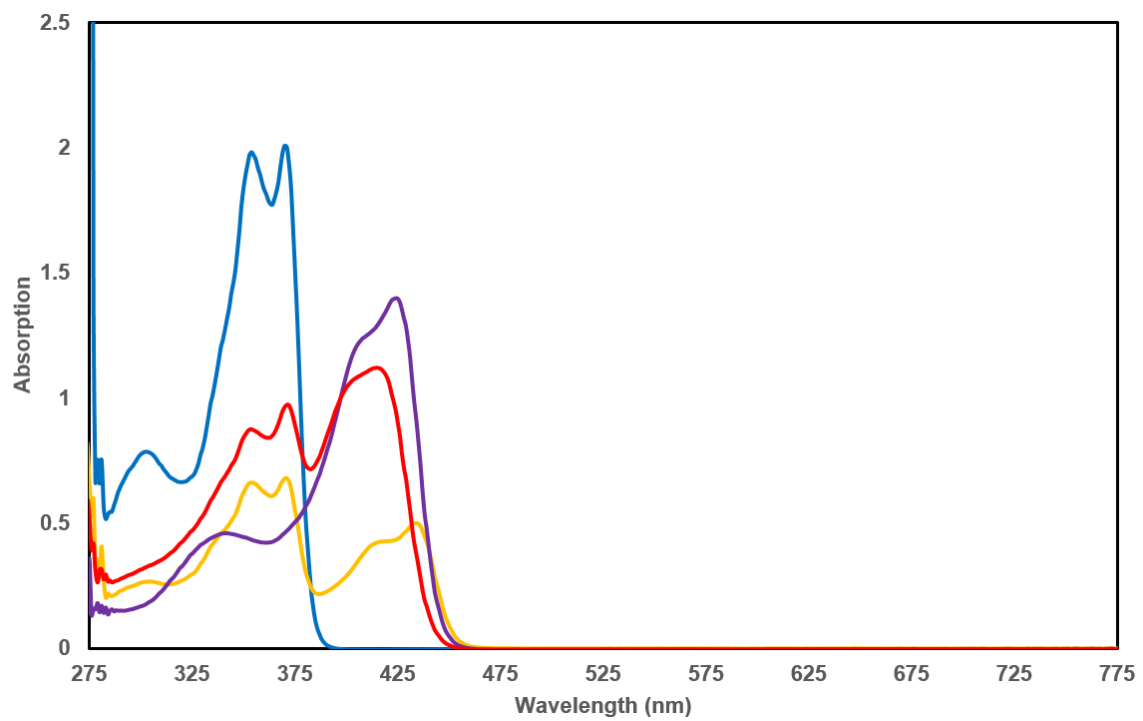
**Figure FD.30.** CV of **D.8**. Conditions: 0.1 M TBAPF<sub>6</sub>, 0.2 mM substrate in acetonitrile, 100 mV/s, internal reference to Fc/Fc<sup>+</sup>.



**Figure FD.31.** Isolated CV of the peak at +0.23 V from **D.8** at 100 mV/s (red), 200 mV/s (orange), 400 mV/s (yellow), and 600 mV/s (green).

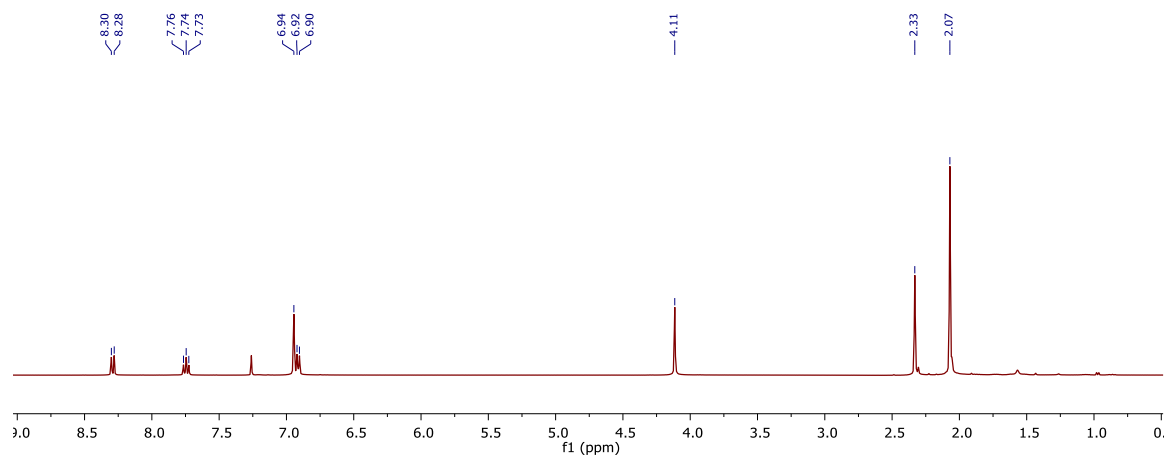
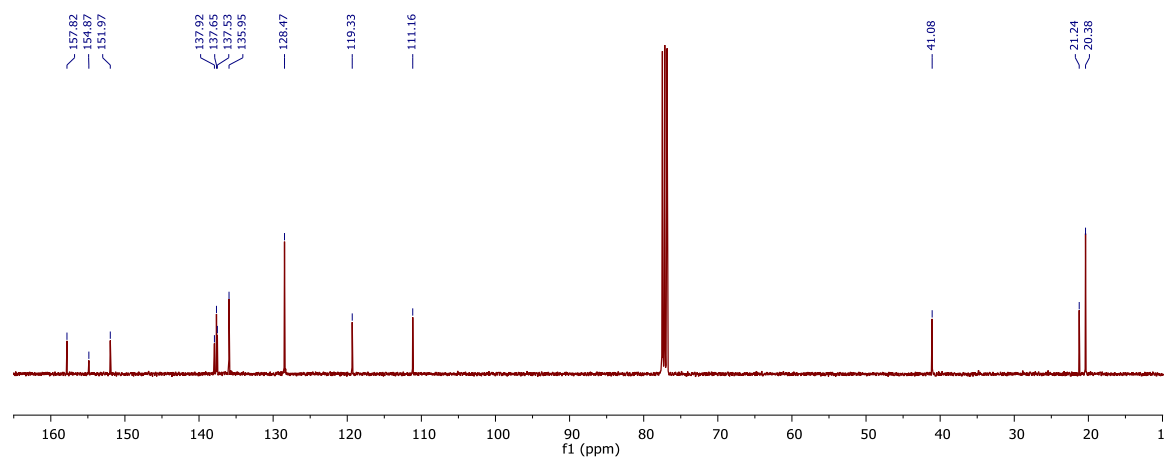
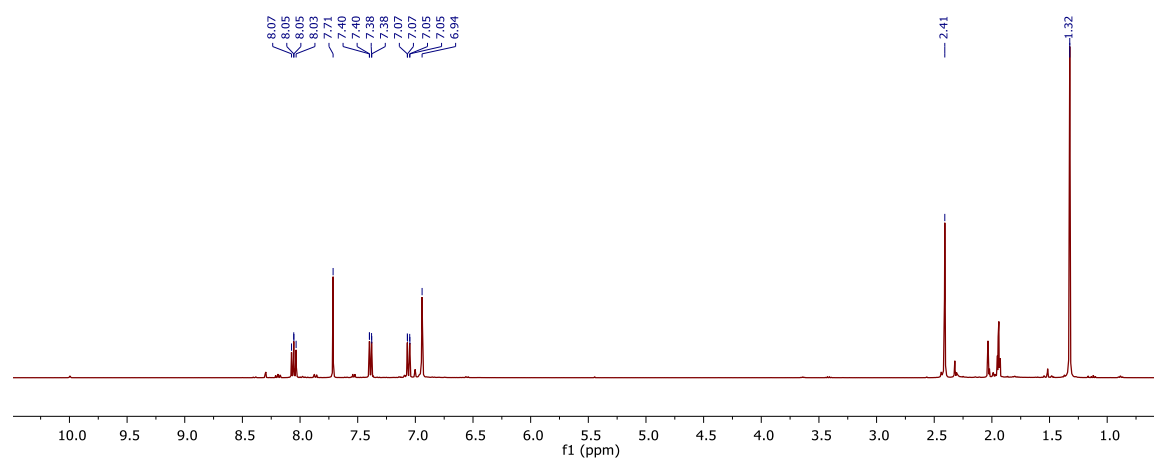


**Figure FD.32.** Current vs. scan rate plot for the feature at +0.23 V for complex **D.8**.



**Figure FD.33.** UV-Vis spectra of **D.1** (blue), the lithium salt of **D.1** (purple), the sodium salt of **D.1** (red), and the potassium salt of **D.1** (orange).

## APPENDIX E

Figure FE.1. <sup>1</sup>H NMR spectrum of **E.1** in CDCl<sub>3</sub>.Figure FE.2. <sup>13</sup>C NMR spectrum of **E.1** in CDCl<sub>3</sub>.Figure FE.3. <sup>1</sup>H NMR spectrum of **E.16** in CD<sub>3</sub>CN.

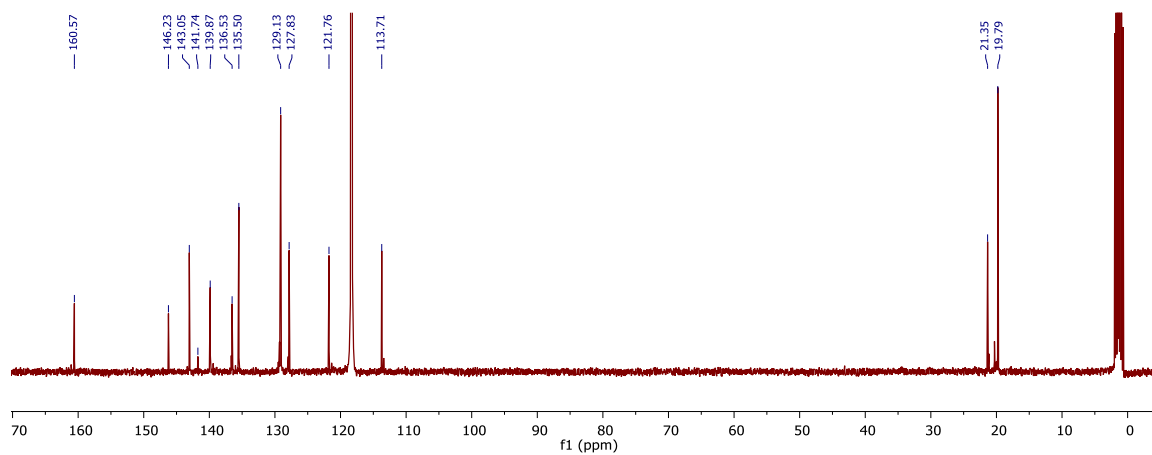


**Figure FE.4.**  $^{13}\text{C}$  NMR spectrum of **E.16** in  $\text{CD}_3\text{CN}$ .

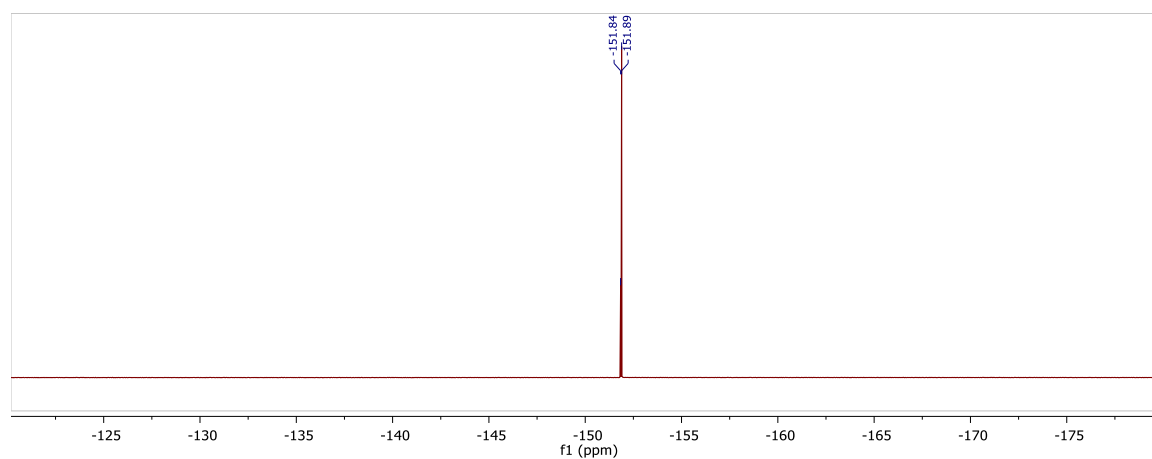


**Figure FE.5.**  $^{19}\text{F}$  NMR spectrum of **E.16** in  $\text{CD}_3\text{CN}$ .

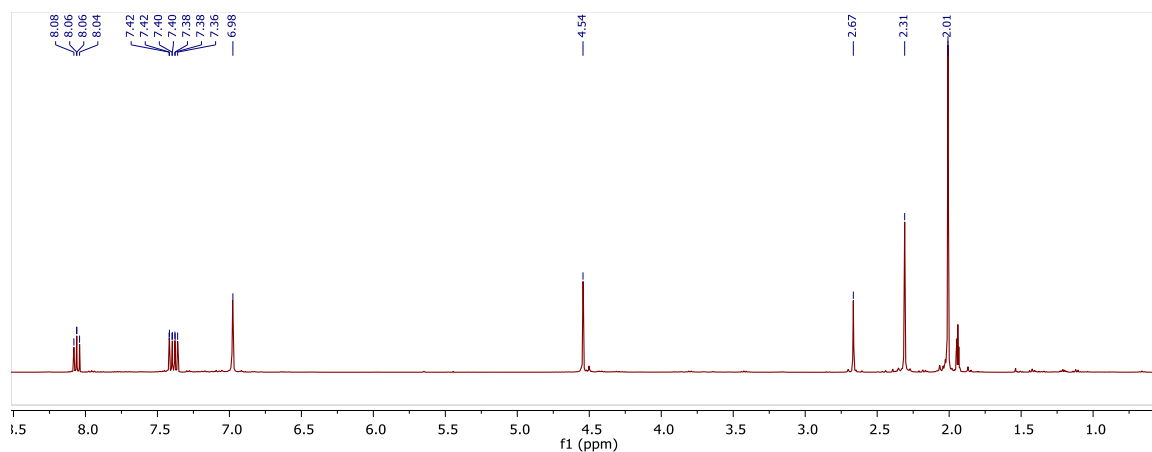


**Figure FE.6.**  $^1\text{H}$  NMR spectrum of **E.18** in  $\text{CD}_3\text{CN}$ .



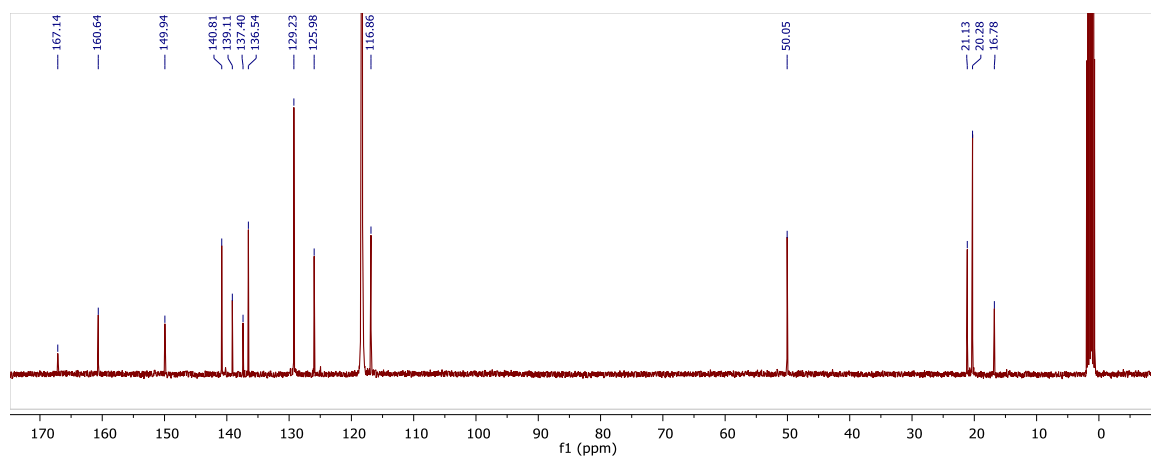


**Figure FE.7.** <sup>13</sup>C NMR spectrum of **E.18** in CD<sub>3</sub>CN.

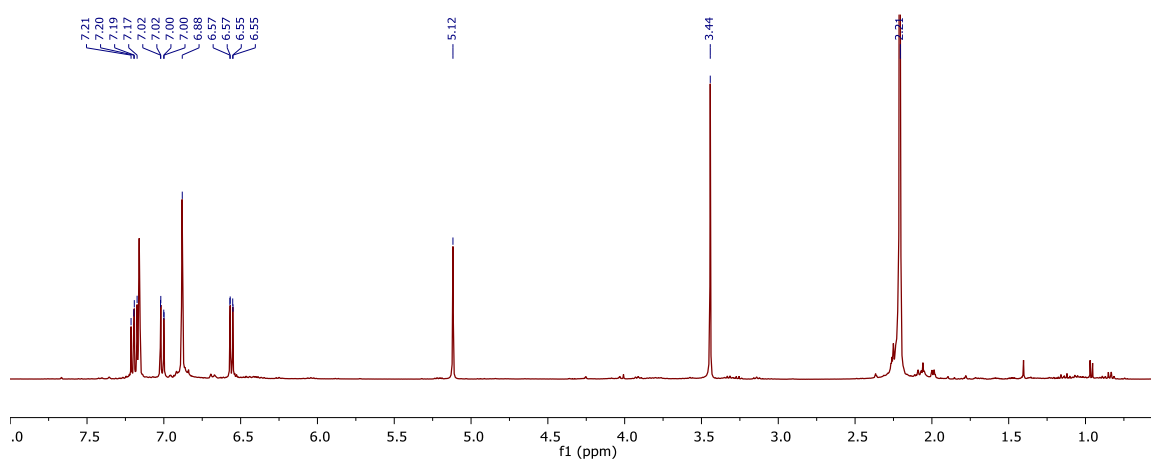


**Figure FE.9.** <sup>1</sup>H NMR spectrum of **E.19** in C<sub>6</sub>D<sub>6</sub>.

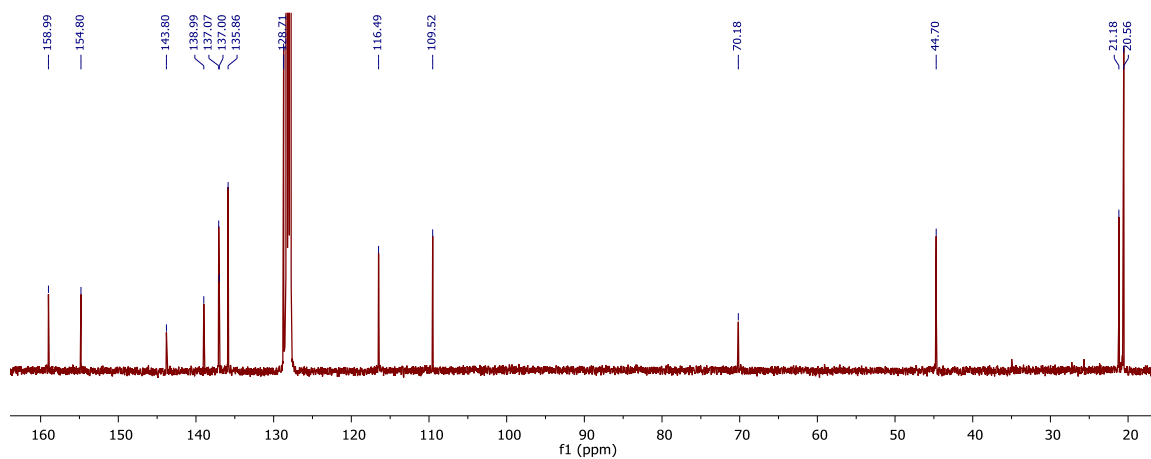


**Figure FE.10.** <sup>13</sup>C NMR spectrum of **E.19** in C<sub>6</sub>D<sub>6</sub>.

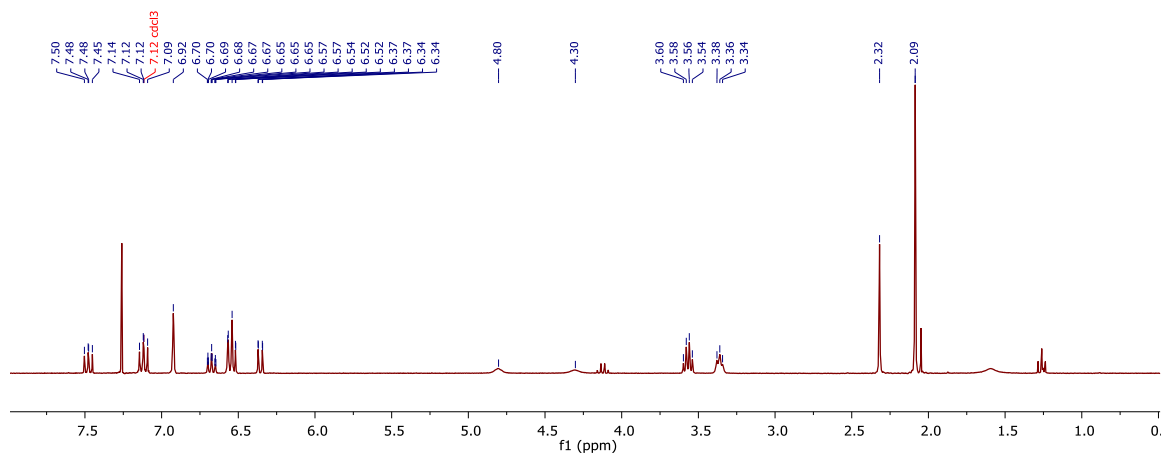


Figure FE.11.  $^1\text{H}$  NMR spectrum of **E.21** in  $\text{CDCl}_3$ .

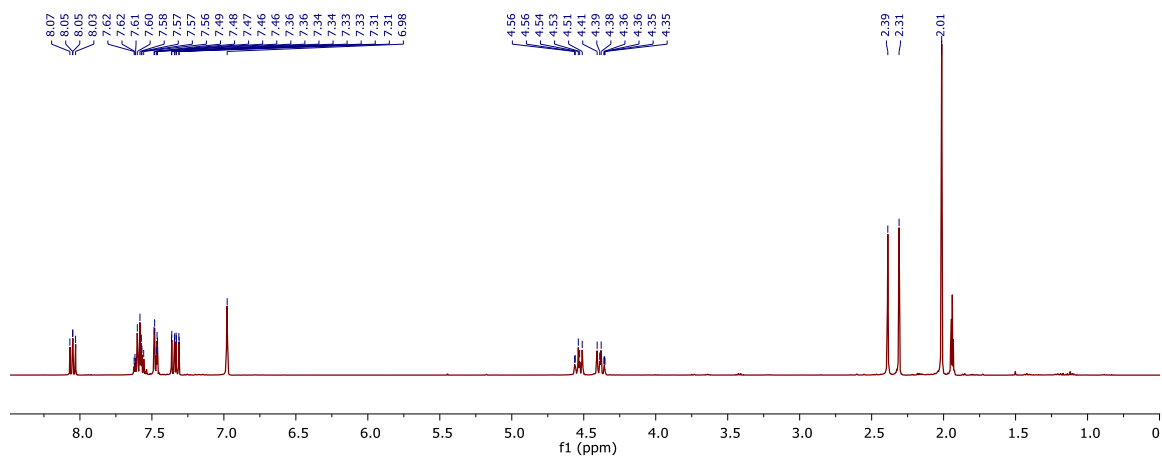


Figure FE.12.  $^1\text{H}$  NMR spectrum of **E.22** in  $\text{CD}_3\text{CN}$ .

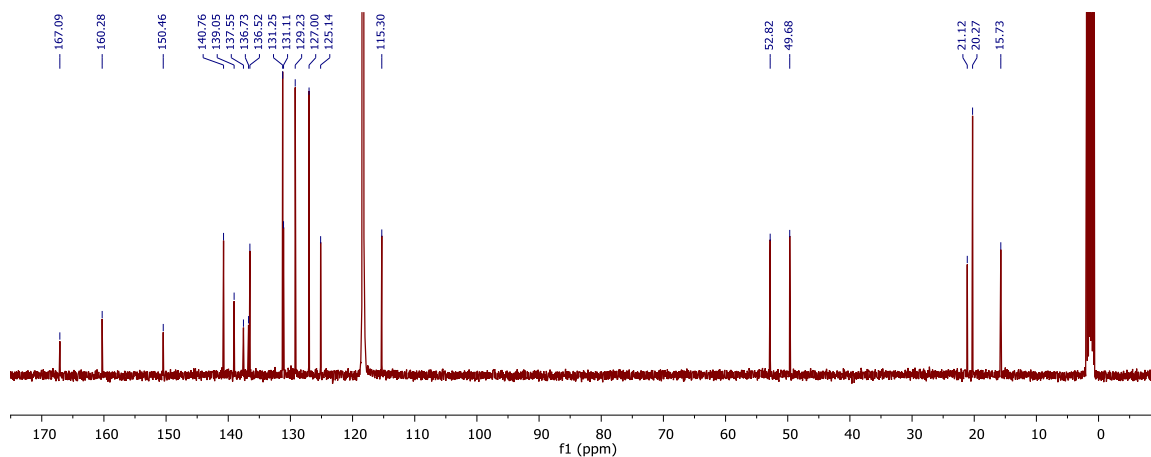


Figure FE.13.  $^{13}\text{C}$  NMR spectrum of **E.22** in  $\text{CD}_3\text{CN}$ .

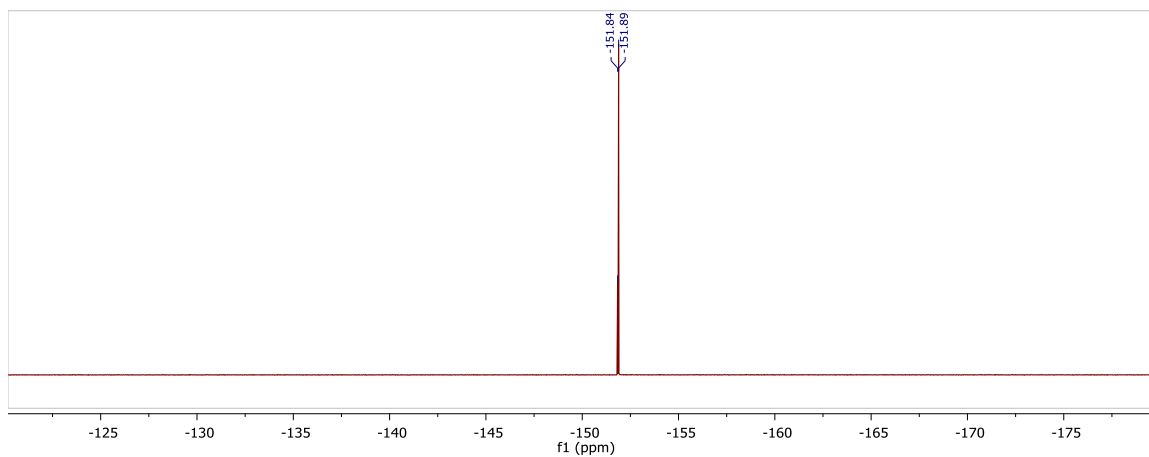


Figure FE.14.  $^{19}\text{F}$  NMR spectrum of **E.22** in  $\text{CD}_3\text{CN}$ .

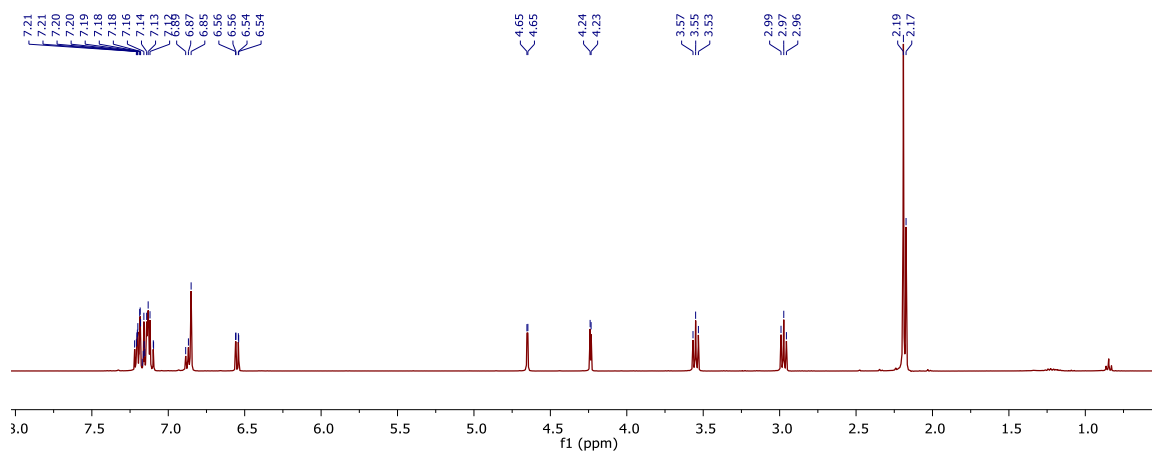


Figure FE.15.  $^1\text{H}$  NMR spectrum of **E.23** in  $\text{C}_6\text{D}_6$ .

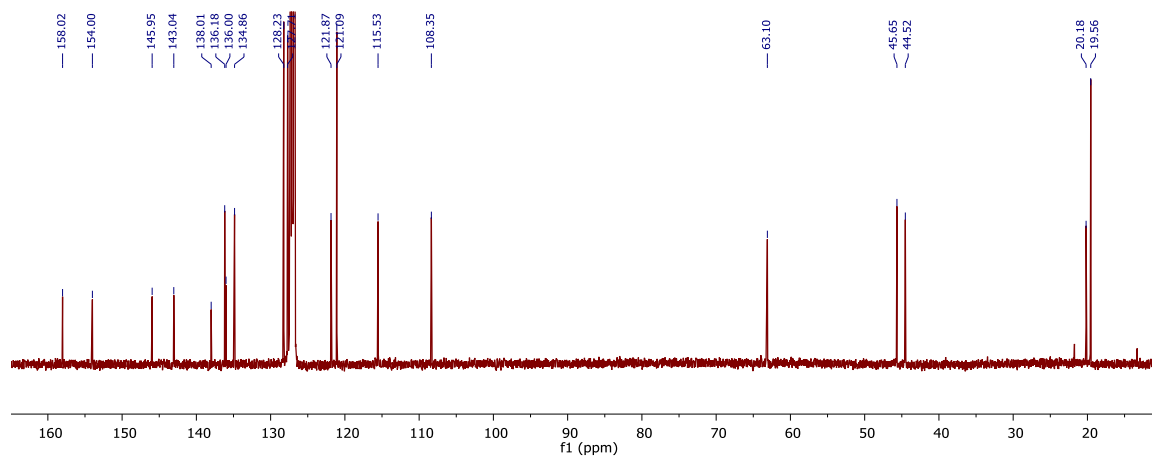
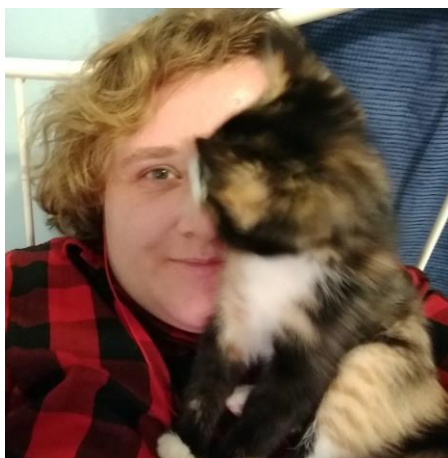


Figure FE.16.  $^{13}\text{C}$  NMR spectrum of **E.23** in  $\text{C}_6\text{D}_6$ .

## ABOUT THE AUTHOR



Jessica Sampson was born in Portsmouth, UK in September 1990 and moved to Newport, OR with her parents at the tender age of 6 weeks. She did all but six months of her K-12 education in Newport, OR and graduated valedictorian from Newport High School in June, 2009. During this period, Jessica spent time developing her skills as a pianist, bassoonist, and recorder and tuba player and participating in a range of ensembles including the Central Coast Chorale and in the orchestra for the musicals *Into the Woods* and *Sweet Charity*. She was also involved in numerous other theatre performances, including three separate productions of *Twelfth Night*. As a result of field trips to the Hatfield Marine Science Center through elementary and middle school, she developed an appreciation for marine life; however, it was not until her freshman chemistry course that she started down the road towards a career in the sciences. In fall 2009 she matriculated at the University of Chicago as a chemistry major. After brief stints in the Ocean Acoustics and Marine Geophysics Group at Oregon State University and as an editorial assistant for the sciences list at the University of Chicago Press, she worked for Prof. Richard Jordan on the development of phosphine-phosphonate Pd(II) catalysts for ethylene polymerization. In June 2013 she graduated from the University of Chicago with a B.S. in Chemistry with honors, then moved cross-country to California to start research in the group of Prof. Theodor Agapie at the California Institute of Technology. During the course of her graduate research, Jessica worked on the development of ligand platforms to support dinuclear olefin polymerization catalysts, second coordination sphere arene- $\pi$  interactions for substrate activation, and intramolecular  $\pi$ - $\pi$  interactions. Following completion of her graduate research, Jessica will start as a postdoctoral researcher in the group of Prof. Brad Carrow at Princeton University. In addition to science, Jessica refuses to stop talking about the ethics of labor practices in academia, robots, cats, lizards, octopi, and video games.

**Jessica Sampson**  
Curriculum Vitae

---

**Education**

California Institute of Technology, Division of Chemistry and Chemical Engineering  
(2013 – 2019)

*Ph.D. in Inorganic Chemistry*

University of Chicago, The College and The Division of the Physical Sciences (2009-2013)

*B.S. Chemistry with Honors*

Newport High School (2005-2009)

*High School Diploma*

**Awards and Honors**

Beta of Illinois, Phi Beta Kappa (2013)

Student Marshal, University of Chicago (2012-2013)

Dean's List, University of Chicago (2009-2013)

Valedictorian, Newport High School (2009)

**Research Experience**

Graduate Research, Prof. Theodor Agapie (2013 – 2019)

Undergraduate Research, Prof. Richard Jordan (2011-2013)

Ocean Acoustics and Marine Geophysics Group, NOAA Vents program (2008-2009, 2010)

Northwestern Aquatic Sciences, Apprenticeships in Science and Engineering (2007)

**Relevant Experience**

Teaching Assistant, Ch102, CCE Division, Caltech (2018)

Safety Officer, Agapie Lab, CCE Division, Caltech (2014-2018)

Computer Manager, Agapie Lab, CCE Division, Caltech (2014-2018)

Outreach, Agapie Lab, CCE Division, Caltech (2013 – present)

Graduate Lab Assistant, Liquid NMR Facilities, CCE Division, Caltech (2014-2017)

Series Organizer, Inorganic-Organometallics Seminar, CCE Division, Caltech (2015-2016)

**Workshops Attended**

CGSC Leadership Course, Chemistry Graduate Student Committee, California Institute of Technology, Pasadena, CA, USA (10/11/2018-10/12/2018)

Safe Zone LGBTQ+ Ally Training, Caltech Center for Diversity, Pasadena, CA, USA (10/9/2018-10/10/2018)

Developing Graduate Student Leadership Skills in Laboratory Safety, ACS Division of Chemical Health and Safety, Boston, MA, USA (8/19/2018)

Creating an Inclusive Classroom Workshop, CTLO and CCD, California Institute of Technology, Pasadena, CA, USA (7/18/2018)

## Publications

3. Alison M. Johnson, Nathan D. Contrella, Jessica R. Sampson, Mingfang Zheng, and Richard F. Jordan. "Allosteric Effects in Ethylene Polymerization Catalysis. Enhancement of Performance of Phosphine-Phosphinate and Phosphine-Phosphonate Palladium Alkyl Catalysts by Remote Binding of  $B(C_6F_5)_3$ " *Organometallics*, **2017**, *36*, 4990-5002.
2. Jessica Sampson, Gyeongshin Choi, Muhammed Naseem Akhtar, E. A. Jaseer, Rajesh Theravalappil, Hassan Ali Al-Muallem, and Theodor Agapie. "Olefin Polymerization by Dinuclear Zirconium Catalysts Based on Rigid Teraryl Frameworks: Effects on Tacticity and Copolymerization Behavior" *Organometallics*, **2017**, *36*, 1915-1928.
1. Nathan D. Contrella, Jessica R. Sampson, and Richard F. Jordan. "Copolymerization of Ethylene and Methyl Acrylate by Cationic Palladium Catalysts That Contain Phosphine-Diethyl Phosphonate Ancillary Ligands" *Organometallics*, **2014**, *33*, 3546-3555.

## Manuscripts in Preparation

5. Jessica Sampson, Ryan Ribson, Brian Sanders, Gyeongshin Choi, and Theodor Agapie. "Photophysics of Copper(I) Complexes Supported by Mesityl-Substituted Di(pyridyl) Pyrrolide Ligands" *Manuscript in Preparation*.
4. Jessica Sampson, Gyeongshin Choi, Muhammed Naseem Akhtar, E. A. Jaseer, Rajesh Theravalappil, Garcia Villalta, and Theodor Agapie. "Early Metal Di(pyridyl) Pyrrolide Complexes with Second Coordination Sphere Arene-Pi Interactions: Substrate Binding and Ethylene Polymerization." *Manuscript in Preparation*.

## Presentations

9. Mary Arrastia and Jessica Sampson. "How to Prepare SOPs" CCE Safety Day, California Institute of Technology, Pasadena, CA, USA 10/5/2018 (oral)
8. Jessica Sampson, Gyeongshin Choi, M. Naseem Akhtar, E.A. Jaseer, Rajesh Theravalappil, Hassan Ali Al-Muallem, and Theodor Agapie. "Transition Metal Complexes Supported by Pyrrolide and Imidazoline Ligands with Pyridine Donors." 256<sup>th</sup> ACS National Meeting, Boston, MA, USA 8/19/2018 (oral)
7. Jessica Sampson and Theodor Agapie. "Development of New Ligands for Olefin Polymerization." Division of Chemistry and Chemical Engineering Seminar Day, California Institute of Technology, Pasadena, CA, USA 11/10/2017 (poster)
6. Jessica Sampson and Marcus Low. "Liquid Nitrogen and Vacuum/Schlenk Line Hazards." CCE Safety Day, California Institute of Technology, Pasadena, CA, USA 11/04/2016 (oral)
5. Jessica Sampson and Theodor Agapie. "Ethylene and  $\alpha$ -Olefin Copolymerization by Bimetallic Zirconium Complexes." Division of Chemistry and Chemical Engineering Seminar Day, California Institute of Technology, Pasadena, CA, USA 10/21/2016 (poster)
4. Jessica Sampson, Muhammad Naseem Akhtar, E. A. Jaseer, Rajesh Theravalappil, Hassan Ali Al-Muallem, Madalyn Radlauer, and Theodor Agapie. "Ethylene and  $\alpha$ -Olefin Copolymerization by Bimetallic Zirconium Complexes." 251<sup>st</sup> ACS National Meeting, San Diego, CA, USA 3/2016 (oral)
3. Jessica Sampson and Theodor Agapie. "Novel Bimetallic Zirconium Complexes for Ethylene and  $\alpha$ -Olefin Polymerization." SoCal Organometallics Meeting, California Institute of Technology, Pasadena, CA, USA 2/22/2015 (poster)

2. Madalyn Radlauer, Jessica Sampson, and Theodor Agapie. "Bimetallic complexes for polymerization catalysis." 248th ACS National Meeting, San Francisco, CA, USA 8/10/14 (oral)
1. Madalyn Radlauer, Jessica Sampson, and Theodor Agapie. "Polymerization catalysis by bimetallic complexes" 248<sup>th</sup> ACS National Meeting, San Francisco, CA, USA 8/10/14 (poster)